MASSIVE NEUTRINOS
in
ASTROPHYSICS
and in
PARTICLE PHYSICS

Moriond Workshop on Massive Neutrinos
in Astrophysics and in Particle Physics

La Plagne — Savoie — France, January 15-21, 1984

MASSIVE NEUTRINOS IN ASTROPHYSICS AND IN PARTICLE PHYSICS

ISBN 2-86332-026-2

Editions Frontieres
B.P. 44
91190 Gif-sur-Yvette
France

Printed in Singapore by Kim Hup Lee
Printing Co. Pte Ltd.

Proceedings of the

FOURTH MORIOND WORKSHOP

La Plagne — Savoie — France, January 15-21, 1984

MASSIVE NEUTRINOS in ASTROPHYSICS and in PARTICLE PHYSICS

edited by
J. Tran Thanh Van

The Fourth Moriond Workshop on

MASSIVE NEUTRINOS IN ASTROPHYSICS AND IN PARTICLE PHYSICS

was organized by

J. TRAN THANH VAN
and F. VANNUCCI



Associated Editor : Mrs O. LEBEY

FOREWORD

The fourth Moriond Workshop of the XIXth Rencontres de Moriond was held at La Plagne, Savoie, (France) from January 15 to January 21 1984.

The main purpose of the Rencontres de Moriond is to discuss recent developments in contemporary physics and also to promote effective collaboration between experimentalists and theorists in similar fields. By bringing together a relatively small number of participants, we hope to develop better humain relations as well as a more thorough and detailed discussion of the contributions in an informal and friendly atmosphere.

The first workshop (1981) was devoted to Lepton pair production, the second one (1982) to New flavour production and the third one (1983) to Antiproton-proton physics and the W discovery. This year, we focus the workshop on the properties of Massive neutrinos and their implication in astrophysics and particle physics. It is hoped that this confrontation of ideas between astrophysicists and particle physicists and between experimentalists and theorists in this rapidly evolving field allows to deepen our knowledge of the basic structure of matter.

I would like to thank the programm committee members : A. De Rujula, E. Fiorini, A. Grant, J. Schneider, J. Walker and especially the coordinator F. Vannucci for the hard work of organizing and preparing the scientific program and the Conference secretaries O. Lebey, Le Van Suu and L. Norry, who have devoted much of their time and energy to the success of the fourth Moriond Workshop.

I am also grateful to Ms V. Cabaud, Mr F. Meignen, Mr O. Nicolet and Mr and Ms Beaucourt who contributed through their hospitality and cooperation to the well-being of the participants, enabling them to work in a relaxed atmosphere.

J. TRAN THANH VAN

CONTENTS

I. INTRODUCTION

B. KAYSER "Introduction to massive neutrinos". 11

F. VANNUCCI "Phenomenology of massive neutrinos". 45

S.P. ROSEN "General CP properties of neutrino mass eigenstates". 53

B. KAYSER "CPT and CP properties of majorana neutrinos and the practical consequences". 59

II. NEUTRINO OSCILLATION

L. LANCERI "Results on neutrino oscillations from the charm collaboration". 73

J. WOTSCHACK "Results from the CDHS ν oscillation experiment at CERN". 85

C. HABER "A search for inclusive oscillations of muon neutrinos in the mass range $30 < \Delta m^2 < 1000\ eV^2$ ". 99

K. SCHRECKENBACH "The source spectrum of reactor anti-neutrinos and its application to neutrino oscillation studies". 125

G. CONFORTO "Beam dump experiments and neutrino oscillations". 133

J. M. THENARD "Search for neutrino oscillations at Bugey reactor". 143

III. NEUTRINO MASSES

M. GRONAU "The high mass frontier : limits on heavy neutrinos". 155

A. OLIN "Search for massive neutrinos in π --> eν decays". 173

P. LECOULTRE "Determination of an upper limit of m_{ν_μ} from π -decay in flight". 179

R. PRIEELS "Searches for heavy neutrinos in meson decays and muon capture". 189

C. MATTEUZZI "An upper limit on the ν_τ mass". 201

C. SANTONI "Search for the decay of heavy neutrinos". 207

J.M. LEVY	"Some neutrinos decays".	217
J. BJORKEN	"Search for neutral, penetrating, metastable particles produced in the SLAC beam dump".	227
K.E. BERGKVIST	"Some notes on a current neutrino mass experiment in Stockholm".	243
R.G.H. ROBERTSON	"The Los Alamos experiment on atomic and molecular tritium".	253
J.W. PETERSEN	"Resolution tests of the Zurich β-spectrometer".	261
K. SCHRECKENBACK	"Search for massive neutrino branches in nuclear beta decays".	267
O. FACKLER	"The calculation of molecular final states and their effect on a precision neutrino mass experiment".	273
O. FACKLER	"An experiment for a precision neutrino mass measurement".	281
H. L. RAVN	"The N/M electron-capture ratio of the neutrino-mass probe ^{163}Ho".	287

IV. NEUTRINOS IN ASTROPHYSICS

G. STEIGMAN	"Massive neutrinos in cosmology".	295
M. SPIRO	"A possible solar neutrino detector based on indium neutrino reaction and using well known techniques".	311
G. WAYSAND	"Detection of low energy solar neutrinos by chambers of metastable superconducting granules".	319
L. STODOLSKI	"Neutrino masses and mixings in supernova bursts".	341
J.P.J. LAFON	"Halos or no Halos : Is there 'missing mass' hidden in (massive or not) halos in flat galaxies".	355
E. SCHATZMAN	"The internal structure of the sun and the solar neutrinos problem".	369
A. DRUKIER & L. STODOLSKI	"Principles and applications of a neutral current detector for neutrino physics and astronomy".	395

V. DOUBLE BETA DECAY

T. KOTANI	"The double beta decay -Neutrino masses and Right handed current-".	397
S. P. ROSEN	"Comment on the light-heavy majorana neutrino mechanism in no-neutrino double beta decay".	425
L. ZANOTTI	"Double beta decay experiment in the Mont Blanc Tunnel".	429
R. EISBERG	"Progress report on the UCSB/LBL neutrinoless double beta decay experiment".	439

VI. EXOTICS

F. PIERRE	"Single photon detection with Cello at Petra".	447
A. ROTHENBERG	"Limits on the number of light neutrinos".	453
D. PERRET-GALLIX	"Amplification of fluxoids by metastable superconducting granules proposal for an all-Beta monopole detector".	461
A. K. DRUKIER	"Search for superheavy magnetic monopoles with use of a superconducting colloid detector".	471

VII.SUMMARY

S.P. ROSEN	"Summary talk".	483

INTRODUCTION TO MASSIVE NEUTRINOS

Boris Kayser
Division of Physics, National Science Foundation
Washington, D.C. 20550



ABSTRACT

We discuss the theoretical ideas which make it natural to expect that neutrinos do indeed have mass. Then we focus on the physical consequences of neutrino mass, including neutrino oscillation and other phenomena whose observation would be very interesting, and would serve to demonstrate that neutrinos are indeed massive. We comment on the legitimacy of comparing results from different types of experiments. Finally, we consider the question of whether neutrinos are their own antiparticles. We explain what this question means, discuss the nature of a neutrino which is its own antiparticle, and consider how one might determine experimentally whether neutrinos are their own antiparticles or not.

I would like to begin this introduction to the subject of massive neutrinos by briefly discussing theoretical prejudices about neutrino mass. Do current theoretical views lead us to expect that neutrinos are indeed massive? If they do, do they tell us how heavy the neutrinos might be? Then, I would like to focus on the physical consequences of neutrino mass. How does neutrino mass lead to neutrino oscillation, and what is the physics of this process? How does one look for massive neutrinos in meson decay, or in neutrino decay? Need one worry about quantum-mechanical subtleties when comparing results from direct searches for neutrino mass with those from neutrino oscillation experiments? Finally, I would like to consider the question of whether neutrinos are their own antiparticles. In physical terms, what precisely does this question mean? Why is it that we do not already know the answer? How does one describe a neutrino which is its own antiparticle in field theory? Will accelerator experiments at higher energies help to tell us whether neutrinos are their own antiparticles? If not, what experiments will help to answer this question?

Prejudices from Theory

From the standpoint of the grand unified theories (GUTS), which seek to unify the description of the weak, electromagnetic, and strong interactions, it is more natural for neutrinos to be massive than to be massless. The reason is trivial. In any grand unified theory, a given neutrino is put together with a charged lepton and with quarks in one large multiplet. Now, if the neutrino becomes a brother of a charged lepton, which, of course, is massive, and of quarks, which, of course, are also massive, then the neutrino itself would have to be exceptional to be massless. Naturally, this is not a proof that neutrinos have mass. One can construct grand unified theories in which the neutrinos are presumed to be massless, and their masslessness is put in by hand. People have constructed such GUTS. However, I think it is clear that, given the basic character of grand unified theories, this is not the natural thing to do. The natural thing in a GUT is for a neutrino to be massive, just as the other particles in its quark-lepton multiplet are.

Assuming, now, that neutrinos are indeed massive as the

grand unified theories suggest, let us ask how heavy they are likely to be. Unfortunately, as far as gauge theories are concerned, the neutrino masses could be anything at all. If you force yourself to make an estimate of the neutrino mass scale which is natural in GUTS, you can do so by insisting that the neutrino mass term in the Lagrangian contain only known, rather tightly constrained ingredients. Let me explain.

There can be two types of neutrino mass terms in the Lagrangian for a theory. The first is the familiar Dirac mass term, of the form

$$\begin{aligned} \mathcal{L}_D &= -M\bar{\nu}\nu = -M(\bar{\nu}_R \nu_L + \bar{\nu}_L \nu_R) \\ &= -M(\bar{\nu}_R \nu_L + \text{h.c.}) \end{aligned} \tag{1}$$

Here, M is the neutrino mass, and $\nu_{L,R}$ are the left- and right-handed projections of the neutrino field, given by

$$\nu_{L,R} = \frac{1 \pm \gamma_5}{2} \nu \ . \tag{2}$$

The second type of mass term is the Majorana mass term, which has the form

$$\begin{aligned} \mathcal{L}_M &= -M(\overline{\nu^c})_R \ \nu_L + \text{h.c.}) \\ &= -M(\nu_L^T C \nu_L + \text{h.c.}) \ . \end{aligned} \tag{3}$$

Here ν^c, the so-called charge-conjugate field, is $C\bar{\nu}^T$, where $C = \gamma_2\gamma_4$ is the charge conjugation matrix and T denotes transpose. In going from the first line of Eq. (3) to the second, we have used the easily verified identities $(\nu^c)_R = (\nu_L)^c$ and $(\nu_L)^c = \nu_L^T C$. As we shall discuss later, a Majorana mass term leads to a neutrino which is its own antiparticle. Note that the Majorana mass term of Eq. (3) has been constructed entirely out of the familiar left-handed neutrino field ν_L. Now,[1] in the standard electroweak model, this field carries weak isospin $I_z = +1/2$, so that the mass term, as written, carries $I_z = +1$. Thus, in order to construct a term which is properly

weak-isospin invariant before symmetry breaking occurs, you have to introduce some additional fields which carry negative I_z. The neutral Higgs field ϕ^0 of the standard model has $I_z = -1/2$, so a term of the form

$$L \sim - (\phi^0)^2 \, \nu_L^T \, C \, \nu_L + \text{h.c.} \tag{4}$$

will do. When the Higgs develops a vacuum expectation value $\langle\phi^o\rangle$, this term will yield one of the Majorana mass term form $- \langle\phi^o\rangle^2 \nu_L^T C \nu_L$, with a constant multiplying $\nu_L^T C \nu_L$ as in Eq. (3). However, since $\langle\phi^o\rangle^2$ has the dimensions $(\text{mass})^2$, it must appear multiplied by an additional constant K with dimensions $(\text{mass})^{-1}$ if we are to have a mass term of the proper dimensions. Now, as explained in Ref. 1, the term (4) cannot occur in the fundamental Lagrangian of the theory, but must be an effective interaction induced by the exchange of some very heavy particles. These particles presumably have masses of order $M_{GUT} \sim 10^{15}$ GeV, the natural mass scale in grand unified theories. Then K must be $\sim f/M_{GUT}$, where f is some dimensionless effective coupling constant. That is, the effective interaction (4) leads to the Majorana mass term

$$L_M = - \frac{f}{M_{GUT}} \langle\phi^o\rangle^2 \, (\nu_L^T C \nu_L + \text{h.c.}) \, . \tag{5}$$

From Eq. (3), the mass of the neutrino is then

$$M \approx f \frac{\langle\phi^o\rangle^2}{M_{GUT}} \, . \tag{6}$$

Since $\langle\phi^o\rangle$ is known to be 300 GeV from the value of the Fermi coupling constant G_F, everything in this expression for the neutrino mass is known except for f, and we learn that

$$M \approx f(0.1 \text{ eV}) \, . \tag{7}$$

If f is smaller than unity, as many coupling constants are, the neutrino weighs less than 0.1 eV.

I repeat that this is only one estimate. Gauge theories can contain other mass terms with much less predictive power, and so

the neutrino masses could be anything at all. However, as Eq. (7) illustrates, these masses could in particular be much less than those to which most current experiments are sensitive. Thus, if people at this Workshop have clever ideas on how to look for masses well below 1 eV , such ideas might be very helpful.

An interesting question about neutrinos is whether they are their own antiparticles. Neutrinos might be Majorana particles, which means that $\bar{\nu} = \nu$, and lepton number is obviously violated. Or, they might be Dirac particles, which means that $\bar{\nu} \neq \nu$, and there is a conserved lepton number. I will explain the Majorana-Dirac distinction more carefully later, when we discuss the experimental possibilities for telling whether neutrinos are of Majorana or of Dirac character. However, as far as theoretical prejudices are concerned, grand unified theories are theories in which lepton number, like baryon number, is in general violated. It is violated, for instance, in the decay $n \to e^- K^+$. Consequently, one would naturally expect that in GUTS neutrinos would be of the lepton-violating Majorana variety, rather than of the Dirac variety. Of course, this is only a theoretical bias, and one can construct grand unified theories in which the neutrinos are Dirac particles, but I think it is more natural in such theories for them to be Majorana particles. Indeed, there has been a lot of discussion, in the context of various grand unified models, about the possibility that neutrinos are of Majorana character. For example, the Gell-Mann, Ramond, Slansky mechanism,[2] which protects neutrinos from becoming as heavy as quarks, is a mechanism in which the neutrinos are Majorana particles. Now the Gell-Mann, Ramond, Slansky mechanism leads one to expect naively that neutrino masses M are of order M_q^2/M_{GUT} , where M_q is a typical quark mass. If we take $M_q \sim 1$ GeV , then $M \sim 10^{-6}$ eV . Let me say yet again that neutrino masses could be anything, but in particular they could be much less than 1 eV , so ideas on how to look for such small masses would be welcome.

Phenomenology of Massive Neutrinos

I would like to turn now to a discussion of the phenomenological consequences of neutrino mass. One of the most interesting consequences is neutrino oscillation. Let us recall what

that is. Imagine a world with just two kinds of neutrinos. (In other words, forget for the moment about the τ and its neutrino.) Suppose that these two neutrinos, which I shall call ν_1 and ν_2, are massive, and that in particular their masses M_1 and M_2 are different. Suppose that in the decay $\pi^+ \to e^+ + \nu_e$, the outgoing neutrino ν_e, which is called the "electron neutrino" by way of definition, is neither of the physical neutrinos ν_1 and ν_2 with definite mass, but a linear combination of them. That is,

$$\nu_e = \nu_1 \cos\theta + \nu_2 \sin\theta , \tag{8}$$

where θ is a mixing angle. Suppose finally that in the corresponding muonic decay, $\pi^+ \to \mu^+ + \nu_\mu$, the outgoing neutrino ν_μ, which is called the "muon neutrino" by definition, is the orthogonal linear combination. That is,

$$\nu_\mu = -\nu_1 \sin\theta + \nu_2 \cos\theta . \tag{9}$$

Note that in hypothesizing that the neutrino which accompanies a specific charged lepton in weak decays is a mixture of neutrino mass eigenstates, we are simply supposing that the leptons behave exactly as we know the quarks do. Namely, from low-energy data we know that, expressed in terms of quarks, the hadronic decays of the W-boson are of the form

$$W^- \to \bar{u} + d_c \tag{10}$$

and

$$W^- \to \bar{c} + s_c . \tag{11}$$

In the decay to the anti up-quark $\bar{u}$ (the analogue of the e^+ in $\pi^+ \to e^+\nu_e$), the accompanying quark d_c is a coherent mixture of the quarks d and s of definite mass:

$$d_c = d \cos\theta_c + s \sin\theta_c . \tag{12}$$

Here, θ_c is the Cabibbo angle. In the decay to the anti

charmed-quark $\bar{c}$ (the analogue of μ^+), the accompanying quark s_c is the orthogonal linear combination:

$$s_c = -d \sin\theta_c + s \cos\theta_c \ . \tag{13}$$

Consider, now, a beam of neutrinos which have momentum p_ν and are born as muon neutrinos in pion decays of the dominant variety $\pi^+ \to \mu^+ + \nu_\mu$. If the suppositions we have made about neutrinos are right, then, at birth, each neutrino in the beam is the particular linear superposition of the neutrinos of definite mass given by Eq. (9). Now, if ν_1 and ν_2 have different masses, then at the given momentum p_ν the ν_1 and ν_2 components of the beam will travel at different speeds, the lighter component getting ahead of the heavier one. Thus, downstream of its point of birth, the beam will no longer consist of precisely the admixture (9) of ν_1 and ν_2, but of some other admixture. That means that the beam is no longer purely ν_μ, but contains a ν_e component as well. Obviously, the ν_e-ν_μ composition of the beam will vary with distance.

This is the phenomenon of neutrino oscillation. Notice that for it to occur, two things must be true. First, the different neutrino mass eigenstates must have different masses, which implies that at least one of them must have a non-zero mass. Secondly, the neutrinos that go with particular charged leptons must be non-trivial mixtures of the mass eigenstates.

Let us now treat neutrino oscillation quantitatively, assuming that there are not just two but N different varieties ("flavors") of charged lepton: e, μ, τ, and however many more there may be. Correspondingly, we assume that there are N physical neutrinos (mass eigenstates) ν_m, with non-degenerate masses M_m. As before, we assume that the neutrinos ν_f of definite flavor (ν_e, ν_μ, etc.) are not the mass eigenstates, but linear combinations of them:

$$\nu_f = \sum_m U_{fm} \nu_m \ . \tag{14}$$

Here U is a unitary mixing matrix which can be taken to be real if CP is conserved.[3]

Consider a beam of neutrinos with a definite momentum p_ν, born in association with a particular charged lepton ℓ_f (such as a muon). If the mass resolution of the experiment is insufficient to tell which neutrino mass eigenstate is actually involved in each event, each neutrino in the beam will be a coherent superposition of the various ν_m. The ν_m component of the neutrino will have energy $E_m = (p_\nu^2 + M_m^2)^{1/2}$. At time $t = 0$, the moment of its birth, the neutrino is a ν_f; that is, it is the linear combination (14) of the ν_m. Thus, at $t = 0$, its wave function is

$$\psi(x,t=0) = \sum_m U_{fm}\nu_m e^{ip_\nu x} . \tag{15}$$

After a time t, this wave function evolves into

$$\psi(x,t) = \sum_m U_{fm}\nu_m e^{ip_\nu x} e^{-iE_m t} , \tag{16}$$

since each ν_m has definite energy E_m. Assuming that the ν_m are very light ($M_m \ll p_\nu$), we may write $E_m \simeq p_\nu + (M_m^2/2p_\nu)$. Under the same assumption, our neutrino, which was born as a ν_f at $t = 0$, will be traveling at roughly the speed of light. Thus, if it was born at $x = 0$, at time t it will be approximately at $x = t$. At that point the wave function is

$$\psi(t,t) \simeq \sum_m U_{fm}\,\nu_m\, e^{-i(M_m^2/2p_\nu)t} . \tag{17}$$

This state is a superposition of all the flavors $\nu_{f'}$. If we use the inverse of Eq. (14), Eq. (17) becomes

$$\psi(t,t) \simeq \sum_{f'} \left[\sum_m U_{fm}U_{f'm}e^{-i(M_m^2/2p_\nu)t}\right] \nu_{f'} . \tag{18}$$

Squaring the coefficient of $\nu_{f'}$ (and noting that $t = x$), we find that the probability of finding the neutrino to have flavor f' at a distance x from its source, if originally it had flavor f, is

$$P[f \to f';x] = \sum_m U_{fm}^2 U_{f'm}^2 + \sum_{m'\neq m} U_{fm}U_{fm'}U_{f'm}U_{f'm'}\cos\, 2\pi \frac{x}{\ell_{mm'}} . \tag{19}$$

Here the oscillation lengths $\ell_{mm'}$ are given by

$$\ell_{mm'} = 2\pi \frac{2p_\nu}{|M_m^2 - M_{m'}^2|} . \tag{20}$$

Note that the oscillating term in $P(f \to f';x)$ comes from interference between the different mass eigenstates in the neutrino wave function.

When x is small compared to the oscillation lengths $\ell_{mm'}$, the effects of oscillation are not yet visible, and the neutrino has essentially its original flavor. When x is comparable to the oscillation lengths, the flavor content of the beam varies with distance in the characteristic oscillatory manner described by Eq. (19). When x is much larger than the oscillation lengths, then in practice the flavor content of the beam no longer varies with distance. The reason is that any actual beam has a finite momentum spread δp_ν, so that from Eq. (20) it also entails a finite spread in the oscillation length corresponding to any pair of mass eigenstates. Suppose, for example, that only two mass eigenstates, ν_1 and ν_2, participate appreciably in the oscillation, so that there is only one oscillation length $\ell = 4\pi p_\nu / |M_1^2 - M_2^2|$. This oscillation length will have a fractional spread $\delta\ell/\ell = \delta p_\nu / p_\nu$, and by the time x reaches

$$x_{wash} = \left(\frac{1}{\delta p_\nu / p_\nu}\right)\ell , \tag{21}$$

the oscillatory term in Eq. (19) will have washed out. Note, however, that after the oscillations in Eq. (19) have washed out,

$$P[f \to f';x] = \sum_m U_{fm}^2 U_{f'm}^2 . \tag{22}$$

While this transition probability no longer varies with distance, it still does reflect the presence of any non-trivial neutrino mixing. A neutrino born as a ν_μ can still be found on detection to be, for example, a ν_τ.

In terms of convenient units, the argument of the cosine in Eq. (19) is

$$2\pi \frac{x}{\ell_{mm'}} = 2.53 \left(\frac{\delta M_{mm'}^2}{1\,eV^2}\right) \frac{(x/1\ km)}{(p_\nu/1\ GeV)} , \tag{23}$$

where $\delta M^2_{mm'} = |M^2_m - M^2_{m'}|$. From this expression, one can draw the obvious conclusions about the sensitivity of accelerator experiments to neutrino oscillation. To mention a non-accelerator experiment, if one studies $\sim$ 1 GeV neutrinos whose distance of travel before detection is the diameter of the earth ($x = 10^4$ km) , then one can evidently probe down to $\delta M^2_{mm'} \sim 10^{-4}$ eV^2 .[4]

Of course, sensitivity to neutrino oscillation depends not only on having an x which is not too small compared to the oscillation lengths, but also on having reasonable values of the U_{fm} (i.e., reasonably large "mixing angles"). Unfortunately, theory offers essentially no clues about the values of the neutrino mixing angles, any more than it predicts the neutrino masses. In the two-neutrino mixing example of Eqs. (8) and (9), if θ is equal to the Cabibbo angle, the amplitude of oscillation will be 20%. That is, there will be distances x at which the flux of neutrinos of the original flavor will be only 80% of its value at $x = 0$, the remaining 20% having gone into another flavor.

Neutrino oscillation is a lovely example of quantum mechanics in action. I would like to illustrate that.[5] Suppose that you perform the neutrino oscillation experiment sketched in Fig. 1. In the neutrino source region, you create neutrinos in association with muons through the decay of pions in flight. Then, downstream, you let the neutrinos interact with a target, and you insist that each neutrino produce, in particular, an electron. This experiment searches, in other words, for $\nu_\mu \longleftrightarrow \nu_e$ oscillations. Suppose that these are found and that, in particular, when the source-to-detector distance x is varied, the oscillatory x-dependence predicted by Eq. (19) is observed.

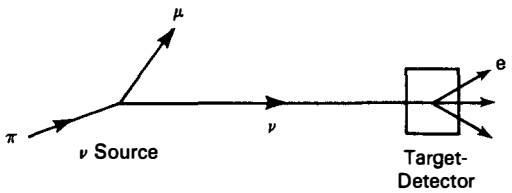


Fig. 1. A neutrino oscillation experiment.

Now imagine adding apparatus at the neutrino source which measures the momenta of the pion and muon in each event. Suppose that these momenta are measured so precisely that they determine the mass-squared of the neutrino, M_ν^2, with an error $\Delta(M_\nu^2)$ less than all $|M_m^2 - M_{m'}^2|$. Then you will know which physical (mass eigenstate) neutrino ν_m actually went down the beam line in each event of the experiment!

Clearly, if you know which mass eigenstate is actually involved in each event, the electron counting rate measured by the detector can no longer oscillate with x. Now only a single physical neutrino, as ordinary a beam particle as a proton, contributes to any given event. You do not have the coherent contributions from several ν_m whose interference with one another was the origin of oscillatory x-dependence.

This disappearance of oscillation with x as a result of momentum measurements which determine M_ν^2 raises an interesting question. Namely, what do these measurements <u>do</u> to destroy the oscillation pattern? The answer to this question is given by the uncertainty principle. To determine M_ν^2, you must measure the momenta of both the pion and the muon. Now, the more accurately the pion momentum is measured, the more uncertain the pion position will be. Consequently, the more uncertain the point where the neutrino is born will be. You might guess that just when the pion momentum is measured accurately enough for $\Delta(M_\nu^2)$ to be less than all $|M_m^2 - M_{m'}^2|$, the uncertainty in the neutrino source point will exceed all the oscillation lengths $\ell_{mm'}$. Obviously, any oscillation pattern will then be obliterated.

This guess is precisely correct. Indeed, we can easily show that, independent of the details of the neutrino source and detector, if measurements made at either place become sufficiently accurate to reveal which ν_m is involved in each event, then the consequent uncertainty in the neutrino source point, or the detection point is that is where the measurements are made, grows larger than all the oscillation lengths. In a given event, the neutrino mass M_ν is related to its energy E_ν and momentum p_ν by

$$M_\nu^2 = E_\nu^2 - p_\nu^2 \ . \qquad (24)$$

If the measurements from which E_ν and p_ν are deduced are made with uncorrelated errors ΔE_ν and Δp_ν, then the error $\Delta(M_\nu^2)$ in the resultant value of M_ν^2 will be

$$\Delta(M_\nu^2) = [(2E_\nu)^2(\Delta E_\nu)^2 + (2p_\nu)^2(\Delta p_\nu)^2]^{1/2} . \tag{25}$$

Now, if we want to know which ν_m is involved in each event, then we must have

$$\Delta(M_\nu^2) < |M_m^2 - M_{m'}^2| \tag{26}$$

for all m,m'. From Eq. (25), we see that the error in p_ν must then satisfy

$$2p_\nu \Delta p_\nu < |M_m^2 - M_{m'}^2| . \tag{27}$$

The uncertainty principle then implies that the neutrino source point, or its detection point if that is where the p_ν and E_ν measurements are made, will have an uncertainty Δx obeying

$$\Delta x > \frac{2p_\nu}{|M_m^2 - M_{m'}^2|} \tag{28}$$

for all m,m'. From Eq. (20), we see that, apart from a factor of 2π, the right-hand side of this relation is precisely the oscillation length $\ell_{mm'}$.

Of course, if the neutrino masses M_m are of order 10 eV or less, and you perform an experiment with $p_\nu > 100$ MeV, there is no danger that you will <u>inadvertently</u> measure p_ν with an accuracy exceeding the critical value given by Eq. (27), thereby accidentally obliterating the oscillation pattern. On the other hand, you may be interested in the opposite limit, where neutrino masses are of order 100 MeV, and the measurements intended to determine these masses do reveal which ν_m is produced in each decay of the parent meson. To search for such heavy neutrinos, you would not look for an oscillation pattern. (Even if $p_\nu > 10$ GeV, when $M_m = 100$ MeV and $M_{m'} \ll M_m, \ell_{mm'} < 10^{-9}$ cm !) Rather, you would try to measure the charged particle momenta in decays such as $\pi^+ \to e^+ + \nu_m$ and $K^+ \to \mu^+ + \nu_m$ accurately

enough to determine the masses of the ν_m . As we have been saying all along, the neutrino which accompanies the charged lepton of flavor f is, with amplitude U_{f1} , the mass eigenstate ν_1 , with amplitude U_{f2} , the mass eigenstate ν_2 , and so forth. Thus, if some of these mass eigenstates are heavy enough, then, for example, in the decay $K^+ \to \mu^+ + \nu_m$ of kaons at rest, the muon momentum spectrum would exhibit several visibly distinct monochromatic lines, corresponding to the masses of the different ν_m .[6]

Searches for heavy neutrinos in leptonic K and π decay have so far yielded limits of order $10^{-5} - 10^{-6}$ on $|U_{em}|^2$ and $|U_{\mu m}|^2$ in rather broad but not exhaustive regions of ν_m mass.[7] Should limits of this magnitude be considered very stringent? In the Kobayashi-Maskawa matrix, the quark sector analogue of the leptonic mixing matrix U considered here, some of the elements could be as small as $10^{-5} - 10^{-6}$. Thus, for all we know, there is mixing in the lepton sector below this level.

If neutrinos have mass, then one expects them to decay through the radiative process $\nu_m \to \nu_{m'} + \gamma$. This process is engendered by loop diagrams such as that in Fig. 2. In the standard model, the lifetime $\tau(\nu_m)$ for radiative decay is extremely long:[8]

$$\tau(\nu_m) > 10^{22} \text{ years} \times \left(\frac{30\text{eV}}{M_m}\right)^5 . \qquad (29)$$

(Relation (29) assumes for simplicity that $M_{m'} << M_m$.) Thus, one need not worry that the composition of a laboratory neutrino beam will be altered by radiative decays. On the other hand, perhaps one can observe the photons coming from such decays of astrophysical neutrinos. To the author's knowledge, the best limit on $\tau(\nu_m)$ from searches for these photons is[9]

$$\tau(\nu_m) > (10^{16} - 10^{18}) \text{ years} , \quad 3 < M_m < 10 \text{ eV} , \qquad (30)$$

based on observations of the Coma and Virgo clusters of galaxies. Obviously, this limit is not yet at the level of the theoretical prediction.

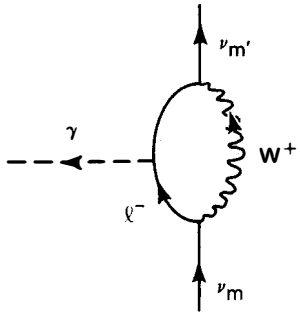


Fig. 2. A loop diagram for radiative decay of a neutrino. The symbol ℓ denotes a charged lepton.

If the mass difference $M_m - M_{m'}$ between two mass eigenstates exceeds the mass of an e^+e^- pair, then in addition to radiative decays, decays of the type $\nu_m \to \nu_e e^- e^+$ are possible. Such decays correspond to the diagram in Fig. 3, which evidently is identical to that for μ decay, except that ν_m replaces the μ and there is a factor of U_{em} at the $\nu_m e^- W$ vertex. Remembering that the μ decay process scales as M_μ^5, we see that

$$\tau(\nu_m \to \nu_e e^- e^+) = \tau(\mu)\left(\frac{M_\mu}{M_m}\right)^5 \frac{1}{|U_{em}|^2} \,. \qquad (30)$$

From a search for this decay in a wide band neutrino beam at CERN, the CHARM collaboration has placed an upper limit on $|U_{em}|^2 \cdot 10]$ For $100 \text{ MeV} < M_m < 490 \text{ MeV}$, this limit is down in the range $10^{-5} - 10^{-6}$, comparable to the limits from π_{e2} decay for lower masses. The CHARM group was able to obtain an even more stringent limit assuming that the heavy ν_m is essentially ν_τ and making an assumption about the rate of ν_τ production in a beam dump. However, the limit I have quoted here is more independent of assumptions.

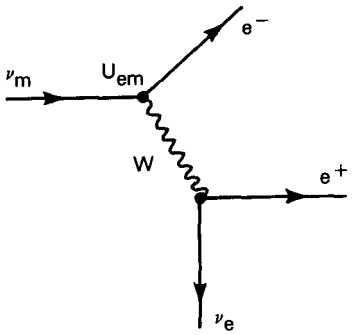


Fig. 3. The decay $\nu_m \to \nu_e e^- e^+$. As shown, the $\nu_m e^- W$ coupling is proportional to U_{em} .

Since they are to be covered in other talks at this Workshop, I shall not discuss the very important experiments which seek to measure neutrino masses directly, either in tritium beta decay, or in electron capture associated with internal Bremsstrahlung. For the same reason, I shall not discuss the astrophysical consequences of neutrino mass, such as the possibility that neutrinos constitute the non-luminous matter in the universe.

I would, however, like to comment on the possible implications of existing tritium results when these are compared with results on neutrino oscillation. When just two mass eigenstates, ν_1 and ν_2 , participate significantly in an oscillation, the U matrix takes the simple form

$$U = \begin{pmatrix} \cos\theta & \sin\theta \\ -\sin\theta & \cos\theta \end{pmatrix} , \tag{31}$$

and Eq. (19) becomes

$$P[f \to (f' \neq f);x] = \sin^2 2\theta \sin^2 \pi \frac{x}{\ell_{12}} , \tag{32}$$

with

$$P[f \to f;x] = 1 - P[f \to (f' \neq f);x] \ .$$

Negative oscillation results are then expressed as correlated limits on the mixing angle θ and the quantity $\delta M_{12}^2 = |M_1^2 - M_2^2|$ appearing in the oscillation length $\ell_{12} = 4\pi p_\nu / |M_1^2 - M_2^2|$. In particular, assuming that just two mass eigenstates are involved, the Gösgen reactor experiment on oscillation in a $\bar{\nu}_e$ beam finds[11] that unless $\sin^2 2\theta \lesssim 0.2$, $\delta M_{12}^2 \lesssim 0.04\ \text{eV}^2$. Now, let us suppose that, as suggested by the ITEP studies of tritium beta decay,[12] $M_{\bar{\nu}_e} \approx 30$ eV . If we continue to assume that "$\bar{\nu}_e$" is comprised essentially of just two mass eigenstates, and that the masses of both of these are near 30 eV , then the Gösgen result leaves us with two possibilities. Either the mixing is small, or else

$$\frac{|M_1 - M_2|}{M_1 + M_2} \lesssim 10^{-5} \ . \tag{33}$$

The latter degeneracy would be interesting, to say the least.[13]

During the Workshop, it was pointed out by Bergkvist[14] and by Robertson[15] that the ITEP group finds its data to be better fitted by two quite different masses than by two roughly equal ones. The best fits are achieved with $M_1 = (80\text{-}115)$eV and $M_2 = (0\text{-}20)$eV .[14],[15] Then $\delta M_{12}^2 \approx 10^4 \text{eV}^2$. Now, in the Gösgen experiment, p_ν is of order 4MeV , and the detector is positioned at either 38m or 46m from the reactor core. Thus, if $\delta M_{12}^2 = 10^4 \text{eV}^2$, the Gösgem detector is more than 3×10^4 oscillation lengths from the $\bar{\nu}_e$ source! It was recalled by Workshop participants that, many oscillation lengths from the neutrino source, a neutrino wave packet will break up into non-overlapping pieces. The author was asked to talk briefly on the question of whether this breakup would make it impossible for the Gösgen experiment to see oscillation or to say anything about neutrino masses and mixing if $\delta M_{12}^2 \approx 10^4 \text{eV}^2$.

I believe the answer to this question is as follows.[16] At a given momentum, the pieces of a neutrino wave packet corresponding to different mass eigenstates ν_m travel at different speeds. For a highly relativistic ν_m , spreading of its piece

of the wave packet can be shown to be negligible. Thus, the wave packet for a neutrino born as, say, a $\bar{\nu}_e$ will indeed split into nonoverlapping pieces when its various ν_m components become more widely separated than the original length h of the packet.[17] Of course, when they no longer overlap, the different ν_m components cannot interfere to make the flavor content of the beam vary with distance.

If there are just two contributing mass eigenstates and one corresponding oscillation length ℓ_{12}, the wave packet will have separated into nonoverlapping pieces by the time $x \sim x_{sep}$, where[16]

$$x_{sep} = (hp_\nu)\ell_{12} \ . \tag{34}$$

Now, if h is bigger than 10^{-8} cm, the size of an atom, and $p_\nu > 1$ MeV, as in all current neutrino oscillation experiments, then $(hp_\nu) \gtrsim 10^3$. However, a typical neutrino beam has a finite momentum spread $(\delta p_\nu / p_\nu) > 1/10$. Thus (see discussion around Eq. (21)), the x-dependence of the flavor content of the beam will have become washed out by the time $x = x_{wash}$, where

$$x_{wash} = \left(\frac{1}{\delta p_\nu / p_\nu}\right)\ell_{12} < 10\ell_{12} \ . \tag{35}$$

Hence, for any macroscopic value of h, separation of pieces of the wave packet at a given p_ν will not eradicate the oscillation with distance until long after it has disappeared anyway due to the broad p_ν spectrum of the beam.

At distances beyond the momentum-spread induced wash out, the transition probability $P[f \to f';x]$ is given by Eq. (22). What happens to this probability after the wave packet breaks up? After breakup, the different ν_m contribute to the event rate incoherently. What is the contribution of a given ν_m to an experiment in which the neutrinos are born in association with the charged lepton ℓ_f, but detected through their production of the differently-flavored charged lepton $\ell_{f'}$? It is the probability U^2_{fm} of creating the ν_m together with an ℓ_f, times the probability $U^2_{f'm}$ that this ν_m will produce an $\ell_{f'}$. Thus, the total event rate is $\sum_m U^2_{fm} U^2_{f'm}$. That is, Eq. (22)

describes $P[f \to f';x]$ correctly both after wash out and after wave packet breakup.

Obviously, through Eq. (22), data from a detector beyond the wash out or wave packet breakup point do provide limits on neutrino mixing, even though there is no x-dependence at such distances. (Of course, comparison of data from two distances which are both beyond the wash out point would show no effect; it is the comparison between one of these distances and $x = 0$ which counts.) In particular, one may ask whether the fits to the ITEP tritium measurements which imply that $\delta M^2_{12} \approx 10^4 eV^2$ are consistent with the Gösgen finding that $\sin^2 2\theta \lesssim 0.2$ for large δM^2_{12}. The answer is that one of the two ITEP solutions quoted by Robertson[15] is consistent with the Gösgen limit, but, assuming that only two mass eigenstates are important, the other solution is not.

Are Neutrinos Majorana or Dirac Particles?

Let us turn now to the question of whether neutrinos are their own antiparticles, beginning with a careful statement of what one means by this question. Suppose there exists a massive neutrino ν_- with negative helicity (indicated by the subscript), as considered at the extreme left of Fig. 4(a). As Fig. 4(a) indicates, CPT-invariance then implies that there must also exist the CPT mirror-image of this particle, a positive-helicity antineutrino. In addition, if ν_- is massive, it travels slower than light, so that by travelling sufficiently fast you can overtake it. If you do, then in your frame it is going the other way, but still spinning the same way as in the original frame. Thus, the Lorentz transformation to your frame turns ν_- into a positive-helicity particle, depicted at the far right of Fig. 4(a). Now, this positive-helicity object may or may not be the same as the CPT mirror-image of ν_-. Let us suppose first that, as imagined in Fig. 4(a), it is not the same. Then it has its own CPT mirror-image, a negative-helicity antineutrino, and altogether there are four states with a common mass. This foursome is called a Dirac neutrino ν^D. In general, a Dirac neutrino will have a magnetic dipole moment, and perhaps even an electric dipole moment. Thus, in the Dirac case, ν_- can be converted into its opposite helicity partner ν_+ not just by a Lorentz

transformation but also through the action of an external $\vec{B}$ or $\vec{E}$ field.

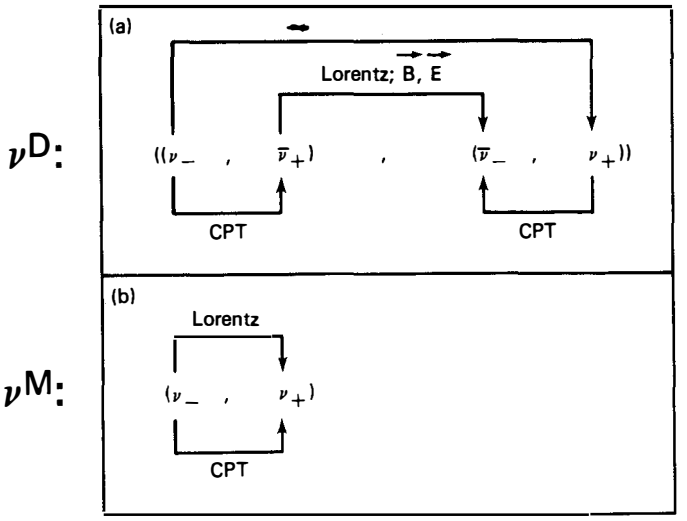


Fig. 4. (a) The four distinct states of a Dirac neutrino ν^D.
(b) The two distinct states of a Majorana neutrino ν^M.

The second possibility, pictured in Fig. 4(b), is that when you reverse the momentum of ν_- by overtaking it, the positive-helicity particle that you obtain is the same as the CPT mirror-image of ν_-. Then there are just two states with a common mass, and this pair of states is called a Majorana neutrino ν^M. In the rest frame, CPT applied to either of the two spin states of such a neutrino simply reverses the spin (due to the time reversal). By a 180° rotation, you can then reverse it again, returning the neutrino to its original state. It is in this sense --- CPT, followed by a 180° rotation --- that a Majorana neutrino is its own antiparticle.

Majorana neutrinos obviously lead to lepton number violation. Given the trivial effect of CPT on a Majorana neutrino, such a particle clearly carries no lepton number, and, brought to

rest, has no memory of whether it was made in a decay such as $\pi^+ \to \mu^+ + \nu$, or one like $\pi^- \to \mu^- + \nu$. In subsequent interactions, this neutrino can produce either a μ^+ or a μ^-.

As long as the mass is not zero, a Dirac neutrino consists of four states $((\nu_-^D, \bar{\nu}_+^D), (\bar{\nu}_-^D, \nu_+^D))$, while in contrast a Majorana neutrino consists of but two (ν_-^M, ν_+^M). Nevertheless, as the mass goes to zero, the distinction between a Dirac and a Majorana neutrino gradually disappears. It appears that the situation can be summed up by what I like to call the

Practical Dirac-Majorana Confusion Theorem:[18]

Assume that all weak currents are left-handed. Assume further that experiments on a given neutrino are always done with one of two incoming states --- a state "ν_-" of negative helicity, or its CPT-conjugate, which we shall call "$\bar{\nu}_+$". (All neutrino experiments have, of course, been done this way.) Then, as the neutrino mass goes to zero compared to the other energy and mass scales in the problem, it gradually becomes more and more difficult to tell experimentally whether "ν_-" and "$\bar{\nu}_+$" are actually $(\nu_-^D, \bar{\nu}_+^D)$, two of the four states of a Dirac neutrino, or (ν_-^M, ν_+^M), the two states of a Majorana neutrino. When the mass vanishes, there is no physical distinction between these two cases.

When a neutrino is massless, it travels at the speed of light, so that one can no longer reverse its helicity by going to another Lorentz frame. Furthermore, if all weak currents are left-handed, the magnetic and electric dipole moments of a neutrino must vanish with its mass,[18] so that external $\vec{B}$ and $\vec{E}$ fields can no longer reverse its helicity either. Thus, the states $(\nu_-^D, \bar{\nu}_+^D)$ get disconnected from their opposite-helicity partners $(\bar{\nu}_-^D, \nu_+^D)$, and the latter states need not even exist. One just has two states, and whether one chooses to call them a Dirac neutrino and its antiparticle, or the two spin states of a Majorana neutrino, is purely a matter of semantics.

As the "confusion theorem" states, the approach to the massless limit is smooth (unfortunately), so that it will be hard to determine whether the light neutrinos with which nature confronts

us are Majorana or Dirac particles. I would like to illustrate this state of affairs by considering neutral-current scattering.

Before doing that, I would like to explain the difference between Majorana and Dirac fields. For those unfamiliar with Majorana particles, the subsequent discussion of neutral-current scattering will then serve as an introductory illustration of how such particles are handled in theoretical calculations.

The Dirac neutrino field ψ^D is given by

$$\psi^D = \sum_{\vec{p},s} \sqrt{\frac{M}{E_{\vec{p}} V}} \left(f_{\vec{p}s} u_{\vec{p}s} e^{ipx} + \bar{f}^{\dagger}_{\vec{p}s} v_{\vec{p}s} e^{-ipx} \right) . \tag{36}$$

Here M, $\vec{p}$, s, and $E_{\vec{p}}$ are, respectively, the neutrino mass, momentum, spin-projection, and energy, u and v are the usual Dirac spinors, f annihilates neutrinos, and $\bar{f}^{\dagger}$ creates anti-neutrinos. A related field which will be useful is the charge-conjugate of ψ^D, $(\psi^D)^c \equiv C(\bar{\psi}^D)^T$. The field $(\psi^D)^c$ is just $\psi^D_{\dagger}$ with $f_{\vec{p}s}$ and $\bar{f}^{\dagger}_{\vec{p}s}$ replaced, respectively, by $\bar{f}_{\vec{p}s}$ and $f^{\dagger}_{\vec{p}s}$; that is, with the roles of particle and antiparticle interchanged.

The Majorana neutrino field ψ^M, which describes the case where particle and antiparticle are identical, may be gotten from the Dirac field simply by setting $\bar{f}^{\dagger}_{\vec{p}s} = f^{\dagger}_{\vec{p}s}$. Thus,

$$\psi^M = \sum_{\vec{p},s} \sqrt{\frac{M}{E_{\vec{p}} V}} \left(f_{\vec{p}s} u_{\vec{p}s} e^{ipx} + \lambda f^{\dagger}_{\vec{p}s} v_{\vec{p}s} e^{-ipx} \right) , \tag{37}$$

where we have included a "creation phase factor" λ in the creation term. This arbitrary phase factor, which in general is present in a Majorana field, corresponds to the possibility of re-defining the one particle state by multiplying it by a phase factor. For some purposes, such as the treatment of neutrinoless double beta decay, it can be convenient <u>not</u> to set $\lambda \equiv 1$.[19]

One may easily show that ψ^M obeys the relation[20]

$$(\psi^M)^c \equiv C(\bar{\psi}^M)^T = \lambda^* \psi^M . \tag{38}$$

Conversely, if one expands any fermion field χ obeying Eq. (38)

in the general form (36), one quickly finds that Eq. (38) implies that $\bar{f}^{\dagger}_{\vec{p}s} = \lambda f^{\dagger}_{\vec{p}s}$. That is, χ is a Majorana field of the form (37), and describes a particle whose antiparticle is itself.

Earlier it was stated that the Majorana mass term (3) leads to a neutrino which is its own antiparticle. Why is that? First of all, any mass term in the Lagrangian, including a Majorana mass term, can be written in the familiar form $-M\bar{\psi}\psi$ whose interpretation we know because we know that it leads to the usual mass term in the Dirac equation. To cast the mass term of Eq. (3) in this canonical form, let us rewrite it in terms of the field ψ defined by[21]

$$\begin{aligned} \psi &= \nu_L + (\nu_L)^c \\ &= \nu_L + (\nu^c)_R \ . \end{aligned} \tag{39}$$

Obviously, the left-handed projection of ψ, ψ_L , is ν_L , while the right-handed projection, ψ_R , is $(\nu^c)_R$. Hence, the mass term (3) may be written as

$$\mathcal{L}_M = -M(\bar{\psi}_R \psi_L + \text{h.c.}) = -M\bar{\psi}\psi \ . \tag{40}$$

Now, since $[(\nu_L)^c]^c = \nu_L$,

$$\psi^c = \psi \ . \tag{41}$$

That is, the field ψ that we would interpret, in view of Eq. (40), as the usual field operator for a spin-1/2 particle, obeys Eq. (38) with $\lambda^* = 1$. This implies, as we have said, that ψ is a Majorana field, and describes a neutrino whose antiparticle is itself.

Let us now contrast the behavior of Dirac and Majorana neutrinos in neutral-current reactions of the form $\nu + A \to \nu + B$, where A is some target, and B is any collection of outgoing particles.[22] At energies well below the Z^0 mass, where all our neutral-current data have been gathered, the standard electroweak model describes any such reaction by an interaction of the form

$$H = [\bar{\psi}\gamma_\mu(1 + \gamma_5)\psi]\, M_\mu(A,B) \ . \tag{42}$$

Here ψ is the neutrino field, which could be either of Majorana or Dirac character, and the bracketed quantity is the neutrino neutral current. The operator $M_\mu(A,B)$ is a neutral current pertaining to A and B, whatever they may be.

From Eq. (36), we see that in the Dirac case the matrix element of the neutrino neutral current is (we set x = 0)

$$\langle \nu_f^D | \overline{\psi^D}\gamma_\mu(1 + \gamma_5)\psi^D | \nu_i^D \rangle = \left[\frac{M^2}{E_f E_i V^2}\right]^{1/2} \bar{u}_f \gamma_\mu(1 + \gamma_5)u_i \ . \tag{43}$$

Note that it is the field $\overline{\psi^D}$ which annihilates the incoming neutrino, and the field ψ^D which creates the outgoing one.

Turning to the Majorana case, we note first that the vector part of the neutrino neutral current, $\overline{\psi^M}\gamma_\mu\psi^M$, now vanishes. The reason is that, regardless of whether ψ is a Majorana or Dirac field, the vector current always satisfies the easily-verified relation

$$\overline{\psi^c}\gamma_\mu\psi^c = -\bar{\psi}\gamma_\mu\psi \ . \tag{44}$$

On the other hand, in the Majorana case Eq. (38) implies that

$$\overline{\psi^c}\gamma_\mu\psi^c = +\bar{\psi}\gamma_\mu\psi \ . \tag{45}$$

Thus,

$$\begin{aligned} \langle \nu_f^M | \overline{\psi^M}\gamma_\mu(1 + \gamma_5)\psi^M | \nu_i^M \rangle &= \langle \nu_f^M | \overline{\psi^M}\gamma_\mu\gamma_5\psi^M | \nu_i^M \rangle \\ &= \left[\frac{M^2}{E_f E_i V^2}\right]^{1/2} (\bar{u}_f\gamma_\mu\gamma_5 u_i - \bar{v}_i\gamma_\mu\gamma_5 v_f) \ , \end{aligned} \tag{46}$$

where the second term in the second line arises from the fact that ψ^M, Eq. (37), as well as $\overline{\psi^M}$, can both annihilate and create neutrinos. Using $v_{\vec{p}s} = C\bar{u}^T_{\vec{p}s}$, we may rewrite Eq. (46) as

$$\langle \nu_f^M | \overline{\psi^M}\gamma_\mu(1 + \gamma_5)\psi^M | \nu_i^M \rangle = \left[\frac{M^2}{E_f E_i V^2}\right]^{1/2} 2\bar{u}_f\gamma_\mu\gamma_5 u_i \ . \tag{47}$$

On the surface, the Dirac and Majorana cases, Eqs. (43) and (47), appear to be quite different. Alas, as the "practical Dirac-Majorana confusion theorem" predicts, this difference evaporates as the neutrino mass goes to zero. Indeed, so long as the incoming (left-handed) neutrino is relativistic, its u spinor satisfies $\gamma_5 u_i \cong u_i$, so that the right-hand sides of Eqs. (43) and (47) cannot be distinguished. That is why the voluminous data on neutral-current scattering have told us nothing about whether neutrinos are Dirac or Majorana particles.

Are there ways of getting around the "Dirac-Majorana confusion theorem"? Suggestions would certainly be welcome. I myself would like to suggest a possibility whose consideration is instructive. Suppose the dominant mass eigenstate in ν_μ has a mass greater than 10 keV .[23] Then, in a 600 GeV pion beam, such as will be available at the Fermilab Tevatron, all neutrinos from the decay $\pi^+ \to \mu^+ + \nu_\mu$ will have laboratory momenta in the forward hemisphere with respect to the beam direction. Consider, now, a ν_μ which is emitted exactly backward, in the pion rest frame, by a pion in such a beam. As depicted in Fig. 5(a), in the pion rest frame the neutrino will have negative helicity (apart from a negligible correction of order M_ν/E^*, where E^* is the energy of the ν_μ in the pion rest frame). However, in the lab. frame the decay will appear as shown in Fig. 5(b). The momentum of the ν_μ will point forward, and its helicity will be positive. Now, if this right-handed ν_μ is a Dirac particle, then it will not interact, because the weak currents are left-handed.[24] On the other hand, if it is a Majorana particle, then, on account of its helicity, it is just what we usually call a $\bar{\nu}_\mu$. Thus, it will interact, but, being a $\bar{\nu}_\mu$, will produce a μ^+, rather than a μ^-. Hence, by determining whether the mounic neutrinos emitted backward in the pion rest frame fail to interact or produce positive muons when they strike a target, we can find out whether they are Dirac or Majorana particles. Also, by observing that some fraction of the neutrinos emitted by fast positive pions exhibit either one of these anomalous behaviors, with the expected dependence on the pion energy, we can demonstrate that the ν_μ does have a non-zero mass. Will such an experiment work?

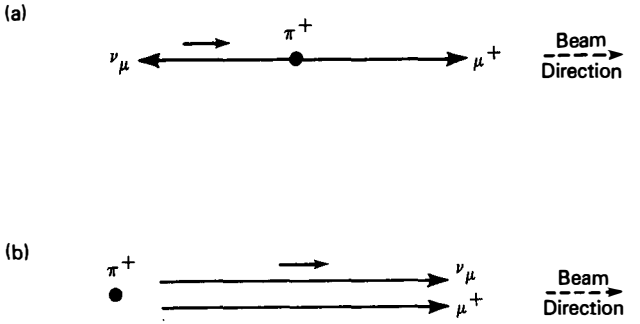


Fig. 5. The decay $\pi^+ \to \mu^+ + \nu_\mu$ of a fast pion into a massive neutrino as seen in (a) the pion rest frame, and (b) the lab. frame. The arrow over the neutrino line represents its spin.

Unfortunately, it will not work. First of all, suppose the neutrinos must travel down a neutrino beam line which is, say, 1 km. long before they intercept the detector which is, say, of order 1 m. wide. Then, to be detectable, they must have laboratory momenta which are not only in the forward hemisphere with respect to the beam direction, but in the forward-most milliradian. Now, let θ^* be the angle, with respect to the beam direction, at which a neutrino is emitted in the pion rest frame. Further, let β_π be the speed of the pion in the lab., and β^* the speed of the ν_μ in the pion rest frame. For the neutrinos with $\theta^* = \pi$ to go forward in the lab., we must have $\beta_\pi > \beta^*$, and we may write

$$\frac{\beta_\pi}{\beta^*} = 1 + \varepsilon \,, \tag{48}$$

where the small quantity ε is given by

$$\varepsilon \simeq \frac{1}{2}\left[\left(\frac{M_{\nu_\mu}}{E^*}\right)^2 - \left(\frac{M_\pi}{E_\pi}\right)^2\right] . \tag{49}$$

If $E_\pi = 600$ GeV , the neutrinos which are in the forward-most milliradian in the lab. are those with $\theta^* \lesssim \frac{5}{6}\pi$, or with $(\pi-\theta^*) \lesssim 4\varepsilon$. Now, the neutrinos with $(\pi-\theta^*) \lesssim 4\varepsilon$ are far too small a fraction of the neutrino flux to be useful. Those with $\theta^* \lesssim \frac{5}{6}\pi$ are a large fraction of the flux, but, as we shall see, the lab. frame helicities of these neutrinos differ only infinitesimally from their pion rest frame helicity of -1 ! Thus, any of these neutrinos will interact like a normal ν_μ , regardless of its Dirac or Majorana character.

The lab. frame helicity h of a neutrino whose pion rest frame helicity h^* is -1 may be found by Lorentz transforming to the lab. frame the left-handed spinor u^* which describes the neutrino in the pion frame. With much less work, it may also be found from a general expression in the literature[25] describing the Lorentz transformation properties of helicity. Either way, one finds that

$$h = -\frac{E_\pi p^* + p_\pi E^* \cos\theta^*}{M_\pi p} , \tag{50}$$

where p^* and p are, respectively, the magnitudes of the neutrino momentum in the pion rest frame and in the lab., and p_π is the momentum of the pion in the lab. From Eq. (50) it is trivial to show that so long as $E^* \cong p^*$, $E_\pi \cong p_\pi$, and θ^* is not near π ,

$$h \cong -1 . \tag{51}$$

Thus, the neutrinos with $\theta^* \lesssim \frac{5}{6}\pi$ will have quite ordinary behavior. Turning to the few neutrinos with θ^* very near π , we expand Eq. (50) in $(\pi-\theta^*)$, assuming that $M_{\nu_\mu} > 30$ keV , so that these neutrinos are forward-going and relativistic in the lab.[24] This yields

$$h \cong 1 - \frac{(\pi-\theta^*)^2}{\varepsilon} . \tag{52}$$

When $\theta^* = \pi$, h is indeed $+1$ as we have said, and it remains near this value until $(\pi-\theta^*) \sim \sqrt{\varepsilon}$. Hence, the uselessly few neutrinos with $(\pi-\theta^*) \lesssim 4\varepsilon$ do have h near $+1$. Equation

(52) suggests that the point beyond which h is quite far from $+1$ is $(\pi-\theta^*) \sim \sqrt{\varepsilon}$. Now, it is easy to show that when even the neutrinos with $\theta^* \approx \pi$ are forward-going and relativistic in the lab., the second term on the right-hand side of Eq. (49) may be neglected, so that $\sqrt{\varepsilon} \sim M_{\nu_\mu}/E^*$. Thus, the point beyond which h is quite far from $+1$ is $p_\perp \sim M_{\nu_\mu}$, where $p_\perp$ is the transverse momentum of the neutrino.

In retrospect, it should not have surprised us that a relativistic neutrino with θ^* not near π has almost exactly the same helicity in the lab. as in the pion rest frame, even though its momentum may point in very different directions in the two frames. We know, after all, that this would be true for a massless particle. Now, the Lorentz transformation from the pion rest frame to the lab. may be viewed as a succession of small transformations, throughout each of which our neutrino remains relativistic. Thus, it behaves very much like a massless particle. This picture only breaks down when θ^* is very near π ($p_\perp \lesssim M_{\nu_\mu}$), so that we are considering a neutrino whose momentum points in almost exactly opposite directions in the two frames of interest. The direction of the momentum of a massless particle can never be exactly reversed by a Lorentz transformation. However, the momentum of a massive particle can be exactly reversed, so when θ^* is sufficiently near π, the massless and massive cases are quite different.[26]

A basic attribute of any particle is its electromagnetic properties. Let us contrast Dirac and Majorana neutrinos in this regard. Of course, they are both electrically neutral, but perhaps they can have dipole moments.

Suppose a Majorana neutrino had a magnetic dipole moment μ_{Mag} and an electric dipole moment $\mu_{E\ell}$. If this neutrino were at rest in a combination of static, uniform magnetic and electric fields, its interaction energy would be $-\mu_{Mag}\langle\vec{s}\cdot\vec{B}\rangle - \mu_{E\ell}\langle\vec{s}\cdot\vec{E}\rangle$. Here $\vec{s}$ is, or course, the neutrino spin operator. Now, under CPT, the $\vec{B}$ and $\vec{E}$ fields go into themselves. However, as we have said, the effect of CPT on a Majorana neutrino is to reverse its spin. Consequently, the dipole interaction energy changes sign under CPT. Thus, if CPT invariance holds, μ_{Mag} and $\mu_{E\ell}$ must vanish.[18]

By contrast, a Dirac neutrino is permitted to have dipole moments. Thus, as mentioned earlier, its helicity can be reversed by the torque,

$$\frac{d\vec{s}}{dt} = \vec{\mu}_{Mag} \times \vec{B} , \tag{53}$$

exerted by an external magnetic field.[27],[28] This helicity-reversal could be detected using the fact that a left-handed neutrino interacts, while a right-handed neutrino does not. Unfortunately, however, the magnetic dipole moment of a neutrino is expected to be quite small. The standard model predicts that for a neutrino of mass M [29]

$$\mu_{Mag} = \frac{3eG_F M}{8\pi^2\sqrt{2}} \simeq 3 \times 10^{-19}\left(\frac{M}{1eV}\right)\mu_{Bohr} . \tag{54}$$

Here μ_{Bohr} is the Bohr magneton. Shrock has considered the possibility of laboratory experiments to detect such a tiny dipole moment, and has concluded that they would not be feasible.[30]

There is only one experimental approach which currently shows promise as a means for determining whether neutrinos are Majorana or Dirac particles. This approach, which is being vigorously pursued, is the search for neutrinoless double beta decay $[(\beta\beta)_{o\nu}]$.[31],[32] In this process, a nucleus would decay to another with two additional protons through the emission of two electrons <u>unaccompanied</u> by any antineutrinos:

$$(A,Z) \longrightarrow (A,Z+2) + 2e^- + 0\bar{\nu} . \tag{55}$$

The decay would be engendered by the diagram in Fig. 6, in which a pair of W bosons, emitted by two neutrons in the parent nucleus, produces the outgoing electrons through the exchange of a virtual neutrino. Of course, we expect that there exist several neutrino mass eigenstates ν_m . Thus, as Fig. 6 indicates, the amplitude for the process is actually a sum over the contributions of all of them, the coupling of a given ν_m to an electron being described by the mixing matrix element U_{em} . Notice that the exchanged neutrino is emitted together with an e^- at one

vertex, and then absorbed to produce another e^- at a second vertex. Considering the first vertex, we would conclude that this "neutrino" is actually a $\bar{\nu}$, but considering the second we would conclude that it is a ν. Thus, for $(\beta\beta)_{o\nu}$ to occur, we must have $\bar{\nu} = \nu$. That is, the exchanged neutrinos ν_m must be Majorana particles.

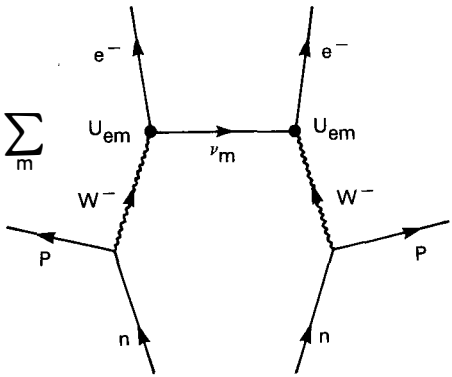


Fig. 6. Neutrinoless double beta decay.

In addition, for $(\beta\beta)_{o\nu}$ to occur, the ν_m must be massive, or else there must be right-handed currents, or both. If all weak currents are left-handed, then each ν_m, behaving like an antilepton at the vertex where it is emitted, is created in a predominantly right-handed state. However, at the vertex where it is absorbed, it behaves like a lepton, and so the current would prefer to absorb it from a left-handed state. The amplitude for the exchanged ν_m to be created left-handed is of order M_m/E_m, so the contribution of this ν_m to $(\beta\beta)_{o\nu}$ is proportional to M_m. However, if there is a right-handed current, then it can readily absorb a right-handed ν_m, and the ν_m contribution no longer depends on a non-zero M_m. Tests which could determine whether $(\beta\beta)_{o\nu}$, once it is observed, is resulting from non-zero masses or from right-handed currents have been proposed by Rosen.[33]

Assuming that there are no right-handed currents, and that to a good approximation CP is conserved in the lepton sector, as it is in the quark sector, the $(\beta\beta)_{o\nu}$ amplitude $A[(\beta\beta)_{o\nu}]$ can be shown to have the form

$$A[(\beta\beta)_{o\nu}] = [\sum_m \frac{\tilde{\eta}_{CP}(\nu_m)}{i} |U_{em}|^2 M_m]\bar{A} \equiv M_{eff}\bar{A} \ . \qquad (56)$$

In correspondence with Fig. 6, this amplitude is a sum over the contributions of the different ν_m . The contribution of each ν_m is proportional to its mass as we have explained, to the square of its coupling to an electron, and, finally, to its CP-parity $\tilde{\eta}_{CP}(\nu_m)$.[34],[35],[3],[36] Note that a Majorana neutrino, being an eigenstate of CPT (followed by a rotation), can have a well-defined value of CP when CP is conserved. However, it turns out that its CP-parity must be imaginary![36],[3] Thus, it is $\tilde{\eta}_{CP}(\nu_m)/i$ which is real. The quantity $\bar{A}$ in Eq. (56) is independent of m , and includes the very non-trivial nuclear matrix element governing neutrinoless double beta decay. Owing to the factor $\tilde{\eta}_{CP}(\nu_m)/i = \pm 1$ in Eq. (56), $(\beta\beta)_{o\nu}$ measures an effective mass, M_{eff} , which is a sum over actual neutrino masses M_m weighted by factors which can be either negative or positive.[37] Thus, an experimental upper limit on $A[(\beta\beta)_{o\nu}]$, translated into an upper limit on M_{eff} through one's knowledge of the relevant nuclear matrix element $\bar{A}$, does not necessarily imply an upper limit on the mass of any one neutrino.

Regardless of whether neutrinos are of Majorana character or not, nuclear double beta decay <u>with</u> the emission of antineutrinos to conserve lepton number,

$$(A,Z) \longrightarrow (A,Z+2) + 2e^- + 2\bar{\nu}_e \ , \qquad (57)$$

certainly does occur. Note, however, that four leptons are emitted in this decay mode, while only two would be emitted in the <u>neutrinoless</u> double beta decay in which we are interested. As a result, phase space favors the latter decay mode by six orders of magnitude! It is this circumstance which makes $(\beta\beta)_{o\nu}$ an especially promising reaction in which to look for evidence that neutrinos are Majorana particles, even though the reaction is

suppressed by the small values of the neutrino masses, and vanishes, in conformity with the "Dirac-Majorana confusion theorem," when the masses go to zero.

The best current limit on M_{eff} comes from a geochemical study which compares the rates for double beta decay (with or without neutrinos) of two different tellurium isotopes.[38] From the geochemical data and ratios of nuclear matrix elements,[39] it is found that[40]

$$M_{eff} < 5.6 \text{ eV} . \tag{58}$$

Hopefully, future experiments will probe the region of even smaller masses.

Summary

From the standpoint of grand unified theories, it is more natural for neutrinos to be massive than massless. Thus, it is a good idea to have this Workshop! However, the neutrinos may be rather light compared to 1 eV . I think it would be worthwhile to give some thought to this possibility. If neutrinos do have mass, then there are fascinating physical consequences, such as neutrino oscillation, and a possibly very important role for neutrinos in astrophysics. Impressive efforts, both past and planned, to measure neutrino masses are discussed in these Proceedings. Laudable attempts to find out whether neutrinos are indeed their own antiparticles, a physically very interesting possibility, are also described.

REFERENCES

1. The argument I will present here is due to S. Weinberg [Phys. Rev. Lett. 43, 1566 (1979)], and E. Witten [Durham NH Workshop (1980), p. 275].
2. M. Gell-Mann, P. Ramond, and R. Slansky, in Supergravity, edited by P. van Nieuwenhuizen and D. Freedman (North Holland), 1979), p. 315.
3. B. Kayser, to be published.
4. D. Ayres et al., Phys. Rev. 29, 902 (1984).
5. The discussion which follows is based on Sec. III. of B. Kayser, Phys. Rev. D24, 110 (1981).
6. Searching for heavy neutrinos by looking for such lines was suggested and urged by R. Shrock [Phys. Lett. 96B, 159 (1980), and Phys. Rev. D24, 1232 (1981)].
7. For summaries, see G. Kane and R. Shrock, in Intense Medium Energy Sources of Strangeness, edited by T. Goldman, H. Haber, and H. Sadrozinski (American Institute of Physics, New York, 1983), p. 123, and F. Vannucci, these Proceedings.
8. A. De Rújula and S. Glashow, Phys. Rev. Lett. 45, 942 (1980).
9. H. Shipman and R. Cowsik, Astrophys. J. 247, L111 (1981).
10. F. Bergsma et al., Phys. Lett. 128B, 361 (1983), and C. Santoni, these Proceedings.
11. F. Boehm, paper presented at the 1983 meeting of the Division of Particles and Fields of the American Physical Society, Blacksburg, September, 1983, and J. Vuilleumier et al., Phys. Lett. 114B, 298 (1982).
12. S. Boris et al., paper presented at HEP83, Brighton, July, 1983.
13. Except for the precise numbers, the above comparison of tritium and oscillation data is due to L. Wolfenstein [Neutrino Mass and Gauge Structure of Weak Interactions, edited by V. Barger and D. Cline (American Institute of Physics, New York, 1983), p. 53.]
14. K. Bergkvist, these Proceedings.
15. H. Robertson, these Proceedings.
16. For further discussion of the wave packet treatment of neutrino oscillation, see Kayser, Ref. 5.
17. S. Nussinov, Phys. Lett. 63B, 201 (1976).
18. B. Kayser, Phys. Rev. 26, 1662 (1982).
19. For discussion of the phases encountered in the field-theoretic treatment of Majorana particles, see Kayser, Ref. 3, and references therein.
20. In the Majorana case, it is a bit dangerous to call $(\nu^M)^c$ the "charge-conjugate field" because the phase factor λ^* relating it to ν^M is arbitrary and has nothing to do with charge conjugation. See Kayser, Ref. 3.
21. We thank G. Senjanovic for explaining this procedure to us.
22. B. Kayser and R. Shrock, Phys. Lett. 112B, 137 (1982).
23. This is considerably less than the current upper limit of 500 keV on M_{ν_μ}, reported at this Workshop by P. Le Coultre.
24. We are assuming the ν_μ is relativistic in the lab., as it will be if $M_{\nu_\mu} > 30$ keV .

25. T.L. Trueman, Lecture Notes on Scattering Theory, Brookhaven National Laboratory internal report, 1965, and G.C. Wick, Ann. of Phys. 18, 65 (1962).
26. Part of the preceding analysis of neutrinos from fast pions was carried out in collaboration with Leo Stodolsky. It is a pleasure to thank Dr. Stodolsky for studying this problem with me, for his physical insight into it, and for his hospitality at the Max Planck Institut für Physik und Astrophysik.
27. K. Fujikawa and R. Shrock, Phys. Rev. Lett. 45, 963 (1980).
28. B. Lynn and G. Feinberg, Columbia University preprint CU-TP-181.
29. B. Lee and R. Shrock, Phys. Rev. D16, 1444 (1977).
30. R. Shrock, Nucl. Phys. B206, 359 (1982).
31. For a more extensive discussion, see T. Kotani, these Proceedings.
32. For a very thorough, up-to-date review of this whole subject, covering the experimental evidence and both the nuclear and particle aspects of the theory, see W. Haxton and G. Stephenson, Jr., Los Alamos National Laboratory preprint LA-UR-84-396 (to be published).
33. S.P. Rosen, in Neutrino 81, edited by R. Cence, E. Ma, and A. Roberts (University of Hawaii, Honolulu, 1981), Vol. 2, p. 76.
34. L. Wolfenstein, Phys. Lett. 107B, 77 (1981).
35. B. Kayser and A.S. Goldhaber, Phys. Rev. D28, 2341 (1983).
36. B. Kayser, these Proceedings.
37. A pair of nearly degenerate Majorana neutrinos with similar couplings to an electron but opposite CP-parities would give nearly cancelling contributions to M_{eff}. Such a pair has been called a pseudo-Dirac neutrino. See L. Wolfenstein, Nucl. Phys. B186, 147 (1981), M. Doi et al., Prog. Theor. Phys. 70, 1331 (1983), and R. Mohapatra, talk given at the LAMPF-II Workshop, Los Alamos, July, 1983.
38. T. Kirsten, H. Richter, and E. Jessberger, Phys. Rev. Lett. 50, 474 (1983).
39. W. Haxton, G. Stephenson, Jr., and D. Strottman, Phys. Rev. D25, 2360 (1982), and Phys. Rev. Lett. 47, 153 (1981).
40. A comparable limit, coming from an experiment on the double beta decay of germanium, was reported at the Workshop. See L. Zanotti, these Proceedings.

PHENOMENOLOGY OF MASSIVE NEUTRINOS

F. Vannucci
LPNHE, Université de Paris, France

ABSTRACT

This paper summarizes the limits obtained, using various methods, in the search for massive neutrinos and their mixings.

There are no reason for the neutrinos to be massless. On the contrary GUT's prefer heavy neutrinos, although they do not give strict predictions. It is then interesting to evaluate the limits that present experiments already put on the parameters involved.

When neutrinos are massive the weak eigenstates ν_e ν_μ ν_τ, which are the neutrinos in the laboratory, are not necessarily identical to the mass eigenstates ν_1 ν_2 ν_3. The two sets are related by a Kobayashi-Maskawa type matrix:

$$\begin{pmatrix} \nu_e \\ \nu_\mu \\ \nu_\tau \end{pmatrix} = \begin{pmatrix} U_{e1} & U_{e2} & U_{e3} \\ U_{\mu 1} & U_{\mu 2} & U_{\mu 3} \\ U_{\tau 1} & U_{\tau 2} & U_{\tau 3} \end{pmatrix} \begin{pmatrix} \nu_1 \\ \nu_2 \\ \nu_3 \end{pmatrix}$$

This is a situation analog to the one existing among quarks, but here the problem to be solved is much more difficult since both matrix elements and masses are unknown, and the limits given by experiments will be on a combination of these parameters.

With this formalism a physical process must be interpreted as an incoherent sum of various channels. For instance $K \to e\nu_e$ is in fact:

$$K \to \sum_i e\nu_i$$

with all ν_i entering if their mass m_i is below the kinematical limit of ~ 500 MeV. Apart from phase space and helicity factors, the different channels will appear with weights $|U_{ei}|^2$. In particular, ν_e produced in tritium decay, where the available energy is only 18 KeV, could be a different superposition of ν_i, namely a different particle, than the one emitted in π or K decays. In the following we will summarize the known limits on the m_i and $|U_{Hi}|^2$, calling ν_H an hypothetical heavy mass eigenstate.

1. DIRECT MEASUREMENTS

Experiments can first put a constraint on the dominant mass eigenstate in a beam: ν_1 for ν_e... This is done by measuring with great accuracy the particles associated with the emitted neutrino: β decay of tritium for ν_1, π decay for ν_2, τ decay for ν_3. This method is most sensitive when the ν carries less energy: at the kinematical end point of the process. The present limits are the following:

$m(\nu_1) \leq 35$ eV[1)]

$m(\nu_2) \leq 500$ KeV[2)]

$m(\nu_3) \leq 160$ MeV[3)]

Here the limit applying on $m(\nu_1)$ comes from the ITEP experiment assuming a massless neutrino.

2. MESON DECAYS

Considering the decay $\pi \to \mu\nu_\mu$, one can look at the main component of the ν beam namely ν_2, and put the limit already quoted. One can also search for heavier ν_H. They would manifest themselves as secondary peaks in the spectrum of the associated charged lepton[4)]. The expected intensity of such a ν_H is $|U_{H\mu}|^2$ with respect to ν_μ. In fact helicity arguments, the fact that ν_H has both right and left handed components, favour ν_H specially in the electronic channels.

Secondary peaks have been searched for in $\pi \to \mu\nu$, $\pi \to e\nu$ and $K \to \mu\nu$ at SIN, TRIUMF and KEK respectively. The absence of signal puts a limit on the mixings $|U_{He}|^2$ or $|U_{H\mu}|^2$ as a function of $m(\nu_H)$. This is shown in fig. 1.

3. DECAYS OF HEAVY NEUTRINOS

If heavy neutrinos exist, they are present in any beam with fluxes proportional to $|U_{H\ell}|^2$. Heavy neutrinos can also be produced directly. For instance $F \to \tau\nu_\tau$ will produce ν_3 which is a good candidate for being heavy. More generally heavy neutrinos can be produced in pairs: $\pi^o \to \nu_H\bar{\nu}_H$ $Z^o \to \nu_H\bar{\nu}_H$ ... and the domain of neutrino masses covered will depend on the production mechanism.

After production these neutrinos will decay[5)]. Different channels will be open depending on the mass. The leptonic channel $\nu_H \to e^+e^-\nu_e$ opens at a mass $\sim$ 1 MeV, heavier masses allow for instance $\nu_H \to e^-\pi^+$. Also radiative decays can be present in particular $\nu_H \to \nu\gamma$, $\nu_H \to \nu\gamma\gamma$. All these decay probabilities are computable, they depend on the mass and the mixings. Again a null result gives a limit in the 2-dimensional plot $m(\nu_H)$, $|U_{H\ell}|^2$. It happens that this method is more powerful than the one discussed previously, just because of the large fluxes available in neutrino beams. Fig. 2 shows results obtained with the CHARM detector using this technique[6)].

4. OSCILLATIONS OF NEUTRINOS

Oscillations are direct transitions between neutrinos of different species. This is possible if neutrinos are massive and if different flavours mix. The probability of oscillations between two states is:

$$P(\nu \to \nu') = \sin^2 2\theta \sin^2 \pi \frac{R}{L}$$

R being the distance over which one measures the oscillation, and L is the oscillation length given by:

$$L = 2.5 \frac{E(GeV)}{\Delta m^2(eV^2)} \text{ (km)}$$

with

$$\Delta m^2 = m_1^2 - m_2^2 \quad .$$

θ is the mixing angle between the two states. The mixing entering in the oscillation $\sin^2 2\theta$ relates to the U elements in the following way:

$$\sin^2 2\theta \sim 4|U|^2 \quad .$$

With more than two neutrinos, there is always a pair between which the oscillation starts. It is the one we consider here.

Oscillations have been searched for in various beams: at reactors, at low and high energy accelerators, with atmospheric or solar neutrinos. The non evidence of oscillations in three new searches[7] completes the limits shown in fig. 3 in the planes Δm^2 vs. $\sin^2 2\theta$ for the three experimental channels $\nu_e \leftrightarrow \nu_\mu$, $\nu_e \leftrightarrow \nu_\tau$, $\nu_\mu \leftrightarrow \nu_\tau$.

But a new result coming from the Bugey reactor experiment[8] seems to give a hint of a positive result with parameters $\Delta m^2 \lesssim 1$ eV^2 and $\sin^2 2\theta \lesssim 10\%$. This is a disappearance experiment. It could indicate an oscillation in the channel $\nu_e \to \nu_\mu$ or $\nu_e \to \nu_\tau$. None of these possibilities are experimentally rejected.

With the formalism presented here these two solutions could mean:

- either $m_2 - m_1 \sim 1$ eV with $|U_{e2}|^2 \sim 2\%$. In that case a BEBC search at low energy[9] should be able to confirm in the near future;
- or $m_3 - m_1 \sim 1$ eV with $|U_{e3}|^2 \sim 2\%$. In that case, if the hierarchy of generations hold, the Jura[10] proposal could shed some useful light on the phenomenon.

The situation concerning the search for heavy neutrinos is summarized in fig. 4. In the plane mixing vs. mass a large region is already explored or will be explored in the near future: the data include results from oscillations together with neutrino decays up to masses reachable with Z^0 decays. The mixing shown here is the one corresponding to the best limit. In fact one should show three different plots with mixings corresponding to e, μ and τ. Still a large region is left for investigation, and in this region appears the possible Bugey singularity.

REFERENCES

1) A. Lyubimov et al., Phys. Lett. 94B (1980) 266 and Proceedings of the 1983 Brighton Conf. on High Energy Physics.

2) P. Le Coultre, Presented at this workshop.

3) C. Matteuzzi, Presented at this workshop.

4) R.E. Schrock, Phys. Lett. 96B (1980) 159.

5) M. Gronau, SLAC Pub 2967 (1982)
F. Vannucci, Preprint LPNHE 83-01.

6) C. Santoni, Presented at this workshop.

7) J. Wotschack, Presented at this workshop.
L. Lanceri, Presented at this workshop.

8) J.M. Thenard, Presented at this workshop

9) M. Baldo Ceolin et al., CERN/PSCC/P33.

10) T.C. Bacon et al., CERN/SPSC 82-20.

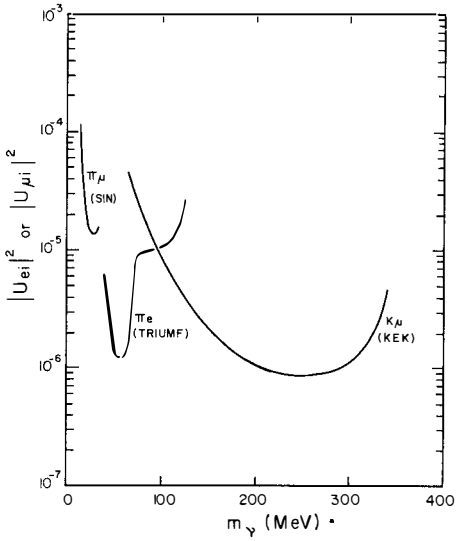


Fig. 1 - Limits on couplings of massive neutrinos obtained in peak search experiments

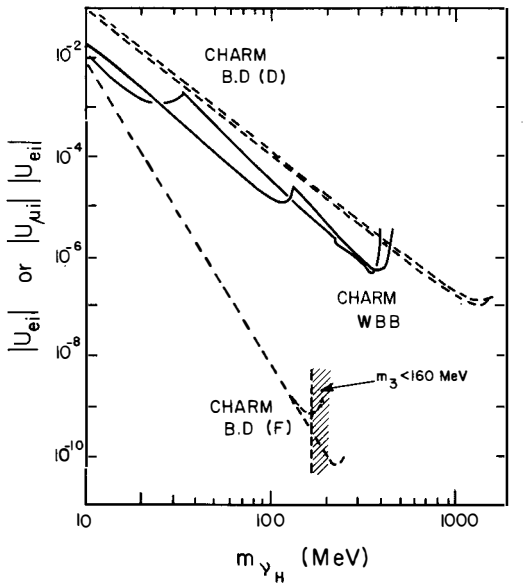


Fig. 2 - Limits obtained in heavy neutrino decays

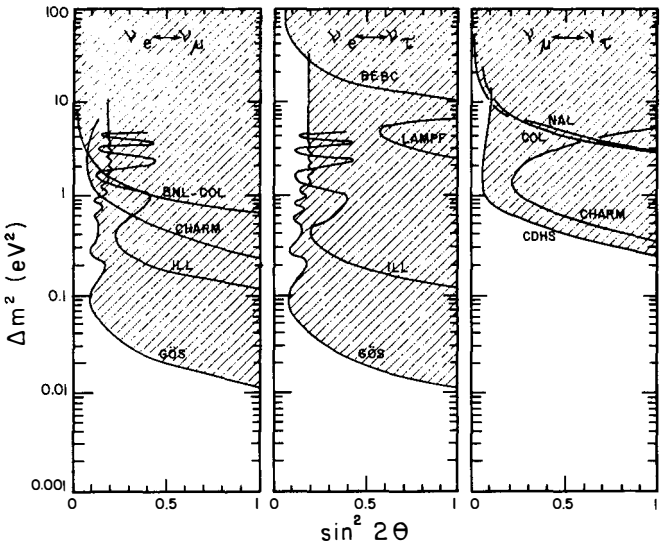


Fig. 3 - Experimental limits achieved in oscillation searches for the three channels $\nu_e\nu_\mu$, $\nu_e\nu_\tau$ and $\nu_\mu\nu_\tau$

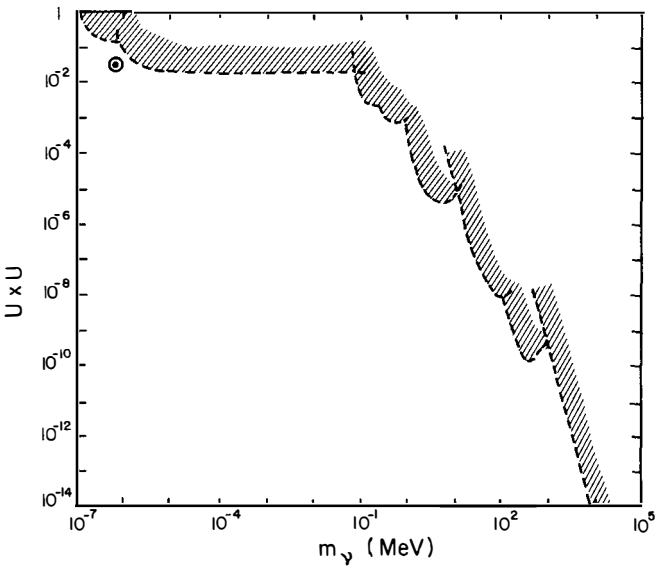


Fig. 4 - Overview of the situation in searches for massive neutrinos

GENERAL CP PROPERTIES OF NEUTRINO MASS EIGENSTATES

S. P. Rosen
T-Division, Los Alamos National Laboratory
Los Alamos, New Mexico 87545



ABSTRACT

We show that the mass eigenvectors of the neutrino mass matrix have definite CP quantum numbers whether or not CP is conserved, and we examine the conditions under which a mixture of even and odd CP eigenstates will occur.

We have heard several discussions of "pseudo-Dirac" neutrinos[1] and other possibilities[2] in which neutrino flavor eigenstates are linear combinations of Majorana mass eigenstates with opposite CP eigenvalues. Because of their opposite CP quantum numbers, these mass eigenstates interfere destructively[3] in the amplitude for no-neutrino double beta decay and thereby give rise to an "effective Majorana mass" which is much smaller than the mean mass of the electron-neutrino. In this talk, I shall consider how eigenstates of CP emerge from the general neutrino mass matrix, and the conditions under which they may have opposite CP eigenvalues.

Let me begin the discussion by examining the case of one generation. For convenience I work with a Dirac neutrino field ψ, and its charge conjugate:

$$\psi_c = \tilde{C\bar{\psi}} \equiv \gamma_2 \psi^* \quad . \tag{1}$$

Under parity ψ will be taken to transform according to the rule

$$\psi \overset{P}{\rightarrow} i\rho \gamma_4 \psi \quad , \quad (\rho = \pm 1) \tag{2}$$

where the imaginary element is deliberately inserted in anticipation of the well-known fact that Majorana neutrinos have imaginary parity[3]. I now form fields

$$\chi (\pm) \equiv \frac{1}{\sqrt{2}} (\psi \pm \psi_c) \tag{3}$$

which, by virtue of eqs. (1) and (2), are eigenstates of both C and CP; in the former case their eigenvalues are ($\pm$ 1) respectively and in the latter ($\pm i\rho$). These are the fields that represent Majorana neutrinos with opposite CP quantum numbers.

The mass matrix can be written down explicitly as

$$\{M_D \bar{\psi}\psi + M_D \bar{\psi}_c \psi_c + M_M \bar{\psi}\psi_c + M_M^* \bar{\psi}_c \psi\} \tag{4}$$

or in matrix form as

$$[\bar{\psi}, \bar{\psi}_c] \begin{bmatrix} M_D & M_M \\ M_M^* & M_D \end{bmatrix} \begin{bmatrix} \psi \\ \psi_c \end{bmatrix} \equiv \bar{\Psi} M \Psi \tag{5}$$

In equation (4), the first term is a Dirac mass term of exactly the same kind as occurs in the quark and charged-lepton mass matrices, and the second term represents the mass of the charge conjugate field explicitly. The third and

fourth terms are the so-called Majorana mass terms coupling the field and its charge conjugate.

Hermiticity of the mass term in eq. (4) ensures that M_D is real, but it places no restriction on M_M. CP invariance, however, would require that M_M be real. Whether or not CP is conserved, the mass matrix M in eq. (5) is Hermitian

$$M^+ = M \tag{6}$$

and its complex conjugate has the additional property

$$C M^* C = M \tag{7}$$

where

$$C = \begin{bmatrix} 0 & 1 \\ 1 & 0 \end{bmatrix} \tag{8}$$

Equation (6) guarantees that the eigenvalues of M are real, and equation (7) implies that the eigenvectors of M have the form:

$$M \begin{bmatrix} a \\ \pm a^* \end{bmatrix} = \lambda \begin{bmatrix} a \\ \pm a^* \end{bmatrix} \tag{9}$$

Consequently the matrix U which diagonalizes M must be of the general form:

$$U = \begin{bmatrix} a & b \\ a^* & -b^* \end{bmatrix}$$

$$U^+ M U = \begin{bmatrix} \lambda_1 & 0 \\ 0 & \lambda_2 \end{bmatrix} \tag{10}$$

It now follows that the eigenvectors of the mass matrix are:

$$\Phi = U^+ \Psi \equiv \begin{bmatrix} a^* \psi + a\psi_c \\ b^* \psi - b\psi_c \end{bmatrix} \tag{11}$$

The upper component of Φ has even CP eigenvalues ($+ i\rho$) and the lower odd CP ($- i\rho$). Thus in the one-generation case, the Majorana mass eigenstates have opposite CP quantum numbers, irrespective of CP conservation.

Let us now generalize this result to the case of N generations by making the following substitutions for the fields ψ and ψ_c:

$$\psi \to \Psi \equiv \begin{pmatrix} \psi_1 \\ \psi_2 \\ \cdot \\ \cdot \\ \psi_N \end{pmatrix}; \quad \psi_c \to \Psi_c \equiv \begin{pmatrix} \psi_{1c} \\ \psi_{2c} \\ \cdot \\ \cdot \\ \psi_{Nc} \end{pmatrix} \tag{12}$$

The elements of M must be replaced by (N x N) matrices with the properties:

$$M_D \to \mathrm{M}_D = \mathrm{M}_D^{+}; \quad M_M \to \mathrm{M}_M = \tilde{\mathrm{M}}_M \tag{13}$$

(+ denotes Hermitian conjugate, and ~ is transpose), and M itself becomes a (2N x 2N) Hermitian matrix:

$$M \to \hat{M} \equiv \begin{bmatrix} \mathrm{M}_D & \mathrm{M}_M \\ \mathrm{M}_M^{*} & \tilde{\mathrm{M}}_D \end{bmatrix} = (\hat{M})^{+} \tag{14}$$

Without loss of generality, we can assume that each component of Ψ transforms with the same phase under parity[4] ($\psi_\ell \to i\rho\, \gamma_4\, \psi_\ell$ for $\ell = 1, 2, \ldots N$), and so $\hat{M}$ will be a real matrix if CP should be conserved.

The matrix C of eq. (8) also becomes a (2N x 2N) matrix:

$$C \to C_N \equiv \begin{bmatrix} 0 & \mathrm{I}_N \\ \mathrm{I}_N & 0 \end{bmatrix} \tag{15}$$

where I_N is an (N x N) unit matrix. It is not difficult to show that in addition to the Hermiticity of $\hat{M}$, the analogue of the property in eq. (7) is also preserved:

$$C_N\, (\hat{M})^{*}\, C_N = \hat{M} \tag{16}$$

Therefore the matrix which diagonalizes $\hat{M}$ must be of the form:

$$\mathrm{U}_N = \begin{bmatrix} \mathrm{A} & \mathrm{B} \\ \mathrm{A}^{*} & -\mathrm{B}^{*} \end{bmatrix} \tag{17}$$

where A and B are (N x N) submatrices (not necessarily unitary), and the mass eigenvectors are:

$$\Phi_N = \mathrm{U}_N^{+} \begin{bmatrix} \Psi \\ \Psi_c \end{bmatrix} = \begin{bmatrix} \mathrm{A}^{*}\, \Psi + \mathrm{A}\, \Psi_c \\ \mathrm{B}^{*}\, \Psi - \mathrm{B}\, \Psi_c \end{bmatrix} \tag{18}$$

Again the upper components have even CP and the lower components odd CP.

When CP is conserved, M_D and M_M are both real, symmetric matrices and the

diagonal form of $\hat{M}$ is given by:

$$\begin{bmatrix} A^{+}\,(M_D + M_M)\,A & , & 0 \\ 0 & , & B^{+}\,(M_D - M_M)\,B \end{bmatrix} \tag{19}$$

The transformation matrices A and B are now real and orthogonal. From this we see that the CP even eigenvectors are associated with the eigenvalues of $(M_D + M_M)$ and the CP odd eigenvectors with $(M_D - M_M)$.

Our final generalization is to introduce the chiral decomposition of the fields into ψ_R, the right-handed multiplet, and ψ_L, the left-handed one. Thus we make the substitutions:

$$\psi \to \begin{pmatrix} \psi_R \\ \psi_L \end{pmatrix}; \quad \psi_C \to \begin{pmatrix} \psi_{CL} \\ \psi_{CR} \end{pmatrix} \tag{20}$$

and replace the (N x N) Dirac and Majorana matrices by (2N x 2N) ones:

$$M_D \to \begin{bmatrix} 0 & D \\ D^{+} & 0 \end{bmatrix} \quad ; \quad M_M \to \begin{bmatrix} R & 0 \\ 0 & L \end{bmatrix} \tag{21}$$

where R and L are symmetric (N x N) matrices. The zeros in eq. (21) correspond to the fact that mass terms can only connect left-handed fields with right-handed ones and vice versa.

Because of the structure of M_D and M_M in eq. (21), it is easy to show that the eigenvalues of $(M_D - M_M)$ must be equal and opposite to those of $(M_D + M_M)$. Since we identify only eigenvectors with positive mass eigenvalues as physical states, it follows that the positive eigenvalues of $(M_D + M_M)$ will have eigenvectors with even CP. The negative eigenvalues of $(M_D + M_M)$ become positive ones for $(M_D - M_M)$ and hence will be associated with odd CP eigenvectors.

In conclusion we see that in general the neutrino mass eigenvectors have definite CP eigenvalues, but the precise mixture of even and odd ones will depend on the detailed structure of the eigenvalue spectrum of $(M_D + M_M)$.[5]

References

(1) T. Kotani, these proceedings.

(2) S. P. Rosen, these proceedings.

(3) B. Kayser, these proceedings.

(4) Any field ψ_R which transforms under parity with a phase $(-\rho)$ can always be replaced by $(\gamma_5\psi_R)$ which transforms with phase $(+i\,\rho)$.

(5) For further details see S. P. Rosen, Phys. Rev. D (to be published).

CPT AND CP PROPERTIES OF MAJORANA NEUTRINOS AND THE PRACTICAL CONSEQUENCES

Boris Kayser
Division of Physics, National Science Foundation
Washington, D.C. 20550



ABSTRACT

The CPT and CP properties of Majorana neutrinos have significant consequences, the most important of which is a potential suppression of the rate for neutrinoless double beta decay. We derive these properties, and find their consequences for double beta decay, and for the radiative decays and electromagnetic interactions of Majorana neutrinos.

As discussed in "Introduction to Massive Neutrinos," in these Proceedings,[1] a Majorana neutrino is its own antiparticle under CPT. This means that the effect of CPT on the state of such a neutrino, ν^M, is given by

$$CPT|\nu^M(\vec{p},s)\rangle = \tilde{\eta}^s_{CPT}|\nu^M(\vec{p},-s)\rangle \ . \qquad (1)$$

Here $\vec{p}$ is the momentum of the neutrino, and s is its spin projection, which reverses, of course, under T. The quantity $\tilde{\eta}^s_{CPT}$ is the phase factor which one expects to encounter in any discrete symmetry transformation such as Eq. (1). As we shall see, $\tilde{\eta}^s_{CPT}$ depends on s.

To the extent that CP is conserved by the weak interactions, a Majorana neutrino is also an eigenstate of CP:

$$CP|\nu^M(\vec{p},s)\rangle = \tilde{\eta}_{CP}|\nu^M(-\vec{p},s)\rangle \ . \qquad (2)$$

Here $\vec{p}$ reverses because of the action of P, and $\tilde{\eta}_{CP}$ is a phase factor representing the intrinsic CP parity of ν^M.

A Majorana neutrino is not an eigenstate of C, because C is badly violated by the weak interactions.[2]

Now, what can one say about the phase factors $\tilde{\eta}^s_{CPT}$ and $\tilde{\eta}_{CP}$, and what are the consequences of the CPT and CP properties of Majorana neutrinos? One of the major consequences is an effect on neutrinoless double beta decay, the process whose observation would signal that neutrinos are Majorana particles. As we shall show, the contributions to this reaction from virtual Majorana neutrinos of opposite CP parity are of opposite sign. If cancellations among these contributions are severe, as expected in some theories, the rate for neutrinoless double beta decay could be far below the level naively expected for neutrinos of given masses.

CP Properties of Majorana Neutrinos

Let us first discuss the CP properties and phases of a Majorana neutrino. Everyone knows that $CP(\gamma) = CP(Z^\circ) = +1$, while $CP(\pi^\circ) = -1$. What is the CP of a Majorana neutrino ν^M? To find out, let us consider the decay $Z^\circ \to \nu^M + \nu^M$, and

make the plausible assumption that CP is conserved in this decay. To see what consequence this has, it is sufficient to suppose that the outgoing neutrinos are nonrelativistic. Now, the final state contains two identical fermions, so it must be antisymmetric. Thus, it must be a $^3P_1$ state, this being the only antisymmetric nonrelativistic state with the same angular momentum J as the Z^o. From Eq. (2), the effect of CP on this two-neutrino state is given by

$$CP|\nu^M\nu^M;{}^3P_1\rangle = \tilde{\eta}_{CP}^2(-1)^L|\nu^M\nu^M;{}^3P_1\rangle \ . \qquad (3)$$

Here the factor $(-1)^L$ is, of course, the consequence for a state of definite L of the momentum-reversal in Eq. (2). Since, in particular, our state has $L = 1$, we see from Eq. (3) that CP conservation in $Z^o \to \nu^M + \nu^M$ requires that $-\tilde{\eta}_{CP}^2 = +1$. From this we learn that the intrinsic CP parity of a Majorana fermion is neither $+1$ nor -1. Rather, it is <u>imaginary</u>![3]

While a Majorana neutrino does not have a well-defined C or P, there may be other Majorana particles for which these quantum numbers are well-defined. Consider, for example, the photino, which is a spin-$\frac{1}{2}$ Majorana fermion predicted by supersymmetric theories to exist as a "super-partner" to the photon. Assuming that the photino participates in interact'ons which are largely C- and P-conserving, one can easily show, just by invoking conservation laws, that the charge conjugation quantum number of a photino (or of any Majorana particle for which C is well-defined) is real. From this result, together with the finding that CP is imaginary, one can infer that the intrinsic parity of any Majorana fermion which <u>has</u> a well-defined parity is imaginary.

An interesting consequence of the fact that the CP parity of Majorana fermions is imaginary is encountered in the radiative decay $\nu_1 \to \nu_2 + \gamma$, where $\nu_{1,2}$ are Majorana neutrinos. To explore the implications of CP conservation in this decay, we consider the cross-channel process $\gamma(q^2) \to \nu_1 + \nu_2$, where $\gamma(q^2)$ is an off-mass-shell photon. Suppose for the moment that the outgoing neutrinos in the latter process are nonrelativistic

and are in a state of definite L , S , and J . Then, in analogy with Eq. (3), the effect of CP , which we shall henceforward call z , on this state is given by

$$z|\nu_1\nu_2;{}^{2S+1}L_J\rangle = \tilde{\eta}_z(1)\tilde{\eta}_z(2)(-1)^L|\nu_1\nu_2;{}^{2S+1}L_J\rangle \ . \qquad (4)$$

Here $\tilde{\eta}_z(i)$ is the intrinsic CP parity of ν_i . Now, because the $\tilde{\eta}_z(i)$ are imaginary, the requirement that the state in Eq. (4) have the same CP as its parent photon implies that

$$-\frac{\tilde{\eta}_z(2)}{\tilde{\eta}_z(1)}(-1)^L = +1 \ . \qquad (5)$$

Thus, since the photon has $J = 1$, the $\nu_1\nu_2$ pair is produced in a P-wave (S- or D-wave) when $\tilde{\eta}_z(2)/\tilde{\eta}_z(1) = +1(-1)$. Now, $\nu_1 \longrightarrow \nu_2 + \gamma$ can involve two possible couplings, electric and magnetic dipole, which yield, respectively, E1 and M1 radiation. On the other hand, one can show that in the nonrelativistic limit of the cross-channel process, an electric dipole coupling would produce P-wave neutrinos, and a magnetic dipole coupling S- and D-wave neutrinos. Hence, when CP is conserved and ν_1 and ν_2 have the same (opposite) CP parity, the radiation in the decay $\nu_1 \longrightarrow \nu_2 + \gamma$ will be E1 (M1) .[4],[3]

Neutrinoless Double Beta Decay

Perhaps the most important consequence of the CP properties of Majorana neutrinos is found in neutrinoless double beta decay $[(\beta\beta)_{0\nu}]$. The observation of this reaction, in which one nucleus decays to another through the emission of two electrons unaccompanied by any antineutrinos, would signal that neutrinos are Majorana particles.[1],[5] The reaction would be engendered by the diagram in Fig. 1, in which a pair of W bosons, emitted by two neutrons in the parent nucleus, produces the outgoing electrons by exchanging a Majorana neutrino. As Fig. 1 indicates, the amplitude for the reaction is the sum of the contributions of all the Majorana neutrino mass eigenstates ν_m which couple to an electron. This coupling is described by the general charged-current weak interaction with neutrino mixing,

$$H(x) = g\sum_m [W_\mu^- i\bar{e}\gamma_\mu(1+\gamma_5)U_{em}\nu_m + W_\mu^+ i\bar{\nu}_m U_{em}^*\gamma_\mu(1+\gamma_5)e] \ . \qquad (6)$$

Here, g is the (real) overall coupling strength, and U is the lepton mixing matrix. Right-handed currents are being neglected for simplicity.

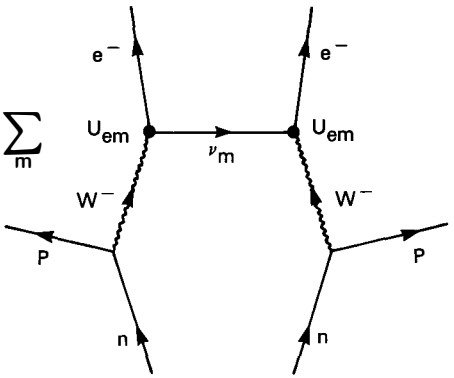


Fig. 1. Neutrinoless double beta decay. Each neutrino ν_m is a Majorana neutrino of definite mass M_m.

When CP is violated, the mixing matrix elements U_{em} can have any phases at all.[6] Now, since it is the first term in the interaction (6) which acts at both electron vertices in Fig. 1, the contribution of a given ν_m to $(\beta\beta)_{o\nu}$ is proportional to U_{em}^2, as Fig. 1 indicates. Thus, when CP is violated, the contributions of the different neutrinos can interfere with arbitrary relative phases.

On the other hand, in the hadron sector CP appears to be rather well conserved, so one can guess that it is also approximately conserved in the lepton sector. Assuming it <u>is</u> conserved, do the contributions of the various ν_m to $(\beta\beta)_{o\nu}$ always add constructively, or may they still interfere destructively, producing a $(\beta\beta)_{o\nu}$ amplitude that is smaller and harder to detect than one would naively expect? Various statements have been made about this question. Doi <u>et al.</u>[7] at one time claimed that destructive interference cannot occur unless CP is violated, and an argument can be given that makes this claim extremely plausible.

Nevertheless, Wolfenstein[8] has asserted that destructive interference already occurs when CP is conserved but the interfering neutrinos have opposite CP parity. Halprin, Petcov, and Rosen[9] agree that destructive interference can occur when CP is conserved, but state that the sign of the interference depends on that in a "Majorana condition" which appears to express the C (rather than CP) properties of the neutrino field. Evidently, there has been some controversy about this matter. Therefore, A.S. Goldhaber and I tried to see if the CP conserving case could be understood in a convincing and simple way.[10] I would like to briefly summarize our analysis and its result.

Disregarding the nucleon lines which generate the W bosons, the process represented by Fig. 1 is just $W^-W^- \longrightarrow e^-e^-$ via Majorana neutrino exchange. To examine this process, it is convenient to go to the cross channel, $e^+W^- \longrightarrow e^-W^+$. To uncover the role played by the CP parities of the neutrinos contributing to the latter reaction, we express its amplitude, $\langle e^-W^+|\, H(x_1)\, H(x_2)\,|e^+W^-\rangle$, explicitly in terms of the intermediate neutrino states:

$$\langle e^-W^+|\, H(x_1)\, H(x_2)\,|e^+W^-\rangle = \sum_{\vec{p},s}^{m} \langle e^-W^+|\, H(x_1)\,|\nu_m(\vec{p},s)\rangle\langle\nu_m(\vec{p},s)|\, H(x_2)\,|e^+W^-\rangle + \cdots \tag{7}$$

On the right-hand side (RHS) of Eq. (7), we have not written out three additional terms which correspond to the three additional ways in which the annihilation of the e^+ and W^-, and creation of the e^- and W^+, can be divided between $H(x_1)$ and $H(x_2)$. The physics of these omitted terms is the same as that of the term we have written out, so we shall discuss only the latter.

If the Hamiltonian $H(x)$ is CP ($\equiv z$) invariant, so that $z\,H(\vec{x},t)z^{-1} = H(-\vec{x},t)$, we have for the first matrix element on the RHS of Eq. (7)

$$\langle e^-W^+|\, H(\vec{x}_1,t_1)\,|\nu_m(\vec{p},s)\rangle = \langle e^-W^+|z^{-1}zH(\vec{x}_1,t_1)z^{-1}z\,|\nu_m(\vec{p},s)\rangle = \tilde{\eta}_z(m)\tilde{\eta}_z^*(e^-)\tilde{\eta}_z^*(W^+)\,\langle e^+W^-|\, H(-\vec{x}_1,t_1)\,|\nu_m(-\vec{p},s)\rangle\ . \tag{8}$$

Here we have employed Eq. (2), and used $\tilde{\eta}_z(m)$, as before, to denote the CP parity of ν_m. The quantities $\tilde{\eta}_z(e^-)$ and $\tilde{\eta}_z(W^+)$ are phase factors encountered when z acts on the (non-self-conjugate) e^- and W^+ states, and will not concern us. Now, in the matrix element on the second line of Eq. (8), H must create an e^+. This is done by the second term in Eq. (6), so this matrix element is proportional to U^*_{em}. However, in the second matrix element on the RHS of Eq. (7), H must absorb an e^+. This is done by the first term in Eq. (6), so this matrix element is proportional to U_{em}. Thus, from Eqs. (7) and (8) combined, the contribution of ν_m to the amplitude for $e^+W^- \longrightarrow e^-W^+$ is proportional to $\tilde{\eta}_z(m)|U_{em}|^2$. Notice that by using CP-invariance to rewrite only the first of the two matrix elements on the RHS of Eq. (7), we have managed to express the ν_m contribution in terms of $|U_{em}|^2$, so that we do not need to know anything about the phases of the U_{em}. Turning to kinematics, let us choose the ν_m spin quantization axis to be along its momentum $\vec{p}$, so that s represents helicity. Then, for given s, either the CP-transformed matrix element in Eq. (8), or its companion matrix element in Eq. (7) to which CP has not been applied, involves a left-handed neutrino. However, except for corrections of the order of the lepton masses, the Hamiltonian (6) conserves lepton helicity, and only couples to an e^+ when it is right-handed. Thus, in both of the matrix elements under discussion, a right-handed neutrino would be preferred. As a result, the contribution of ν_m is proportional to its mass, M_m.

We conclude that when CP is conserved, the amplitude for $e^+W^- \longrightarrow e^-W^+$, and consequently that for $(\beta\beta)_{o\nu}$, is proportional to the quantity

$$\sum_m \tilde{\eta}_z(m)|U_{em}|^2 M_m \equiv i\, M_{eff} \,. \tag{9}$$

(We recall that the CP parities $\tilde{\eta}_z(m)$ are imaginary, so that the effective mass M_{eff} defined by this equation is real.) We see that, unfortunately, neutrinos with opposite CP parity do interfere destructively. Wolfenstein was right, and M_{eff} can easily be smaller than any of the actual masses M_m of the

neutrinos.

We saw earlier that when CP is conserved, the radiative decay $\nu_1 \to \nu_2 + \gamma$ will yield pure E1 (M1) radiation when ν_1 and ν_2 have the same (opposite) CP parity. Thus, in principle, we need not depend on any theoretical model to tell us whether two neutrinos will interfere constructively or destructively in $(\beta\beta)_{o\nu}$. We need only measure the polarization of the photon emitted in the radiative decay of the heavier of these two neutrinos to the lighter! We will then know the relative CP parity of the two neutrinos, and hence how their virtual contributions to $(\beta\beta)_{o\nu}$ will interfere.

Of course, such a measurement is likely to be out of the question, and so we do need to depend on theoretical models. Having demonstrated that neutrinos can in principle interfere destructively in $(\beta\beta)_{o\nu}$, we now ask whether they actually do so in reasonable, popular models. Unfortunately, the answer is yes. There are popular grand unified theories which were constructed without $(\beta\beta)_{o\nu}$ in mind in which different Majorana neutrinos not only have opposite CP parities but cancel one another's contributions to $(\beta\beta)_{o\nu}$ quite thoroughly. Chang and Pal have found[11] that in some realizations of SO(10) grand unified theory, M_{eff} is an order of magnitude below the lightest of the actual neutrino masses M_m. Thus, it seems best that any negative experimental search for $(\beta\beta)_{o\nu}$ be interpreted, not as an upper bound on the mass M_m of any one physical neutrino, but as an upper bound on the effective mass M_{eff}.

CPT Properties and their Consequences

We turn now to the CPT properties and phases of a Majorana particle, and their implications. Since it is so easy to do so, we shall be very general, and study a "Majorana" (i.e., CPT self-conjugate) particle of arbitrary spin J. Consider, in its rest frame, such a particle with $J_z = s$. In analogy with Eq. (1), the effect of $CPT \equiv \zeta$ on the state $|J,s\rangle$ of this particle is defined to be

$$\zeta|J,s\rangle = \tilde{\eta}^s_\zeta |J,-s\rangle \ . \qquad (10)$$

Here $\tilde{\eta}^s_\zeta$ is a phase factor, and we are allowing for the possibility that, for given J, it depends on s. To determine the important characteristics of this CPT phase factor, it is useful to introduce the operator

$$b \equiv e^{-i\pi J_y}\zeta \ . \tag{11}$$

Obviously, when b acts on $|J,s\rangle$, the 180° rotation $e^{-i\pi J_y}$ undoes the spin-reversal caused by ζ. Thus,

$$b|J,s\rangle = \tilde{\eta}^s_b|J,s\rangle \ , \tag{12}$$

where $\tilde{\eta}^s_b$ is some new phase factor. Now, b, like ζ, is an antiunitary operator. (This implies that for any state $|A\rangle$ and coefficient λ, $b[\lambda|A\rangle] = \lambda^* b|A\rangle$.) Hence,

$$b^2|J,s\rangle = b[\tilde{\eta}^s_b|J,s\rangle] = (\tilde{\eta}^s_b)^* b|J,s\rangle = (\tilde{\eta}^s_b)^*\tilde{\eta}^s_b|J,s\rangle \ . \tag{13}$$

That is, $b^2 = 1$ when acting on the states $|J,s\rangle$. From the definition (11), this implies that

$$\zeta^2 e^{-2i\pi J_y} = 1 \ . \tag{14}$$

Here we have used the fact that ζ commutes with rotations. (Note that the spin-reversal in Eq. (10) implies that ζ anticommutes with $\vec{J}$, and its antiunitarity implies that it also anticommutes with i, so that it commutes with $e^{-i\pi J_y}$.)

The 360° rotation in Eq. (14) brings a particle back to its original state, multiplied by the famous phase factor $(-1)^{2J}$, whose presence in the case where $J = 1/2$ has been verified by elegant neutron interferometry experiments. From Eq. (14), we learn that when ζ^2 is applied to any Majorana (i.e., CPT self-conjugate) particle, it returns it to its original state multiplied by exactly the same phase factor:[12]

$$\zeta^2 = (-1)^{2J} \ . \tag{15}$$

One may think of the application of $(CPT)^2$ to a Majorana

particle at rest as a jerky rotation through 360° . What we have just found is that this operation introduces exactly the same phase factor as the actual rotation.

From Eq. (10) and the antiunitarity of ζ ,

$$\zeta^2|J,s> = \zeta[\tilde{\eta}_\zeta^s|J,-s>] = (\tilde{\eta}_\zeta^s)^*\zeta|J,-s> = (\tilde{\eta}_\zeta^s)^*\tilde{\eta}_\zeta^{-s}|J,s> \ . \quad (16)$$

Therefore, Eq. (15) implies that

$$\tilde{\eta}_\zeta^{-s} = (-1)^{2J}\ \tilde{\eta}_\zeta^s \ . \quad (17)$$

Thus, the CPT phase factor $\tilde{\eta}_\zeta^s$, unlike most discrete symmetry phase factors with which we are familiar, depends on s .

Our knowledge of this s-dependence can be used, for example, to derive the most general expression for the matrix element of the electromagnetic current of a Majorana neutrino.[10],[13] The electromagnetic interaction is, of course, $H^{EM} = J_\mu^{EM} A_\mu$. Now, it is easy to convince oneself by semi-classical arguments that $\zeta A_\mu \zeta^{-1} = -A_\mu$. Therefore, if H^{EM} is to be CPT-invariant, it must also be true that $\zeta J_\mu^{EM}\zeta^{-1} = -J_\mu^{EM}$. Consider, now, the matrix element $<\nu^M(\vec{p}_f,s_f)|J_\mu^{EM}|\nu^M(\vec{p}_i,s_i)>$, where ν^M is a Majorana neutrino. From the antiunitarity of ζ , the fact that $\zeta J_\mu^{EM}\zeta^{-1} = -J_\mu^{EM}$, and Eq. (1) we have

$$\begin{aligned} &<\nu^M(\vec{p}_f,s_f)|J_\mu^{EM}|\nu^M(\vec{p}_i,s_i)> \\ &\quad = <\zeta[\nu^M(\vec{p}_i,s_i)]|\zeta J_\mu^{EM}\zeta^{-1}|\zeta[\nu^M(\vec{p}_f,s_f)]> \\ &\quad = -(\tilde{\eta}_\zeta^{s_i})^*\,\tilde{\eta}_\zeta^{s_f}\ <\nu^M(\vec{p}_i,-s_i)|J_\mu^{EM}|\nu^M(\vec{p}_f,-s_f)> \ . \end{aligned} \quad (18)$$

(We are now referring to the CPT phase factor in Eq. (1) as $\tilde{\eta}_\zeta^s$, of course.) Now, Lorentz invariance and current conservation imply that

$$\begin{aligned} &<\nu^M(\vec{p}_f,s_f)|J_\mu^{EM}|\nu^M(\vec{p}_i,s_i)> = \\ &\quad = i\bar{u}_f\left[F\gamma_\mu + G(q^2\gamma_\mu - \not{q}q_\mu)\gamma_5 + M\sigma_{\mu\nu}q_\nu + Ei\sigma_{\mu\nu}q_\nu\gamma_5\right]u_i \ . \end{aligned} \quad (19)$$

Here u is a Dirac spinor, $q = p_f - p_i$, and F, G, M, and E are form factors depending on q^2. Expressing the right-hand side of the CPT constraint (18) in a similar form, we find after some manipulation that

$$-(\tilde{\eta}_\zeta^{s_i})^* \tilde{\eta}_\zeta^{s_f} \langle \nu^M(\vec{p}_i,-s_i)|J_\mu^{EM}|\nu^M(\vec{p}_f,-s_f)\rangle =$$

$$= \{(\tilde{\eta}_\zeta^{s_i})^* \tilde{\eta}_\zeta^{s_f}(-1)^{s_i - s_f}\}\, i\bar{u}_f[-F\gamma_\mu + G(q^2\gamma_\mu - \not{q} q_\mu)\gamma_5$$

$$-M\sigma_{\mu\nu}q_\nu - Ei\sigma_{\mu\nu}q_\nu\gamma_5]\, u_i \ . \qquad (20)$$

From Eq. (17), we see that the combination of phase factors in curly brackets in Eq. (20) is $+1$ for any s_i, s_f. Thus, comparing Eqs. (19) and (20), we conclude that $F = M = E = 0$. Consequently, the most general expression for the matrix element of the electromagnetic current of a Majorana neutrino is

$$\langle \nu^M(\vec{p}_f,s_f)|J_\mu^{EM}|\nu^M(\vec{p}_i,s_i)\rangle = i\bar{u}_f[G(q^2)(q^2\gamma_\mu - \not{q} q_\mu)\gamma_5]u_i \ . (21)$$

There is only one form factor G, and the coupling is of axial vector type. A Majorana neutrino not only is electrically neutral, but also has no electric charge distribution (which would have been described by the form factor F, had it not vanished). Nor does it have magnetic and electric dipole moments (which would have been the $q^2 = 0$ values of the form factors M and E, had they not vanished).

Using these same CPT techniques, one can also find the most general expression for the matrix element of the neutral weak current of a Majorana neutrino,[3] and the most general form for the coupling to gravity of such a particle.[14]

Summary

A Majorana neutrino is its own antiparticle under CPT, and, approximately, under CP as well. However, it is not its own antiparticle under C.

The CP parity of a Majorana particle is imaginary. For any Majorana particle for which the ordinary parity is well-defined, that too is imaginary.

Majorana neutrinos of opposite CP parity make opposing contributions to $(\beta\beta)_{o\nu}$. As a result, this reaction measures an effective mass, M_{eff} , which could be smaller than all of the actual masses of the neutrinos.

For any CPT ($\equiv \zeta$) self-conjugate particle of spin J , $\zeta^2 = (-1)^{2J}$. As a result, the CPT phase factor $\tilde{\eta}^s_\zeta$ obeys the relation $\tilde{\eta}^{-s}_\zeta = (-1)^{2J}\tilde{\eta}^s_\zeta$. The s-dependence described by this relation can be used to find the most general expressions for $\langle \nu^M | J^{EM} | \nu^M \rangle$ and for other interesting quantities.

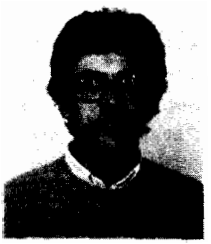
REFERENCES

1. B. Kayser, these Proceedings.
2. B. Kayser, Phys. Rev. D26, 1662 (1982).
3. For a discussion of CPT, CP, and C phases, and their effects, in Majorana particles processes, see B. Kayser, to be published.
4. B. McKellar, Los Alamos preprint LA-UR-82-1197, J. Nieves, Phys. Rev. D26, 3152 (1982), and P. Pal and L. Wolfenstein, Phys. Rev. D25, 766 (1982).
5. T. Kotani, these Proceedings.
6. The CP-violating phases which may occur in the U matrix are discussed by J. Schechter and J. Valle [Phys. Rev. D22, 2227 (1980)], A. Barroso and J. Maalampi [Phys. Lett. 132B, 355 (1983)], and J. Bernabeu and P. Pascual [Nucl. Phys. B228, 21 (1983)]. The last authors also discuss the CP-conserving case.
7. M. Doi et al., Phys. Lett. 102B, 323 (1981).
8. L. Wolfenstein, Phys. Lett. 107B, 77 (1981).
9. A. Halprin, S. Petcov, and S.P. Rosen, Phys. Lett. 125B, 335 (1983).
10. B. Kayser and A.S. Goldhaber, Phys. Rev. D28, 2341 (1983).
11. D. Chang and P. Pal, Phys. Rev. D26, 3113 (1982).
12. The simple derivation of this result given here may be found in Refs. 10 and 3. For earlier derivations and work, see P. Carruthers, Phys. Lett. 26B, 158 (1968), and Spin and Isospin in Particle Physics (Gordon and Breach, New York, 1971), E. Wigner in Group Theoretical Concepts and Methods in Elementary Particle Physics, edited by F. Gürsey (Gordon and Breach, New York, 1964), p. 37, and G. Feinberg and S. Weinberg, Nuovo Cimento 14, 571 (1959).
13. J. Nieves, Ref. 4, and B. McKellar, Ref. 4, originated the general approach which we shall now follow. However, their calculations needed revision to take into account the non-trivial s-dependence which we have just derived.
14. A. Khare and J. Oliensis, Argonne preprint ANL-HEP-PR-83-62.

RESULTS ON NEUTRINO OSCILLATIONS FROM THE CHARM COLLABORATION

CHARM Collaboration [1])
(CERN-Hamburg-Amsterdam-Rome-Moscow)

Presented by L. Lanceri [2])
CERN, Geneva, Switzerland



ABSTRACT

We searched for oscillations of muon neutrinos using two similar fine-grained neutrino detectors, having fiducial masses of 36 tons and 120 tons, placed at 123 m and 903 m from the beginning of the CERN low energy neutrino source. The average energy of the selected neutrino events was 1.5 GeV. Events initiated by ν_e's have been searched for and an upper limit of 2.7%, at 90% confidence level, is obtained for the fraction of ν_μ's transformed into ν_e's. For complete mixing this corresponds to a limit $\Delta m^2 \leq 0.20$ eV^2 for the transition $\nu_\mu \rightarrow \nu_e$ and to a minimum value of the mixing parameter $\sin^2 2\theta = 0.04$. In the same data sample oscillations of ν_μ's to ν_τ's, and possibly heavier neutrinos, do not appear. In this case for complete mixing the limit is $\Delta m^2 \leq 0.29$ eV^2.

---

[1]) Members of the collaboration are: F.Bersgma, J.Dorenbosch, M.Jonker, C.Nieuwenhuis (Amsterdam); J.V.Allaby, U.Amaldi, G.Barbiellini, L.Barone, A.Capone, Y.Eisenberg, W.Flegel, L.Lanceri, M.Metcalf, J.Panman, D.Perret-Gallix, R.Plunkett, C.Santoni, F.Vannucci, K.Winter (CERN); I.Abt, J.Aspiazu, F.W.Büsser, H.Daumann, P.D.Gall, T.Hebbeker, F.Niebergall, P.Schütt, P.Stähelin (Hamburg); P.Gorbunov, E.Grigoriev, V.Kaftanov, V.Khovansky, A.Rosanov (Moscow); A.Baroncelli, B.Borgia, C.Bosio, M.Diemoz, U.Dore, F.Ferroni, E.Longo, L.Luminari, P.Monacelli, F.deNotaristefani (Rome).

[2]) On leave of absence from INFN, Trieste, Italy.

1. INTRODUCTION

The hypothesis that neutrinos might be massive and the lepton number conservation law might be violated [1] is receiving considerable theoretical and experimental attention. We do not know of fundamental reasons for neutrino masses being exactly zero and for the exact conservation of the leptonic number, and precise predictions from theory are missing. Some experimental facts reinforce however these expectations: for instance, the solar neutrino flux is not fully understood [2] and evidence for non-zero neutrino mass has been reported by an experiment at ITEP [3].

If neutrino mass eigenvalues are non-degenerate and the lepton flavour is not conserved, neutrino flavour eigenstates are non-trivial linear superpositions of mass eigenstates. From the different evolutions in space and time of the mass eigenstates or "stationary states" it follows that in a beam of neutrinos of energy E (in GeV) and initially pure flavour α (α = e,μ,τ,..), after a distance L (in km) a component of flavour β (β = e,μ,τ,..) develops, so that ν_β can be found with a probability :

$$P(\nu_\alpha \rightarrow \nu_\beta) = \sin^2 2\theta \, \sin^2(1.27\Delta m^2 L/E) \quad . \qquad (1)$$

Δm^2 is the difference between the squares of the mass eigenvalues (in eV^2) and θ is the mixing angle in the usual two-flavor parametrization [1], assumed here for simplicity.

The detection of a variation in the flavour composition of a neutrino beam, or "neutrino oscillation", is therefore a clear signature for massive neutrinos. The squared mass eigenvalues difference Δm^2 and the mixing angle θ can be measured in such an experiment. The ratio L/E determines the range of masses to which the experiment is sensitive. The sensitivity to the mixing angle is limited by the systematic uncertainties in the knowledge of the initial flux of the neutrino beam, for the experiments detecting neutrinos of flavor α and looking for the "disappearance" of a fraction of them. Experiments looking for the "appearance" of neutrinos of flavour β on the other hand may be limited by the backgrounds.

2. THE CERN BEAM AND THE CHARM DETECTORS

In 1983 a new facility dedicated to neutrino oscillations experiments came into operation at CERN. A new 19.2 GeV proton beam was extracted from the CERN Proton Synchrotron (PS) and directed onto a 60 cm long , 8 mm diameter beryllium target. The produced pions and kaons were allowed to decay in a 48 m long, 2.8 m high, and 5 m wide tunnel, followed for muon filtering by a 50 cm concrete wall, a 4 m thick iron absorber, and earth. The low energy ($\langle E_\nu \rangle \simeq$ 1.5 GeV) muon neutrino beam thus produced pointed at the three existing detectors, BEBC,

CDHS and CHARM, placed in the Super Proton Synchrotron (SPS) neutrino beam line, at about 900 m from the described target.

The CHARM fine-grained calorimeter [7] consists of several subunits each formed by a layer of 20 scintillator counters, a layer of 256 streamer tubes, a marble slab, and a layer of 128 proportional drift tubes (PDT's). The marble slabs have 3m x 3m lateral dimensions and are 8 cm thick. They are surrounded by a 45 cm wide iron frame, which is instrumented with PDTs only. Sixty such subunits constituted the "far detector", at an average distance from the target of 903 m. The far detector fiducial mass was approximately 120 tons. Eighteen subunits corresponding to a fiducial mass of 36 tons were placed at 123 m from the target. They are referred to as the "close detector". Twenty 4m x 4m wide and 8 cm thick plates of iron, interleaved with PDT layers, were added to the eighteen calorimeter subunits of the close detector, to increase the efficiency in the containment of long muon tracks. They formed the close detector "muon catcher".

A sketch of the neutrino beam line with the two CHARM detectors is shown in fig.1. The close detector orientation with respect to the PS neutrino beam axis reproduced the orientation of the far detector, which could not be moved from its alignment along the SPS neutrino beam line. The PS neutrinos entered therefore the detectors at an angle of 22° with respect to their longitudinal axis. In the small solid angles covered by the detectors, the neutrino beam flux varied to a good approximation as $1/L^2$, L being the distance from the target. The ratio of fluxes in one subunit of the far and one subunit of the close detector are therefore approximately given by the ratio of solid angles :

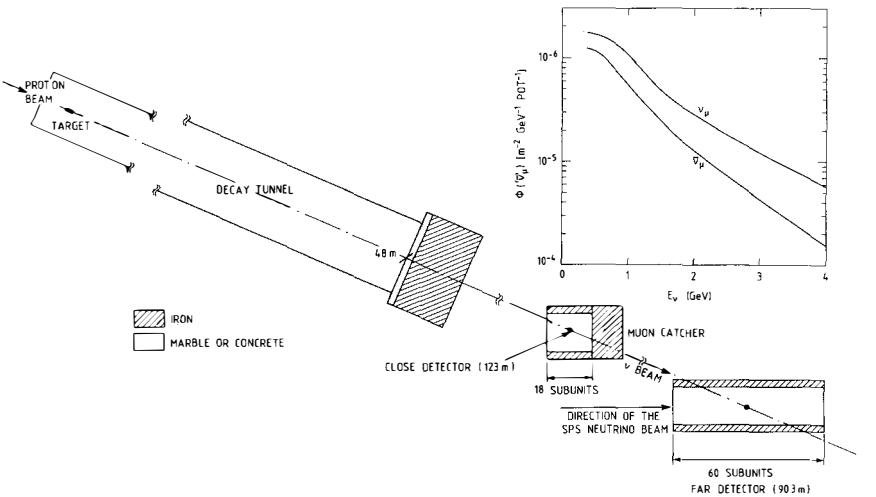


Fig. 1: Sketch of the neutrino beam derived from the CERN Proton Synchrotron and the close and far CHARM detectors. The insert shows the computed ν_μ and $\bar{\nu}_\mu$ fluxes at the far detector.

$$\Delta\Omega_F/\Delta\Omega_C = (123/903)^2 = 0.0187 \qquad (2)$$

Small deviations from this law are due to the finite size of the neutrino source, and have been carefully investigated by Monte Carlo simulations.

The effects of the re-interactions of pions and kaons in the target, and of the interactions in the air and walls of the decay tunnel of the protons non interacting in the target have been studied in detail. The expected ratio of fluxes in a far and in a close detector subunit, computed as a function of the neutrino energy, is shown in fig.2. Taking into account the efficiency of the CHARM detectors and integrating over the accepted energy range, we computed the expected ratio of integrated event rates per detector subunit:

$$r_{exp} = (0.96 \pm 0.015)(\Delta\Omega_F/\Delta\Omega_C) = 0.0178 \pm 0.0003 \; . \qquad (3)$$

The 1.5% error on the expected ratio was estimated by varying all the relevant parameters in the Monte Carlo simulation. Of course, the uncertainties in the knowledge of the flux cancel out to first order in the ratio (3); measuring the interaction rates simultaneously with two detectors placed at different distances from the target is therefore an important improvement with respect to one-detector neutrino oscillation searches.

The insert of fig.1 shows the computed muon neutrino and antineutrino energy spectra. The contamination of electron neutrinos in the beam was estimated to be less than 0.5% of the total flux.

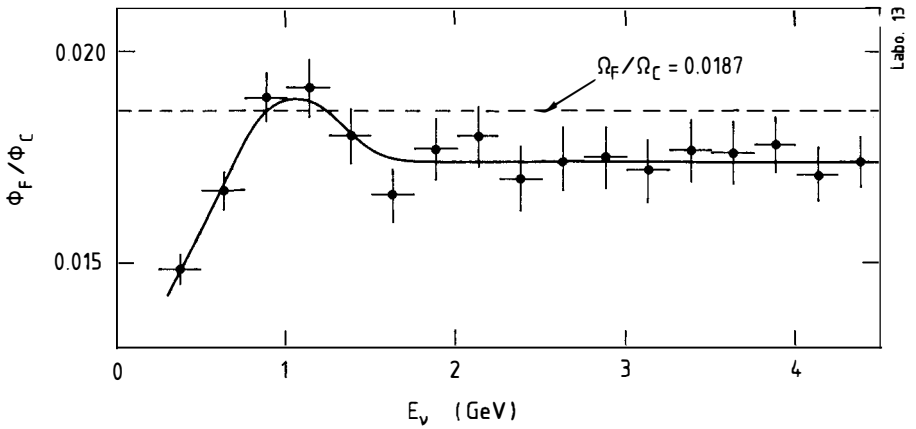


Fig. 2: Computed ratio of fluxes in the close and far detector as a function of the neutrino energy.

3. DATA TAKING AND EVENT FILTERING

In normal running conditions the proton beam intensity was about 1.2×10^{13} protons on target per burst, at a repetition rate of 1.2 Hz. Each burst was composed of twenty short (15 nsec) bunches separated by 105 nsec, for a total duration of 2.2 μsec. Our trigger selected in each of the two detectors events in which at least three scintillators were hit. Approximately one event in ten bursts was recorded per detector, in a 20 μsec gate containing the beam burst. This rate was dominated by cosmic rays in the far detector and by beam-related entering tracks in the close detector. The event timing with respect to a beam signal was recorded to allow the separation and subtraction of the cosmic rays induced background, while the fine-grained detector gave all the informations necessary for the rejection of entering tracks.

We recorded data for a total of 9.8×10^{18} protons on target. The present analysis is based on a subset of 8.7×10^{18} protons, in which both the close and the far detectors were simultaneously operating with good efficiency.

The characteristics of the CHARM detector allowed us to perform a ν_μ disappearance experiment, by measuring the rates of ν_μ induced charged current (CC) events in the two detectors, and to perform a ν_e appearance experiment by searching for candidates of ν_e induced CC events. To this end we selected contained events characterized either by a clear isolated track originating in the detector volume, accompanied at most by some small hadronic activity at the origin (signature for a ν_μ CC event), or by a narrow and compact shower, compatible with the known behavior of low energy electromagnetic showers in our detector (signature for a ν_e CC event). Both types of events were accepted by a filter program based on the following criteria:

1. At least four contiguous scintillator layers hit were required.

2. A good fit of a straight line to the average position of the hits in each PDT layer and in each streamer tube layer was required; from this line and the scintillator information a starting and an end point and a length ℓ (in number of subunits) were reconstructed for each event.

3. The length had to be $\ell \leq 15$ subunits and the starting and end points had to be compatible with an interaction vertex in marble and a stop in marble or surrounding iron.

Additional fiducial volume conditions (15 subunits in the close detector and 57 subunits in the far) and track angle limits were introduced to improve the rejection of background events due to traversing cosmic rays and beam-related entering muons. The cosmic background was also reduced by rejecting events out of time with respect to the beam signal. The algorithm rejected complicated events having several prongs and/or diffused showers, but retained some neutral

current (NC) events characterised by a compact shower. According to a Monte Carlo simulation based on experimental bubble chamber results, a fraction of 20% NC events contaminated the sample of selected events in the range $4 \leq \ell \leq 15$.

With these criteria 2043 events in the close detector and 270 events in the far detector were selected. The absolute prediction of our Monte Carlo simulation of beam and detectors for the far detector rate was of ~ 220 events, in good agreement with the measured value. A special run, in which the target was removed from the proton beam, was dedicated to the study of the effects of the interactions of the protons escaping the target in the decay tunnel air and end wall. The measured rate of close detector contained events in these conditions was about 17% of the normally observed rate. The Monte Carlo calculation, giving 15%, reproduces this result reasonably well.

4. THE ν_e APPEARANCE SEARCH

All the selected far detector contained events and a subsample (850) of those of the close detector were visually scanned searching for candidates of ν_e quasi-elastic CC events, characterised by a single electromagnetic shower. The following criteria were applied:

1. We required a minimum length of 5 subunits and a maximum in the pulse height in the scintillator layers at least 3 subunits after the vertex.

2. The sum of the scintillator pulse heights in the second, third and fourth layer after the vertex had to be larger than that of 9 minimum ionizing particles (mip).

3. The pulse height in the last scintillator layer had to be smaller than 3 mip.

With these criteria 19 (66) events were observed out of 270 (850) events scanned for the far (close) detector. The raw shower energy spectra of these events are shown in fig.3.

The ratio of efficiencies $\varepsilon_e/\varepsilon_\mu$ for finding ν_e CC events (filter algorithm and scanning criteria) and ν_μ CC events (filter algorithm alone) was computed by Monte Carlo, and turned out to be (100 ± 12)%. The algorithm alone had a higher efficiency for electrons ($\varepsilon_e/\varepsilon_\mu = 2.25 \pm 0.1$) due to the containment conditions and the requirement $\ell \leq 15$, which affected mainly muon tracks; on the other hand the scanning criteria had an efficiency for electrons $\varepsilon_e = (45 \pm 5)\%$. After correcting for these efficiencies and for the different lengths of the two detectors (a 7% effect), the ratios between events interpreted as ν_e and ν_μ CC events were:

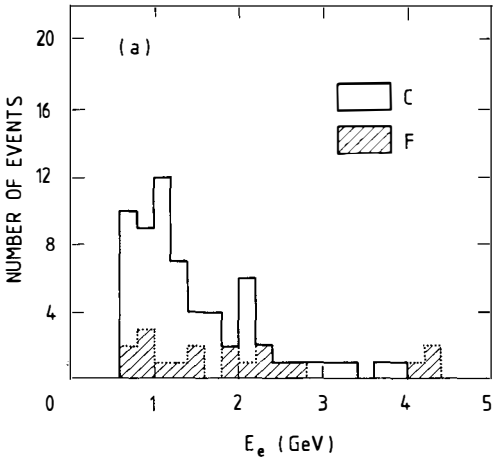


Fig. 3: Observed distributions of the electron energies of ν_e candidates in the close and in the far detector.

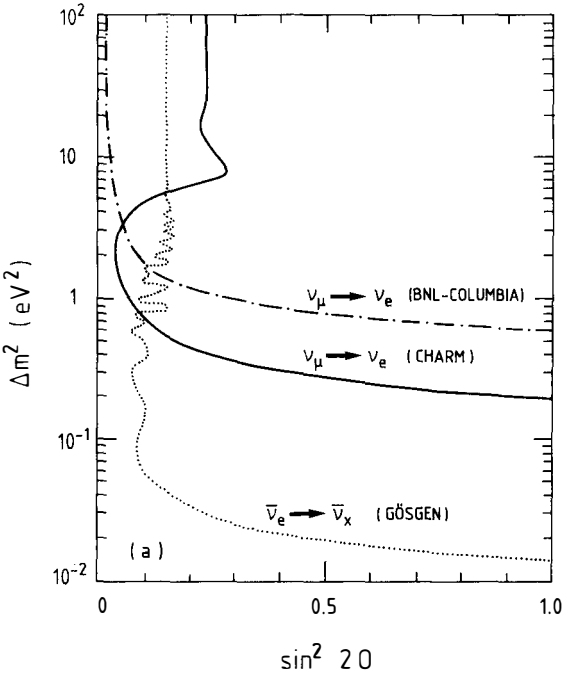


Fig. 4: The 90% confidence limit obtained in the appearance experiment $\nu_\mu \rightarrow \nu_e$ is compared with the best previously obtained limits for oscillations of the types: $\nu_\mu \rightarrow \nu_e$ (Baker et al., ref. 4) and $\bar{\nu}_e \rightarrow \bar{\nu}_x$ (J.L. Vuilleumier et al., ref. 6).

$$\begin{aligned} &\text{close detector :} \quad R_C = (\nu_e/\nu_\mu)_C = (9.2 \pm 1.1 \pm 1.1)\% \\ &\text{far detector} \quad : \quad R_F = (\nu_e/\nu_\mu)_F = (8.9 \pm 2.0 \pm 1.0)\% \end{aligned} \tag{4}$$

The second error is systematic and accounts for the uncertainties in the efficiency computations; it is strongly correlated in the close and the far detector. The computed contamination of ν_e in our beam being smaller than 0.5%, eq. (4) indicates that the observed ratios are due to the contamination of NC events with an electromagnetic-like component, or to very fast oscillations at high Δm^2, resulting in an average effect in both detectors. By subtraction of the close and far detector results, one obtains an upper limit of 2.7% at 90% confidence level for the amount of $\nu_\mu \rightarrow \nu_e$ oscillation between the close and the far detector. The comparison of the two electron candidates energy spectra (fig.3) by a maximum likelihood method taking into account the computed beam energy spectrum and detector acceptances provides the 90% confidence level limit shown in fig.4.

For full mixing ($\sin^2 2\theta = 1$) our best limit is $\Delta m^2 > 0.20$ eV^2 (at 90% c.l.) while our best sensitivity in the mixing angle is $\sin^2 2\theta = 0.04$, at $\Delta m^2 = 2.0$ eV^2.

5. THE ν_μ DISAPPEARANCE SEARCH

As discussed in section 4, we did not observe oscillations of muon to electron neutrinos in our beam. What about other neutrino flavors? Neutrinos associated with the τ or possible heavier leptons are, in our beam, below the threshold for the production of their lepton partners and only undergo neutral current interactions. A signature for the oscillations of muon neutrinos into these neutrino flavors is therefore given by the measurement of a ratio of close to far detector CC events rates different from the one expected in the absence of oscillations, and given by eq. (3). In contrast, the neutral current event rates are independent of the presence of oscillations.

We searched for such effects in our samples of 2047 close detector and 270 far detector contained events, selected according to the criteria described in section 3. Corrections for dead times, event losses and cosmic ray background were applied. Then the event rates per unit fiducial mass were computed as functions of the number of subunits traversed in each event. Finally the ratios of these rates in the close and in the far detector were compared with those computed by Monte Carlo.

The dead time fractions were 5.7% in the close and 1.9% in the far detector. The errors in their measurement were neglegible. Events with superimposed tracks or spurious hits ("double events") were in some cases lost by the filter algorithm; we excluded them from the analysis. By scanning random samples of close and far detector events we determined the fraction of "double events" to

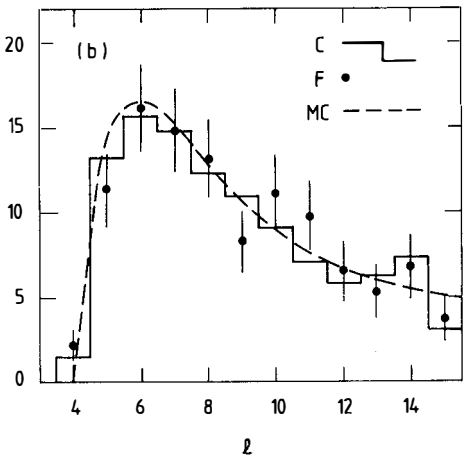


Fig. 5: Distribution of the length ℓ (in number of subunits) of ν_μ events selected in the close and far detector. The number of events in each bin is corrected for the effective fiducial mass and normalised to the far detector solid angle. The dotted line indicates the Monte Carlo prediction, normalised to the total number of events observed in the close detector.

be (11.3 ± 3.1)% and (7.0 ± 2.0)% respectively. The cosmic ray background was neglegible in the close detector and contributed 3.4% of the far detector contained events. This contribution was estimated using the events recorded out of time with respect to the beam.

In our two detectors different fiducial masses, corresponding to (16-ℓ) subunits in the close and (58-ℓ) subunits in the far detector, were available for events of reconstructed length ℓ (in number of traversed subunits, see section 3). To compare the observed numbers of events of given length ℓ we weighted them by 1/(16-ℓ) and 1/(58-ℓ) respectively for the far and close detector. Fig.5 shows the two weighted distributions as functions of ℓ. In the figure the close detector spectrum is multiplied by the ratio of solid angles (1) to approximately compensate for the neutrino fluxes. The ratio r_{obs} of the integrals of the two spectra is:

$$r_{obs} = 0.0171 \pm 0.0010 \pm 0.0009 \ , \quad (4 \leq \ell \leq 15) \qquad (5)$$

The first error is statistical while the second accounts for the systematic uncertainty resulting from the measurement of the event length ℓ.

This result must be compared with the Monte Carlo expectation discussed in section 2, eq. (2). The ratio of the two ratios should be compatible with one in the absence of oscillations and is in our case:

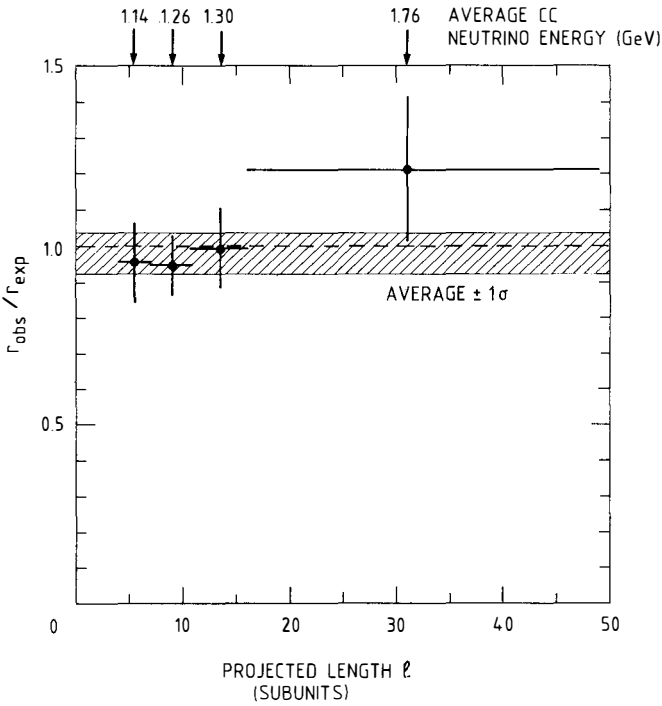


Fig. 6: The ratio r_{obs}/r_{exp} measured in the disappearance experiment is plotted versus the length ℓ (in number of subunits) of the events.

$$r_{obs}/r_{exp} = 0.96 \pm 0.06 \pm 0.05 \ , \ (4 \leq \ell \leq 15) \qquad (6)$$

We also subdivided the ℓ-interval in 3 bins and separately computed the measured to expected rates ratio for each of them. The results are shown in fig.6. The fourth point, which appears in the figure, was obtained by considering longer events, with a relaxed containment condition in the close detector, where tracks were allowed to leave the calorimeter and stop in the muon catcher. The observed length of these events was corrected for the different density of the catcher with respect to the rest of the detector and expressed as an "effective equivalent length" ℓ (in subunits). Corrections and weights similar to those discussed above for shorter events were applied.

The results of this search are compatible with no disappearance of muon neutrinos. To express them in terms of the parameters Δm^2 and $\sin^2 2\theta$ of eq.(1), we computed the expected ratios of rates r_{exp} as functions of Δm^2 and $\sin^2 2\theta$ in the four ℓ-bins. In this computation the CC events spectra in the far and close

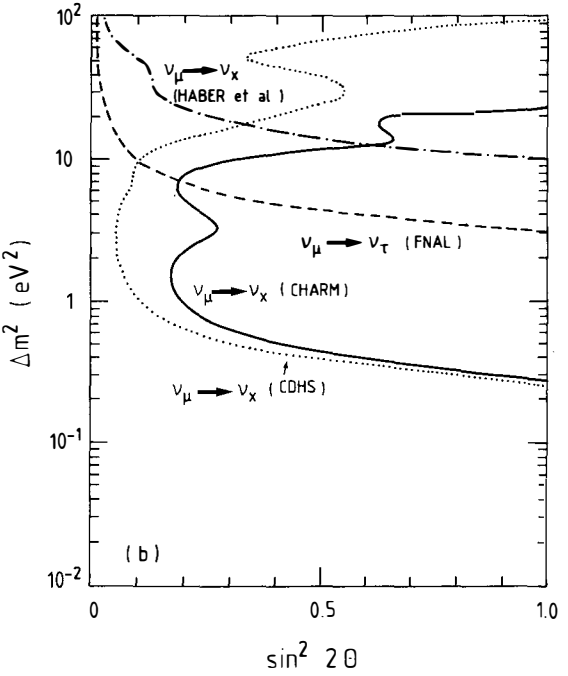


Fig. 7: The 90% confidence limit obtained in the disappearance experiment is compared with previous limits on ν_μ oscillations to ν_τ (Ushida et al., ref. 5) and $\nu_\mu \rightarrow \nu_x$ (CDHS Collab., ref. 8 and Haber et al., ref. 5).

detector were varied according to the changes in ν_μ fluxes determined by the oscillation parameters, while the NC contamination of our sample (i.e. 20% in the interval $4 \leq \ell \leq 15$, according to our Monte Carlo) was assumed to be independent of the oscillation parameters, and acted as a background insensitive to changes in neutrino flavor. We then computed:

$$\chi^2 = \Sigma_i \frac{[r_{exp,i} - r_{obs,i}]^2}{\sigma_i^2} \qquad (7)$$

where the errors σ_i included the statistical error on $r_{obs,i}$ and a 5% systematic error (eq.(6)). From the variation of χ^2 we derived the 90% confidence level limit shown in fig.7. The best limits we obtain are $\Delta m^2 < 0.29$ eV^2 for full mixing and $\sin^2 2\theta < 0.18$ for $\Delta m^2 \approx 1.5$ eV^2. We checked that for an increase by 50% of the neutral currents contamination in the Monte Carlo calculation the best limit in Δm^2 increases by less than 0.02 eV^2.

6. CONCLUSIONS

No evidence for oscillations of muon neutrinos was found in a search using the CHARM detector and the new CERN low energy neutrino beam. The result on the appearance of electron neutrinos, studied for the first time with a two-detector experiment, improves on existing limits for small mixing angles in the mass range $0.8 \leq \Delta m^2 \leq 3.5$ eV^2. The results of the ν_μ disappearance search are in agreement with the limit obtained in the same beam by the CDHS Collaboration [8], and both improve by an order of magnitude on previous experiments in the small Δm^2 region.

REFERENCES

1. B. Pontecorvo, Zh. Eksp. Teor. Fiz. 34 (1958) 247
   [Sov. Phys. JETP 7 (1958) 172].
   B. Pontecorvo, Zh. Eksp. Teor. Fiz. 53 (1967) 1725
   [Sov. Phys. JETP 26 (1968) 984].

2. G. Zatsepin, Proc. Int. Conf. Neutrino '82, Balatonfured, Suppl., p. 53 (1982).

3. S. Boris et al., Proc. Int. Europhysics Conf. on High Energy Physics, Brighton (UK), p.386 (1983).

4. N.J. Baker et al., Phys.Rev.Lett. 47 (1981) 1576.

5. N. Ushida et al., Phys. Rev. Lett. 47 (1981) 1694.
   C. Haber et al., Fermilab. preprint, FERMILAB-CONF-83/57-Exp. (1983).

6. Caltech-SIN-TUM Collaboration, J.L. Vuilleumier et al., Phys. Lett. 114B (1982) 298.

7. A.N. Diddens et al., CHARM Collaboration, Nucl. Instr. and Methods 176 (1980) 189.
   A.N. Diddens et al., CHARM Collaboration, Nucl. Instr. & Meth. 178 (1980) 27.
   M. Jonker et al., CHARM Collaboration, Phys. Scr. 23 (1981) 677-679.

8. F. Dydak et al., CDHS Collaboration, Phys. Lett. B134 (1984) 281.

RESULTS FROM THE CDHS*) ν OSCILLATION EXPERIMENT AT CERN

Jörg Wotschack
CERN, Geneva, Switzerland



ABSTRACT

Results from the CDHS low energy ν oscillation experiment at the CERN PS are reported. The experiment looks for the disappearance of ν_μ measuring simultaneously the ν flux at 130 and 885 m distance from the target. No significant deviation from the expected flux ratio has been found. The experiment excludes therefore oscillations of the type $\nu_\mu \rightarrow$ anything in the range $0.26 < \Delta m < 90$ eV^2 for maximal mixing. The best limit on the mixing angle $\sin^2 2\theta$ is 0.05 for $\Delta m^2 \approx 2.5$ eV^2.

---

*) CERN-Dortmund-Heidelberg-Saclay-Warsaw Collaboration

1. INTRODUCTION

For the oscillation experiment the CDHS neutrino detector, which was designed to cope with high energy neutrinos from the CERN Super Proton Synchrotron (SPS), has been used in a very non-standard way: Neutrinos were provided by the Proton Synchrotron (PS) instead of the SPS; their energies were only a few GeV; no attempt was made to measure the hadronic energy, and the muon momenta were determined from range rather than from the track curvature in the magnetic field. The iron modules were not magnetized and the driftchambers were switched off. In addition, two detectors have been used instead of one.

Since the formalism of neutrino oscillations has been discussed before in this Workshop (see F. Vannucci's talk in these proceedings) it will not be discussed again here.

The probability that a neutrino ν_a oscillates into a neutrino ν_b is

$$P_{\nu_a \to \nu_b} = \sin^2 2\theta \cdot \sin^2(1.27 \cdot \Delta m^2 \cdot \frac{L}{E}),$$

where L is the distance of flight in meters and $\Delta m^2 = |m_{\nu_i}^2 - m_{\nu_2}^2|$ in eV^2.

Since this probability depends on both the mixing angle θ and Δm^2, results are usually presented in a two-dimensional plot in Δm^2 and $\sin^2 2\theta$.

No experiment so far has convincing evidence for the existence of oscillations. The present best limits for the different oscillation channels are shown in figure 1. By far the smallest Δm^2 values down to $\Delta m^2 = 0.017$ for $\sin^2 2\theta = 1$ have been explored by a reactor experiment measuring the $\bar{\nu}_e$ flux at some distance from the reactor core[1]. Since these experiments look for the disappearance of $\bar{\nu}_e$, i.e. $\bar{\nu}_e \to$ anything, they set at the same time a limit on $\overset{(-)}{\nu}_\mu \leftrightarrow \bar{\nu}_e$ oscillations.

Using ν_μ as initial neutrino state, the present limits are much less restrictive. Here the best limits have been obtained for the transition $\nu_\mu \to \nu_e$ by the BNL-Columbia 15' FNAL bubble chamber experiment[2] looking for an abnormal ν_e admixture in the ν_μ beam. No excess of ν_e has been found leading to the limits as shown in figure 1. From the same negative result conclusions on the oscillation $\nu_\mu \to \nu_\tau$ can be drawn if one uses the 16% branching ratio $\tau \to e\nu\bar{\nu}$. Of course the limits are poorer than for the ν_e case giving $\Delta m^2 \approx 2.5\ eV^2$ for maximal mixing. The same limit has also been reached by an emulsion experiment at FNAL[3] looking directly for τ decays. Among about 700 charged current interactions no τ has been observed.

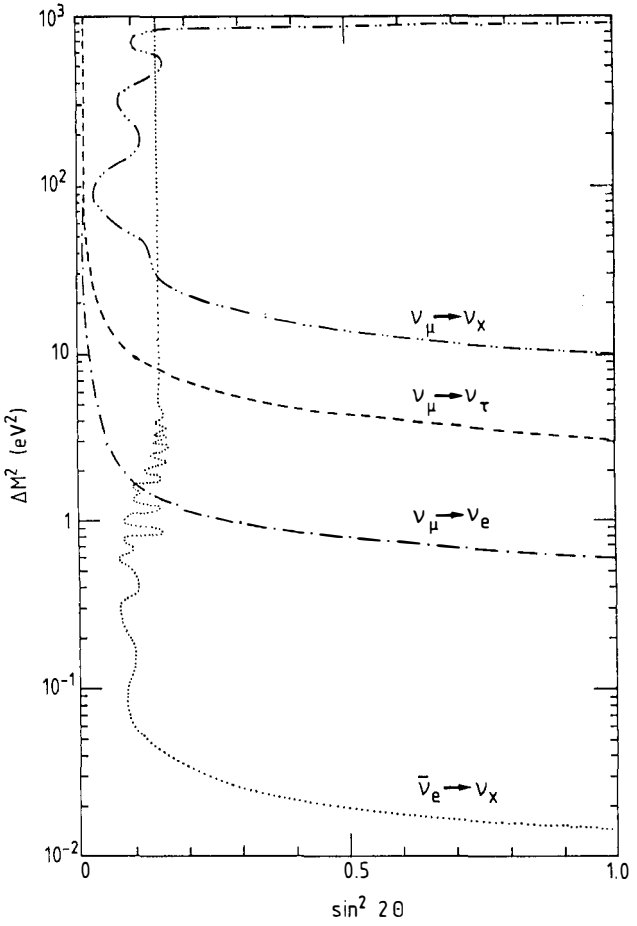


Figure 1: Present best limits on the mixing angle parameter $\sin^2 2\theta$ and the mass difference squared, Δm^2, for different oscillation channels. Results on $\bar{\nu}_e \rightarrow \nu_x$ are from the Gösgen reactor experiment[1], on $\nu_\mu \rightarrow \nu_e$ from an FNAL 15' bubble chamber for experiment[2], on $\nu_\mu \rightarrow \nu_\tau$ also from[2] and from an FNAL emulsion experiment[3]. The only limit on $\nu_\mu \rightarrow \nu_x$ comes from the CCFR experiment at FNAL[4].

In contrast to these experiments which look for the appearance of new neutrino flavours, the CDHS oscillation search looks for a change in the primary ν_μ flux. This method - although statistically much more demanding - has the clear advantage of not being restricted to $\nu_\mu \rightarrow \nu_e$ and $\nu_\mu \rightarrow \nu_\tau$ oscillations. It also allows oscillations into so far unknown types of neutrinos to be detected. The only existing result on such an inclusive search comes from the CCFR high energy ν_μ disappearance experiment[4] which however is only sensitive to mass differences squared in the range 20 - 900 eV^2.

2. EXPERIMENTAL SET-UP

Oscillations of ν_μ into other types of neutrinos lead to a change of the ν_μ flux with distance from the neutrino origin. The idea is therefore to measure the ν_μ flux at two positions using ν_μ charged current events as signature. In order to become independent of an absolute flux determination the measurement was done simultaneously. The same acceptance and systematics are assured by using two detectors as identical as possible.

Neutrinos are produced in a bare target beam with a ν flux approximately proportional to L^{-2} where L is the distance from the target.

The general layout of the experiment on the CERN site is shown in figure 2. A new low energy neutrino facility has been constructed at the PS with a beam line pointing towards the existing CDHS West Area detector which sits at 885 m from the new target. The second detector is implanted at 130 m distance from the target.

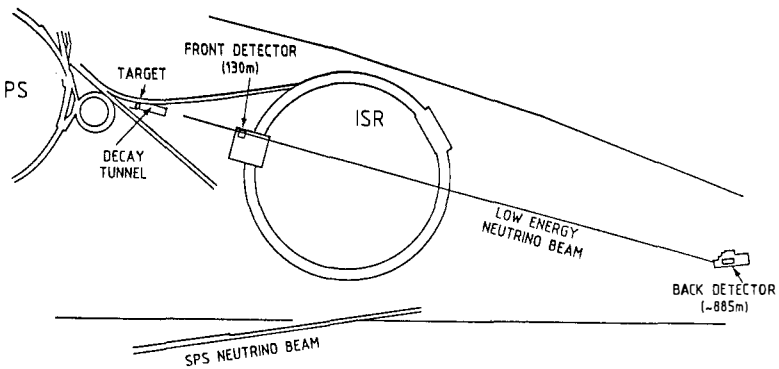


Figure 2: Layout of the CERN neutrino oscillation facility at the PS. Indicated are the positions of the two CDHS detectors at 130 and 885 m from the target.

Protons of 19.2 GeV are provided from the PS every 1.2 sec in 20 bunches each 5-10 ns wide and separated by 105 ns. The target is a 60 cm long rod of Beryllium 8 mm in diameter. It is followed by a 52 m tunnel to allow the kaons and pions produced in the target to decay. The muons, produced at the same time, and the remaining hadrons are absorbed in 4 m of iron and 70 m of molasse behind the decay tunnel.

There is no focussing behind the target. The neutrino beam has, therefore, a divergence much larger than the solid angle subtended by the two detectors. This results in a neutrino flux which is almost constant over the detector surface, independent of the neutrino energy, as long as the neutrino energies are larger than 1 GeV. The neutrino spectrum peaks at about 1 GeV and decreases proportionally to e^{-E_ν} at higher energies.

The layout of the two detectors is shown in figure 3. Both detectors are inclined by 22^o with respect to the beam axis. They are composed of modules constructed of circular iron plates, 3.85 m in diameter, interleaved with plastic scintillator hodoscopes. Three distinct types of modules were used. Their main difference is the iron sampling width in the beam direction and the horizontal and vertical granularity of the hodoscopes. Type I modules have 2.5 cm iron sampling but five consecutive scintillators are viewed by the same photomultiplier leading to an effective sampling of 12.5 cm of iron. The horizontal and vertical granularity is 15×15 cm^2. Type II modules are sampled every 5 cm of iron. The vertical resolution is 45 cm and no information on horizontal position is available. The same structure is used in the type III modules only here the sampling width is 15 cm. The back detector is formed of 10, 5, and 6 modules of the three types respectively, while the front detector consists of two modules of each type, see figure 3.

The trigger is based on the projected range of iron traversed by the most penetrating particle of the event. Trigger planes were constructed by adding all of the signals of single planes in the type I modules and of groups of three consecutive planes in the type II modules. The modules of type III were not used in the trigger. The thickness in iron per trigger plane is 12.5 cm and 15 cm correspondingly. An event is registered if three out of four adjacent trigger planes have a signal larger than 1/5 of that released by a minimum ionizing particle. With this condition full trigger efficiency is achieved for events with projected ranges longer than 40 cm. The two detectors were linked and controlled and readout by a single computer ensuring identical life- and downtimes.

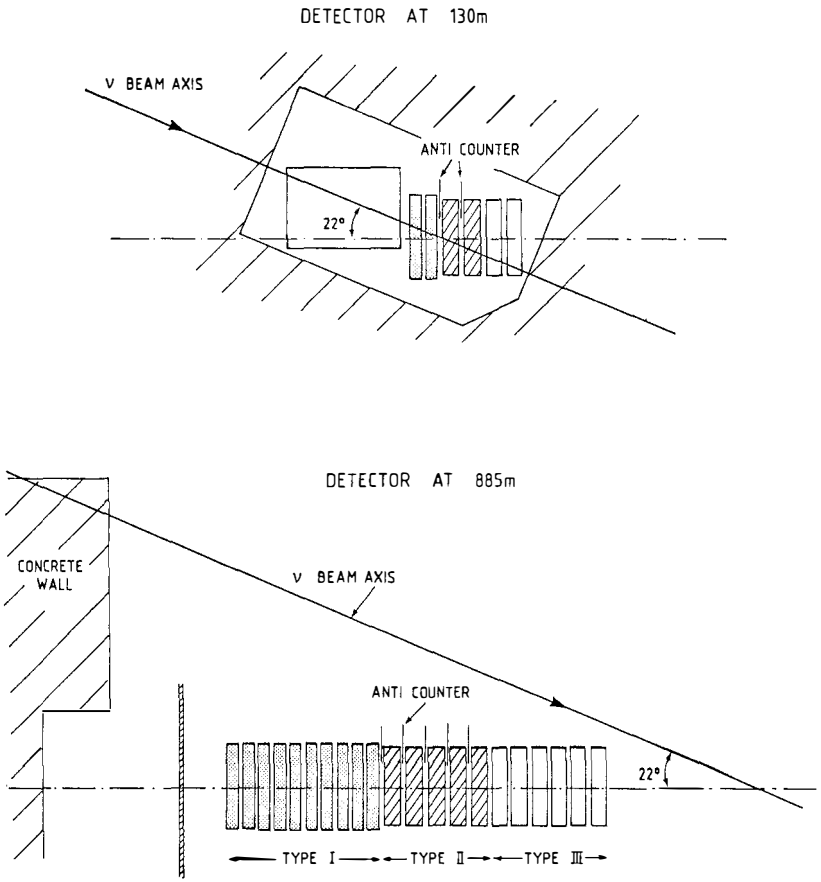


Figure 3: Layout of the two detectors of the CDHS neutrino oscillation experiment. The front detector is sitting in a 6 m deep hole, completely surrounded by concrete. This is simulated at the back detector by erecting an 8 m thick concrete wall in front of the detector.

An offline reconstruction program assigned the geometrical vertex position to each event and determined the event range in iron, projected onto the detector axis. The last plane of an event was either defined by the point where the most penetrating particle came to rest or left the detector. Also the vertical angle and - for the type I modules - the horizontal angle of the track of the most penetrating particle (usually a muon) has been determined.

3. DATA AND BACKGROUNDS

Data were taken during six weeks in February and March 1983. The useful number of protons on target was 7×10^{18} with bursts of typically 10^{13} protons every 1.2 sec. Events were taken in a 3 μs gate around the 2.1 μs long neutrino spill. The corresponding data rates in the front and back detector were 1/5 and 1/70 beam correlated events per burst and 1/250 and 1/60 cosmic ray events. The deadtime due to these rates were (9±1)% and (2±0.2)%. In order to determine the background from cosmic ray events and to monitor the detector performance, data were also taken in a second gate, outside the spill and 600 μs long.

There were two main sources of background to the experiment: cosmic ray events and muons from neutrino interactions in the material surrounding the detectors. The cosmic ray background can be neglected in the front detector but is, however, as big as the signal in the back detector. The majority of cosmic ray events could be easily eliminated by requiring that the event vertex was inside the detector and that the vertical angle of the muon track with the detector axis was less than 45^{o}. A remaining background of 0.5% in the front detector and about 9% in the back detector has been subtracted statistically using the rates measured in the out of spill gate.

The neutrino induced muons entering the detector from the outside are beam correlated and their relative importance is much larger in the front detector than in the back. To ensure the same background muon environment in both detectors an 8 m thick concrete wall had been piled up in front of the back detector simulating the concrete surrounding the front detector, see figure 3. Once created, these muons were then rejected by using the first planes of the detectors as anti-counters. Muons entering the detector through the sides were rejected in the type I modules by requiring that the vertex was not more than 1.6 m away from the detector axis. In the type II modules events were rejected if they started in the top or bottom layers of scintillators or if there was a signal in the anti-counter installed in front of each module on the side facing the beam.

In addition to these cuts, events were only retained if their vertex was inside the fiducial volume which was chosen so that differences between the two

detector set-ups were minimal. For each type of modules only events originating in the volume from the second plane of the first module to the first plane of the last module were accepted. The corresponding fiducial volumes are nine modules of type I and four modules of type II in the back detector and one module of each type in the front detector.

After all cuts approximately 22,000 and 3,300 events were left in the front and back detector respectively, with a contamination of 50 and 300 cosmic ray events.

4. RESULTS

In the analysis the following principles were applied. Events were classified according to their range in iron. This minimizes any dependence on pulse-height calibration in the two detectors. A minimal projected range of four and ten planes in the modules of type I and II, respectively, ensured full trigger efficiency and, at the same time, reduced the contribution of neutral current events to the event sample to less than 5%. The average neutrino energy of the accepted events was about 3 GeV in both detectors. Events starting in modules of type I and II were analysed separately. Only relative rates in the two detectors were used.

Small differences in the neutrino spectrum and in the detector geometry were corrected for with the help of Monte Carlo generated events. This simulation included hadron production and neutrino interaction cross sections. It also included effects such as secondary proton interactions and hadron absorption in the target, as well as hadron production in the decay region and in the beam dump. Neutrino interactions in the material surrounding the detectors, neutral current interactions, and minor differences in the functioning of the two detectors were also taken into account. The typical correction to the goemetrical scaling (the ratio of the distances squared divided by the number of fiducial modules) is 5%.

Table 1 gives the final event numbers and their ratios for the two types of modules. The errors are statistical only. Also given are the expected back/front ratios of the neutrino flux assuming L^{-2} scaling and the result of the Monte Carlo calculation for the case of no oscillations.

TABLE 1

Detector Type	Loc.*)	Distance²/fid. vol.	Number of events		
			Data	MC	Data/MC
I	F	$129.1^2/1$	10180	8863	
	B	$880^2/9$	2005	1685	
	B/F	0.1937	0.1970±0.0048	0.1901±0.0014	1.036±0.030
II	F	$130.7^2/1$	13120	12252	
	B	$887^2/4$	1156	1019	
	B/F	0.0868	0.0881±0.0027	0.0832±0.0007	1.059±0.040

*) F = Front, B = Back

The systematic uncertainties of the experiment were estimated by varying the parameters of the analysis over the expected range of uncertainty and studying the effect on the ratio of events in the two detectors. The most serious contributions came from the dead-time correction, the differences in event reconstruction efficiency and the performance of the two detectors, and the number of events entering the fiducial volume from outside, but not identified as such. Each of these uncertainties was found to be 1%. The second serious group of uncertainties came from our imperfect knowledge of the hadron production energy and transverse momentum spectra, the hadron absorption in the target, the hadronic spectra from secondary proton interactions, the effect of proton interactions downstream of the target and possible trigger inefficiencies. Each of them was estimated to be at most 0.5%. Finally uncertainties in neutrino cross-sections and the cosmic ray event subtraction were found to contribute less than 0.5%. By adding all of these contributions in quadrature, the overall systematic uncertainty in the ratio of the event rates in the two detectors was estimated to be 2.5%.

From the integrated rates in Table 1, taking into account the systematic uncertainty, limits on Δm^2 and $\sin^2 2\theta$ can be obtained as shown in figure 4.

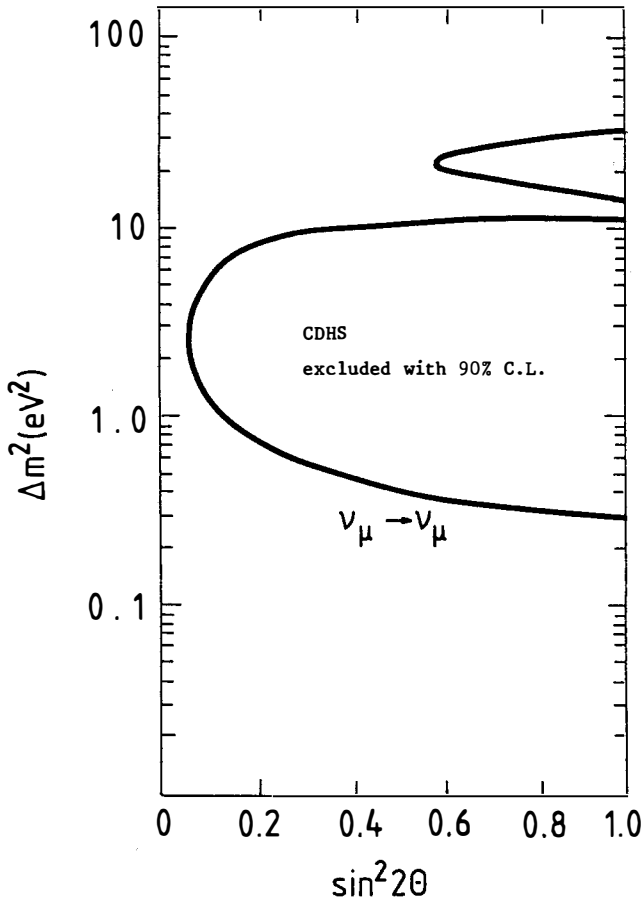


Figure 4: Limit on neutrino oscillations $\nu_\mu \rightarrow$ anything in terms of Δm^2 and $\sin^2 2\theta$ as obtained by comparing integrated event rates in the two detectors. The region on the right side of the curve is excluded (90% C.L.).

Small Δm^2 oscillations would result in a suppressed flux of neutrinos in the back detector giving a back/front smaller than unity. For $\Delta m^2 \gtrsim 10\ eV^2$, however, the back/front ratio can become unity or even larger and an analysis using integrated event numbers is not sensitive.

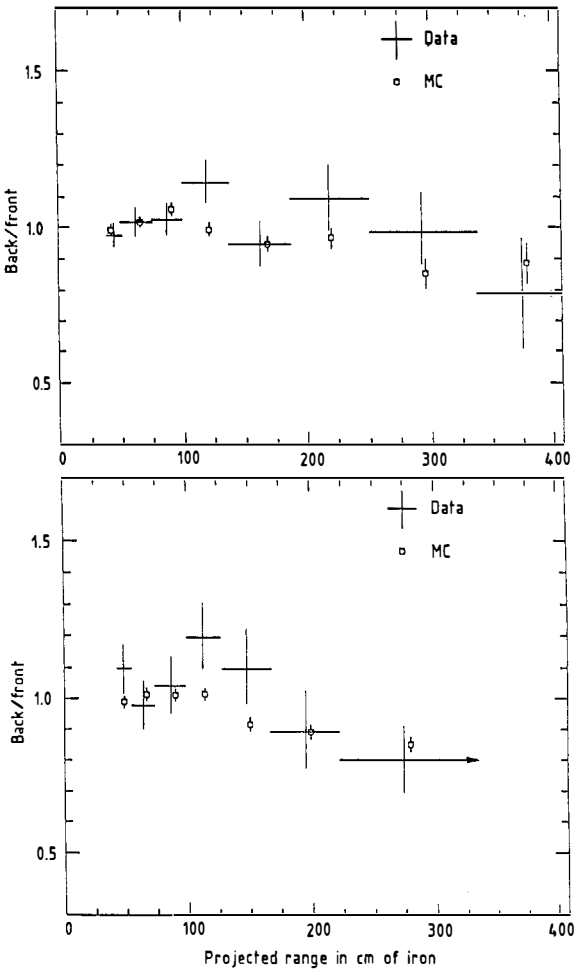


Figure 5: Ratio of event rates in the back and front detector as as function of the projected range of the events in iron. Data ratios and the corresponding Monte Carlo ratios are shown in 5a) for events starting in modules of type I and in 5b) for events starting in type II modules.

More information than from the integrated rates can be obtained by looking at the ratio of events as a function of their projected range in iron. Figures 5a and 5b show the back/front ratios for data and Monte Carlo events in the two types of modules, respectively. The ratio of data and MC is given in figure 6 together with the expected variation of this ratio as a function of range for different assumptions of Δm^2 and $\sin^2 2\theta$. In the case of no oscillations this ratio should be unity independent of range. The data show no significant signs of an oscillation. From the event rates in the two detectors as a function of range, including the 2.5% systematic error, limits on ν_μ oscillations can be set in terms of $\sin^2 2\theta$ and Δm^2, as shown in figure 7. The area to the right of the curve is excluded at the 90% confidence level. For maximal mixing Δm^2 values between 0.26 and 90 eV^2 are excluded. The most restrictive limit on the neutrino mixing angle parameter $\sin^2 2\theta$ is 0.05 at $\Delta m^2 = 2.5$ eV^2. A comparison with the best limits obtained in earlier experiments, see figure 1, shows that the best Δm^2 limit for $\nu_\mu \rightarrow \nu_e$ oscillations has been improved by a factor of two. The improvement in the transition $\nu_\mu \rightarrow \nu_\tau$ is about a factor ten and for the oscillation $\nu_\mu \rightarrow$ anything the limit on Δm^2 has been ameliorated by a factor of $\sim$60.

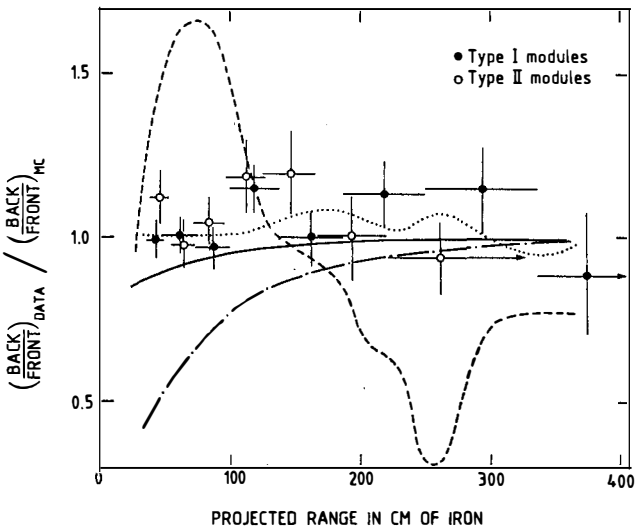


Figure 6: Ratio of Monte Carlo corrected event rates in the back and front detector as a function of projected range in iron. Events starting in the two types of modules are given separately. Also shown are curves indicating the expected behaviour of these ratios in the case of oscillations for different choices of Δm^2 and $\sin^2 2\theta$. _____ $\Delta m^2 = 1$ eV^2 and $\sin^2 2\theta = 0.2$; -·-·- $\Delta m^2 = 1$ eV^2 and $\sin^2 2\theta = 1$; ····· $\Delta m^2 = 32$ eV^2 and $\sin^2 2\theta = 0.2$; ----- $\Delta m^2 = 16$ eV^2 and $\sin^2 2\theta = 1$.

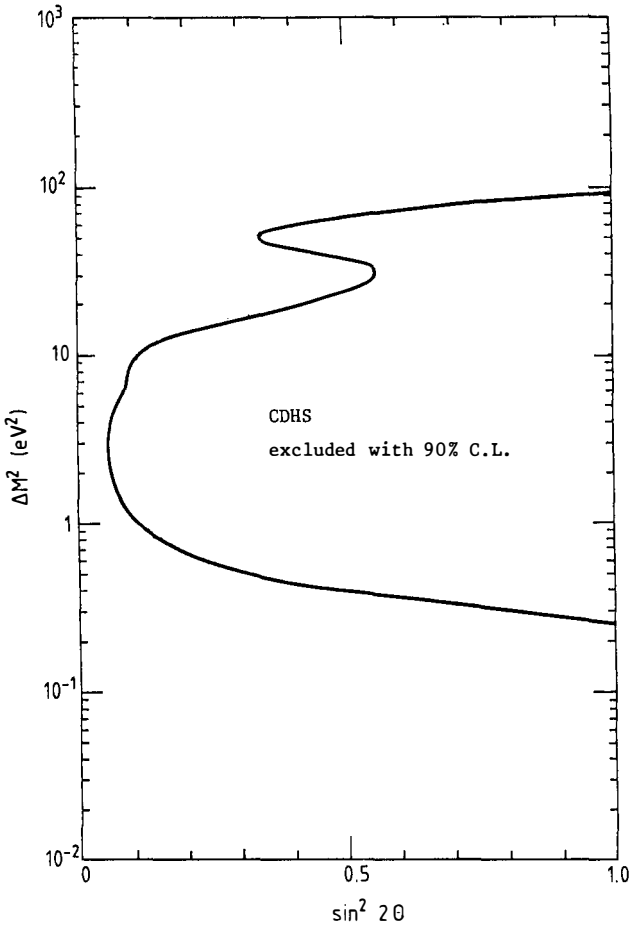


Figure 7: Final limits set by the experiment on $\nu_\mu \rightarrow$ anything obtained from a fit to the ratio of event rates as a function of projected range in iron. The area to the right side of the curve is excluded with 90% C.L.

REFERENCES

1) J.L. Vuilleumier et al., Phys. Letters 114B (1982) 298; see also K. Schreckenbach's talk in these proceedings.

2) N.J. Baker et al., Phys. Rev. Letters 47 (1981) 1576.

3) N. Ushida et al., Phys. Rev. Letters 47 (1981) 1694.

4) C. Haber et al., Fermilab preprint, FERMILAB-CONF-83/57-EXP (1983); see also C. Haber's talk in these proceedings.

A SEARCH FOR INCLUSIVE OSCILLATIONS OF MUON NEUTRINOS IN THE MASS RANGE, $30 \lesssim \Delta m^2 < 1000$ eV^2

C. Haber, P. Auchincloss, R. Blair, M. Ruiz*, F. Sciulli, M. Shaevitz, W.H. Smith, R. Zhu**
Columbia University, New York, NY 10027 USA

D. Garfinkle, F.S. Merritt, M. Oreglia, P. Reutens
University of Chicago, Chicago, IL 60637 USA

R. Coleman, H.E. Fisk, B. Jin**, D. Levinthal†, W. Marsh, P.A. Rapidis, H.B. White, D. Yovanovitch
Fermi National Accelerator Laboratory, Batavia, IL 60510 USA

A. Bodek, F. Borcherding, N. Giokaris‡, K. Lang‡, I.E. Stockdale
University of Rochester, Rochester, NY 14627 USA

presented by C. Haber



ABSTRACT

A search for inclusive ν_μ oscillations has been performed in the Fermilab narrow band neutrino beam using two similar detectors running simultaneously at two distances from the neutrino source. The data show no positive signal and rule out oscillations of ν_μ into any other single type of neutrino for $30 < \Delta m^2 \lesssim 1000$ eV^2 and $\sin^2 2\theta > 0.02$-0.20.

INTRODUCTION

In recent years the possibilities of massive neutrinos and lepton number non-conservation have received renewed interest. Neutrinos with masses between 0.0001 and 10 eV have been proposed within the context of certain Grand Unified Theories.[1] Astrophysicists have discussed primordial neutrinos with masses in the range 1-100 eV. These have been suggested as an important component of the total mass density of the universe and as a constituent of the dark matter which is thought to be bound to large astronomical objects.[2] These considerations and the rather weak existing experimental constraints have motivated a new series of direct measurements of neutrino masses. Such experiments are sensitive to mass effects in the kinematics of certain weak decays. For ν_μ and ν_τ the results of these measurements have been only the improved limits, $M_{\nu_\mu} < 500$ keV,[3] and $M_{\nu_\tau} < 160\text{-}173$ MeV.[4] A group studying the electron spectrum in ^3H beta decay has however twice reported positive evidence for non-zero $\bar{\nu}_e$ mass, 14 eV < $M_{\bar{\nu}_e}$ < 46 eV, at the 90% C.L.[5] All these measurements are close to the maximum sensitivity attainable in experiments which look for mass effects in decay kinematics. In addition to kinematical effects, however, the existence of neutrino mass can imply other hitherto unobserved physical phenomena which are in principle more sensitive to the effects of a small neutrino mass. These include neutrino decays, lepton number non-conserving transitions and neutrino oscillations. In this paper we present results from the first experiment to search for inclusive oscillations of muon neutrinos at a high energy (30 GeV < E_ν < 240 GeV) accelerator.

PHENOMENOLOGY OF NEUTRINO OSCILLATIONS

If neutrinos have non-zero masses then it is likely that the interaction by which their mass is generated is different than the usual weak interaction. Such an interaction may violate lepton number conservation. In this case the eigenstates of the weak interaction, ν_e, ν_μ, ν_τ, ... $\nu_{\ell n}$, would be different from the mass eigenstates. We may call these eigenstates, ν_1, ν_2, ν_3, ... ν_n. One expects though that:

$$\nu_{\ell_i} = \sum_{j=1}^{n} U_{ij}\nu_j \qquad (1)$$

where ν_{ℓ_i} is the weak interaction eigenstate associated with the i^{th} charged lepton and U_{ij} is some unitary neutrino mass mixing

matrix. If in addition, the masses

$$m_{\nu_1} \neq m_{\nu_2} \neq m_{\nu_3} \neq \ldots m_{\nu_n}$$

then as a weak interaction eigenstate evolves in time, the different mass eigenstates of which it is superposed will propagate with different phases. At some later time t, the probability,

$$\begin{aligned}
\text{Probability}(\nu_{\ell_i}(t)=\nu_{\ell_i}(o)) &= |\langle\nu_{\ell_i}(t)|\nu_{\ell_i}(o)\rangle|^2 \\
&= \Big|\sum_{k=1}^{n}\langle\nu_k|e^{-iE_k t}U_{ik}\cdot\sum_{j=1}^{n}U_{ij}|\nu_j\rangle\Big|^2 \\
&= \Big|\sum_{jk=1}^{n}e^{-iE_k t}U_{ik}^{*}U_{ij}\langle\nu_k|\nu_j\rangle\Big|^2 \\
&= \Big|\sum_{j=1}^{n}e^{-iE_j t}|U_{ij}|^2\Big|^2 \qquad (2)
\end{aligned}$$

which may in general differ from one. If we simplify the situation and imagine that only two states (e.g. ν_μ and ν_x) are mixed rather than n, we arrive at an expression for the probability that a neutrino remain with the same flavor some distance D from the decay of its parent:

$$\text{Probability}(\nu_\mu\rightarrow\nu_\mu) = 1-\sin^2(2\theta)\sin^2\left(\frac{1.27\ \Delta m^2 D}{E_\nu}\right) \qquad (3)$$

where θ is the mixing angle between the two eigenstates; Δm^2 is the difference in the masses squared $m_1^2-m_2^2$, in eV^2; D is the distance from decay point to detector in kilometers and E_ν is the neutrino energy in GeV. This expression describes the phenomenon of two state neutrino oscillations:[6] as a particular flavor neutrino travels from its decay point, it may be detected as some other type of neutrino with a harmonic probability. (In what follows, we restrict ourselves to this two-state case.) We note that this striking effect depends only upon the assumption that the mass difference is non-zero and that some mixing of the weak interaction eigenstates occurs. Furthermore, this effect can be sensitive to the existence of masses which are smaller than those accessible in direct decay experiments.

OSCILLATION EXPERIMENTS

A number of experiments have searched for neutrino oscillations. These experiments have been of two classes. The first class, which is called exclusive or appearance experiments, uses a neutrino beam of known composition and searches for the presence of other

types of neutrinos. Exclusive experiments are sensitive to particular oscillation channels such as $\nu_\mu \rightarrow \nu_e$ or $\nu_\mu \rightarrow \nu_\tau$. Here the probability of a ν_e appearing at some point D along a ν_μ beam, for example, is given by:

$$\text{Probability}(\nu_\mu \rightarrow \nu_e) = \sin^2(2\theta)\sin^2\left(\frac{1.27\ \Delta m^2 D}{E_\nu}\right) \quad . \qquad (4)$$

The second class, inclusive or disappearance experiments, searches for a depletion in the flux of a particular type of neutrino. Such experiments are sensitive to all exclusive channels as well as oscillations into new exotic neutrinos. These may include sterile non V-A interacting neutrinos or a neutrino associated with a new charged lepton which is too massive to be produced at available energies. For a given beam, the inclusive probability is given by Eq. (3) above.

The inclusive and exclusive oscillation probabilities depend upon both the neutrino energy, E_ν, and the distance, D, from the decay point of the parent particle to the detector. Oscillations may thus be detected in either of two ways. One approach is to compare the energy variation of measured event rates at a fixed distance from the neutrino source with some expected behavior. An alternate method is to compare the energy variations in event rates at different distances from the neutrino source. The second approach would be equivalent to the first if one set of event rates could be measured at precisely the neutrino source.

The sensitivity of an experiment to the parameters which determine the oscillation, Δm^2 and $\sin^2 2\theta$, is set by geometry, neutrino energy, and statistical and systematic errors. The value of Δm^2 sets the frequency of the oscillation. The maximum value of D/E, the ratio of distance to neutrino energy, available in an experiment therefore determines a lower limit on sensitivity to Δm^2. Table 1 lists some common neutrino sources, typical maximum values of D/E, and the corresponding sensitivity to Δm^2.

Experiments which compare event rates at a fixed distance to some expected behavior have been performed at accelerators and nuclear reactors. These measurements have important systematic limitations. In the case of exclusive experiments, one is comparing measured rates due to anomalous flavors of neutrinos in a beam to a calculated background rate. In general, this background is only known to within some uncertainty. Inclusive single distance experiments which have been performed at reactors rely

TABLE 1

SOURCE	NEUTRINO	E(MEV)	D/E(M/MEV)	SENSITIVITY
SUN	ν_e	0. -4.	10^{11}	10^{-11} EV
REACTOR	$\bar{\nu}_e$	0. -8.	1-2	0. 01 EV
ACCELERATOR (PS, AGS)	$\nu_\mu, \bar{\nu}_\mu$	500-3000	. 1-. 03	0. 50 EV
ACCELERATOR (FNAL, SPS)	$\nu_\mu, \bar{\nu}_\mu$	$3X10^{3}$ - 2. 5X10	. 03-. 004	10^{1} EV

TABLE 2

NEUTRINO DETECTORS

	LAB E	WONDER BLDG
TOTAL MASS	1000 TON	200 TON
TARGET FIDUCIAL MASS	116 TON	48 TON
TRANSVERSE TOTAL(INCH)	120"X 120"	60"X 60"
TRANSVERSE FIDUCIAL	78. 04"X 78. 04"	50"X 50"
TARGET DENSITY (GR/CM)	4902. 96	4725. 40
TOROID P_T	3 X 0. 8 GEV	1. 2 GEV
MUON MOMENTUM RESOLUTION	11%	16%
EHAD RESOLUTION	89/√E	89/√E
DISTANCE TO DECAY REGION CENTER	1116 M	715 M
SPARK CHMBR RESOLUTION	0. 5 MM	0. 5 MM

upon calculations of reactor neutrino energy spectra and knowledge of the low energy interaction cross section. The spectrum of neutrinos, which are emitted by a nuclear reactor, results from a superposition of the beta decays of many separate fission products. Studies of the beta spectra of these fission products along with measurements of associated reactor electron spectra have led to calculations of absolute neutrino flux at nuclear reactors. There exist uncertainties in these calculations since the beta spectra of all these fission products are not known. The low energy $\bar{\nu}_e$ interaction cross section can be related to the neutron lifetime. To the extent to which the flux calculations can be trusted and the neutron lifetime is known, one may predict absolute event rates at a nuclear reactor. At accelerators, one expects a linear energy dependence for the total cross section. Depletions in flux due to inclusive oscillations will appear in the measured cross section for a particular neutrino as apparent deviations from the expected energy dependence. Especially at higher energies, there may however be other "unknown physics" which also affects the expected energy dependence of the total cross section.

The systematic uncertainties which limit measurements done at a single distance from the neutrino source cancel out in experiments which compare variations in event rates at more than one distance.

Recently published results from an inclusive search using one detector placed alternately at two locations along a $\bar{\nu}_e$ beam at the Gosgen power reactor[7] exclude positive signals in a region indicated by a previous measurement.[8]

FERMILAB E701

The experiment described in this paper (Fermilab E701) searches for inclusive oscillations of muon neutrinos in the energy range 30 GeV < E_ν < 240 GeV by operating two similar detectors simultaneously in the same accelerator neutrino beam. Event rates for the charged current deep inelastic scattering process

$$\nu_\mu + \text{nucleon} \rightarrow \mu^- + X \ ,$$

(where X is some unspecified hadronic state) are compared at the two detectors as a function of neutrino energy.

NEUTRINO BEAM

Data were collected between January and June of 1982 in the Fermilab dichromatic neutrino beam.[9] This beam was produced by allowing approximately 10^{13} 400 GeV protons, extracted from the accelerator during a 2 ms spill to impinge upon a 1-ft long BeO target. The resulting secondaries, pions, kaons, and protons were sign and momentum selected by a series of magnets and collimators into a narrow momentum bite ($\Delta p/p = \pm 10\%$), parallel focused ($\Delta\theta = 0.0002$ radian) beam of charged hadrons. These hadrons were then allowed to traverse a 350-meter long evacuated decay region. Therein some fraction of the pions and kaons decay into muons and neutrinos. This decay region was followed by a 6.1-meter long steel and aluminum beam dump to absorb the remaining hadrons. A 545-meter steel and earth muon shield separates the beam dump from the first neutrino detector. The second detector was placed after another 401 meters of earth. Figure 1 displays the layout of the Fermilab neutrino beam used for E701. Access ports at two locations in the decay region and directly after the beam dump contain intensity and profile monitors for hadrons and muons.[10]

The neutrinos in the dichromatic beam resulted primarily from the decays, $\pi \rightarrow \nu_\mu \mu$ (B.R. = 100%); $K \rightarrow \nu_\mu \mu$ (B.R. = 63.5%); $K \rightarrow \pi^o \nu_\mu \mu$ (B.R. = 3.2%); and $K \rightarrow \pi^o \nu_e e$ (B.R. = 4.82%). The muon neutrino energy spectrum for hadrons of 200 GeV is shown in Figure 2. Since the momentum bite of the beam was rather narrow, most of the neutrinos, which came from two-body decays, lay in one of two energy bands. We called those which result from pion decay ν_π, and those which result from kaon decay ν_k. The neutrinos from three-body decay represented a small contamination to the dichromatic spectrum. An additional source of neutrinos came from decays near the hadron production target before momentum and sign selection had occurred. These formed a wide band background which is also shown in the figure.

For the two-body decays, kinematics impose a correlation between the neutrino energy and the decay angle with respect to the parent particle's direction in the lab frame. Because of this, the neutrino energy and the radius of the event vertex at the neutrino detector are also correlated. In Fig. 3 the total measured neutrino energy is plotted against the radius of the interaction vertex for two settings of the hadron beam transport. The higher

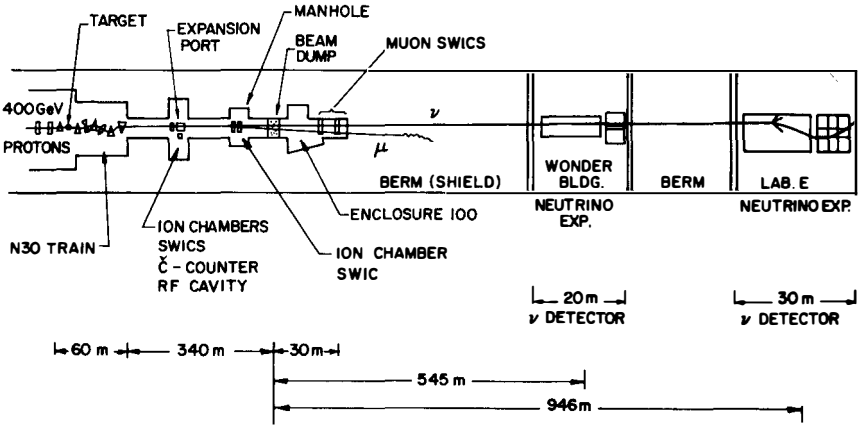


Fig. 1 Layout of Fermilab neutrino area.

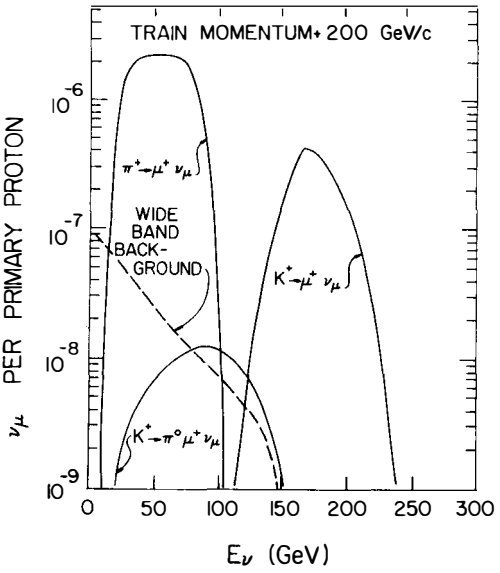


Fig. 2 Neutrino energy spectrum of the dichromatic beam set to select +200 GeV momentum secondaries.

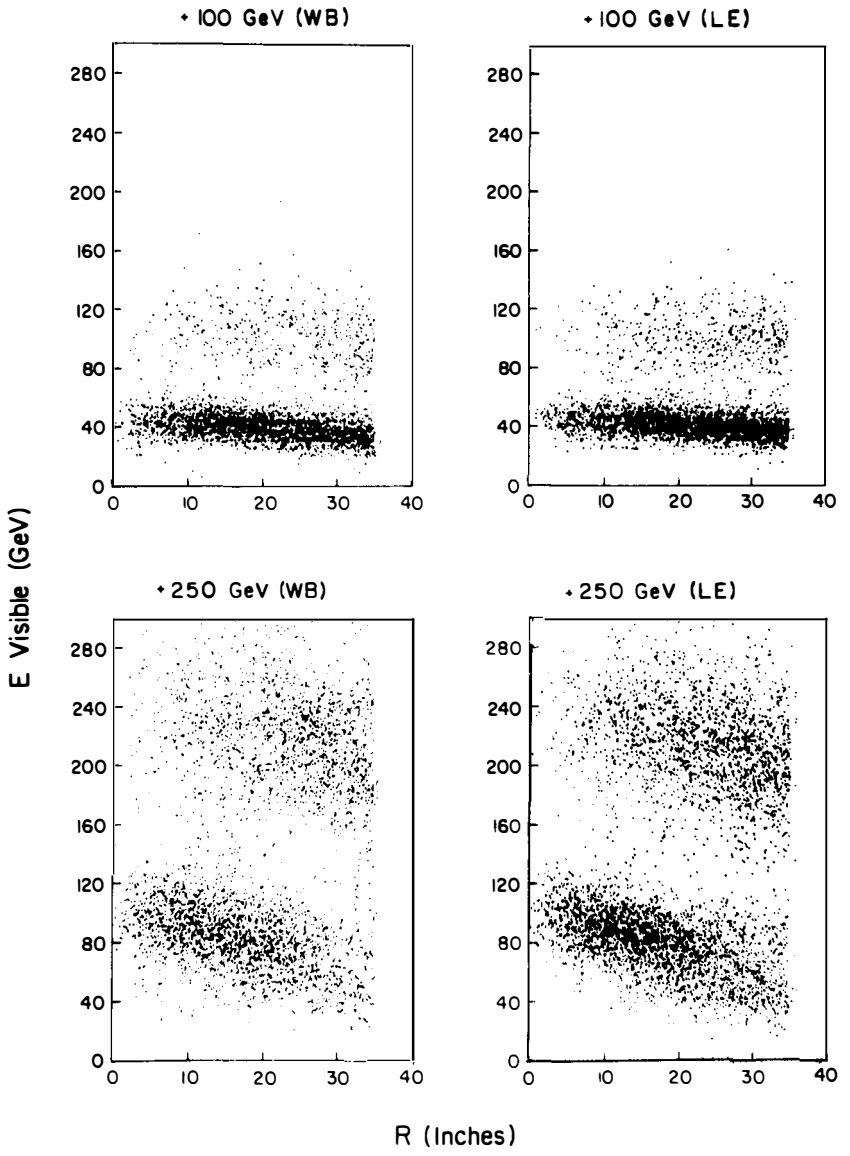


Fig. 3 Visible neutrino energy vs. radius (inches) of event interaction vertex at the two detectors for two settings of the secondary beam momentum selection. Wonder Building radius scaled to Lab E by 1.56.

energy bands are ν_K events while the lower energy bands are ν_π events. This plot shows that the measured total energy allows a clean separation between ν_π and ν_K events.

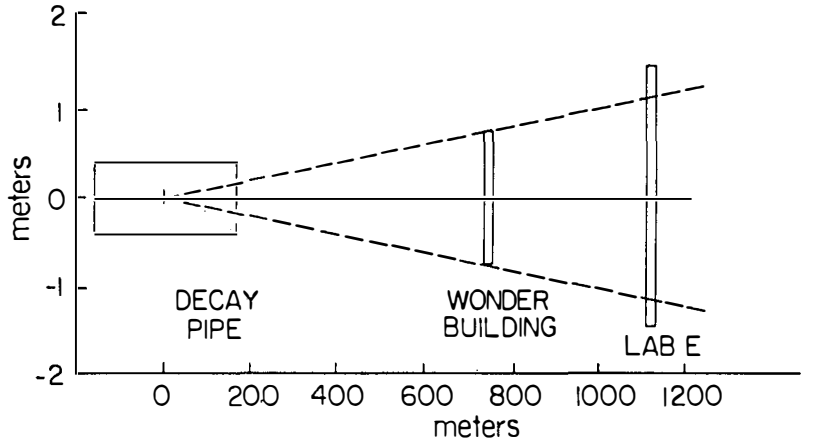
NEUTRINO DETECTORS

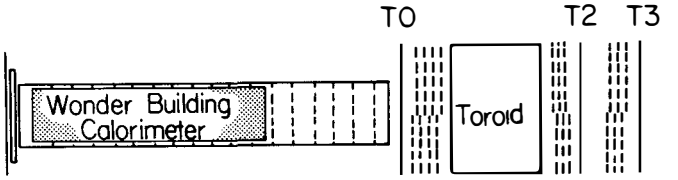
The first neutrino detector was located at 715 meters from the center of the decay region at a site known as the Wonder Building. The second detector was located at Lab E, 1116 meters from the decay region center. Both detectors were of similar design and construction. They were optimized to study, at high energy, the deep inelastic charged current scattering process.

Neutrinos interacted in a massive combined target calorimeter constructed out of steel plates and scintillator. The Lab E detector target consisted of 444 tons of 3 m x 3 m x 5 cm thick steel plates, fifty-six 3 m x 3 m liquid scintillation counters (located after every 10 cm of steel) and twenty-six 3 m x 3 m spark chambers (located after every 20 cm of steel). The Wonder Building target consisted of 108 tons of 1.5 m x 1.5 m x 5 cm steel plates, fifty-six 1.5 m x 1.5 m acrylic scintillation counters (located after every 10 cm of steel) and seventeen 1.5 m x 3.0 m spark chambers (located after every 30 cm of steel).

Hadronic energy was measured by observing scintillator pulse height downstream of the interaction vertex. Both detectors sampled the hadronic shower with the same spacing. Counters were calibrated by observing the response to minimum ionizing muons and the Lab E detector was also calibrated by an external hadron beam of known energy. The energy resolution was found to be $0.89/\sqrt{E}$. Small shifts in the calorimeter gain with time were monitored using a light flasher system.

The muon was tracked through steel by the spark chambers interspersed in the target. These spark chambers were read out magnetostrictively with a transverse position resolution of 0.5 mm. The muon sign and momentum were measured in a magnetized steel toroidal spectrometer downstream. The Lab E spectrometer included three 1.6-m long toroids, with 1.8 m outer radius and a 12.7 cm hole for the coils. The P_T kick of each toroid was 0.8 GeV (total $P_T \simeq 2.4$ GeV). Each toroid was followed by five 3 m x 3 m spark chambers. The Wonder Building spectrometer had one toroid, 2.4 m long, with an outer radius of 1.5 m and a 12.7 cm radius hole. This magnet was preceded by four 3 m x 3 m spark chambers and





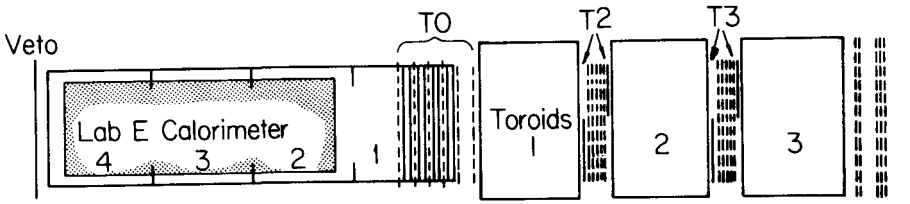


Fig. 4 A plan view (a) of the neutrino source and the two detectors. The average width of the secondary beam in the decay pipe is approximately 0.2 meters. The upstream (b) and downstream (c) detectors are shown also.

TABLE 4

BEAM SET	TYPE	BIN INCH	ENERGY GEV	WIDTH %	LABE EVTS	WONB EVTS	DATA* RATIO	ERROR	MC ** RATIO	ERROR	MC*** RATIO	ERROR
250	PION	0-20	82.86	.1949	2413	2279	1.059	0.030	1.031	.0051	1.043	.0051
250	PION	20-40	63.00	.3081	1430	1452	0.985	0.037	1.015	.0085	1.026	.0085
250	KAON	0-50	209.60	.1146	2865	2806	1.021	0.027	0.993	.0045	0.997	.0085
200	PION	0-20	70.51	.1710	3684	3522	1.046	0.025	1.027	.0056	1.037	.0056
200	PION	20-40	55.05	.2394	2595	2567	1.011	0.028	1.021	.0081	1.027	.0081
200	KAON	0-50	176.25	.1118	2989	3007	0.994	0.026	0.974	.0053	0.984	.0053
165	PION	0-20	61.01	.1506	2204	2157	1.022	0.032	1.005	.0060	1.035	.0060
165	PION	20-40	49.78	.2046	1915	1929	0.993	0.033	1.031	.0080	1.030	.0080
165	KAON	0-50	151.28	.1117	1478	1581	0.935	0.035	0.974	.0065	0.959	.0065
140	PION	0-20	53.62	.1453	2983	3063	0.974	0.025	1.026	.0069	1.031	.0069
140	PION	20-40	45.20	.1634	3168	3115	1.017	0.025	1.029	.0080	1.036	.0080
140	KAON	0-50	128.50	.1150	1727	1729	0.999	0.034	0.974	.0075	0.999	.0075
100	PION	0-20	40.76	.1268	1646	1670	0.986	0.034	1.020	.0080	1.020	.0080
100	PION	20-40	36.42	.1452	2130	2090	1.019	0.031	1.005	.0081	1.005	.0081
100	KAON	0-50	96.08	.1090	705	703	1.003	0.054	0.965	.0110	0.965	.0110

* DATA CORRECTED FOR NORMALIZATION DIFFERENCES.
** NOMINAL MONTE CARLO CORRECTIONS INCLUDING UPSTREAM BACKGROUND.
*** "STRETCHED" MONTE CARLO CORRECTIONS INCLUDING UPSTREAM BACKGROUND.

followed by six 3 m x 3 m spark chambers. The total P_T kick was 1.2 GeV. Figure 4 shows the two detectors, and their properties are summarized in Table 2.

The trigger used in this analysis was designed to select only charged current interactions where the muon momentum could be analyzed. It required at least one minimum ionizing track in the target, and a signal from a trigger counter located after the first magnet, in anti-coincidence with a veto counter located just upstream of the apparatus. Analysis of events satisfying this trigger should yield the muon energy E_μ, the muon angle θ_μ, and the hadronic energy E_H. These three variables completely specify the event kinematics. In addition, the radial interaction vertex allows one to infer the total neutrino energy from the beam design.

ANALYSIS

Before describing the analysis of the data, we may estimate the particular limitations of this experiment. With a separation between the Lab E and Wonder Building detectors of 301 meters, the maximum value of D/E is 0.01. This corresponds to minimum Δm^2 sensitivity of 10 eV^2. At high Δm^2, when the oscillation becomes rapid, we expect a cutoff from two effects. Since the decay region has a length of 350 meters, any oscillation of shorter wavelength will become averaged over. This corresponds to a Δm^2 of 1700 eV^2. This experiment has roughly 10% total energy resolution. If we attempt to resolve energy variations which are too rapid, we expect to lose sensitivity also. This implies for E701 an upper Δm^2 cutoff of approximately 1000 eV^2.

Data were taken with the hadron beam transport set to select positive secondaries at momenta of 250, 200, 165, 140, and 100 GeV . Transverse fiducial cuts were set such that the two detectors subtended close to the same geometrical flux (see Fig. 4). To ensure the detectors received a simultaneous neutrino flux, events occurring in a particular detector were included in the analysis only if the other detector were operational and taking data. Spark chamber deadtime limited the acceptance to one event per accelerator spill in each detector. As a result, a relative deadtime correction was applied to the counting rates. Table 3 lists the flux in targeted protons received by the two detectors during the experiment.

The oscillation analysis is based upon a comparison of event rates at the two detectors as a function of neutrino energy. The

TABLE 3

FLUX IN PROTONS ON TARGET $X10^{16}$

	250	200	165	140	100	SUM$X10^{18}$
LAB E						
TOTAL LIVE	96.3	57.2	44.9	53.6	41.5	2.9
GOOD RUNS	88.9	54.0	40.8	53.3	40.2	2.8
GOOD STEER	87.3	54.0	39.4	52.7	39.8	2.7
WOND BLDG TAKES DATA	48.4	44.4	30.9	40.2	32.7	2.0
WOND BLDG						
TOTAL LIVE	101.2	61.6	51.2	54.8	44.2	3.1
GOOD RUNS	66.4	61.4	43.8	50.3	38.3	2.6
GOOD STEER	65.4	61.3	42.7	50.0	38.2	2.6
LAB E TAKES DATA	51.5	47.4	35.4	40.2	34.9	2.1

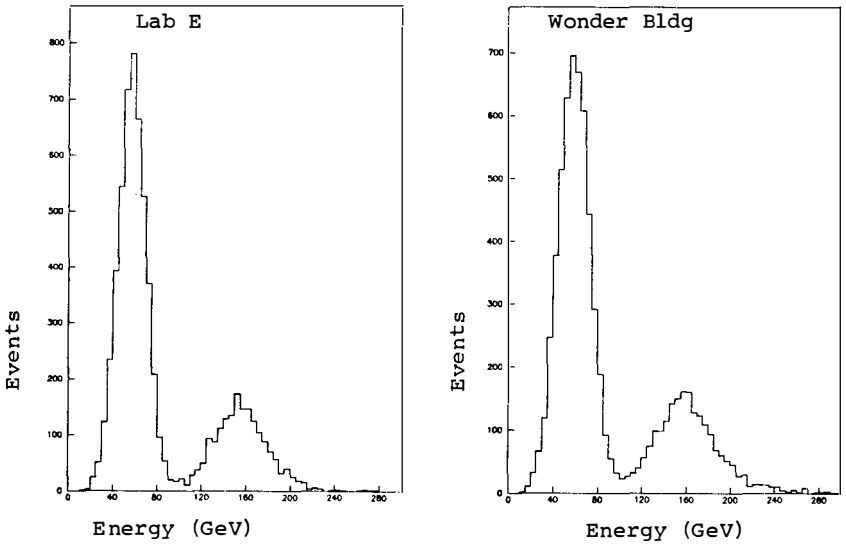


Fig. 5 Measured energy distributions in Lab E and the Wonder Building for a +165 GeV momentum setting of the secondary beam.

dichromatic beam is particularly suited to this, since once events are separated between ν_π and ν_k, the radial interaction vertex is directly related to the neutrino energy. The measured total energy in charged current events allows a clean separation between ν_π and ν_k. The two detectors were observed to agree in their measurements of total energy to within $\pm$ 3.1% across the range 30 GeV < E_ν < 240 GeV accessible to this experiment. Figure 5 shows histograms of total measured energy for a +165 GeV setting of the hadron beam transport. In both apparati, the peaks from ν_π and ν_k are seen to be clearly distinct.

Once the π/k separation is done, at each setting the events are further separated into radial bins about the beam center. (These centers are determined at each setting from the transverse vertex distributions of high energy ν_π events to an accuracy of $\pm$ 0.25 in.) Because of the energy angle correlation in the narrow band beam, these radial bins are effective energy bins also. In the far (Lab E) detector, there are two bins for ν_π, one from 0 in. - 20 in., and one from 20 in. - 40 in.; for ν_k there is one bin from 0 in. - 50 in. These bins and the typical energy variation can be seen in Fig. 6. The geometrical bin boundaries in the near (Wonder Bldg) detector are determined by scaling the radii in the far detector by the ratio of the distances of the two detectors from the decay region center (DWB/DLE = 0.6407). This scaling is based upon the assumption that the beam may be treated as if it originated at the center of the decay region. Corrections based upon this assumption will be discussed later. The energy distribution for each bin is determined by a Monte Carlo simulation of the neutrino beam. The mean energies and standard deviations as calculated for each bin are shown in Table 4.

The event samples are further restricted by a series of cuts. The steering of the incident neutrino beam was determined by monitoring the position of the hadron beam in the decay region. Events for which the beam center deviates from a 2-in. square at Lab E are dropped from the analysis. A set of fiducial cuts ensures containment of showers and the equality of solid angle subtended by the two detectors. A longitudinal cut upon the event vertex eliminates 30% of the downstream target volume. A transverse cut upon the event vertex of $\pm$ 25 in. x $\pm$ 25 in. is imposed about the axis of the smaller Wonder Bldg detector.

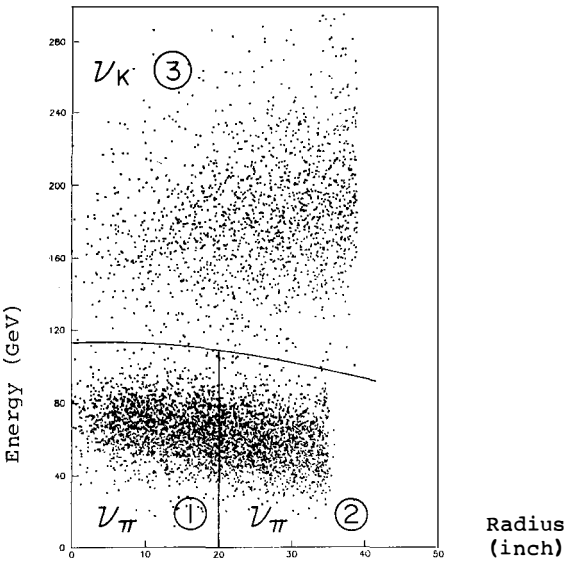


Fig. 6 Lab E measured neutrino energy vs. radial vertex of event for the +165 GeV momentum setting of the secondary beam. Radial bin boundaries used in oscillation analysis are indicated on the figure.

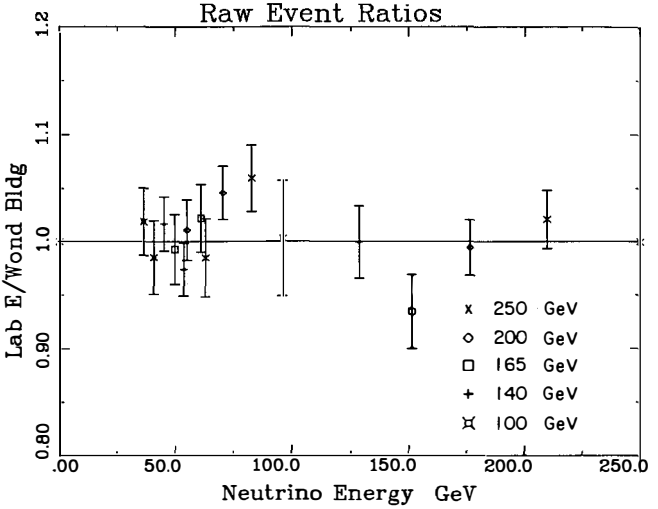


Fig. 7 Raw event ratios (Lab E/Wonder Building) vs. neutrino energy. The events have been corrected for normalization differences only. The five highest energy points are from ν_K. The symbols indicated the different secondary momentum settings.

The transverse cut at Lab E is determined by scaling as the decay region center to detector distance ratios. In addition ν_π (ν_k) are required to have a vertex within 22.5 in. (25 in.) of the beam center in the Wonder Building. This radius cut is also scaled to the Lab E detector. Cuts upon the muon track define a simple geometrical trigger. These include an angle cut of 0.2 radians and a straight line extrapolation of the target track to the trigger counter (T2) within its active area. Events for which the muon travels within the toroid hole for more than 20% of its path length in the spectrometer are also cut.

The detectors had an equal number of steel plates. Each event is translated in software from the detector of occurrence to the other along a line joining its interaction vertex to the decay region center. Its vertex is placed in the corresponding steel plate. The events are required to pass all cuts in both detectors. In this way the acceptances are forced to be equal. The resulting event sample is listed in Table 5.

Before counting rates can be compared, sets of corrections must be applied. The first set results from small normalization differences between the two detectors. These include a relative target density ratio of 1.036 ± 0.013, relative deadtime corrections which range between 1-13%, and a relative veto deadtime correction which is $1\text{-}3 \pm 0.3\%$. Events and ratios following these corrections are shown in columns 6-9 of Table 4 and in Fig. 7. The uncertainties in these normalization differences as well as the factors listed in Table 6 contribute to an overall systematic error estimated to be 1.5%. A small off-line event reconstruction inefficiency was eliminated by visually scanning and reconstructing events failing to satisfy fitting criteria and including them in the data sample.

A second set of corrections (0-4%) result from the assumption all neutrinos could be treated as if they originated at the decay region center. Factors which determine the effective mean decay position include exponential decay, solid angle and parallax (because of the finite length of the decay region), hadron beam angular divergence, and upstream (wide band) background. Since we scale from the decay region center, relative rates at the far detector are enhanced (decreased) as the mean decay position moves upstream (downstream).

TABLE 5

RAW EVENT TOTALS BEFORE AND AFTER CUTS

ENERGY		250	200	165	140	100	SUM
PION:							
FID VOL	LE	4765	7763	4838	8304	4952	30622
	WB	4693	7628	5135	7791	4943	30190
ALL CUT	LE	3794	6120	3747	6388	3722	23771
	WB	3732	6089	4086	6178	3760	23845
KAON:							
FID VOL	LE	3260	3410	1693	2290	937	11590
	WB	3224	3495	1963	2162	968	11812
ALL CUT	LE	2833	2931	1359	1808	698	9629
	WB	2806	3007	1581	1729	703	9826

TOTAL AFTER CUTS: LAB E= 32400
WOND BLDG=33671

TABLE 6

SOURCES OF SYSTEMATIC ERROR

SOURCE	FACTOR*	ERROR
TARGET DENSITY	1.036	.003
RELATIVE DEADTIME	1.0- 1.13	.01
VETO DEADTIME	1.01- 1.03	.003
BEAM CENTERS	----	.003
Z POSITION OF DETECTORS	----	.001
WIDE BAND BACKGROUND	----	.003

*CONTRIBUTION TO NORMALIZATION
DIFFERENCE IF RELEVANT,
FACTOR MULTIPLIES
LAB E/WONDER BLDG.

TABLE 7

CORRECTIONS FOR UPSTREAM (WIDE BAND) BACKGROUND

LAB E/WOND BLDG

SET	TYPE	BIN	CORR
250	PION	0"-20"	1.008
250	PION	20"-40"	1.011
250	KAON	0"-50"	1.001
200	PION	0"-20"	1.005
200	PION	20"-40"	1.007
200	KAON	0"-50"	1.000
165	PION	0"-20"	1.004
165	PION	20"-40"	1.004
165	KAON	0"-50"	1.000
140	PION	0"-20"	1.004
140	PION	20"-40"	1.004
140	KAON	0"-50"	1.000
100	PION	0"-20"	1.007
100	PION	20"-40"	1.005
100	KAON	0"-50"	1.001

Wide band background from decays near the production target were measured by closing a collimator in the hadron beam transport. This collimator absorbed all hadrons before their entrance to the decay region. All interactions observed during this time are from wide band background. The relative acceptance difference of the two detectors given our binning procedure can be calculated assuming these neutrinos to originate from a point source at the target. Corrections, listed in Table 7, based upon this are applied to the event ratios.

The other effects, all of which relate to neutrinos originating in the decay region, were calculated using a Monte Carlo simulation of the neutrino beam. For kaons, this calculation predicts that exponential decay and parallax are dominant in determining the mean decay position, shifting it downstream 15-25 meters. For the higher energy pions, the neutrino decay angle is of the same order as the hadron beam divergence. Since the hadron beam divergence originates at the entrance to the decay region, this property of the beam moves the apparent mean decay position upstream making the relative rate in the far detector to near detector larger for the inner ν_π radial bin. This effect is largest at the 250 GeV setting and diminishes with secondary beam energy as the lab decay angle grows.

In the beam simulation, particle production in p-Be collisions, based upon the data of Atherton et al,[11] is used as input to a magnetic ray tracing program, TURTLE.[12] This program includes surveyed positions of all hadron beam elements and measured magnet currents as input parameters. The emerging hadron beam is allowed to decay and the resulting neutrinos are interacted in the detectors. These events are then fully reconstructed and passed through an identical analysis as the data.

This simulation of the hadron beam is checked by a number of observations. Data from profile monitors in the decay pipe and in the muon shield allow a comparison between predicted and measured spatial distributions. In addition, the hadron beam angular divergence was measured. This was done by sampling the beam with a 6 ft long, 0.5 in. square collimator which was step scanned transversely across the entrance to the decay region. The total transverse size of the hadron beam at that point was approximately 2.0 in. x 4.5 in. The resulting downstream spatial profiles could be used to infer the total angular spectrum since each collimator

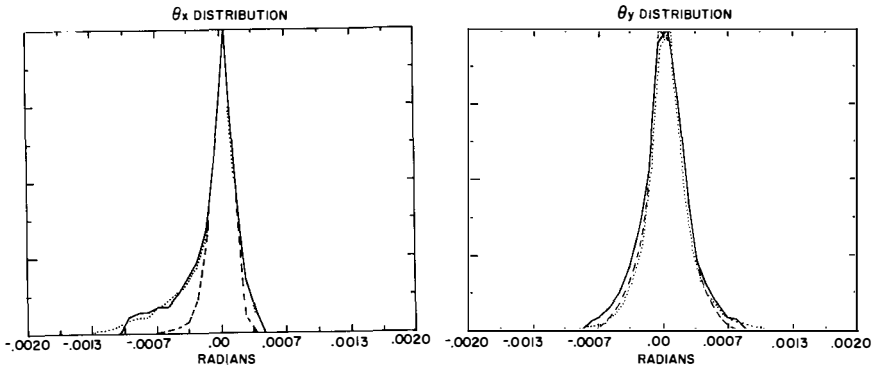


Fig. 8 Angular distribution of the secondary beam for a momentum setting of +165 GeV, at the entrance to the decay region. (a) θ_x and (b) θ_y. The solid curve is the measured distribution. The dashed curve is the Monte Carlo prediction. The dotted curve is the prediction of the "stretched" Monte Carlo.

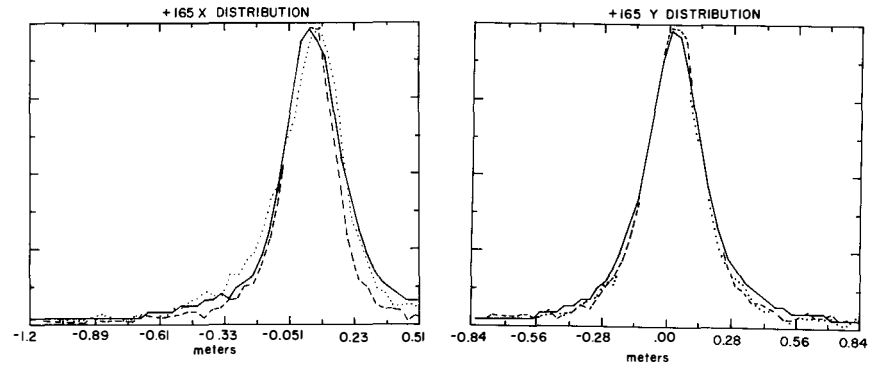


Fig. 9 Spatial distribution of muons for a secondary beam momentum setting of +165 GeV. These distributions are taken 29 meters of air downstream of the decay region beam dump (see Fig. 1). (a) X and (b) Y distributions. Solid curve is the measured distribution. The dashed curve is the Monte Carlo prediction. The dotted curve is the prediction of the "stretched" Monte Carlo.

position represented essentially a point source of hadrons.

The measured and simulated angular distributions are observed to agree for the central 80% of the beam phase space. The real angular distribution includes a tail at wide angle which the Monte Carlo fails to predict. Figure 8 shows this comparison. To evaluate the importance of this contribution to the corrections, some input parameters to the beam transport code are varied and beam angles are increased until a new angular distribution is obtained which more closely reproduces the entire measurement. This "stretched" beam (Fig. 8) is also used to simulate the experiment. In Fig. 9 we show muon distributions as measured and predicted by the two Monte Carlo models. Table 4 contains correction factors for the data obtained with both sets of Monte Carlo events. Factors for the wide band background are also included in these corrections. Although the "stretched" beam predicts slightly larger corrections, the disagreement is at the $< 1\%$ level. Figure 10 shows event ratios corrected by the nominal (not stretched) Monte Carlo vs. energy.

TEST OF OSCILLATION HYPOTHESES

In the absence of neutrino oscillations the data shown in Fig. 10 should each be unity. To test the data for consistency with various neutrino oscillation hypotheses, the following approach is adopted. For a pair of parameters, (Δm^2 and $\sin^2 2\theta$) the Monte Carlo events described in the preceding section are weighted by their oscillation probability calculated with their generated energy and decay point. These events are analyzed and appropriately summed. A χ^2 function is formed with the measured event ratios uncorrected by Monte Carlo (column 8, Table 4). A possibly different normalization factor for each energy setting is included with an error of 1.5% (see previous discussion of systematics). The χ^2 function is minimized with respect to these five factors. The χ^2 function is given by:

$$\chi^2 = \sum_{i=1}^{5} \sum_{j=1}^{3} \frac{\left(R_{ij}^{meas} - f_i^{norm} \cdot R_{ij}^{MC}(\Delta m^2, \sin^2 2\theta)\right)^2}{\sigma_{ij}^2} + \sum_{i=1}^{5} \frac{\left(f_i^{norm} - 1\right)^2}{\sigma_{norm}^2}$$

Here R_{ij} are the measured or predicted ratios of counting rates (Lab E/Wonder Bldg) from the i^{th} energy setting and the j^{th} radial bin. The total absolute error, including event statistics and Monte Carlo statistics is given by σ_{ij}. The normalization factors

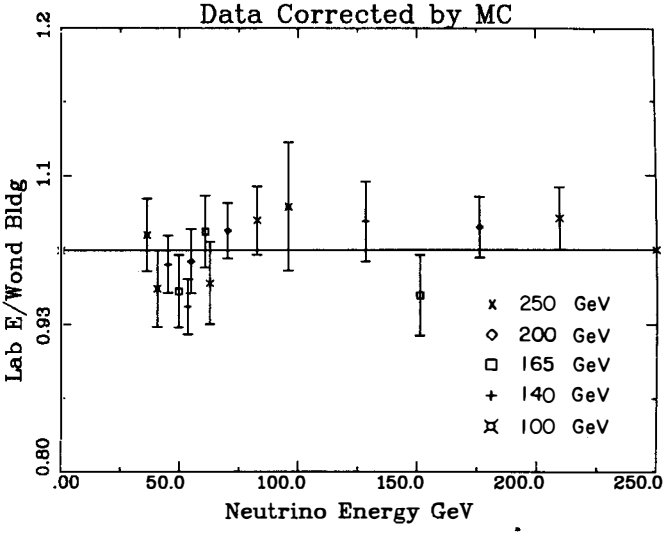


Fig. 10 Event ratios (Lab E/Wonder Building) vs. neutrino energy. The data include corrections for normalization differences, corrections for wide band background, and Monte Carlo corrections for effects of the secondary beam distribution in the decay region.

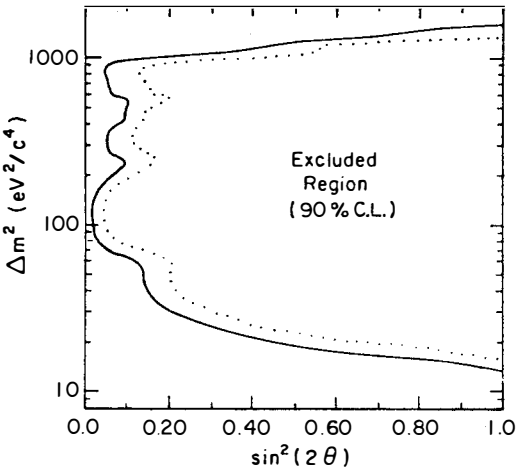


Fig. 11 90% C.L. limits on possible inclusive oscillations of muon neutrinos as a function of Δm^2 and $\sin^2 2\theta$, calculated using the likelihood ratio test (solid curve). The region to the right of the curve is excluded. These limits are calculated including systematic errors and errors on the secondary beam divergence. The limits obtained with Pearson's χ^2 test are also shown (dotted line).

are f_i^{norm} and σ_{norm} is 1.5%.

The event sums in each detector are expected to be gaussian distributed. In general though, the ratios of these sums may not be. For equal errors in numerator and denominator, $\ell n(R)$ is expected to be more gaussian than R.[13] In addition to the χ^2 described above, we have done an analysis using a χ^2 function formed with $\ell n(R)$ rather than R. We find however that for a given hypothesis (Δm^2 and $\sin^2 2\theta$), the two χ^2 are consistent.

The χ^2 for the hypothesis of no oscillations is acceptable, (χ^2 = 11.5 for 15 D.F.) and, therefore, the data cannot be used to support a claim of a finite value for Δm^2 and $\sin^2 2\theta$. However, a certain region of the Δm^2 and $\sin^2 2\theta$ plane can be excluded. We have calculated this region at the 90% C.L. using the maximum likelihood ratio test.[14] This test allows one to compare a particular Δm_o^2 and $\sin^2 2\theta_o$ hypothesis to all other two parameter fits. By Monte Carlo, the distribution $P(\lambda)$, of the quantity,

$$\lambda = -2\ell n\{\frac{\mathcal{L}(\Delta m_o^2, \sin^2 2\theta_o)}{MAX\mathcal{L}(\Delta m^2, \sin^2 2\theta)}\} = \chi^2(\Delta m_o^2, \sin^2 2\theta_o) - \chi^2_{minimum} \quad ,$$

may be found for a given event statistics. Here $\mathcal{L}(\Delta m_o^2, \sin^2 2\theta_o)$ is the likelihood function for the given hypothesis. That λ below which 90% of $P(\lambda)$ lies indicates an equi-χ^2 contour relative to the best fit. For our statistics we find for this point λ = 4.6 and for our data χ^2_{min} = 8.65 for Δm^2 = 1352 eV^2 and $\sin^2 2\theta$ = 0.50. Alternately, a Pearson χ^2 test [15] for 15 D.F. may be used to gauge a particular two parameter hypothesis against all other N parameter (e.g. 3 component, 4 component maxing, etc.) fits. Usually this absolute test will yield a more restrictive limit than the maximum likelihood ratio test. Since we have considered only two parameter oscillations in our analysis we present limits based upon the ratio test. We also include (as a dotted curve) limits calculated using the Pearson χ^2 test. Most other inclusive oscillation experiments have analyzed their data using a likelihood ratio test[7)16)17)], and therefore our likelihood ratio limit should be used when comparing to their results.

The effect of systematic uncertainties in the angular divergence of the hadron beam which is evaluated with the two Monte Carlos cannot readily be included in the χ^2 function since

they correlate different radial bins. We calculate 90% confidence level limits as described above using Monte Carlo events from both beam models; at each Δm^2 we take the worse limit. The excluded region is shown in Fig. 11.

In the region of sensitivity, these data show no evidence for oscillations of muon neutrinos. In the interval 30 eV $<$ Δm^2 $<$ 1000 eV^2, the mixing must be less than 0.02-0.20. If only one neutrino has mass then, 6 eV $<$ M_ν $<$ 33 eV is excluded. If two neutrinos have similar mass (i.e. Δm = 5 eV), then we exclude 3 eV $<$ M_ν $<$ 100 eV. This excluded region covers much of the mass range proposed by cosmological models.

This is a unique experiment in that a search for inclusive oscillations in this Δm^2 region can only be performed by a long baseline experiment at high energies. (The only other inclusive search using a ν_μ beam has been performed at lower energies, excluding oscillations for smaller values of Δm^2.[16])

We thank Directorate and Staff of the Fermi National Accelerator Laboratory, the Accelerator Division, and the Neutrino Department, and especially S. Pordes, for invaluable support. We also acknowledge the excellent technical assistance of C. Chizzo and K. Gray. This research was supported in part by the U. S. Department of Energy and the National Science Foundation.

REFERENCES

Present addresses:

* Department of Physics, University of Florida.
** Institute for High Energy Physics, Beijing, P.R. China.
† Department of Physics, Florida State University.
‡ Fermilab, Batavia, IL.
‡ On leave: Institute of Nuclear Studies, Warsaw, Poland.

1) R. Barbieri et al, Phys. Lett. 90B, 91 (1980).
A. Masiero, M. Roncadelli, Phys. Rev. D25, 2612 (1982).
E. Witten, Phys. Lett. 91B, 81 (1980).
2) V.C. Rubin, Science 220, 1339 (1983).
P.H. Frampton, P. Vogel, Phys. Rpts. 82, 339 (1982).
3) H.B. Anderhub et al, Phys. Lett. 114B, 76 (1982).
R. Abela et al, SIN Newsletter 15, p. 26.
4) C. Matteuzzi (these proceedings).
5) V.A. Lubimov et al, Phys. Lett. 94B, 266 (1980). See also,
M. Shaevitz, Lepton-Photon Symposium, Ithaca, NY (1983).
6) S.M. Bilenky, B. Pontecorvo, Phys. Rpts. 41, 225 (1978).
7) J.L. Viulleumier et al, Phys. Lett. 114B, 298 (1982).
8) F. Reines et al, Phys. Rev. Lett. 45, 1307 (1981).
9) D. Edwards, F. Sciulli, Fermilab TM-660, 1976 (unpublished).
10) R. Blair et al, Nevis Report #1309 (submitted to NIM).
P. Auchincloss et al, Fermilab FN-382,1983 " " " .

11) H.W. Atherton et al, CERN Preprint CERN 80-07 (1980).
12) D. Carey, NAL-64, 2041.000 Fermilab (1978).
13) A. Bodek, NIM 117, 613 (1974).
14) W.T. Eadie et al, Statistical Methods in Experimental Physics (North-Holland Publ. Co., Amsterdam 1971), p. 230.
15) A.G. Frodesen, O, Skjeggestad, H. Tøfte, Probability and Statistics in Particle Physics (Universitets-Forlaget, Bergen 1979), p. 415.
16) F. Dydak et al, Phys. Lett. 134B, 3,4 (1984).
17) J.M. Thenard (LAPP, Annecy-Bugey Reactor Collaboration) private communication.

THE SOURCE SPECTRUM OF REACTOR ANTINEUTRINOS AND ITS APPLICATION TO NEUTRINO OSCILLATION STUDIES

K. Schreckenbach
Institut Laue Langevin, 38042 Grenoble, France

F. von Feilitzsch
Physik Department der TU München, 8046 Garching, Germany

A.A. Hahn
Caltech, Pasadena, USA
present address: University of California at Irvine, CA 92717, USA

Precise measurements of cumulative beta spectra from ^{235}U and ^{239}Pu neutron induced fission were performed at the magnetic beta spectrometer BILL at the ILL reactor. Following a conversion of these spectra into the correlated antineutrino spectra the source spectrum of $\bar{\nu}_e$ of nuclear reactors could be constructed. These results are discussed in the context of neutrino oscillations experiments with reactor neutrinos.

The interpretation of experiments with reactor antineutrinos, such as the search for neutrino oscillations, depends on a knowledge of the $\bar{\nu}_e$ source spectrum from the reactor. This spectrum is composed of a superposition of $\bar{\nu}_e$ spectra from beta decaying fission products in the reactor core. Most such $\bar{\nu}_e$ are found below 10 MeV.

In principle one may construct the reactor $\bar{\nu}_e$ spectrum from experimental and theoretical data for the individual fission products, but in practice this is very difficult. Several hundred fission products with many beta branches are involved. It is not surprising that the various calculations of this type differ considerably from each other (see comparison in ref. 1,2).

An alternative experimental method of determining the reactor $\bar{\nu}_e$ source spectrum is to measure the composite beta spectrum from fission products for each of the fissile isotopes making a significant contribution to the reactor power. To make such measurements one may simulate a small reactor which is transparent to the emitted beta particles, but contains the fission products. To this end we have used the arrangement shown in fig. 1. In a constant neutron flux, fission is induced in the layer of fissile material, which is sandwiched between the 7.5 μm Ni catcher foils for the fission products. The time for the beta activities to reach saturation is a function of the beta half lifes of the fission products. After an exposure time of a few hours saturation is achieved for those beta decays with endpoint energies $E_o \gtrsim 3$ MeV. The emitted beta particles are measured on-line and normalized per fission. The resulting experimental beta spectrum has to be converted into the correlated $\bar{\nu}_e$ spectrum, a delicate task if a precision of a few percent is demanded. Finally for a given reactor core the $\bar{\nu}_e$ spectrum has to be constructed according to the contribution of the various fissile isotopes (mainly ^{235}U, ^{239}Pu, but also ^{241}Pu, ^{238}U) to the reactor power.

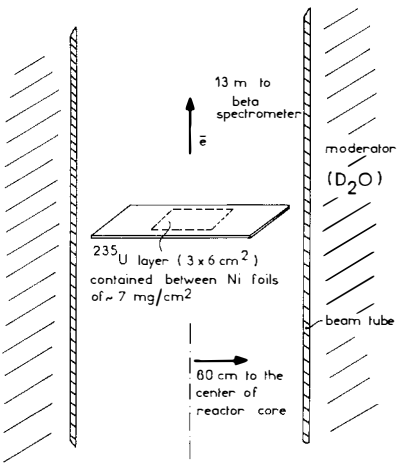


Fig. 1 Schematic view of the target site at the BILL spectrometer

We have performed measurements of the composite beta spectra of ^{235}U and ^{239}Pu fission products[1,2] using the magnetic spectrometer BILL[3] at the High Flux

Reactor, Grenoble. The in-pile target site is illustrated in fig. 1. After a 13 m flight path in the evacuated beam tube the electrons are analysed in the two subsequent iron-core magnets of the spectrometer, a geometry which prevents scattered electrons reaching the electron counter. The absolute rates per fission were determined by comparison with well-known thermal neutron reaction cross sections. Contributions from electrons other than the beta particles from fission products were estimated to contribute less than 1% to the spectrum for $E_\beta > 1.5$ MeV.

In the near future it is planned to make an improved measurement of the beta spectrum from ^{235}U fission (extension to higher energies; new absolute calibration) and a measurement of the spectrum from ^{241}Pu.

For the conversion of the experimental beta spectrum into the correlated $\bar{\nu}_e$ spectrum, we have approximated the experimental beta spectrum above 1.5 MeV by $\sim$ 25 allowed branches P_i with amplitudes a_i:

$$N_\beta(E_\beta) = \sum_i a_i \, P_\beta^{(i)}(E_\beta, E_o^{(i)}, \bar{Z}(E_o^{(i)})) \qquad (1)$$

$\bar{Z}$ denotes the mean proton number for branches with endpoint energy $E_o^{(i)}$ (see ref. 2). This decomposition was accomplished using the Fermi-Kurie representation of the spectrum, in which allowed transitions take the form of a straight line. The composite $\bar{\nu}_e$ spectrum can then be constructed easily by converting the individual branches:

$$N_\nu(E_\nu) = \sum_i a_i \, P_\beta^{(i)}(E_o^{(i)} - E_\nu, E_o^{(i)}, \bar{Z}(E_o^{(i)})) \qquad (2)$$

It was found that this conversion became insensitive to the number of branches, if it was larger than about 20. The conversion method is obviously sensitive to the shape of P_β used in eqs. (1) and (2). Thus, at the level of a few percent, the result of the conversion depends on higher order corrections to the shape of allowed transitions and on possible contributions of first-forbidden transitions. Radiative corrections were included following the theory of Sirlin[4], giving a correction of $(E_\nu - 4)\%$, E_ν in MeV, for the converted spectrum. Weak magnetism and higher order Coulomb terms depend on the nuclear structure of the fission products involved and have not been included in our conversion procedure.

One simple test of this procedure is to compare the spectra N_β^{exp} and N_ν^{exp} we derive with calculated spectra N_β^{cal} and N_ν^{cal}, where the conversion is done explicitly by summing up separately the $\bar{\nu}_e$ and betas from the individual fission products. For relativistic beta decays the following relation is a good

approximation:

$$P_\nu(E_\nu) \approx P_\beta(E_{tot}-\Delta E) \qquad (3)$$

$$E_{tot} = E_\beta + m_e c^2 \; ; \quad \Delta E \text{ Coulomb term}$$

Thus the composite spectra N_β and N_ν are correlated in the same manner. Correlated deviations between calculated spectra N^{cal} and the experimental spectra N^{exp} are shown in fig. 2. It proves that our conversion is close to that of N_β^{cal} to N_ν^{cal}.

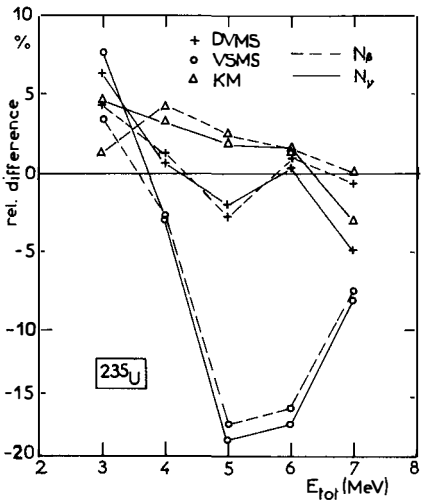


Fig. 2 Relative differences of the N_β and N_ν spectra of the present work to various calculations: DVSM[5], VSMS[6] and KM[7]. The deviations $(N^{exp}-N^{cal})/N^{exp}$ between N_β and N_ν are the same within a few percent.

In connection with short-range ν oscillations it may be worthwhile to discuss one general feature of the reactor $\bar{\nu}_e$ source spectrum. To a good approximation the "Kurie plot" $K_\nu(0)$ of the $\bar{\nu}_e$ source spectrum is simply the quadratic sum of straight lines corresponding to individual, allowed beta branches. For our purpose with the approximation (3) the Fermi function can be taken at $E_\beta \simeq E_\nu - m_e c^2$, and a fixed value of Z may be chosen. It may be readily verified that no turning points can occur in $K_\nu(0)$ since

$$\frac{d^2K_\nu(0)}{dE_\nu^2} = \frac{\text{const}}{\sum_i a_i (E_o^{(i)}-E_\nu)^2} > 0 \qquad (4)$$

for all E_ν. Fig. 3 indicates the form of $K_\nu(L)$ for the $\bar{\nu}_e$ spectrum of ^{235}U and shows the effect of a two neutrino oscillation (see eq. (5)) on the spectrum. Thus it is clear that independently of any detailed knowledge of the source spectrum, the observation of turning points in the $K_\nu(L)$ spectrum recorded at some distance L from the reactor would provide a signature for the occurrence of neutrino oscillations. It is self-evident that this analysis is rather qualitative and would demand a measurement of **high statistical accuracy** with an $\bar{\nu}_e$ detector.

The best analysis for the occurence of ν oscillations involves a detailed comparison of ν spectra taken at different distances L from the reactor core

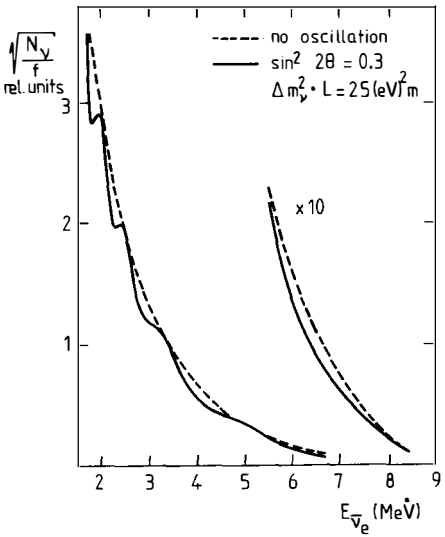


Fig. 3 Approximate Kurie representation of the $\bar{\nu}_e$ spectrum from ^{235}U fission. The effect of ν oscillations with the given paramaters is illustrated.

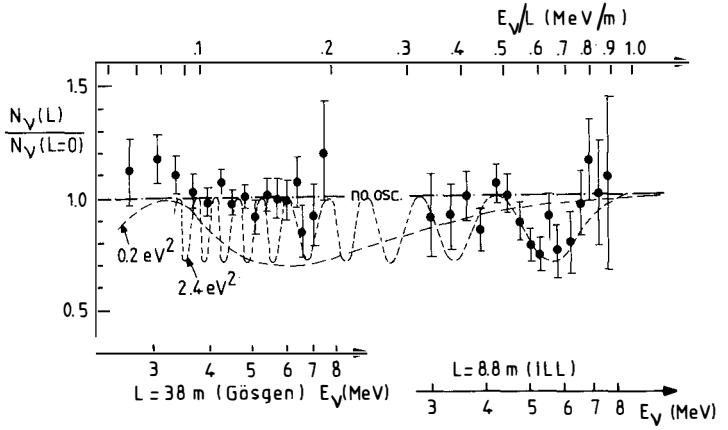


Fig. 4 $\bar{\nu}_e$ yields measured at a distance L from the ILL[8] and Gösgen reactor[9], normalised to the corresponding $\bar{\nu}_e$ source spectra.

including the source spectrum L=0. The impact of the L=0 spectrum on this analysis is shown in figs. 4 and 5 . For two neutrino oscillations it can be

shown that

$$N_\nu(L)/N_\nu(0) = 1 - \frac{\sin^2 2\theta}{2}\,(1 - \cos(2.5\ \Delta m^2_\nu \cdot L/E_\nu) \qquad (5)$$

$$[(eV)^2 \cdot m/MeV]$$

Hence spectra measured at various distances from the reactor core can be compared in a common representation as function of E_ν/L. In fig. 4 are shown the normalized spectra $N_\nu(L)/N_\nu(0)$ as observed in $\bar{\nu}_e$ detectors at the ILL and Gösgen reactors with $N_\nu(0)$ taken from the present measurements. For a common mixing parameter $\sin^2 2\theta = 0.3$ several possible oscillation curves are given. It should be noted that this figure must not be taken too literally since part of the assigned errors is correlated and the theoretical curves do not take the finite resolution of the detector system (detector size and resolution, core size) into account.

The present status of the ILL-Gösgen experiments[10] is summarized in fig. 5. For fast oscillations ($\Delta m^2_\nu \gtrsim 10\ eV^2$ for our case) individual oscillations were no longer detectable and for all E_ν an average value

$$N_\nu(L)/N_\nu(0) = 1 - \frac{\sin^2 2\theta}{2} \qquad (6)$$

is observed. In this case the experiment is reduced to a comparison of the neutrino flux at distances $L \neq 0$ and $L = 0$. The present data allow the disappearance of at most 8% of the $\bar{\nu}_e$ flux (90% c.L.) and hence give for $\Delta m^2_\nu \gtrsim 10\ eV^2$ a limit of $\sin^2\theta \lesssim 0.16$. This limit holds for high values of m_{ν_i}, up to the point where phase space corrections become important (above ~ 4 MeV). Eq. (6) is also valid for the case where we have incoherence of the interfering mass eigenstates.

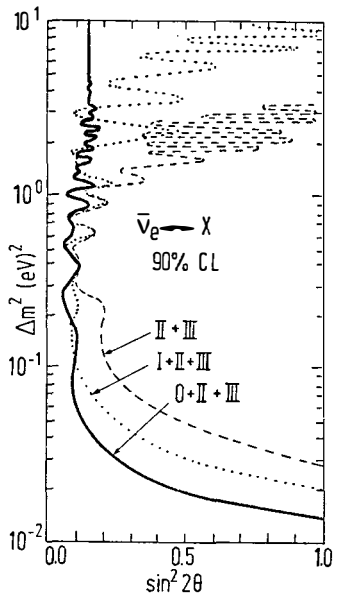


Fig. 5 Exclusion plots from the ILL-Gösgen experiments. 0: source spectrum; I: ILL, 8.8 m; II: Gösgen, 38 m; III: Gösgen, 46 m.

It should be noted that the high Δm^2_ν limit depends on a knowledge of the life time τ_n of the neutron, since the inverse neutron decay reaction $\bar{\nu}_e + p \to n + e^+$ was used for the detection of the $\bar{\nu}_e$ in the ILL-Gösgen experiments. The corresponding cross section is approximately proportional to $(E_\nu - Q)^2/\tau_n$, where $Q = 1.8$ MeV. A value of $\tau_n = 912 \pm 18$ sec[11] was adopted in the present evaluation, but some care

must be taken in the light of recent new values for τ_n [12]. If we take this additional uncertainty into account then $\sin^2 2\theta \lesssim 0.2$ ($\equiv \sin^2\theta < 0.05$) is presently a safe limit for $\bar{\nu}_e \to X$ and $\Delta m^2_{\nu\bar{\nu}} \gtrsim 10\ eV^2$ at a 90% confidence level.

The authors wish to acknowledge stimulating discussions with F. Böhm, W. Gelletly, W. Jaus, H.V. Klapdor, H. Kwon, R.L. Mössbauer, P. Vogel, J.L. Vuilleumier and V. Zacek. The technical assistance of the ILL reactor staff and of G. Blanc is much appreciated.

References

1) K. Schreckenbach, H.R. Faust, F. von Feilitzsch, A.A. Hahn, K. Hawerkamp and J.L. Vuilleumier, Phys. Lett. 99B, 251 (1981)
2) F. von Feilitzsch, A.A. Hahn and K. Schreckenbach, Phys. Lett. 118B, 162 (1982)
3) W. Mampe et al., Nucl. Instr. Meth. 154, 127 (1978)
4) A. Sirlin, Phys. Rev. 164, 1767 (1969)
5) B.R. Davis et al., Phys. Rev. C19, 2259 (1979)
6) P. Vogel et al., Phys. Rev. C24, 1543 (1981)
7) H.V. Klapdor and J. Metzinger, Phys. Rev. Lett. 112B, 22 (1982)
8) H. Kwon et al., Phys. Rev. D24, 1097 (1981)
9) J.L. Vuilleumier et al., Phys. Lett. 114B, 298 (1982)
10) R.L. Mössbauer, First ESO-CERN Symposium, November 1983
11) Review of Particles Properties, Phys. Lett. 111B, 91 (1982)
D.H. Wilkinson, Nucl. Phys. A377, 474 (1982)
12) P. Bopp et al., Workshop on "Reactor Based Fundamental Physics", Institut Laue Langevin, Grenoble, Nov. 1983, Proceedings to be published in Journal de Physique

BEAM DUMP EXPERIMENTS AND NEUTRINO OSCILLATIONS

Gianni Conforto *

Istituto Nazionale di Fisica Nucleare, Firenze, Italy

Abstract: Electron - muon universality requires the electron - to muon - neutrino flux ratio in prompt neutrino experiments to be unity independently of the production mechanism. The presently available data indicate that the confidence level for this to be true is only $2 \cdot 10^{-4}$. The consistency of the measurements at various dump - detector distances suggests an interpretation of the data in terms of neutrino oscillations. When this hypothesis is tried on the most recent ('81 - '82) data a fit is obtained with the parameters

$$\Delta m^2 = (360 \pm 40)\ eV^2$$
$$\sin^2(2\alpha) = 0.32\ ^{+0.18}_{-0.08}$$

and a confidence level of about 30%. The results of older prompt neutrino as well as those of other experiments are shown to be in agreement with this result. It is concluded that electron - to tau - neutrino oscillations represent a completely reasonable interpretation of the present prompt neutrino data.

1. Introduction.

There is no a priori reason to believe neutrinos to be massless. If they are not, the weak eigenstates

$$\nu_\alpha = \nu_e, \nu_\mu, \nu_\tau, \ldots$$

are, in the general case, linear combinations of the mass eigenstates

$$\nu_i = \nu_1, \nu_2, \nu_3, \ldots.$$

This leads to the possibility of neutrino oscillations [1]. The relevant notations and formulae are introduced in section 2.

Beam dump or, more appropriately, prompt neutrino experiments [2, 3] are best suited to the study of neutrino oscillations with "large" mass differences ($|m^2(\nu_i) - m^2(\nu_j)| \approx 100 - 1000\ eV^2$). The principle of and the available data from these experiments are presented in section 3.

A fit to these data in terms of neutrino oscillations is described in section 4. The discussion of the results and the conclusions are offered in section 5.

2. Essentials of neutrino oscillations.

In the simplifying case in which oscillations are assumed to occur only between two neutrino species, the probability of an initial ν_α of energy E being equal to a ν_β at a distance L is [1, 2]

$$P(\nu_\alpha \to \nu_\beta) = \sin^2(2\alpha)\ \sin^2(1.27 \cdot \Delta m^2 \cdot \frac{L}{E}) \qquad [1]$$

where: α is the "mixing angle"

$\Delta m^2 = m^2(\nu_1) - m^2(\nu_2)$ in eV^2

L in km

E in GeV.

For $\Delta m^2 \gg E/L$, the formula above reduces to

$$P(\nu_\alpha \to \nu_\beta) = 0.5 \cdot \sin^2(2\alpha). \qquad [2]$$

An experimental upper limit in $P(\nu_\alpha \to \nu_\beta)$ excludes a region in the plane $\sin^2(2\alpha)$, Δm^2 which is not limited at large Δm^2. The present experimental situation [4] is depicted in Figure 1.

3. Beam dump neutrino experiments.

Beam dump experiments [2, 3] are the tool used to investigate the properties of "prompt" neutrinos produced in the (semi) - leptonic decays of short - lived particles.

They are realized by making the high energy proton beam from an accelerator interact in a target, the "dump", several interaction lengths thick. Copiously pro-

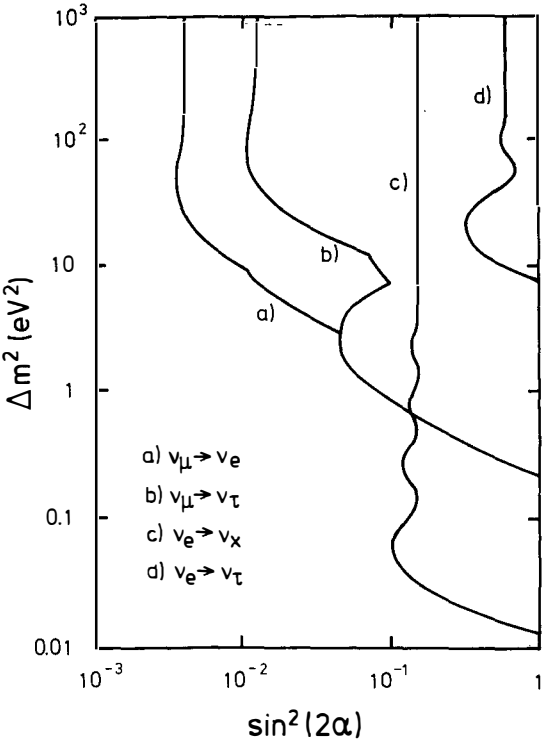


Fig. 1

Fig. 1. Present limits (90% confidence level) to neutrino oscillations. Regions to the right of the curves are excluded.

duced long - lived pions and kaons are mostly reabsorbed in the dump, thus largely reducing the yield of ordinary neutrinos from their decays. This allows the detectors, placed downstream of a muon filter, to be sensitive to the much weaker source of prompt neutrinos. Prompt neutrino rates are obtained either by "subtraction" of the calculated non - prompt component or by "extrapolation to infinite density" of the event rates measured at various dump densities.

All experimental observations indicate that prompt neutrinos originate from the production and subsequent semi-leptonic decays of charmed particles. Thus, electron - muon universality requires the prompt electron - to muon - neutrino (and antineutrino) flux ratio, $\nu_e + \bar{\nu}_e / \nu_\mu + \bar{\nu}_\mu$ or in short ν_e / ν_μ, to be unity independently of the charmed particles production mechanism.

Several measurements of ν_e / ν_μ exist in the literature [5-8] and new results have been reported in the last Summer Conferences [9-12]. Table I contains a summary of these results.

Table I

Experimental determinations of the electron - to muon - neutrino flux ratio ν_e / ν_μ. The years indicated are those in which the data were taken. L is the distance between the dump and the detector. When two errors are quoted the first is statistical, the second systematic.

Experiment	Reference	L(m)	ν_e / ν_μ
CDHS '77	5	890	0.6 ± 0.2
BEBC '79	6	820	$0.59 \, ^{+ 0.35}_{- 0.21}$
CDHS '79	7	890	$0.64 \, ^{+ 0.22}_{- 0.15}$
CHARM '79	8	910	$0.48 \pm 0.12 \pm 0.10$
BEBC '82	9	400	$1.35 \, ^{+ 0.65}_{- 0.35}$
CDHS '82	10	470	$0.83 \pm 0.13 \pm 0.12$
CHARM '82	11	490	$0.59 \pm 0.11 \pm 0.08$
FFMOW '81-'82	12	56	$1.09 \pm 0.09 \pm 0.10$

At first sight it appears that"no conclusion can yet be drawn from the preliminary results of the new experiments; while in 1979 all three experiments at CERN were consistent with a mean value of the ν_e ($\bar{\nu}_e$) to ν_μ ($\bar{\nu}_\mu$) flux ratio of 0.55 $\pm$ 0.08, the 1982 results are not consistent with each other and, if nevertheless combined, also not consistent with the 1979 results" [3].

Indeed, a fit to the hypothesis $\nu_e / \nu_\mu = 1$, assuming Gaussian errors and combining quadratically statistical and systematic errors, yields a confidence level C.L. = 2×10^{-4}.

Of course, it is completely legitimate to ascribe all deviations of ν_e / ν_μ from unity to some hidden systematic effects and wait for better measurements to clarify the situation. However, it is equally legitimate to investigate whether our present knowledge could not be better described by a different hypothesis. At a closer inspection, the data show the remarkable regularity that while all measurements performed at similar values of L are in quite good agreement, different determinations of ν_e / ν_μ are obtained for the various values of L. This is born out by the results of Table II and graphically displayed in Figure 2.

Table II

Determinations of the electron - to muon - neutrino flux ratio ν_e / ν_μ for various values of the dump - detector distance L. These results are obtained by weighted - averaging those of Table I at similar values of L. Statistical and systematic errors have been combined in quadrature. C.L. is the χ^2 - confidence level.

Experiment	L(m)	ν_e / ν_μ	C.L. (%)
CERN '77-'79	820-910	0.57 ± 0.09	∿ 100
CERN '82	400-490	0.74 ± 0.10	10
FFMOW '81-'82	56	1.09 ± 0.13	-

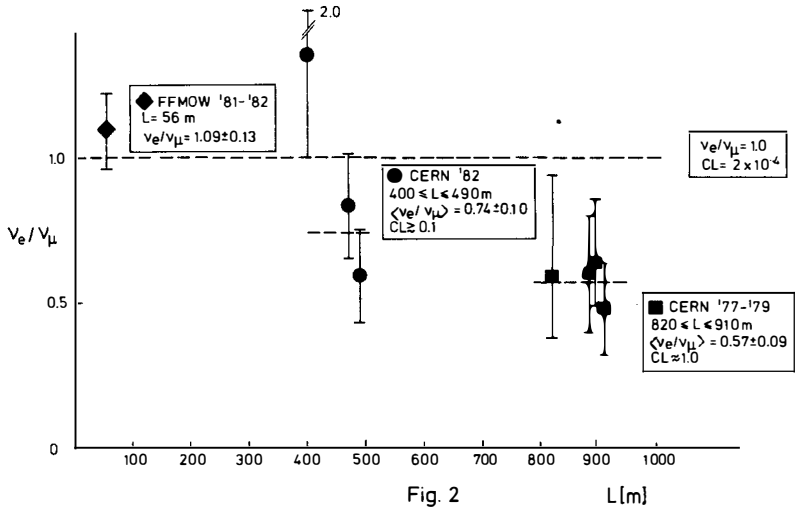


Fig. 2

Fig. 2. The electron - to muon - neutrino flux ratio ν_e / ν_μ plotted as a function of the dump - detector distance L. Dashed lines indicate the weighted averages of the various determinations of ν_e / ν_μ at similar values of L.

4. The fit of the oscillation hypothesis.

A variation of ν_e / ν_μ with L is very suggestive of an oscillatory phenomenon. Since in this case the relevant parameter is L / E (see equation 1), to investigate further this possibility only the recent data on ν_e / ν_μ as a function of E (references 3, 10 and 12) have been used. The limits on muon - neutrino induced oscillations shown in Figure 1 are very tight. This justifies the simplifying

assumption that all deviations of ν_e / ν_μ from unity are due to the electron - neutrino oscillating into a third kind of neutrino, ν_x. It then follows from formula [1] that the electron - to muon - neutrino flux ratio is given by

$$\nu_e / \nu_\mu = 1 - \sin^2(2\alpha) \sin^2\beta \qquad [3]$$

with

$$\beta = 1.27 \cdot \Delta m^2 \cdot L / E. \qquad [4]$$

The experimental determinations of ν_e / ν_μ are averages over various neutrino energy intervals. To account for this, under the assumption of no significant variation of the event energy spectra within each interval, formula [3] becomes

$$\left[\nu_e / \nu_\mu\right]_{E_1 \leq E \leq E_2} = 1 - \frac{\sin^2(2\alpha)}{\beta_2 - \beta_1} \int_{\beta_1}^{\beta_2} \sin^2\beta \, d\beta \qquad [5]$$

A fit of equation [5] to the data of references 3, 10 and 12 yields the result

$$\Delta m^2 = (360 \pm 40)\ eV^2$$

$$\sin^2(2\alpha) = 0.32\ ^{+\ 0.18}_{-\ 0.08}$$

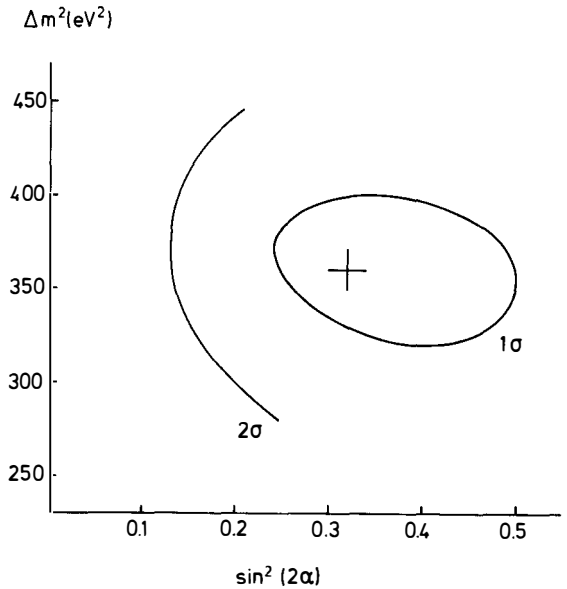


Fig. 3

Fig. 3. The one and two standard deviation contours in the $\sin^2(2\alpha)\Delta m^2$ plane obtained by fitting equation [5] to the ν_e / ν_μ data of references 3, 10 and 12.

with an about 30% confidence level. The one and two standard deviation contours for this solution are shown in Figure 3.

5. Discussion and conclusions.

The existing data on ν_e / ν_μ as well as the result of the fit are displayed in Figure 4.

Only statistical errors have been considered, since presumably systematic errors, by affecting equally all results of the same experiment, do not change the shape of the curve. Although some systematic effects seem to be present (e.g. the CHARM '82 points are always lower than those of CDHS '82) the general consistency of the results within the statistical error bars is quite good as indicated also by the confidence level of the fit.

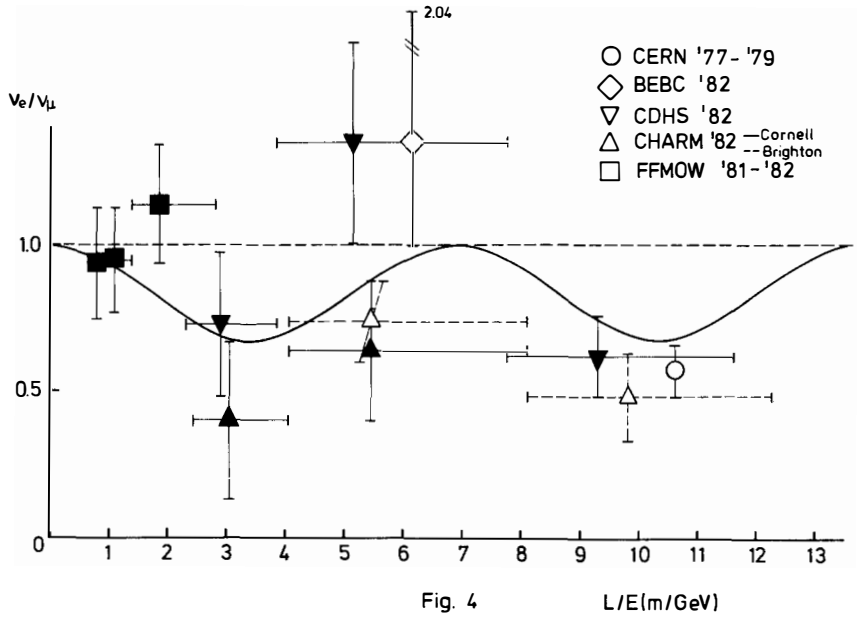


Fig. 4

Fig. 4. Existing determinations of ν_e / ν_μ as a function of L / E. The black points only have been used as input data. Horizontal bars indicate the L / E interval relevant to each value of ν_e / ν_μ. The continuous line represents the result of the fit.

The black points in Figure 4 represent the input data to the fit. Two FFMOW '81-'82 points at L / E < 0.7 m / GeV (E_ν > 80 GeV) have not been used in view of their closeness to L / E = 0. Two data points above L / E ≈ 12 m / GeV (20 < E_ν < 40 GeV), one from CDHS '82 and the other from CHARM '82, have also been discarded as they

correspond to very wide L / E intervals. Between the two existing analyses of the same CHARM data, the one presented at the Cornell Symposium [3] has been selected because of its more readily usable form. The ν_e / ν_μ values of BEBC '82 and CERN '77-'79 (see Table II) are averaged over the whole energy range covered by the experiment and therefore cannot be dealt with by the fitting procedure in its present form. They are plotted in Figure 4 with no horizontal bars at values of L / E corresponding to the average event energy.

All the information not used as input to the fit is in excellent agreement with its result. In addition to the one shown in Figure 3, the fit finds another solution with the first ν_e / ν_μ minimum in the neighbourhood of $L / E \approx 10$ m / GeV. This possibility is however fairly unlikely in view of the rather poor agreement with the BEBC '82 point.

Limits on the probability of an electron - neutrino turning into another type of neutrino are obviously relevant to this analysis. The most stringent result of this type [2, 4] is the one from an experiment at the Goesgen nuclear reactor [13] shown in Figure 1. For large masses the 90% confidence limit is $\sin^2(2\alpha) < 0.15$ and, assuming Gaussian errors, $\sin^2(2\alpha) < 0.28$ at the three standard deviation level. The use of a more recent value for the neutron lifetime could rise the 90% confidence limit to $\sin^2(2\alpha) < 0.2$ [14]. Although the compability with the results of prompt neutrino experiments (see Figure 3) is admittedly rather marginal, no serious inconsistency exists at present.

Curve d) in Figure 1 shows that our current knowledge is totally compatible with the possibility of all deviations of ν_e / ν_μ from unity being due to electron - to tau - neutrino oscillations. It could be objected that the argument ceases to be self - consistent at this point since in some cases (notably the CDHS experiment) the electron - neutrino event rate is not measured directly but rather derived from the observed rate of muon - less events and that this procedure does not discriminate between electron - and tau - neutrino induced events. In fact, it is easy to prove that because all tau - neutrino interactions have at least one neutrino in the final state and because of the $E > 40$ GeV cut introduced in the analysis the effect is very small compared to the statistical errors. Thus, there is no contradiction between the electron - to tau - neutrino oscillation hypothesis and the experimental result that the two methods of determining the electron - neutrino induced rate, when applied to the same set of data (as in the CHARM experiment), yield compatible results, at least at high energy [2].

In conclusion, electron - to tau - neutrino oscillations represent a completely consistent and perhaps even the most reasonable interpretation of the present data.

Acknowledgements. I am very grateful to M. Lusignoli, L. Maiani (Rome) and B. Monteleoni (Firenze) for many illuminating discussions and constructive criticism. I am deeply indebted to U. Rehder (DESY) for her careful drawing of the figures and patient typing of the manuscript.

References

* Address after April 1984: CERN, Geneva, Switzerland

1) S.M. Bilenki and B. Pontecorvo, Phys. Reports 41, 225 (1978)
2) G. Conforto, Proceedings of the 8th International Workshop on Weak Interactions and Neutrinos, Javea, Spain, September 5 - 11, A.Morales Editor, World Scientific, Singapore 1983, p. 43.
3) K. Winter, Proceedings of the 1983 International Symposium on Lepton and Photon Interactions at High Energy, D.G. Cassel and D.L. Kreinick Editors, F.R. Newman Laboratory of Nuclear Studies, Cornell University, Ithaca N.Y., 1983, p. 177.
4) M. Shaevitz, ibid. p. 132.
5) T. Hansl et al., Phys. Lett. 74B, 139 (1978)
6) P. Fritze et al., Phys. Lett. 96B, 427 (1980)
7) M. Jonker et al., Phys. Lett. 96B, 435 (1980)
8) H. Abramowicz et al., Zeitschrift für Physik 13, 179 (1982)
9) A. Parker, Proceedings of the International Europhysics Conference on High Energy Physics, Brighton U.K., July 1983, J. Guy and C. Costain Editors, Rutherford Appleton Laboratory, Chilton, Didcot 1984, p. 310.
10) P. Perez, ibid. p. 316.
11) A. Capone, ibid. p. 312. See also reference 3.
12) B. Roe, ibid. p. 318
13) J.L. Vuillemier et al., Phys. Lett. 114B, 298 (1982)
14) K. Schreckenbach, private communication.

Search for $\overline{\nu}_e$ oscillations at Bugey reactor*

presented by

Jean-Michel THENARD
(LAPP ANNECY LE VIEUX)

ABSTRACT : A high statistic experiment for search of neutrino oscillations has been carried out near a nuclear power plant at Bugey (France), at two distances from the core (13.6 and 18.4 metres). We mesure the neutrino spectrum with the inverse beta decay reaction $\overline{\nu}_e + p \rightarrow n + e^+$. The apparatus is described and the data analysis presented. Some preliminary results at the two positions are shown.

RESUME : Une expérience à haute statistique pour la recherche d'oscillations neutrinos a été réalisée sur le site du Bugey (France), près d'un réacteur nucléaire à deux distances du coeur, 13.6 et 18.3 mètres. Les principales caractéristiques de l'appareillage ainsi que l'analyse de données sont décrites. Des résultats préliminaires relatifs aux deux positions sont donnés.

*Members of the Collaboration are :
Y.DECLAIS, H.DE KERRET, H.PESSARD, J.M.THENARD (LAPP-ANNECY).
J.F.CAVAIGNAC, A.HOUMADA, D.H.KOANG, B.VIGON (ISN-GRENOBLE).
G.GIRARDI (LAPP-Th-ANNECY), part time.

I. NEUTRINO OSCILLATIONS.

Since the prediction of existence of neutrinos, the question of their mass has been raised[1][2]. More recently the grand unified theories, predicts non conservation of baryon and lepton members[3]. Furthermore, in cosmology massive neutrinos would explain the energy deficit in inverse. It would also explain the red shift observed in halo around galaxies.

Neutrino oscillations would imply the two aspects :

.non degeneracy of neutrinos : one of them should have a non-zero mass

.lepton member or lepton flavor is not conserved (depending of neutrino type : Dirac or Majorana).

The hypothesis is that the weak interaction eigenstates $|\nu_e>$, $|\nu_\mu>$ are superpositions of mass eigenstates of the Hamiltonian. The composition of one pure neutrino beam type will evolue with time. It is classical to consider the simplified case where the two neutrino type oscillation is favoured. The neutrino fluw of one type is modulated along the distance L between source and detection by the probability of finding same neutrino at the distance L :

$$P(L/E_\nu) = 1-\sin^2 2\theta \, \sin^2 1.27 \, \Delta m^2 \frac{L}{E_\nu}$$

E_ν neutrino energy (MeV)

L distance (Meters)

Δm^2 is the difference of the squared masses of the two states of neutrinos (MeV)

Δm^2 fixe the oscillation length (period of oscillation)

θ is the mixing angle between two neutrinos and fixes the amplitude of oscillation.

In nuclear reactor experiments we have a pure source of electron-antineutrino with an energy range up to 10 MeV. In this experiment we look for disappearance of $\overline{\nu_e}$: this tests all the possibilities of $\overline{\nu_e}$ oscillations (either the energy balance in reaction is too low to create μ,τ and we can not detect ν_μ, ν_τ, or in Majorana case we could not detect the wrong helicity neutrino).

Using the inverse beta decay reaction we measure the antineutrino spectra at two distances so we can compare

- The spectra of $\overline{\nu_e}$ detected each position to the predicted spectrum issued from calculations using the spectra of the fission products present in the core (more than 260 isotopes with known decay scheme are involved in decays).
- The spectra of $\overline{\nu_e}$ in the two positions. As we will see further this comparison in much free of large systematic errors than the first method.

II. SITE AND DETECTOR.

A. Site : the EDF power plant is located at Bugey near Lyon (France). Four 900 MW pressurized water reactors are running on the site. We took care of background coming from the 3 other reactors.
The reactor under which we installed our apparatus has unique features :

1) Underground position : a foundation raft allowed us to place the detector at close distances from the core in a radiation controlled area :

position 1 : 13,63 $\overline{\nu_e}$ flux $2.0 \times 10^{13}/cm^2 sec$
position 2 : 18.30 $\overline{\nu_e}$ flux $1.1 \times 10^{13}/cm^2 sec$

2) Easy movement between two positions : the active detector can be moved from position 1 to position 2 without changing any part of this apparatus : we will see that different measurements along time permit to cross check the general stability (calibrations, backgrounds).

3) Shielding : the two positions are located below superstructure of the core and completely isolated from the core vessel by 2,5 meters of heavy concrete.

position 1 is shielded by the Uranium of the active core :
30 meters equivalent water
position 2 is just below vapor generator :
18 meters equivalent water.

B. Apparatus : the apparatus we have built has two functions : detection and background rejection.

1) Detector : we use the inverse beta decay reaction to detect the antineutrino events

$$\overline{\nu_e} + p \rightarrow n + e^+ \quad (Q = 1.8 \text{ MeV} \pm \varepsilon)$$

.Neutron detection : The neutron (mean recoil energy 20 KeV) si signed in He(3) proportional counters after thermalisation in the target. The neutron is detected by the capture reaction

$$n + He^3 \rightarrow p + t + 760 \text{ KeV} \quad (\sigma_{capture} = 5500 \text{ barn})$$

The energy deposited in He(3), by this reaction is recorded to clean up neutron from γ background.

Four of these helium counters are interspaced with five planes of 6 target cells. There is no localisation of neutron in He(3) counters. The absolute detection efficiency has been measured with a calibrated antimoine Beryllium source. 204 points of measurement have been done over the whole sensitive volume of the detector

$$\varepsilon_{meas} = 25.33 \pm 2 \%$$

.targets and positron energy measurement : The 5 planes of cells target are made with 6 lucite target cells filled with liquid scintillator (NE 135 C).

The total volume of active oil is 321.14 l 2.016 10^{28} protons.

The total volume of lucite is 476 l 10^{28} protons.

Each target cell is viewed by two photomultipliers. On each side recorded independently in ADC via a multiplexeur. To avoid pile up of low energy background (511 KeV) over good position candidate in ADC, only a group of 12 PM containing the target with deposited energy over hardware threshold of 800 KeV is recorded in the computer.

2) Background rejection :

a) At the two positions, passive background shielding is done by low identical cubic structures which surround the detector. Each face of the cube consists, from inside to outside, of 7 cm thick of low activity lead, 10 cm of liquid scintillator (veto counters), 25 cm of borated water and 10 cm of lead.

b) Active rejection : Each veto counter viewed by one photomultiplier are used to reject cosmic muon induced events. Vetos flag of 10 µs, 500 µs, 1 ms, 1,5 ms duration are associated with the sum of vetos.

In position 1, vetos count 155 hits/sec.

In position 2, vetos count 176 hits/sec.

The scintillator in target (NE 135 C) permits to use pulse shape discrimination (PSD) to reject fast neutron generated by Cosmis rays from good events. Furthermore we read out independently the 4 photomultipliers of a target cell. This permits to reject γ background issued from material around photomultiplier. In the ADC we store the 3 gammas backward in time after neutron arrival in He3 counters to reject events with multiple correlated gammas (cosmic background in surrounding lead).

3) Trigger and readout :

During the data taking, the single counting rates above the hardware thresholds, were typical 350/sec in the targets (mainly gammas) and 1.5/sec in He3 counters for neutrons. For the veto counters they were 155/sec at Position 1 and 176/sec at Position 2. All the single rates were independent of the reactor operation.

The deposited energy, timing and localisation of the neutron and of the three preceding gammas (γ_1 ,γ_2, γ_3) were written on magnetic tape as well as other relevant informations : reactor power, computer deadtime, veto flags of different durations (15, 498, 896, 1440 µsecs), and single rates from camac scalers. The data recording was triggered by a neutron event satisfying He3 pulse-height threshold and veto criteria. In normal data taking, where the

498 μsecs length veto signal was included in the trigger, the trigger rate was 0.31/sec at both positions.

III. ANALYSIS.

A. Monte-Carlo : We compute the energy response $\varepsilon(E_\nu)$ of the whole detector by folding in the spatial neutron efficiency with the complete simulation of the targets (neutrino interactions in lucite, cells edge effects, positron annihilations at rest and in flight, light collection). The kinematical correction to the measured neutrino energy due to the neutron recoil energy[4] is included.

The expected positron spectra $N(E_\nu)$ have been determined by a comprehensive Monte-Carlo simulation. The reactor geometry is fully detailed, rhe measured radial and longitudinal neutron density distributions are used. For each fuel assembly, the different contributions of the four fissile isotopes to the energy production were deduced from the daily state of burn-up provided by EDF[5]. From this calculation, mean values are :

	U^{235}	U^{238}	Pu^{239}	Pu^{241}
Position 1	62.1%	7.6%	26.4%	3.9%
Position 2	47.9%	8.2%	36.9%	7.0%

For U^{235} and Pu^{239}, we take as input for the initial neutrino spectrum the measurement of[6]. Among calculations giving results on the unmeasured U^{238} and Pu^{241} isotopes, we have used those of[7] which are in good agreement with the measurements for U^{235} and Pu^{239}. Due to the low energy tail (edge effects) of the detector energy response and to our statistical significance in the high energy part of the spectrum (up to 8.3 MeV neutrino energies), we need to extrapolate the spectrum of each isotope from 8 to 10 MeV, using the Klapdor at al.calculations[8] which extend up to 9 MeV. In the determination of the expected spectrum, we have separated in the errors on the initial spectrum, the normalization error (4.8%) from the point-to-point errors which affect the shape of the neutrino energy distribution. We use for the neutron lifetime $\tau_{\bar{n}} = 900$ sec[9]. The uncertainty on the cross-section from τ_n is taken as 2.0% reflecting the spread between the experimental measurements. The positron yield is given by :

$$Y(\Delta^2,\theta,L,E_\nu) = \varepsilon(E_\nu) \times N(E_\nu) \times \int_L P_{\nu_e \to \nu_e}(\Delta^2,\theta,\ell/E_\nu)\,d\ell$$

B. Data reduction :

a) Selection :

	Rejection	Rate (Position 1)
Trigger rate		0,31/sec
To select for good neutrinos events we ask for :		
- single He3 counter signal in the neutron window and no veto signal during the 896 preceedings μsec	2	
- good position : the first gamma recorded must have an energy bigger than 1.5 MeV, no 15 μsec associated veto, the four PM of the target should be matched (this rejects 20 % of the gammas which could be be residual activity and HV lakage in sockets)	1.5	
- adjacence between He3 and one unique target	10	
- time between neutron and positron signal less than 200 μsec	1.2	
- PSD signal out of first neutron window which is determined as final event example for each data taking period	1.1	
- no gammas in other targets during 200 μsec after good positron	1.03	
		20.7 evts/hr

b) Corrections factors :

The spectra normalized in time are corrected for the dead times (data acquisition and veto counting every fifteen minutes (1.03 and 1.11), for losses of events due to the PSD (1.01) and $\gamma_1\gamma_2$ time cuts (1.016) and for the losses of events due to the neutron-positron time cut (from the observed $n\gamma$ time distribution in the final two positions sample we get a correction factor of 1.26).

C. Data taking : We took datas from february 1982 to June 1983 :
The table shows the experimental conditions during the data taking.

	Feb.82		Jan.83				June 83
Data Set	Pos1 A	Pos2 A	Pos2 B	Pos2 C	Pos2 OFF	Pos 1 OFF	Pos 1 B
Power (Mwth)	2755.8	2739.1	1636.4	2249.6	-	-	2782.7
Eff.time(Hrs)	1197.6	1401.6	1103.7	623.5	529.2	738.5	936.4
Events/hour	28.27	15.38	10.78	13.43	3.87	3.91	28.57
Nb events	25589	17597	9520	6791	1787	2605	21820

(The events/hour rates are corrected for dead-time and losses, not for neutron efficiency).

a) Survey of apparatus stability : The He(3) efficiency was monitored one day every week using events with 15 μs veto flag, which are mainly induced neutrons cosmic rays and with a Am bi source every month (This source was also used to follow with high statistic the neutron efficiency between the two positions).

The energy calibration was measured with Am/Be gamma source every month.

EDF staff provide us the burn up (fuel evolution) every day.

One tape was written in normal conditions and one for cosmic runs per week.

Figure (1) shows the ratio of energy spectro of the two data sets measured at position 1. The good agreement demonstrates that all effects due to the variation of the energy calibration and apparatus stability have been well controlled over 17 months. At the second position, the reactor was operating at different powers by 100 KeV energy in figure (2). The linearity observed in every energy bin, shows a correct control in particular of the effective time and reactor mean power. For an optimal use of all the information, we extract the positron energy spectrum for the second position from a linear fit of the four data sets available. The ration between fitted reactor off and measured reactor off was flat which shows no sensible background evolution with time.

IV. RESULTS AND COMMENTS.

Figures (3) and (4) shows the experimental position spectra for reactorroncand reactor off position 1 and position 2. The figure (5) shows the ration Data/Expected for the two positions versus L/E.

The figures (6) and (7) shows the ratios Data/Monte-Carlo versus the positron energy. This ratio is different from 1 and not flat as it would be expected for no oscillation. This is statistically significant with errors of the order of 2 % per bin for position 1 (Only statistical errors have been quoted). One natural possible explanation would be a neutrino oscillation. Neither position 2 results no other results constraints this conclusion due to low statistic limitations.

Comments : Differents sources of uncertainties can affect this first position ratio.

a) Normalisation errors : these overall errors are the combination of errors on initial measured $\overline{\nu}_e$ spectrum (4,8 %)[6], measurement of thermal power (1%), neutron cross section (2,2 %) which is poorly known, solid angle (1,5 %), neutron efficiency (1,8 %), relative neutron efficiency with time (1,5 %), number of protons in target (1,8 %), background from the other reactors (0,2 %) and effects of the different analysis cuts and corrections (2,6 %).

Some of these errors will decrease as the analysis progress (specialy solid angle and neutron efficiency where new measurement will appear soon).

The combined overall normalisation error is 10 % which is much bigger than the statistical point to point error.

b) Second source of error is the knowledge initial spectra uncertainties :

.Two isotopes (U^{235} and Pu^{241}). $\overline{\nu_e}$ emission spectra have not been measured some calculations have been done. Figure (8) shows the ratio of expected positron spectra for two hypothesis (Kopeykin, Vogel). All the preceeding plots have been done using Kopeykin's neutrino spectra.

.The $\overline{\nu_e}$ spectra for (U^{235} and Pu^{229}) have been measured up to 8 MeV/c. Due to resolution in target we used to extrapolate this spectra up to 10 MeV/c. How to exptraolate ? We have used "a la Klapdor" extrapolation. Is it the best ?

.Radiatives corrections on measured isotopes spectra and on the cross section $\sigma_{\nu p}$ are only applied as a corrective factor.

.Effect of non isotropic distribution of neutron emitted in $\nu p \rightarrow e^+ + n$ is under study with neutronic program. This could affect by a few percent the absolute normalisation for detector edges.

.Burn-up : from[13] it is possible to study the effects of evolution with time. Figure (9) shows the effect for full year reactor running, calculated by Monte-Carlo.

.Absolute calibration of positron energy : a systematic shift of order of 50 to 100 KeV between experimental spectrum based on our absolute energy calibration (done with gamma sources) and simulated spectrum could exist (Bremsstrahlung and compton scattering could specially cause trouble).

The impact of all these effects have been simulated and lead to distorsion of same order as observed on the datas.

These effects would not effect the ratio position 1/position 2. Furthermore many of the systematic errors will disappear in this ratio (only power, relative neutron efficiency, cuts, burn-up errors will contribute for 2.5 %).

The work is now underway to compare directly the spectra at the two positions 1 and 2 and better conclusion could be drawn.

CONCLUSIONS.

High statistical datas from reactor experiment are available. Data shows a significant deviation from no Υ oscillation neutrino.

Better knowledge of the systematical uncertainties are needed before any final conclusion. The direct comparison of the spectra at two positions would be soon available and will give better answer about neutrino oscillations.

REFERENCES.

(1) Z.Maki, M.Nakasawa and S.Sakata, Prog. Theor. Phys. 23 (1962)870.

(2) B.Pontecorvo, Zh.Eksp. Teor. Fiz. 53 (1967)1717 [traduction : Soviet Phys. JETP 26 (1968)894].

(3) J.N.Bahcall and H.Primakoff, Phys. Rev. D.18 n°9 (1978)3463.

(4) P.Vogel, CERN Preprint Th-3727.

(5) Calculations from Division Calculs Nucleaires of Electricité de France.

(6) K.Schreckenbach et al., Phys. Lett. 99B, (1981)251.
F.Von Feilitzch et al., Phys. Lett. 118B, (1981)162.

(7) V.I.Kopeykin, Sov. J.Nucl. Phys. 32, (1980)1507.

(8) H.V.Klapdor and Metzinger, Phys. Rev. Lett. 48, (1982)127.

(9) D.H.Wilkinson, Progr. Pep. Nucl. Phys. 6, (1980)325.

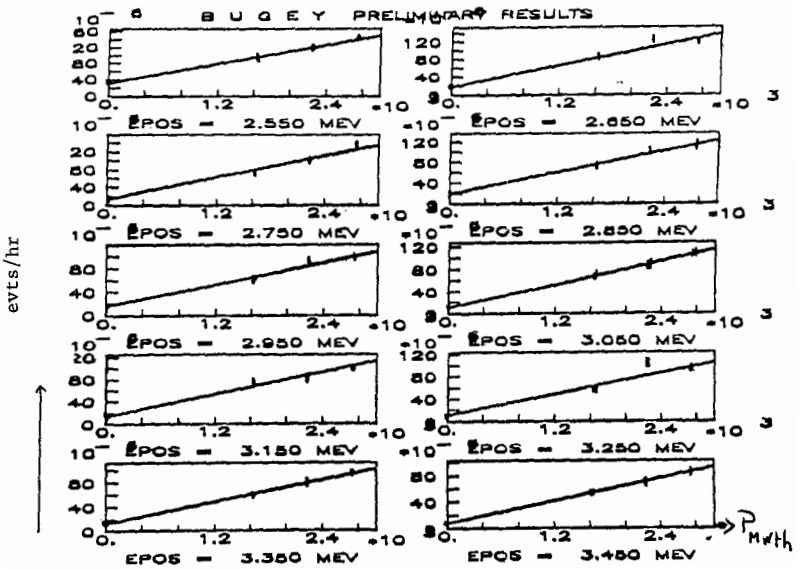


Figure 1 : Position 2, events/hour versus thermal reactor power

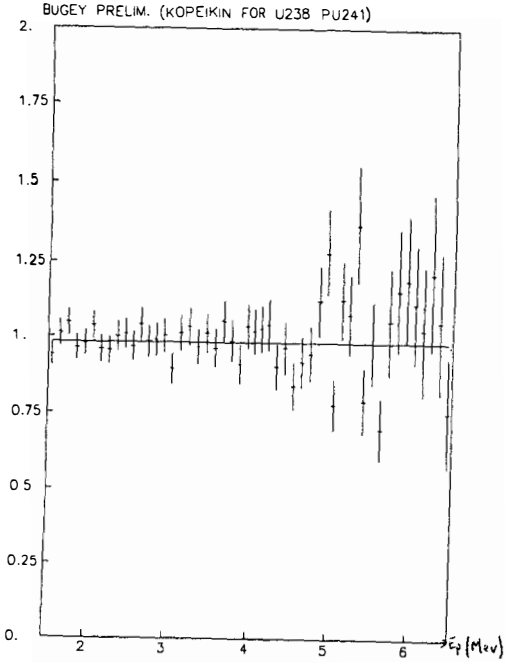


Figure 2 : Ratio between positron spectra in Campaign A over Campaign B in Position 1.

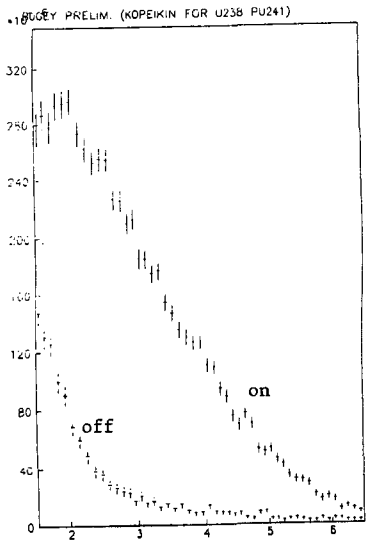


Figure 3 : Positron energy spectra position 1

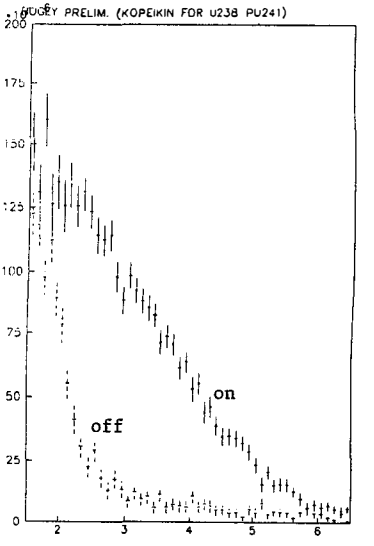


Figure 4 : Positron energy spectrum position 2

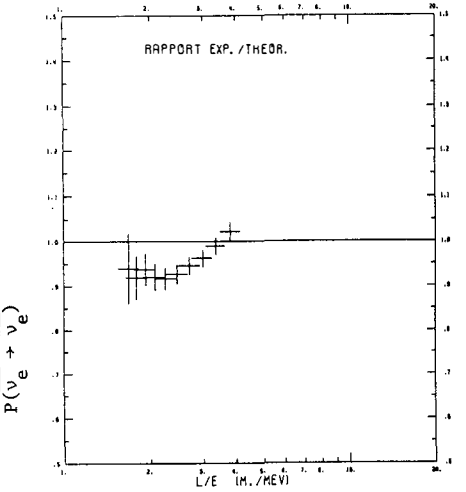


Figure 5 : Transition probabilities as function of L/E_ν position 1

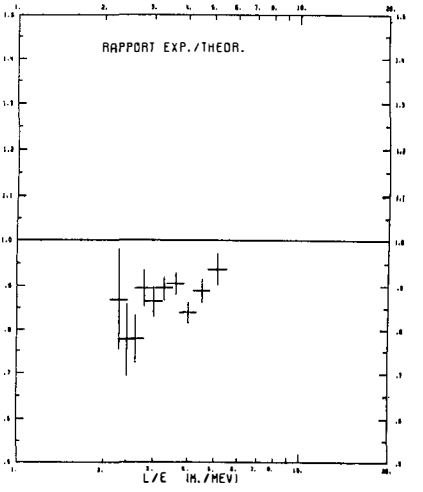


Figure 6 : position 2

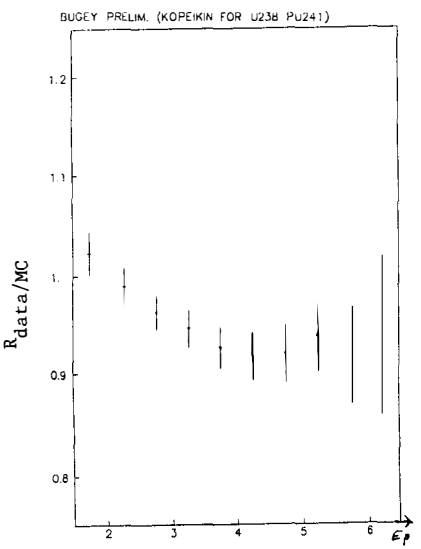


Figure 7 : Data/expected positron spectra, position 1

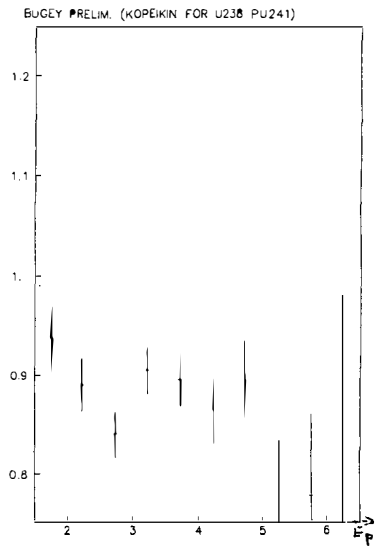


Figure 8 : Data/expected positron spectra, position 2

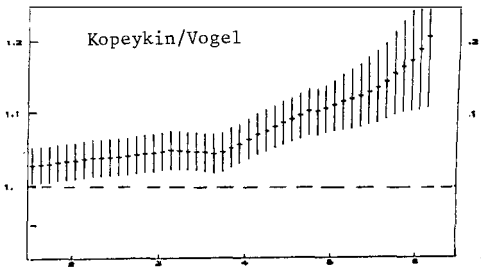


Figure 9 : Ratio between expected spectra with Kopeykin and Vogel hypothesis for unmeasured isotopes.

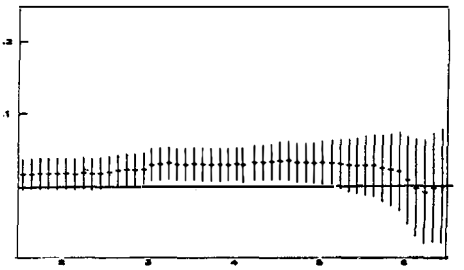


Figure 10 : Effect on expected positron spectra for two fuel composition corresponding to position 1 and 2 data taking

THE HIGH MASS FRONTIER:

LIMITS ON HEAVY NEUTRINOS

Michael Gronau*
Department of Physics, Syracuse University
Syracuse, N.Y. 13210



ABSTRACT

The theoretical motivation for a search for heavy neutrinos is discussed followed by the presentation of typical model dependent expectations for the mixing of the latter with ordinary neutrinos. Present mass and mixing limits on such heavy neutral leptons are based on search for secondary peaks in π and K leptonic decays and on the absence of neutrino decay signatures in neutrino beams from conventional sources and beam dumps. While these limits are quite poor for masses above 1 GeV, we describe methods to extend the limits to masses in the many GeV region. Such limits may be derived from search in b decays, high statistics neutrino experiments, search in ep colliders, W and Z decays and finally - decays of very heavy gauge bosons (if such exist in the TeV region) when produced in multi-TeV pp and $\bar{p}p$ colliders.

---

*on leave from Technion, Haifa, Israel.

I. Theoretical motivation

Whereas the rest of this meeting is devoted dominantly to light neutrinos, today we will investigate the "high mass frontier". In this review a variety of methods will be described to search for heavy neutrinos.[1] Some of these studies were already made in experiments[2] and others may be carried out soon or in the future.

A search, in the mass range of order 10 MeV to 1 GeV and much beyond it, may be motivated by two independent sequences of arguments:

a) The present upper limits on the masses of the e, μ and τ neutrinos (60 eV, 500 KeV and 250 MeV respectively) deteriorate considerably with generation number. If a fourth charged lepton is to be discovered, in e^+e^- collisions or in W, Z decays for instance, the direct limit on the mass of its neutrino will most probably lie in the few GeV region. Search for neutrinos in the mass range of order 10-100 MeV (in which ν_τ may have its mass) up to a few GeV (in which a higher generation neutrino may exist) is therefore of considerable interest.

b) The second motivation is based on the frequently asked question: "Where are the right-handed neutrinos?" The remarkable observation that neutrinos have been observed only in left-handed forms, whereas all other observed fermions appear in both left and right chirality states, has led to two types of interpretation: The first one, for which SU(5) GUT is an example[3], attributes this observation to the fundamental handedness of the interactions. Thus in SU(5) the reducible $\bar{5}+10$ representation, believed to give rise with its fermion content to all the possible gauge interactions, contains only a left-handed neutrino. An alternative view, suggested by an SO(10) based GUT[4], is that this phenomena is merely a consequence of a left-right asymmetry in the neutrino mass spectrum. SO(10) accommodates the left-handed neutrino and its right-handed partner (and to this matter indeed unifies all quarks and leptons) in a single irreducible 16 representation. The masses of the right-handed neutrinos are expected to be extremely heavy[5] if they originate from a GUT scale but could be in the region of 100 GeV[6] or even of order 1 GeV[7] if they are related to some intermediate mass scale. In particular, if this mass scale is that of parity restoration in the left-right symmetric $SU(2)_L \times SU(2)_R \times U(1)$ theory[6,8], one may envision a situation[7] in which $m(W_R)$=1-10 TeV[9] and $m(\nu_{eR})$ =1-10 GeV. Such circumstances

are not at all disfavored by our experience with ratios of gauge boson (W_L) to fermion (u quark) masses (or alternatively - the ratio of gauge to Yukawa couplings).

II. Expectations for the mixing of heavy neutrinos with light ones

In certain grand unified theories, such as the ones referred to in Sec. Ib, heavy neutrinos N_a (a more appropriate term for these objects would be "heavy neutral leptons") exist which are almost pure isosinglets under weak SU(2). In the weak isodoublet states n_i (i=e,μ,τ) these heavy mass eigenstates mix very slightly with the familiar light neutrinos ν_i

$$n_{iL} \simeq \nu_{iL}(1-\frac{1}{2}\sum_a |U_{ia}|^2) + \sum_a U_{ia}N_{aL} \qquad (1)$$

Here and throughout this entire talk we will disregard possible mixing among light neutrinos. The charged and neutral weak current involving neutrinos are (ℓ_i=e,μ,τ)

$$J^\mu_{cc} = \sum_i \bar{n}_{iL}\gamma^\mu \ell_{iL} \qquad J^\mu_{nc} = \sum_i \bar{n}_{iL}\gamma^\mu n_{iL} \qquad (2)$$

Let us now concentrate on two types of models to which eqs. (1) and (2) apply, to anticipate the possible values of the heavy neutrino masses (M_N) and their mixing with the light neutrinos (U_{iN}).

a) Massive Majorana neutrino model

In the version of the type of models suggested in Refs. 5 and 6, in which mixing among generations is disregarded for simplicity, the light and heavy neutrinos are described by Majorana fields and are the eigenstates of the mass matrix

$$M_i = \begin{pmatrix} 0 & \mu_i \\ \mu_i & M_{N_i} \end{pmatrix} \quad i=e,\mu,\tau \qquad (3)$$

where $M_{N_i} >> \mu_i$. The mass eigenvalues are approximately M_{N_i} (a Majorana mass) and μ_i^2/M_{N_i} (μ_i=a Dirac mass). The mixing parameters are

$$U_{iN_i} \simeq -\mu_i/M_{N_i} \qquad (4)$$

The Dirac mass μ_i may be related in grand unified theories to the corresponding charge 2/3 quark mass, divided by 3 to account for renormalization group corrections.[10] To allow for a factor 3 uncertainty in such estimates we take

$$\mu_i = (m_{q_i}/3)3^{\pm 1} = \begin{matrix} 0.5\text{-}5 \text{ MeV} & q_1=u \\ 150\text{-}1500 \text{ MeV} & q_2=c \\ 2.5\text{-}25 \text{ GeV} & q_3=t \end{matrix} \qquad (5)$$

where we have arbitrarily taken m_t=25 GeV.
Eqs. (4) (5) with the present upper bounds on neutrino masses lead to the allowed regions of (M_N, $|U_{iN}|^2$) as described in Fig. 1a. Note that lower heavy neutrino masses and smaller mixing parameters would be allowed if μ_i is related to the corresponding charged lepton mass rather than the quark mass.[7]

In the model of Ref. 6 the heavy neutrino may couple to the corresponding charged lepton via the exchange of W_R or by W_L-W_R mixing (ξ). The corresponding mixing parameters, supplementing those of eq. (4), are $m^2(W_L)/m^2(W_R)$ and ξ respectively for which rather stringent upper limits exist.[9]

b) Massless neutrino model

The light neutrino may be strictly massless due to some discrete symmetry.[11] The heavy neutrinos obtain their Dirac mass by mixing with additional weak isosinglets. In this model, extensively studied in Ref. 12, a light neutrino may mix with more than just one heavy neutrino. The mixing parameters U_{iN_j} may again be expressed in terms of the charge 2/3 quark masses and are again inversely proportional to the heavy neutrino masses. The explicit expressions may be found in Ref. 12. They lead to the allowed regions of (M_{N_j}, $|U_{iN_j}|^2$) as shown in Fig. 1b.

Altogether we conclude from Figs. 1a and 1b, which describe the possibilities within the two different types of models, that heavy neutrinos in the 1-10 GeV mass range could exist with mixing to light neutrinos which might be extremely small. One should note at this point that for $M_{N_i} > m_\pi$ there are some model-independent universality constraints on the mixing parameters which imply[1,12]

$$\sum_i |U_{eN_i}|^2 \lesssim 4.3\% \qquad \sum_i |U_{\mu N_i}|^2 \lesssim 0.8\% \qquad (6)$$

A considerably weaker constraint applies to $U_{\tau N_i}$.

III. Lifetime estimates and typical branching ratios

It follows from eqs. (1) (2) that in the decays of a heavy neutrino both charged and neutral weak currents can contribute.

This is shown in Fig. 2, in which the same mixing parameters U_{iN} appears in the W and the Z-mediated diagrams. The total decay rate may be expressed in terms of the muon decay rate

$$\frac{\Gamma_N}{\Gamma_\mu} = \sum_i |U_{iN}|^2 \Phi_i(M_N) \left(\frac{M_N}{M_\mu}\right)^5 \qquad (7)$$

where Φ_i counts the effective number of unit-strength charged-current channels. Using the explicit matrix element and phase space expressions with appropriate fermion masses, the following somewhat simplified best-fit expressions are obtained for heavy neutrinos mixing with the three types of light neutrinos:[1]

$$\tau_{N_e} = 4.15\times10^{-12}\ \text{s}\ (M_N/1\ \text{GeV})^{-5.17}|U_{eN}|^{-2}$$
$$\tau_{N_\mu} = 4.49\times10^{-12}\ \text{s}\ (M_N/1\ \text{GeV})^{-5.19}|U_{\mu N}|^{-2}$$
$$\tau_{N_\tau} = 1.08\times10^{-11}\ \text{s}\ (M_N/1\ \text{GeV})^{-5.44}|U_{\tau N}|^{-2} \qquad (8)$$

These expressions apply to $M_N \lesssim 50$ GeV beyond which W, Z propagators (and later on decays into real W, Z's) start to be important. As an illustration of the lifetimes one may expect Fig. 3 shows lines of fixed τ_{N_μ} in the $(M_N, |U|^2)$ plane. One may view this figure in conjunction with the mass and mixing values expected in specific models (Figs. 1a, 1b) to appreciate the enormous range of possibilities. The average decay path length may range all the way from sub-millimeters to hundreds of meters.

Branching ratios into various classes of final states may be similarly estimated. Typical values, for the range $M_N \lesssim 50$ GeV, are given below

type of mode	$\ell^+\ell^-\nu$	neutrinos	ℓ^-+hadrons	ν+hadrons
branching ratio	0.2	0.1-0.2	0.4-0.5	0.2

These values depend crucially on the existence of the neutral current couplings of the heavy neutrinos to the light ones. At this point we wish to stress that in general the presence of such couplings will diminish the detected decay signal of N into a charged-current mode (such as $\ell^+\ell^-\nu, \ell^-$+hadrons). Moreover, it turns out that the decay $N_e \to e^+e^-\nu_e$, for instance (searched for in one of the experiments described later on), suffers from destructive interference between the charged and neutral current amplitudes. Its branching ratio for M_N=1-2 GeV is found to be 8% rather

than the purely charged-current value of 20%.

In the following we will use eqs. (1) (2) to study various phenomena in which heavy neutrinos may be detected. In some of these studies (such as that of the beam dump results) the limits on the mixing which we derive are more conservative than those based on purely charged current decays of N. On the other hand other phenomena (such as the production of N's in neutrino interactions) rely heavily on the mere existence of these neutral current couplings. In the more naive view (Ia) that the heavy neutrinos are members of a higher generation isodoublet and mix with the light ones, just as quarks do, such couplings are expected to be GIM suppressed.

IV. Present mass and mixing limits

a) Secondary peaks in π, $K \to \ell\nu$ (ℓ=e,μ)

If $M_{N_i} < M_{\pi(K)} - M_\ell$ then eq.(1) would lead to secondary peaks in the momentum spectra of the lepton ℓ with rates proportional to $|U_{\ell N_i}|^2$ [13]. The nonobservation of such peaks in several such experiments, the branching ratio measurements of π, $K \to e\nu$ and a study of muon decay have led to the limits shown in Fig. 4. The limits extend to M_N=160 and 310 MeV for $|U_{eN}|^2$ and $|U_{\mu N}|^2$ respectively and are at best of order 10^{-5}-10^{-6}. Some improvement of these limits is expected from future experiments.[15]

b) Heavy neutrino decays in conventional beams

If the neutrino weak eigenstate (1) contains a (tiny) component of a heavy mass eigenstate, again with $M_N < M_{\pi(K)} - M_\ell$, then neutrino beams from π and K decays will contain a fraction of heavy neutrinos which may decay in flight.[16] Since the relative abundance of the heavy neutrinos in the beam is proportional to $|U_{\ell N}|^2$ and so is also their decay rate (into $e^- e^+ \nu_e$, $e\mu\nu$, $e\pi$ etc.) one may wonder whether the decay signature remains feasible for small mixing parameters. To argue that indeed this is the case we have compared in Ref. 16 the heavy neutrino (energy E_N in GeV) decay rate to the $\nu_\mu e$ neutral current interaction rate (at energy E, on a target with density ρ) for equal decay and interaction length.

$$\frac{\Gamma(N \to e^- e^+ \nu)}{\Gamma(\nu_\mu e \to \nu_\mu e)} \simeq 3 \times 10^{12} |U|^4 \frac{(M_N/M_\mu)^6}{\rho E E_N} \text{ (kinematic helicity factor)} \quad (9)$$

The very large coefficient, of order 10^{12}, is an indicator of the

high sensitivity of a neutrino decay search in the mass range $M_\pi < M_N < M_K$ to very small mixing, typically of order 10^{-5} to 10^{-6} or smaller. In fact eq.(9) may be used to infer bounds on $|U_{eN}|^2$ from previous measurements of the $\nu_\mu e$ cross section at high energies.[17] At high energies the e^+e^- pairs from $N \to e^+e^-\nu_e$ would emerge in the forward direction with a very small opening angle, mostly smaller than the angular resolution of an electron shower in the detector. Such events could not be distinguished from the $\nu_\mu e$ scattering events. A rather conservative bound may therefore be obtained by quite safely assuming that the decay rate is just smaller than the measured rate of $\nu_\mu e \to \nu_\mu e$ (which agrees with the standard model prediction). When applying this limit to each of the two experiments of Ref. 18 one derives the bounds $|U_{eN}|^2 < 10^{-6}\text{-}10^{-5}$ for $160 < M_N < 480$ MeV as shown in Fig. 4.[19] Some improvement of these limits was made by a reanalysis of the combined neutrino and antineutrino data of the second on Ref. 18,[20] and is also shown in Fig. 4. Using a reported sample of anomalous μe events observed at a low energy neutrino experiment[21] the limits on $|U_{\mu N}|^2$ may be extended up to $M_N = 380$ MeV with values in the vicinity of 10^{-6}.[17]

It was pointed out in Refs. 16, 17 that an improvement of these limits (obtained as by products) by a couple of orders of magnitude is expected to be achieved through a direct search for neutrino decay in flight (in particular in low-energy neutrino beams) by specially designed decay detectors. A high energy neutrino decay experiment is currently under progress[22] and a low energy experiment is scheduled for this summer.[23]

c) Heavy neutrino decays from beam dump sources

In order to consider the mass range $M_N > M_K$ heavier sources of N's must be considered, for instance charmed meson decays. Charm production and subsequent leptonic decays were observed in beam dump experiments by the interaction of the (prompt) decay neutrinos. The detected leptons have properties (e.g. rates, energy and transverse-momentum spectra) which agree with the hypothesis of charm production. A conservative assumption, in analogy with the one made in subsection b, is that if heavy neutrinos emerge from the decay of charmed hadrons their own decay rates into electrons and muons is just smaller than the observed lepton rates. This then leads to bounds of order $10^{-6}\text{-}10^{-5}$ on both

$|U_{eN}|^2$ and $|U_{\mu N}|^2$ for $0.5<m_N<1$ GeV.[24]

Recently the results of a beam dump experiment with a decay detector were reported by K. Winter.[22] In ref. 1 we made a parallel analysis of the same experiment, the result of which I wish to present here in order to stress the assumptions involved in such a study. The quantities required for the analysis include the following:

1. The D (F) production cross section and their x,p_T distribution. (We use $\sigma=27\mu b$ at $E_{lab}=400$ GeV and a distribution $(1-x)^4 e^{-2m_T}$.)[25]

2. The branching ratios of $D\to N\ell$ and $D\to(S=-1)N\ell$ ($F\to N\ell$) as a function of M_N. (We use $f_D=f_K$[26] for the former and the spectator model for the latter.)

3. The branching ratio of the particular decay mode of N which is searched for (8% for $e^+e^-\nu_e$).

4. The geometric acceptance (we find an average value of 2%).

5. The decay probability of N within the detector, which depends on its average decay path L, on the detector length Δ and on its distance from the beam dump ℓ_1; $P_d=e^{-\ell_1/L}(1-e^{-\Delta/L})$. ($\Delta=35$m, $\ell_1=480$m).

The resulting region of M_N and $|U_{eN}|^2$ excluded by the absence of a detectable decay $N\to e^+e^-+\ldots$ is shown by the combined solid curve (based on $D\to Ne$) and dotted curve (based on $D\to(S=-1)N\ell$) of Fig. 5. Also shown in this Figure are the limits quoted in Ref.22, which were based on somewhat less conservative assumptions (for 1,2,3). If analyzed in terms of the sequence $D\to N\mu$(+ strange) $N\to\nu_\mu e^+e^-$ (allowed via the neutral current), this experiment may be used to derive similar however somewhat weaker bounds on $|U_{\mu N}|^2$. (the branching ratio into $e^+e^-\nu_\mu$ is merely 2%.) In order to obtain bounds on the latter parameter independent of the existence of heavy-to-light neutral currents, decays into muons must be searched for. Note the large $|U|^2$ region which may not be excluded, since heavy neutrinos would decay before reaching the detector. This region may be partially filled in by beam dump experiments with a relatively short distance ℓ_1.[28]

V. Future expected mass and mixing limits

a) b production and an ideal beam dump experiment

In principle b production in hadronic collisions may extend the limits to higher values of M_N. In practice however there exists

no evidence yet for this process. Estimates of $2\sigma(B)$ at 400 GeV range from 10 to 100 nb.[1,27] The CHARM experiment[22] may be analyzed in terms of b decays viewed in the spectator model as $b \to cN\ell$. The dashed-dotted and dashed lines in Fig. 5 indicate the excluded regions for B cross section of 100 and 10 nb respectively. The limits of Fig. 5 may be considerably extended by an "ideal dump" experiment, which would have all other parameters as the CHARM experiment, except ℓ_1 reduced from 480 m to 50 m, geometric acceptance increased to 10% and beam momentum doubled to 800 GeV/c. The range of parameters that may be excluded in such an experiment is shown in Fig. 6. It extends up to M_N=2.5-3 GeV for values of $|U|^2$ down to about 10^{-6}, however does not include relatively large values of $|U|^2$.

b) B decays in e^+e^- annihilation

Since e^+e^- annihilation provides copious sources of b quarks and since the decay of the heavy neutrinos may be detected here close to the point of production, these experiments may fill in the large $|U|^2$ region. As an illustration of the potential limits derivable from this type of experiment we have studied in Ref. 1 the actual case of B production at the $\Upsilon'''(4S)$.[29] The result of this study, based on a sample of 8.4×10^4 $B+\bar{B}$'s and on the assumption that no $\ell^{\pm}$+3 prong secondary vertex is detected at a distance of 3 mm to 8 cm from the production point, are shown in Fig. 7. An increase of statistics by an order of magnitude may fill in the large $|U|^2$ gap of Fig. 6, up to M_N=1.7 GeV.

c) High statistics neutrino experiments

If neutral currents couple light neutrinos to heavy ones, as assumed in eqs. (1), (2), then the latter may be produced in neutrino interactions. The production rate is simply given by the ordinary neutral current cross section times $|U|^2$ and a mass dependent threshold factor. This factor, calculated in Ref. 1, indicates a strong suppression for masses much above 5 GeV at present neutrino energies. In high statistics neutrino experiments one might expect the order of a million neutral-current events. These experiments may therefore search the region $|U|^2 > 10^{-6}$, $M_N < 5$ GeV.

As seen in Fig. 3 the expected N-lifetimes in this region range from 10^{-5}s (M_N= 1 GeV, $|U|^2=10^{-6}$) to 10^{-13} s (M_N=5 GeV, $|U|^2=10^{-2}$). Corresponding to these values one may encounter one of the three possibilities: Decays in the shielding hundreds of

meters upstream of the detector, decays within the detector of heavy neutrinos produced in the detector and instantaneous decays. In the first case the events are characterized by a limited total effective mass and in the last one the detected lepton will exhibit unusual kinematical behavior. For Majorana N's one may expect wrong-sign single leptons. A search for wrong-sign μ^+ in neutrino scattering was carried out quite a few years ago.[30] Based on the limits of this experiment we crudely estimate that Majorana N's with $M_N \lesssim 3$ GeV, $|U_{\mu N}|^2 \gtrsim 10^{-3}$-$10^{-2}$ may be excluded. To figure out what kind of limits may be derived when searching for a second (decay) vertex in the detector, we considered in Ref. 1 a detector of length 10 m and a nominal energy of 100 GeV. If no more than one event out of 10^4 or 10^6 neutral-current events is observed with the second vertex at least 10 cm from the primary one, one would obtain the contours of bounds shown in Fig. 8. We see that these experiments may investigate the hitherto unsearched domain $M_N \lesssim 3$-5 GeV, $|U|^2 > 10^{-5}$-10^{-3}.

d) Charged lepton scattering on nucleons

Fast muons from π and K decays are highly polarized. The V-A amplitude of the process μ+nucleon$\to$N+... is suppressed by the wrong helicity of the muons and may not provide very useful limits on the mixing $U_{\mu N}$. This process may be used however to search for V+A couplings[31] and some bounds on $m(W_R)/m(W_L)$ might be obtained thereby. In ep colliders electrons are expected to appear with both longitudinal polarization, and it seems feasible to collect a sample of at least 10^4 ep$\to\nu_e$+... events in an experiment with $\sqrt{s} \gtrsim 200$ GeV.[32] An experiment which is sensitive to a single N event - detected by a secondary vertex if M_N=several GeV, or by some anomalous lepton structure if M_N is heavier - may set bounds of order 10^{-4} on $|U_{eN}|^2$,

e) W and Z decays

The decay rates of $W\to\ell\bar{N}$ and $Z\to\nu\bar{N}$ are given by the corresponding rates into $\ell\nu$ and $\nu\bar{\nu}$ times $|U|^2$ and a kinematic suppression factor. The decay $Z\to N\bar{N}$ is suppressed by $|U|^4$ (eqs. (1) (2)), unlike the case of a higher generation isodoublet where it suffers merely from the mild kinematic suppression.[33] In a large $p\bar{p}$ colliding beam experiment one may expect 10^4W decays into $e^{\pm}\nu$, which may explore the region $|U|^2 \gtrsim 10^{-4}$ for masses which are substantial fractions of M_W. Similarly e^+e^- collisions at $\sqrt{s}=M_Z$ may

eventually accumulate the order of 10^6 Z's. This may enable extending the limits on the mixing down to 10^{-5}. The decays $Z \to \nu\bar{N}$, $\bar{\nu}N$ would be spectacular with their unbalanced jets.

f) W_R and Z_2 decays

One of the motivations of a search for heavy neutrinos, pointed out in the introduction, is the hunt for the right-handed neutrino. Theories which accommodate such fermions (i.e. SO(10) GUT) have a right handed W_R and a second Z_2, which decay into ℓN and $N\bar{N}$ respectively unsuppressed by mixing.[34] In Ref. 1 we estimated the production of W_R and Z_2 in multi-TeV pp and $\bar{p}p$ colliders. As an illustration - it is found that for a $\bar{p}p$ experiment at $E_{c.m.}$=40 TeV, sensitive at the $\sigma B = 10^{-39} cm^2$ level, one may envision production of W_R up to $m(W_R)$=10 TeV. The decay N's could be just nearly as heavy.

VI. Two Concluding remarks

a) The hunt for the right-handed neutrino, which may also serve to search for a high generation heavy neutrino, has just started. In a decade or two we may reach four orders of magnitude beyond the present mass limit of 1 GeV.

b) Since $M_\nu \propto M_N^{-1}$ (eq. (3)) the search for heavy neutrinos described in this talk is intimately related to the major effort made in attempting to improve the limits on light neutrino masses.

Acknowledgement

Much of this talk is based on work done with C.N. Leung and J.L. Rosner, to both I deeply thank for an enjoyable collaboration. I also wish to thank Francois Vannucci for providing me an opportunity to present this talk and Jean Tran Thanh Van for his warm hospitality and for a very successful meeting. This work was supported by the U.S. Department of Energy under contract no. DE-AC02-76ER03533.

References

1. This talk is based to a major extent on a recent work with C.N. Leung and J.L. Rosner, University of Chicago report EFI 83/63, January 1984. This paper contains an extensive list of references for previous phenomenological and experimental studies of neutral heavy leptons.
2. See for instance talks by R. Prieels, A. Olin, F. Vannucci, M. Levi, and C. Santoni at this meeting.
3. H. Georgi and S.L. Glashow, Phys. Rev. Lett. 32, 438 (1974).
4. H. Georgi, in Particles and Fields - 1974, Proceedings of the Meeting of the APS Divisions of Particles and Fields, Williamsburg, Virginia, edited by C.E. Carlson (AIP, New York, 1975), p.575; H. Fritzsch and P. Minkowski, Ann. Phys. N.Y., 93, 193 (1975).
5. M. Gell-Mann, P. Ramond and R. Slansky, in Supergravity, edited by D.Z. Freedman and P. van Nieuwenhuizen (North-Holland, Amsterdam, 1979), p.315; T. Yanagida, in Proceedings of the Workshop on Unified Theory and Baryon Number of the Universe, edited by O. Sawada and A. Sugamoto (KEK, Tsukuba, Japan, 1979).
6. R.N. Mohapatra and G. Senjanovic, Phys. Rev. Lett. 44, 912 (1980); Phys. Rev. D23, 165 (1981).
7. M. Gronau and S. Nussinov, Fermilab-Pub-82/52-THY, 1982 (unpublished); M. Gronau and R. Yahalom, Nucl. Phys. B236, 233 (1984).
8. J.C. Pati and A. Salam, Phys. Rev. D10, 275 (1974).
9. G. Beall, M. Bander and A. Soni, Phys. Rev. Lett. 48, 848 (1982); G.C. Branco, J.M. Frere and J.M. Gerard, Nucl. Phys. B221, 317 (1983); H. Harari and M. Laurer, Fermilab Report FERMILAB-Pub-83/59-THY, July 1983 (unpublished).
10. A.J. Buras, J. Ellis, M.K. Gaillard and D.V. Nanopoulos, Nucl. Phys. B135, 66 (1978).
11. D. Wyler and L. Wolfenstein, Nucl. Phys. B218, 205 (1983).
12. C.N. Leung and J.L. Rosner, Phys. Rev. D28, 2205 (1983).
13. R.E. Shrock, Phys. Lett. 96B, 159 (1980); Phys. Rev. D24, 1232 (1981).
14. a) D.A. Bryman et.al., Phys. Rev. Lett. 50, 1546 (1983).
    b) R.E. Shrock, Ref. 13, based on K. Heard et.al., Phys. Lett. 55B, 327 (1975) and J. Heintze et.al., Phys. Lett. 60B, 302 (1976).
    c) R. Abela et.al., Phys. Lett. 105B, 263 (1981).
    d) R.E. Shrock, Phys. Rev. D24, 1275 (1981).
    e) R.S. Hayano et.al., Phys. Rev. Lett. 49, 1305 (1982).
    f) C.Y. Pang et.al., Phys. Rev. D8, 1989 (1973).
15. R. Prieels and A. Olin, talks at this meeting.
16. D. Toussaint and F. Wilczek, Nature 289, 777 (1981); M. Gronau, SLAC report SLAC-PUB-2967, Aug. 1982 (unpublished).

17. M. Gronau, Phys. Rev. D28, 2762 (1983).

18. R.H. Heisterberg et.al., Phys. Rev. Lett. 44, 635 (1980); M. Jonker et.al., Phys. Lett. 105B, 242 (1981); 117B, 272 (1981).

19. See eqs. (11) (12) of Ref. 17.

20. F. Bergsma et.al., Phys. Lett. 128B, 361 (1983) and C. Santoni at this meeting.

21. H. Faissner et.al., Z. Phys. C10, 95 (1981).

22. K. Winter, talk at the 1983 International Symposium on Lepton and Photon Interactions at High Energies, Cornell University, August 1983; C. Santoni at this meeting.

23. F. Vannucci and M. Levi, talks at this meeting.

24. M. Gronau, Proceedings of the International Workshop on Electroweak Interactions at High Energies, DESY, Hamburg, September 1982, edited by R. Kogerler and D. Schildknecht (World Scientific Publishing Company) p.143 and Ref. 17.

25. R.C. Ball et.al., UM HE 83-11 and UM HE 83-13. There is some uncertainty about the magnitude of the cross section and the x distribution; B. Roe, private communication and J. Walker, at this meeting.

26. C.H. Albright, R. Shrock and J. Smith, Phys. Rev. D20, 2177 (1979); E.G. Floratos, S. Narison and E. de Rafael, Nucl. Phys. B155, 115 (1979); H. Krasemann, Phys. Lett. 96B, 397 (1980).

27. F. Halzen, Proceedings of the 21st International Conference on High Energy Physics, Paris, France, July 1982, edited by P. Petiau and M. Porneuf (Les Editions de Physique, 1982) p. C3-381.

28. e.g. the experiment of Ref. 25.

29. M. Gronau, N. Horwitz and J. Rosner, CLEO Internal Note, CBX 84-6, January 1984.

30. M. Holder et.al., Phys. Lett. 74B, 277 (1978). I thank M. Shaevitz and J. Wotschak for informing me about this experiment.

31. K. Winter, Phys. Lett. 67B, 236 (1977); A.R. Clark, Phys. Rev. Lett. 46, 299 (1981).

32. T.A. O'Halloran, Jr., Proceedings of the 1982 DPF Summer Study of Elementary Particle Physics and Future Facilities, Snowmass, Colorado, 1982, p.82.

33. R. Shrock, Proceedings of the 1982 DPF Summer Study, Snowmass, p.261; F. Vannucci at this meeting; V. Barger, W.Y. Keung and R.J.N. Phillips, University of Wisconsin preprint MAD/PH/152 (1984); R. Thun, Univ. Michigan, UM HE 83-21.

34. W.Y. Keung and G. Senjanovic, Phys. Rev. Lett. 50, 1427 (1983).

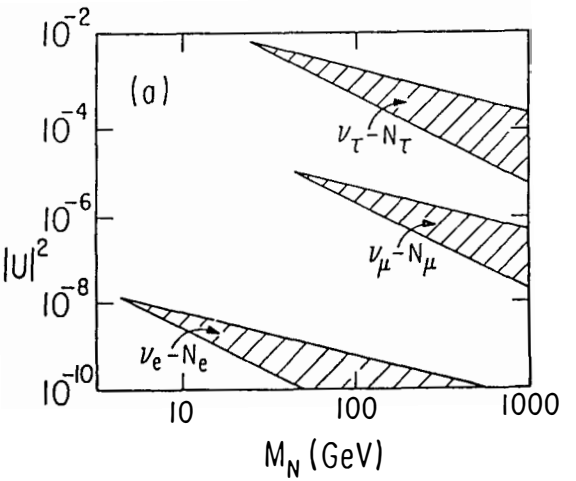


Fig. 1a. Boundaries of allowed regions of $(M_N, |U|^2)$ in the type of models suggested in Refs. 5, 6.

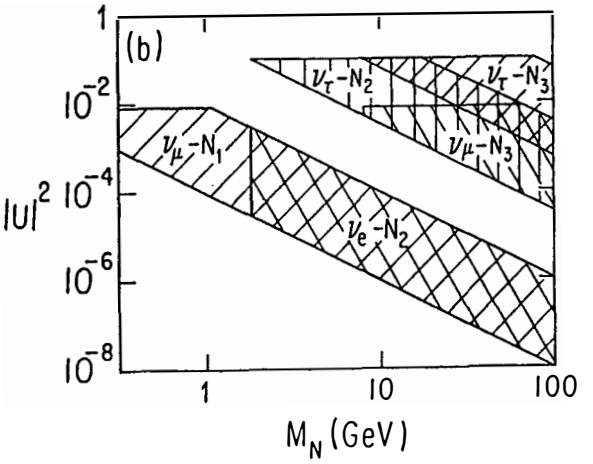


Fig. 1b. Boundaries of allowed regions of $(M_N, |U|^2)$ in the model of Ref. 12.

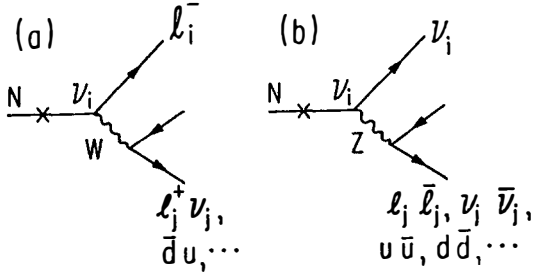


Fig. 2. Typical decays of a heavy neutrino via (a) charged current (b) neutral current.

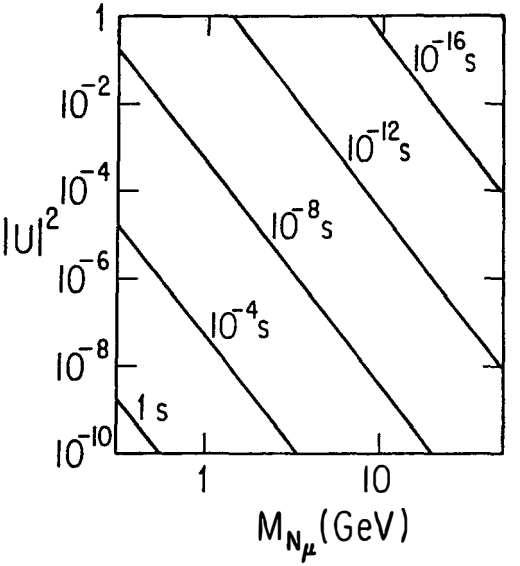


Fig. 3. Lines of fixed lifetime of a heavy neutrino mixing with ν_μ (eq.(8)).

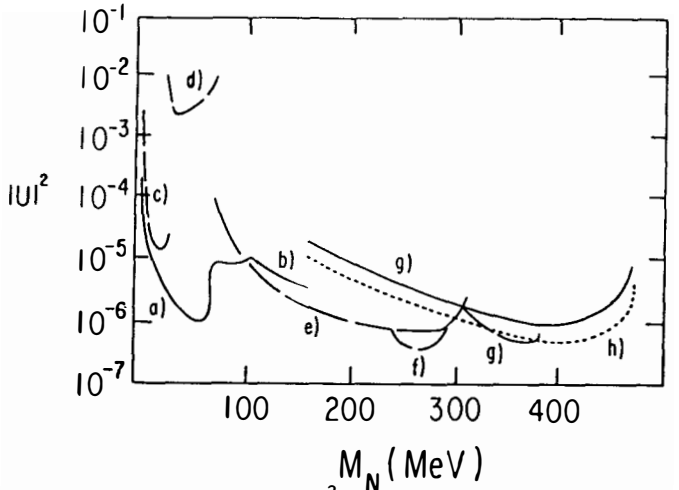


Fig. 4. Limits on $|U_{eN}|^2$ (solid line and dotted line) and on $|U_{\mu N}|^2$ (dashed line): a)-f) Ref. 14; g) study in Ref. 17 based on experiments of Ref. 18; h) Ref. 20.

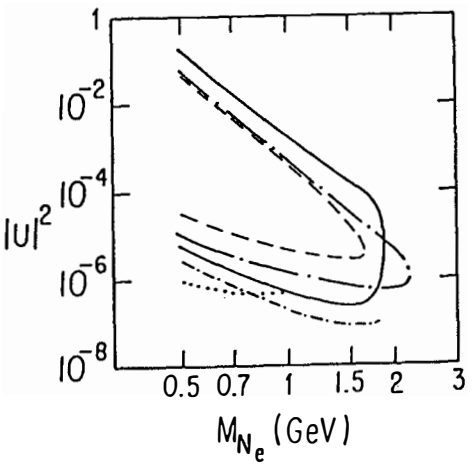


Fig. 5. Reanalysis of the experiment of Ref. 22. Solid line: D→Ne. Dotted line: D semileptonic decay. Dashed-dotted line: B semileptonic decay, $\sigma(B)+\sigma(\bar{B})=100$ nb. Dashed line: B semileptonic decay, $\sigma(B)+\sigma(\bar{B})=10$ nb. Shortly dashed-dotted line: Ref. 22.

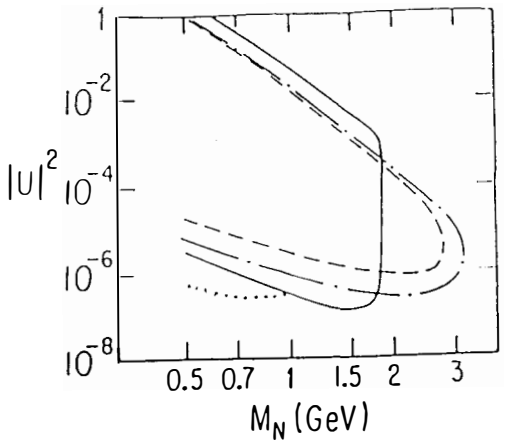


Fig. 6. "Ideal" beam dump experiment with same parameters as those of Ref. 22 except ℓ_1=50m, p_L=800 GeV, geometric acceptance=10%. Curves as in Fig. 5.

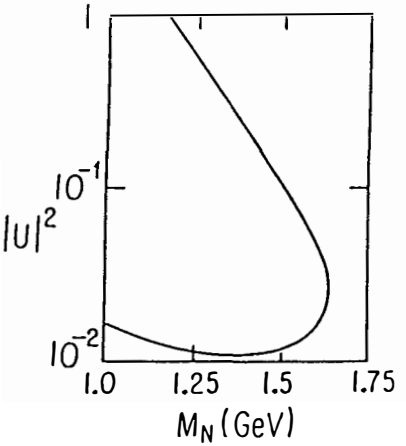


Fig. 7. Limits obtainable from B-production at the T''' (4S).

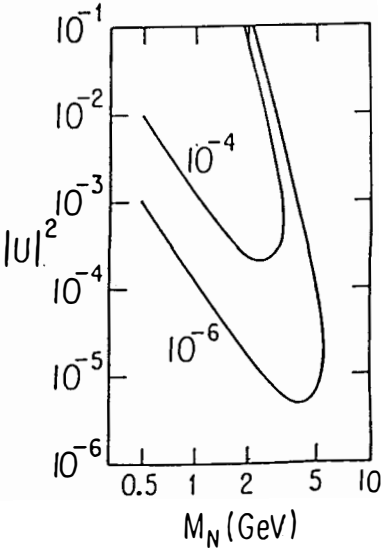


Fig. 8. Limits obtainable from a high-statistics neutrino experiment with 10^4 or 10^6 neutral-current events.

SEARCH FOR MASSIVE NEUTRINOS IN $\pi \to e\nu$ DECAYS

A. Olin
TRIUMF and U. of Victoria

ABSTRACT

The positron spectrum from the decay $\pi^+ \to e^+\nu_e$ has been examined for evidence of secondary peaks arising from an admixture in the ν_e weak eigenstate of massive neutrinos associated with the τ or other heavy leptons. Neutrinos of mass 30-120 MeV would provide a positron peak distinguishable from the $m_\nu = 0$ peak in our experiment. We have established limits on the intensity of such peaks and the resulting constraint on the neutrino mixing parameters. The branching ratio $\Gamma((\pi^+ \to e^+\nu_e)/\Gamma(\pi^+ \to \mu^+\nu_\mu))$ obtained in our measurement constrains the mixing parameters over the range m_ν = 4-60 MeV.

The feasibility of a branching ratio measurement of improved accuracy and greater sensitivity to secondary peaks will also be discussed.

Our group has been studying $\pi \to e\nu$ decay through the measurement of the $(\pi^+ \to e^+\nu)/(\pi^+ \to \mu^+\nu)$ branching ratio and through the search for secondary peaks in the positron spectrum. Both measurements, as discussed by Schrock,[1] may be used to set limits on an admixture of massive neutrinos coupled to the ν_e weak eigenstate. The $\pi \to e\nu$ decay is a sensitive experimental test because of helicity suppression, which reduces the rate by a factor of $m_e^2/m_\mu^2 \approx 40000$. This suppression is greatly reduced in a branch with $m_\nu > 5$ MeV.

The branching ratio may be calculated directly from the weak current to be

$$R = \frac{\Gamma(\pi \to e\nu)}{\Gamma(\pi \to \mu\nu)} = \frac{m_e^2}{m_\mu^2}\left(\frac{m_\pi^2 - m_e^2}{m_\pi^2 - m_\mu^2}\right)^2 \frac{G_e^2}{G_\mu^2} = 1.278\times10^{-4} \ .$$

The radiative correction σ to this decay were first calculated by Kinoshita.[2] Exactly the same result was obtained by Goldman and Wilson[3] and Marciano and Sirlin[4] using a gauge model which eliminated the cut-offs required by Kinoshita. The theoretical prediction in the standard model is the

$$R' = R(1 + \sigma) = (1.233 \pm 0.004) \times 10^{-4}$$

where the error is an estimate of the contribution from the pion substructure. R' would also be affected by a breakdown in μ - e universality ($G_e \neq G_\mu$) or the presence of unknown particles (charged higgs, leptoquarks, etc.) which have a pseudoscalar coupling to the weak current.[5]

Our group is undertaking a new measurement of R in which we expect to improve on our previous results, especially the bounds on neutrino mixing. I will first briefly discuss our recent experiment, emphasizing the systematic uncertainties, and then discuss the wrinkles by which we hope to improve things.

The experimental arrangement is shown in Fig. 1.[6] The pions are stopped in B4-B6, and the B3 and B7 scintillators serve to contain the resulting $\pi \to \mu$ rare decays. The positron energy was measured in a large NaI(Tl) detector. The scintillators T1, T2, T3 but not the NaI(Tl) detector were included in the trigger in order to obtain an energy independent efficiency for $E_e > 1$ MeV. Figure 2 shows the positron energy spectrum for t = 2-28 ns after the pion stop, including the $\pi \to e\nu_e$ peak and the $\mu \to e\nu\bar{\nu}$ spectrum. The two low energy peaks are the zero-energy pedestal and the positron annihilation line. Figure 3 shows the time distributions for events in the $\pi \to e\nu$ and $\mu \to e\nu\bar{\nu}$ energy regions.

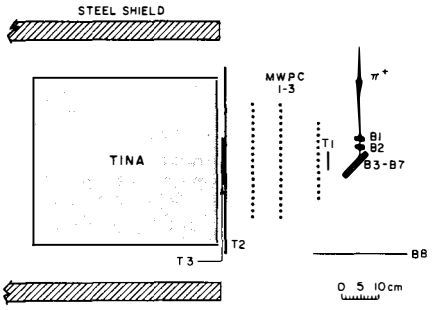


Fig. 1. Setup for the TRIUMF $\pi \to e\nu$ experiment. Scintillators B1-B8 detect pion stops, T1-T3 detect decay positrons, and TINA is the large NaI(Tl) crystal described in the text.

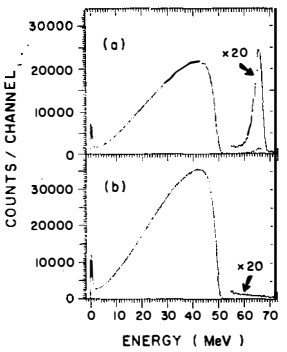


Fig. 2. (a) Observed decay positron energy spectrum for bin 1 (t = 3 to 28 ns). (b) Observed decay positron energy spectrum for bin 2 (t = 176.5 to 201.5 ns).

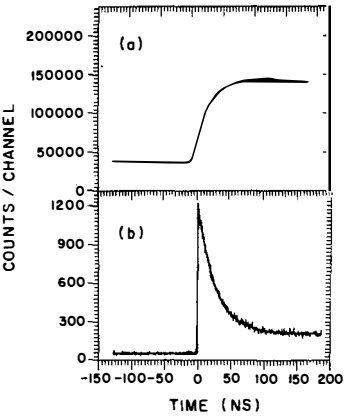


Fig. 3. Timing spectra and fits (solid lines). (a) $\pi \to \mu \to e$ events in the range 0-53 MeV; (b) $\pi \to e\nu_e$ events in the range > 53 MeV. A pileup background due to $\pi - \mu - e$ events was also present.

The timing spectra were fitted for the amplitudes of the $\pi \to e$, $\pi \to \mu \to e$, and $\mu \to e$ decay contributions, $A\pi_e$, $A\pi_{\mu e}$, and $A_{\mu e}$. Small additional terms were fitted to account for effects due to pileup and to the scintillator refiring times. The branching ratio is

$$R = \frac{A\pi_e}{A\pi_{\mu e}} = (1.219 \text{ to } 0.014) \times 10^{-4} .$$

The important systematic uncertainties are from the tail of the $\pi \to e\nu$ peak (0.75%) and from multiple Coulomb scattering (0.4%). In our new experiment we aim for a factor of 4 reductions in these uncertainties.

Suppose that the mixing of weak and mass eigenstates (for three generations) is given by

$$\nu_\alpha = U_{\alpha i}\nu_i \quad (i=1,2,3,\ \alpha=e,\mu,\tau) .$$

The ratio of the branching ratio compared to the no mixing value is[1)]

$$\frac{R}{R_o} = \frac{1 - |U_{e_3}|^2(\rho_e - 1)}{1 - |\nu_{\mu_3}|^2(\rho_\mu - 1)} \qquad 0 < m_{\nu_3} = 33 \text{ MeV}$$

where ρ is the level density and helicity suppression factor. At higher m_{ν_3} the $\pi \to \mu\nu_3$ is kinematically forbidden, so

$$\frac{R}{R_o} = \frac{1 + |U_{e_3}|^2(\rho_e - 1)}{1 - |U_{\mu_3}|^2} \qquad 33 \text{ MeV} < m_{\nu_3} = 55 \text{ MeV} .$$

At even higher m_{ν_3} the $\pi \to e\nu_3$ decays would fall under the Michel positrons and would not contribute to the branching ratio, so

$$\frac{R}{R_o} = \frac{1 - |U_{e_3}|^2}{1 - |U_{\mu_3}|^2} \qquad m_{\nu_3} > 55 \text{ MeV} .$$

Mixing of neutrinos in these mass ranges would produce secondary peaks in the positron spectrum with amplitude $\frac{\pi \to e\nu_3}{\pi \to e\nu_1} = |U_{e_3}|^2 \rho e$. Figure 4 illustrates how we searched for secondary peaks in our data. In 4b we have removed the Michel positrons using the delayed decay spectrum, and in 4c the $\pi \to e\nu$ peak is removed. The residuals were smoothed using a Fourier transform (Fig. 4d) and the significance of a peak at each maximum was evaluated using a Monte Carlo technique. The resulting limit on the yield and mixing is shown in fig. 5.

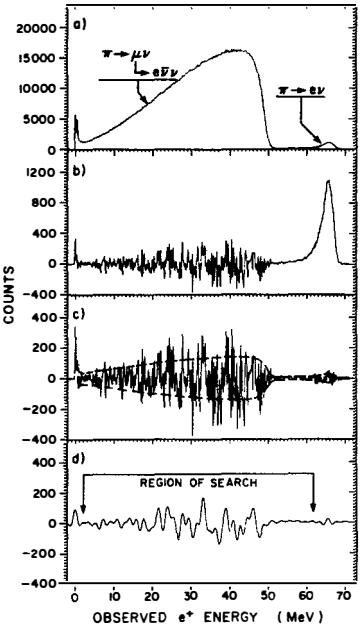


Fig. 4. Analysis of the positron spectrum for secondary peaks: a) The full spectrum 2-22 ns after the pion stop; b) The spectrum of $\pi \to \ell$ decays obtained after subtraction of the normalized μ-decay distribution; c) The spectrum of residuals after subtraction of the calculated $\pi \to e\nu$ line shape. The dashed line envelope indicates the magnitude of the statistical uncertainty ($\pm 1\,\sigma$) centred on zero; d) The residual spectrum after smoothing.

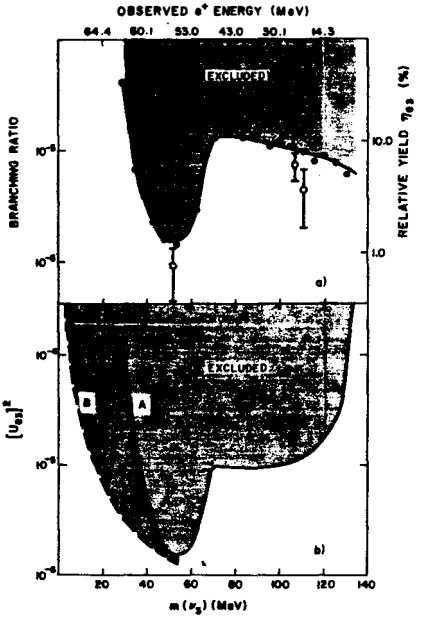


Fig. 5a. a) The 90%-CL upper limit for pion decay to a neutrino of mass $m(\nu_3)$. The open points are peaks identified in the data which were not to be statistically significant. The solid points represent the limits of the sensitivity of the peak search algorithm. b) The 90%-CL limit on the neutrino mixing parameter $|V_{e_3}|^2$. Curve A was obtained from the search for monoenergetic peaks; curve B from the branching ratio measurements.

The leading systematic uncertainty in the branching ratio measurement is the $\pi \to e\nu$ lineshape, which we determine by using a $\Delta p/p = 1\%$ electron beam available from the channel. Radiative corrections, Bhabha scattering, etc. are included using a Monte Carlo calculation. To improve on this we aim to measure

directly the $\pi \to e\nu$ lineshape from a subset of the data of our run.[1]) This can be done by distinguishing between $\pi \to e$ and $\pi \to \mu \to e$ decays in the target scintillator according to the total energy deposited. This scheme is illustrated schematically in fig. 6 for 1 MeV resolution in the target scintillator. A suppression of 100 in the Michel positrons will reduce the lineshape uncertainty

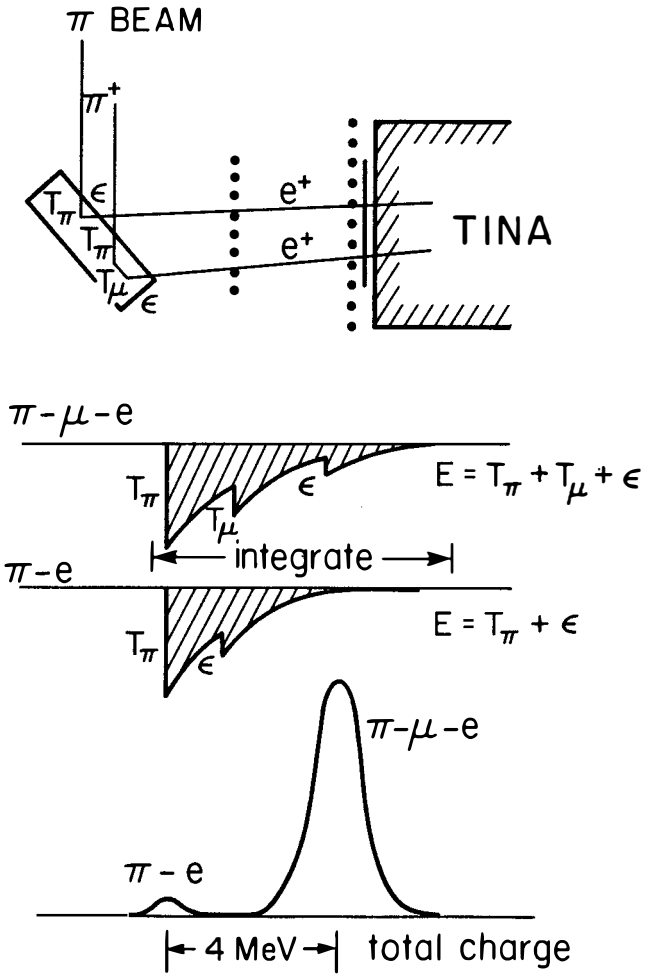


Fig. 6. Total energy measurement in the target scintillator. Typical pulses from pions stopping in the target scintillator are shown schematically. The total charge spectrum shows a clear separation of the $\pi \to e$ and $\pi \to \mu \to e$ decays.

contribution to the 0.2% level. The next largest correction, multiple scattering, may be greatly reduced by replacing some of the scintillators with low mass wire chambers.

The feasibility of this technique has been investigated recently in a short test run. The resolution obtained in the target scintillator was only 1.9 MeV - this will be improved by using better photo tubes and light guides. Nevertheless, as can be seen in fig. 7, a supression of ~ 500 was achieved at a loss of 30% of the $\pi \to e\nu$ decays. We are highly encouraged by this result, and are planning a full-scale run for this summer. In terms of our sensitivity to neutrino admixtures, we hope to achieve a $\times$ |3 improvement on the bounds in the 10-55 MeV mass region, and $\times$ |200 for mases of 55-120 MeV.

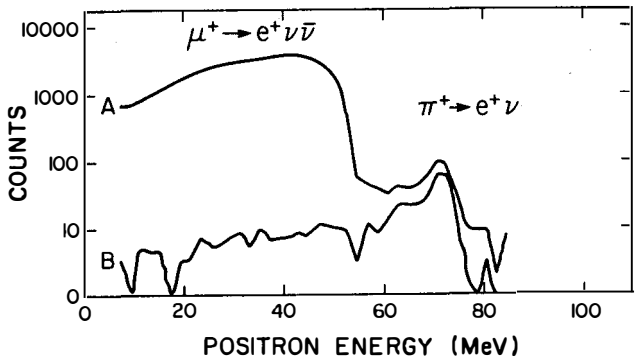


Fig. 7. Positron spectrum from π decay observed in the test run. Curve A is the full spectrum, while curve B shows the effect of the cut on the energy deposited in the target scintillator.

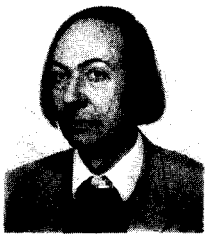
REFERENCES

1. R.E. Shrock, Phys. Rev. D 24, 1232 (1981).
2. T. Kinoshita, Phys. Rev. Lett. 2, 477 (1959).
3. T. Goldman and W. Wilson, Phys. Rev. D 15, 709 (1977).
4. W. Marciano and A. Sirlin, Phys. Rev. Lett. 36, 1425 (1976).
5. O. Shanker, Nucl. Phys. B204, 375 (1982).
6. A more complete description of these results may be found in D.A. Bryman, R. Dubois, T. Numao, B. Olaniyi, A. Olin, M.S. Dixit, D. Berghofer, J.-M. Poutissou, J.A. Macdonald and B.C. Robertson, Phys. Rev. Lett. 50, 7 (1983), Phys. Rev. Lett. 50, 1546 (1983).
7. T. Numao, TRIUMF experimental proposal 248.

DETERMINATION OF AN UPPER LIMIT OF m_{ν_μ} FROM π-DECAY IN FLIGHT

H.B. Anderhub, J. Boecklin, H. Hofer, F. Kottmann, P. LeCoultre, D. Makowiecki, H.W. Reist, B. Sapp, P.G. Seiler

Presented by P. LeCoultre
Institut für Hochenergiephysik, Eidg. Technische Hochschule
CH-8093 Zürich



ABSTRACT

An upper limit for m_{ν_μ} has been determined from the forward π-decay in flight at SIN. The kinematical analysis and the inherent calibrations lead to the result: $m_{\nu_\mu} < 0.50$ MeV/c^2 (90% CL). Improvements of the experiment to reduce this limit are also discussed.

It is possible to determine the mass of the muonic neutrino either from three-body decays - where one gets the mass from the measured spectra via theory - or from two-body decays, which give the mass squared from a purely kinematical analysis. We chose the second case, but instead of measuring the momentum of the muon from π-decay at rest, we determined both momenta, that of the pion and that of the muon from π-decaying in flight in the very forward direction. The decay in vacuo has the advantage not to depend on uncontrolled energy losses in the π-stop region. Analyzing the kinematics of the forward pion-decay in flight, gives a very reliable result, due to the possibilities to calibrate and monitor the apparatus with undecaying pions or muons during data taking.

Let us first have a look at our apparatus (fig. 1). For the kinematical analysis one needs the measurement of the momenta and the decay angle. The latter is measured in our set-up with two sets of proportional chambers

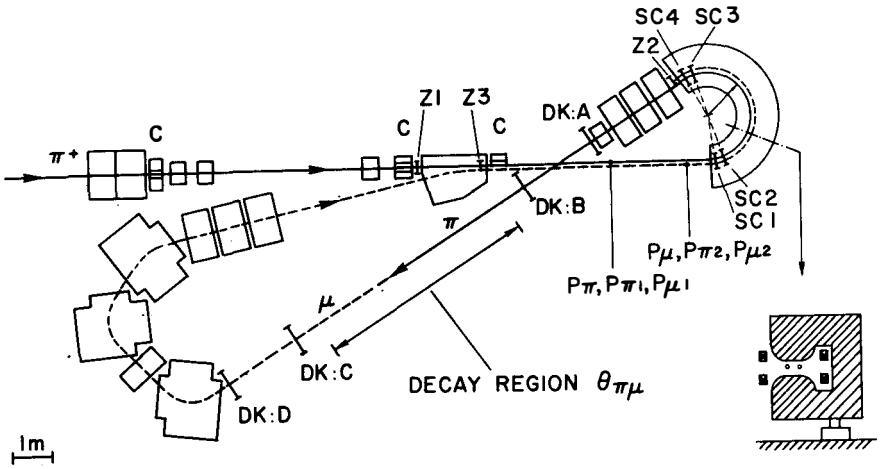


Fig. 1. Apparatus

(DK A,B,C,D), on both ends of the so-called "decay-region". In order to localize the decay point somewhere inbetween these two sets of chambers, the time-of-flight (TOF) method is used. Due to the fact that the muons have a slightly larger velocity than the pions we are able to determine the decay point to ±1.25 m according to our TOF-resolution of 140 psec. One scintillator, Z1, is placed in front of a collimator in the injection region and the second, Z2, at the exit of the figure-8-beam arrangement. The π- and μ-momenta are measured in the same spectrometer consisting of a 210° C-shaped magnet and four very thin spark cham-

bers (SC 1,2,3,4). In this way the systematic error on the momentum difference $p_\pi - p_\mu$ is minimal. - Calibrations of all the detectors can be done with undecaying pions and muons travelling along the whole beam-line.

Let us now discuss the principle of our method: The neutrino momentum p_ν is given by the momentum difference of the pion and the muon. It can be calculated if one knows all the quantities p_π, θ, m_π^2, m_μ^2, $m_{\nu_\mu}^2$. Assuming a vanishing neutrino mass the calculated neutrino momentum p_ν^o can be compared to the measured one. Their difference is

$$p_\nu - p_\nu^o \simeq \left.\frac{\partial p_\nu}{\partial (m_{\nu_\mu}^2)}\right|_{\substack{m_{\nu_\mu}=0 \\ p_\pi = \langle p_\pi \rangle}} \cdot \langle m_{\nu_\mu}^2 \rangle$$

got from the expansion of p_ν in $m_{\nu_\mu}^2$. This approximation is valid on the 10^{-4}. $(p_\nu - p_\nu^o)$ level for small decay angles $\frac{\partial p_\nu}{\partial m_{\nu_\mu}^2}$ depends only weakly on $p_\pi, \theta, m_\pi, m_\mu$ and its error has therefore only a small influence $m_{\nu_\mu}^2$.

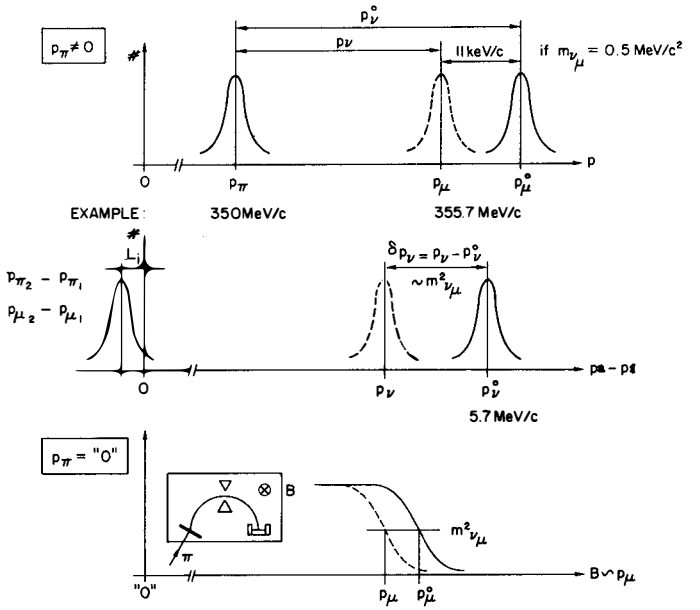


Fig. 2. The two methods to determine an upper limit for m_{ν_μ} from π-decay in flight (2a+b) or from π-decay at rest (2c)

Fig. 2a illustrates the method: From a measured pion momentum one calculates the expected muon momentum p_μ^o for the vanishing ν-mass. The shift of the measured one is due to a finite neutrino mass in this drawing. If $p_\pi = 350$ MeV/c, then p_μ^o will be approximately 355.7 MeV/c. For a muonic neutrino mass of 0.5 MeV/c^2 a shift of 11 keV/c should be observed.

As mentioned before we measure the pion and muon momenta in the same spectrometer and the crucial measured quantity is of course their difference. We therefore shall always plot momentum differences (fig. 2b). The momentum-difference spectrum corresponds now to the above mentioned ν-momentum spectrum. The peak to the left corresponds to the momentum difference spectrum of pions - or muons - which go twice through our spectrometer without decaying. They give us a measurement of the energyloss of these particles in our detectors and the shape of the spectrum. Therefore a precise knowledge of the corrections to be applied on the neutrino momentum shift is available.

After the pion momentum has been determined between SC 2 and 3, the pions loose energy in SC 3 and 4 and in DK A and B before they decay. The muons loose the similar amount of energy in DK C and D and in SC 1 and 2 before their momentum is determined (the SC's and DK's are all built identical). The measured neutrino momentum has to be corrected for this effect.

One easily can show that our corrected neutrino momentum is then given by $p_\nu^c = p_\mu - p_\pi - \frac{1}{2}(p_{\pi_2} - p_{\pi_1} + p_{\mu_2} - p_{\mu_1})$, where $p_{\pi,\mu_{1,2}}$ corresponds to the momentum of the calibration π,μ on their first und second path through the spectrometer. In order to reduce possible non-linearities in the chambers, read-out system etc. we chose a particular beam layout, calibration events with momenta and geometrical paths through the spectrometer which coincide practically with the ones of our good decay events.

Fig. 3 shows this special configuration: the trajectories of decay and calibration events go through point P_1 in SC 3 on their first pass and through P_2 on their second pass. As a consequence the systematics of the corrected neutrino momentum p_ν^c in P_1 and P_2 cancel out. - The momenta are $p_{\pi_1} = p_\pi$ and $p_{\mu_2} = p_\mu$. We get $p_\nu^c = \frac{1}{2}[(p_{\mu_2} - p_{\pi_2}) + (p_{\mu_1} - p_{\pi_1})]$. The corrected ν-momentum is then proportional to $(d_1+d_2)/4$ with d_1 and d_2 being the two shown distances in SC 2. The systematic error on p_ν^c due to the spark chambers is therefore proportional to 1/4 of the systematical error on d_1+d_2.

Contrary to this now discussed peak shifting method, measuring the muon momentum of the pion decay at rest allows only to observe the muon spectrum

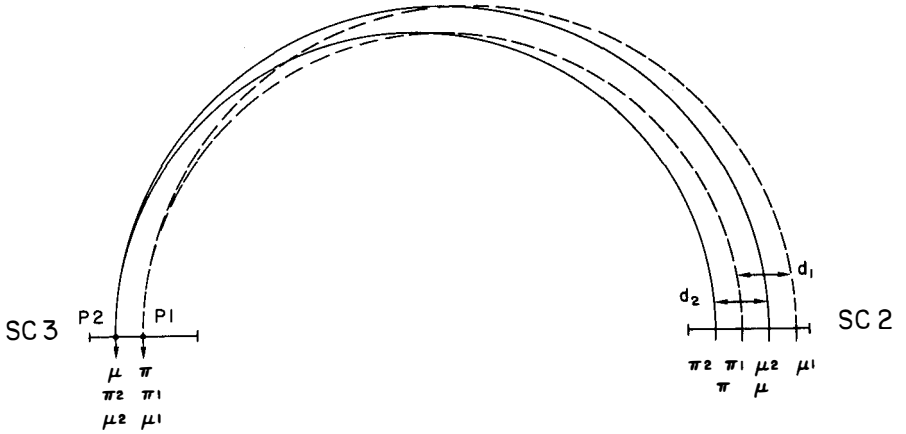


Fig. 3. Particular beam lay-out to reduce systematics

(fig. 2c), but not the energy losses of the muon. According e.g. to the other SIN experiment[1] the muon momentum is scanned in a magnetic spectrometer by variing the field. As shown, one observes the edge of the muon spectrum. The shift is proportional to $m^2_{\nu_\mu}$. Because there is no calibration, the shape and that contribution to the shift coming from the energy losses, have to be extracted via a carefully calculated π-stop distribution and a muon energy loss distribution in the π stopping scintillator.

Discussion of the calibrations:

First the TOF-measurement: In our set-up non decaying pions and muons can travel along the whole beam-line system. They give two calibration peaks in our TOF-spectrum. We therefore can monitor the stability of the TOF-measurement and correct for eventual shifts. The TOF interval of events with their decay-point within the decay-region can be defined relative to these calibration peaks.

Again with the help of throughgoing particles we obtained the distribution of the spatial angles for straight tracks, giving an angular resolution of 0.84 mrad inherent to our proportional chamber system (fig. 4a). Fig. 4b shows the data for decay-events (fulfilling the TOF condition). The points agree with the calculated distribution (solid line), which is obtained by folding the dotted spectrum with the calibration spectrum. In other words: the dotted spectrum is the spectrum of the true decay angles. - The mean decay angle (unfolded

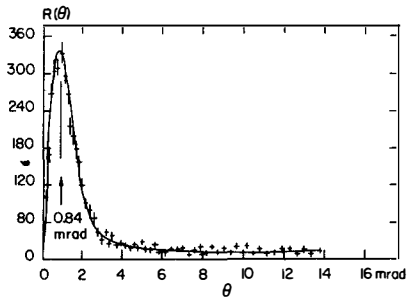


Fig. 4a. Distribution of spatial angles for straight tracks

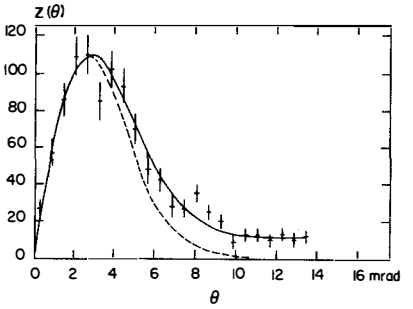


Fig. 4b. Spectrum of decay angles

spectrum) is determined to be $\langle\theta\rangle = (3.35 \pm 0.15)$ mrad for measured angles between 0. and 13.5 mrad.

Remarks about the resulting momentum-difference spectra: First about the momentum differences of the pion calibration events (the muon case is analogue) (fig. 5a): it is asymmetric and it has a structured tail due to the detector geometry. - The same is true for decay events (fig. 5b): here the asymmetry is more pronounced, due to the finite decay-angles. The determination of the relative positions of the two peaks is possible, because one is able to reproduce their shapes by a calculation.

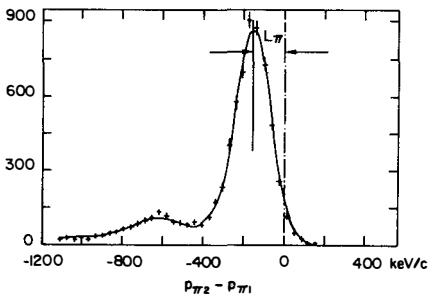


Fig. 5a. Momentum difference spectrum of calibration events (shown for pions; it is similar for muons)

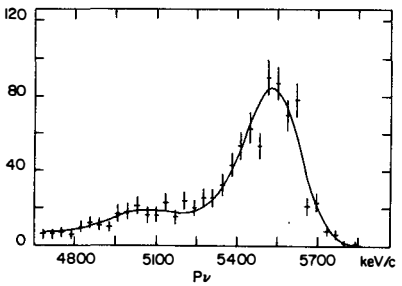


Fig. 5b. Neutrino-momentum spectrum

For the calibration peak a model for the momentum-loss in the chamber gas, windows, wires and support grids allowed to fit the curve perfectly well and therefore also to determine the momentum loss L of the pions or muons in the

detectors, needed to correct the neutrino momentum.

The shape of the decay event distribution is obtained from kinematical calculations using the π-momentum and decay-angle distributions, folding the resulting spectrum with the shape of a calibration spectrum.

Thanks to the measured momentum losses L_i we are now able to express p_ν^c as follows: $p_\nu^c = p_\nu^o - L_\nu + \frac{1}{2}(L_\pi + L_\mu)$, where L_ν also contains - besides of momentum losses - the effect of the neutrino mass. We finally found a corrected neutrino momentum shift of $\delta p_\nu^c = 6.4$ keV/c.

We estimated the systematics on this value by determining the variations of the $L_{\pi,\mu}$ values with respect to the track position in the spark chambers. Here we found, thanks also to the particular beam layout discussed before, a systematic error of 11.4 keV/c for the ν-momentum shift.

In table 1 we list all errors (90% CL) which have an influence on δp_ν^c. We notice that the major contribution is due to the just discussed "chamber non-linearity". Statistics is the second point in importance, the third is due to the error of the decay-angle measurement.

TABLE 1. Error summary (90% CL)

Errors on p_ν^o :		Influence on δp^c
pion mass	Δm_π = 1.5 keV/c	0.16 keV/C
muon mass	Δm_μ = 0.4 keV/c	0.06
decay angle	$\Delta\theta_{\pi\mu}$ = 0.15 mrad	
	$\langle\theta\rangle$ = 3.35	5.32
pion momentum	$\Delta\langle p_\pi\rangle$ = 26. keV/c	0.40
Errors on p_ν^c :		
from statistics		7.13
from "chamber non-linearity"		11.40
from others		1.35
Errors on $p_\nu^c - p_\nu^o$:		
from $\Delta\langle B\rangle = 5.10^{-5}\langle B\rangle$		0.55
Total error		$\Delta(\delta p_\nu^c)$ = 14.54 keV/c (90% CL)
		= 8.81 keV/c (68% CL)

We end up with $\delta p_\nu^c = (6.4 \pm 14.5)$ keV/c, which yields a negative mean value of the neutrino mass squared: $\langle m_{\nu_\mu}^2 \rangle = (-0.14 \pm 0.20)$ MeV/c^2 (68%CL). Putting the probability distribution to zero for negative $m_{\nu_\mu}^2$, we get for the upper limit of the neutrino mass

$$m_{\nu_\mu} \leq 0.50 \text{ MeV/}c^2 \text{ with 90\% CL.} \quad ^{2)}$$

An interesting question is how to improve this result. In table 2 we show - assuming $\langle m_\mu \rangle = 0$ - how much the error on δp_ν has to be to give the upper limits indicated in the next column. E.g. what would it mean, if we try to reach 200 keV/c^2? δp_ν should then be less than 1.8 keV/c.

TABLE 2. Needed precision on δp_ν versus upper limit of m_{ν_μ}:

$\Delta(\delta p_\nu)$ for $\langle m_{\nu_\mu} \rangle = 0$	m_{ν_μ} - upper limit (90% CL)
11. keV/c	500 keV/c^2
4.	300.
1.8	200.
0.4	100.

In the error list (table 1) three main contributions exist which one now has to reduce to about 1 keV/c:

a) The largest contribution comes from the non-linearity of the spark chambers and their readout system. We could replace these chambers by microstrips and get an improvement on $\Delta\delta p_\nu$ of 1 to 2 orders of magnitude. Our chambers were only 2 mg cm^{-2} thick. Microstrips can't yet been made thinner than $\sim$ 50 mg cm^{-2}. But the multiple scattering in the spectrometer is still of minor importance at this level because of the angular focussing property of our 180° spectrometer.

b) The statistics, the second point of importance, would be easy to improve. In the experiment presented to-day we had only some 1000 decay events and 10'000 calibration events. With the good resolution of the microstrips the center of the distributions would be determined more precisely already by this amount of events.

c) The third point, the angular resolution, is the hardest: Namely 1 keV/c uncertainty of the ν-momentum shift corresponds to an angular uncertainty of

0.1 mrad for a $\langle\theta\rangle$ of 1 mrad at p_π = 350 MeV/c. $(\Delta\theta)^2$ is a sum of three contributions:

$$(\Delta\theta)^2 = (\Delta\theta_{\text{mult.scatt.}})^2 + (\Delta\theta_{\text{system}})^2 + (\Delta\theta/N)^2.$$

The only factor of concern is the contribution of the multiple scattering. Replacing the proportional chambers also by microstrips, would give a $\Delta\theta_{\text{mult.scatt.}}$ of 1 to 2 mrad, which is definitely too large. In principle a correction can be applied, but it's not trivial to correct for a factor $\sim$ 20. Therefore thinner chambers are needed. E.g. thin drift chambers with 0.1 mm resolution and less than 1 cm of gas thickness should work.

Increasing the pion momentum is useless, because δp_ν is proportional to p_π:

$$\Delta(\delta p_\nu) \sim p^3\theta\Delta\theta \sim p_\pi^3(\Delta\theta)^2 = p_\pi^3 \left(\frac{14.\text{const.}}{p_\pi \beta_\pi}\right)^2 = p_\pi \cdot \text{const.}$$

Decreasing the pion momentum is of no help, because the multiple scattering of the particles in the microstrips of the spectrometer starts then to become important. All these considerations lead to the conclusion, that the method of the π-decay in flight is limited mainly by the multiple scattering in the detectors used for the decay-angle measurement.

Investigations how to realize the improvements have to go on and may be we become convinced to do a second step. But is a factor 2 to 3 worthwhile the effort? I think it is.

REFERENCES

1) Daum et al., Phys. Rev. D20, 2692 (1979)

2) Anderhub et al., Phys. Lett. 114B, 76 (1982)

SEARCHES FOR HEAVY NEUTRINOS IN MESON DECAYS AND MUON CAPTURE

R. Prieels : Institut de Physique, Université Catholique de Louvain, 2 Chemin du Cyclotron, B - 1348 Louvain-la-Neuve, Belgium

ABSTRACT

Searches for heavy neutrinos can be performed measuring the momentum of the charged lepton emitted in two-particle meson decays. Similarly, the nuclear recoil in muon capture can also reveal finite neutrino masses.

The advancement of a new detector to be used in muon capture on ^3He is exposed. A progress report on an experiment on $\pi \rightarrow e\nu$ decay is also presented.

1. INTRODUCTION

The assumption of mixed neutrinos mass eigenstates in the flavor-states is the key condition of eventual neutrino oscillations[1]. The mixing enters through the unitarity U matrix as :

$$|\nu_\ell\rangle = U_{\ell i}|\nu_i\rangle$$

It was the merit of Shrock[2] to call attention to a class of experiments with would allow to observe eventual neutrino-mixing induced by non-diagonal matrix-element as small as 10^{-6}. This methods consists essentially in a precision spectroscopy of the charged particle emitted in conjunction with the neutrino of a given flavour-state. A mixture of different mass eigenstates would be revealed by peaks of "anomalous" momentum in the charged-particle spectrum ; their positions being related to the mass of the neutrino eigenstates and their intensities to the square of the non-diagonal matrix-element. The region of neutrino-mass and mixing investigated in these decay experiments is complementary to the region sampled by the oscillation experiments in their appearance or disappearance mode. This is shown in Fig. 1 where we clearly see the "micromixing" reached by the spectroscopic method to be compared to the "millimixing" sensitivity of the oscillation experiments. The limitation however of the former method is the poor minal mass (1 MeV) that can be observed due to the finite energy resolution of the measuring devices.

The sensitivity to the mixing in the meson decay is related to the suppression of the V-A constraint as the neutrino mass increases. The intensities of the charged lepton lines in the momentum spectrum are equal to

$$|U_{\ell i}|^2 \rho m_{\nu_i}$$

where $\rho_{m_{\nu i}}$ contains phase space and V-A suppression effects and is shown in Fig. 2.

Table 1 gives examples of decays with the maximum neutrino mass that can be reached. Let us precise here that those decays give informations on different non diagonal elements of the U matrix.

TABLE 1

matrix el.	meson decay or reaction products	max. -mass	ref.
$U_{\mu i}$	$\pi^+ \to \mu^+ + \nu_\mu$	30 MeV	3,4)
	$K^+ \to \mu^+ + \nu_\mu$	390 MeV	5)
	$K^+ \to \mu^+ + \nu_\mu + \nu + \bar{\nu}$	450 MeV	6)
	$\mu^- + {}^3He \to {}^3H + \nu_\mu$	100 MeV	7,8)
U_{ei}	$K^+ \to e^+ + \nu_e$	490 MeV	9)
	$\pi^+ \to e^+ + \nu_e$	130 MeV	10,11)
	$e^- + A \to A' + \nu_e$	2-3 MeV	

2. MUON CAPTURE IN HELIUM 3

A research for massive neutrinos in muon capture is developed by the LOUVAIN-SIN collaboration at SIN. It was noted[7] that pion and kaon decay are practically unable to observe possible heavy neutrinos on the rather extended mass range of 30-90 MeV and that a measurement of the triton recoil spectrum from the reaction $\mu^- + {}^3He \to {}^3H + \nu_\mu$ should allow to bridge this gap. In the same paper[7], an analysis of an old precursor muon capture experiment[12] set new limits for the muon-flavor mixings in the 30-90 MeV mass range. Fig. 3 shows this experimental result on which bounds were calculated. The aim of the currently developed experiment is to lower these limits by an order of magnitude. This is shown with the already known results in the Fig. 4.

Improvements of the pioneer experiment can be done in two ways : first by the use of a beam with better focusing which is expected to decrease by a factor of ten the noise in the spectrum region of interest and secondly in improving the resolution to 1 % by building a new detector. The tool chosen for the determination of the kinetic energy of the triton is a gas scintillation proportional chamber (GSPC) filled with ^3He [13-16].

If a particle is stopped in a gas, it looses its energy either by ionizing or exciting the gas atoms. In collision processes, isomeric molecular excited states He_2^* are formed and emit their typical far-ultraviolet radiation. The photons produced by atoms excited during the stopping process are called the primary light. If the primary electrons produced by ionization are drifted into a region of high enough electric field, new excited atoms will be formed. This means that an amount of radiation

(secondary light) proportional to the number of primary electrons and thus to the kinetic energy of the stopped particle will be produced.

Two problems were encountered in building this helium-GSPC detector.

The first one is, in contrast to a Xenon-GSPC type detector, that there is a mismatch of the emission spectrum (600-1000 Angstrom) with the sensitive region of the photomultiplier. We observed that a small addition of nitrogen (100-5000 ppm) can play the role of the normally used wavelength shifter through a transfer of excitation to nitrogen which have an emission band of (3000-3800 Angstrom) adapted with a photomultiplier equipped with a quartz window.

Secondly, with his quenching properties, nitrogen will prevent the UV-light to reach the wall of the counter where these hard photons from He_2^* can cause photoeffect, liberate new electrons and initiate a long discharge process. Still better quenching can be obtain with a supplementary addition of CH4 in small amount. This allows us to reach better stability and higher rate. A schematic drawing of this detector is shown in Fig. 5. The actual achieved resolution is of 4 % and improvements are still under way. Performance in a muon beam will be tested in March 1984.

3. PION MESON DECAY IN ELECTRON AND NEUTRINO

Neutrino mass limits from this meson decay already exist from a by-product of a TRIUMF branching ratio measurement[17] of the $\pi^+ \to e^+\nu$ and $\pi^+ \to \mu^+\nu$ decays. A dedicated experiment is under way performed by a LOUVAIN-ZURICH-LAUSANNE collaboration at SIN. Fig. 6 shows the already published result and the goal limits of our experiment. Let us note here that the limit "b" from the branching ratio measurement is model dependent as it is calculate with the assumption of no pseudoscalar contribution. I will report here on the status of our experiment.

Let us remind here that the method consists in detecting an eventual abnormal peak in the momentum spectrum of the positron emitted in the $\pi^+ \to e^+\nu$ decay. This peak would occur at a momentum lower than 70 MeV/c and eventually even lower than 50 MeV/c. Two points has then to be considered in order to achieve the best result. First a good energy resolution : the better it is, the more sensitive we will be on the mixing parameter of an eventual heavy neutrino. Secondly, to detect with great sensitivity a positron peak below 50 MeV/c, it is crucial to reduce the 10000 times more abundant positron background coming from the pion-muon decay

chain building up the known Michel spectrum.

The different live times of pion and muon already help if one restricts the observation time to the 30 first nanoseconds. This is shown in Fig. 7 taken from ref. [10]. But this is not enough and an extra rejection is needed.

If the pions are stopped into a scintillator we can perform an analysis of the resulting pulse. If one integrate the charge of the rising part of the pulse and also, separately, the falling part of the same signal. the ratio of both areas will be a constant whatever the energy release is during the stopping process. If, however, the pion decays whilest in the scintillator and if the produced muon looses its energy inside the scintillator too, then the electronic pulse shape will be deformed and the previous ratio will change depending on the instant of the decay. This phenomenon is shown in Fig. 8 where the higher edge corresponds to single particle events and the lowest one to double particle events the second being produced later than the rise time of the first pulse. If on the other hand the thickness of the scintillator is such that the energy release of one electron remains always small, this effect does not affect the pulse-distribution. Clearly, selecting "single-events", a separation of about one nanosecond can be achieved[18].

To get a good energy resolution we choosed to use the magnetic pair-spectrometer of the LAUSANNE-ZURICH-MUNICH collaboration as a single particle momentum analyzer. Fig. 9 shows a drawing of our setup where "T" is our scintillator target. The energy resolution obtained from a part of our data by a retracing method is illustrated in Fig. 10. The combined effects of both energy resolution improvements and Michel spectrum suppression is illustrated in the spectrum shown in Fig. 11a comparing it to Fig. 7. From pour data shown in Fig. 11a we subtracted an adjusted Michel spectrum deformed according to our acceptance ; the resulting spectrum is shown in Fig. 11b.

Data are still under analysis ; the overall amount of $\pi \to e\nu$ events recorded to date is about 6000.

We are indebted to Dr. J.P. Deutsch for many useful discussions.

4. REFERENCES

1) B. Bontecorvo, ZhETH (USSR) 53, 1717 (1967)
   A.K. Mann and H. Primakoff, Phys. Rev. D15, 655 (1977)
   J.N. Ng, Nucl. Phys. B191, 125 (1981)
2) R.E. Shrock, Phys. Lett. 96B, 159 (1980)
3) R. Abela et al., Phys. Lett. 105B, 263 (1981)
4) R.C. Minehart et al., preprint 1984
5) R.S. Hayano et al., Phys. Rev. Lett. 49, 1305 (1982)
6) C.Y. Pang et al., Phys. Rev. D8, 1989 (1973) quoted in ref. 5
7) J.P. Deutsch et al., Phys. Rev. D27, 1644 (1983)
8) J.P. Deutsch et al., SIN proposal R-82-14
9) J. Heintze et al., Nucl. Phys. B149, 365 (1979)
10) D.A. Bryman et al., Phys. Rev. Lett. 50, 1546 (1983)
11) R. Prieels et al., SIN proposal R-81-09
12) D.R. Clay et al., Phys. Rev. 140, B586 (1965)
13) C.A.N. Conde and A.J.P.L. Policarpo, Nucl. Instr. and Meth. 53, 7 (1967)
14) W. Herold et al., Nucl. Instr. and Meth. 217, 277 (1983)
15) W. Herold, ETH Thesis Nr. 7133
16) R. Ferreira Marques, ETH Thesis Nr. 7111
17) D.A. Bryman et al., preprint 1983
18) C. Amsler et al., SIN Newletters 15, NL28 (1983)

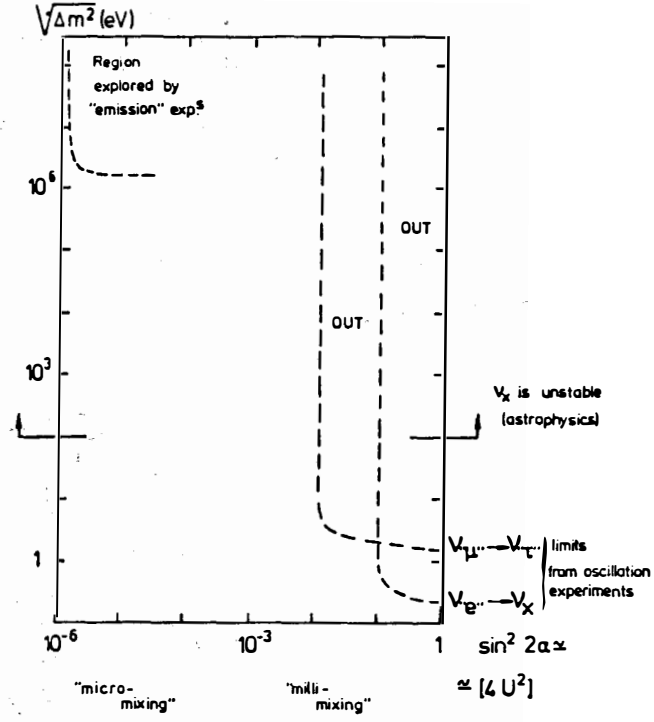


Figure 1.

Qualitative comparison of the sensitivity-region of the neutrino oscillation experiments and the "emission-type" experiments.

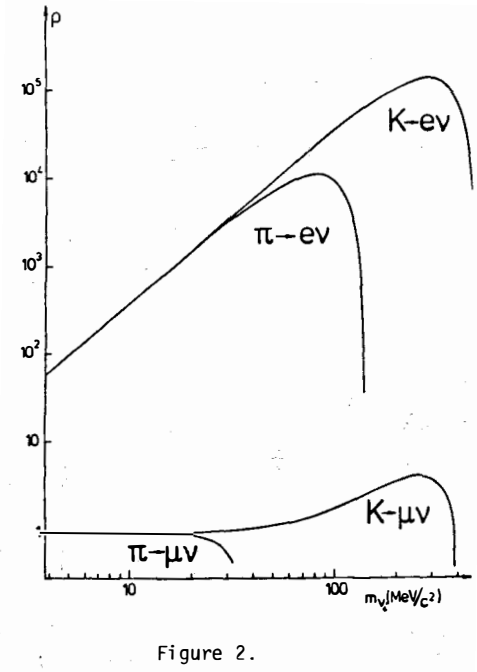


Figure 2.

Sensitivity enhancement factor for observing "anomalous" peaks, corresponding to components with neutrino masses different from zero in the decay of kaons and pions.

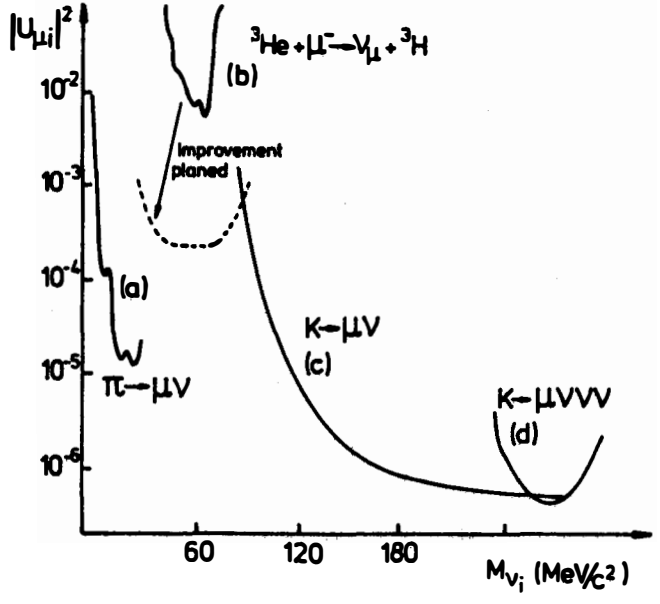


Figure 3.

Bounds of $|U_{\mu i}|^2$ vs neutrino mass; The goal limit of the running experiment is indicated is dashed lin. Other bounds shown in the figure are from : a) $\pi \rightarrow \mu\nu$ heavy neutrino search (ref. 3), b) an analysis of the muon-capture experiment (ref. 7,12), c) $K \rightarrow \mu\nu$ heavy neutrino search (ref. 5), d) $K \rightarrow \mu\ \nu\ \bar{\nu}\ \nu$ decay experiment (ref. 6).

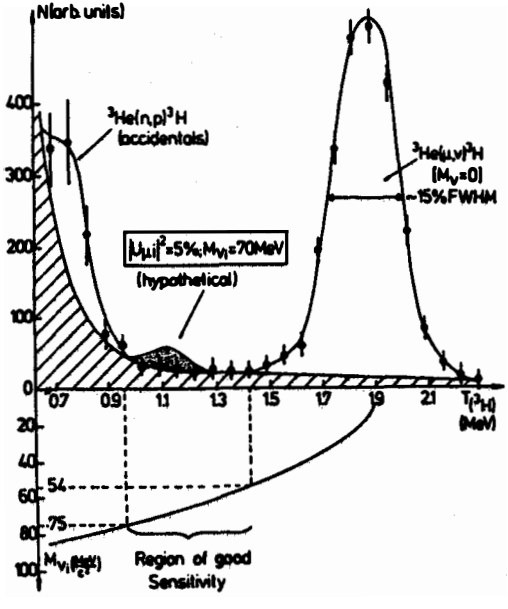


Figure 4.

Triton-recoil-energy spectrum observed by the authors of ref. 12 and relationship between this energy and the mass of a corresponding neutrino. The peak drawn as a dotted area illustrates the effect of a hypothetical heavy neutrino of $m_{\nu i}$ = 70 MeV/c^2 emitted with a mixing strength of $|U_{\mu i}|^2$ = 0.05.

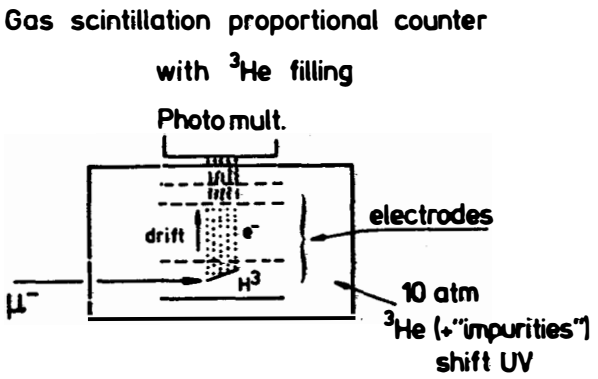


Figure 5.

Sketch of the gas detector developed to measure the recoil energy of ^{3}H in the reaction $\mu^- + {}^3He \rightarrow {}^3H + \nu$.

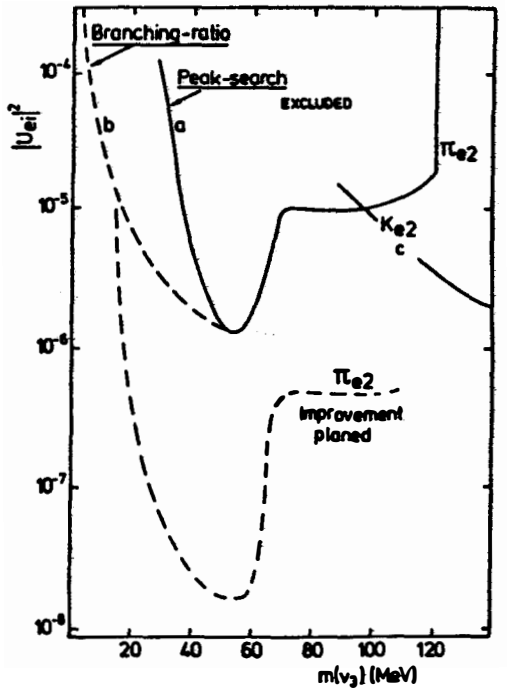


Figure 6.

Bounds on $|U_{ei}|^2$ vs neutrino mass. The goal limit of the described experiment is shown at the bottom of the figure. Are also shown, the bounds from : a) the neutrino beak search from $\pi \rightarrow e\nu$ decay (ref. 10), b) the branching ratio measurement $\pi \rightarrow e\nu/\pi \rightarrow \mu\nu$ (ref.17) c) the Ke2 results (ref. 9).

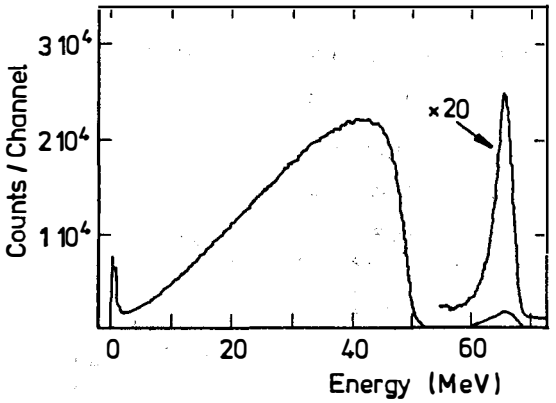


Figure 7.

Positron energy spectrum from $\pi \rightarrow e\nu$ decay obtained at Triumf in an observation window (3-28 ns) after stopping of the pion.

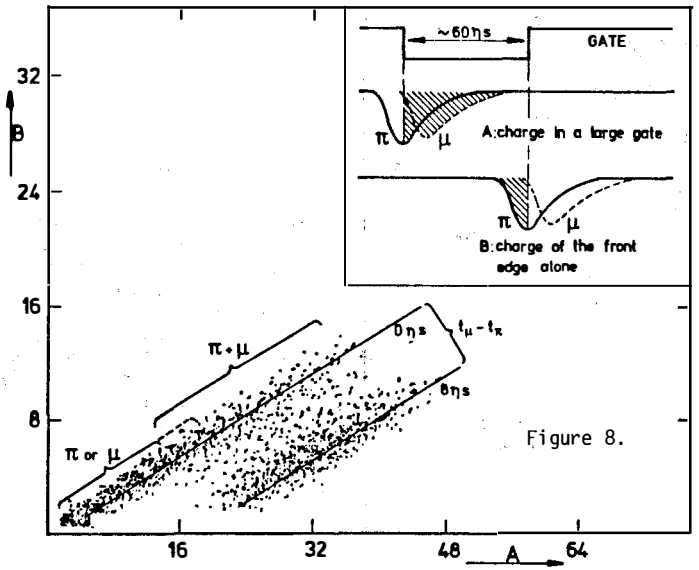


Figure 8.

Biparametric plot of the two samplings from the target detector. The left edge corresponds to "single particle", whereas the right one corresponds to double particles events separated by more than the rise time of a single pulse. A separation of two pulses within one nanosecond can be achieved.
The insert shows the gating scheme for a typical π-μ sequence. The shaded areas indicates the part of the signal integrated.

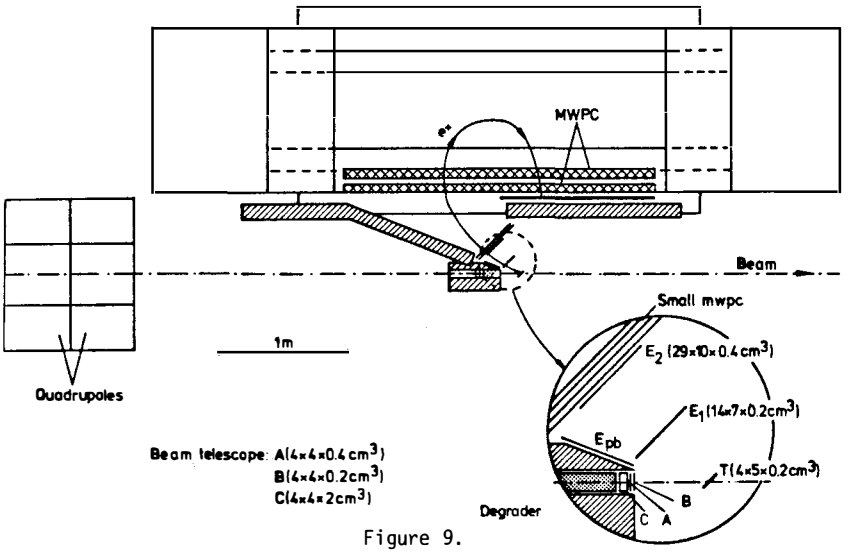


Figure 9.

Setup of the $\pi \to e\nu$ experiment of the LOUVAIN-ZURICH-LAUSANNE collaboration. Pions are stopped in the scintillator target "T" and the emitted positrons are momentum analyzed by a transformed pair-spectrometer.

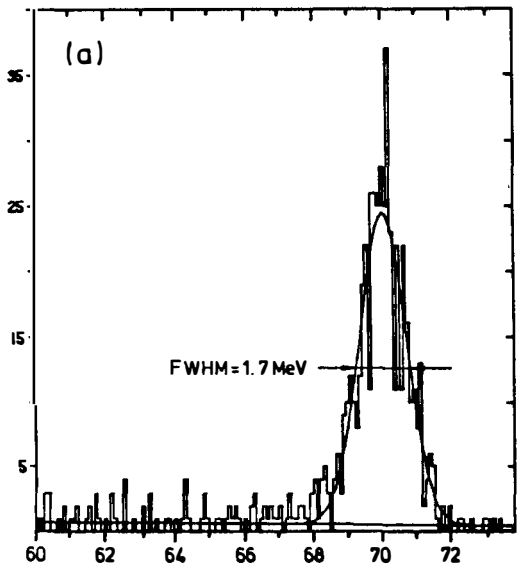


Figure 10.

Positron momentum spectrum of $\pi \to e\nu$ decay between 60 and 75 MeV/c. The momentum is computed by a retracing method.

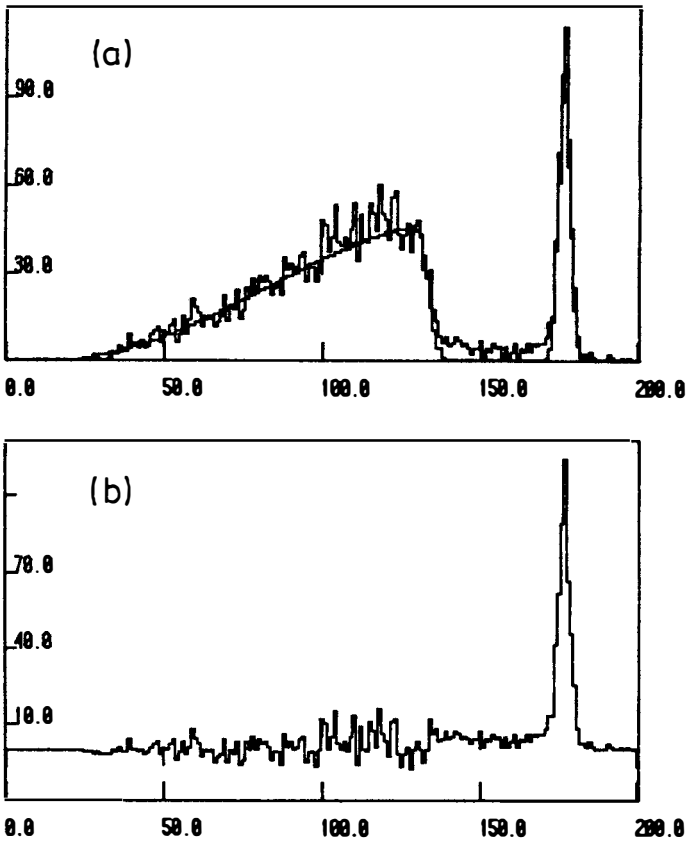


Figure 11.

a) Total positron energy spectrum computed by a retracing method after cuts to reduce the π - μ - e cascade contribution. These positrons are emitted within the 30 first nsec. after the pion stop. "Michel" to "$\pi \rightarrow e\nu$" ratio is 6.4 ; total $\pi \rightarrow e\nu$ events are 441 with a resolution of 1.7 MeV/c FWHM.
b) Experimental spectrum obtained after substraction of a fitted "Michel" spectrum folded with an approximate response function.

AN UPPER LIMIT ON THE ν_τ MASS*

Clara Matteuzzi
Stanford Linear Accelerator Center
Stanford University, Stanford, California 94305

ABSTRACT - An upper limit on the ν_τ mass was set studying the four-pion invariant mass distribution in the decay $\tau \to 3\pi^\pm\pi^0\nu_\tau$, in the Mark II detector at PEP.[1] The limit is $m_{\nu_\tau} < 164$ MeV/c^2 at the 95% confidence level.

RESUMÉ - Nous avons utilisé la désintégration du lepton τ en $3\pi^\pm\pi^0\nu_\tau$, pour établir une limite supérieure de la masse du ν_τ. Notre résultat est $m_{\nu_\tau} < 164$ MeV/c^2 a 95% niveau de confiance.

*Work supported by the Department of Energy, contract DE-AC03-76SF00515.

The ν_τ is the less well known object among all the known types of neutrinos: its interactions have not yet been observed, differently from ν_e and ν_μ, and the measurements of its mass are quite poor. Previous measurements have given upper limits of 250 MeV/c^2. This value was determined from a study of the electron spectrum[2] from the decay $\tau \to e\nu_e\nu_\tau$ and from a study of the pion spectrum[3] from the decay $\tau \to \pi\nu_\tau$. For comparison, the upper limit on the ν_μ mass is 0.500 MeV/c^2 at the 90% confidence level[4], and the ν_e mass has been measured[5] to lie between 14 and 46 eV/c^2 at the 99% confidence level. The measurement reported here sets a new upper limit on the ν_τ mass from the study of the four-pion invariant mass spectrum in the decay $\tau \to 3\pi^\pm\pi^0\nu_\tau$. This decay mode is more sensitive to the ν_τ mass since the invariant mass of the four-pion state approaches the τ mass. Furthermore, the invariant mass is not affected by radiative corrections.

The data were taken with the Mark II detector at the e^+e^- storage ring PEP at a center of mass energy of 29 GeV. At this energy, the reaction $e^+e^- \to \tau^+\tau^-$ has a very peculiar topology, the τ's being produced back to back, and their decay giving a final low multiplicity. The reaction is therefore well separated from $e^+e^- \to q\bar{q} \to$ hadrons, the averaged charged multiplicity of which being $\sim$ 11 particles. The Mark II detector has been described in detail elsewhere.[6] We briefly describe the apparatus relevant to this analysis. It contains two charged particle tracking devices, a high precision drift chamber (the vertex chamber)[7], and a large drift chamber with seven layers of axial drift cells divided into an inner band of four layers and an outer band of three layers. The main drift chamber consists of 16 layers of sense wires at radii between 41 and 145 cm. Both tracking chambers are immersed in a 2.3 kG solenoidal magnetic field. For high momentum charged particles, the rms momentum resolution σ_p/p, is approximately 0.10p, where p is measured in GeV/c.

The central electromagnetic calorimetry is provided by eight rectangular lead-liquid-argon modules which surround the magnet coil. These modules are approximately 14 radiation lengths thick and provide an energy resolution of $14\%/\sqrt{E}$, where E is the energy measured in GeV.

The integrated luminosity of the data used in this analysis was 158 pb^{-1} and corresponds to a sample of 16300 produced $\tau^+\tau^-$ pairs.

We selected events as $\tau^+\tau^-$ candidates if they had a total detected energy larger than 8 GeV and exactly four charged particles with zero total charge. Each event was divided into two hemispheres by a plane perpendicular to the thrust axis and was required to have three charged particles in one hemisphere recoiling against a single charged particle in the other. The accolinearity

angle, defined as the angle between the total momenta of the particles in each hemisphere, had to be smaller than 50°. To select well measured events, we required each charged track to have signals in at least 14 layers of the two drift chambers, and to approach the vertex within 2 cm in the plane transverse to the beam direction and within 15 cm along the beam direction. We also required the total energy of the three charged particles to be less than 15 GeV. Events with a low-mass pair of tracks, one of which was identified as an electron, were rejected since this pair was most likely from a π^0 Dalitz decay or from a photon which converted close to the interaction point. Electrons were identified[8] by the calorimeters when the electron energy was greater than 1 GeV and by the time of flight counters when the electron energy was less than 350 MeV.

At least two photons were required to accompany the τ decay that contained three charged particles. Each photon was required to be detected well inside the fiducial volume of the calorimeter modules to have a measured energy greater than 250 MeV, and to be separated by at least 20 cm in the calorimeter from all charged tracks with energy deposit in the liquid argon smaller than the minimum ionizing energy. To discriminate further against backgrounds due to charged particle interactions in the calorimeters, photons with measured energies less than 600 MeV were required to have a ratio of energy deposited in the rear layers to that deposited in the front layers of less than 1.5. Additional requirements were applied if the photon shared energy with other particles in one or two of the calorimeter coordinates.

A fit to the π^0 mass was performed by adjusting the photon energies. To eliminate contributions from higher π^0 multiplicity decays, we also required that no more than one π^0 could be reconstructed from all combinations of the detected photons--that is, that at most one combination had $\chi^2 < 10$.

Figure 1 shows the $\gamma\gamma$ invariant mass distributions after the above event selection requirements. There is a clear π^0 signal with little background. There were 64 events in which the fit had a confidence level larger than 10% and these were retained. The fitted values for the photon energies were subsequently used in the calculation of the four-pion invariant mass.

The total energy of the $3\pi^{\pm}\pi^0$ state was required to be greater than 8 GeV for $m_{4\pi} > 1.5$ GeV/c^2. This requirement loses 7% of the τ events, while rejecting 50% of the hadronic background. Figure 2 shows the invariant mass distribution for the 60 events which survived all of the event selection criteria. There are no events between 2.0 and 2.5 GeV/c^2, showing that the hadronic background is very small. The background in Fig. 2 from hadronic events was determined from a Monte Carlo simulation to be 3% in the total sample, and (10 ± 10)% in the

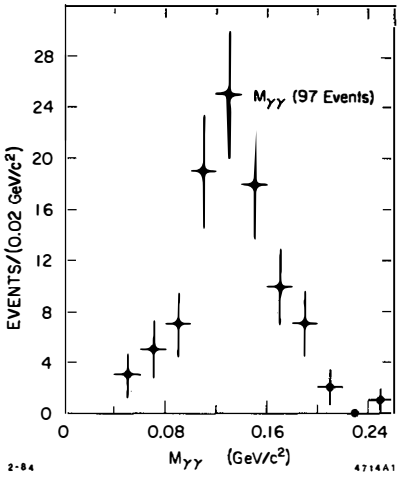


Fig. 1: γ-γ invariant mass distribution for the $3\pi^{\pm}\pi^0$ candidates before requiring the confidence level for a fit to the π^0 hypothesis to be greater than 10%.

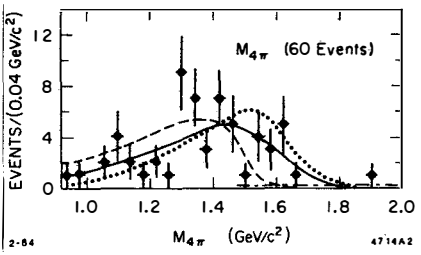


Fig. 2: $3\pi^{\pm}\pi^0$ invariant mass distribution for the selected decays. The curves are drawn for m_{ν_τ}=0 (solid) and 250 MeV/c^2 (dashed) and with the assumption that the four-pion state is dominated by a p' resonance of mass 1570 MeV/c^2 and width 510 MeV/c^2. The dotted line is pure phase space decay. The dashed-dotted line represents the hadronic background.

region $m_{4\pi} > 1.5$ GeV/c^2. The resolution in invariant mass was determined from the Monte Carlo simulation as a function of $m_{4\pi}$. Its average value is (53 ± 5) MeV/c^2 in the range $m_{4\pi} > 1.5$ GeV/c^2.

The upper range of the $m_{4\pi} > 1.5$ GeV/c^2, was compared to the expected behavior[9] for different values of the ν_τ mass and different assumptions about the four-pion state. Only the upper part of the $m_{4\pi}$ spectrum is sensitive to the ν_τ mass. The value of 1.5 GeV/c^2 was chosen because it gives the best compromise between sufficient sensitivity and adequate statistics. A maximum likelihood method was applied to determine an upper limit from the 15 events in the $m_{4\pi} > 1.5$ GeV/c^2 region. The hadronic background was taken to be distributed uniformly over the invariant mass range, as suggested by the Monte Carlo simulation.

If the $\tau \to 3\pi^{\pm}\pi^0\nu_\tau$ decay is assumed to have a pure phase space distribution, the upper limit on the ν_τ mass is 155 MeV/c^2 at the 95% confidence level. If, as is more likely, the four-pion state is assumed to be dominated by a ρ' resonance[10] of mass 1570 MeV/c^2 and width 510 MeV/c^2, the limit is also 155 MeV/c^2. The results are not very sensitive to the various assumptions about the four-pion state since, in all cases, the $m_{4\pi}$ spectrum close to the τ mass is largely determined by the available phase space. The solid curve in Fig. 2 shows the calculated spectrum with the ρ' hypothesis and with $m_{\nu_\tau} = 0$. It is in good agreement

with the data.

We checked the stability of the results by varying some of the parameters involved in the fit. If the experimental resolution in invariant mass is 20% worse than we have assumed, then the limit increases by 8%. If the fraction of background is increased from 10% to 30%, then the limit also becomes 8% worse. If the range of the invariant mass spectrum used in the fit is enlarged to $m_{4\pi} > 1.3$ GeV/c^2 instead of $m_{4\pi} > 1.5$ GeV/c^2, nothing is added to the sensitivity and the limit does not change.

When we take into account the systematic uncertainties in our knowledge of the hadronic background, our experimental resolution, and the mass and width of the ρ' resonance, we obtain an upper limit on the mass of the τ neutrino of 164 MeV/c^2 at the 90% confidence level.

REFERENCES

1) The MARK II experiment is run by a collaboration of SLAC, LBL, and Harvard University:

G. S. Abrams, D. Amidei, A. R. Baden, A. M. Boyarski, J. Boyer, M. Breidenbach, P. Burchat, F. Butler, D. L. Burke, J. M. Dorfan, G. J. Feldman, G. Gidal, L. Gladney, M. S. Gold, G. Goldhaber, L. Golding, G. Hanson, D. Herrup, R. J. Hollebeek, W. R. Innes, J. A. Jaros, I. Juricic, J. A. Kadyk, A. J. Lankford, R. R. Larsen, B. W. LeClaire, M. Levi, N. S. Lockyer, V. Lüth, C. Matteuzzi, M. E. Nelson, R. A. Ong, M. L. Perl, B. Richter, M. C. Ross, P. C. Rowson, T. Schaad, H. Schellman, D. Schlatter, P. D. Sheldon, W. B. Schmidke, G. H. Trilling, D. Wood, J. M. Yelton, C. de la Vaissiére, and C. Zaiser

2) W. Bacino et al., Phys. Rev. Lett. 42, 749 (1979).

3) C. A. Blocker et al., Phys. Lett. 109B, 119 (1982).

4) H. B. Anderhub et al., Phys. Lett. 114B, 76, 1982. See also P. Le Coultre communication at this Conference.

5) V. A. Lyubimov et al., Sov. Phy.-JETP 54, 616 (1982).

6) R. H. Schindler et al., Phys. Rev. D24, 78 (1981).

7) J. A. Jaros, in Proceedings of the International Conference on Instrumentation for Colliding Beam Physics, SLAC-Report 250, Edited by W. Ash, Stanford, California (1982), p. 29.

8) M. E. Nelson et al., Phys. Rev. Lett. 50, 1542 (1983).

9) P. Tsai, Private communication.

10) A. Cordier et al., Phys. Lett. 109B, 129 (1982).

SEARCH FOR THE DECAY OF HEAVY NEUTRINOS

CHARM Collaboration

F. Bergsma, J. Dorenbosch, M. Jonker and C. Nieuwenhuis
NIKHEF, Amsterdam, The Netherlands

J. V. Allaby, U. Amaldi, G. Barbiellini, L. Barone, C. Berger, A. Capone, W. Flegel, L. Lancieri, M. Metcalf, J. Panman, C. Santoni and K. Winter
CERN, Geneva, Switzerland

I. Abt, J. Aspiazu, F. W. Büsser, H. Daumann, P. D. Gall, F. Niebergall, K. H. Ranitzsch, P. Schütt and P. Stähelin
II. Institut für Experimentalphysik, Universität Hamburg, Hamburg, Fed. Rep. Germany

P. Gorbunov, E. Grigoriev, V. Kaftanov, V. Khovansky, and A. Rosanov
Institute for Theoretical and Experimental Physics, Moscow, USSR

A. Baroncelli, B. Borgia, C. Bosio, M. Diemoz, U. Dore, F. Ferroni, E. Longo, L. Luminari, P. Monacelli, F. de Notaristefani, P. Pistilli, L. Tortora and V. Valente
Istituto Nazionale di Fisica Nucleare, Rome, Italy

Presented by C. Santoni



ABSTRACT

No evidence for heavy neutrinos with a mass in the range 10-1750 MeV decaying into two electrons and one light neutrino was found in a search performed in the horn-focused wide-band neutrino beam and in the neutrino beam produced by the dump of 400 GeV protons in a copper target. The wide-band beam experiment is sensitive to neutrinos with a mass below 490 MeV, and for masses greater than 250 MeV yields an upper limit at 90% c.l. on the square of the neutrino mixing angle of $\approx 10^{-6}$. In the beam-dump experiment an upper limit on the square of the neutrino mixing angle of $\approx 10^{-10}$ was obtained in the neutrino mass range around 170 MeV, assuming that the neutrino associated with the τ lepton is massive. If no assumption is made on the nature of the heavy neutrino, a limit of $\approx 10^{-7}$ is obtained in the mass range around 1500 MeV.

A search for heavy neutrinos decaying into two electrons and one light neutrino was performed by the CHARM Collaboration using the 400 GeV wide-band neutrino beam and the neutrino beam produced by the dump of 400 GeV protons.

If neutrinos are massive, their weak (flavour) eigenstates are linear combinations of the mass eigenstates [1,2]:

$$\nu_l = \Sigma\, U_{li}\, \nu_i \qquad (l = e,\mu,\tau,\ldots,\ i = 1,2,3,\ldots) \tag{1}$$

A neutrino beam can then contain, in addition to its major part of light neutrinos, a minor component of heavy ones. As shown in Fig. 1, such neutrinos may be originated in the decay of pseudoscalar mesons M (π,K,D,F,...), produced by the interaction of protons with the target, and then decay in the detector.

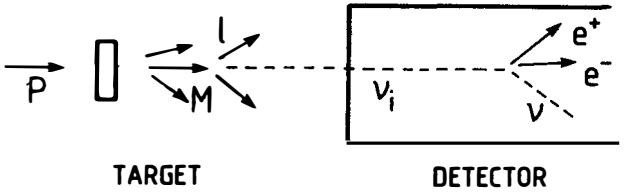


Fig. 1 Production and decay of heavy neutrinos.

Heavy neutrinos are produced with a rate [1,2]:

$$\frac{\Gamma(M\to\nu_i[m]+l+X)}{\Gamma(M\to\nu[0]+l+X)} = \rho|U_{li}| \ . \tag{2}$$

The factor ρ depends on the neutrino mass m. In the case of purely leptonic decay, it takes into account the fact that, for finite neutrino mass, there is less suppression due to helicity conservation than in the case of a zero-mass neutrino (as an example: for a neutrino mass of 200 MeV, $\rho \approx 10^5$ in the case of the $K \to e\nu$ decay and $\rho \approx 4$ for the $K \to \mu\nu$ decay).

Neutrinos with a mass larger than a few mega-electronvolts can decay into a light neutrino and two electrons. For neutrinos with mass larger than 110 MeV other decay channels are open ($\nu_i \to e\mu\nu$, $\nu_i \to e\pi$, ...). The probability for heavy neutrino decay is proportional to the square of the neutrino mixing angle $|U_{li}|$ defined in eq.(1) [1,2].

The number of heavy neutrino decay events expected in the detector is given by:

$$N_{ev} = \Phi\, P_{dec} \approx |U_{l'i}U_{li}|^2 \ , \tag{3}$$

where Φ is the heavy neutrino flux and P_{dec} is the probability for the neutrino to decay in the detector; $U_{l'i}$ and U_{li} are the neutrino mixing angles entering respectively into the meson and the heavy neutrino decay probability.

Heavy neutrinos decaying into a pair of electrons [1,2]:

$$\nu_i \rightarrow e^+e^-\nu_e \ , \tag{4}$$

were searched for in the CHARM experiment. This decay mode was considered because the CHARM detector can identify electromagnetic showers [3] and, moreover, it allows a search for massive neutrinos in a wide mass range. The lifetime of the decay (4) is scaled from the muon-decay lifetime and is given by:

$$\tau_i = |U_{ei}|^2 \ (m_\mu/m_i)^5 \ \tau_\mu \ . \tag{5}$$

In the wide-band neutrino beam experiment, heavy neutrinos produced in the decay of π's and K's were searched for. The search for "two-electron events" was performed in a sample of 1.3×10^6 neutrino and 1.4×10^6 antineutrino interactions collected in the fine-grain CHARM calorimeter [3]. The neutrinos and antineutrinos were produced by 1.4×10^{18} and 5.7×10^{18} protons on target, respectively. The events induced by reaction (4) would appear in the calorimeter as muonless narrow showers, which are a characteristic of electromagnetic showers [3], with a small angle θ between the shower axis and the direction of the incoming neutrino beam and with more than two minimum ionizing particles at the shower origin. A total of 1100 electromagnetic events with a visible energy E between 7.5 and 50 GeV and a value of the variable $E^2\theta^2$ below 0.54 GeV^2 were selected. These events come from:

a) elastic and quasi-elastic charged-current events induced by the electron-neutrino contamination of the beam,

b) events induced by the scattering of neutrinos on electrons,

c) neutral-current events with a γ or a π^0 in the final state produced by coherent scattering of muon neutrinos on nuclei [4],

d) neutrino decay events, if any.

These classes were separated making use of the variables $E^2\theta^2$ and E_f, where E_f is the energy deposited in the first scintillator plane following the shower vertex. As shown in Fig. 2, showers initiated by the decay of massive neutrinos into two electrons or by a γ or π^0 from process (c) almost always have a value of E_f larger than that released by one minimum ionizing particle (6 MeV), whilst a large fraction of the showers due to single electrons induced by processes (a) and (b) give an energy deposition corresponding to one minimum ionizing particle. The total number of events due to processes (a) and (b) was obtained from the subsample of the events with $E_f < 8$ MeV by a study of the event distribution versus the variable $E^2\theta^2$ as shown in Fig. 3a. Fig. 3b shows the $E^2\theta^2$ distribution for the events with $E_f > 8$ MeV after subtraction of

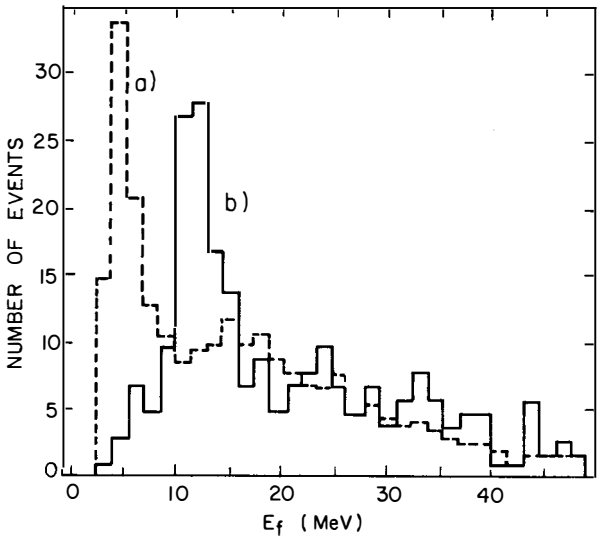


Fig. 2 Measured distribution of the energy deposition in the first scintillator plane after the vertex. a) single-electron-induced showers, b) showers induced by two electrons, γ or π^0. The contamination due to electon-induced shower is estimated to be 15%.

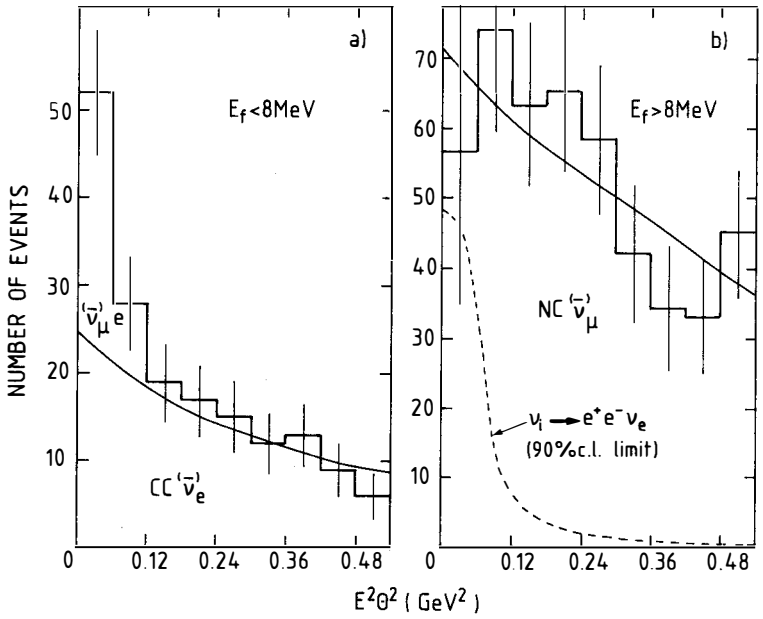


Fig. 3 Distributions of the candidate events observed in the WBB as a function of $E^2\theta^2$.

single-electron events which have radiated a photon converted in the target plate preceding the scintillator. The solid curve represents the contribution due to process (c). The number of events attributed to heavy neutrino decay is compatible with zero. For neutrino masses below 140 MeV, 1 ± 41 events are attributed to neutrino decay in the cas of a muon partner, and 1 ± 49 events in the case of an electron partner. For larger neutrino masses, acceptance effects change the sensitivity by a factor of ≈ 0.5. In Fig. 3b the dashed curve represents the expected distribution for the decays of neutrinos having a mass of 240 MeV normalized to the 90% c.l. limit.

In the beam-dump experiment, heavy neutrinos produced in the decay of short living particles (D's and F's) were searched for. The layout of the beam-dump experiment [5] is shown in Fig. 4. A scintillation counter plane of 6×4.8 m^2 active area (SC1) defines the beginning of the decay volume. The decay region is parallel to the neutrino beam line at a mean distance of 5 m, corresponding to an angle with respect to the incident proton beam of 10 mrad. The detector covers a solid angle of 3.9×10^{-5} sr. One module of the CHARM fine-grain calorimeter was displaced to the end of the decay region. The performance of this module is well understood [3] and has been tested in many experiments. The energy of electromagnetic cascades is measured in this module, which is 6 radiation lengths deep, with a resolution of $\Delta E/E < 0.30$ for shower energies $E > 5$ GeV. The decay volume is subdivided into three regions, using two sets of proportional tubes (P1 and P2) [3] (see Fig. 4). Each set consists of four planes of proportional drift tubes, covering a surface of 4×4 m^2, preceded by a lead plane of 1/2 radiation length thickness. The wires in the first two planes of each set are horizontal and in the last two planes vertical. The planes of a set are separated by 15 cm. In order to improve the angular resolution of the shower and to better reconstruct the decay point, a

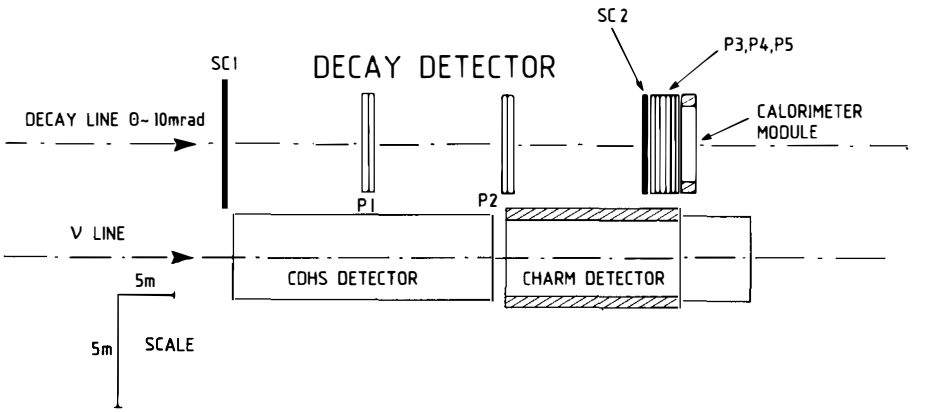


Fig. 4 Layout of the decay beam-dump experiment.

low-density detector was added in front of the CHARM calorimeter module. This was made of three sets of proportional tubes (P3, P4, and P5), covering an area of 4 x 4 m^2. In front of these was placed a scintillation counter plane of the same area (SC2). The estimated angular resolution for an electromagnetic shower is a few milliradians.

The signature of the events induced by reaction (4) would be one or two electromagnetic showers with their origin in the decay region. The detector was exposed to a neutrino flux produced by 1.7 x 10^{18} protons on a solid copper target [6] and 0.7 x 10^{18} protons on a copper target laminated with an effective density of 1/3 of solid copper [6]. In the combined exposures, 21,000 events were collected satisfying the following trigger requirements: no hits in the scintillator plane SC1 and a hit in at least four scintillator planes of the calorimeter module. These events include: cosmic-ray events (a track not pointing to the scintillator plane SC1), parasitic events (tracks from neutrino interactions in the CDHS and CHARM detectors or in the floor), beam-associated muons, and neutrino interactions. In order to check the performance of the decay detector the events recognized as neutrino interactions and having the shower vertex after the scintillator plane SC2 were used. In this part of the decay detector 340 ± 45 neutrino interactions were observed. Based on the number of neutrino interactions observed in the CHARM calorimeter, and taking into account the different mass and the different angle with respect to the proton beam [5], 440 ± 50 neutrino interactions were expected.

Events recognized to be cosmic rays entering the detector, parasitic events, and beam-associated muons were eliminated from the sample. The decay candidates were required to have at least one hit in the scintillator plane SC2 (corresponding to a decay region of 35 m length), and a shower energy larger than 3 GeV. The sample was scanned to look for candidates which are consistent with having two electrons. The scanning criteria were: in the case of a single hit in the scintillator plane SC2, the pulse height was required to be larger than that corresponding to the energy released by the passage of 1.5 minimum ionizing particles (9 MeV), and not more than two tracks in the proportional-tube sets P3, P4, and P5. No event satisfies these criteria.

From these two negative results limits on the mixing angle values were obtained.

In the wide-band neutrino beam experiment, the expected number of neutrino decay events in the detector is proportional to $|U_{ei}|^4$ or to $|U_{\mu i}U_{ei}|^2$, depending on whether the heavy neutrino is produced with an electron or a muon, in the decay of π's and K's. The heavy neutrino flux was computed using the wide-band beam Monte Carlo simulation program [7]. The absolute normalization was obtained from the number of neutrino interactions collected in the calorimeter.

In the beam-dump experiment, assuming that the heavy neutrinos are originated in the D's decay, the expected number of events is proportional to $|U_{ei}|^4$ or to $|U_{\mu i}U_{ei}|^2$ as in the case of the wide-band experiment. If one assumes that heavy neutrinos are produced in the leptonic decay of the F meson ($F \to \tau\nu$) and in the subsequent τ decay, and that the weak eigenstate ν_τ couples mainly with a single-mass eigenstate ν_i: $|U_{l',i}|^2 = |U_{\tau i}|^2 = 1$, the number of events expected in the detector is proportional to $|U_{ei}|^2$. The last assumption is justified by the present limit on the τ neutrino mass: 250 MeV [8]. The flux of heavy neutrinos was computed by assuming: $BR(D \to \mu\nu[0]) = 7 \times 10^{-4}$, $BR(D \to e\nu[0]) = 15.4 \times 10^{-9}$ and $BR(D \to lX\nu[0]) = 0.1$ in the case of the D source [9] and $\sigma_F/\sigma_D = 0.2$ and $BR(F \to \nu_\tau\tau) = 0.03$ in the case of the F source [10]. The factor ρ in (2) for the semileptonic decay of the D's has been computed making use of the 'Spectator' model [11]. The normalization was obtained from the number of prompt single-muon events observed in the CHARM calorimeter (1380 ± 250) [12]. These events are mainly induced by ν_μ coming from D decay. In the acceptance calculation the production of D and F mesons was simulated by a Monte Carlo program, assuming a distribution for the Feynman variable x corresponding to $(1-x)^4$ and a transverse momentum distribution proportional to $\exp(-2\,p_t)$. Cascade production was taken into account.

The limits at 90% c.l. on $|U_{ei}|^2$ and on $|U_{\mu i}U_{ei}|$ in the neutrino mass range 10-1750 MeV are shown in Figs. 5a and 5b. The result coming from the 'D decay' assumption is still preliminary. The limits on $|U_{\mu i}U_{ei}|$ cannot be directly

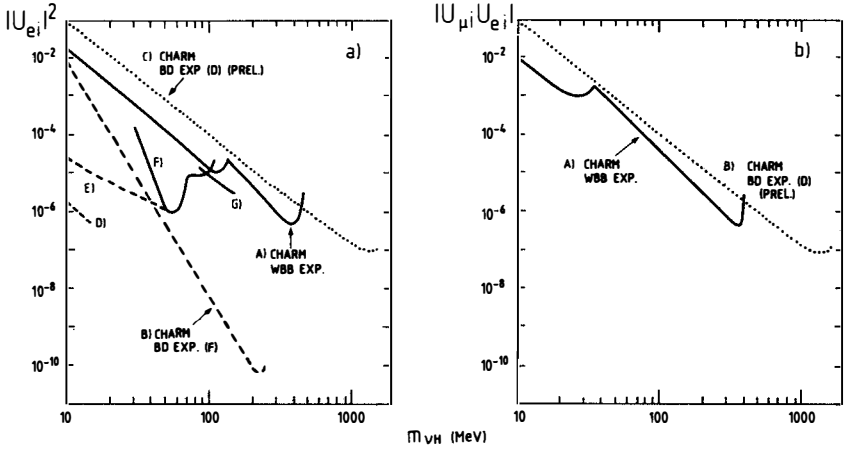


Fig. 5 a) Limits at 90% c.l. on $|U_{ei}|^2$ as a function of neutrino mass:
A) wide-band beam (WBB) experiment, B) beam-dump (BD) experiment [F decay], C) beam-dump (BD) experiment [D decay], D) limits from solar neutrino measurements [13], E),F) limits from the measurements of the $\pi \to e\nu$ decay [14], G) limits from the measurements of the $K \to e\nu$ decay [15].
b) Limits at 90% c.l. on $|U_{ei}\,U_{\mu i}|$ as a function of neutrino mass:
A) wide-band beam (WBB) experiment, B) beam dump (BD) experiment [D decay].

compared with published limits because they refer only to $|U_{ei}|^2$ [13-15] and $|U_{\mu i}|^2$ [16,17]. It should be noted that if the mixing angles are > $0.1[10^{-3}]$ then the wide-band neutrino-beam experiment [the beam-dump experiment] is no longer sensitive to neutrino masses larger than 350 [1200] MeV, since the beam would be heavily attenuated by decays before reaching the CHARM detector which is ≈ 900 [≈ 500] m from the neutrino source.

In conclusion, there is no evidence for the decay into two electrons of heavy neutrinos with mass in the range 10-1750 MeV. The wide-band beam experiment is sensitive to values of $|U_{ei}|^2$ and $|U_{\mu i}U_{ei}|$ of ≈ 10^{-6} for neutrino masses around 250 MeV. In the beam-dump experiment an upper limit at 90% c.l. on $|U_{ei}|^2$ of 10^{-10} was obtained in the neutrino mass range around 170 MeV assuming that the ν_i produced by the F 'identifies' with the ν_τ. If the heavy neutrinos are produced by the D, preliminary limits on $|U_{ei}|^2$ and $|U_{\mu i}U_{ei}|$ of ≈ 10^{-7} are obtained for neutrino masses around 1500 MeV.

In the summer of 1983 the beam-dump detector have been exposed to the wide-band beam. An improvement of 1-2 orders of magnitude in the limits on the mixing angle values is expected.

REFERENCES

1. R. E. Shrock, Phys. Rev. D24 (1981) 1232.

2. M. Gronau, Stanford preprint SLAC-PUB-2967, August 1982.

3. M. Jonker et al. (CHARM Collaboration), Nucl. Instrum. Methods 200 (1982) 183.

4. K. Lackner, Nucl. Phys. B153 (1979) 526.

5. M. Jonker et al. (CHARM Collaboration), proposal CERN/SPSC/81-21, SPSC/P142 Add. 1, 12 March 1981.

6. M. Jonker et al. (CHARM Collaboration), proposal CERN/SPSC/80-31, SPSC/P142, 25 April 1980 (WA65).

7. C. Visser, NUBEAM, CERN Hydra Application Library (1979).

8. W. Bacino et al., Phys. Rev. Lett. 42 (1979) 749.
A more stringent limit on the ν_τ mass (170 MeV) has been presented at this conference by C. Matteuzzi.

9. E. L. Berger, L. Clavelli and N. R. Wright, Argonne preprint ANL-HEP-PR-82-32, July 1982.

10. D. Haidt, CERN 83-02 (1983), p. 63.

11. R. E. Shrock, Phys. Rev. D24 (1981) 1275.

12. Preliminary results from the CHARM Collaboration (unpublished).

13. D. Toussaint and F. Wilczek, Nature 289 (1981) 777. The limits are obtained from: K. Beurmann et al., Acta Phys. Acad. Sci. Hung. 29, Suppl.1 (1970) 173; T. Cline and G. Porreca, Acta Phys. Acad. Sci. Hung. 29, Suppl.1 (1970) 145; R. Mewaldt et al., Proc. 14th Int. Cosmic Ray Conf., Munich, 1975 (MPI für Extraterrestrische Physik, Munich, 1975), vol.1, p. 349.

14. D. A. Bryman et al., TRIUMF preprint TRI-PP-82-43 (1982), submitted to Phys. Rev. Lett..

15. D. Berghofer et al., Proc. Int. Conf. on Neutrino Physics and Astrophysics, Maui, Hawaii, 1981 (eds. R. J. Cence, E. Ma and A. Roberts) (Univ. of Hawaii, Honolulu, 1981), vol. 2, p. 67. The limits are obtained from the $K \to \nu e$ decay measurements: K. Heard et al., Phys. Lett. 55B (1975) 327; J. Heintze et al., Phys. Lett. 60B (1976) 302.

16. R. Abela et al., Phys. Lett. 105B (1981) 263.

17. R. S. Hayano et al., Phys. Rev. Lett. 49 (1982) 1305.

SOME NEUTRINOS DECAYS

Jean-Michel LEVY

LPNHE, Université Pierre et Marie Curie
Tour 12 - 3e étage
4, place Jussieu
75230 Paris Cedex 05

INTRODUCTION

Massive neutrinos mixing with weak interaction eigenstates are expected to decay into various channels depending on their masses and their mixing pattern. In what follows we review some of these decay modes in the simplest possible frame ; in general, we shall consider only the addition of right handed neutrino fields to the spectrum of the standard Glashow-Salam-Weinberg theory of weak interactions, thereby allowing for the existence of Dirac masses generated through the coupling of these fields and their left-handed mates with the usual Higgs doublet and its charge-conjugate, as is the case for quarks.

We feel that this rather conservative attitude is justified both by the huge number of possibilities allowed as soon as one deviates from the simplest pattern, which precludes any attempt to exhaustiveness in a restricted space, and by the latest experimental findings which seem to point to the absence of Majorana neutrinos (non observation of neutrinoless double β decay)[1] and to a (very)small mass for the electron-neutrino[2] which would then arise from a Dirac term.

After a review of the most simple decay possibilities in this restricted frame, we shall briefly describe a forth coming experiment designed to detect some of these.

Notation : the weak group eigenstates are denoted with a greek index while the mass eignestates are indicated by a latin index. Symbollically $\nu_k = \sum_\beta U_{k\beta}\nu_\beta$ with $\beta = e,\mu,\tau...$ and U the leptonic mixing matrix.
In the sequel, $\nu_h(\nu_\ell)$ will stand for a heavy (light) neutrino mass eigenstate.

I. THE SIMPLEST : $\nu_H \to e^-e^+\nu_\ell$.

The decay, analogous to μ decay, is allowed in tree approximation if the mixing matrix element U_{he} is non zero and it corresponds to the graph of fig. 1a.

Neglecting m_ℓ with respect to m_h and m_e one finds for the width :

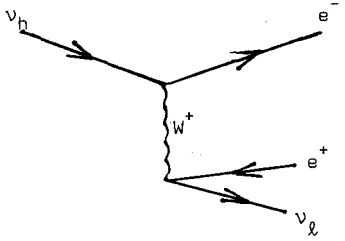
$$\Gamma(\nu_h \to e^+e^-\nu_\ell) = \frac{G^2 m_h^5}{64\pi^3} f(r) \left| U_{he}U^*_{\ell e} \right|^2 \qquad (1.1)$$

with $r = \frac{4m_e^2}{m_h^2}$ and $f(r) = \sqrt{1-r}\ (\frac{1}{3} - \frac{7r}{6} - \frac{r^2}{24} - \frac{r^3}{16}) + r^2(1 - \frac{r^2}{16})\ \mathrm{Tanh}^{-1}(\sqrt{1-r})$

If $r \ll 1$ this is like the standard μ decay formula and gives a lifetime of

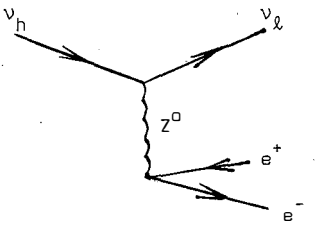
$$\tau(\text{sec}) = 2.9.10^{4}\left(\frac{m_h}{\text{MeV}}\right)^{-5} / \left|U_{he}U^{*}_{\ell e}\right|^{2} \qquad (1.2)$$

There are a priori also neutral current graphs contributing (fig. 1b) but in our restricted frame they add up to zero when one sums over the weak interaction eigenstates coupling to Z°, due to the unitarity of U. In some models, however [3], like the much studied left-right symmetric alternative to the standard theory, such graphs may contribute. If one assumes only h-e and ℓ-e couplings, the sum results in a decay width given by formula (1.1) times a factor $\frac{1+a^2}{8}$ where $a = 1+4\sin^2\theta_w$ and θ_w is the weak mixing angle. Thus, there is destructive interference between the neutral and charged current pieces



$\times U_{he}\,U^{*}_{\ell e}$

(a)



$\times \sum_{\beta} U_{h\beta}U^{*}_{\ell\beta} = \delta_{h\ell} \to 0$

(b)

Fig. 1. Graphs contributing to $\nu_h \to \nu_\ell\, e^- e^+$. In fact, graphs (b) cancel in the simplest scheme considered here.

The same cancellation forbids decays like $\nu \to 3\nu$ in our scheme. Again, this is not true in the lift-right symmetric theory.

II. THE MOST DISCUSSED $\nu_h \to \gamma\nu_\ell$

This is the analogue of the much looked for decay $\mu \to e\gamma$ and is of great importance in cosmology.

The decay goes through one loop according to the graphs shown in fig. 2 but is strongly suppressed due to the GIM mechanism[4]. It has been computed by many authors[5] with the following result :

Let $r = (m_\ell / m_h)^2$ and $X_\beta = (m_\beta / m_w)^2$

then $$\Gamma(\nu_h \to \nu_\ell \gamma) = \frac{\alpha G^2}{32\pi^4} m_h^5 (1-r)^3 (1+r) \left| \sum_\beta U_{h\beta} U^*_{\ell\beta} F(x_\beta) \right|^2 \qquad (2.1)$$

For known charged leptons $X_\beta \ll 1$ and $F \simeq -\frac{3}{4} + \frac{3x}{8}$ so that the sum in the right hand side is $\sum_\beta \simeq 3/8\, X_\tau\, U_{h\tau} U^*_{\ell\tau}$ giving a lifetime of

$$\tau(\text{sec}) = 5.4.10^{13} \left(\frac{m_h}{\text{MeV}}\right)^{-5} / |U_{h\tau} U^*_\tau|^2 \qquad (2.2)$$

This could only be reduced by the existence of a very heavy charged lepton in our frame (see however[6] for a scheme giving rise to less desperatly long lifetimes).

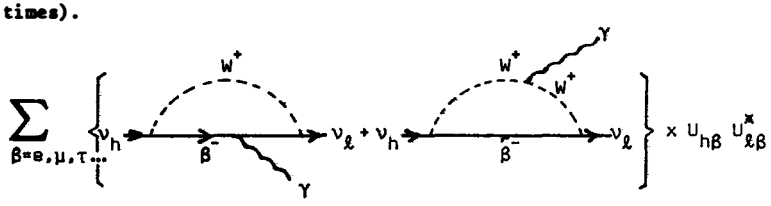


Fig. 2. The decay $\nu_h \to \gamma\nu_\ell$; graphs with one or two W propagator replaced by unphysical higgses must be added when one works in a renormalizable gauge.

III. THE LATEST $\nu_h \to \gamma\gamma\nu_\ell$.

This mode is interesting because it turns out that the GIM suppression which is expected a priori to play the same role as in the one γ decay is in fact ineffective. It has been known for a long time[9] that the leading contribution comes from the first diagram of Fig. 3 which is a factor $(\frac{M_w}{m_\beta})^2$ above the others. Using only this graph one gets the following width[7]

$$\Gamma(\nu_h \to \gamma\gamma\nu_\ell) = \frac{\alpha^2 G^2}{32\pi^5} m_h^9 \int_0^{(1-\sqrt{r})} ds((1-r)^2 - s(1+r))s^2 \lambda^{1/2}(1,s,r) \, |I|^2 \quad (3.1)$$

where $r = (m_e/m_h)^2$ and $I = \sum_\beta U_{h\beta} U_{\ell\beta} F(\frac{sm_h^2}{m_\beta^2}) \frac{1}{m_\beta^2}$

and $F(z) = \int_0^1 dx \int_0^{1-x} dy \frac{xy}{1-zxy}$ (3.2)

The very different magnitudes of the terms in the sum over β is what makes the GIM suppression being itself suppressed. The term with $\beta = e$ dominates for all values of m_h.
However, the m_h^9 factor is deceiptive and the approximation[7)8)] $F(z) \simeq F(0) = \frac{1}{24}$, which would lead to the conclusion that this mode overtakes $\nu_h \to e^+e^-\nu_\ell$ for sufficiently high m_h is quite illegitimate but for r very close to 1 when the rate is very low anyway.

We find[10)] that F (3.2) can be expressed in terms of elementary functions with the following result :

$$F(z) = -\frac{1}{2z} + \frac{2}{z^2}\left[\sin^{-1}(\frac{\sqrt{z}}{2})\right]^2 \qquad z \leq 4$$

$$F(z) = -\frac{1}{2z} + \frac{\pi^2}{2z^2} - \frac{2}{z^2}\left[\cosh^{-1}(\frac{\sqrt{z}}{2})\right]^2 + \frac{2i\pi}{z^2}\cosh^{-1}(\frac{\sqrt{z}}{2}) \qquad z \geq 4$$

Keeping only the term with $\beta = e$, setting $m_\ell = 0$ and integrating numerically one finds the lifetime given in fig. 4, several orders of magnitude above that due to $\nu_h \to e^+e^-\nu_\ell$ which remains the dominant mode if $U_{he} \neq 0$.

If, however, for some reason $U_{he} = 0$ then there is a kind of competition between the one and two photons channels (the latter being now dominated by the μ-loop). This is depicted in fig. 5. Note that the comparison has an absolute meaning only in the case of three generations, for then $|U_{h\mu}U^*_{\ell\mu}| = |U_{h\tau}U^*_{\ell\tau}|$ if $U_{he} = 0$.

The same kind of competition occurs for $m_h \lesssim 1$ MeV if $U_{he} \neq 0$ and if the mixing coefficients for e and τ are of the same order of magnitude (fig. 6)

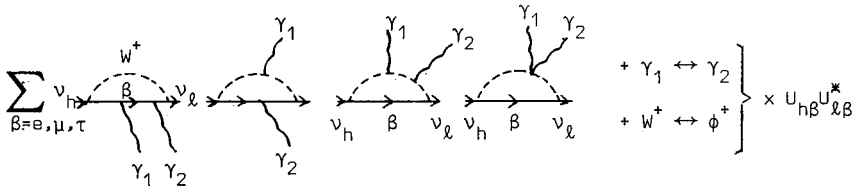


Fig. 3. The leading contribution is given by the first diagram and that with the photons exchanged alone.

IV. THE MOST OPTIMISTIC

Going to higher neutrino masses new channels open ; one finds first $\nu_h \to \mu^- e^+ \nu_e$ and/or $\nu_h \to e^- \mu^+ \nu_\mu$, then for example, $\nu_h \to \ell^- \pi^+$. The amplitude of this last mode is quite easy to relate to that of $\pi \to \nu\ell$ and one gets (neglecting m_e).

$$\Gamma = \frac{G^2 f^2 \cos\theta_c}{16\pi} m_h^3 \left(1 - \left(\frac{m_\pi}{m_h}\right)^2\right) |U_{he}|^2 \qquad (4.1)$$

with $f\cos\theta_c \simeq 128$ MeV. It is interesting in that in spite of the m_h^3 factor it dominates the $e^+e^-\nu_\ell$ mode for all reasonable values of m_h as soon as it is kinematically allowed, as is shown in fig. 7.

V. LOOKING AT NEUTRINOS DECAYS [11]

The CERN experiment P.S. 191 is specifically designed to look for some of the decay modes which we have reviewed. It will use a "low energy" (1 GeV) neutrino beam from the Proton Synchrotron (mainly ν_μ) which will be given 17 meters to decay before a calorimeter made of iron plates and planes of flash tubes in which the electromagnetic showers from ℓ's or γ's will develop and be measured (see Fig. 8). To make sure that charged particules originate from a point in the decay space and to reconstruct their trajectories, several planes of flashtubes will be placed between the muon shield and the calorimeter, the intervening space being filled with helium bags in order to minimize the amount of matter (Fig. 9).

This experiment should be sensitive to a massive component in the ν_μ beam down

to masses of a few MeV. In any case, it will give limits on the products of mixing matrix coeffcients several order of magnitudes lower than those given by searches for secondary peaks in the charged lepton spectra of pseudoscalar meson leptonic decays[12] (see[13]).

The kind of constraints which can be expected from the absence of $e^-e^+\nu$ events for ν_h originating from $\pi \to \mu\nu$ and ν_μ oscillating to ν_h looks like

$$|U_{he}U_{h\mu}|^2 < \frac{2.8.10^4 \mathrm{Log}^{1/c}}{N_\pi\, \alpha(m_h) m_h^6} \frac{E}{L}$$

when c is the required confidence level, N_π is the number of π in the hadron beam, E and L are the neutrinos energy and the decay length and

$$\alpha(m_h) = \frac{\Gamma(\pi \to \mu\nu;\ m_\nu = m_h)}{\Gamma(\pi \to \mu\nu;\ m_\nu = 0)} = \frac{r_\mu + r_\nu - (r_\mu - r_\nu)^2}{r_\mu (1-r_\mu)^2} \lambda^{1/2}(1, r_\mu, r_\nu)$$

with $r_{\mu,\nu} = (m_{\mu,\nu}/m_\pi)^2$, and 100 % efficiency has been assumed.

Note that one has to discriminate both between the decay and the production processes. In the hypotheses of massive and mixed neutrinos, a ν_μ originating from $K \to \mu\nu$ is not the same as that originating from $\pi \to \mu\nu$.

CONCLUSION

In the current activity for the determination of neutrino masses, neutrino decays play an important role in that, although they cannot compete with oscillations for the detection of very small masses, they are sensitive to much smaller mixing coefficients than any previous method of investigation in the region of higher masses.

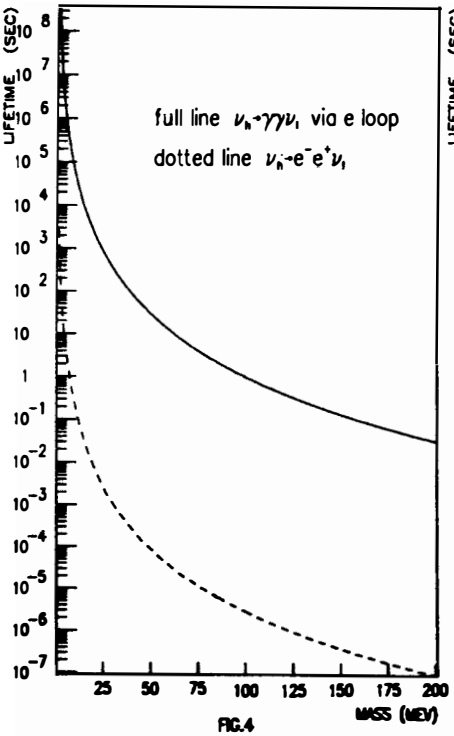


FIG.4

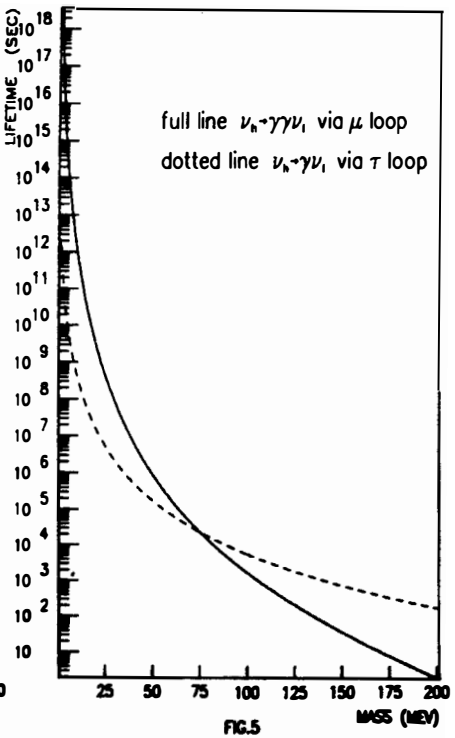


FIG.5

Fig. 4. *Comparison of heavy neutrinos lifetimes due to decaus via* $e^- e^+ \nu_\ell$ *and* $\gamma\gamma\nu_\ell$. *The times must be divided by* $|U_{he}\, U^*_{\ell e}|^2$.

Fig. 5. $U_{he} = 0$ *is assumed here. The lifetime due to two* γ *decay is in units of* $|U_{h\mu}\, U^*_{\ell\mu}|^2$. *sec. Whilst that due to one* γ *decay is in units of* $|U_{h\tau}\, U^*_{\ell\tau}|^2$. *sec. The comparison has an absolute meaning only in the case of three generations.*

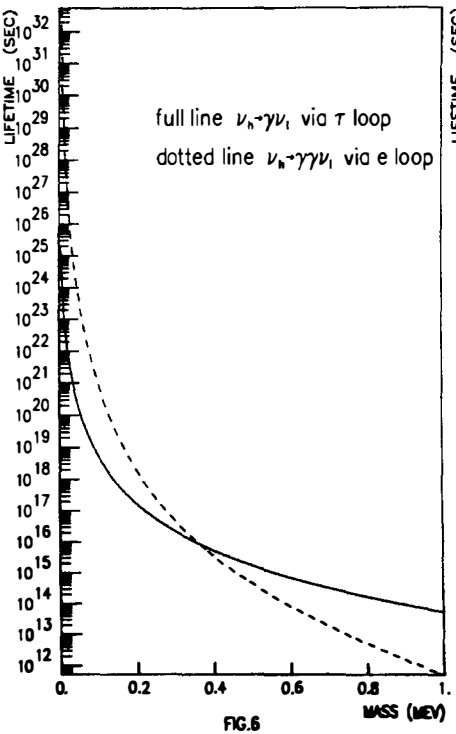


FIG.6

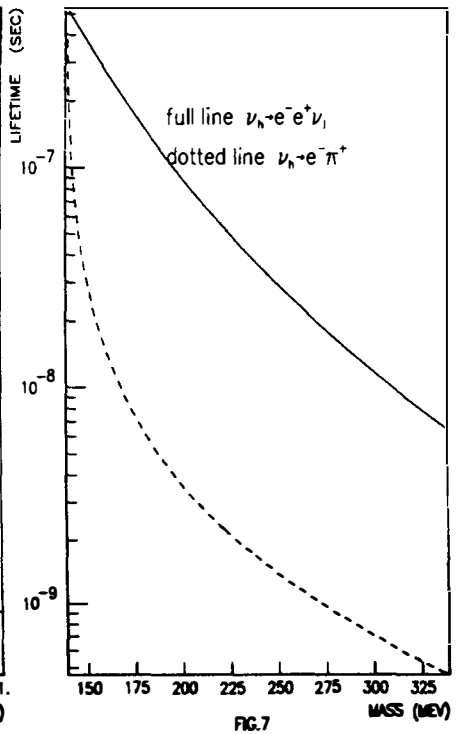


FIG.7

Fig. 6. Comparison of one and two photons neutrinos decays for $U_{he} \neq 0$ *under the* $e^-e^+\nu_\ell$ *threshold. The comparison makes sense only if* $|U_{he}\, U^*_{\ell e}| \simeq |U_{h\tau}\, U^*_{\ell\tau}|$

Fig. 7. There is no $|U_{\ell e}|$ *factor in the* $e^-\pi^+$ *decay width formula. Hence this mode is strongly favoured if there exists a neutrino of mass above 140 MeV.*

REFERENCES

1) T. KIRSTEN et al , Phys. Rev. Lett. 50, 474 (1983)
F.T. AVIGNONE et al, Ibid 50, 721 (1983)

2) V. LUBIMOV, Proceedings of the International Europhysics Conference on High Energy Physics. Brighton, July 83, p.386 (Published by Rutherford Appleton Lab.).

3) M. GRONAU, contribution at this conference .

4) S.L. GLASHOW, J. ILIOPOULOS, L. MAIANI, Phys. Rev. D2, 1258 (1970).

5) e.g. E. MA, A. PRAMUDITA, Phys. Rev. D24, 1410 (1981), P.B. PAL and L. WOLFENSTEIN, Phys. Rev. D 25, 766 (1982).

6) A. ZEE, Phys. Lett. 93B, 389 (1980).
S. T. PETCOV, Phys. Lett. 115B, 401 (1982).

7) J.F. NIEVES, Phys. Rev. D28, 1664 (1983).

8) F. VANNUCCI, LPNHE preprint 83-01.

9) M.K. GAILLARD AND B.W. LEE, Phys. Rev. D3, 897 (1974).

10) J.M. LEVY, unpublished.

11) D. PERRET-GALLIX et al., CERN/PSCC 83-12 (1983).

12) R.S. HAYANO et al, Phys. Rev. Lett. 89, 1305 (1982).
R. ABELA et al., Phys. Lett. 105B, 263 (1981).
D.A. BRYMAN et al, TRIUMF Preprint TRI-PP 82-43 (1982).

13) F. VANNUCCI, Contribution at this conference.

SEARCH FOR NEUTRAL, PENETRATING, METASTABLE PARTICLES PRODUCED IN THE SLAC BEAM DUMP*.

SLAC Experiment E-137†
Presented by J. Bjorken

Abstract

A search was made for neutral objects which might be produced by 20 GeV electrons incident on the SLAC beam dump, penetrate the downstream natural shielding, and decay upstream of an electromagnetic shower calorimeter. With about 30 coulombs of electrons dumped, no candidate events were found above an energy of ~2 GeV. Preliminary analysis implies the 95% confidence level limit on the product of mass and lifetime of light axion-like bosons decaying primarily into two photons to be greater than 0.8 keV-sec. Preliminary limits on photino parameters are also given.

†Collaboration members are:

J. D. Bjorken, (Fermi National Accelerator Laboratory, Batavia, Il. 60510), S. Ecklund and W. R. Nelson, (Stanford Linear Accelerator Center, Stanford, Ca. 94305), A. Abashian, L. Mo, and P. Rassman, (Dept. of Physics, Virginia Polytechnic Institute, Blacksburg, Va. 24061), C. Church, (Datec, Inc., 7601 Manchester Ave., Hanover Park, Il. 60103), and T. Nunamaker, (Nanometrics, Inc., 451 South Blvd., Oak Park, Il. 60302).

I. INTRODUCTION

In this note we report preliminary results of SLAC Experiment E-137. It was a search for neutral objects which might be produced by 20 GeV electrons incident on the SLAC beam dump, penetrate the downstream natural shielding, and decay upstream of an electromagnetic shower calorimeter. A primary motivation for this experiment was to search in a general way for axion-like, pseudo-Nambu-Goldstone-bosons. It turns out that the experiment sets useful bounds on the production of photinos, particles slightly more related to the subject matter of this workshop (They at least have the right spin). While the experiment is not a very sensitive probe of "conventional" massive neutrinos, there does exist a proposed follow-up search at Fermilab which is relevant to the topic of this workshop. That proposal, which has a "stage one" approval pending cost review and addition of more personnel, will make a similar search downstream of the Fermilab beam dump.

II. THE EXPERIMENT

We shall not enter here into a detailed discussion of the underlying phenomenology and motivation for experiment E-137, since it deals mainly with properties of conjectured axion-like entities. Suffice it to say that a search experiment as speculative as this one most probably will, in the unlikely case of a positive result, find something unanticipated and not what was proposed. For example, the first SLAC beam dump experiment[1] was motivated by possible existence of sequential heavy neutrinos, but became most relevant to axion searches[2]. Our experiment E-137, primarily motivated by axions, turns out to be relevant to photino searches.

We should mention features of this beam-dump experiment quite unique to SLAC. There is of course the high intensity of the primary beam, with a yield of approximately one coulomb of 20 GeV electrons delivered per (very good) day. The 1.6 μsec pulse length (180 pulses/sec) allows good cosmic-ray rejection. But most importantly the electrons, positrons, and photons which are produced in the dump (a large tank of water) have traverse momenta $\lesssim$ 20 MeV, much lower than in hadronic showers. This collimation, together with production mechanisms even more collimated, implies that beams of the sundry hypothetical

X-particles will be well collimated. This in turn allows a long decay region without significant loss of acceptance. The E-137 apparatus is located about 380 m downstream of the dump, with 200 m of available decay path in front of the detector. This geometry is typical of hadron dump experiments with more than an order of magnitude higher energy.

Typical collimated production mechanisms are shown in Fig. 1. They include coherent photoproduction of bosons which could then decay into $\gamma\gamma$ or e^+e^-, bremstrahlung of bosons from electrons followed by decay into e^+e^-, or annihilation of positrons upon atomic electrons, either resonantly (again followed by e^+e^- decay) or nonresonantly into a pair of particles such as photinos. (The photinos purportedly decay into γ + goldstino).

A sketch of the experimental layout is shown in Fig. 2. The SLAC primary beam was transported through end-station A, site of the classic deep-inelastic electron-scattering experiments. At that point a remotely controllable target could be inserted into the beam to generate beam-associated "sky shine" background. Charged pions photoproduced in this target emerged into the airspace viewed by the detector, where they interacted, producing at the detector mainly muons (along with a few photons) coming from decaying pion secondaries. These were useful for timing purposes as well as for checking out and monitoring detector performance. During dump running, the target was of course removed, and the primary electron beam was transported, without steering, to the primary beam dump located in the berm at the downstream end of the SLAC research area.

The detector itself was an 8-layer, 8 radiation-length shower calorimeter. Each layer consisted of a hodoscope of 0.5 m x 1.5 m x 1cm scintillation counters, one radiation length of iron or aluminum converter, and a plane of multiwire proportional chambers. For the first phase of the experiment (~10 Coulombs dumped), each plane was a 2 x 3 mosaic of the 1m x 1m chambers used in the Fermilab experiment of Heisterberg et. al[3]. which measured ν_μ e elastic scattering; aluminum radiator was used. For the final phase of the experiment (~20 Coulombs dumped) new 3m x 3m chambers of similar design were installed, and the radiator was replaced by steel.

Clearly good angular resolution (<<50 mrad) was essential, and this capability was obtained from the multiwire proportional chambers. As shown in Fig. 3, the two cathode planes of the chambers consist of delay lines milled from copper-clad G10, one for horizontal readout, the other for vertical. Each delay line was tapped at several points (5 for the 1m x 1m chambers and 24 for the 3m x 3m chambers), and the cathode signals were fed into CCD's operating at 50 MHz. The CCD, acting as a fast shift register, subdivided an incoming pulse into 20 nsec segments, and stored the charge of each segment into consecutive CCD "buckets". When a trigger from the scintillator hodoscope occurred, the CCD clock rate was reduced to 20 MHz until the charges in the 36 CCD "buckets" could be read out and digitized in sequence by one ADC. This provided essentially analogue information on the cathode pulse size and shape, with a spatial resolution of ~3 mm for the 3m x 3m chambers and ~8 mm for the original 1m x 1m chambers.

Two triggering schemes were used in parallel. The first emphasized energy and required that the total pulse height (per plane) in three out of any four adjacent planes be above a preassigned threshold. The threshold shower energy for this trigger was 400 MeV. The second trigger, which emphasized directionality, was highly efficient even for horizontal muons, and required at least four out of eight 0.5m x 1.5m x 1cm scintillators in a given row (i. e. having the same transverse location in the apparatus) to fire. Here the discriminator thresholds were set well below minimum ionizing.

The experiment was proposed and approved in 1980. The first run, with 9.5 coulombs of electrons dumped, occurred in January of 1982. The final run, with 20.4 coulombs of electrons dumped, occurred in November and December of 1982. In February 1984 the scintillator hodoscope was calibrated in the SLAC test beam.

The running conditions turned out to be quite clean. With the 1/4" aluminum target inserted into the beam, the trigger rate was ~3 x 10^6/coulomb, dominated by low energy muons. The energy spectrum of these beam-associated triggers is shown in Fig. 4a. Essentially nothing is found above an energy of 3 GeV. With the target removed, the triggers were dominated by cosmic rays with a rate ~10^3/coulomb. The energy spectrum is considerably harder, as shown in Fig. 4b. Of course the angular distribution is much broader, leading to easy rejection of

almost all these triggers. Examination of the time distribution of the low energy component of the spectrum does reveal a beam-associated signal. If the energy spectrum of that beam-associated signal is the same as for "target-in" data, there should be in the data sample less than 0.2 beam-associated triggers per coulomb with energy above 3 GeV.

A typical event as seen by the multiwire proportional chambers is shown in Fig. 5. The angular resolution for showers is difficult to estimate directly from the data because the incident direction is not known. Fits to the tracks give an estimated angular resolution of $\lesssim$10-20 mrad(FWHM), which, as will be seen in the next section, is very comfortable.

III. ANALYSIS and RESULTS

After the final run in late 1982, the data was scanned via computer-generated visual displays. Candidates of interest would be single or double showers which pointed in the general direction of the beam dump. It will come as no surprise that no signal was found. However, the limits we quote should still be regarded as preliminary pending completion of more work on estimating production cross-sections and efficiencies. Here we report on results from the final 20 Coulomb run. During that run ~23,000 triggers were written on tape. After cuts for energy (>1 GeV) and timing, ~6000 triggers survived. The overwhelming majority of these candidates were readily categorized as muons and cosmic ray showers. After the scan, where events which were observed to be grossly nondirectional were rejected, 189 events remained. These were measured, and after cuts requiring vertical and horizontal angles less than 300 mrad, only 24 events remained. These are shown in Fig. 6. One sees that only one event lies within a reasonable fiducial region of horizontal angle less than ±100 mrad and vertical angle less than 30 mrad (the approximate horizon of the shielding berm as seen by the detector). Just from the multiwire proportional chamber data this surviving event may be regarded as pointing toward the dump. But it has too low an energy; 2 GeV was the optimistic threshold cut already suggested in the proposal. The scintillator data implies that this event is caused by a muon which radiated a photon in the front portion of the detector and penetrated

the entire eight planes. We thus end up with no convincing candidate events.

A second line of analysis was also used which avoids possible subjectivity associated with the visual scanning. (However, in a search experiment such as this, and with the complex topology of the typical cosmic ray triggers, we believe there is no substitute for making the full scan.) In this alternative analysis, we required that the observed energy exceed 3 GeV, that the signal be in time with the beam, and that at least 2/3 of the energy be within a single scintillator row, as would be expected for almost all horizontal showers. Only 36 events passed these criteria, and the event sample overlapped the preceding sample of 189 obtained from the visual scan, again leading to no candidate events.

As already mentioned, we have not completed the full analysis, especially with regard to questions of resolution and efficiency, and to calculations of yields for a variety of conjectured particles. We here restrict ourselves to two reasonably topical candidate phenomena: light axions and photinos.

A) Axions

We assume the axion is photoproduced via the Primakoff effect, decays predominantly into two photons, and is of low mass (<30 MeV). Under these circumstances the experimental yield depends only upon lifetime and mass, and our preliminary estimate is

$$M_X \tau_X > 0.8 \text{ keV-sec.} \qquad \text{(preliminary; } M_X < 30 \text{ MeV; 95\%CL)}$$

In this estimate we have conservatively assumed the threshold energy for detection to be 3 GeV. The expected energy spectrum is proportional to the track-length distribution of photons in the water beam dump. This was computed via the EGS shower simulation program[4] (Fig. 7), and one sees that ~30% of the expected axion flux above 1 GeV actually lies above 3 GeV. Thus our quoted limit (which scales with the square root of the flux) is not inordinately sensitive to the cut in energy.

For a given mass, the axion lifetime must of course be long enough for the particle to penetrate the shielding berm before decaying. However, in that edge of the parameter domain, previous beam dump experiments are at least as sensitive as this experiment.

The classical Peccei-Quinn-Weinberg-Wilczek (PQWW) axion[5] has by now been convincingly ruled out experimentally[6]. The sensitivity of this experiment to a PQWW axion[7] is marginal, and is shown in Fig. 8. Were the PQWW axion to exist, experiment E-137 might have seen it. But E-137 never could have ruled out the whole mass range of 200-400 keV which was of interest two or three years ago[8]. However, it still remains important to search for generic axion-like entities (i. e. pseudo-Nambu-Goldstone-bosons) associated with perhaps some totally unanticipated spontaneous symmetry-breaking scheme remote from present experience. The present result most improves previous bounds on parameters if the axion-like entity is not coupled to currents containing known lepton or quark degrees of freedom.

B) Photinos

Some phenomenological supersymmetry schemes[9] have posited a light photino decaying into photon and goldstino. In this experiment, photino pairs may be produced in e^+e^- annihilation (on atomic electrons) via scalar-electron (selectron) exchange. The yield thus depends not only on photino mass and lifetime but also - quite sensitively - to the selectron mass[10]. The photino lifetime in turn depends[11] upon the scale $\Lambda=\sqrt{d}$ of supersymmetry breaking, conjectured to perhaps be in the range of 100 GeV to 10 TeV.

The positron spectrum was again computed via EGS. When convoluted with production cross-section and decay lifetime our estimated limit from this experiment is

$$\frac{\mu^3}{M^2\Lambda^2} < 6 \text{ mm. (95\% CL)}$$

where μ = photino mass $<<30$ MeV
M = selectron mass
Λ = supersymmetry breaking scale

The condition that the photino survives a journey through the shielding berm must also be met. This is, roughly

$$\frac{\mu^3}{\Lambda^2} \geq 60 \text{ eV}$$

The opacity of these results must be even greater to the reader than to this author; a more transparent way of viewing them is shown in Fig. 9. To our knowledge the region excluded by this experiment has not been covered by previous measurements.

IV. FUTURE PLANS

The running of SLAC experiment E-137 is complete. Final analysis should be finished within a few months, with the remaining work consisting of refining the estimates of production cross-sections and detection efficiencies.

Meanwhile a new proposal for a similar experiment at Fermilab has been submitted and in principle approved in November 1983, pending an increase in group size and an acceptably small cost estimate. This experiment, E-635, is similar in concept to the SLAC experiment as well as to previous dump experiments such as carried out by the CHARM collaboration[12]. In brief, the E-137 apparatus, supplemented by a solid iron toroid magnet and some extra radiation lengths of electromagnetic calorimetry, will be placed 300 m downstream from Lab C, where resides the large neutral-current experiment of F. Taylor et. al. This locale is about 560 m from the new Fermilab beam dump. The purpose of the experiment is again to search for low mass (<1-3 GeV) neutral particles which might be produced in the hadronic shower and which might decay in the 300 m region upstream of the detector. The signature for the trigger will be either electromagnetic energy deposition or a dimuon with vertex in the decay volume. A candidate particle might be an axion-like pseudo-Nambu-Goldstone-boson X of mass M_X~200 MeV - 2 GeV decaying into dimuons, with decay constant $F_X \sim 10^4$ TeV. For such a particle we estimate that the sensitivity (per proton dumped) is a factor >30 better than previous experiments such as the CHARM or (thus far unpublished) CDHS experiments. The experiment will be sensitive to other decay modes such as $\gamma\gamma, e^+e^-, \mu^\pm e^\mp$, etc. It will of course also be a sensitive search for heavy neutrinos, and will hopefully be ready well before the beam dump (ca. 1986-1987).

V. ACKNOWLEDGMENT

We thank W. K. H. Panofsky and the SLAC staff for generous support and assistance. Special thanks go to Finn Halbo for superb engineering support and to the accelerator operations crew, who delivered beam of record intensity under difficult operating conditions.

REFERENCES

1. SLAC Experiment E-56, M. Schwartz, spokesman. A description may be found in the thesis of A. Rothenberg, SLAC report SLAC-147, 1972 (unpublished) and in reference 2.
2. T. Donnelly et. al., Phys. Rev. D18, 1607 (1978).
3. R. Heisterberg et. al., Phys. Rev. Lett. 44, 635 (1980).
4. R. Ford and W. R. Nelson, SLAC Report SLAC-210(1978)
5. R. Peccei and H. Quinn, Phys. Rev. Lett. 38, 1440 (1977) Phys. Rev. D16, 1971 (1977) S. Weinberg, Phys. Rev. Lett. 40, 223 (1978). F. Wilczek, Phys. Rev. Lett. 40, 279 (1978).
6. C. Edwards et. al., Phys. Rev. Lett. 48, 903 (1982). M. Sivertz et. al., Phys. Rev. D26, 717 (1982). M. Adam et. al., Phys. Rev. D27, 1665 (1983). B. Niczyporuk et. al., Z. Physik C17, 197 (1983).
7. We use the expression for axion lifetime given in Reference 2 and standard formulae for Primakoff production in making this estimate.
8. For a review, see Y. Declais, Proceedings of the 21st. International Conference on High Energy Physics, July 1982, Paris, France, ed. P. Petiau and M. Porneuf.
9. Phys. Lett. 86B, 272 (1979); also see P. Fayet, Proceedings of the 21st. Conference on High Energy Physics, July 1982, Paris, France, ed. P. Petiau and M. Porneuf.
10. The production cross section is given by P. Fayet, Phys. Lett. 117B, 460 (1982).
11. N. Cabibbo, G. Farrar, and L. Maiani, Phys. Lett. 105B, 155 (1981).
12. F. Bergsma et. al. (CHARM collaboration), Phys. Lett. 128B, 361 (1983).

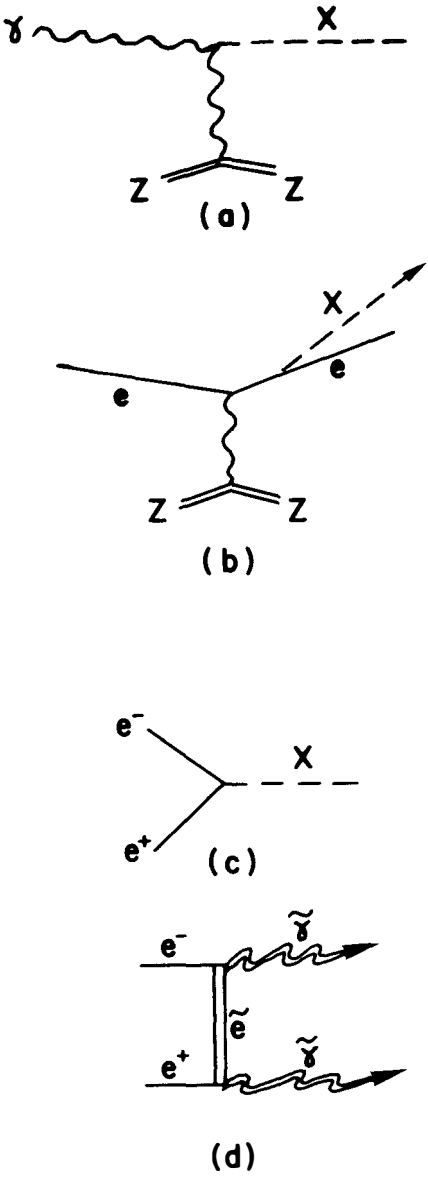


Fig. 1. Collimated production mechanisms for neutral bosons: (a) Primakoff photoproduction, (b) bremsstrahlung from electrons, (c) resonant annihilation of positrons on atomic electrons, and (d) nonresonant production (by positrons on atomic electrons) of photino pairs via selectron exchange.

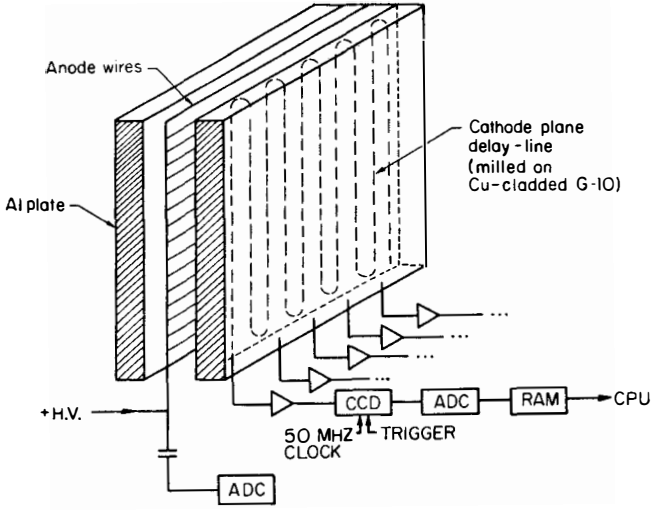


Fig. 3. Schematic of the delay-line multiwire proportional chambers and the CCD electronics.

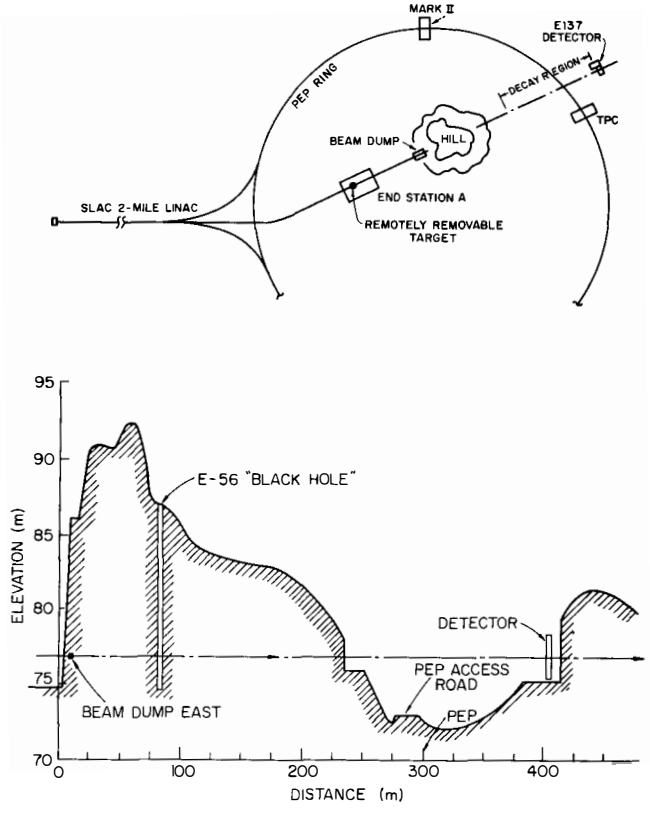
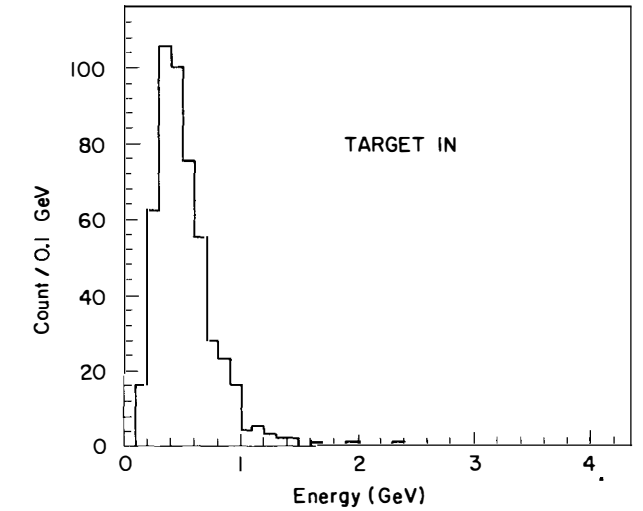


Fig. 2 Layout of SLAC experiment E-137.



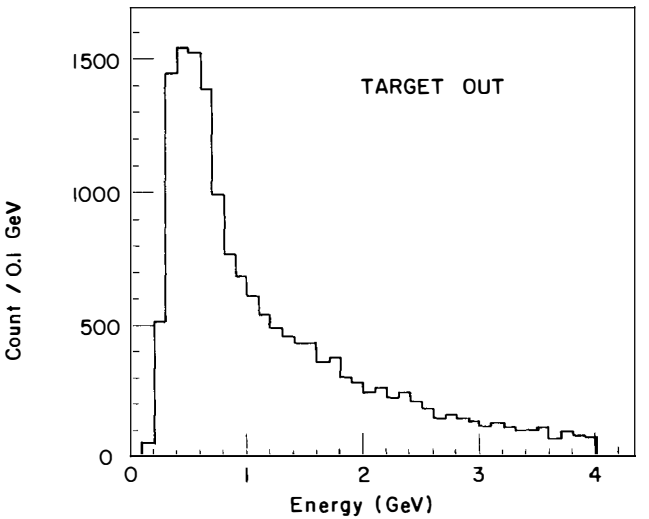


Fig. 4. Energy spectrum of experimental triggers as determined from total scintillator pulse height: (a) beam-associated skyshine with removable Al target in beam, and (b) beam dump running with target removed.

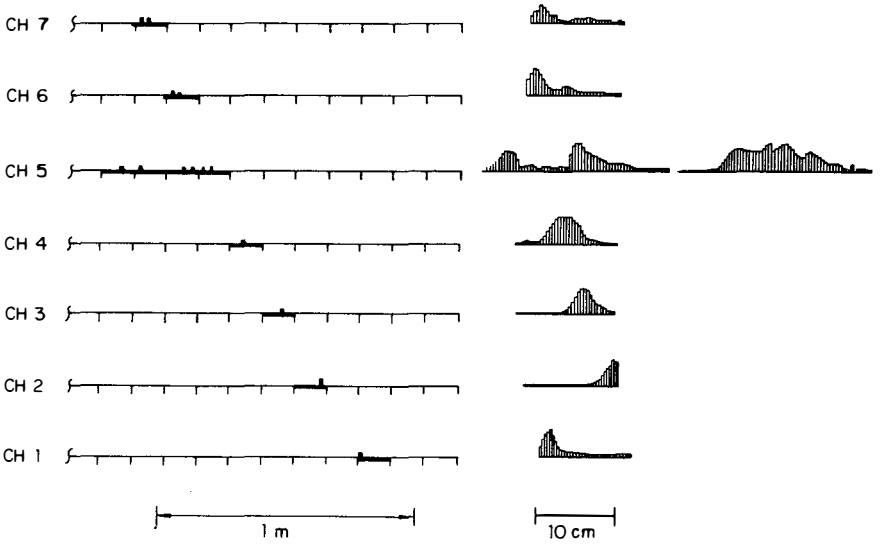


Fig. 5. Typical event as seen by the 3m x 3m multiwire proportional chambers. On the left is the top view of the chambers. The ticks locate the taps on the delay line. The bold-faced region is that portion of the chamber read by the CCD's which is shown expanded on the right, where the observed pulse shape is exhibited. The peak values have been plotted on the layout at the left.

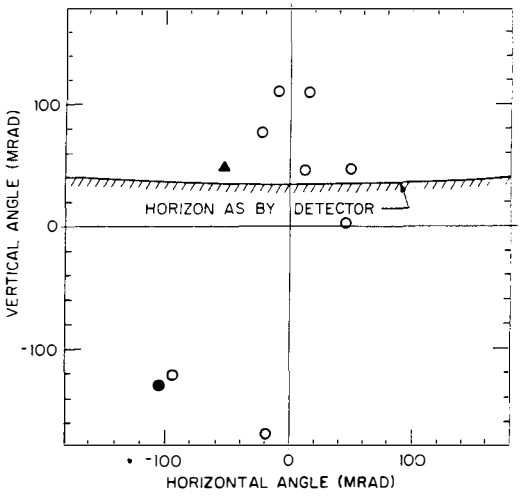


Fig. 6 Scatter plot of the angular distribution of candidate events. Only the bold-faced point has energy >3 GeV ; the triangular point has energy >2 GeV, but unambiguously does not point toward the dump. The three points apparently emergent from below the horizon are actually cosmic rays entering the detector from the rear.

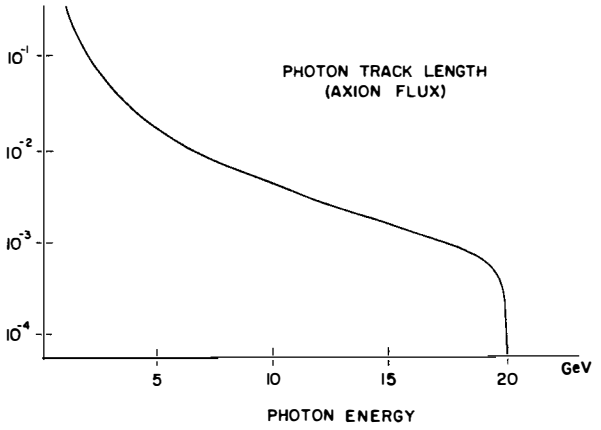


Fig. 7. Track length distribution of photons in the dump whose emission angle subtends the E-137 detector. This distribution is directly proportional to the flux of low mass hypothetical axions into the detector.

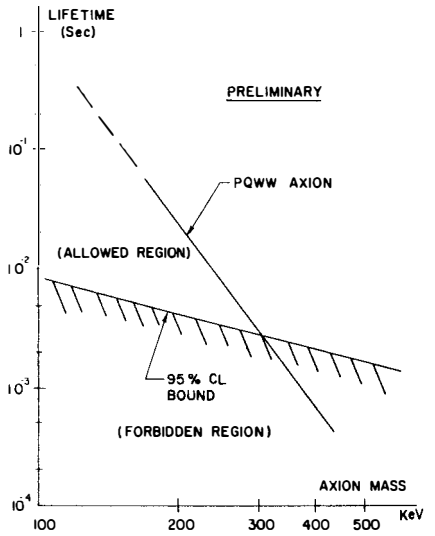


Fig. 8. Preliminary limits on hypothetical axion properties from experiment E-137. It is assumed the axion decays predominantly into $\gamma\gamma$.

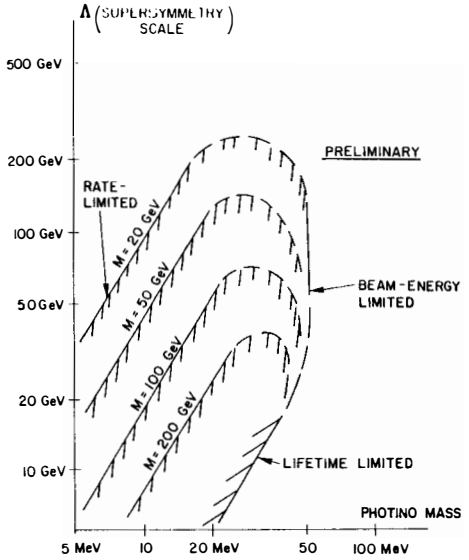


Fig. 9. Preliminary limits on photino properties from experiment E-137. The dotted region of the boundaries are as yet only roughly estimated and will soon be refined.

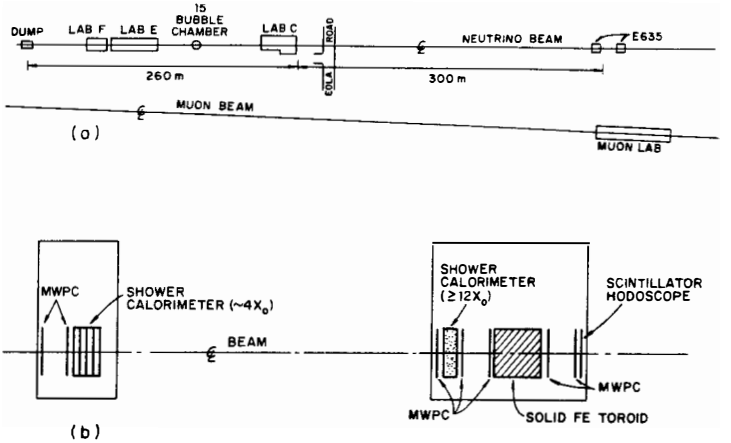


Fig. 10. Layout of Fermilab beam dump experiment E-635: (a) general plan, and (b) detailed layout. The two portions of the experiment are separated by about 20 m.

SOME NOTES ON A CURRENT NEUTRINO MASS EXPERIMENT IN STOCKHOLM

Karl Erik Bergkvist
Research Institute of Physics, S-104 05 Stockholm, Sweden



ABSTRACT

Somewhat in keeping with the notion of workshop on the label of the present gathering we give some brief views and remarks related to a preparatory stage of a new neutrino mass experiment. Basic means is the upper endpoint behaviour of the tritium β-spectrum; in outline the new experiment much follows our earlier work on the same topic (Nucl. Phys. B39, 317 (1972)). The very high luminosity offered by combined electrostatic and magnetic β-spectroscopic methods remains a central experimental feature. Improved sensitivity with respect to neutrino mass is being looked for by further attention to the background problem and to the detector 0-effect. Preliminarily, progress by a factor of between five and ten has been achieved on these areas. The details of the production of the new tritium source have not yet been settled. No real cure for the interpretation uncertainty associated with the atomic interplay is presently included in the outline of the new experiment. As a step-one aim we just wish to reach the minimum level of accuracy where indications can be obtained as to the reproducibility of the observed endpoint behaviour implied by the neutrino mass statements by Lubimov et al. The intricate general problem of how to strictly handle the atomic interplay will be postponed to a second - conceivably much different and more elaborate - second step.

At the Research Institute of Physics in Stockholm we are presently preparing a new neutrino mass experiment based on the upper endpoint behaviour of the tritium β-spectrum. At least initially the new experiment will follow in general outline our earlier work on the same issue some decade ago[1]. Using the experience then gained, our new effort is intended to be a kind of least effort which is not judged obviously insufficient for gaining independent indications as to the correctness of the finite-mass claim by Lubimov et al.[2-4]. When initiating our new effort some years ago judgements as to how to proceed were based on the Russian results from 1980 and 1981[2,3], amounting to a most probable neutrino mass around 35 eV under the assumption that the atomic interplay of the free atom could be used when interpreting the data. On this basis it seemed quite reasonable to start a new effort essentially along the lines of our earlier experiment, looking for possibilities to improve the old measures in a quantitative way rather than trying to introduce qualitatively different steps. The more recent Russian results from 1983[4] have somewhat reduced*, and made a bit more subtle**, the effect to be looked for by other investigators. In our case the new situation may make it necessary to elaborate somewhat further on the source technique than was initially anticipated.

In our current plans we have not yet included any actual remedy for the uncertainty in the atomic interplay in the source. In the personal view of the present writer, the main uncertainty as to whether the neutrino mass is finite presently does not stem primarily from uncertainties in the atomic interplay but rather from the risk of unrecognized systematic effects in the delicate measures involved in the work by Lubimov et al. Any independent experimental support for the implied observed spectrum behaviour will drastically reduce the latter uncertainty and strongly strengthen the evidence that the neutrino mass is indeed finite. Upon this view rests our present, modest-ambition effort. As to the possibility of proceeding later to an experiment capable of furnishing genuinely compelling evidence little can be said at present in our case. There are other, more extensive experiments discussed at this workshop[5,6] which - from the outset - aim at such a decisive test. In spite of various obvious virtues in these more elaborate projects, over-all it is still not entirely clear to the present writer that the appropriate combination of intensity, resolution and low background can indeed

* It should be noted that in Refs 2 and 3 no allowance is made for the intrinsic width of the reference line. The more recent results of Ref. 4 do take this width into account, assuming a Lorentzian intrinsic line shape. The effect of shake-up processes, qualitatively obviously of potential concern, still awaits a quantitative assessment.

** Improved fit of the data of Ref. 4 is obtained with a two-mass hypothesis (V.A. Lubimov, private communication).

ultimately be reconciled with the type of source needed for an accurate knowledge of the atomic interplay and of other types of energy exchange in the source which affect the β-spectrum. The very great difficulties of the compelling proof again - we feel - make a stepwise approach to the problem reasonable.

Since our current effort owes so much to our earlier experiment the reader is referred to that work for an underlying more detailed discussion. Various improvements realized at the present preparatory stage will be defined with respect to the earlier experiment. For comparisons with other current efforts, the present notes, together with Ref. 1, should provide proper information. Needless to say, before improvements have been implemented in actual runs, figures remain preliminary.

The 1980 and 1981 results by Lubimov et al. of a probable neutrino mass around 35 eV were obtained with about 40 eV resolution and based on data collected during about 3000 hours. In our earlier work, with the same resolution, we were able to assess an upper limit for the mass of around 55 eV from about 100 hours of data collection. Without analyzing things in quantitative details, it seems reasonable that if some modest further improvements in the performance of our earlier system can be achieved, and if this is combined with more prolonged data taking, a relevant level of accuracy should be within reach for seeing an indication of the presence of the claimed finite mass - making similar assumptions about the magnitude of the spread in final-state energy due to atomic interplay. In the preparatory work done, it may be motivated to comment briefly on the following points:

1. The high-luminosity system generally
2. The source arrangement
3. The aperture defect corrector
4. The reduction of the scattered background
5. The detector arrangement
6. The production of the tritium source.

1. The high-luminosity β-spectroscopic methods employed in our earlier neutrino mass experiment are applicable to a variety of basic spectrometer configurations. Primarily as a means of saving time we have chosen to adhere as much as possible to the lay-out used in the earlier measurement (cf. Fig. 1); in particular the iron-yoked $\pi\sqrt{2}$ magnetic component has been retained. It is a hope rather than a conviction that this component will ultimately withstand the more stringent requirement with respect to linearity and absence of remanence of our new

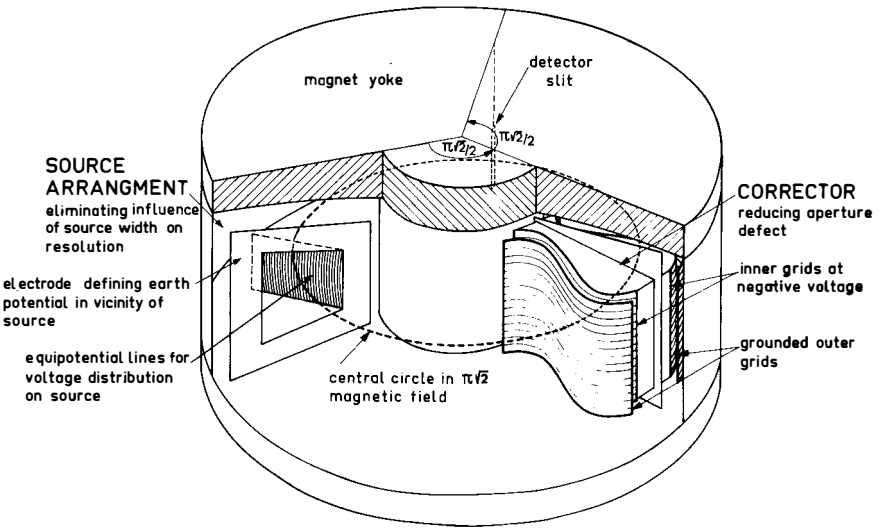


Fig. 1. Basic outline of electrostatic-magnetic β-spectrometer as used in our earlier work[1].

experiment. A somewhat more elaborate system of trim coils have been introduced and, electronically, the accuracy in the very setting of the magnetic and electric fields involved have been adequately improved. The general system layout selected allows a very high luminosity to be achieved.

2. The source arrangement primarily has to furnish the appropriate potential distribution over the source area while keeping unwanted particle optical effects from the electric field in the source region as small as possible. For the present application we have developed a new arrangement comprising three interchangeable 20 x 10 cm^2 sources (Figs 2 and 3). Each source can be put in working position without breaking the vacuum or the magnetic field setting. Apart from the main tritium source the arrangement involves a reference source - supplying an appropriate conversion line - and a particle optical diagnostics source. The latter contains two small electron guns allowing the particle optical performance of the complete system at around 18 keV to be checked by means of a fluorescense screen at the detector slit position.

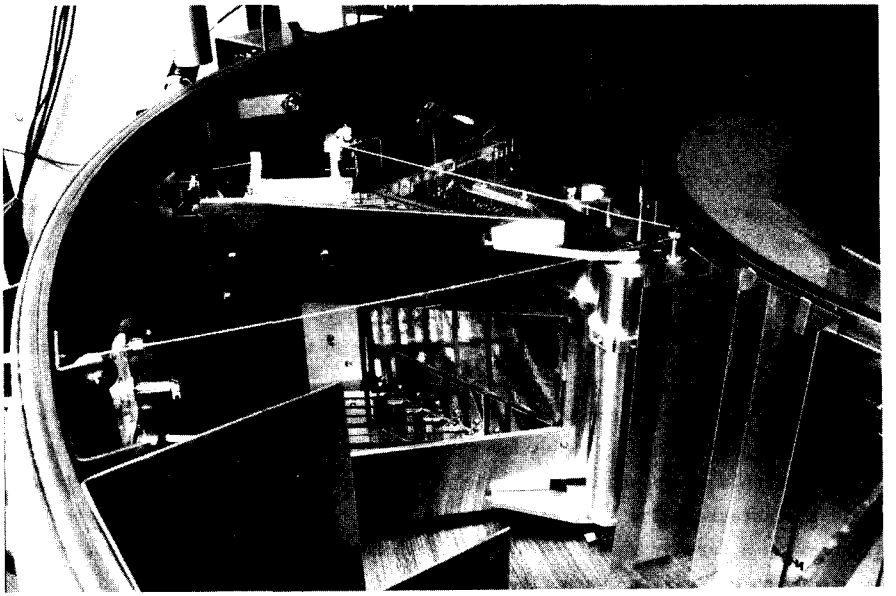


Fig. 2. Front view of the new source arrangement. The old tritium source from Ref. 1 is mounted in working position.

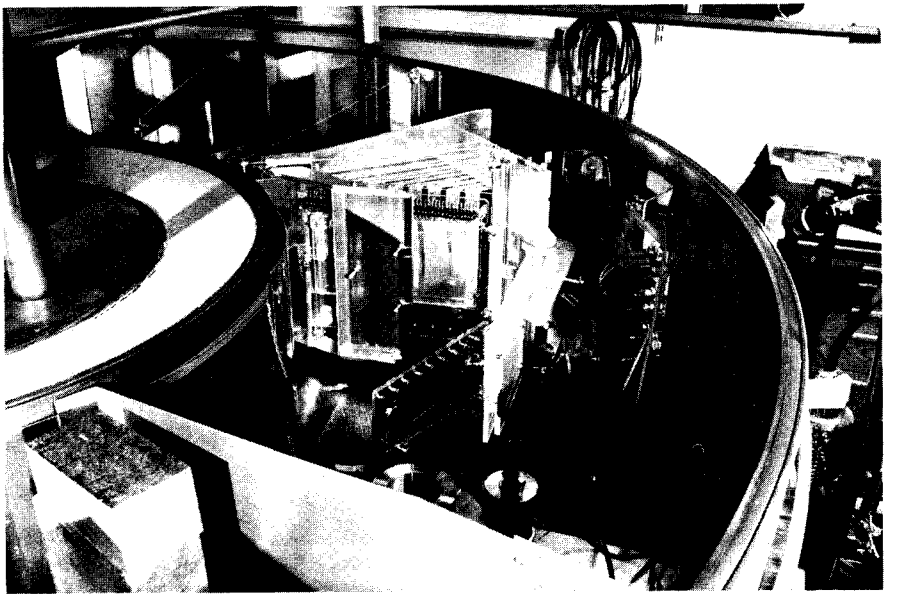


Fig. 3. Rear view of the new source arrangement. In retracted positions are seen the reference source (upper) and the electron gun source (lower).

The 20 x 10 cm^2 source size is intended for work with about 40 eV instrumental resolution. When higher resolution is desired, appropriately smaller sources can easily be accommodated within the same basic mechanical arrangement by means of suitable adaptors.

In addition to meeting the obvious requirements with respect to mechanical precision, particle optical performance and electric reliability, the new source arrangement is also designed with a view of keeping the background at the endpoint as small as possible.

3. The aperture defect corrector in the high-luminosity system in our earlier general applications has been of an electrostatic type (cf. Fig. 1). In the present effort, strictly concerned with the small focused energy of the tritium β-spectrum upper endpoint, it has been possible to replace the electrostatic corrector with a corresponding magnetic device producing both less obstruction and less scattering. The smaller scattering of this origin has been of importance in achieving a further reduction of the background intensity at the endpoint, compared with our earlier work. The new magnetic corrector is pictured in Fig. 4.

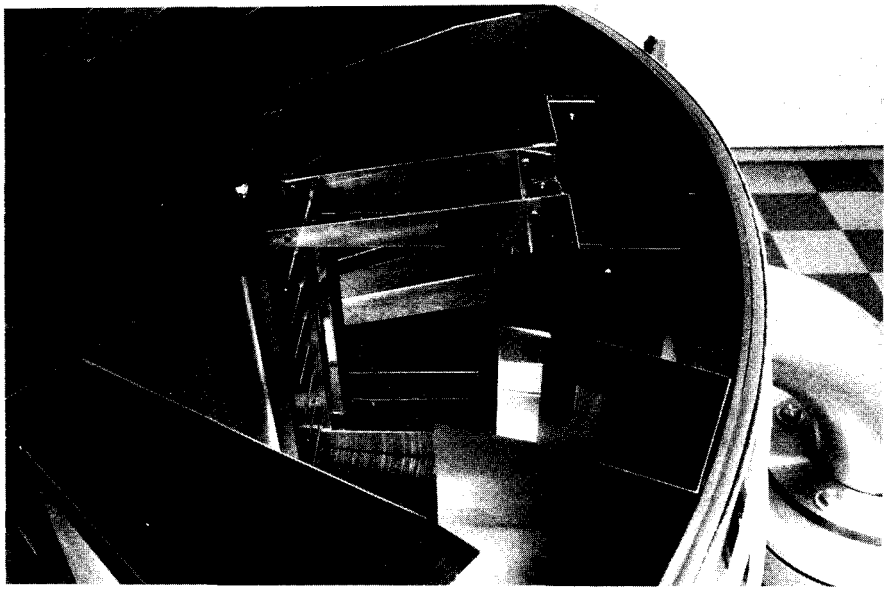


Fig. 4. The new magnetic aperture defect corrector.

The current loops, some 30 mm apart and of about 0.5 mm diameter carry around 2 amps at 18 keV focused energy. The magnetic corrector shown provides adequate performance at a resolution of about 40 eV. With a reduction in aperture size (now $\sim$ 0.4 % of 4π) and revised current loops higher resolutions can be reached.

4. The background at the endpoint is obviously a key issue in the present type of experiment. The total background may be divided in scattered background - proportional to the source strength - and detector 0-effect. The ultimate possibilities as to how far a scattered background can be reduced is hard to assess in any type of spectrometer, the result so much depending on the details of the execution of the whole system. Being of one-cycle focusing type, our system is not inherently as efficient in keeping the scattered background small as some of the multi-cycle focusing systems resorted to in several other current efforts on the neutrino mass issue[2-7]. Still, the scattered background can be said to be sufficiently controlled when it roughly matches the detector 0-effect. In our earlier experiment we reached such a point after a reduction by a factor of 50, starting from an admittedly modest situation of background control. In the present effort it has seemed reasonable - as a first step - to try to proceed by something like an order of magnitude on the topic of scattered background and detector 0-effect. So far a factor of around five has been achieved in the further reduction of scattered background. To get this result the new magnetic aperture defect corrector has been instrumental. Any genuinely intrinsic limitation for at least some still further progress has not yet been identified, but increasingly more demanding attention to details may be needed. It should be recalled in this context that with the very large source involved the potential gradient on the source gives the properly focused particles an energy spread of about 2.5 keV. Hence a strongly energy discriminating detector is not an obvious cure for an even further reduction of the scattered background in our case.

5. The detector arrangement in our current experiment comprises an array of three adjacent proportional counters (cf. Fig. 5). The above mentioned goal of reducing the 0-effect by a factor of ten has been reached primarily by reducing as much as possible the cross section area of each chamber, this area now amounting to about 3 x 4 mm^2. Neither this area, nor the height of about 16 cm of the sensitive volume can be much further reduced when source areas of some 20 x 10 cm^2 are to be used. Although electrically separated, the chambers share a common gas enclosure. This arrangement makes it possible to stack the three counters sufficiently close to each other for not coming in conflict with the rather limited extension of the useful focal plane of the high-luminosity system[8]. The system of separate chambers, rather than a conventional multiwire

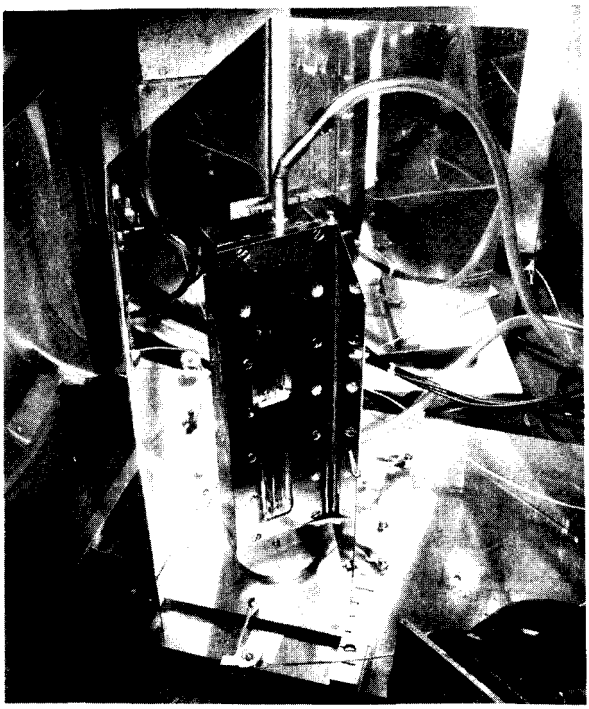


Fig. 5. The new detector arrangement.

single chamber, has been chosen to admit the best possible definition of the responce function in the analysis of the measured spectrum.

In order to keep corrections for window thickness manageably small, the counters are operated with thin ($\sim$ 80 $\mu g/cm^2$) windows and hence, low pressures (some 40 mm of Hg). Inevitably, because of the small cross section area of the chambers, this means absorbing only a minor part of the 18 keV energy of the endpoint ß-particles. Preamplifier noise has to be considered when finding the best compromise between thin window and decent pulse size. Clearly only experience from actual runs will fix things in this regard. Similarly, the achievement of appropriate stability of operation can not be judged until such a stage is reached.

6. The preparation of the tritium source at present somehow amounts to choosing the least unsatisfactory solution among various schemes concievable. The preparatory work of the new experiment so far has been done with the tritium source

from our earlier experiment. This source is no longer suitable for actual data taking on the endpoint behaviour. The old source was obtained by an ion-pumping technique. A similar procedure - with refinements where such can be conceived of - currently seems the most promising path to take for pursuing step one as defined in the introductory remarks. Needless to say, ideas as to getting some real break-through on the issue of the source problem in general are continuously being looked for.

References

1. K.E. Bergkvist, Nucl. Phys. B39, 317 (1972).
2. V.A. Lubimov et al., Phys. Letters 94B, 266 (1980).
3. V.A. Lubimov et al., Sov. Phys. JETP 54(4), 616 (1981)
4. V.A. Lubimov et al., Contribution to the 1983 High Energy Physics Conference in Brighton, England.
5. T.J. Bowles et al. (Los Alamos exp.). Talk by R.G.H. Robertson at this workshop.
6. O. Fackler et al. (Livermore exp.). Talk by O. Fackler at this workshop.
7. W. Kündig et al. (Univ. Zürich exp.). Talk by J.W. Petersen at this workshop.
8. K.E. Bergkvist, Ark. Fys. 27, 383 (1964)

THE LOS ALAMOS EXPERIMENT ON ATOMIC AND MOLECULAR TRITIUM

R. G. H. Robertson, T. J. Bowles, J. C. Browne, T. H. Burritt, J. A. Helffrich, D. A. Knapp, M. P. Maley, M. L. Stelts, and J. F. Wilkerson,
(presented by R. G. H. Robertson)
Physics Division,
Los Alamos National Laboratory Los Alamos, NM 87545, U.S.A.



Abstract: An apparatus is under construction at Los Alamos that will allow the measurement of the β spectra of free tritium atoms and molecules. It consists of an RF dissociator, a long cylindrical decay region open at both ends, a pumping restriction, and a toroidal magnetic spectrometer.

The fact that the mass of the neutrino could be inferred from the electron spectrum in β decay was first pointed out by Fermi.[1] Recently a group at ITEP have carried out highly sensitive experiments[2] on ^3H and have concluded that the mass of $\bar{\nu}_e$ is greater than 20 eV. These experiments were made possible largely through the development by Tret'yakov[3] of a toroidal magnetic spectrometer of high luminosity. Only a region of about $2m_\nu$ at the end point is sensitive to neutrino mass, and only about 2×10^{-8} of the total decay intensity lies in the last 40 eV (in the absence of neutrino mass).

A number of concerns have been raised about the ITEP experiments, perhaps the most basic being the problem of the final states. A free tritium atom decays to the daughter $^3He^+$, leaving the ion in excited states for which the energy levels and branching ratios are simply and precisely calculable in the "sudden approximation" (see Fig. 1). Williams and Koonin[4] have shown that this corresponds to the first Born approximation, and that the second Born terms are at the level of 0.1%. However, in the ITEP experiments, the tritium was not free but bound in valine molecules. Kaplan, Smutnii, and Smelov[5] have

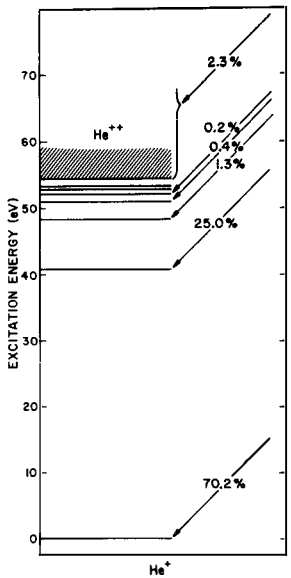


Fig. 1

Branching in the decay of atomic tritium to final states in $^3He^+$ and $^3He^{++}$.

calculated the energy levels and branching ratios for valine I and valine II, but the accuracy of these difficult calculations is not known, and radiolysis may have altered the structure of the source molecules in any case. At present, it appears to us that only tritium atoms, and probably T_2 molecules (see the report by O. Fackler at this conference), can be treated confidently.

The basis of a practical source of free atomic tritium was suggested to us by D. Kleppner. Tritium gas is dissociated in an RF discharge and admitted to a long tube pumped at both ends. Provided that recombination does not occur too rapidly, an equilibrium pressure of T atoms exists in the tube as set by the influx and the conductance of the tube. The tube is placed on the axis of a solenoid so that β's spiral along the field lines toward one end or the other. Obtaining a dense source requires a long, narrow tube, but this in turn raises the probability of recombination at the wall because each atom strikes the wall thousands of times before escaping. It has been known[6] for some time that Pyrex glass and quartz exhibited low recombination probabilities "per bounce" (reaching a minimum of about 2.5×10^{-5} at 120 K). However, these materials are insulators, and the possibility of unknown charges accumulating on their surfaces was troubling. We conducted tests on a variety of materials in the form of tubes using a dissociator coupled to the tube, a chopper to modulate the emergent beam, and a mass spectrometer. Surfaces of Si, Ge, B, and Al were studied, with Al exhibiting very desirable properties (no doubt owing to the native layer of Al_2O_3 on all Al surfaces). In Fig. 2 the recombination probability per bounce, γ, is plotted as a function of temperature. Uncertainties are of the order of 10% for the largest measured γ, but rise to ~100% near the minimum. A clear isotopic effect is seen.

Based on these observations we are constructing a source tube of aluminum 4 m long and 3.8 cm diameter. It is anticipated that an integrated free-atom density close to 10^{16} cm^{-2} with a molecular contamination of ~15% can be reached. The molecular fraction will be measured on-line by VUV absorption spectroscopy.

The source tube is placed in a solenoidal magnetic field of about 1.5 kG with a small axial gradient, provided by a superconducting solenoid. At one end a pinch coil reflects most of the β's starting with a velocity component directed towards that end; as a result about 98% of the β's reach the weak-field end of the solenoid.

An important feature of our experiment is that the entire source is biased at a negative potential which can be as large as -20 kV. The principal reason for shifting the spectrum to higher energies is to eliminate as a source of background tritium that enters the spectrometer. The price paid, of course, is that somewhat higher resolving power is required in the spectrometer.

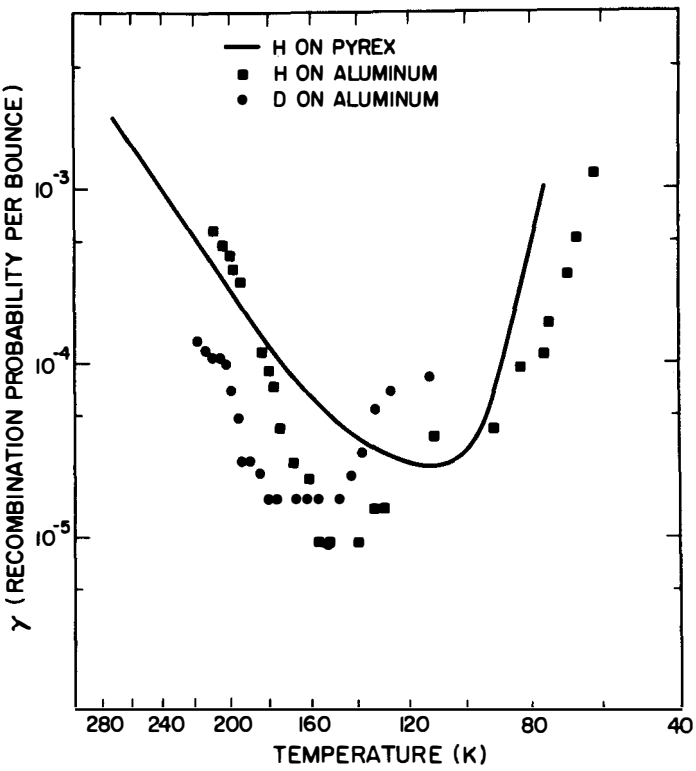


Fig. 2

Recombination of H and D on surfaces of Pyrex glass and aluminum. The Pyrex data are taken from Ref. 6.

Between the source and the spectrometer (see Fig. 3) is a pumping restriction to reduce the flow of tritium into the spectrometer. The restriction consists of two tubes operated at 60 K and, between them, a good-geometry cryopump. A second cryopump follows the restriction.

One of the most interesting aspects of the problem is extraction of the β's from the relatively large field of the source through a collimator and into the low-field spectrometer. Given that in order to enter the spectrometer, all β's must pass through a collimator of radius r_c at an angle less than ψ_s, we find two general theorems: 1) there is a maximum radius R_4 in the solenoid beyond which no β can originate and still enter the spectrometer; and 2) the maximum

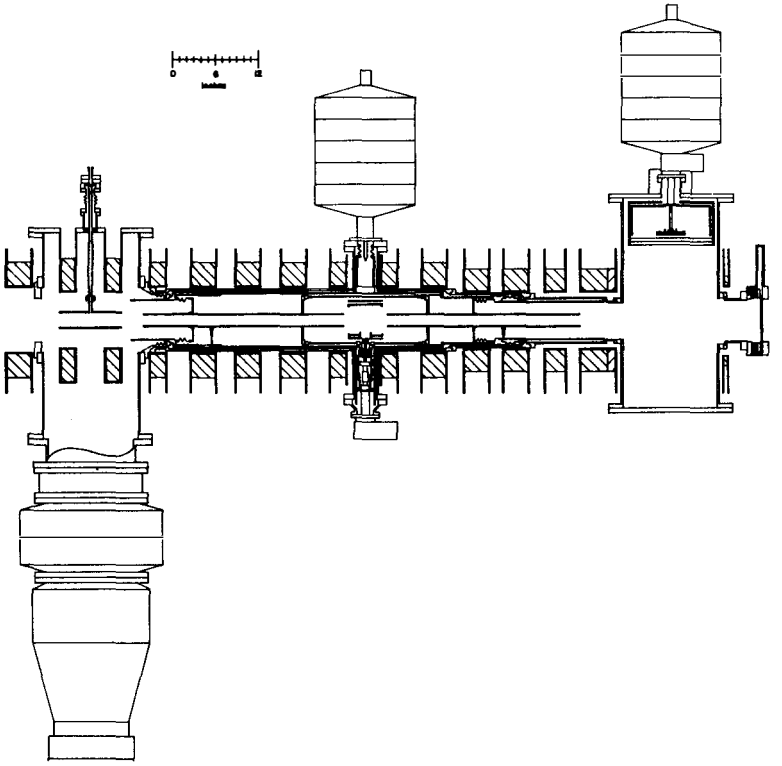


Fig. 3

Pumping restriction between source and spectrometer.

fraction of rays originating within R_4 that can be transmitted to the spectrometer is given by

$$\eta = \frac{6x\rho + 2\rho^2}{3R_4^2} \quad ,$$

where $x = \frac{r_c p'}{p} \sin \psi_s \quad ,$

and ρ is the (maximum) radius of orbits in the field. This is valid for $\rho < 2x$. The electron momenta before and after acceleration are p and p′ respectively. The expression for R_4, the limiting radius, is

$$R_4 = \rho\left[1 + \left(1 + \frac{2x}{\rho}\right)^{1/2}\right] \quad .$$

These results follow from conservation of the canonical angular momentum.

The significance of the first theorem is, of course, that any electrons originating from tritium adsorbed on the walls of the apparatus (in particular, the source tube) can be rejected absolutely, independent of aberrations or imperfections in the optical system. In practice the β′s are focussed through the collimator with an efficiency about 50% of the theoretical maximum by means of a set of coils.

Acceleration of the β′s occurs at the end of the source tube. The acceleration field extends over a finite distance, penetrating the finned tube extension and potentially causing spectrum distortion. However, only a small fraction ($<10^{-3}$) of detected decays occur in this region of varying potential, and so the distortion is insignificant. Scanning the spectrum can be performed in several ways, but the preferred method is to vary the source potential and maintain all other potentials and fields fixed. While this causes a (calculable) variation in extraction efficiency, there is significant advantage to presenting the spectrometer and focal plane detector with fixed energy particles.

The spectrometer is modeled on the design of Tret′yakov.[3] A side view is shown in cross-section in Fig. 4, and specific design parameters have been given previously (see Ref. 7). We have modified Tret′yakov's design in two principal respects: The focal length of the spectrometer is about twice as large, and particles enter the toroidal field at angles between 20 and 30°, rather than between 85 and 95° to the axis. Matching the atomic source to the spectrometer is then greatly simplified. The resolution of the spectrometer is determined mainly by source size and is calculated to be $p/\Delta p = 3000$ FWHM for a 1-cm diameter source, when an exit slit is employed to remove the contribution of detector position resolution.

The electron-optical properties of the system can be studied in several ways. A 40-kV electron gun is mounted at the pinch end of the source and can be used to measure resolution, transmission, aberrations, scattering, and source thickness contributions. A very convenient check on the general behavior of the

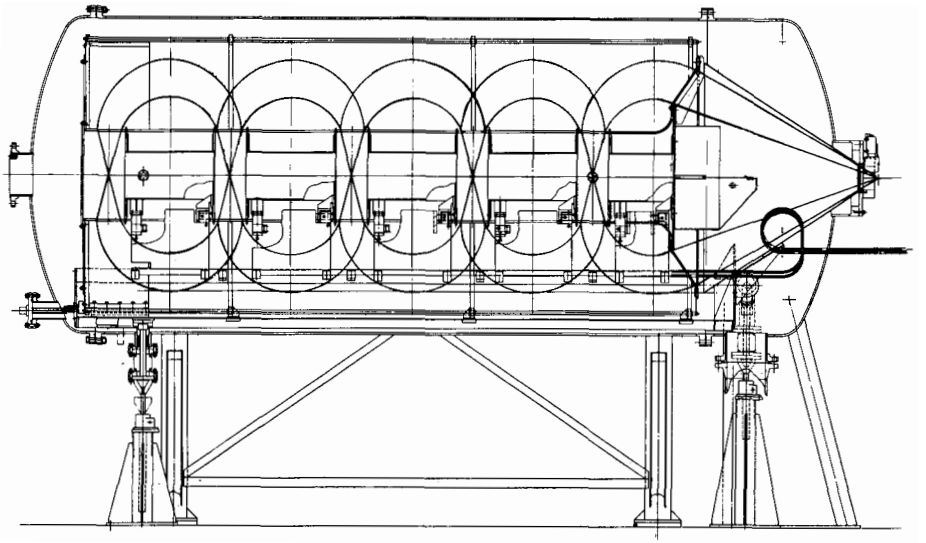


Fig. 4

Toroidal spectrometer.

source and spectrometer is to use 1.8-hr ^{83m}Kr, a daughter of 83-day ^{83}Rb. This isotope is gaseous, short-lived, and emits a 17.8 keV conversion line.

In a test setup we have produced intense beams (~10^{18} atoms/sec) of H and D with high dissociation fractions (<90%). These have been transmitted through Al tubes having characteristic "bounce numbers" N_c near 3000 without significant recombination. Based on these data, we estimate source densities of about 10^{16} atoms/cm^2 and count rates approaching 1 Hz in the last 100 eV of the spectrum, about 20 times higher than used by the ITEP group. Measured background rates in

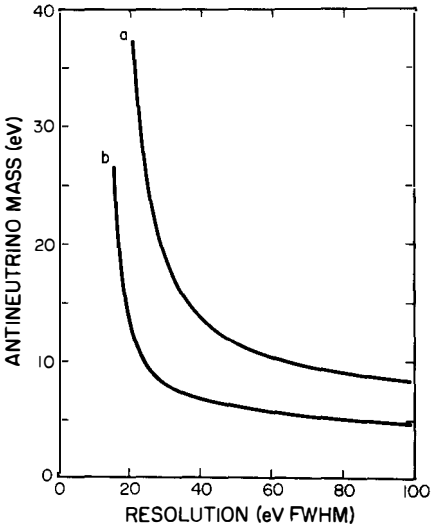


Fig. 5

Limits (2σ) on mass obtainable in 10^6 seconds running for a background rate of 2×10^{-3} sec^{-1}, a) source strength 1×10^{15} cm^{-2}, b) source strength 1×10^{16} cm^{-2}.

a prototype focal plane detector are of order 2×10^{-3}, and Fig. 5 shows the limits that can be placed on the neutrino mass in about 2 weeks running.

REFERENCES

1. E. Fermi, Z. Phys. 88, 161 (1934).

2. S. Boris, A. Golutvin, L. Laptin, V. Lubimov, V. Nagovizin, E. Novikov, V. Nozik, V. Soloshenko, I. Tichomirov, and E. Tret'yakov. (ITEP preprint 1983); V. A. Lyubimov, E. G. Novikov, V. Z. Nozik, E. F. Tret'yakov, V. S. Kozik, and N. F. Myasoedov, Sov. Phys. JETP 54, 616 (1981).

3. E. F. Tret'yakov, Izv. Akad. Nauk. SSR, Ser. Fiz. 39, 583 (1975).

4. R. D. Williams and S. E. Koonin, Phys. Rev. C 27, 1815 (1983).

5. I. G. Kaplan, V. N. Smutnii, and G. V. Smelov, Sov. Phys. JETP 84, 833 (1982).

6. B. J. Wood and H. Wise, J. Chem. Phys. 66, 1049 (1962).

7. T. J. Bowles, R. G. H. Robertson, M. Maley, J. C. Browne, T. Burritt, J. Toevs, M. Stelts, J. Helffrich, D. Knapp, and A. G. Ledebuhr, AIP Conference Proceedings No. 99, 17 (1983).

RESOLUTION TESTS OF THE ZURICH β-SPECTROMETER

W.Kundig, J.W.Petersen, R.E.Pixley, H.Stussi, and M.Warden
Physics Institute, University of Zurich, CH-8001 Zurich, Switzerland

ABSTRACT

The Zurich β-spectrometer to determine the electron antineutrino mass from the ^{3}H decay is described, and the determination of the spectrometer resolution function is discussed.

1. Introduction

The precision measurement of the tritium β-spectrum near its endpoint seems to offer the best chance of determining the mass of the electron antineutrino. The most succesfull experiment to date was reported by Lubimov et. al. from the Institute of Theoretical and Experimental Physics (ITEP) in Moscow. The group reported[1] in 1980 a neutrino mass of $14 \leq m_\nu \leq 46$ eV at the 99 % confidence level. At the Brighton conference (1983) new measurements with greatly improved resolution and lower background were reported[2] confirming their original result. Although the ITEP group has presented a very careful work, the importance of the results necessitates an independant confirmation. The questionable points of the Russian experiment are the use of a complicated organic source and an incomplete knowledge of the spectrometer resolution function. We are currently working on a β-spectrometer which allows better resolution at larger count rates and an improved control of the spectrometer resolution function.

2. Spectrometer

The spectrometer shown in Fig.1 is of the Tretyakov type[3], modified with a retarding field surrounding the source. The spectrometer has cylindrical symmetry.

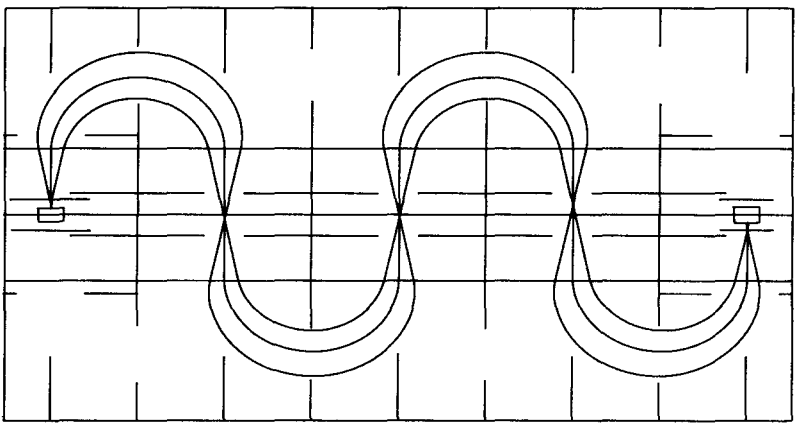


Figure 1. Scale drawing of spectrometer. The distance from the source to the detector is 2.65 m.

The use of an extended source (area = 150 cm^2) is made possible by applying a voltage across the source[4], which is composed of ten rings, each 1 cm wide. The source is at high voltage surrounded by a grid near ground potential. The retarded electrons are subsequently analyzed in the magnetic spectrometer. The detector is a 10 cm long, position-sensitive proportional counter. Post acceleration is employed so that the electrons can penetrate the detector window. The spectrometer is located in an iron-free hut at the Swiss Institute of Nuclear Research (SIN). The earth's field in the spectrometer is compensated to better than 1 mG.

A measurement is made by stepping the retarding voltage with the magnet field held constant. Thus the detector sees only electrons of one energy, and the problem of the energy dependent detector efficiency is thereby eliminated. Furthermore the resolution and luminosity can be adjusted by simply changing the analyzing energy of the magnet. With this type of spectrometer the resolution (FWHM), the transmission, and the energy interval covered by the source and the detector are all proportional to the analysing energy of the magnetic spectrometer. In addition the transmission is roughly proportional to the reciprocal of the initial electron energy. For the tritium measurements the magnet analyzing energy will be set in the range 1.0 - 2.2 keV. For E_{mag} = 1 keV and a retarding voltage of 17.5 kV the resolution (FWHM) is 10 eV, the transmission 0.4 %, and the energy interval covered by source and detector is 50 eV. For measurements of the energy spectrum of conversion electron sources it is convenient to use magnet energies as low as 150 eV corresponding to a resolution of 1.2 eV.

Due to the low relative resolution of the magnetic spectrometer needed ($\Delta E/E$ = 1 %) the constructional demands on accuracy are not critical. For the same reason the source and the detector can be large. For the detector the large dispersion (= 2.09 mm/eV at E_{mag} = 1 keV) leads to relaxed requirements on position resolution so that a resistive wire charge division method becomes sufficient.

An obvious disadvantage of detecting retarded electrons is the lack of discrimination against background from ^3H contamination.

3. Resolution function

The spectrometer resolution function (SRF) is the spectrum recorded in the detector when monoenergetic electrons are emitted from the source, and is a crucial property needed for the tritium measurement. One might think that the SRF could be obtained directly using a conversion electron source

having a sufficiently small natural width. Unfortunately, this proves to be difficult due to the occurrence of close-lying sattelites of the conversion lines produced by accompanying shake-off excitations[5].

We have adopted the following rather complicated procedure: First a high resolution measurement (FWHM = 1.2 eV) is used to determine the energy distribution of the emitted conversion electrons. The resolution function is only of minor importance for this step. Then measurements at a resolution suitable for the tritium experiment are used to check Monte Carlo calculations of the SRF at these energies. This is done by folding the Monte Carlo SRF with the source energy spectrum determined in step one, and comparing this with the measured spectra.

We illustrate this procedure with a measurement of the 7290 eV K-conversion electrons emitted in the decay of the 14403 eV state in ^{57}Fe. The natural width of this line is 1.5 eV. The source was prepared by evaporating 0.1 $\mu g/cm^2$ $^{57}CoCl_2$ onto a single source ring. Figure 2 shows the spectrum measured at a magnet energy E_{mag} = 150 eV. The FWHM of the Monte

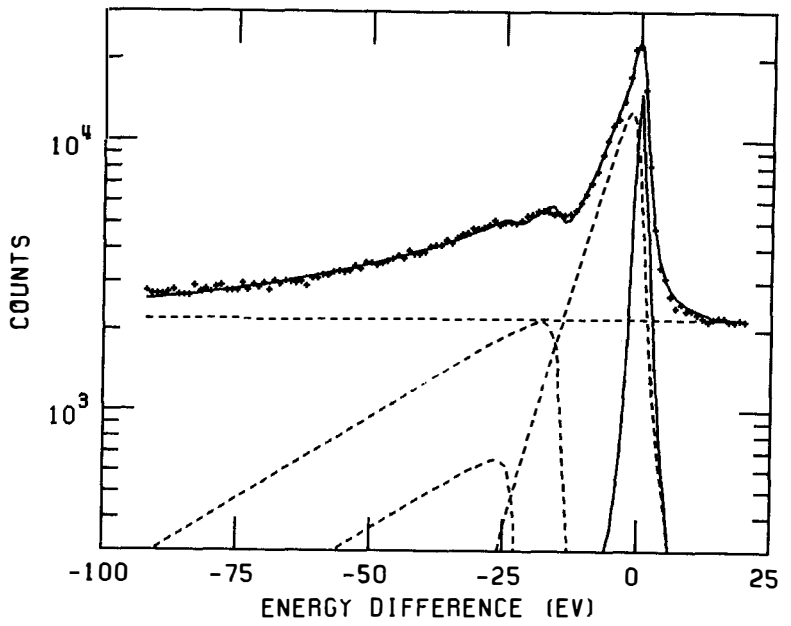


Figure 2. The 7290-eV, K-conversion electron spectrum measured at E_{mag} = 150 eV. Shake-off sattelites and background are shown dashed. The total function and the no-energy-loss peak are shown solid.

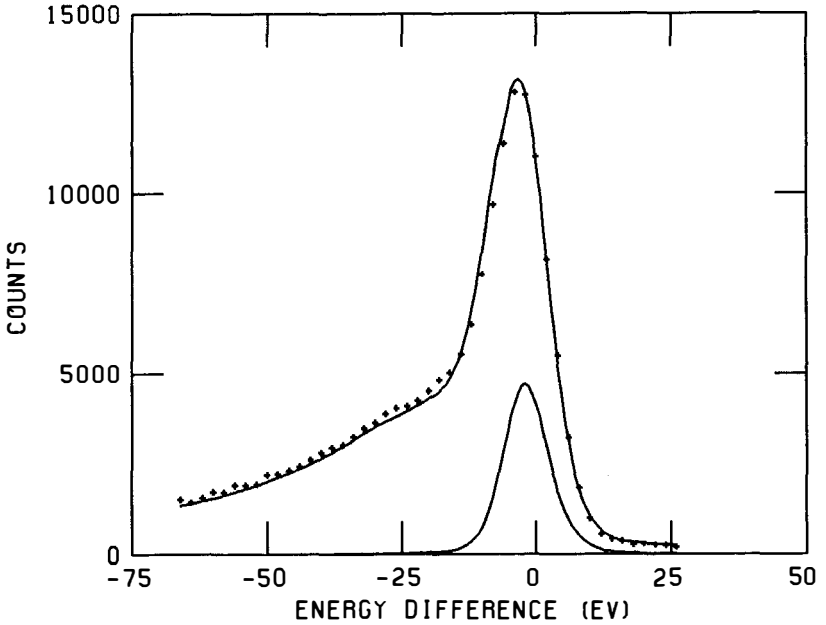


Figure 3. Spectrum measured with E_{mag} = 1200 eV. The curves are the fitted function and the no-energy-loss peak.

Carlo SRF at this energy is 1.2 eV. The distinct structures observed in the spectrum are ascribed to a number of shake-off sattelites. A 12-parameter function composed of three sattelites , the no-energy-loss peak , and the background folded with the Monte Carlo SRF for this energy has been fitted to the experimental data. The large number of free parameters does not allow any conclusions on the validity of the calculated SRF at this energy. On the other hand, the good agreement between fit and data means that we have found an adequate representation of the source energy spectrum to be used for the resolution measurements at higher magnet energies.

Figure 3 shows a spectrum measured with the same source at E_{mag} = 1200 eV corresponding to a resolution of 9.6 eV. The curve is the Monte Carlo SRF for this energy folded with the source energy distribution as obtained above. Only three free parameters (total height, position and background) have been used. the agreement is good and gives us confidence that the SRF can be calculated with sufficient accuracy for the magnet energies to be used in the tritium

measurements.

We point out that shake-off sattelites have not been taken into account in the ITEP experiment. This results in a spurious tail in their resolution function which will lead to systematic errors (towards larger neutrino masses) when fitting their data. These systematic errors can be comparable to the mass reported.

Aknowledgement

The support of the Swiss National Science Foundation is acknowledged. We are also grateful to SIN for generous support of the experiment.

References

1. V.A.Lubimov, E.G.Novikov, V.S.Nozik, E.F.Tretyakov, V.S.Kosik, Phys.Lett.94B (1980) 266.
2. S.Boris,A.Golutvin,L.Laptin,V.Lubimov,V.Nagovizin,E.Novikov,V.Nozik, V.Soloshenko,I.Tichomirov,E.Tretyakov, presented at the Brighton Conference on Neutrino Physics, 1983.
3. E.F.Tretyakov, Izvestiya Akademii Nauk SSSR. Seriya Fizicheskaya 39 (1975) 583.
4. K.E.Bergkvist, Nucl.Phys. B39 (1972) 317.
5. F.T.Porter, M.S.Freedman, F.Wagner,Jr., Phys.Rev. C3 (1971) 2246, and references cited there in.

SEARCH FOR MASSIVE NEUTRINO BRANCHES IN NUCLEAR BETA DECAYS

K. Schreckenbach, G. Colvin
Institut Laue Langevin, 38042 Grenoble, France

F. von Feilitzsch
Physik-Department der TU München, 8046 Garching, Germany



A search for heavy neutrino branches in nuclear beta decays was performed by a comparative measurement of the β^+ and β^- spectral shape of the ^{64}Cu decay, using the magnetic spectrometer BILL at the ILL reactor. A massive neutrino branch would have shown up in both spectra at the corresponding energies $E_\beta = Q_\beta - m_\nu$, where Q_β is the beta end point energy for $m_\nu = 0$. No evidence was found for a massive neutrino branch in the range $m_\nu = 30$ keV to 500 keV, but stringent upper limits were established, ranging to 4×10^{-3} relative to the main $m_\nu \cong 0$ branch. Our results are compared with the various limits from other experiments.

The possibility of non-zero neutrino rest masses and mixing of massive neutrinos is still an open question both from the experimental and theoretical side. Experimentally neutrino masses $m_{\nu_e} < 60$ eV, $m_{\nu_\mu} < 500$ keV, $m_{\nu_\tau} < 250$ MeV[1] are not excluded. For the description of neutrinos as superpositions of neutrino mass eigenstates (and hence neutrino mixing) there is to our knowledge no firm experimental evidence.

In our work we have studied the question of neutrino mixing in a kinetic experiment searching for an admixture of a heavy neutrino mass eigenstate to the main light component in the electron neutrino. In the low energy regime K capture of a nucleus and the nuclear $\beta^{\pm}$ decay are suitable for these investigations. In a two body decay such as K capture satellite peaks corresponding to heavy neutrino branches would occur in the recoil spectrum of the atom in analogy to the $\pi^+ \to \mu^+ \nu_i$ decay[2], for example. Although low limits may be extracted from a possible peak structure, the method is restricted to m_ν not much smaller than the Q value of the K capture reaction due to the $(Q_{EC}^2 - m_{\nu_i}^2)$ dependence of the atomic recoil energy. A wider range of neutrino masses (compared to the reaction Q value) can be covered regarding the $\beta^{\pm}$ decay of a nucleus, since in such a three body decay the maximum energy of the charged lepton depends linearly on m_ν. A superposed heavy neutrino mass eigenstate would show up in the momentum spectrum of the beta particle as a "kink"[3,4]. In the present experiment we refer to the search for such kinks in the electron or positron spectrum in the nuclear beta decay for mass eigenstates in the range 30 to 500 keV.[5] For the simplified case of two neutrino mixing, the weak interaction eigenstates of ν_e can be described as

$$| \nu_e > = \cos\theta | \nu_1 > + \sin\theta \; | \nu_2 >$$

where θ is the mixing angle and $|\nu_i>$ are the mass eigenstates (i = 1, 2). A beta-decay comprising two branches with neutrinos ν_1 and ν_2 would show a momentum spectrum N_β for the emitted beta particles of

$$N_\beta = N_\beta(\nu_1) \cos^2\theta + N_\beta(\nu_2) \sin^2\theta$$

which for the case of an allowed beta-decay and $m_{\nu_1} \simeq 0$ has the form

$$N_\beta \propto f \delta^2 \cos^2\theta \qquad \delta < m_{\nu_2}$$

$$N_\beta \propto f\delta^2 \cos^2\theta + f\delta(\delta^2 + m_{\nu_2})^{1/2} \sin^2\theta \qquad \delta > m_{\nu_2}$$

where $f = p_e^2 F$ (p_e is the electron momentum and F the Fermi function), and $\delta = E_o - E_\beta$ (E_o is the end point energy for $m_\nu = 0$). In the Kurie representation

$(K = \sqrt{[N_\beta / f]})$ and small admixtures, $\sin^2\theta$, the observed Kurie plot will be

$$K \propto \delta \cos\theta + (\sin^2\theta/2 \cos\theta)\ (\delta^2 - m_{\nu_2}^2)^{1/2}, \qquad \delta > m_{\nu_2}$$

Thus the Kurie plot shows a distinct deviation from linearity for $\delta > m_{\nu_2}$, and thus provides a sensitive search for massive neutrino branches in the spectral shape of beta decay. To limit problems arising from background structure and to have a firm signal in the case of a massive branch, a comparative investigation of the positron and electron spectrum of the decay of ^{64}Cu ($t_{1/2}$ = 12.07 h) was undertaken with a magnetic spectrometer. The isotope ^{64}Cu has the advantages that both decay modes have single end point energies and are allowed beta decays (see fig. 1). Also the positron spectrum will be free from lines and edges. Therefore a massive branch of mass m_{ν_2} would be present as a kink in <u>both</u> spectra at energies $E_{\beta^+} = E_o(\beta^+) - m_{\nu_2}$ and $E_{\beta^-} = E_o(\beta^-) - m_{\nu_2}$, assuming the mass symmetry $m_\nu = m_{\bar{\nu}}$. Thus the presence of a kink at corresponding energies in both spectra would be a firm signature for a massive neutrino branch in the beta decay.

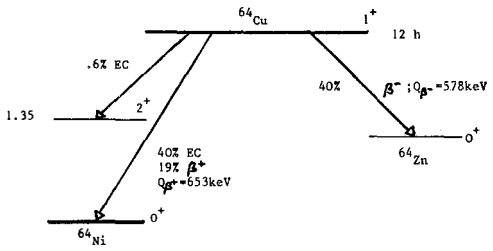


Fig. 1 Scheme of the $\beta^{\pm}$decay of ^{64}Cu.

The instrument used for this measurement was the high resolution iron-core spectrometer "BILL" situated at the HFR Grenoble[6]. A resolution of $\Delta p/p = 6 \times 10^{-4}$ was achieved. Approximately 3×10^8 events were recorded for each spectrum in the range δ = 0 - 500 keV. To determine the extent to which a massive neutrino branch occured in the experimental spectra, a derivative method was used which took into account the expected shape of a massive neutrino branch[5]. In the Fermi-Kurie representation of the spectra a straight line was defined by the zero level at E_o and the average value over a region of 10 keV above a hypothetical kink. In the region 40 keV below this hypothetical kink the extrapolated values of this line were compared with the experimental points for a possible amplitude of a heavy ν branch. Fig. 2 shows the theoretical shape of branches with $\sin^2\theta = 0.03$ for the cases m_ν = 360 keV and 100 keV, respectively. The reduced phase space for massive neutrinos is taken into account. The search for kinks was swept through the whole spectrum and exclusion plots for possible amplitudes of massive

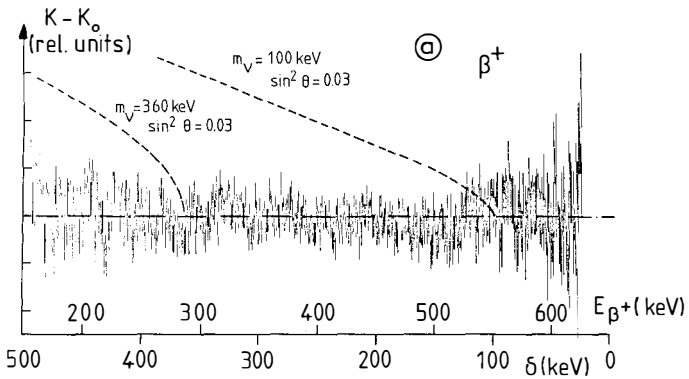


Fig. 2 Straightened and horizontally turned Kurie plot of the β^+ spectrum of the ^{64}Cu decay with statistical error bars (per keV window). Hypothetical $\sin^2\theta = 0.03$ branches with m_ν = 360 keV and 100 keV are shown.

ν branches were constructed separately from the β^+ and β^- spectrum. The statistical accuracy of the present data defined the lowest limit which could be achieved. Fig. 3 summarizes the final limits for massive neutrino branches from the present work. The combined limit is somewhat higher than the statistical limits due to non-statistical fluctuations in the data. No massive neutrino branches were detected.

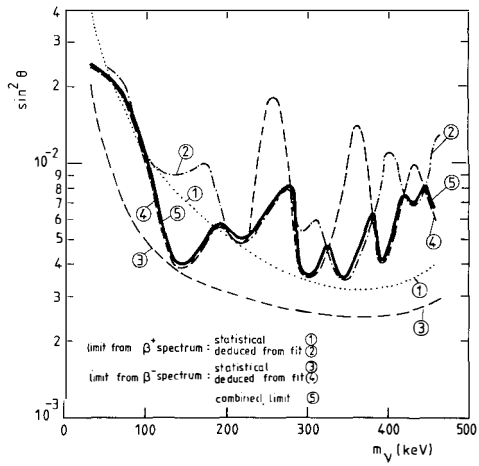


Fig. 3 Exclusion plots for massive neutrino branches deduced from present measurements. The solid line shows the achieved limits of the combined analysis of the β^+ and β^- spectra (90% confidence). The region above this line is excluded by these measurements.

For the case of electron neutrinos being composed of a dominant mass eigenstate with $m_{\nu_1} \approx 0$ and a second mass eigenstate with m_{ν_2} in the range 10 keV to 1 MeV, the limits from various experiments are shown in fig. 4. Since our result is valid for any neutral heavy particle emitted in the nuclear beta decay, only limits of a similar general signature are given, including

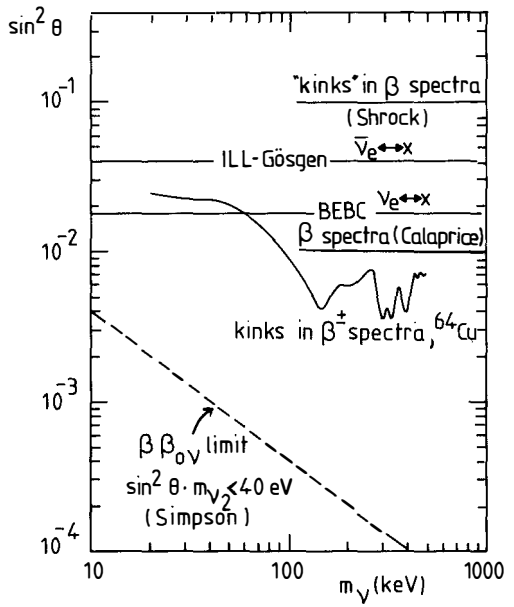


Fig. 4 Various experimental limits for heavy neutrino admixtures in the electron neutrino.

neutrino oscillation experiments of the type $\nu_e^{(-)} \rightarrow X$. The results from kinks in nuclear beta decays by Calaprice and Millener[7] and by Shrock[3] are not yet published in detail. Below m_{ν_2} = 10 keV Simpson[8] derived limits from the tritium beta decay. The BEBC experiments[9] gave the lowest limit from neutrino oscillation experiments, however questions arose concerning the statistical relevance of this result. The ILL-Gösgen limit stems from a flux measurement of reactor $\bar{\nu}_e$ at a distance from the reactor core relative to the $\bar{\nu}_e$ flux at the origin (disappearance experiment)[10]. With a safe limit of neutrino-less double beta decay ($\beta\beta_{0\nu}$) experiments, Simpson[11] derived the very stringent limit $\sin^2\theta\, m_{\nu_2} \lesssim 40$ eV. But it should be noted that this limit is based on the assumption of neutrinos being majorana particles and of constructive interference of neutrinos in the $\beta\beta_{0\nu}$ decay.

The authors are grateful to the ILL reactor staff and to G. Blanc for technical assistance. Part of the work was supported by the BMFT.

References

1) V.A. Lubimov et al., Phys. Lett. 96B, 159 (1980)
K.E. Bergquist, Nucl. Phys. B39, 317 (1972)
H. Anderhub et al., Phys. Lett. 114B, 76 (1982)
W. Bacino et al., Phys. Rev. Lett. 42, 749 (1979)
2) R. Abela et al., Phys. Lett. 105B, 263 (1981)
F.P. Calaprice et al., Phys. Lett. 106B, 175 (1981)
3) R.E. Shrock, Phys. Lett. 96B (1980) 159
4) B.H.J. McKellar, Phys. Lett. 97B, 93 (1980)

5) K. Schreckenbach, G. Colvin and F. von Feilitzsch, Phys. Lett. 129B, 265 (1983)
6) W. Mampe et al., Nucl. Instr. Meth. 154, 127 (1978)
7) F.P. Calaprice and D.J. Millener, Phys. Rev. C27, 1175 (1983)
8) J.J. Simpson, Phys. Rev. D24, 2971 (1981)
9) O. Erriquez et al., Phys. Lett. 114B, 298 (1982)
10) J.L. Vuilleumier et al., Phys. Lett. 114B, 298 (1982)
K. Schreckenbach, F. von Feilitzsch and A.A. Hahn in "The source spectrum of reactor antineutrinos and its application to ν oscillation studies", contribution to this workshop.
11) J.J. Simpson, Phys. Lett. 102B, 35 (1981)

THE CALCULATION OF MOLECULAR FINAL STATES AND THEIR EFFECT ON A PRECISION NEUTRINO MASS EXPERIMENT

O. Fackler*, M. Mugge†, H. Sticker*, N. Winter‡, R. Woerner‡

* Rockefeller University
† Fermilab
‡ Lawrence Livermore Laboratory

ABSTRACT

We are performing an experiment to determine the electron neutrino mass with the precision of a few electron volts by measuring the tritium beta decay energy distribution near the endpoint. At the few electron volt level, a major consideration in the choice of a tritium source is the effect of excited final atomic or molecular states on the beta decay distribution. It is important to choose a source for which the initial and final states can be accurately calculated. We have chosen frozen tritium as our source since the states of molecular tritium and those of the HeT^+ daughter ion have electronic wavefunctions that can be calculated with high accuracy. We describe the effects of final excited states on the neutrino mass determination and the results of these calculations in this paper.

The choice of a source for our tritium beta decay experiment (described in an accompanying paper) is extremely important. Several problems need to be addressed in choosing the best source. The first is that if the neutrino mass is zero, the fraction of decays within 2 eV of the endpoint is only 2.6×10^{-12}. This small fraction necessitates a source of high activity, but one that is thin in order to keep the dE/dx loss of the emerging beta small. Even if the neutrino has a small finite mass, the major distortion of the spectrum occurs within a few neutrino masses from the endpoint.

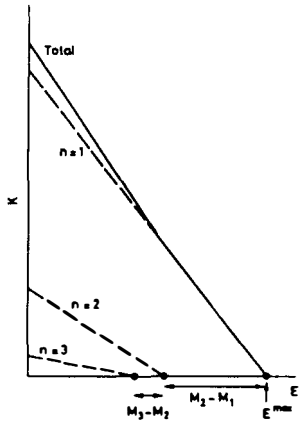


Fig. 1a

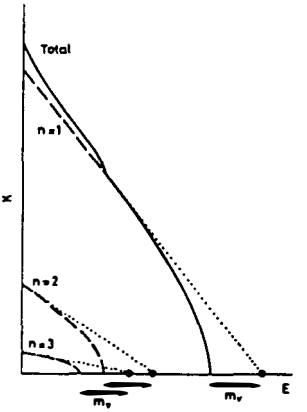


Fig. 1b

The second problem is that the decaying atom or molecule remains in one of many excited states. These excited states degrade the beta energy and give rise to a number of branches in the tritium beta decay spectrum each with different endpoint energies. The sum of these branches gives rise to the distorted measured spectrum. The effect of these different excited final states on the Kurie plot for a zero mass neutrino is shown in Fig. 1a and for a finite mass neutrino in Fig. 1b. These figures show that a precision neutrino mass experiment must accurately account for these final states. Unfortunately the transition probabilities and energy levels of the final states are not calculable with sufficient precision for most complex molecules or tritium binding processes which might serve as sources.

These two considerations, along with others, led us to chose pure molecular tritium (T_2) frozen at liquid helium temperatures as our source. This source is ideal because it has:

1) a very high specific activity -- the highest possible for a given dE/dx loss, and

2) a very low intermolecular binding energy (on the order of 1/400 eV), which means that the electronic wavefunction is essentially that of the free T_2 molecule.

We have done the final state calculations for free molecular tritium although the actual source is frozen tritium. Nevertheless, the tritium molecular wavefunction in the frozen solid is very close to the molecular wavefunction of the free molecule. We can understand this fact qualitatively by noting that the tritium melting temperature implies that the intermolecular binding energy is very much less than the orbital electron binding energy. Consequently we can expect a very small perturbation on the molecular wavefunction because of intermolecular binding forces.

More quantitively, the electron probability density at the half nearest molecular neighbor distance is approximately 3×10^{-4} of the maximum. This small electronic overlap gives rise to a negligible distortion of the molecular wavefunction. The depth of the internuclear potential well is approximately 1,600 times deeper than the intermolecular potential well. This difference in binding energies also indicates a very small perturbation of the molecular wavefunction in the solid.

A theoretical calculation of the change in the T_2 electronic wavefunction resulting from the effects of binding tritium in the crystal lattice was done by L. Stolarzik, Warsaw (Reported to us by H. Monkhorst, University of Florida). He symmetrically orthogonalized the wavefunctions and found that the fractional change in the wavefunction, $\Delta\psi/\psi$, is approximately 0.07%. This small change is not surprising since the inductive forces which bind the tritium molecules in the solid are typically one to two orders of magnitude smaller than the exchange forces which govern molecular binding.

The experimental evidence for a very small change in the electronic wavefunction resulting from the binding in the solid comes from Raman spectra in gaseous and solid hydrogen. The vibrational energy levels are

determined by the shape of the internuclear potential well and the shape of this well is determined by the electronic wavefunction. The typical measured shift in the vibrational energy levels resulting from the binding in solid hydrogen is about 1/2000 eV. Since this energy shift is very small compared with the typical vibrational energy level spacing of about 0.1 eV, this is evidence for a very small perturbation in the molecular wavefunctions resulting from the intermolecular binding in the solid. Furthermore, the molecular binding forces are so weak that the rotational states are hardly perturbed and the molecules can rotate as though they were nearly free.

Hence, conservatively, we can conclude that the uncertainty in the transition probabilities due to intermolecular binding in the solid is less than 0.5% and much smaller for the energy level uncertainties.

Because this essentially free tritium molecule is a two electron system, the final molecular excited state effects can be accurately calculated. The probability for a molecular transition to occur upon beta decay is given by

$$P_{if} = \left|\int \psi_f^* T_{op} \psi_i \, d\tau\right|^2$$

where ψ_f and ψ_i are the final and initial state wavefunctions and T_{op} is the operator taking the initial state into the final state upon beta decay. With a high degree of accuracy, we can partially make the Born-Oppenheimer approximation and separate the molecular wavefunction into the electronic wavefunction, Φ^{el}, and the nuclear wavefunction, $\chi^{nuc}_{\nu,j}$, which depends on both the vibrational quantum number, ν, and the rotational quantum number, j.

$$\psi = \Phi^{el} \chi^{nuc}_{\nu,j}$$

Since T_{op} does not depend on the electronic coordinates, the transition probability can then be rewritten as

$$P_{if} = \left|\int A_{if} \chi_f^* T_{op} \chi_i \, d\tau\right|^2$$

where

$$A_{if} = \int \Phi^{*}_{el}(\vec{r})\Phi(\vec{r})d\vec{r}.$$

The electronic wavefunctions are determined by a complete configuration interaction calculation. The internuclear potential energy for each of the excited states is calculated along with the electronic wavefunctions. The nuclear wavefunctions are determined for each of these electronic states by solving Schroedingers equation for that potential energy function. For the bound states, the nuclear wavefunctions are determined for each vibrational and rotational quantum number.

As will be discussed later, the initial state $\psi_i = \Phi_i^{el} \chi_{\nu,j}^{nuc}$ for the T_2 molecule can be accurately taken as the ground electronic state and the $\nu = 0$, $j = 0$ nuclear motion state. On the other hand there will be a distribution of final states in each degree of freedom.

Figure 2 shows the final state potential energy curves for the HeT^+ daughter ion as a function of the helium-tritium internuclear distance for the first twenty eight states. Most of these molecular states have the wrong electronic configuration to have any appreciable transition probability. The transition probabilities for these states are shown as a function of the $He\text{-}T^+$ internuclear separation in Figure 3. This figure shows that at the initial T_2 internuclear separation, 1.4 A. U., there are only five electronic states, including the ground state, which have sufficiently large transition probabilities to give rise to distinct branches in the Kurie plot. As is expected from the closeness of the T_2 and the HeT^+ ground state internuclear separations, most of the probability occurs for a transition to the HeT^+ ground state. The probability of finding the HeT^+ ion in the ground state after the decay is approximately 60% which is to be compared with 70% in the decay of an isolated tritium atom. Note that the calculations accurately reproduce the atomic tritium transition probabilities for large internuclear separations.

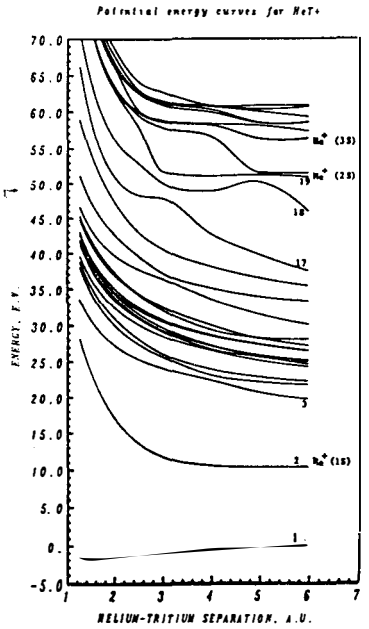


Fig. 2

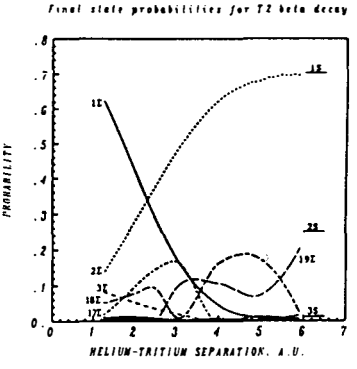


Fig. 3

Unlike the atom, however, the HeT^+ molecule in its ground state has two additional degrees of freedom which can absorb energy from the decay beta. These two additional degrees of freedom are the vibrational and rotational states.

At the liquid helium temperature of our source, only the lowest vibrational and the lowest rotational states are populated. However, after the decay, when one of the atoms has been given an impulse from the decay beta, most of the possible vibrational and rotational states will be populated. Fortunately, even near the endpoint of the beta decay spectrum where the maximum momentum transfer to the nucleus can occur, the energy transferred to the nucleus is too small to dissociate the HeT^+ daughter ion.

The HeT^+ is primarily excited to a high vibrational state when, near the endpoint of the beta decay distribution, the decay beta is emitted nearly aligned with the internuclear axis. Conversely, the HeT^+ ion is

left in a highly excited rotational state when the decay beta is emitted nearly perpendicular to the internuclear axis. This coupling between the beta decay and the vibrational and rotational states is shown in Fig. 4 as a high density of states near the top of the potential well.

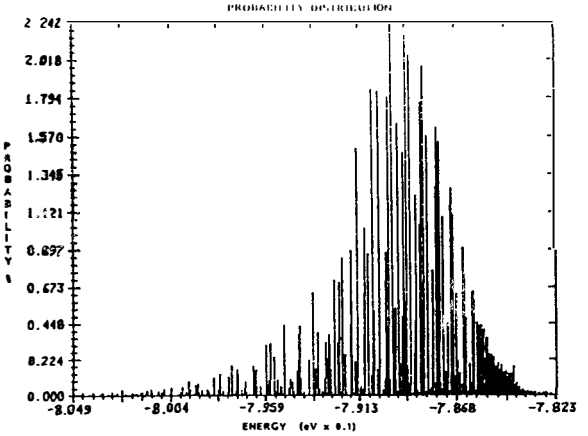


Fig. 4

The probability of finding the HeT^+ in in a particular vibrational and rotational state versus the energy of these states are shown in Figure 4. The full width of this distribution is about 2 eV and the full width at half height is on the order of 1 eV. As a consequence of this small spread, the ground state branch in the Kurie plot is smeared by only an average of 1 eV. This additional spread is a small penalty to pay for the ease of using molecular rather than atomic tritium.

Our conclusion is that frozen tritium is an ideal source because:
1) The molecular final state effects are well calculable and the uncertainties in these calculations due to calculational accuracy and intermolecular binding effects result in an uncertainty in the determination of the neutrino mass of less than 1 eV.
2) It is pure tritium and consequently it is the most intense source for a given dE/dx loss.

We would like to thank the many people at Fermilab, Lawrence Livermore Laboratory and Rockefeller University for their greatly

appreciated help. We would also like to thank J. Tran Thanh Van and the organizers of this Rencontre de Moriond for their warm hospitality.

AN EXPERIMENT FOR A PRECISION NEUTRINO MASS MEASUREMENT

O. Fackler[+], M. Mugge[*], H. Sticker[+], R. Woerner†

* Fermilab
† Lawrence Livermore National Lab
\+ Rockefeller University

Abstract

We describe an experiment which is designed to determine the electron neutrino mass to better than 2 eV. Key features of the experiment are a high activity frozen tritium source and a high resolution electrostatic spectrometer designed to make a careful measurement of the tritium beta decay end point spectrum. The goal is to determine the neutrino mass to better than 1 eV statistically in a four day run. A series of these runs will allow study of potential systematics. The construction phase is nearly complete and preliminary data will be taken in late spring.

It has been over fifty years since Pauli postulated a new highly penetrating particle that could explain the continuous energies observed in beta decay. Early observation that the neutrino mass is small led many to believe it was massless. In recent years, a number of suggestions have been advanced that neutrinos have mass. These suggestions range from a possible explanation of the paucity of solar neutrinos, the gravitational attraction of galactic clusters and nebulae, and the distribution of luminous matter within galaxies.

In 1972, Bergkvist[1] set an upper limit to the electron neutrino mass of 60 eV. A Russian group[2] in 1980 claimed evidence of a non-zero neutrino mass in the 14-46 eV range. This result along with results from neutrino oscillation experiments stimulated a great deal of work on various methods of measuring a possible non-zero neutrino mass.

Our experiment is designed to make a high resolution measurement of the tritium beta decay spectrum near the end point. Our design goal is to determine the neutrino mass better than 1 eV statistically in a four day run. This time period allows numerous groups of runs to study potential systematic errors at the 2 eV level or below.

We chose frozen tritium as our source for two reasons. First, it is a source with fully calculable final states. Second, pure tritium offers the highest possible activity for a given dE/dx loss.

1) K. Bergkvist, Nucl. Phys. B39, 317 (1972)
2) V.A. Lubimov et al, Phys. Lett 94b, 266 (1980)

The source thickness is continuously variable allowing study of the dE/dx effects. As one goes to a thicker source with a higher counting rate, the electron energy spectrum is of course degraded.

The apparatus is shown in Figure 1. A gate valve separates the source region on the left from the rest of the apparatus. With the valve closed, we rotate the source to a horizontal position and introduce gaseous tritium in the bottom of the tank. This produces a uniform layer of frozen tritium on the source which is then rotated back down vertically. The gate valve is then opened, illuminating an adjustable collimator. The accepted electrons pass through the aperture of a cryopump and in to the spectrometer region.

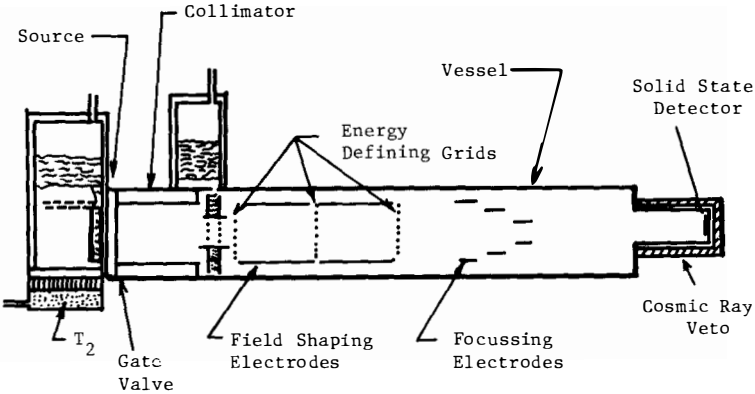


FIGURE 1 Schematic view of the apparatus. The source at the left rotates from its vertical position to a horizontal position as shown by dotted lines.

The spectrometer consists of three parallel grid planes and field shaping electrodes. The electrons enter a uniform retarding electric field and only those electrons whose energy is above the potential of the center grid plane pass through the center grid. The grid consists of parallel wires whose diameter and spacing are chosen such that the depth of the potential well between wires is less than 2 volts. Depending on the angular acceptance of the collimator chosen, the effective energy resolution of the collimator plus spectrometer is adjustable from 0.7 eV up to 3.0 eV. Those electrons which pass through the center grid are then accelerated back to their original energy and pass through the last grid plane.

Electrons next enter a focussing region consisting of three concentric rings. These rings electrostatically focus the electrons onto a solid state detector which has an energy resolution of ~ 1 KeV. This resolution aids in reducing backgrounds.

The vacuum vessel containing the experiment is 7-1/2 meters long by 0.9 meters in diameter. It is designed to operate at 10^{-12} torr in order to prevent frozen gas buildup on the cryogenic source. At these pressures, we can run for 4 days and only increase the dE/dx loss in the source by 0.1 ev. Other environmental considerations for the vessel include cooling to liquid nitrogen temperatures in order to reduce the radiative heat load on the source and cryopump and heating to bakeout the whole system. These have necessitated both cooling panels for liquid nitrogen and sufficient insulation to keep the liquid nitrogen consumption at acceptable levels. Additionally, a magnetic shield is

incorporated with the insulation to give a measured magnetic field in the fiducial region of the vessel of less than two milligauss.

Figure 2 shows a Monte Carlo simulation of a beta energy spectrum for a four day run. The spectrometer measures an integral event distribution. The upper curve shows this distribution for a neutrino mass of 5 eV versus the lower curve with a mass of 0 eV. Counting times are increased as one nears the end point so that the errors are kept small. For example, in the 5-10 eV bin away from the end point, the 0 and 5 eV mass curves differ by 25 standard deviations.

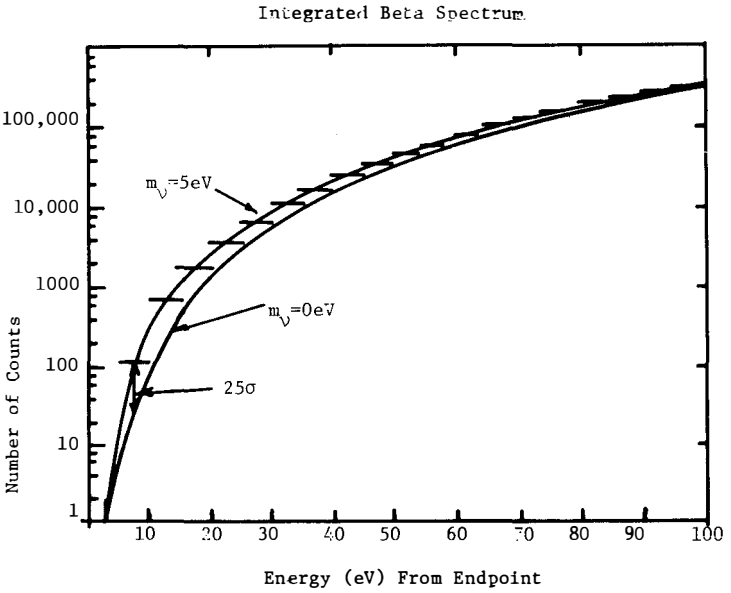


FIGURE 2 A Monte Carlo simulation of the experiment including all anticipated resolutions and physics effects. The upper curve is the expected one for a 5eV neutrino mass and the lower curve is for a 0eV neutrino mass. Error bars are about the width of the bars except in the lowest bin.

We are currently setting up the experiment at Lawrence Livermore National Laboratory. We are studying backgrounds from electrostatic components of the experiment and expect to put an ion implanted source in during late spring to study potential tritium induced backgrounds. We plan by late summer to complete the cryogenic components of the experiment.

We appreciate the support of many people at Fermilab, Lawrence Livermore National Laboratory and Rockefeller University. We thank J. Tran Thanh Van and F. Vannucci for a very stimulating meeting.

---

*Work performed under the auspices of the U.S. Department of Energy by Lawrence Livermore National Laboratory under contract number W-7405-ENG-48, by Fermilab and by Rockefeller University.

THE $^{N}/_{M}$ ELECTRON-CAPTURE RATIO OF THE NEUTRINO-MASS PROBE ^{163}Ho.

H.L. Ravn [1], J.U. Andersen[2], G.J. Beyer[1]★, A. De Rújula[1], P.G. Hansen[2], B. Jonson[1], E.Laegsgaard[2].

1) CERN, Geneva, CH-1213 Geneva 23

2) Institute of Physics, University of Aarhus, DK-8000 Aarhus C.



ABSTRACT

As a step towards the application of ^{163}Ho in experiments to determine the electron neutrino mass the total-absorption spectrum of the ^{163}Ho electron capture decay was investigated. By means of a ^{163}Ho doped silicon semi-conductor detector a direct measurement of the $^{N}/_{M}$ capture ratio was made. The $^{N}/_{M}$ capture ratio was found to be 2,27 ± 0,4. From this we deduce a $Q_{EC} = 2{,}84\ ^{+0{,}16}_{-0{,}10}$ keV.

★ Visitor from Zentralinstitut fur Kernforschung, Rossendorf bei Dresden, DDR

Introduction.

The shape near the upper endpoint of the continous inner bremsstrahlung spectrum (IB) in electron capture beta-decay (EC) contains information on the neutrino mass [1] in a similar way as the high energy part of the tritium betaspectrum [2,3,4].

This has stimulated our general interest in nuclei that undergoes electron-capture decay with the "right" Q value. The ideal cases for observation of a neutrino-mass effect are nuclei with a low Q value situated just below the binding energy of an atomic s-state of the daughter atom. In these cases the strongly resonant behaviour of the bremsstrahlung near the x-ray energies results in a huge magnification of the interesting endpoint region.

From the chart of the nuclides we have chosen the three radioactive nuclei ^{193}Pt, ^{163}Ho and ^{157}Tb as the best candidates for our long range objective to measure the electron-neutrino mass via the shape of their IB spectra.

The isotope ^{193}Pt with a Q_{EC} value of 56,6 ± 0,3 keV was used for the first detailed test of the De Rújula [1] extended Glauber-Martin [5,6] theory. The high Q value permitted a series of bremsstrahlung - x-ray coincidence measurements by means of a standard Ge - Si(Li) photon spectrometer [7]. It could be shown that the low energy internal bremsstrahlung originates in P-wave capture, the predicted spectral shapes were in striking agreement with theory and for the absolute intensities the agreement was even quantitative. A Kurie plot of the ^{193}Pt IBEC spectrum provided a new improved limit $m_\nu < 500$ eV.

We then turned our attention to the experimentally much more difficult case of ^{163}Ho. In a first experiment with gas proportional counters [8], a mono-atomic layer source of ^{163}Ho with a known number of atoms, permitted efficient counting of M shell radiations with energies just above 1 keV. From the resulting partial M capture half-life $T^M_{1/2} = (4{,}0 \pm 1{,}2) \times 10^4$ y we deduced $Q_{EC} = 2{,}58 \pm 0{,}10$ keV and a total half-life $T_{1/2} = (7 \pm 2) \times 10^3$ y.

In order to judge the feasibility of ^{157}Tb in future experiments related to the neutrino mass more precise values of the decay parameters were determined.[9]. The $Q_{EC} = 62{,}9 \pm 0{,}7$ keV obtained from electron capture ratios leaves

a transition energy of 8,4 ± 0,7 keV for the decay to the 54,5 keV excited level in ^{157}Gd. This is very close to the 2s resonance energy of 8,376 keV. Experiments which attempt to observe the IBEC spectrum in coincidence with photons or conversion electrons de-exciting the 54,5 keV level are in progress. The minute branching ratio of $(1,1 \pm 0,1) \times 10^{-3}$ found for this level may offset the enhancement of the near resonance point bremsstrahlung in which case ^{163}Ho remains the best m_ν probe.

In the present paper we report on the M/N capture ratio obtained in a first attempt to measure the IBEC spectrum of ^{163}Ho by means of total absorption spectrometry. By implantation of ^{163}Ho into the sensitive volume of a silicon semi-conductor detector we obtain, due to the low energies involved in the ^{163}Ho decay, a calorimetric measurement. The internal source counting technique, widely used in electron capture studies [10], further more takes advantage of the process of electron ejection in electron capture (EEEC) which in this case dominates over the IBEC spectrum by almost three orders of magnitude [11].

The experiment is similar to the one with a tritium-implanted Si(Li) detector carried out by Simpson [4]; the advantage of the Ho experiment would be in the M,N peaks that would make the spectrum self-calibrating (cfr. Dixon et al. [12]) and in the intensity at the end-point. The difficulties, which will become clear from the following, are associated with the behaviour of implanted Ho in silicon.

Experimental

In the following only a brief account of the experimental details is given (a full report will be published later) [13].

The ^{163}Ho prepared by neutron irradiation of ^{162}Er in the reactor at Kf Z Rossendorf [14] was ion implanted through a 3 mm Ø defining mask into a number of silicon crystals shaped as guard ring counters. The implantations were carried out in the Aarhus Institute of Physics. Two energies were used, 500 keV and 2 MeV, obtained by means of the 600 kV implantation unit and the 2 MV van de Graaf, respectively. The crystals were kept at an annealing temperature of 330 °C while the about 10^{11} ^{163}Ho were implanted along a channeling direction. The implanted dose was maintained by a Faraday cup. After implantation of the $^{11}B^+$ and $^{31}P^+$ contacts at 5 kV and 50 kV, respectively, on the two faces of the crystals, the counters were annealed at 300 °C for 1/2 hour. The counters were operated at liquid-nitrogen temperature.

Results.

A. Status of the Ho doped detector development.

The behaviour of the detectors was rather independent of the ^{163}Ho implantation energy. A representative energy spectrum obtained with a counter doped at 500 keV is shown in fig. 1.

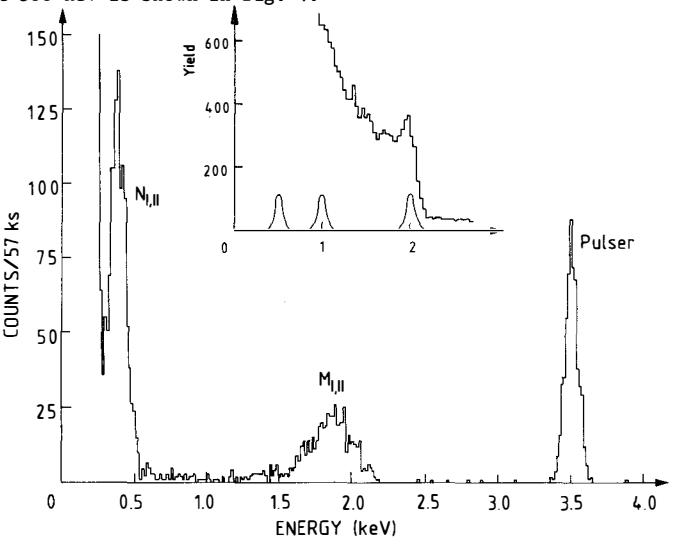


Fig. 1. Total absorption spectrum showing the ^{163}Ho M and N capture peaks at 2,05 keV and 0,4 keV respectively. The inset illustrates the response of the Ho doped silicon semi-conductor detector before drifting with backwards bias.

As tested with an external ^{55}Fe K x-ray source, which also served to determine the energy scale, no difference could be found between ^{163}Ho doped counters and undoped ones.

The initial response of the detectors to the ^{163}Ho decays, shown in the inset of fig.1. indicates very incomplete charge collection in the region of the implanted ^{163}Ho atoms. Only the sharp drop of the end-point and the weak indication of a peak at the correct energy of 2,05 keV, the M_I binding energy of dysprosium showed that ^{163}Ho was being detected. The spectrum shown in fig. 1. was obtained after a treatment of the detectors over 12 hours with a forward bias. The $M_{I,II}$ peak now is clearly resolved and the $N_{I,II}$ line of only 419 eV also appears at the low energy side of the spectrum.

This first observation of beta decay by N capture completely resolved from M capture events illustrates how the ^{163}Ho experiment is self-calibrating with respect to energy scale and resolution. The half-width of the $M_{I,II}$ peak is $\sim$ 380 eV compared with 75 eV for the pulser. The peak appears below the expected value of 2,05 keV, thus indicating that effects of incomplete charge collection remain. Over the days following the forward bias treatment the resolution of the detector unfortunately gradually returned to the initial condition shown in the inset of fig.1. Despite the fact that the detector could be redrifted, an attemt to collect sufficient statistics for a neutrino mass measurement is at the present development stage too difficult.

B. $^{N}/_{M}$ capture ratio and Q_{EC}.

A $^{N}/_{M}$ shell capture ratio of 2,27 ± 1 ± 0,4 is obtained directly from fig.1. The error limits represent statistical and possible systematic errors, respectively. This value allows to calculate a new more precise value of Q_{EC}. For this we follow the notation of Bambynek et al. [10], according to which the capture rate to a given filled sub-shell x is proportional to the square of the ^{163}Ho - ^{163}Dy nuclear transition matrix element and the usual statistical rate function:

$$f_x = \frac{\pi}{2} \beta_x^2 B_x (Q_{EC} + E_x)^2 m_e^{-2} c^{-4}$$

where:

β_x is the amplitude of a Coulomb wave function

B_x is the overlap and exchange correction factor

E_x is the energy of an electron in shell x (a negative number)

$m_e^{-2} c^{-4}$ is the square of the neutrino momentum.

The quantities β_x, B_x are tabulated in ref. [10]. As can be seen from that paper the values for B_x depend somewhat on the method of calculation. We use here, rather arbitrarily the recalculated values based on a method due to Bachcall. After some extrapolation, both along the atomic number Z and along the main quantum number n (namely to get a value for the Q_I shell), we arrive at the estimated B(K) = 0.993, $B(L_I)$ = 1.032, $B(M_I)$ = 1.080, $B(N_I)$ = 1.183, and $B(Q_I)$ = 1.3. The correction factors for the M_{II}, N_{II}, O_{II} states were assumed to be unity. From the $(N_I + N_{II})/(M_I + M_{II})$ ratio we then calculate

$Q_{EC} = 2.84 \begin{smallmatrix} + 0.16 \\ - 0.10 \end{smallmatrix}$, where the lower limits include possible systematic errors. The $(O_I + O_{II})/(N_I + N_{II})$ ratio, which is almost independent of Q_{EC}, becomes 0.176.

C. The partial M-capture half-life.

Since the present experiment measures the implanted dose of mass 163 atoms we can repeat the determination of the partial M-capture half-life. Together with the disintegration rate observed in the $M_I + M_{II}$ peak we obtain $T^M_{1/2} = 28\ 500 \begin{smallmatrix} + 6000 \\ - 10\ 000 \end{smallmatrix}$ y

The assymetric error limit takes into account the extrapolation of the M tail to zero. From the mass spectrum observed during implantation a correction of 5 % has been applied to correct for the presence of ^{163}Dy in the beam.

Discussion.

The new Q_{EC} of $2{,}84 \begin{smallmatrix} + 0{,}16 \\ - 0{,}10 \end{smallmatrix}$ replaces but is consistent with the previous value [8] 2,3 ± 1 keV and 2,58 ± 0,10 keV. The latter value which was based on a semi-empirical estimate of the nuclear matrix element, can be refined further on the bases of more precise values of the partial M-capture half-life. Although the new direct measurement $T^M_{1/2} = 28\ 500 \begin{smallmatrix} + 6000 \\ - 10000 \end{smallmatrix}$ y is consistent with the earlier values of 40 000 ± 12 000 y [8] and 45 000 ± 15 000 y [15] an even better value may be obtained from the very precise total half-life of 4570 ± 50 y determined by Baisden et al.[16]. In an obvious notation we must have $T^M_{1/2}(1+ \frac{N}{M} (1 + \frac{O}{N})) = 17\ 400 \pm 2300$ y, where the shell ratios quoted above have been used. Returning now to the use of an estimated nuclear matrix element M (as in [1]). The correction was quoted in the wrong order in ref. [8]. Calculated by Drs. Bengtsson and Ragnarsson, to whom our best thanks are once again due, the quantity $u_p^2 u_n^2$ was 0.508 for ^{151}Ho and 0.354 for ^{163}Ho. The analysis of ref. [1] remains correct. We find from this $T^M_{1/2}$ a $Q_{EC} = 2.86 \pm 0.14$ keV, where the lower limit includes a possible 30 % error on $|M|$ [15]. It will be seen that the half-life [16], our new N/M ratio and the matrix element deduced [8] from data for ^{161}Ho form part of an internally consistent set.

Our conclusions lean heavily on calculations of N capture, a process observed for the first time in our work and very sensitive to the finer

details of the atomic calculation. For this reason and also owing to the difficulties of the experiment, the exact Q_{EC} could still differ somewhat from 2.85 keV. The value is low enough for ^{163}Ho to retain its place as an interesting candidate for neutrino mass experiments though not as near to the resonance points (2.05 and 9.05 keV) as one had hoped for originally.

References.

[1] A. De Rújula, Nucl. Phys. A374 (1982) 619.

[2] K.E. Bergkvist, Nucl. Phys. B39 (1972) 317; Phys. Scripta 4 (1971) 23.

[3] V.A. Lyubimov, E. G. Novikov, V.Z. Nozik, E.F. Tretyakov and V.S. Kosik, Phys. Lett. 94B (1980) 266.

[4] J.J. Simpson, Phys. Rev. D23 (1981) 649.

[5] R.J. Glauber and P.C. Martin, Phys. Rev. 104 (1956).

[6] P.C. Martin and R.F. Glauber, Phys. Rev. 109 (1958) 1307.

[7] B. Jonson, J.U. Andersen, G.J. Beyer, G. Charpak, A. De Rújula, B. Elbek, H.Å. Gustafsson, P.G. Hansen, P. Knudsen, E. Laegsgaard, J. Pedersen and H.L. Ravn, Nucl. Phys. A396 (1983) 479.

[8] J.U. Andersen, G.J. Beyer, G. Charpak, A. De Rújula, B. Elbek, H.Å. Gustafsson, P.G. Hansen, B. Jonson, P.Knudsen, E. Laegsgaard, J. Pedersen and H.L. Ravn, Phys. Lett. 113B (1982) 72.

[9] G.J. Beyer, A. De Rújula, R.-D. von Dincklage, H.Å. Gustafsson, P.G. Hansen, P. Hoff, B. Jonson, H.L. Ravn and K. Risager, Nucl. Phys. A408 (1983) 87.

[10] W. Bambynek, H. Behrens, M.H. Chen, B. Crasemann, M.L. Fitzpatrick, K.W.D. Ledingham, H. Genz, M. Mutterer and R.L. Intemann, Rev. Mod. Phys. 49 (1977) 77 - 221.

[11] A. De Rújula and M. Lusignoli, Phys. Lett. 118B (1982) 429.

[12] W.R. Dixon, W.F. Davidson, R.S. Storey and D.M. Rehfield, Phys. Lett. 108B (1982) 265.

[13] E. Laegsgaard, J.U. Andersen. G.J. Beyer, A. De Rújula, P.G. Hansen, B. Jonson and H.L. Ravn. The Capture Ratio $^{N}/M$ In The EC Beta Decay Of ^{163}Ho. To be published.

[14] G.J. Beyer and H.L. Ravn. Preparation of Extremely Pure Samples of ^{163}Ho and ^{193}Pt. To be published.

[15] S. Yasumi, G. Rajasekaran, M. Ando, F. Ochiai, H. Ikeda, T. Ohta, P.M. Stefan, M. Maruzama, N. Hashimoto, F. Fujioka, K. Ishii, T. Shinozuka, K. Sera, T. Omori, G. Izawa, M. Yagi, K. Masumoto and K. Shima. Phys. Lett. 122B (1983) 461; S. Yasumi, Report at the Brighton Conference on High-Energy Physics (July 1983).

[16] P.A. Baisden, D.H. Sisson, S. Niemeyer, B. Hudson, C.L. Bennett and R.A. Naumann. Phys. Rev. C 28 (1983) 337.

MASSIVE NEUTRINOS IN COSMOLOGY

Gary Steigman, Bartol Research Foundation



Abstract

Neutrinos are produced copiously during the early evolution of the Universe and survive in great abundance as relics from the big bang. If neutrinos have a small mass (> few eV) and are stable, they may dominate the present Universe. The survival of light (< MeV) and heavy (> MeV) neutrinos from the early Universe will be described and constraints from cosmology placed on their masses. Stable, light neutrinos with $M_\nu \sim 25\text{–}75$ eV are not inconsistent with limits to the universal mass density but do present problems for the evolution of the observed large scale structure of the Universe. A speculative scenario involving heavier ($M_\nu \sim 100\text{–}250$ eV) unstable neutrinos is described. The assets and liabilities of this new scenario are outlined. Nucleosynthesis constraints on the number of neutrino families ($N_\nu < 4$) are reviewed.

Introduction

This elementary overview of the role played by neutrinos, especially massive neutrinos, in cosmology is intended for the interested neophyte. This article is not a detailed and comprehensive review of neutrino astrophysics; many such excellent reviews already exist. As the goal is to provide enough information to bring the beginner up to speed, the extensive literature in this field is only referenced sporadically. My apologies to those whose work I've drawn upon without deserved attribution. It is the hope that the reader will leave this article with the desire – and the background – to seek out recent and future work in this exciting area of modern physics.

A perspective on recent developments in neutrino cosmology is provided by the following brief overview of the history – as it is known to me – of the subject. Shortly after the modern era in cosmology was ushered in with the discovery of the blackbody background radiation, Gershtein and Zeldovich[1] set the first cosmological limit to neutrino masses. As will be described later, the higher the universal mass density, the faster the Universe expands and the younger it is today. Gershtein and Zeldovich[1] correctly noted that lower limits to the age of the Universe led to upper limits to the possible mass density contributed by massive neutrinos and, hence, to upper limits to the sum of the masses of all neutrinos. Despite some crude estimates and numerical errors, they[1] found a limit to the mass of the μ-neutrino (only the e- and μ-neutrinos were known then) $M_{\nu\mu} < 400$ eV.

Neutrino cosmology languished for several years until the early 1970s and the work of Cowsik and McClelland[2] and Marx and Szalay[3]. From limits to the deceleration of the expansion of the Universe (the higher the mass density, the more rapidly the expansion decelerates) they set limits to the sum of neutrino masses in the range ~ 50–100 eV. More important, they were the first to propose massive neutrinos as a solution to the dark mass in clusters problem. Following the pioneering work of Zwicky[4], it has been

clearly established[5] that, on large scales (larger than those of the visible parts of galaxies), the gravitational potential in which the observed tracers (galaxies) move, is dominated by material which is nonluminous (to the optical astronomer, nonluminous means not shining in the optical, or blue, part of the spectrum). The dark mass problem is especially serious on the scale of rich clusters of galaxies.[5] Cowsik and McClelland[2] and Szalay and Marx[3] noted that neutrinos with masses of order 10 eV could account for the mass of clusters and, they wouldn't shine

There was another lapse of several years before activity started up once again on the role of massive neutrinos in cosmology[6]. In 1979, Tremaine and Gunn[7] noted - as had Cowsik and McClelland[2] - that phase space considerations excluded light neutrinos from shallow potential wells. Although relatively light neutrinos (~ few eV) could supply the dark mass in clusters, they could not supply the dark mass in galactic halos where the potential wells are less deep. In contrast, neutrinos heavy enough to cluster in galactic halos (M_ν ~ few tens of eV) would supply too much dark mass. Tremaine and Gunn[7] concluded, correctly, that neutrinos could not supply the dark mass on all scales in the Universe. They also inferred, incorrectly, that neutrinos could not dominate the Universe. Schramm and Steigman[8] pointed out that in rich clusters of galaxies, most baryons are dark. X-ray emission from rich clusters signals the presence of hot gas (nucleons and electrons). The hot gas, whose contribution to the total mass of the cluster outweighs that of the galaxies, is "dark" since it is shining in the x-ray but not the optical part of the spectrum. In environments other than that of rich clusters, this baryonic mass may be truly dark. Since some of the dark mass is baryonic, neutrinos need not supply <u>all</u> the dark mass. More importantly, Schramm and Steigman[8] noted that since primordial nucleosynthesis constrained[9] the nucleon mass density to be no more than ~20% of the critical mass density, should observations point to a higher total mass

density, something other than nucleons - perhaps massive neutrinos - would be required.

If, indeed, massive neutrinos do dominate the universal mass density, they play a very significant role in the growth of perturbations and the formation of large scale structure in the Universe. Because of their weak interaction, neutrinos ceased scattering off other particles very early on ($t \sim 1$ sec.) and have "free-streamed" ever since; they do, of course, gravitate. Free streaming neutrinos will mix regions of high and low density and, by an analogue of Landau damping, erase perturbations on small scales[10]. The lighter the neutrino, the faster it is moving (at a given temperature or time in the evolution) and the further it will free stream. If, indeed, ours is a neutrino dominated Universe, then the neutrino can neither be too light (or structure on all interesting scales would have been erased) nor too heavy (or there would have been too much dark mass). These considerations have led to a "favorite" mass for the heaviest neutrino in the vicinity of 30 eV.

With this historical overview as introduction, let us now turn to the details. In the next section the survival of "light" relic neutrinos is described and constraints are put on the possible masses of such neutrinos. Next, the fate of "heavy" relic neutrinos is outlined and constraints on the masses of such neutrinos are derived. In both cases we will only be concerned with stable neutrinos (i.e.: neutrinos whose lifetimes exceed the present age of the Universe) for an excellent review of the constraints on the lifetimes of massive, unstable neutrinos, see the article by Turner[11]. In the subsequent section we describe the role of light neutrinos in primordial nucleosynthesis and use the abundances of the light elements to limit the number of kinds of such neutrinos. Next, the "standard" neutrino scenario (one, most massive species of neutrino with M_ν of order 30 eV) is summarized and the problems it faces are outlined. This article concludes with the description of a new, speculative scenario[12] which, although facing difficulties of its own, solves some of the problems of the standard scenario.

"Light" Relic Neutrinos

Much of the material in this and subsequent sections appears in the author's review article[13] which the reader is advised to consult for further details and the appropriate references.

The total density drives the cosmic expansion rate during early epochs: $t^{-1} \propto \rho^{1/2}$. Early on the total density is dominated by extremely relativistic particles so that $\rho = \rho_{ER} \propto T^4$ where T is the temperature. As a result, the age and temperature of the early Universe are related by $t \propto T^{-2}$; for $t \sim 1$ sec, $T \sim 1$ MeV.

During early epochs ($T > 1$ MeV) neutrino pairs are produced and annihilate via the neutral current weak interaction: $e^+ + e^- \leftrightarrow \nu_i + \bar{\nu}_i$ where $i = e, \mu, \tau, ---$; for e-neutrinos, charged current interactions contribute as well. At very early times and high temperatures ($T > M_Z$) the interaction rate grows linearly with temperature: $\Gamma_\nu = n_e \sigma_\nu \propto T^3 \times T^{-2} \propto T$. Since the expansion rate (t^{-1}) grows as T^2, the number of interactions in an expansion timescale increases as the Universe expands and cools: $\Gamma_\nu t \propto T^{-1}$. For $T \lesssim T_{GUT}$, neutrino pairs are in equilibrium ($\Gamma_\nu t >> 1$). As the Universe cools below the Glashow-Weinberg-Salam transition, the W and Z bosons become massive and the cross sections change: for $T < M_Z$, $\Gamma_\nu \propto T^3 \times T^2$ and $\Gamma_\nu t \propto T^3$. The interaction rate decreases until, at $T =$ few MeV, it becomes comparable with the expansion rate. For $T <$ few MeV, $\Gamma_\nu t < 1$ and equilibrium can no longer be maintained; the neutrinos "freeze-out".

Our discussion here pertains to "light" neutrinos which are relativistic at freeze-out: $M_\nu <$ few MeV. In equilibrium ($T >$ few MeV), photons, electrons and neutrinos all have the same temperature. It is convenient to compare the neutrinos (relativistic fermions) to the photons (relativistic bosons). In equilibrium, the number densities and the energy densities are

related by

$$n_\nu/n_\gamma = 3/4\ (g_\nu/2); \quad \rho_\nu/\rho_\gamma = 7/8\ (g_\nu/2). \tag{1}$$

In equation (1), g_ν is the number of neutrino helicity states ($g_\nu = 2$ for a Majorana neutrino and its antineutrino).

After freeze-out no new neutrino pairs are produced and no relic pairs annihilate. Until $e^\pm$ pairs begin annihilating no extra photons are produced so that (1) is valid for $T > M_e$. During this epoch ($M_\mu \gtrsim T \gtrsim M_e$) $T_\gamma = T_e = T_\nu$ and,

$$\rho_{TOT} = \rho_\gamma + \rho_e + \rho_\nu = \frac{43}{8}\,\rho_\gamma\left[1 + \frac{7}{43}\,(N_\nu - 3)\right], \tag{2}$$

where N_ν is the total number of light ($\lesssim$ few MeV), two component neutrino flavors.

For $T < M_e$, $e^\pm$ pairs annihilate heating the relic photons. The relic neutrinos, having already decoupled cannot share in the energy (more properly, the entropy) released by the $e^\pm$ annihilation. As a result, for $T \lesssim M_e$, the relic photons are hotter than the relic neutrinos,

$$(T_\nu/T_\gamma)^3 = 4/11; \quad n_\nu/n_\gamma = 3/4\ N_\nu\ (T_\nu/T_\gamma)^3 = (3/11)N_\nu. \tag{3}$$

Today, then, when $T_\gamma \approx 2.7K$, $T_\nu \approx 1.8K$ and, whereas in every cubic centimeter there are 400 relic photons, there are 109 relic neutrinos of each species in the same volume. There are comparable numbers of light relic neutrinos and relic photons. To put this in perspective, the nucleon to photon ratio is some nine orders of magnitude smaller[9]: $\eta \equiv N_N/N_\gamma \lesssim 10^{-9}$. If neutrinos have a small but finite mass, they may dominate the present universal mass density.

$$\rho_\nu/\rho_N = M_\nu n_\nu/M_N n_N \approx 3\ M_\nu(\mathrm{eV})\eta_{10}^{-1} \gtrsim M_\nu/3\ \mathrm{eV}. \tag{4}$$

In (4), $n_{10} \equiv 10^{10} n$ and M_ν is the sum of all neutrino masses weighted by $g_\nu/2$. For M_ν in excess of a few eV, $\rho_\nu > \rho_N$ and the present Universe is Neutrino Dominated.

The present expansion rate is measured by the value of the Hubble parameter,

$$H_0 = 100 h_0 \text{ kms}^{-1}\text{Mpc}^{-1}; \; H_0^{-1} \simeq 10 h_0^{-1} \times 10^9 \text{ yr}. \tag{5}$$

In (5), h_0 has been introduced to account for the current observational uncertainty in H_0; it is likely that $1/2 \lesssim h_0 \lesssim 1$. Related to the present expansion rate is the critical density which separates those underdense ($\lesssim \rho_c$) models which expand forever from those overdense ($> \rho_c$) models whose expansion will ultimately be halted to be followed by collapse.

$$\rho_c = 3H_0^2 (8\pi G)^{-1} \simeq 10^4 h_0^2 \text{ eV cm}^{-3}. \tag{6}$$

It is convenient to compare all densities to ρ_c; Ω_i is the ratio of ρ_i to ρ_c. For light relic neutrinos we have,

$$\Omega_\nu = \rho_\nu/\rho_c \simeq \left(\frac{M_\nu}{100\text{eV}}\right) \frac{\theta^3}{h_0^2} . \tag{7}$$

In (7), $\theta \equiv T_\gamma/2.7\text{K}$; it is likely that $1 \lesssim \theta \lesssim 1.11$. Note that if, as is suggested by "inflationary" models $\Omega_{TOT} = 1$ and, if nucleons and neutrinos are the stuff of the Universe, then: $M_\nu \text{ (eV)} \simeq 100 h_0^2 (1 - \Omega_N)$.

If, indeed, the sum of the light neutrino masses exceeds a few eV, we live in a neutrino dominated Universe. As Gershstein and Zeldovich[1], Cowsik and McClelland[2] and Marx and Szalay[3] have noted, there are constraints on how large the mass of the most massive neutrino may be. At present, the age constraint[1] is most severe. The age of the Universe is less than the Hubble age, $t_0 \leq H_0^{-1}$; the higher the present density, the younger the Universe (for $\Omega_0 = 1$, $t_0 = 2/3\ H_0^{-1}$). From the ages of the stars in globular star clusters, the Universe appears to be at least 10–13 billion

years old. If, in fact, $t_o \gtrsim 10\text{–}13 \times 10^9$ yr, the combination $\Omega_\nu h_o^2$ is constrained to be $\lesssim 1/4 - 3/4$ which implies (see (7)) $M_\nu \lesssim 25\text{–}75$ eV. Note that if, as in the inflationary models, $\Omega_o = 1$ then,

$$M_\nu \text{ (eV)} \lesssim \frac{44}{\theta^3} \left(\frac{10^{10} \text{ yr}}{t_o}\right)^2. \tag{8}$$

Although the overall constraint on the mass density contributed by light relic neutrinos will permit a relatively high mass, we must be careful to avoid too much dark mass on scales where neutrinos and nucleons are mixed (i.e.: on scales where dissipation has not occurred, permitting nucleons to settle relative to the non-interacting neutrinos). On such scales, since all neutrinos are dark and not all nucleons shine: $M_{Dark}/M_{Lum} \gtrsim M_\nu/M_N \approx \Omega_\nu/\Omega_N \approx 3M_\nu(\text{eV})\, n_{10}^{-1}$. There is little evidence for dissipation on the scale of rich clusters where $M_{Dark} \lesssim (10\text{–}30)\, M_{Lum}$ so that $M_\nu(\text{eV}) \lesssim (3\text{–}10)\, n_{10} \lesssim 20\text{–}100$ for $n_{10} \lesssim 7\text{–}10$[9].

As mentioned in the Introduction, free steaming neutrinos will damp perturbations and erase structure from the Universe[10]. The mass scale for damping is [10],

$$M_D \approx 3 \times 10^{18}\, M_\nu^{-2} M_\theta \approx 3 \times 10^{14}\, (\Omega_\nu h_o^2)^{-2}\, M_\theta. \tag{9}$$

For $\Omega_\nu h_o^2 \lesssim 1/4 - 3/4$, $M_D \gtrsim (5\text{–}50) \times 10^{14}\, M_\theta \gtrsim M_{clusters}$. In the case that $\Omega_o = 1$, $h_o \lesssim 2/3$ and $M_D \gtrsim 7 \times 10^{14}\, M_\theta$. Here's the problem. Except for the high end of the permitted range ($\Omega_\nu h_o^2 \sim 3/4$, $M_\nu \sim 75$ eV) structure is erased on all interesting scales ($M_D \gtrsim M_{cluster}$). Detailed numerical simulations of the development of structure in the neutrino dominated scenario confirm this indication of trouble[14]. It seems that the large scale structure requires $\Omega_\nu h_o^2 \gtrsim 1$ whereas the age constraint on the density demands $\Omega_\nu h_o \lesssim 3/4$. The scenario of a Universe dominated by relatively light, relic neutrinos is in trouble!

"Heavy" Relic Neutrinos

If some species of neutrinos has a mass in excess of ~ 10 MeV, our previous discussion must be modified. Such neutrinos will become nonrelativistic while still in equilibrium and, for $T < M_\nu$, $n_\nu/n_\gamma \propto \exp(-M_\nu/T) << 1$. The freeze-out abundance of relic neutrinos is now quite small (see Lee and Weinberg[6] and Dicus, Kolb and Teplitz[6]; also ref. 13).

$$n_\nu/n_N \simeq 60\, M_\nu^{-3}(10/n_{10}) > 60\, M_\nu^{-3}. \tag{10}$$

In (10), and subsequently in this section, M_ν is measured in GeV. The ratio of neutrino to nucleon mass densities is therefore,

$$\Omega_\nu/\Omega_N \simeq 70\, M_\nu^{-2}(10/n_{10}) > 70\, M_\nu^{-2}. \tag{11}$$

In units of the critical mass density, the mass density contributed by heavy relic neutrinos is,

$$\Omega_\nu \simeq 2.4\, h_o^{-2}\, [M_\nu(\mathrm{GeV})]^{-2}. \tag{12}$$

In this case ($M_\nu > 10$ MeV), neutrinos with $M_\nu < 8$ GeV will dominate the total mass density; much heavier, stable neutrinos will play no significant cosmological role. As before, the age constraint requires that $\Omega_\nu h_o^2 < 1/4 - 3/4$ so that, for stable relic heavy neutrinos, $M_\nu > 2$–3 GeV. Lighter neutrinos must be unstable.

Heavy relic neutrinos have a very small damping scale and will cluster on very small scales (<< galaxy). To avoid too much dark mass on small scales requires a lower bound to M_ν. If, for example, dissipation has not played a significant role in the formation of elliptical galaxies or some small groups of galaxies[15] then, $M_\nu < M_{Dark} < 3\, M_{Lum} < 3\, M_N$, so that $\Omega_\nu < 3\, \Omega_N$ and $M_\nu > 5$ GeV.

Before summarizing the constraints on stable, massive neutrinos and the problems facing the "standard" neutrino dominated scenario, let us make a brief digression to consider the important role played by light neutrinos during the epoch of primordial nucleosynthesis.

Nucleosynthesis and N_ν

Shvartsman[16] originally noted that since the amount of helium-4 produced in big bang nucleosynthesis increases with increasing energy density, primordial nucleosynthesis can be used to limit the total density at early epochs. At nucleosynthesis the total density is given by equation (2) so that a limit for ρ_{TOT} corresponds to a constraint on N_ν[17]. In fact, N_ν in equation (2) really accounts for <u>all</u> particles which are relativistic at the time of nucleosynthesis (M < few MeV).

$$N_\nu = \sum_F{}' (g_F/2)(T_F/T_\nu)^4 + 8/7 \sum_B{}' (g_B/2)(T_B/T_\nu)^4. \qquad (13)$$

In (13), F(B) are all relativistic fermions (bosons) with statistical weight g_F (g_B) and temperature T_F (T_B). For those particles which have frozen-out earlier than the neutrinos, $T_{F,B} \leq T_\nu$. The prime on the sums in (13) indicate that photons and $e^\pm$ pairs are omitted.

The ^{4}He abundance depends on N_ν, on the neutron half-life $\tau_{1/2}$ and, weakly on the nucleon abundance η[9]. For $N_\nu = 3 \pm 1$, $\tau_{1/2} = 10.6 \pm 0.2$ min and $1 < \eta_{10} < 10$, the ^{4}He abundance by mass, Y, is well fit by [18]

$$Y = 0.227 + 0.011 \ln\eta_{10} + 0.013 (N_\nu - 3) + 0.015 (\tau_{1/2} - 10.4). \qquad (14)$$

From the observed abundances of deuterium and helium-3 we are led to a lower limit to the nucleon abundance[9] $\eta_{10} > 3$-4 (if η were smaller, D and ^{3}He would be overproduced). For $\eta_{10} > 3$ and $\tau_{1/2} > 10.4$ min.,

$$Y \geq 0.239 + 0.013 (N_\nu - 3). \qquad (15)$$

It is difficult, given the observational data at present, to infer an accurate value of the primordial abundance of ^4He[19]. Currently, the best estimates suggest[19]: $Y_p = 0.24 \pm 0.01$ and $Y_p < 0.25$. From equation (15) and this upper limit to Y_p we are led to: $N_\nu < 4$. At <u>most</u> there could be one more family of neutrinos This limit to the number of lepton families is complementary to that obtained from the width of the Z° boson[18]. The Z° width counts all particles with $M < M_Z/2$ which couple directly to the Z°; nucleosynthesis counts all particles with M < few MeV, regardless of their couplings.

Problems With The Standard Scenario

We have seen that relic neutrinos will dominate the universal mass density if the sum of all neutrino masses lies in the range of a few eV to a few GeV. That is, for 3 eV < M_ν < 8 GeV, $\Omega_\nu > \Omega_N$. Neutrinos with masses in most of this range must be unstable lest they contribute too much density at present. For example, if M_ν > 25–75 eV, $\Omega_\nu h_o^2 > 1/4 - 3/4$ and the Universe would be too young; for $M_\nu < 5$ GeV, $\Omega_\nu > 3\ \Omega_N$ and there would be too much dark mass in the Universe. Heavy, stable neutrinos with masses in the narrow window of ~ 5–8 GeV may be allowed by cosmology, but they are uninteresting. For light, stable neutrinos in the allowed range of a few eV to 25–75 eV, detailed modeling of the neutrino dominated scenario suggests problems[14]. The following dilemma is at the root of the difficulties.

Perturbations on a scale ~ $5h_o^{-1}$ Mpc are entering the nonlinear regime today[20]. In the neutrino dominated scenario, such scales would have been damped by free streaming unless the neutrino is sufficiently massive: $M_\nu > 250\ h_o$ eV. For such massive neutrinos, $\Omega_\nu h_o^2 > 2.5\ h_o$ and, even for h_o as low as 0.4, $\Omega_\nu h_o^2$ exceeds unity and the Universe is too young. Alternately, neutrinos with masses in the allowed range (< 25–75 eV) damp perturbations on scales which are too large (> 16–50 Mpc).

To summarize, relic neutrinos with masses of several tens of eV could account for the dark mass inferred from large scale dynamics. However, such neutrinos will free stream during the earlier evolution of the Universe, damping perturbations required for the observed large scale structure of the Universe. The standard neutrino scenario seems terminally ill.

A Speculative Scenario

The density parameter Ω, the ratio of the total density to the critical density is epoch dependent. For spatially open models which expand forever, $\Omega \to 0$ as $t \to \infty$. For spatially closed models which ultimately collapse, $\Omega \to \infty$ as the maximum expansion is approached. Since the present value of Ω is observed to be within an order of magnitude of unity, it is "natural" to assume that $\Omega_0 = 1$[21]. $\Omega_0 = 1$ is predicted by the inflationary models[22]. As compelling as these hints are, there is a problem. Studies of the large scale dynamics on scales up to several tens of Mpc find $\Omega_0 = 0.2 \pm 0.1$[23]. If, indeed, Ω_0 is unity, there are at least two possibilities. Perhaps the visible galaxies are poor tracers of the total mass; perhaps we are only seeing the tip of the iceberg. The other possibility is that the dominant contribution to the total mass density is more smoothly distributed than the observed galaxies. If extremely relativistic (ER) particles dominate the present mass density then, by virtue of their high speeds they will be smoothly distributed on all scales up to the present horizon and it will be possible to have $\Omega_0 = \Omega_{NR} + \Omega_{ER} = 1$.

Recently, M. S. Turner, L. M. Krauss and the author[12] have proposed that the Universe is dominated by the relativistic decay products of a heavy relic particle - perhaps a heavy neutrino. Although more general scenarios are possible[12] let us here restrict our attention to the case where the nonrelativistic (NR) component is ordinary nucleons (N) and the heavy,

decaying particle (X) is to be identified with a heavy neutrino. In a majoran[24] or familon[25] model the heavy neutrino will decay at an epoch whose redshift is z_d to a light neutrino plus a neutral, massless Nambu-Goldstone boson. In the following, we use X to denote the heavy neutrino as well as its decay products.

The nucleon density evolves with redshift (z) as

$$\rho_N \simeq 10^4\, \Omega_N h_o^2 (1+z)^3 \text{ eV cm}^{-3}. \tag{16}$$

After X-decay, $z < z_d$, while the decay products are ER,

$$\rho_X \simeq 10^4\, \Omega_X h_o^2\, (1+z)^4 \text{ eV cm}^{-3}, \tag{17}$$

where $\Omega_N + \Omega_X = 1$. Before X-decay, $z > z_d$, the massive Xs are NR and,

$$\rho_X \simeq 10^4\, \Omega_X h_o^2\, (1+z_d)(1+z)^3, \tag{18a}$$

$$\rho_X = M_X n_X = M_X n_X n_\gamma. \tag{18b}$$

For X= ν, the X abundance is $n_X = n_\nu = 3/11$. From (18a and b) we find

$$M_X(\text{eV}) = 26 \Omega_X h_o^2 n_X^{-1} (2.7\text{K}/T_{\gamma o})^3 (1+z_d). \tag{19}$$

For $\Omega_X h_o^2 < 1/4$ (see below), $M_X(\text{eV}) < 24(1+z_d)$. Note that the present momenta of the decay products is < 12 eV/c so that the lighter neutrino should be less massive than ~10eV.

Such a scenario has several assets. Firstly, we have arranged the numbers to satisfy our prejudice that $\Omega_o = 1$. Being relativistic today, the dominant matter ($\Omega_X > 0.8$, $\Omega_N < 0.2$) is distributed smoothly. This allows for $\Omega_o = 1$ even though for the clumped (i.e.: NR) matter, $\Omega_{dyn} \simeq 0.2$. Our scenario, in addition, "improves" the "standard" neutrino scenario. Recall that the standard neutrino model required a "high" mass to make the damping scale sufficiently small but, a "low" mass to be in accord with constraints on

the total mass density. Here, we have our cake and eat it too! The early evolution of our model ($z>z_d$) is dominated by the mass of the heavy neutrino (eq. 19) so that the damping scale is

$$M_{DX} \simeq 3 \times 10^{14} M_\odot \, (4/1+z_d)^2. \tag{20}$$

This may be in accord with the observed large scale structure if $z_d>3$.

In our model, perturbations in the linear regime will grow from the epoch, z_{eq}, of X domination to z_d. The total growth factor is

$$\gamma = (1+z_{eq})/(1+z_d) \simeq 7 \times 10^3 (h_o/\tfrac{1}{2})^2 \, (2.7K/T_{\gamma_o})^4. \tag{21}$$

All mass scales which enter the horizon up to z_{eq} will experience adequate growth. The mass--in nucleons--within the horizon at z_{eq} is

$$M^{eq}_{N,H} \simeq 3 \times 10^{14} M_\odot (10/1+z_d)^3. \tag{22}$$

The observed large scale structure suggests $1+z_d<10$.

The decaying neutrino scenario with $3<z_d<9$ ($M_\nu \simeq 100$–240eV) offers several advantages vis-a-vis galaxy formation over the stable neutrino scenario. Indeed, as White, Frenk and Davis[14] showed, to account for the observed large scale structure in the standard neutrino model requires $h_o \simeq 2.5 \, \Omega_o^{-1}$, which, for $\Omega_o<1$, is excluded. In our model, if for the moment we neglect the effect on the large scale structure of the X decays, $\Omega_o \rightarrow$ " Ω " $\simeq \Omega_N + \Omega_X(1+z_d)$. For $h_o<1/2$ (see below) and $\Omega_N \lesssim 0.2$, $z_d > 4$–5 may resolve this difficulty.

Along with its attractive assets, the decaying neutrino scenario is burdened with significant liabilities. The most serious threat to our model is the age problem. In our scenario, the Universe is radiation dominated (RD) today. A radiation dominated Universe expands faster and is younger than a matter dominated Universe. For $\Omega_o=1$, a RD Universe is half the Hubble age.

$$t_o = 1/2H_o^{-1} \simeq 5 h_o^{-1} \times 10^9 \text{yr}. \tag{23}$$

Since our model is only partially RD ($\Omega_N \simeq 0.05$–0.2), $t_0 H_0 \simeq 0.51$–0.57. In any case, since the ages of the oldest stars exceeds 10 billion years, our model fails unless $h_0 < 1/2$; this possibility is not excluded.[26)]

In our model, bound systems of Xs and nucleons have formed by $z_{GF} > z_d$. When the Xs decay do these systems unbind? On scales from galaxies up to, perhaps, clusters, the nucleons would have dissipated during the initial collapse. Such scales may be nucleon dominated before X decay and therefore will not unbind. Even initially X-dominated scales may not fly apart when the Xs decay. If the dynamical timescale is short compared to the decay time, the systems may "puff up" adiabatically. For $t_{dyn} \sim 10^8$–10^9 yr., this requires $1+z_d < 3$–10.

In summary, the decaying neutrino scenario permits $\Omega_0 = 1$, explains why $\Omega_{obs} \simeq 0.2$ and provides a better account for the observed large scale structure than the standard, stable neutrino scenario. However, when the heavy ($M_\nu \sim 100$–250 eV) neutrino decays, bound systems may fly apart. Also, the resulting RD Universe expands rapidly and is young today. Do the assets cover the liabilities? The bottom line awaits more detailed calculations and more accurate observational data.

Acknowledgements

Much of the work described here has been published elsewhere and I am indebted to numberous colleagues and collaborators from whom I've learned so much. Dave Schramm and Mike Turner must be singled out for special thanks. This research is supported at Bartol by DOE grant DE-AC02-78ER-05007.

References

1) S.S. Gershtein and Ya. B. Zeldovich, JETP Lett. 4, 120 (1966).
2) R. Cowsik and J. McClelland, Phys. Rev. Lett. 29, 669 (1972); Ap. J. 180, 7 (1973).
3) G. Marx and A.S. Szalay, Proc. Neutrino '72, Vol. I, 123 (1972); A.S. Szalay and G. Marx, Astron. and Astrophys. 49, 437 (1976).
4) F. Zwicky, Helv. Phys. Acta 6, 110 (1933).
5) S.M. Faber and J.S. Gallagher, Ann. Rev. Astron. and Astrophys. 17, 135 (1979).
6) B.W. Lee and S. Weinberg, Phys. Rev. Lett. 39, 165 (1977); D.A. Dicus, E.W. Kolb, and. V. Teplitz, Phys. Rev. Lett. 39, 168 (1977); J.E. Gunn, B.W. Lee, I. Lerche, D.N. Schramm and G. Steigman, Ap. J. 223, 1015 (1978); G. Steigman, C.L. Sarazin, H. Quintana and J. Faulkner, Astron. J. 83, 1050 (1978).
7) S. Tremaine and J.E. Gunn, Phys. Rev. Lett 42, 407 (1979).
8) D.N. Schramm and G. Steigman, GRG 13, 101 (1981); Ap. J. 243, 1 (1981).
9) J. Yang, D.N. Schramm, G. Steigman and R.T. Rood, Ap. J. 227, 697, (1979); K.A. Olive, D.N. Schramm, G. Steigman, M.S. Turner and J. Yang, Ap. J. 246, 547 (1981); J. Yang, M.S. Turner, G. Steigman, D.N. Schramm and K.A. Olive, Ap. J. (In Press June 1984).
10) J.R. Bond, G. Efstathiou and J. Silk, Phys. Rev. Lett. 45, (1980); I. Wasserman, Ap. J. 248, 1 (1981).
11) M.S. Turner, Proc. Neutrino '81, Vol. I, 95 (1981, R. J. Cence, E. Ma and A. Roberts eds.).
12) M.S. Turner, G. Steigman and L.M. Krauss, Phys Rev. Lett., In Press (1984).
13) G. Steigman, Ann. Rev. Nucl. Part. Sci. 29, 313 (1979).
14) S. White, C. Frenk and M. Davis, Ap. J. (Lett.) 274, L1 (1983).
15) P. N. Appleton and R. D. Davies and in Int. Kin. & Dyn. of Gals. (IAU Symp. No. 190, E. Athanassoula ed.) p. 95 (1982).
16) V.F. Shvartsman, JETP Lett. 9, 184 (1969).
17) G. Steigman, D.N. Schramm and J.E. Gunn, Phys. Lett. 66B, 202 (1977).
18) D.N. Schramm and G. Steigman, Phys. Lett., In Press (1984).
19) G. Steigman, Bartol Preprint BA-84-1 (To appear in the Proceedings of the Yerkes Workshop on Nucleosynthesis) (W.D. Arnett and J.W. Truran eds).
20) M. Davis and P.J.E. Peebles, Ap. J. 267, 465 (1983).
21) R.H. Dicke and P.J.E. Peebles in General Relativity: An Einstein Centenary Survey. (S.W. Hawking and W. Israel eds; Cambridge Univ. Press, Cambridge 1979).
22) A.H. Guth, Phys. Rev. D23, 347 (1981).
23) Ref. 5; W. Press and M. Davis, Ap. J. 259, 449 (1982); M. Aaronson, J. Huchra, J. Mould, P.L. Schechter and R.B. Tully, Ap. J. 258, 64 (1982); M. Davis and P.J.E. Peebles, Ann. Rev. Astron. and Astrophys. 21, 109 (1983).
24) Y. Chikashige, R. Mohapatra and R. Peccei, Phys. Rev. Lett. 45, 1926 (1980).
25) F. Wilczek, Phys. Rev. Lett. 49, 1549 (1982); D. Reiss, Phys. Lett. 115B, 217 (1982).
26) A. Sandage and G.A. Tammann, Ap. J. 256, 339 (1982); Proceedings of the CERN/ESO Meeting On Particle Physics and Cosmology (1984).

A POSSIBLE SOLAR NEUTRINO DETECTOR BASED ON INDIUM NEUTRINO REACTION AND USING WELL KNOWN TECHNIQUES

M. SPIRO
Département de Physique des Particules Elémentaires, CEN-Saclay,
91191 Gif-sur-Yvette Cedex, France.

ABSTRACT

The interest for using Indium as a target for solar neutrino is stressed again. A possible solar neutrino detector using well known techniques (liquid scintillator and multiwire chambers) is described. It would be a large size heavy detector but it appears feasible and modular.

In 1976, Raghavan [1] suggested that Indium might be the most suitable target for a solar neutrino detector, and tried to design a possible detector on ν_eIn reaction [2], [3].

In my talk I want first to show you that Indium is still very attractive for solar neutrino detection and second that it might be possible nowadays to design a modular detector based on very well known standard techniques. Such a detector however will be very heavy at full scale.

There is a working group at Saclay [4]. Other solutions are also being studied, which are listed at the end.

SOLAR NEUTRINO DETECTION

Three main nuclear reactions [5] in the sun are neutrino sources:

Nuclear reaction	ν_e flux on earth ($cm^{-2} sec^{-1}$)	ν_e energy range
(1) $pp \rightarrow de + e^+ + \nu_e$	6×10^{10}	100 ÷ 420 keV
(2) $^7Be + e^- \rightarrow {}^7Li + \nu_e$	4.3×10^9	861 keV (monoenergetic)
(3) $^8B \rightarrow {}^8Be + e^+ + \nu_e$	5.6×10^6	5 ÷ 14 MeV

Other reactions contribute to the ν_e flux but with a much lower rate in their particular own ν_e energy range. At this stage it must be stressed that the ν_e flux from reaction (1) is almost model independent (< 10% uncertainty) while the ν_e flux from reaction (3) which depends on the amount of ^8B in the sun is sensitive to the whole stellar nuclear reaction chain leading to ^8B production and can then vary by a factor 2 according to the sun stellar model.

Up to now the only experiment which recorded solar neutrino events [6] is the R. Davis experiment based on transmutation of ^{37}Cl into ^{37}Ar. However this reaction has a high threshold which makes it only sensitive to the ν_e flux from reaction (3).

The experiment found 3 times a lower flux than expected in the sun standard model. This discrepancy can be attributed either to neutrino oscillations based on 3 neutrino species or to wrong predictions from the sun standard model. A detector sensitive to all 3 reactions and allowing to separate the 3 kind of sources will be able to disentangle the puzzle. If a constant discrepancy factor for the 3 kind of fluxes is found then neutrino

oscillations would be the only known possible explanation for the present time. If the discrepancy only remains for the ν_e flux from reaction (3) it is then most likely to be due to solar nuclear reactions leading to ^8B production [7]. So, by measuring solar neutrino fluxes from each of the 3 nuclear reactions, one provides with informations of considerable interest for both astrophysics and elementary particle physics :

- for astrophysics it is a very powerful way to study the interior of the sun.
- for elementary particle physics an experiment with solar neutrinos will be extremely sensitive to neutrino oscillations due to the enormous distance between the sun and the earth and the low energy of these neutrinos. It will be possible to test mass differences of the order of 10^{-6} eV.

The idea of using Indium for detecting solar neutrinos from the proton proton primary reaction in the sun has been suggested since a long time by R.S. Raghavan [1]. The basic reaction is the β inverse decay of ^{115}In to the 614 keV excited state of Sn :

$$\nu_e + In \rightarrow Sn^{**}(7/2^+) + e^- \qquad (4)$$

This reaction (4) has a threshold of 120 keV so that :

$$E_e \simeq E_\nu - 120 \text{ keV}$$

The electron energy spectrum obtained from folding the solar neutrino spectrum with the cross sections of reaction (1), (2) and (3) is given in fig.1. Such a ν_e In reaction is then mostly sensitive to reaction (1) and (2) and will then give information complementary to the Davis experiment.

Reaction (4) is followed by a double desexcitation of Sn^{**}

$$Sn^{**}(7/2^+) \rightarrow \gamma\,(100 \text{ keV}) + Sn^{*}(3/2^+) \qquad (5)$$
$$Sn^{*}(3/2^+) \rightarrow \gamma\,(500 \text{ keV}) + Sn(1/2^+) \qquad (6)$$

The half life time of $Sn^{**}(7/2^+)$ is 3.26 μs. The life time of $Sn^{*}(3/2^+)$ is less than 10^{-10} sec.

In reaction (5) the photon internal conversion probability is $\simeq$ 50 % .

The delayed concidence signature will be the only way to remove the background coming from Indium radioactivity :

$$^{115}In \rightarrow {}^{115}Sn + e^- + \overline{\nu_e} \qquad (7)$$

The half life of ^{115}In is $5x10^{14}$ years. The maximum energy of the electron is 490 keV. It is clear that unless great care is taken the accidental coincidence rates could make the experiment unfeasible. These features have been discussed in great details by R.S. Raghavan and by Booth [2], [3], [8].

THE DETECTOR

Although all parameters have to be optimized, we present here a tentative description of what could be one possible solar neutrino Indium detector.

It is based (fig.2) on a stack of 1 m^2 multiwire proportional chamber with 3 mm gap and with common cathodes made of 5 μm mylar on which are deposited on both sides 5 μm thick Indium strips, 2 or 3 mm wide. 340 chambers are stacked in that way (2 m long stack) providing with an elementary cell of 25 kg of Indium. The read out of the coordinates is arranged to provide separately x, y and z coordinates which means that all same x wires or strips (< 500) are "ored" and in the same way that all same y and all same z are "ored". This leads to $\simeq$ 1000 electronic channel read out.

Ten cm's MWPC stacks will have to be interleaved with 10 cm thick tank of liquid scintillator to allow for the 500 keV γ detection from reaction (7) (Sn^* deexcitation). This corresponds to 2 tons of scintillator and will bring the volume of an elementary cell to 4 m^3.

PERFORMANCES

Event identification

By using only photon internal conversion in reaction (1) to identify an event, two tracks must be seen in a gate of 10 μsec, coming from the same Indium source point. The Indium source point can be located within 1 mm^3. Furthermore in coincidence with the second electron (photon internal conversion) there should be a pulse in the photomultipliers coming from the 500 keV γ (or another track in the chamber far away from the 2 coincident tracks).

Resolution on the energy of the incident ν_e is poor but should allow separation between reaction (1) and (2). Monte-Carlo is under way.

Efficiency

The efficiency for Indium radioactivity β^- detection is $\simeq$ .8.

The efficiency to solar ν_e In reaction detection has been calculated by taking into account :

- probability of photon internal conversion in reaction (6) : .45
- probability that both electrons from the ν_e reaction and from the photon internal conversion traverse a gap : .66
- probability of detecting the 500 γ from reaction (7) : .8
- dead time after reaction (4) : .90

This leads to .0015 event per day for an elementary cell of 4 m^3, 2 tons of scintillator and 25 kg of Indium.

Background

The number of "events" made of 2 accidental radioactivities at the same location (1 mm^3 of Indium) within 10 μsec is 3. per day for an elementary cell.

Additional rejection comes from the requirement of an extra γ in coincidence with the second electron to be observed, which means that in order to fake a ν_e event a third radioactivity should take place in coincidence ($\simeq$ 100 nsec) with the second one, or what is more likely, the second radioactivity β^- has to produce a bremstrahlung γ of energy > 200 keV. This probability plus the reduced efficiency for detecting the second β^- which has produced a bremstrahlung γ gives an additional factor of 10000 to 50000 depending on the energy resolution of the scintillator plus light collection system [2].

This leads to a signal/noise ratio of 5 to 25. However at this stage a lot of further studies and optimizations are needed to estimate this ratio.

CONCLUSION

The detector we describe offers a powerful background rejection and uses only well known techniques. It appears feasible. However the main drawbacks are the modest efficiency (.21) which induces a need of 2.5 tons of Indium to get .15 event per day, the big corresponding amount of scintillator ($\simeq$ 200 tons) and the corresponding overall size of the detector (400 to 800) m^3). Nevertheless it seems to us that such a possibility could be seriously worked out. Specially an attracting feature in that spirit is the modularity of the detector.

Other much more compact techniques are being also investigated at Saclay. Two of them may be promissing :

- Low pressure chambers with BaF^2 + Indium, U.V. scintillator windows.

- Solid chemical Indium compound window with good mobility and long absorption lengths (few mm's) for ionization electrons coupled to multiwire proportional chambers.

These two possibilities are at the stage of feasibility studies at the present time.

Aurouet, Blumenfeld, Michau, Micolon, Soirat, Thevenin are also involved in one part or another of the studies.

REFERENCES

[1] R.S. Raghavan, Phys. Rev. Letters 37 (1976) 259
[2] R.S. Raghavan, Brookhaven Solar Neutrino Conference, 1978
[3] R.S. Raghavan, Hawaii Neutrino Conference, "Neutrino 81" Vol.I, p.27
[4] M. Bourdinaud, G. Chardin, M. Cribier, R. Hubbard, P. Mangeot, B. Pichard, J. Rich and M. Spiro
[5] Bahcall et al., review of Modern Physics 54 n°3 (1982) 8
[6] R. Davis Jr. et al., Proc. of the Purdue Conf. "Neutrinos-78" (ed. by E.C. Fowler), p.53
[7] E. Schatzmann, private communication
[8] - N. Booth, Oxford preprint.

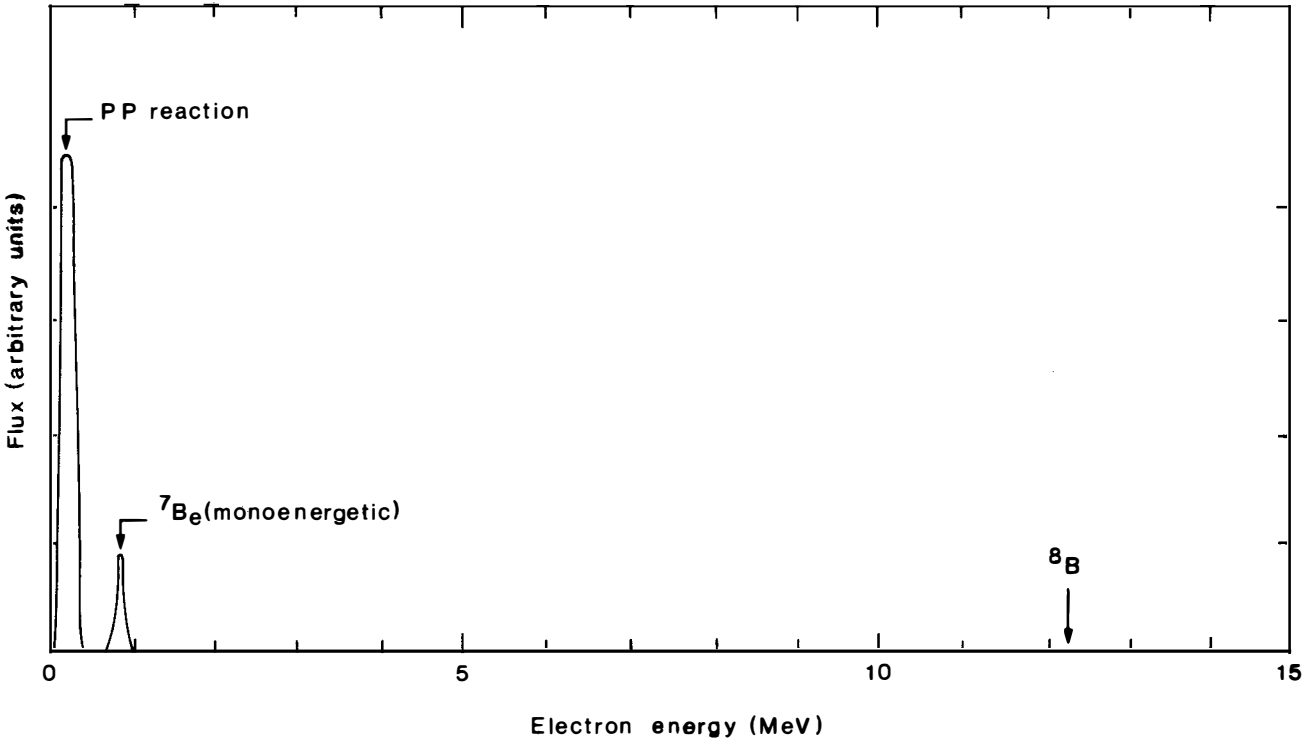
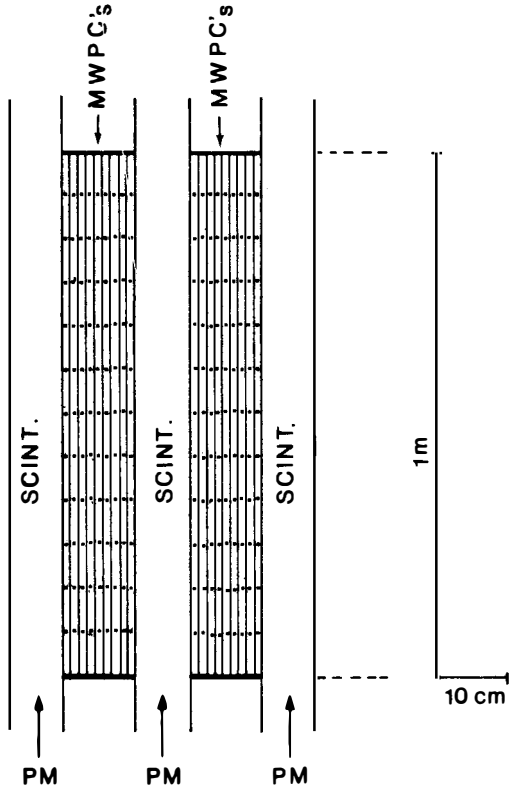


Fig.1 - Expected electron energy spectrum induced by solar neutrinos.



MWPC': 1 m^2

Cathode : 5 μ mylar + 5 μ In strips on both sides

Cathode to cathode : 6 mm

Fig.2 - Sketch of the basic elements in the detector.

DETECTION OF LOW ENERGY SOLAR NEUTRINOS BY CHAMBERS OF METASTABLE SUPERCONDUCTING GRANULES

G. WAYSAND
Groupe de Physique des Solides de l'Ecole Normale Supérieure
Tour 23 - Université Paris VII - 75251 PARIS Cedex 5 - France

ABSTRACT :

A brief reminder about solar neutrino detection is presented in order to stress the necessity of low-energy and real-time solar neutrino detection. It is shown, in section 2, that two independent possible solutions exist for that purpose. Both of them are using as target and detectors large volumes of metastable superconducting granules. These solutions are :
a) the inverse β decay reaction of neutrinos with indium.
b) the detection of the recoil energy of a nuclei of the granule under the impact of a neutrino (coherent scattering discussed hereafter by Stodolsky).

In the Indium case, the energy threshold is 128 keV, in the coherent scattering it can, in principle, be lower than the 420 keV corresponding to the maximum energy of the neutrino produced by the proton-proton reaction.

In section 3, with the indium solution in mind the basic properties of metastable superconducting granules are presented and in 4, the sketch of a potential small scale detector is presented.

* the reader of this paper is also invited to look at the communication of L. Gonzales Mestres and D. Perret-Gallix in these proceedings about the detection of magnetic monopole with superconducting granules but of larger size ($\phi \sim 30\mu$).

I. BRIEF SURVEY OF THE SOLAR NEUTRINOS

The proton-proton chain reaction in the sun is represented on Fig. 1 where the reactions which are producing neutrinos are framed. Near by each of these frames, the energy spectrum of the produced neutrinos is handwritten.

Once emitted, these neutrinos can reach the earth. Figure 2 represents the results of the well-known Bahcall evaluation for each of these neutrinos emitting reactions. The important point is that the neutrinos coming from the proton-proton reactions are much more abundant than all the others.

Unfortunately, the only existing experiment does not detect them. This experiment of Davies relies on the property of Cl^{37} (which represents 25 % of the natural chloride) to capture a neutrino. In this reaction, Cl^{37} is transformed in Ar^{37} which is detected by the electron emitted when it desexcites. The energy threshold of this reaction is 814 keV, far above the maximum energy of 420 keV of a neutrino coming from a proton-proton reaction. Looking at Fig. 2, one can see that, with such an energy threshold, the Davies experiment is sensitive only to neutrinos produced in the B^8 decomposition. These neutrinos are only 10^{-4} of the neutrino flux at the surface of the earth. In the running device, the chloride is combined with carbon and there is about 10^{30} chloride atoms in 615 tons of C_2Cl_4 at 1600 meters underground. Between two and three Argon atoms are obtained per week. It is four times less than predicted by the standard model of the sun.

If one admits the experimental findings, the discrepancy with theoretical predictions can be assigned to one of the terms of the following alternative :
- either the standard model of the sun is incorrect and, for example, turbulence must be taken into account (see Schatzman's paper in these proceedings) ;
- or neutrinos oscillations are responsible of the small value of the observed neutrino flux. If this is true, not only a lower energy threshold of detection is necessary but also a real-time signal must be obtained (to study the variation of the neutrino flux with the earth-sun distance), the gallium experiment where Ga^{71} is transformed in Ge^{71} has a lower threshold : 236 keV but not the real time read-out which can only be obtained by the Indium experiment. In addition to real time read-out, the indium reaction provides also a lower energy threshold : 128 keV.

II. TWO REAL-TIME METHODS FOR SOLAR NEUTRINOS DETECTION

2.1. Inverse β-decay of In 115

This reaction was proposed by R.S. RAGHAVAN.

$$^{115}In + \nu \rightarrow {}^{115}Sn + e^- \xrightarrow{3.26\mu s} e_1 + \gamma_2$$

All over the range of atomic masses from 111 to 131, one observes a β decay from the $9/2^+$ state of the Indium isotopes to the $7/2^+$ state of In. At the lower atomic masses of this range, Sn is transformed in Indium, whereas at the high atomic masses, the reverse process occurs. At the atomic mass 115, the two levels are separated by only 128 keV ; the $9/2^+$ state is the stable of ^{115}In, whereas the $7/2^+$ state just above is an excited state of 115 Sn with a lifetime of 3.26 µsec. This reaction has a low energy threshold and offers a complete real time read out.
Therefore, the measure of the energy E_ν of the incoming neutrino becomes possible by the knowledge of e_ν, energy of the capture electron :

$$e_\nu = E_\nu - 128 \text{ keV}$$

The identification of the e_ν pulse is ensured by a triple delayed coïncidence :

$$e_\nu \xrightarrow{3.26\mu s} e_1 + \gamma_2$$

associated with a spatial localisation of e_ν and e_1.

If e_ν is used to start a clock and $e_1 + \gamma_2$ stops it. The spectrum of the time delay between these two events is exponential with a time constant of 3.26 µsec. In practice, this spectrum is above a continuous background caused by random coïncidences of events opening and closing the timing. Such an event can be a correct start by e_ν but followed by a 600 keV photon from the surrounding medium. This γ-ray simulates the $(e_1+\gamma_2)$ event by a Compton cascade and stops the clock. This is why the triple delayed coïncidence must be completed by the geometrical condition that all the events e_ν , e_1, γ_2 took place in the same elementary volume. The reduction of random events is in that case proportional to the achieved spatial resolution.

The Bell Labs-MIT collaboration has studied the classical detection solutions but all of them are voluminous and heavy : in this type of devices, the indium is a target. It must be divided and immersed in a detecting substance (specially, if one wants to detect the low energy electrons which have a very small mean free path. Therefore, the dilution of indium is large and the volume of the device must be large itself.

This difficulty disappears if the target is itself the detector. This is the case when indium is divided into microspheres in conditions where a metastable superconducting can exist. In such a situation, the target is the detector, higher filling factor can be reached.

2.2. Coherent diffusion of neutrinos

In this case, the target and the detector are also confused and a real time

is possible in principle. Since the problem is dealt extensively in another paper of this conference I will deal only with the immediate practical aspects of this proposal.

The basic argument is that, in spite of the weakness of the recoil energy of the neutrino, it is large enough to allow in the microsphere where the transition occurs, an energy release large enough for the nucleation of the phase transition from the metastable superheated state to the normal (resistive) state.

The average recoil energy of a nuclei of atomic mass A is :

$$\bar{E}_A = \frac{2}{3A} E_\gamma^2$$

and might provided to a 10μ sphere of diameter placed in a helium bath at 1.2°K a heating of a few 10^{-3}K. This process is not limited to solar neutrino and therefore is the principle for a neutral current detector. The cross section of the reaction is not so small because it varies with the square of the number N of neutrons in the nuclei of the target

$$\sigma = 0.42 \times 10^{-44} N^2 E_\nu^2 \qquad \text{(in cm}^2 \text{ if } E_\nu \text{ is in MeV)}$$

The dark side of this principle of detection is that the only caracteristic signature of the neutrino is that one and only one microsphere will change of state. The change of state of a single isolated granule can, as well, be induced by natural radioactivity of the device. The noise background can only be estimated on a detector of a size large enough.

For tin granules 4μ in diameter at 50 mK and for a heating of 10mK, it seems, according to experimental data that under a reactor of the Laue-Langevin type (ILL-Grenoble) with an average neutrino emission of 2,3 MeV one event per day will be detected by this method for 1,5 kg of tin (which represents a detector of one liter with of filling factor in volume of about 20 %).

III. METASTABLE SUPERCONDUCTING GRANULES

3.1. Generalities

Type I superconductors present a $T<T_c$, critical temperature of apparition of superconductivity, a first order transition in magnetic field. Therefore, metastable states can, by principle, by observed : supercooling and superheating. Supercooling is observed when the magnetic field in which the metal is immersed is decreased from values higher to $H_c(T)$, the thermodynamical critical magnetic field to zero. When the metal remains in the normal state, under $H_c(T)$ up to $H_{sc}(T)<H_c(T)$, we are in the supercooling regime, H_{sc} is the supercooling critical field. The condensation of electrons in Cooper pairs, responsible of the superconducting state

is delayed exactly like the vapour condensation can in the high mountains, be delayed even if the saturated value is overcome. The supercooled phase is easily observed even on a bulk metal. The reverse regime, superheating can be seen only if the metal is divided in small spheres without surface defects favorising the magnetic field penetration. This is because the main feature of type I superconductors is that they expel completely the magnetic field from their volume : they are perfectly diamagnetic. This is called also the Meissner effect. Therefore, if a sphere with good surface aspect is in a magnetic field increased from zero, it will remain superconducting above $H_c(T)$ until a field $\frac{2}{3} H_{SH}(T)$ is reached when the metastability is broken. (The demagnetization factor of a sphere is 3/2, this is why only 2/3 H_{SH} can be reached in the superheated regime).

With the actual mode of fabrication of granules, the superheating is easily observed for sphere under 35 μ in diameter down to a submicron diameter (a few 1000Å at 1°K) when the first order transition disappears because the sphere diameter is of the order of the penetration depth of the magnetic field at the surface of the sphere. The supercooling state is used for particle detection because a small amount of energy deposition triggers the apparition of the normal state.

3.2. Observation of the change of state :

In spite of the zero resistivity of the superconducting state, the resistance measurements cannot be used for the observation of the phase transition because the presence of electrical contacts will favorise the penetration of the magnetic field and the superheated regime will not exist. Therefore, one uses the disparition of the Meissner effect for the observation of the change of state : at the output of an inductance of width L surrounding a granule of radius R, a flux variation will appear at the change of state : $\Delta\phi = \pi \frac{R^3}{L} H$ where H is the applied field. The penetration time Δt of the magnetic field in the granule is short, thus the voltage $\frac{\Delta\phi}{\Delta t}$ is detectable. A superconducting granule is a monostable system, it will be active again only if, for a short time (10^{-6}sec) the magnetic field is lowered under H_{SC}.

A correct first glance at superheated superconducting granules is to consider them as similar to other well-known detectors of high energy physics based on metastability : bubble chambers, emulsions... but with the possibility of a real time electronic read-out of the breakdown of the metastable state. One can "read" in a volume where a grain has changed of state. Also, with some care, one can get an information about the energy release in the granule but before to evaluate the energy threshold, we must examine the diamagnetic interactions between granules.

3.3. Diamagnetic interactions between granules

Because supercooling and superheating are metastable states, the flux variation due

to their disparition is a delta function and the hysterisis cycle in magnetic field of a single isolated granules is rectangular. However, for detecting purpose, large volumes and high filling factors in granules are necessary. If one thinks that for a filling factor of 10 % in volume, the average distance between granules is of the order of their diameter, it is easy to realize that the expulsion of the magnetic field from these granules creates large distorsion of the applied external field. Each granule can be replaced by a magnetic dipole interacting whith the other. It turns out that the equatorial fields of the granules in a volume are distributed from around $2/3\ H_C$ to $2/3\ H_{SH}$. The superheated branch of a collection of granules is a S shaped curve. Therefore, for a given applied field, there is a distribution of equatorial fields. In such a situation, one can only obtain average information on energy threshold because in a (H,T) phase diagram the representative zone of the system at a temperature T is not a point but a segment of straight line T = constant parallel to the H axis.

Another effect due to diamagnetic interactions is that two granules in contact are no more metastable if the contact zone favorises the magnetic field penetration. In other terms, percolating granules are not metastables. This is reflected by the variation of the number of superheated granules as a function of the filling factor of a constant volume. Experimental results shows that up to 20 % this number is proportional to the filling factor but, above which it saturates around 26 %.

3.4. Energy threshold of the superheated state in a spherical granule

When the change of state happens, a heterogeneous nucleation of the normal state occurs by partial heating of the granule. The dynamic of the change of state depends on :

a) the thermal diffusion of the initial heating caused by the incident particle. Its coefficient is $D_T = \frac{K}{C_p}$ where K is the thermal conductivity and C_p the specific heat, both at the normal state.

b) the propagation of the normal state which is not theoretically known but experimental results showed that it is reasonable to estimate it to be of the order of magnitude of D_S which is the speed of diffusion of the superconducting state :

$$D_S = \frac{\xi^2(T)}{2\tau_S} = \frac{8\xi_0\ kT_C}{1{,}83\ n}$$

where ξ is the coherence length of the Cooper pair, ξ_0 is its value at 0°K, τ_S is the Cooper pair lifetime.

c) the speed of penetration of the magnetic field which is determined by the decay time of the eddy currents opposing the penetration of H. Pure metals like type I superconductors having a low resistivity, the decay time is always longer than the

propagation of the normal state and the thermal diffusion. Therefore, the change of state is controlled by these two last phenomena. Let us take a temperature of 2°K, then we have the following table for D_T and D_S of the main type I superconductors :

	D_T cm²/s	D_s cm²/s
Sn	3×10^4	360
In	2.7×10^3	250
Hg	200	300

In the case of Indium and Tin, heat propagates faster than the normal state. This is an argument for a simple model where the normal zone is isothermal. This simplistic picture does not allow the detailed description of the change of state but will allow a crude evaluation of the energy threshold of the superheated state. Let us admit also in a very crude manner that the change of state will happen only if the normal zone reach at least one point of the equation. Indeed, in other terms, the particle has to heat only a fraction of the granule, from the external magnetic field can provide additional energy because eddy current will start to heat the granule. This will help the change of state of that part of the granule which remains superconducting. In the case where the energy deposited by the particle is localized in one "point" (a volume comparable to ξ^3, ξ is the coherence length, we have $\xi \ll R$), the average partial volume, turns out to be $2/3\ \pi R^3$. If $\int_o^\ell \frac{\partial E}{\partial r}\, dr$ is the energy deposited by the particle, the average normal zone has a temperature increased by :

$$\Delta T = \frac{\int_o^\ell \frac{\partial E}{\partial r}\, dr}{2/3\ \pi R^3 C_p}$$

and reaches $T+\Delta T$ where the superheated critical field $H_{SH}(T)$ is decreased down to :

$$H_{SH} + \frac{\partial H_{SH}}{\partial T}\ \Delta T$$

If this new value of H_{SH} is lower than the applied field at the equator, the change of state will happen. Thus, for a given irradiation at a given field, H there is a maximum field H_m such as $H_c<H_m<H_{SH}$ above which it is not possible for any granule in the detecting volume to change of state. H_m is given by :

$$\Delta H = H_m - H = \frac{\partial H_{SH}}{\partial T}\ \Delta T$$

It is this quantity that we can observe and not ΔT. After a time of irradiation, long enough for all the granules of a collection to flip to the normal state, the

field which was kept constant during the irradiation is increased.

At the beginning, nothing happens, because of the granules immediately above the applied field had flipped under irradiation. When $H + \Delta H_{exp}$ is reached, flipping granules are anew observed. ΔH^{+}_{exp} is not exactly equal to ΔH because it is an average estimation, however crude experimental results have already provides an agreement with the above model within a factor three. (ΔH_{exp} is three times larger than ΔH).

If the signal/noise ratio for the change state is good enough, additional information about energy loss can, in principle, be obtained by pulse amplitude analysis. Conventional electronics does not allow such a refinement. In the Indium solar neutrino detector the counting of the number of granules flipped by the capture electron will provide the energy analysis.

3.5. Sketch of a metastable superconducting detector

Granules are mixed in paraffin wax. This suspension is spread upon kapton foils on epoxy cards upon which read-out loop were printed by usual techniques for printed circuits. The alloy of the read out loop is itself superconducting, its magnetic critical field is larger than H_{SH}. The read-out loop can have a great variety of shapes ; to get localization, we used long loops. In that case, the value of the inductance is proportional to the length of the loop, but the signal is inverse to the width L.XY screens are obtained if a slice of granules in paraffin is sandwiched between two planes of orthogonal families of loops. The thickness of the layer is about half the width L. The feasibility of such a device has been demonstrated for a 81x81 mm^2 screen with a 1.27 mm period. Another device with hybrid electronics is under construction with a spatial resolution of 0.6 mm (128 x 128 pixels) and two additional linear detectors with a resolution between 50 μ and 150 μ.

Electronic read-out : we are using charge preamplifiers with field effect transistors at the input part in a so called "cold resistance" set up. This preamplifier is connected with the pick-up coil through two transformers for impedance adaptation purpose. The first one is immediately at the output of the pick-up coil, it is made with superconducting wires. The second is at the preamplifier input at room temperature. This technique, now available in hybrid version, seems to have reached its limit, at least as long as the electronics remains at room temperature. The best performance is the detection of a granule of 15μ in diameter in a pick-up coil 300 microns wide with a 10 cm loop long. Such a solution is excluded for large volumes, required for solar neutrino detection. Another technology exists : Josephson devices.

IV. POSSIBLE SOLAR NEUTRINO PROGRAM

The popularity of Josephson devices has reached the high energy communauty with the Cabrera attempt to identify a signal in a Josephson magnetometer with the trace of a magnetic monopole. Cabrera used a Josephson RF system, which, in spite of its RF denomination is limited in frequency towards 200 kHz in commercially available systems.

A second family of Josephson devices exists which are true interferometers because they include two junctions in a loop coupled to an external coil (in our case, the pick up coil surrounding the granules). These devices are called DC SQUID.

SQUID = Superconducting Quantum Interferometric Device

They do not require external radio frequency modulation . They are limited in frequency by their self-inductance and can work with short pulses. In the best conditions, their sensitivity compete with RF SQUID :

$10^{-4}\phi_o$

when $\phi_o = 2\times10^{-7}$ g×cm² is the quantum flux unit.

In our case, $\Delta\phi \sim 2\times10^{-5}$ gauss cm²

$\Delta\phi \sim 200\ \phi_o$

with only $10^{-1}\phi_o$, we are better by a factor 2×10^{-3} in signal/noise. This allows to read granules of 2,5 μ in diameter in a loop 2 mm wide.

Following Raghavan, we can estimate the figure of merit $\frac{S}{N}$ of an indium detector for solar neutrino. The background is mainly due, according to him to the γ- rays coming from the stuff around indium. It is estimated at 2×10^{-7}/keV/g/sec. From where

$$\text{figure of merit} = \frac{S}{N} = \frac{20}{nC}$$

n = mass of indium in the elementary cell (in our case, the volume of an address $X_iY_jZ_k$) et C the indium concentration in the total system. With a filling factor of 20 %, a figure of merit equal to one is obtained for an elementary cell of 9,1 mm³.

A one liter detector will therefore provide a sufficient rejection with cells of 8 mm³. It can be a stock of 5000 cells realized by 50 planes X and 50 planes Y with 2 mm wide pick up coils, 10 cm long, the spacing betwen plane being 2 mm. Such a detector made with tin can be tested nearby a reactor, made with indium, it will allow the detailed noise study for a full size solar neutrino detector with metastable superconducting granules.

REFERENCES

SOLAR NEUTRINOS

(1) J.N. BAHCALL, Nulc. Phys. 71, 267 (1965).
(2) J.N. BAHCALL, Rev. Mod. Phys. 50, 881 (1978)

^{115}In REACTION

(4) R.S. RAGHAVAN, Phys. Rev. Lett. 37, 259 (1976).
(5) M. DEUTSCH et R.S. RAGHAVAN, Proposal to develop a Detector for Solar Neutrinos. - M.I.T. - 17 mai 1979.
(6) R.S. RAGHAVAN - Direct detection and spectroscopy of solar neutrinos using indium. Talk given at the University Wisconsin Miniconference on the Neutrino Mas. - Oct. 2-5, 1980.

RECOIL ENERGY

(7) A. DRUKIER et L. STODOLSKY - Principles and applications of a neutral current detector for neutrino physics and astronomy.
(Preliminary version 23 juin 1983 - unpublished).
Paper n° : MPI-PAE/PTh 36/82.

SUPRACONDUCTIVITE (main references)

(8) C. VALETTE, Thèse série A n° 846 - Orsay - 1971 (non publiée)
(9) C. VALETTE and J.P. BURGER - Journal de Physique 30, 562 (1969).
(10) H. BERNAS, J.P. BRUGER, G. DEUTSCHER, C. VALETTE, S.J. WILLIAMSON Phys. Lett. 24A, 721 (1967).
(11) A.K. DRUKIER, C. VALETTE, G. WAYSAND, L.C.L. YUAN, F. PETERS. Lettere al Nuovo Cimento, 14, 300, (1975).
(12) R.L. CHASE, CH. GRUHN, A. HRISOHO, C. VALETTE, G. WAYSAND. Fast electronics for a metastable superconducting detector. Proceedings 2nd Ispra nuclear electronics symposium - Stresa 29, (1975). Publication Euratom - EUR 5370 E aux soins de la Communauté Européenne.
(13) C. VALETTE, G. WAYSAND - Proceedings XXth Cospar 38 (1977), North Holland.
(14) D. HUEBER, C. VALETTE, G. WAYSAND - Cryogenics, 21, 387 (1981).
(15) D. HUEBER, C. VALETTE, G. WAYSAND - Proceedings LT 16, Physica, 1088, 1229 (1981).
(16) C. VALETTE, G. WAYSAND, D. STAUFFER - Solid State Com. 41, 305 (1982).
(17) A. HRISOHO, G. WAYSAND, Instrumental limit and number of effective granules in superheated superconducting detectors.
A paraître dans Nucl. Instr. Meth.

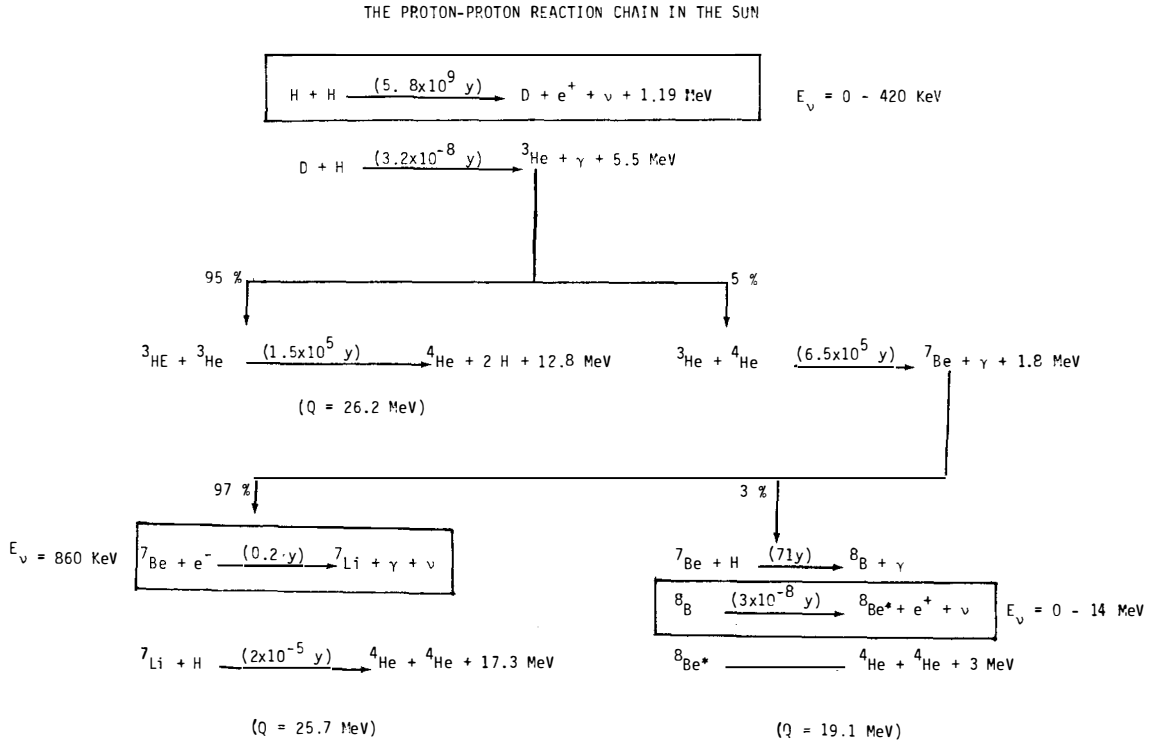


Figure 1 : The chain of nuclear reactions in the sun. The framed equations produce neutrinos. E_ν represents the energy of the emitted neutrinos. The range of variation is written for each of the neutrino producing reactions.

ENERGY SPECTRUM OF SOLAR NEUTRINOS

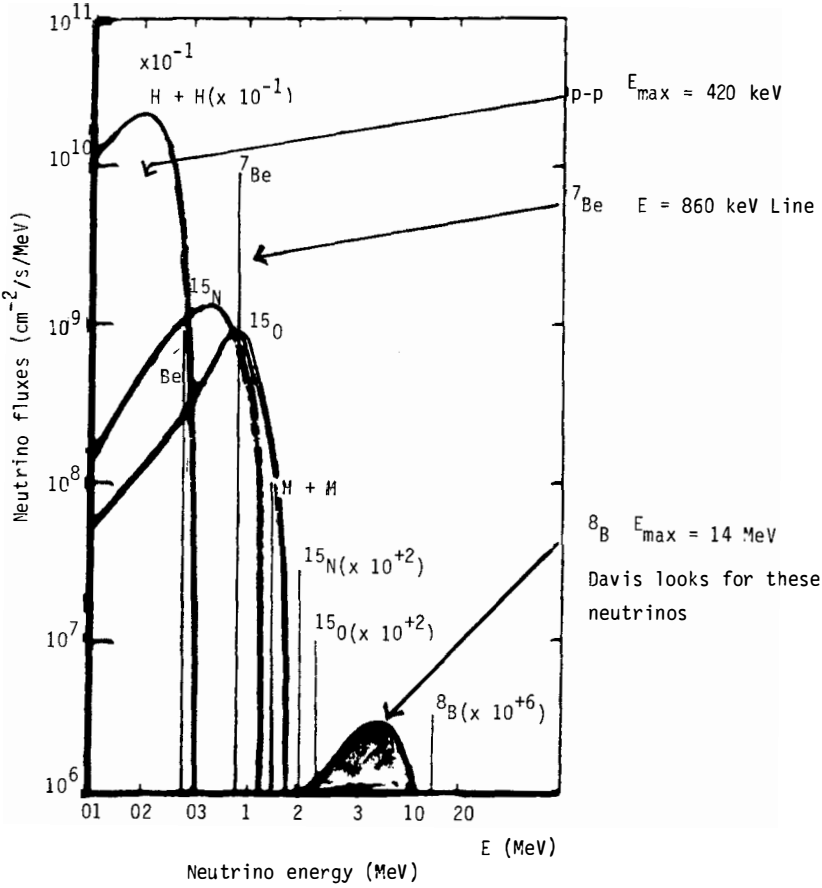


Figure 2 : Energy spectrum of the solar neutrino on the ground surface of the Earth. The flux scale is logarithmic. The shadowed zone represents the part of the spectrum detected by the Davis experiment with ^{37}Cl (threshold : 814 keV). These neutrinos are only 10^{-4} of the total flux on Earth surface.

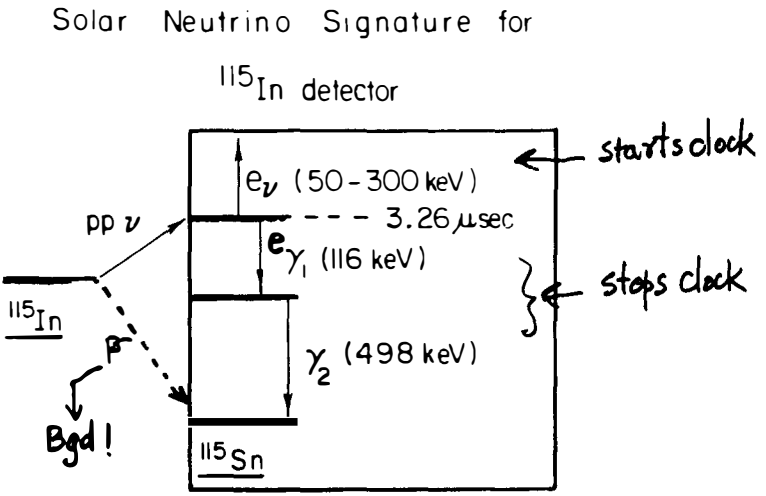


Figure 3 : Inverse β decay of ^{115}In in ^{115}Sn.

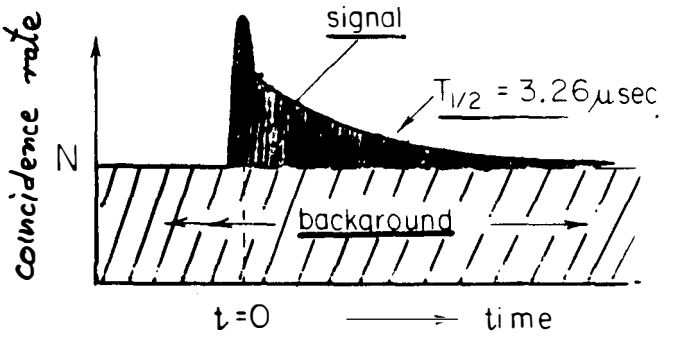


Figure 4 : Delay spectrum between e_ν dans $(e_1 + \gamma_2)$ when a solar neutrino reacts with a ^{115}In nuclei.

$$\overline{E_A} = \frac{2}{3A} E_\nu^2$$

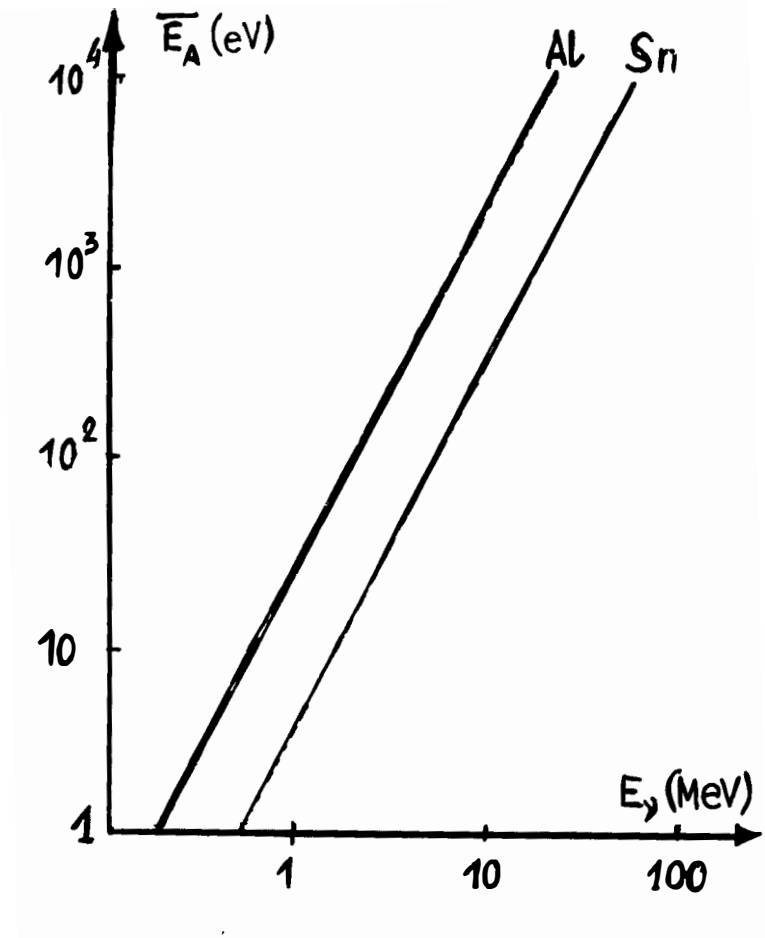


Figure 5 : Average recoil energy of a nuclei of superconducting metal under neutrino impact.

METASTABLE SUPERCONDUCTING POSITION DETECTORS

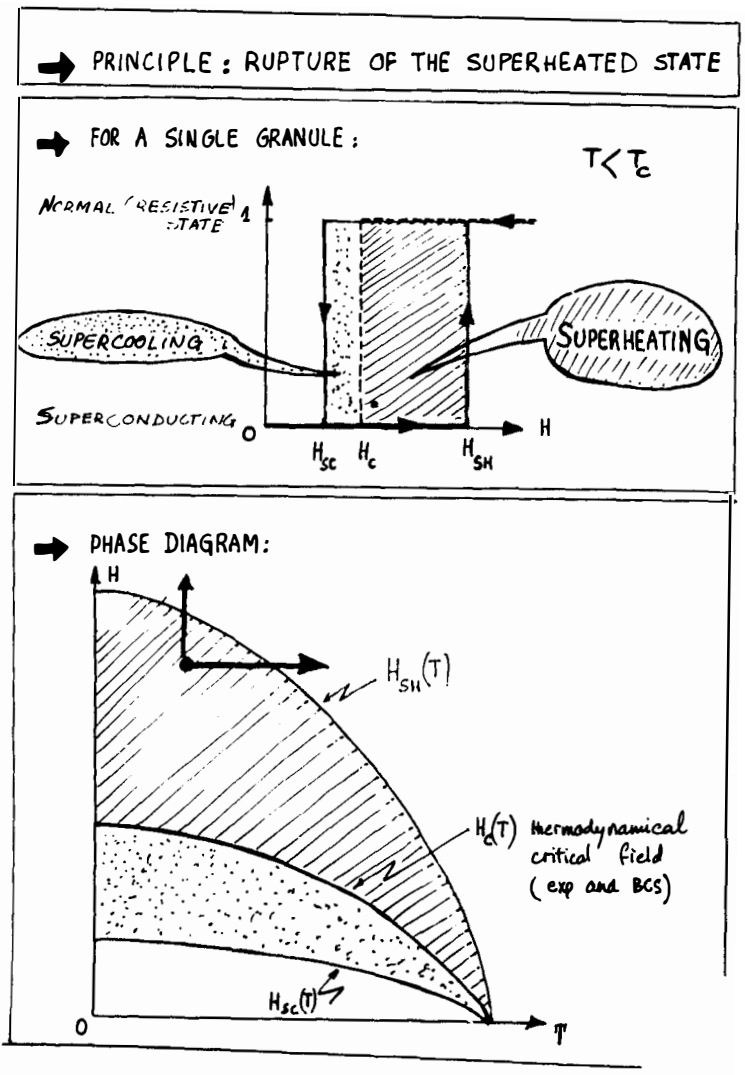
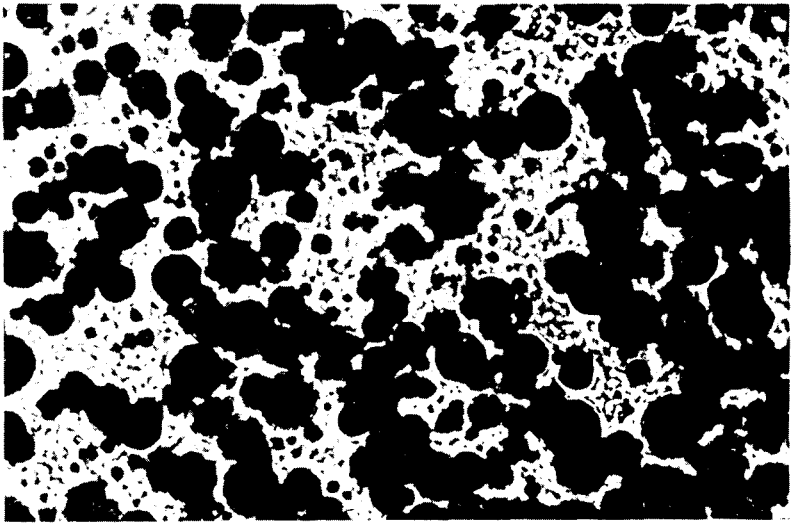
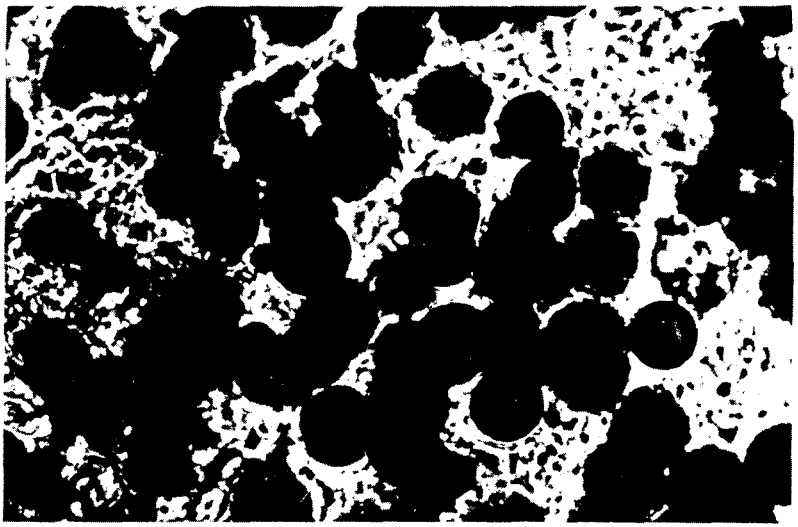


Figure 6 : Phase diagram of metastable superconducting system.
a) Upper graph : for a given temperature T, the hysterisis cycle of the susceptibility with the magnetic field.
b) Lower graph : the phase diagram itself : the horizontal arrow leaves the superheated zone for the normal (resistive) one.



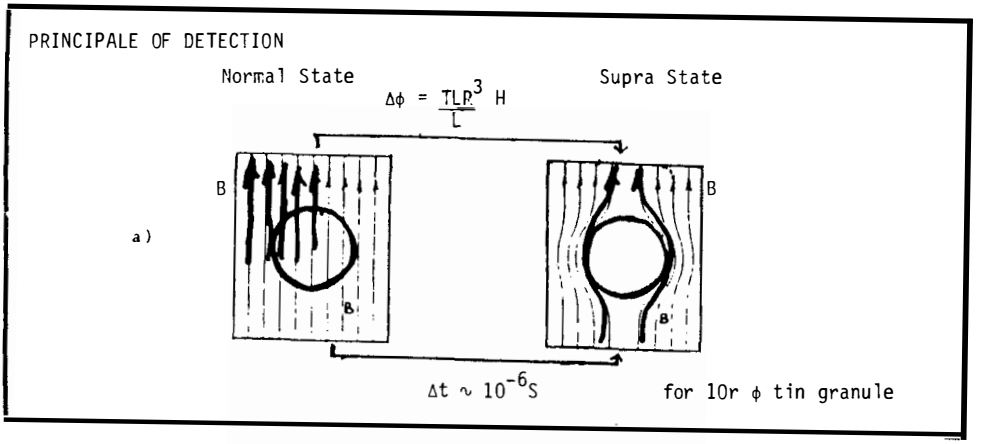
FILLING: 10% ; Collection [12, 25 µ]

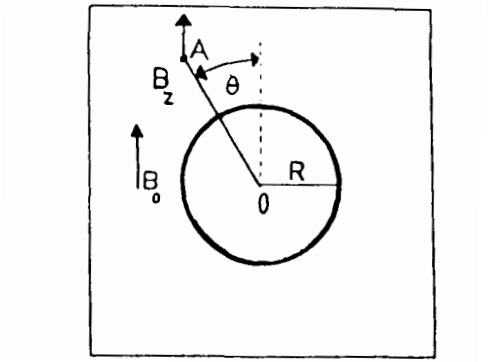


Collection [25,33 µ]

0 25 50 microns

Figure 7 : Collection of tin microspheres dispersed in paraffin wax (filling factor 10 %).





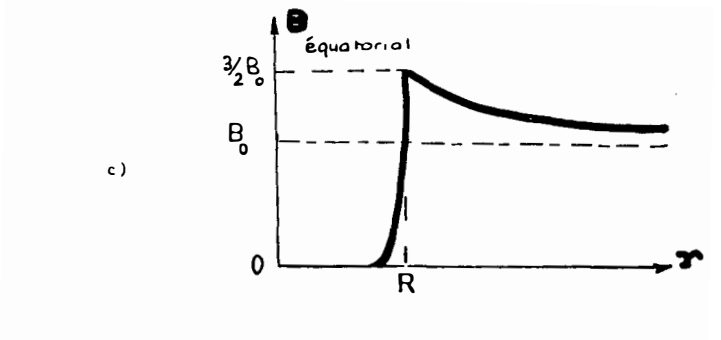
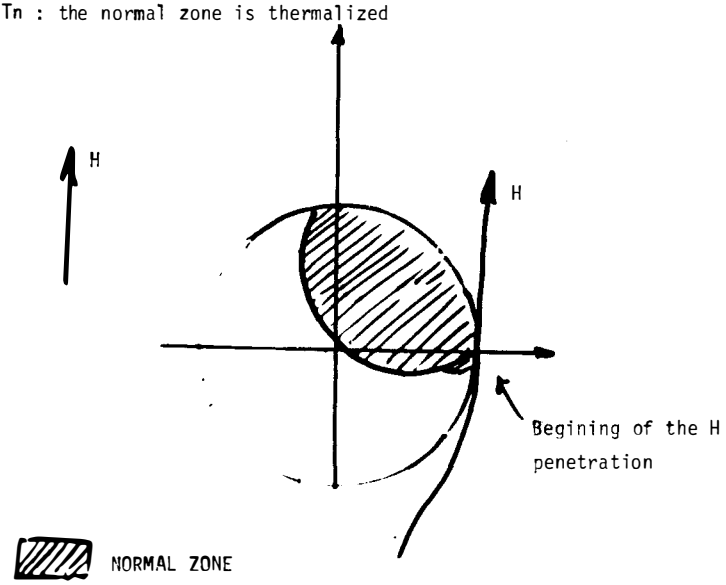


Figure 8 : Perfect diamagnetism of a sphere of type I superconductor.

1)

In Sn & Tn : the normal zone is thermalized



2)

This local heating is

$$\Delta T \simeq \frac{\int_0^{\ell} \frac{\partial E}{\partial r}\, dr}{\frac{2}{3}\pi R^3 Cp}$$

which is equivalent to a jump ΔH in magnetic field defined by

$$\Delta H = Hm - H = \frac{\partial H_{sh}}{\partial T}\,\Delta T$$

Figure 9 : The model of partial heating of a granule.

Therefore, for a given irradiation at H fixed there is a maximum field Hm : $H \leqslant Hm \leqslant H_{SH}$ above which the granules cannot change of state

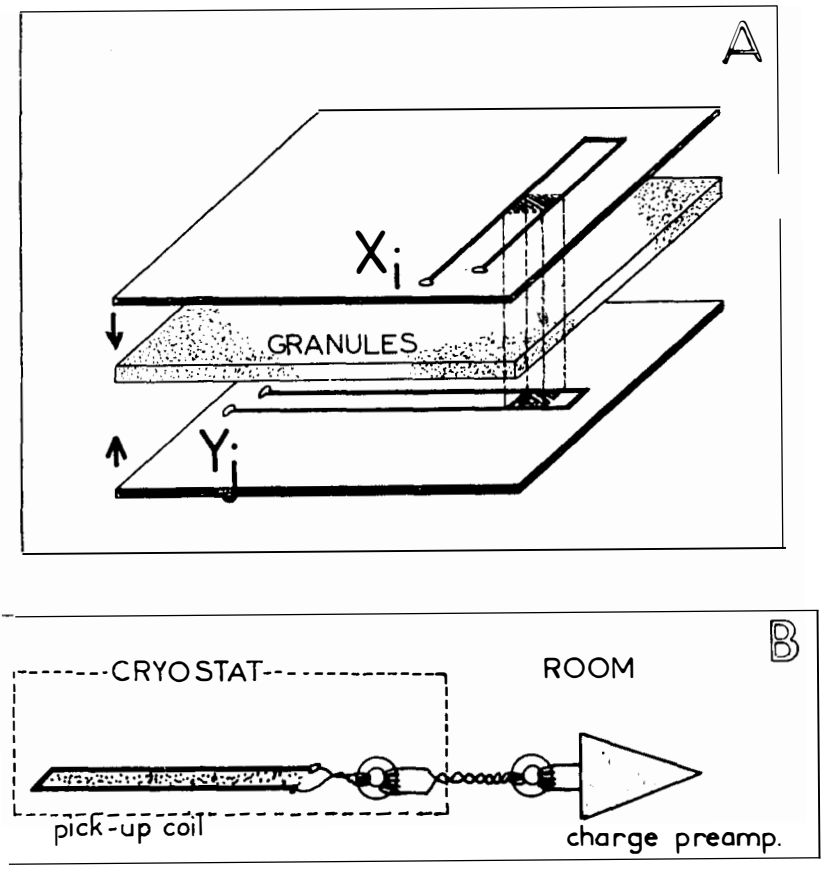


Figure 10 General sketch of a detector :

a) geometry for an XY localization
b) coupling of the pick up coil with the preamplifier.

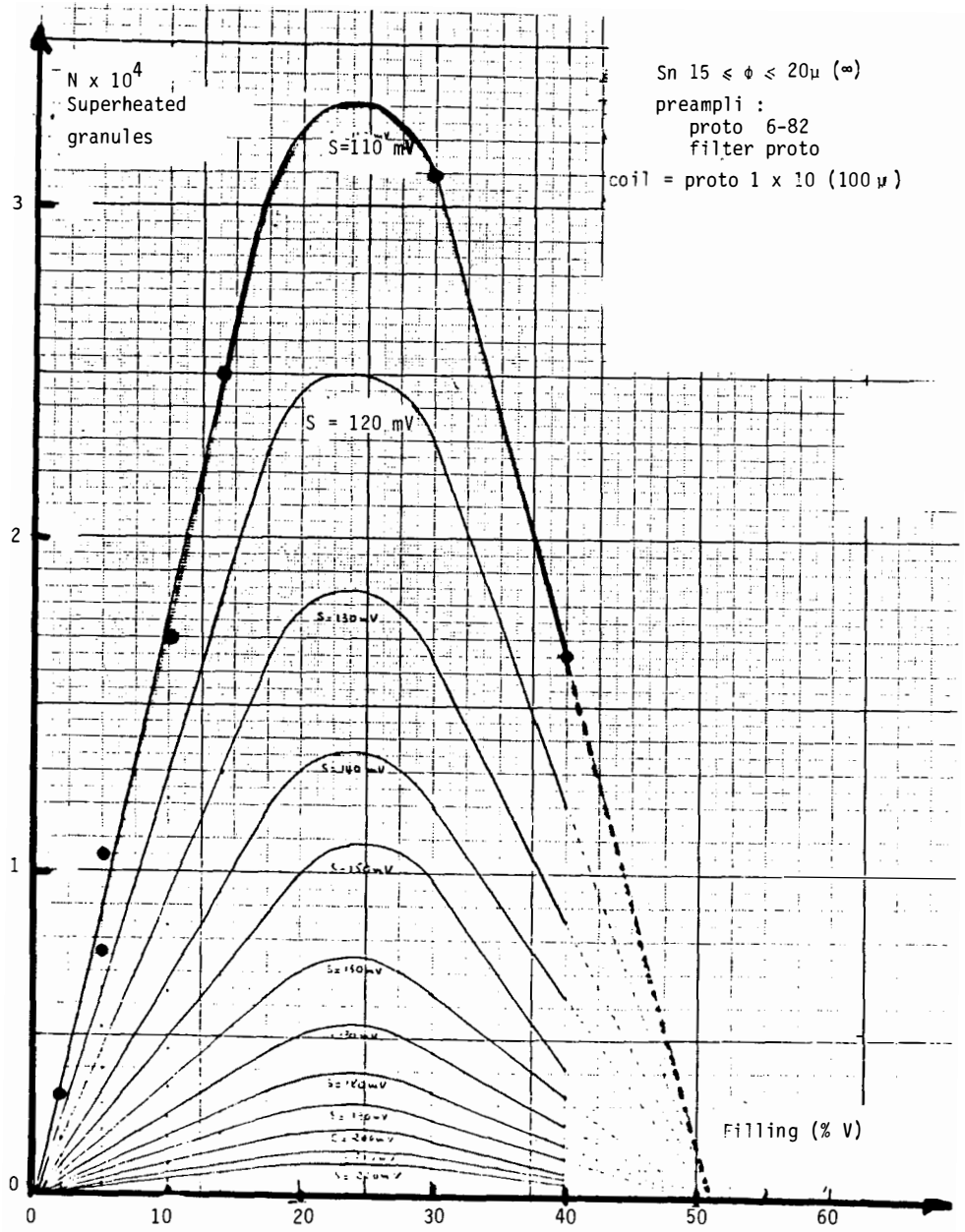
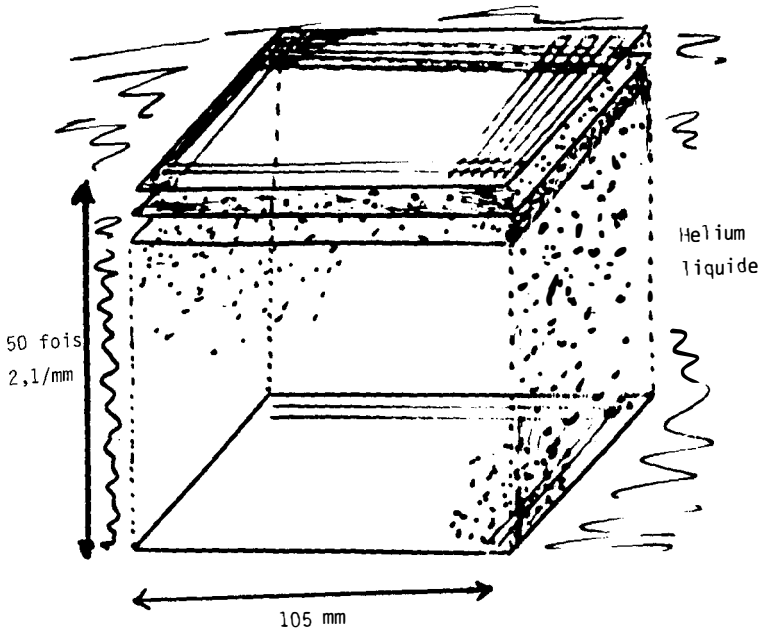


Figure 11 Variation of the number of superheated granules as a function of the filling factor.



Détecteur de V_{utile} ∿ 1 Litre

Sn ou In ∿ 1 à 2 Kg

Chaque plan comprend 50 boucles et 50 boucles Y

Cellule Elementaire ∿ 8 mm^3

Figure 12 Sketch for a one liter detector for solar neutrinos

ALLURE GENERALE

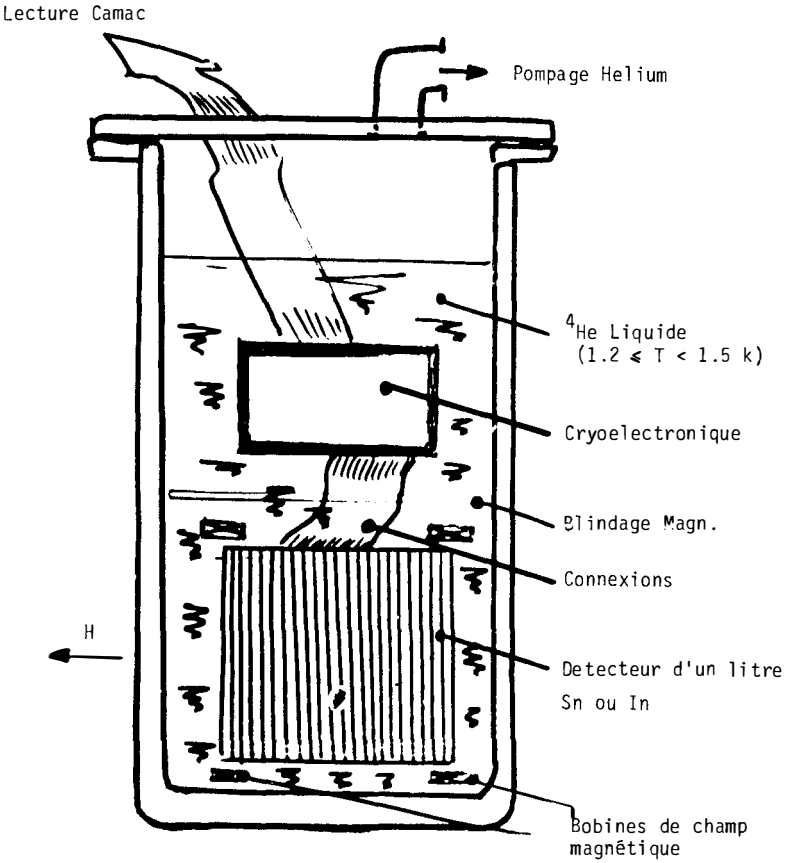


Figure 13 Full system for a one liter detector.

NEUTRINO MASSES AND MIXINGS IN SUPERNOVA BURSTS

L. Stodolsky
Max-Planck-Institut für Physik und Astrophysik
- Werner-Heisenberg-Institut für Physik -
Munich (Fed.Rep.Germany)

Neutrino bursts from supernova explosions would offer a novel opportunity to study the masses and mixings of neutrinos. We examine, on the basis of a definite supernova model, the various effects which might exist and how they could be observed.

Because the flight time for neutrinos from a supernova to the earth will in general be very long, on the order of 10 kpc for a supernova in the galactic center, even small neutrino masses can result in substantial effects on the neutrino flight time to the earth. Here I would like to briefly report on some calculations using a hopefully realistic supernova model.[1] The work is largely from P. Reinartz's diploma thesis. More details can be found there and in our paper (MPI-PAE/PTh 50/83).

A neutrino of mass m, energy E, coming from a distance d, has a flight time to the earth

$$t = d(1 + (m/E)^2/2 \qquad (1)$$

for light neutrinos we expect $m/E \ll 1$, ($\hbar = c = 1$ units). We note that unlike electromagnetic radiation, the interstellar medium may be treated as having zero refractive index for neutrinos, in view of their weak interaction. Thus for two neutrinos m_1 and m_2 of the same energy the time separation is

$$\delta_t = d(m_2^2 - m_1^2)/(2E^2) \qquad (2)$$

which, for E = 10 MeV and $m_2^2 - m_1^2 = (10\ \text{eV})^2$ for example, gives

$$\delta_t = 50\ \text{msec/kpc} \qquad (3)$$

In addition to Zatsepen's original idea on pulse spreading,[2] there are a number of other effects which may be observable in present or planned neutrino detectors, yielding important information about the neutrino:[3),4)]

A) The existence of neutrinos with finite and distinct masses can give a set of time separated pulses, with characteristics depending on the type of detector.

B) Neutrino mixing can show up as separate pulses for a neutrino of a <u>given</u> type.

C) A time-energy correlation should exist for the individual events since the more energetic neutrinos arrive first. Different neutrino masses could be seen through this effect even when there are not well separated pulses in time.

D) If the neutrinos are incoherent, which is the case unless mass difference are extremely small, mixing will cause an increase in the relative amounts of $\bar{\nu}_e$ / ν_e, relative to what is expected from the supernova itself.

E) For very small mass differences (10^{-10} eV) so the oscillation length is just on the order of the distance to the earth, there can be coherence effects to be observed through oscillation of a given neutrino type with respect to detected energy.

We illustrate these points with some plots.

The distribution in time and energy for the initial neutrino burst without any propagation effects are shown in Fig. 1 and 2 respectively. The normalization is for observation at the earth at a distance of 10kpc. The average energies of ν_e, $\bar{\nu}_e$, ν_μ, $\bar{\nu}_\mu$ are 12, 12, 18 and 18 MeV respectively. The total flux is $4.0 \cdot 10^{11}/cm^2$ for ν_e, $2.6 \cdot 10^{11}/cm^2$ for ν_μ (equal for μ) and $0.6 \cdot 10^{11}/cm^2$ for $\bar{\nu}_e$.

To take into account possible neutrino flavor mixing we shall use a simple model in which there are mass eigenstates ν_1 and ν_2, masses m_1 and m_2 such that

$$\begin{aligned} |\nu_e> &= \cos\theta\ |\nu_1> + \sin\theta\ |\nu_2 \\ |\nu_\mu> &= \sin\theta\ |\nu_2> + \cos\theta\ |\nu_2 \end{aligned} \qquad (4)$$

and similarly for the antiparticles.

All our calculations are for d = 10 kpc. Since according to Eq. 1, the time delay relative to light flight time is $\alpha\ dm^2$, one can scale to other distances by changing all masses such that dm^2 remains constant.

First to give an idea of how a finite mass leads to a spreading of the pulses, we show the time distribution which results when each neutrino is given a mass of 2 eV. This is given as the dotted line in Fig. 1. Dramatic effects result when the mass of the heavier neutrino is set large but still substantially less than the present experimental limit of a few hundred keV. In Fig. 3, we show no mixing and m_{ν_μ} = 1 keV. The ν_μ's arrive an hour after the ν_e's. The width of the ν_μ pulse also illustrates the spreading effect due to the mass: the ν_e's appear as a delta function at t = 0 on the scale of the plot.

Above masses around one eV separated pulses appear for $m_2/m_1 \sim 10$. This is shown in Fig. 4A, 4B and 4C. There is no mixing and m_1 = 1 eV and m_2 = 15, 30 and 100 eV. For m_2 = 1 keV the delay of the second pulse reaches 10^3 sec (Fig. 3). The shoulder at the end of the ν_e curves is due to the second "after burning phase" in the supernova which is thought to follow the first big pulse.

Note that even if a distinct second peak should not appear, the time distribution of the total neutrino signal will be much longer than that of the original pulse (Fig. 1). Below we shall explain how using the energy-time correlation for the neutrinos, one might identify distinct masses even if the peaks are not distinctly separated.

Turning to point B), we now examine what can be learned when the neutrino type is distinguished. Particularly interesting here is $\bar{\nu}_e$, which could be seen in water Cerenkov or liquid scintillator detectors

examining Fig. 5.[7]

The maximal effect in the two state case would be reached with $\theta = 45°$, and $\bar{\nu}_e / \nu_e$ cannot exceed about 1/2, since $\bar{\nu}_e$ is small to begin with. With 3 states the limit becomes about 2/3. CPT is assumed[6] so that the magnitudes of the particle and anti-particle mixings are the same.

We now consider the situation of long wave trains, where there could be coherence. Here there still can result a situation which observationally is like complete incoherence if the neutrino source is spread out in size compared to the oscillation length. In this case emission from different points of the source leads to different interference effects which average each other out at the detector. With a supernova, of say 10 km dimensions, and E = 10 MeV, this would imply that

$$m_2^2 - m_1^2 \quad \frac{2.5(E/\text{meV})}{L/m} \simeq 2.5.10^{-4}(\text{eV})^2 \qquad (7)$$

For example, masses on the order 10^{-2} eV or less are required for coherence over the surface of the star.

If the masses are this small, $\sim 10^{-2}$ eV, then for 10 kpc the particles arrive with a time delay $\sim 10^{-6}$ sec or ~ 100 m. Thus the length of the wave trains need only be on this order for interference effects to be possible, in principle.

However, this coherence will not to observable due to the energy spread of the neutrinos, which leads to a further washing out of interference effects. Neutrinos of different energies will have different oscillation lengths L, differing by δL. If interference effects are to be visible, we must have

$$\frac{d}{L} \lesssim \frac{\delta L}{L} \quad 1 \qquad (8)$$

Since d is astronomical, L must be very big, that is the neutrino mass differences extremely small. For example, assuming that the energy resolution in $\bar{\nu} + P \rightarrow n + e^+$ is $\delta E/E \sim 0.1$, we could divide the data into samples with $\delta/L \sim 0.1$. For d = 10 kpc this implies $\delta m^2 \sim (10^{-10}\ \text{eV})^2$. This mass difference is of course tiny, but on the other hand only 5 orders of magnitude smaller than that for K°'s. In this case interference would manifest itself through oscillations in the number of a given neutrino type, say ν_e or $\bar{\nu}_e$, detected as we vary the energy observed. A different pattern for ν_e and $\bar{\nu}_e$ can then result from CP violation, without necessarily requiring CPT violation. Observation of such interference effects would be direct, and probably the only possible evidence for such tiny mass differences. In Fig. 9 we show a hypo-

and identified perhaps by the free neutron or the positron annihilation from $\bar{\nu}_e + P \rightarrow n + e^+$. Since $\bar{\nu}_e$ is emitted in one pulse, if it arrives as two or more pulses, this is direct evidence for neutrino mixing. In Fig.5 we show the $\bar{\nu}_e$ pulse (E^2-weighted) for $m_1 = 1$ eV, $m_2 = 15$ eV and $\theta = 0°$, 25°, 45°.

The time-energy correlation, point C), is interesting because if it exists it shows that neutrino mass is the origin of separate pulses or time delay and not, say, "bounces" in the supernova. Furthermore it may permit greater sensitivity to separate mass eigenstates, even if the pulses are not well spread or separated in time. Here it is important to note that we have simply assumed for simplicity that there was no time-energy correlation in the original burst, which in reality is undoubtedly not true in detail. Thus for finer effects this would have to be studied with a more detailed supernova model.

The main point is that the more energetic neutrinos will arrive first. This is shown in Fig.6 where the average energy of the detected neutrino (with E^2 weighting) is shown as a function of time, with a single neutrino of mass 3 eV.

We now consider the time-energy correlation with distinct neutrino masses. Here an interesting effect arises in that even if there are not distinct pulses in time, the arrival of the second, more massive, neutrino will lead to a jump in the number of energetic neutrinos on the heels of the low energy "laggards" of the first neutrino.

The same arguments apply of course for three distinct states. Fig. 7 shows the case $m_e = 1$ eV, $m_\mu = 10$ eV, $m_\tau = 30$ eV, without mixing.

We expect different phenomena in the two extremes of coherence or incoherence. If we have complete incoherence, then the particle content of the radiation at the earth in terms of ν_e, ν_μ ... will simply be given by the mixing angles. Thus, for example a ν_e at the star could result, for $\theta = 45°$, in 50% ν_μ at the earth. The most striking consequence of this situation would be an increase in the $\bar{\nu}_e$ content at the earth with respect to ν_e, while ν_e will be reduced by its mixing into ν_μ and ν_τ. The magnitude of the effect depends of course on the size of the mixing angles, but since at emission $\bar{\nu}_e / \nu_e$ is expected to be 1/10, there could easily be a noticeable effect [7]. Fig. 8 shows the change in ν_e for $\theta = 45°$. This would be, therefore, a way to establish mixing even if there are not clearly separated pulses. The increase in $\bar{\nu}_e / \nu_e$ naturally also holds with separated pulses as may be seen by

thetical case where the oscillation length L for 10 MeV is the earth-supernova distance. Naturally, if L becomes greater than the distance to the supernova, the oscillations disappear again for earthbound detectors. Hence even given very small neutrino mass differences, these differences would have to be in a very narrow "window" to lead to observable oscillations at the earth.

We conclude by reviewing what seem to be the most important points concerning neutrino detector configurations so that the most can be gotten out of the supernova event, should it be observed.

First, obviously, it would be beneficial to have good statistics, many neutrino conversions in the detector, so that the various distributions in energy and time can be found. The large proton decay detectors if adaptable to neutrinos, for example, could give on the order of hundreds of events.

Secondly, timing information, say at the msec level is important in following the development of the burst.

Energy resolution, as might be possible using the electron or positron from $\nu + N \rightarrow N + e$ would be very useful in establishing the time-energy correlation connected with a neutrino mass and in allowing one to look for neutrino oscillations. Distinction of the neutrino type, particularly $\bar{\nu}_e$, in order to look for the "repeated appearances" and the increase in the $\bar{\nu}_e / \nu_e$ ratio characteristic of mixing, as well as the "neutral current" detector sensitive to ν_μ and ν_τ as well,[5] would complete the picture. Just because supernovas are so spectacularly rare it would be a shame if one came and it were not fully exploited.

We would like to thank R.D. Peccei for discussions, and we are grateful to W. Hillebrand for advice on supernova models.

References

1) J.R.Wilson, Am.N.Y.Acad.Science 358 (1980);
J.P.Schinder and S.T.Shapiro, Ap.J. 259, 311 (1982);
D.Freedman et al., Ann.Rev.Nucl.Science 27, 167 (1977); and
W.Hillebrand, private communication;

2) G.T.Zatsepin, ZhTEF Pis Red 8, 333 (1968);
see a detailed discussion in
T.Piron, Phys.Lett. 102B, 299 (1981);

3) The extraction of more information on neutrinos from a supernova seems to have occured to a number of people including at least:

N.Cabbibo, Acad.Lincei, Int. Meeting on Astrophysics and Elementary Particles, Common Problems (1980);
J.M.LeSecco, Proceedings Neutrino Mass Miniconference, Telemark, Wisconsin (1980), Univ. of Wisconsin, p. 191;
L.Stodolsky, München-Crakow Seminar (1982) (unpublished) and ref. 5;

4) For example, in the possible event seen by
K.Lande, G.Bozoke, W.Frati, C.K.Lee, E.Fenyes and O.Saavedra, Nature 251, 485 (1974), the narrowness of the bursts (μ sec) was used to set tight mass limits. Unfortunately such narrow bursts are incompatible with current supernova models. If we nevertheless assume that some unknown event in the galactic center produced these very narrow bursts, we might try to attribute the four (or more) distinct bursts as due to neutrino mixing. In this case we would have (at least) four neutrino mass eigenstates. With $E \simeq 15$ Mev, d = 10 kpc, the timing information reported would imply $m_{21}^2 = = 1.3 \cdot 10^{-3}$ ev^2, $m_{32}^2 = 1.9 \cdot 10^{-3}$ ev^2, $m_{43}^2 = 1.9 \cdot 10^{-3}$ ev^2 for the mass difference. Those numbers do not appear a priori unreasonable. On the other hand each pulse should spread if there is a mass, and one can show that $\Delta t / \delta t \simeq 2\ \delta E/E$, where Δt is the spread within a pulse and δt the spacing between pulses. Since the timing information indicates $\Delta t / \delta t \simeq 10^{-3}$, the neutrinos would have to have been very monochromatic: $\delta E/E \sim 10^{-3}$. Since we know of no such astrophysical source, we conclude that the mixing explanation is implausible.

5) A.Drukier, L.Stodolsky, preprint MPI-PAE/PTh 36/82;to be published in Phys.Rev.;

6) N.Cabbibo, Phys.Lett. 72B, 333 (1978);

7) R.Silberberg and M.M.Shapero, Proceedings 1980 Int. Dumand Symposium, ed. V.J.Stenger, suggest that oscillations would lead to a greater ν_e luminosity at the supernova itself. It has been pointed out, however, that in dense nuclear matter neutrino oscillations should be suppressed, L.Wolfenstein, Phys.Rev. D20, 2634 (1979). The oscillations in flight, as we consider them, however, still can lead to an increase in the ν_e's.

Figure Captions

Fig. 1 Neutrino time distributions as the neutrinos leave the star; solid lines) and as they arrive at the earth with a common mass of 2 eV (dotted lines). Curves for $\bar{\nu}_\mu$, $\bar{\nu}_\tau$ and $\bar{\nu}_\tau$ or other light neutrinos ($m < 10$ MeV) would be the same as that shown for ν_μ. Normalization is flux at the earth.

Fig. 2 Energy distributions assumed for ν_e and ν_μ. That for $\bar{\nu}_e$ is the same as ν_e while other light neutrinos are the same as ν_μ.

Fig. 3 Time distribution for observation at the earth when ν_e (at t=0) has a negligible mass and ν_μ a mass of 1 keV. The plot illustrates both the delay and spreading of the pulse due to a mass (no neutrino mixing). The flux has been weighted by the factor $(E/15\ \text{MeV})^2$ to take into account the E^2 dependence of possible detection reactions.

Fig. 4 Illustration of multiple peaks in the time distribution, when ν_e has a mass of 1 eV and ν_μ of 15, 30 or 100 eV (a, b and c), (no mixing). The shoulder in ν_e is due to the "late burning" phase.

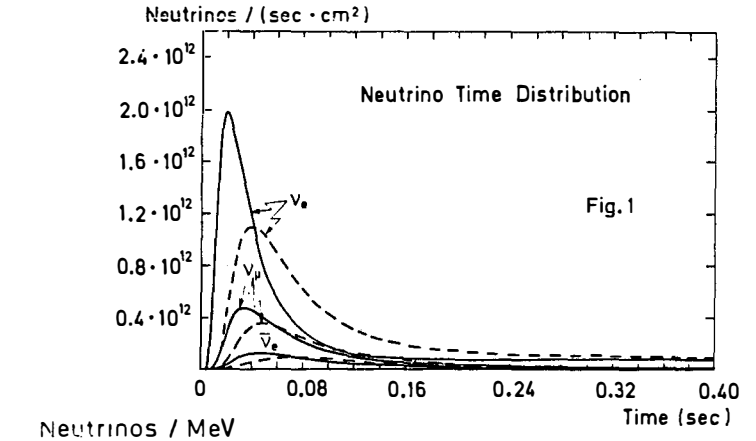
Fig. 5 Illustration of "repeated appearances" of $\bar{\nu}_e$ for $m_1 = 1$ eV and $m_2 = 15$ eV with various mixing angles. The second bump can be higher than the first with $\theta = 45°$ due to the E^2 weighting and the higher energy of ν_μ at emission.

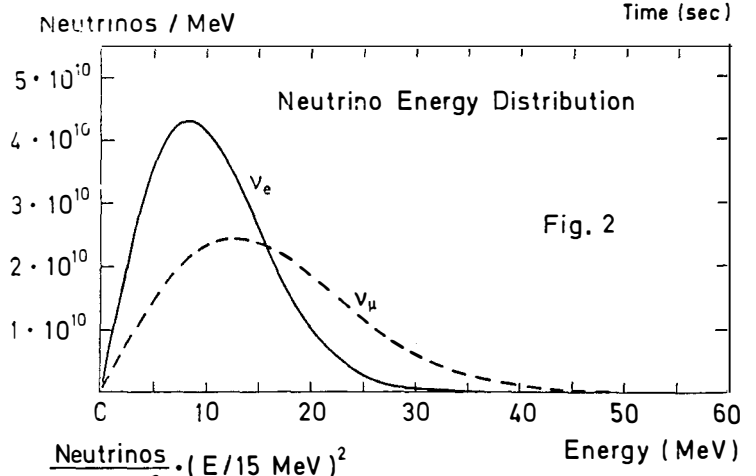
Fig. 6 Average energy versus time, showing the earlier arrival of the most energetic neutrinos with a single neutrino mass of 3 eV (E^2 weighting).

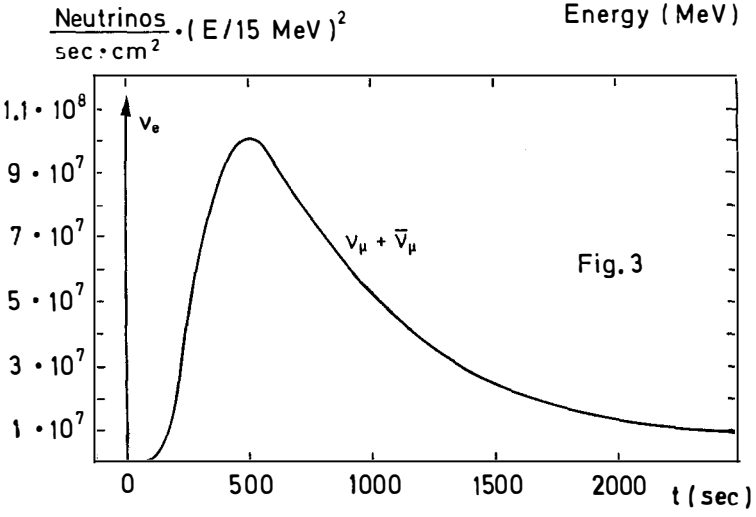
Fig. 7 Average energy versus time with three distinct neutrino masses of 1 eV, 10 eV, and 30 eV for ν_e, ν_μ and ν_τ.

Fig. 8 Illustration of the observability of mixing, even if there are not distinct peaks in time or coherence between different mass eigenstates, by observing the increase of $\bar{\nu}_e$. The mass m_1 and m_2 have been taken $<<1$ eV and $\bar{\nu}_e$ is shown with no mixing and maximal mixing.

Fig. 9 Most favourable case for observation of oscillations, when the supernova-earth distance is just one oscillation length for 10 MeV neutrinos.


Neutrinos / (sec · cm²)
2.4 · 10¹²
2.0 · 10¹²
1.6 · 10¹²
1.2 · 10¹²
0.8 · 10¹²
0.4 · 10¹²
Neutrino Time Distribution
Fig. 1
νe
νμ
ν̄e
0
0.08
0.16
0.24
0.32
0.40
Time (sec)


Neutrinos / MeV
5 · 10¹⁰
4 · 10¹⁰
3 · 10¹⁰
2 · 10¹⁰
1 · 10¹⁰
Neutrino Energy Distribution
Fig. 2
νe
νμ
0
10
20
30
40
50
60
Energy (MeV)


Neutrinos / sec · cm² · (E/15 MeV)²
1.1 · 10⁸
9 · 10⁷
7 · 10⁷
5 · 10⁷
3 · 10⁷
1 · 10⁷
νe
νμ + ν̄μ
Fig. 3
0
500
1000
1500
2000
t (sec)

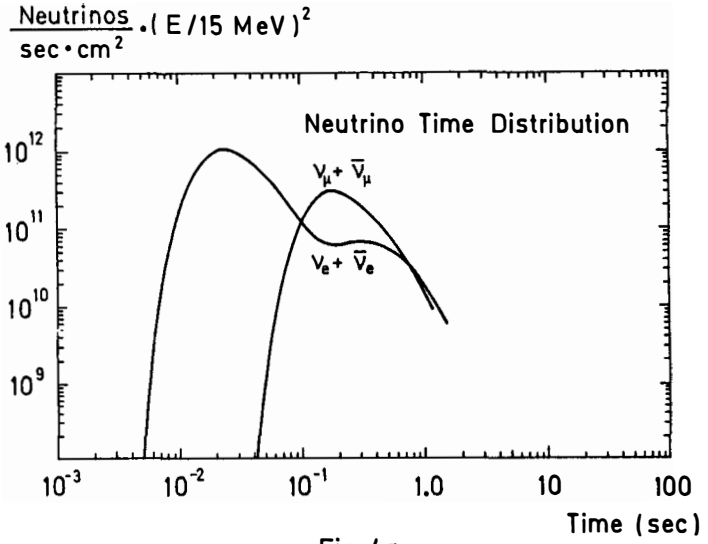

Neutrinos / sec • cm² • (E / 15 MeV)²
Neutrino Time Distribution
$\nu_\mu + \bar{\nu}_\mu$
$\nu_e + \bar{\nu}_e$
10^{12}
10^{11}
10^{10}
10^{9}
10^{-3}
10^{-2}
10^{-1}
1.0
10
100
Time (sec)

Fig. 4a

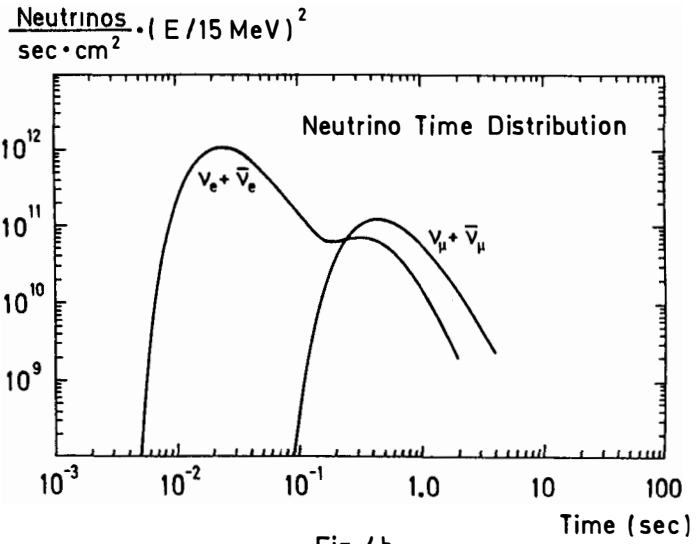

Neutrinos / sec • cm² • (E / 15 MeV)²
Neutrino Time Distribution
$\nu_e + \bar{\nu}_e$
$\nu_\mu + \bar{\nu}_\mu$
10^{12}
10^{11}
10^{10}
10^{9}
10^{-3}
10^{-2}
10^{-1}
1.0
10
100
Time (sec)

Fig. 4b

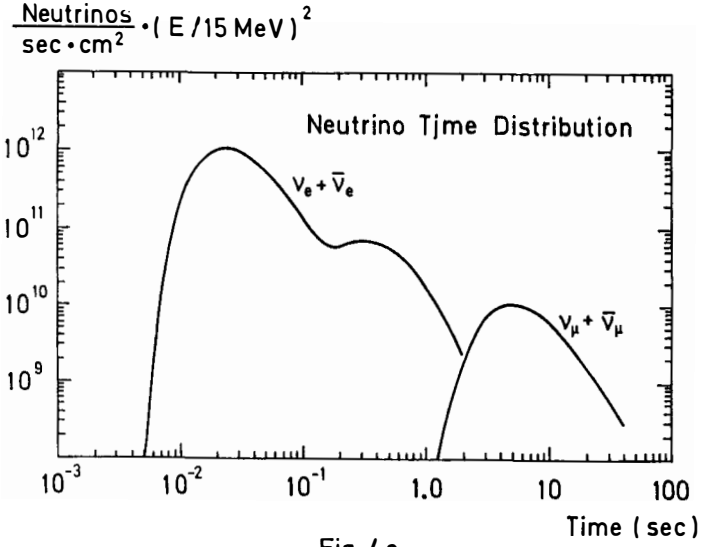

Neutrinos / sec • cm² • (E /15 MeV)²
Neutrino Tjme Distribution
$\nu_e + \bar{\nu}_e$
$\nu_\mu + \bar{\nu}_\mu$
10^{12}
10^{11}
10^{10}
10^{9}
10^{-3}
10^{-2}
10^{-1}
1.0
10
100
Time (sec)

Fig. 4 c

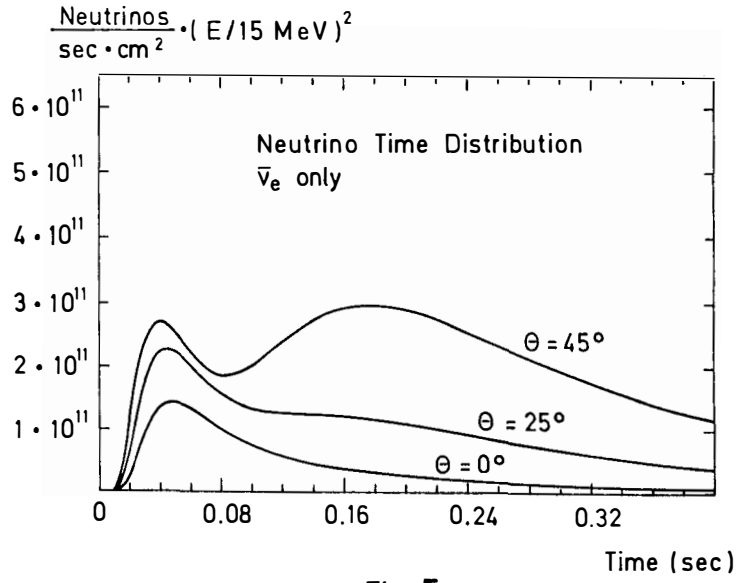

Neutrinos / sec • cm² • (E/15 MeV)²
Neutrino Time Distribution
$\bar{\nu}_e$ only
$6 \cdot 10^{11}$
$5 \cdot 10^{11}$
$4 \cdot 10^{11}$
$3 \cdot 10^{11}$
$2 \cdot 10^{11}$
$1 \cdot 10^{11}$
Θ = 45°
Θ = 25°
Θ = 0°
0
0.08
0.16
0.24
0.32
Time (sec)

Fig. **5**

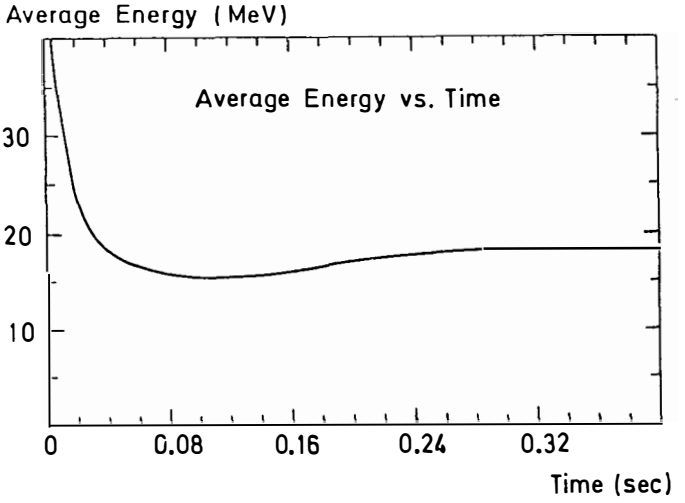

Average Energy (MeV)
Average Energy vs. Time
30
20
10
0
0.08
0.16
0.24
0.32
Time (sec)

Fig. 6

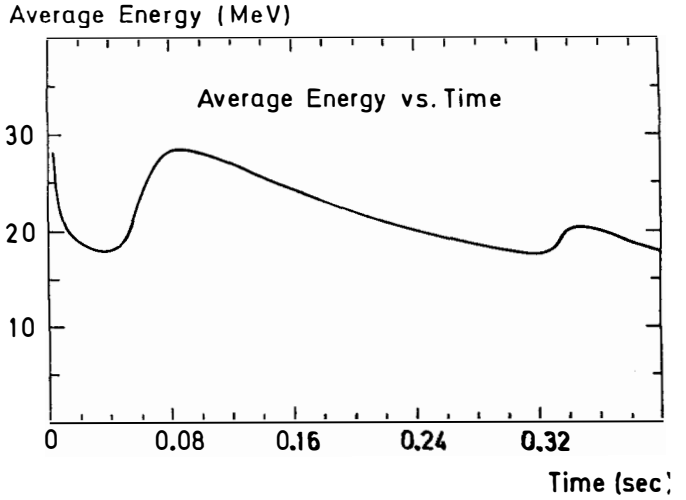

Average Energy (MeV)
Average Energy vs. Time
30
20
10
0
0.08
0.16
0.24
0.32
Time (sec)

Fig. 7

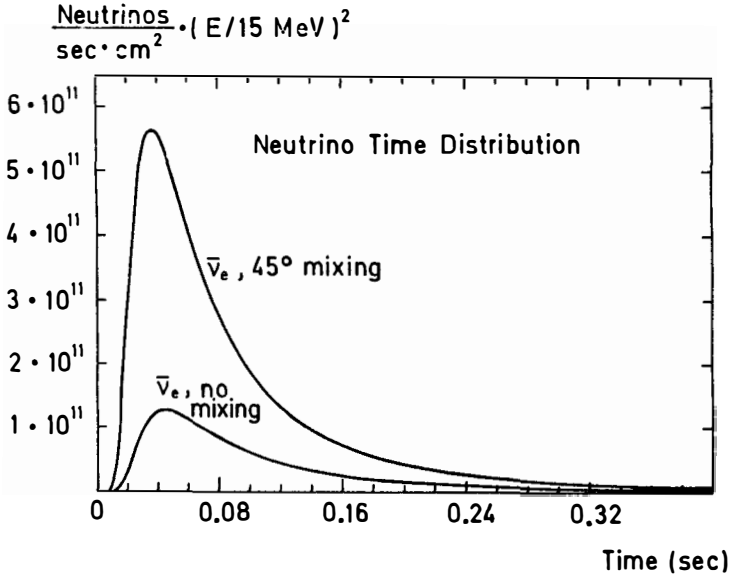

Neutrinos / sec · cm² · (E/15 MeV)²
Neutrino Time Distribution
$\bar{\nu}_e$, 45° mixing
$\bar{\nu}_e$, no mixing
6 · 10¹¹
5 · 10¹¹
4 · 10¹¹
3 · 10¹¹
2 · 10¹¹
1 · 10¹¹
0
0.08
0.16
0.24
0.32
Time (sec)

Fig. 8

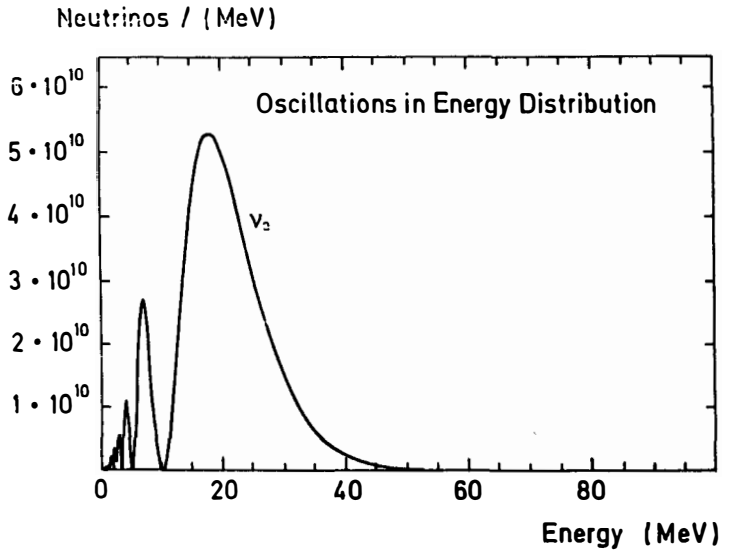

Neutrinos / (MeV)
Oscillations in Energy Distribution
ν_2
6 · 10¹⁰
5 · 10¹⁰
4 · 10¹⁰
3 · 10¹⁰
2 · 10¹⁰
1 · 10¹⁰
0
20
40
60
80
Energy (MeV)

Fig. 9

HALOS OR NO HALOS : Is there "missing mass" hidden in (massive or not) halos in flat galaxies ?

Jean-Pierre J. LAFON
Observatoire de Paris-Meudon
Département Recherches Spatiales/LA 264
92195 Meudon Principal Cedex



ABSTRACT : It has often be too easily accepted that a large amount of "adequate" invisible matter should be invoked to explain some phenomena observed in galactic systems. However, the existence of (massive or not) dark halos surrounding the observable matter is not so obvious, in particular as a result of the flatness of rotation curves at large radial distances.

I INTRODUCTION

Since the problem of the total mass in the Universe has appeared as crucial for its future evolution, the determination of the amount of matter contained in systems at various volume scales has been considered with particular attention. This paper is devoted to this problem for flat galaxies.

In spite of a lot of papers published during the last fifty years, the structure and the dynamics of flat galaxies (among which our Milky Way) is not clearly elucidated. It is only generally accepted that the behaviour of such systems is dominated by non-collisionnal stellar dynamics i.e. each star (and the gas) moves in the gravitationnal potential determined by all the other stars. The stars behave like a "non collisionnal gravitationnal plasma". However, this particular "non neutral plasma physics" is not well known. This is the reason why the amount and the distribution of mass in flat galactic discs are matters of discussions; an important question is : is all (or almost all the matter) in the visible stars or is there an important invisible component? Many arguments have been raised in favor of or against the presence of a (more or less) massive hidden component.

In the next section we summerize the main arguments and in the others we discuss the problem of the slope of the rotation curves. The conclusion is that the question is not so simple and that, contrary to what is too smarly stated, the observed flat rotation curves can be those of galaxies wit <u>or without</u> halos.

II WHY MASSIVE HALOS AND WHAT IN THEM ?

The arguments usually invoked in favor of the presence of a large amount of non visible mass around galactic discs are :

** Stability of such discs against the formation of bars, spiral arms, ... (Ostriker et al., 1974; Berman and Mark, 1979; Sellwood, 1983)

** Excitation of warps in galaxies (Bertin and Casertano. 1982)

** The Oort problem (Oort, 1960) : the discrepancy between the counted density at the sun "that implied by dynamics".

** The orbits of very distant stars supposed belonging to galactic systems (Hawkins, 1983)

** The orbits of satellite galaxies around the Milky Way (Lin and Lynden-Bell, 1977)

** Binary galaxy statistics (Turner, 1976)

** The stability of the Local Group (Kahn and Woltjer, 1959)

** The differential variation of the mass to light ratio with radial distance (Gilmore and Hewett, 1983)

** The flatness of rotation curves at large radial distances.

However, the existence of halos is still open to discussion because, first, same arguments do not apply in all cases, and then there are not enough correlated data showing that the same halo enables to give a correct interpretation of the data concerning same objects.

Of course, the nature of the matter these eventual halos can be made of is also open to discussion; various possibilities have been considered : gas, snowballs, dust and rocks, Jupter-like bodies, low mass stars, dead stars, neutron stars, massive neutrinos, gravitinos, monopoles, ... (discussion in a paper by Hegyi and Olive (1983)).

Hereafter we consider the problem from a dynamical point of view for individual galaxies.

III THE PROBLEM OF VISIBLE MASS AND ROTATION CURVES

The amount of mass can be determined from observational data of two types : the rotation curve and the light curve. Both can be determined for steady-state axisymmetric flat systems. In the case of non axisymmetric systems, except for very irregular systems, bars, spiral arms, rings and other similar systems can be considered as transient perturbations involving a small part of the total amount of matter, superposed on an axisymmetric average state. Then, the rotation curve is that curve which gives the velocity $v(r)$ of any test mass eventually travelling along a circular orbit centered at the center of the galaxy and of radius r in the mean plane of the flat system versus the radial distance r.

The rotation curve can be interpreted directly in terms of the gravitationnal potential ϕ through the gravitationnal acceleration γ since, for circular motion,

$$\gamma = v^2(r)/r$$

Then, if one assumes that the stars move in the gravitationnal potential due to them, γ and ϕ can be interpreted in terms of the mass density ρ using the Poisson equation :

$$\Delta\phi = 4\pi G\rho$$

Comparing the mass density distribution to the light curve one can find the spatial variation of the mass to light ratio.

Until last years, the rotation curve was measured for fairly small radial distances, say a tenth of kiloparsec from the center of the galaxy; it was supposed that these curves should show decreasing tails according to Kepler's law ($v(r) \propto 1/\sqrt{r}$) at larger radial distances since, there the test body was probably submitted to the attraction of a point-like mass (Figs 1 and 2). Theoretical models of curves withe Keplerian tails where fitted to the data (Fig. 2), for instance using formulas like those of Brandt and Scheer (1965).

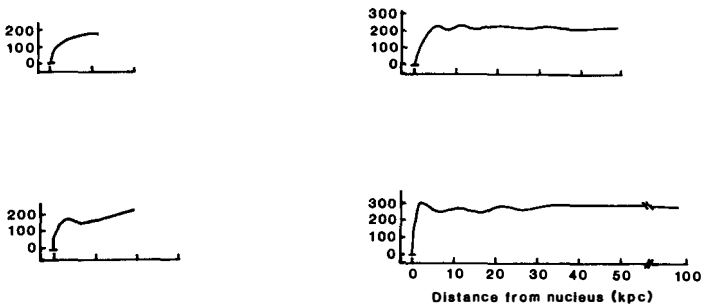
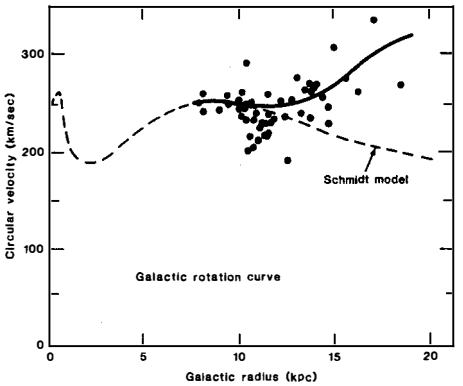


Figure 1. From Rubin, 1983. Rotation curves.



Rotation curve of the Milky Way The filled circles represent data and the solid line a fourth-order least-squares fit to the data. The dashed line is the rotation curve from the Schmidt mass model The Schmidt model fits the rotation curve from the atomic hydrogen data inside the solar circle well, but does not fit the data beyond 12 kpc from the center.

Figure 2
From Blitz et al., 1983

Recent observations show that for much larger radial distances, the rotation curves usually remain flat : the circular velocity does not decrease like $1/\sqrt{r}$ (Figs 1 and 2). This is often interpreted as revealing the presence of a highly massive invisible halo surrounding the flat system and governing its motion. The following discussion is devoted to this question : Are halos necessary and/or sufficient to produce flat rotation curves? We shall see that, contrary to what is too often thought, the rotation curves can be flat both for systems with or without halos (massive or not).

IV PROPERTIES OF SYSTEMS WITH SPHERICAL SYMMETRY

We now investigate the rotation curves of systems with dynamics governed by a mass system with spherical symmetry.

1/ *Point mass*

First consider a point mass M at the center O of the system. In such a system, Newton's law reads

$$\phi(r) = -GM/r \qquad \gamma = -GM/r^2 = v^2/r$$
$$v(r) = \sqrt{(GM/r)} \propto 1/\sqrt{r}$$

This is illustrated by the system of the planets.

2/Spherical mass distribution

Now assume that the mass is distributed in space in such a way that the total mass within a sphere of radius r is m(r). Then, using the Gauss theorem, one finds

$$Gm(r)/r^2 = v^2(r)/r$$
$$v(r) = \sqrt{(Gm(r)/r)} \propto \sqrt{(m(r)/r)}$$

If m(r) tends to some limit m_0 when $r \to \infty$, $v(r) \propto 1/\sqrt{r}$, but, conversely, if the rotation curve remains flat at large distances, $v(r) \simeq$ cst leads to $m(r) \propto r$.

Thus, it is important to notice that, if produced by a massive spherical halo, a flat rotation curve implies a halo with space density decreasing like $1/r^2$ and so an <u>infinite mass</u>.

Remark : A homogeneous halo (constant density) corresponds to a mass within the distance r , m(r), equal to $(4/3)\pi\rho r^3$ (where ρ denotes the constant density) and so to a circular velocity $v(r) = r\sqrt{((4/3)G\pi\rho)} \propto r$, which characterizes a ri-

gid rotation.

V EFFECTS OF FLATTENING

Now let us compare the rotation curves produced by the mass distributed 1/ with spherical symmetry 2/ with axisymmetry in an equatorial plane according to the same law m(r) where m(r) respectively denotes the mass inside a sphere of radius r in the former case and that inside a circle of radius r in the latter case. There is a fundamental difference between these two cases. In the former case the acceleration to which a test star is submitted is equal to

$$\gamma(r) = v^2(r)/r = Gm(r)/r^2$$

so that $v^2(r) = \sqrt{(Gm(r)/r)}$

is a local function of r, whereas in the latter case v(r) depends on the whole mass distribution profile m(r) from r = 0 to r ∞, that is inside and outside the circle of radius r.

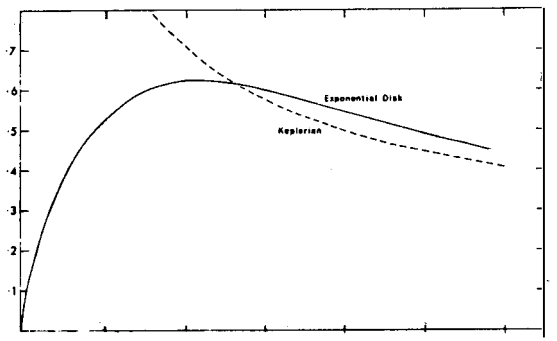
For instance, in the case of an exponential distribution of matter (space density ∝ exp(-r/h), m(r) tends to a limit and v(r) becomes Keplerian as soon as r is of the order of the length scale h, whereas in the case of an exponential disc m(r) tends to a limit at radial distances of the same order but v(r) becomes Keplerian at much larger distances (see Freeman, 1970), since

$$v^2(r) = \frac{1}{2}\left(\frac{r}{h}\right)^2 \{I_o\left(\frac{r}{h}\right)K_o\left(\frac{r}{h}\right) - I_1\left(\frac{r}{h}\right)K_1\left(\frac{r}{h}\right)\}$$

where I_o, K_o, I_1, K_1 denote Bessel's functions. (Fig. 3)

Thus, for a given rotation curve, the ratio of the amount of matter contained contained within a radial distance r in a flat model to that in a spherically symmetric model cannot easily compared to 1. Numerical models are necessary.

Lequeux (1983) has compared the distribution of mass corresponding to simple phenomenological models of rotation curves. He has plotted the ratio Y of the mass m(r) inside a sphere of radius r in some models with rotation curves like those indexed by 1 and 2 on Fig. 4 to that in a spherical model with



Exponential disc : $m(r) \propto \{h^2 - (h^2 + hr)\exp(-\frac{r}{h})\}$

Figure 3 - Rotation curves; from Freeman, 1970

same rotation curves versus the radius a of the which separates the two first linear branches with different slopes (measured in units of the radius R at which the slope of curve 2 changes). Model 1 has a still flat rotation curve at large radial distances whereas model 2 has a Keplerian rotation curve for r > R.

Fig. 4 shows that Y is of course equal to 1 in the case of the spherical model, smaller than 1 in the other cases, and smaller in case 2 than in case 1 for any a/R between 0 and 1.

It follows that flat rotation curves can be obtained for flat systems of smaller mass than spherical systems with same rotation curves.

VI DYNAMICAL EFFECTS OF FLATTENING

Other indications of dynamical effects of flattening have recently been pointed out separately by Tohline and Kalnajs (1983).

Tohline (1983) has shown that using numerical simulations he could obtain flat rotation curves and that "cold discs" (i.e. discs of stars mainly in quasi-circular orbits) can be stabilized against bar or spiral arm formation without dark halos if dynamics is governed by interactions between two bodies

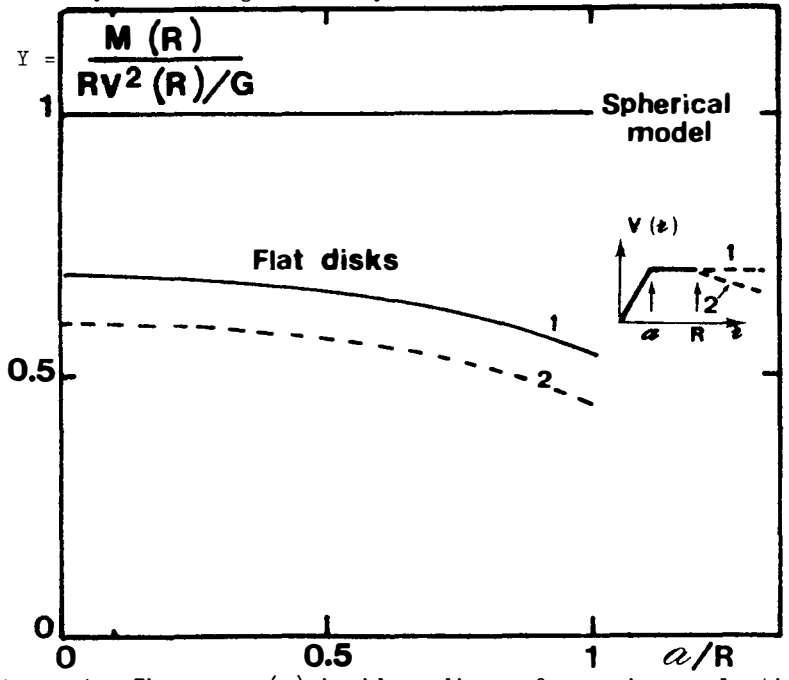


Figure 4 - The mass m(r) inside radius r for various galactic models : spherical model (horizontal line at the top), and flat disk models with rotation curves as defined in the insert Model 2 has a Keplerian rotation curve fo r > R (Lequeux, 1983)

of the form $\frac{Gm_1m_2}{r^2}\{1 + \frac{r}{a}\}$ (where m_1 and m_2 are the masses of the bodies and a is of the order of the kiloparsec), instead of the purely Newtonian interaction law. Typically the correction term is the solution of a two dimensional Poisson equation and describes the attraction between two parallel infinitely long rods.

Kalnajs (1983) could fit data for rotation curves and light curves corresponding to constant mass to light ratios, for three galaxies with only a disk component and for another with a disk and a small bulge component.

Finally, from the results mentioned in Sects V and VI we can conclude that flattening is important for dynamics. Finally, the usual arguments invoked in favor of the presence of massive halos, especially the flatness of the rotation curve at large radial distances are not sufficient and do not enable to decide clearly.

VII DYNAMICALLY SELF CONSISTENT MODELS

Thus, it is necessary to build up dynamically self consistent models in which the potential is that determined by the mass distribution through the Poisson equation and the mass distribution is governed by the motion of each star in the potential determined by all the others.

This can be done using numerical simulation of a large number of individual particles, or, as dicussed hereafter, using a statistical description of the systems based on distribution functions.

The models that will now be considered are concerned with with self consistent, axisymmetric, steady state three dimensionnal though flat star systems. We analyse the possible states : stability is not investigated.

These models are fully dynamical, i. e. each star moves in the potential du to the others and the possible orbits are populated according to distribution functions of the form Yf where *** f is a function with a functional form satisfying conditions expressing physical properties detailed hereafter

*** y is a function equal to 1 if the maximum radial distance reached by a star is lower than some finite radius R determining the space dimension of the system, and equal to 0 in other cases.The length R is a function of the parameters appearing in f. This last condition introduces a smooth and natural cut-off in the distribution function that tends to 0 when $r \to R$.

The first paper of a series devoted to such models appeared in 1976 (Lafon, 1976). The distribution function adopted is a sum of "coarse grain" distribution functions describing "well-mixed" systems i.e. systems for which all continuous smooth functions (mean velocity, mass density, ...) at each point is independent of the "phase" of each star on its orbit but depends only on the population of the orbits reaching this point ((Lafon, 1976; Mello and Brody, 1972; Lynden-Bell, 1967). It can be expressed under the form

$$Yf(\xi,E) = Y \sum_i \alpha_i \exp(a_i E + b_i \xi)$$

with $\xi = rv/\sqrt{(2\varepsilon_o)}$ $\quad E = (u/2\varepsilon_o)^2 + (\xi/r)^2 + (\phi(r)/\varepsilon_o)$

where u, v, $\phi(r)$, ε_o respectively denote the radial and the tengential velocity components, the gravitationnal potential, some energy unit. It is also assumed that this function satisthe following physical conditions, likely, at least as a zero order approximation, as results from observations:

$$f > 0 \qquad \partial f/\partial E < 0 \qquad \partial f/\partial \xi \neq 0$$

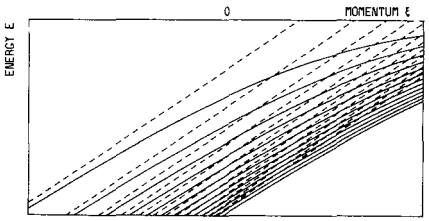
For distribution functions with one term or two terms with opposite signs in the sum, this respectively implies functions of the form (Lafon, 1976) :

$$f(\xi,E) = \alpha \exp(aE + b\xi) \qquad 1$$

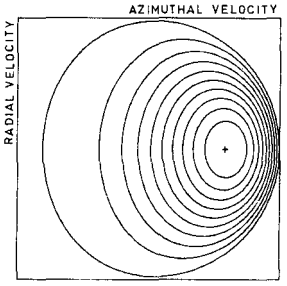
$$f(\xi,E) = \alpha \exp(b\xi)\,(\exp(a_1 E) - \exp(a_2 E)) \qquad 2$$

with $\alpha > 0$, $a < 0$ and $\alpha > 0$, $a_1 < a_2 < 0$ respectively; b was taken arbitrarily positive (changing its sign reverses the rotation of the system).

Iso-f curves corresponding to a function of the latter form are shown on Fig. 5. They look like those derived from observations.



Form of iso-f curves in the ξ, E-plane for distribution functions f



Form of iso-f curves in the u, v-plane for distribution functions f

Figure 5 - Iso-f curves from Lafon, 1976

Numerical models have been constructed for distribution functions of both forms. Typical results are shown on Figs 6 to 17. A special system of units was used used for these curves in order to allow scale changes.

*** Unit of length : arbitrary

*** Unit of potential : B, the potential at the center of the system; $B = \varepsilon_o \phi(0)$

*** Unit of mass : M, that generating a potential equal to B at the distance A; $M = BA/G$

*** Subsequent unit of velocity : v_o, that of a star with kinetic energy per unit mass equal to B; $v_o^2/2 = B$

All the curves correspond to systems with a total mass equal to 1. Parameters for Figs.6 to 9, 10 to 13, 14 to 17 are displayed in tables 1, 2, 3 respectively.

These results point out the following features :

*** The systems are strongly non linear and self-consistent; rotation curves very similar in the inner part are obtained for fairly different distribution functions. The inner part of the rotation curve is also insensitive to the central mass density. Same remark concerning the curve representing the percentage p(r) of the total mass within the circle of radius r. At the same time, the central density is highly sensitive to the parameters a_1, b of the distribution function.

*** The rotation curve is always flat, sometimes uprising at large radial distances, never Keplerian, without massive halo. The flatness seems linked to the smoothness of the decrease of the distribution function close to the edge of the system. The non Keplerian behaviour appears as an effect of the non circular, highly elliptic with very small ξ reaching large radial distances , which are always present and should never be neglected in the outer parts of the system : less populated non circular orbits leads to smaller circular rotation velocities.

*** This is consistent with a steep density decrease in the outer parts of the system.

Table 1 - Data for Figs 6 to 9 Lafon, 1976

Figure	Curve	a	b	Radius	Total Mass
	1	−5	3.764	1.049	1
	2	−5	3.852	1.304	1
	3	−5	3.814	1.547	1
	4	−5	3.680	1.804	1
	5	−5	3.426	2.055	1
	6	−5	2.850	2.410	1
	7	−5	1.252	2.893	1
	dashed	−5 Ng	2.850	2.397	1
	crosses	−5 Ng	2.850	3.	1.25

Table 2 - Data for Figs 10 to 13 Lafon, 1976

Figure	Curve	a_1	a_2	b	Radius	Total Mass
	1	−3	−0.5	3.868	1.203	1
	2	−3	−0.5	3.808	1.337	1
	3	−3	−0.5	3.205	1.976	1
	4	−3	−1.	4.	1.698	1
	5	−3	−1.	3.617	2.159	1

Table 3 - Data for Figs 14 to 17 Lafon, 1976

Figure	Curve	a_1	a_2	b	Radius	Total Mass
	1	−4	−0.5	4.338	2.789	1
	2	−4	−0.5	4.	3.220	1
	3	−4	−1	4.703	2.884	1
	4	−4	−1	4.127	3.704	1
	5	−4	−1	4.	3.826	1

VIII CONCLUSION

To summerize, observationnal data such as rotation curves and light curves cannot be interpreted in terms of stellar dynamics and galactic structure in a simple direct way : the "inversion problem" is complicated and must be investigated cautiously. In particular, fairly different stellar systems can correspond to curves with very similar arcs.

Then, though the presence of a (massive or not) dark halo cannot be excluded a priori, it is not possible to infer this presence from the only topology (flatness) of the rotation curve.

Additionnal models fitting observationnal data both with rotation curves and light curves related in a self consistent dynamical way are necessary in each particular case. Such models are being investigated now.

ooooo ooooo ooooo

REFERENCES

BERMANN R.H., MARK J.W.-K., Astron. Astrophys., 77, 1979, 31
BERTIN G., CASERTANO S., Astron. Astrophys., 106, 1982, 274
BLITZ L., FICH M., KULKARNI S., Science, 220, 1983, 1233
BRANDT J.C., SCHEER L.S., Astron. J., 70, 1965, 471
FREEMAN K.C., Astrophys. J., 60, 1970, 811
GILMORE G., HEWETT P., Nature, 306, 1983, 669
HAWKINS M.R.S., Nature, 303, 1983, 406
HEGYI J., OLIVE K.A., Phys. Letters, 126B, 1983, 28
KAHN F.D., WOLTJER L., Astrophys. J., 130, 1959, 705
KALNAJS A.J., IAU Symp. 100, Internal kinematics and dynamics of galaxies, E. Athanassoula ed., D. Reidel, 1983, 87
LAFON J.-P.J., Astron. Astrophys., 46, 1976, 461
LEQUEUX J., Astron. Astrophys., 1983 (preprint)
LIN D.N.C., LYNDEN-BELL D., Month. Not. Roy. Astr. Soc., 181, 1977, 59
LYNDEN-BELL D., Month. Not. Roy. Astr. Soc., 136, 1967, 101
MELLO P.A., BRODY T.A., Amer. J. Phys., 40, 1972, 1239
OORT J., Bull. Astron. Inst. Neth., 15, 1960, 45

OSTRIKER J.P., PEEBLES P.J.E., Astrophys., 186, 1973, 467
RUBIN V.C., Science, 220, 1983, 1339
SELLWOOD J., The origin and evolution of galaxies, B.J.T. Jones and J.E. Jones ed., D. Reidel, 1983, 247
TOHLINE J.E., IAU Symp. 100, Internal kinematics and dynamics of galaxies, E. Athanassoula ed., D. Reidel, 1983, 205
TURNER, Astrophys. J., 208, 1976, 304

oooooooooooooooo

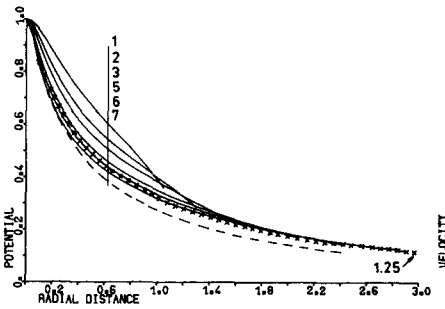


Figure 6

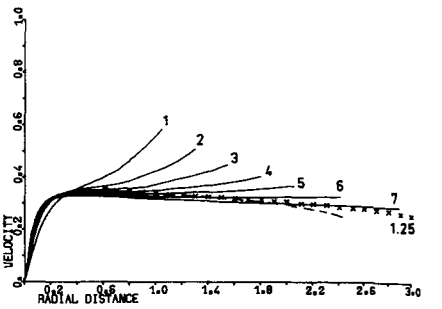


Figure 8

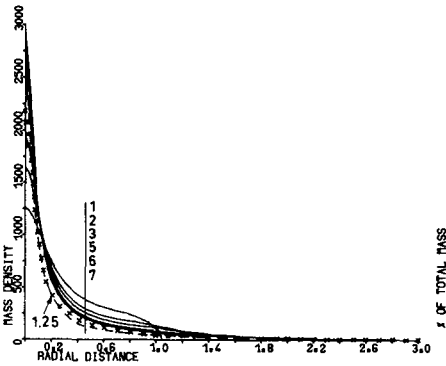


Figure 7

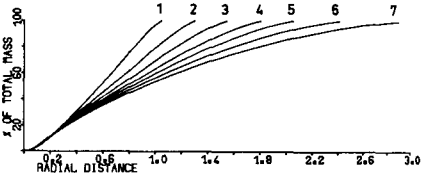


Figure 9

6 Potential versus radial distance for models based on distribution functions of the form 1 using the data given in Table 1 The dashed lines correspond to Ng's (1967) results for models with total mass equal to 1. The crosses correspond to Ng's model with mass 1.25

7 Surface density versus radial distance for models based on distribution functions of the form 1 using the data given in Table 1 The dashed lines correspond to Ng's (1967) results for models with total mass equal to 1. The crosses correspond to Ng's model with mass 1.25

8 Rotation curves for models based on distribution functions of the form 1 using the data given in Table 1 The dashed lines correspond to Ng's (1967) results for models with total mass equal to 1. The crosses correspond to Ng's model with mass 1.25

9 Percentage of total mass within a circle of radius r as a function of r for models based on distribution functions of the form 1 using the data given in Table 1 The dashed lines correspond to Ng's (1967) results for models with total mass equal to 1. The crosses correspond to Ng's model with mass 1.25

Note : NG E.W., Astrophys. J.,150, 1967, 787

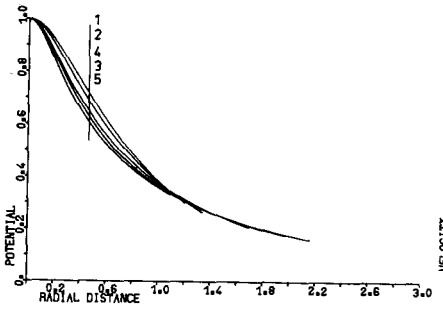


Figure 10

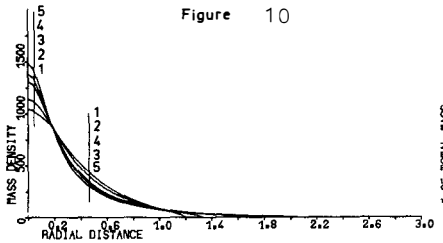


Figure 11

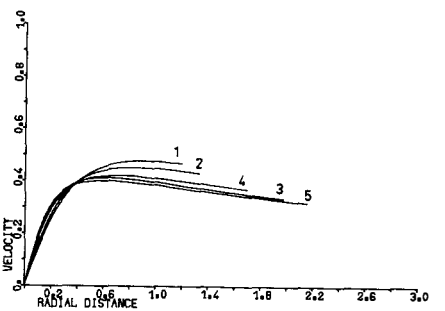


Figure 12

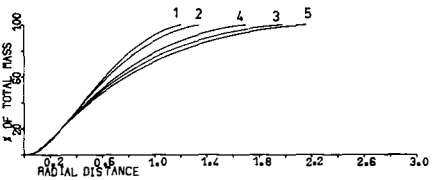


Figure 13

10 Potential versus radial distance for models based on distribution functions of the form 2 using the data given in Table 2

11 Surface density versus radial distance for models based on distribution functions of the form 2 using the data given in Table 2

12 Rotation curves for models based on distribution functions of the form 2 using the data given in Table 2

13 Percentage of total mass within a circle of radius r as a function of r for models based on distribution functions of the form 2 using the data given in Table 2

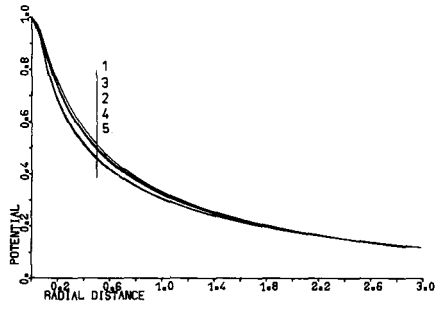


Figure 14

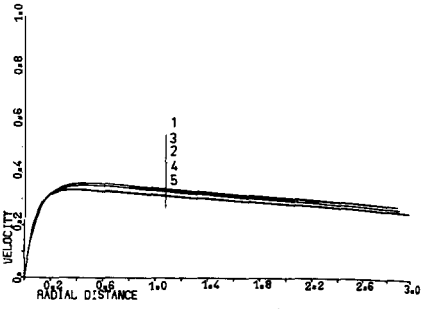


Figure 16

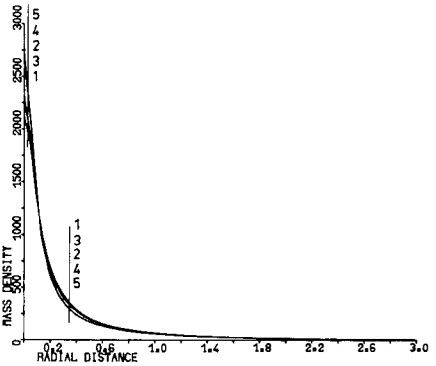


Figure 15

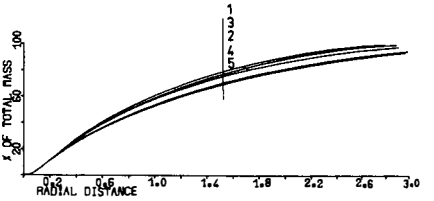


Figure 17

14 Potential versus radial distance for models based on distribution functions of the form 2 using the data given in Table 3

15 Surface density versus radial distance for models based on distribution functions of the form 2 using the data given in Table 3

16 Rotation curves for models based on distribution functions of the form 2 using the data given in Table 3

17 Percentage of total mass within a circle of radius r as a function of r for models based on distribution functions of the form 2 using the data given in Table 3

THE INTERNAL STRUCTURE OF THE SUN AND THE SOLAR NEUTRINOS PROBLEM

E. SCHATZMAN

Observatoire de Nice - BP 139 - 06003 NICE CEDEX



ABSTRACT

The observed neutrino flux (Davis experiment) is known to be too small by a factor 3 to 4 compared to the predicted flux.

Here is given a review of the physical processes which determine the properties of the solar model : equation of state, absorption coefficient, nuclear cross-section, thermonuclear reaction rate, convection. Standard models give a solar neutrino flux around 7.6 S.N.U. (Solar neutrino Units = 10^{-36} reaction $atom^{-1}$ sec^{-1}). Non-standard models are briefly discussed.

Stellar rotation generates meridional circulation and differential rotation which themselves produce shear flow instabilities. This suggest the presence of a mild turbulence and mixing by turbulent diffusion. Astrophysical confirmation of turbulent diffusion mixing is given. Turbulent diffusion mixing can explain the neutrino deficiency by a change of chemical composition of the central regions of the sun.

Solar sismology, surface abundance ratio and neutrino deficiency suggest a strongly radius-dependent coefficient of turbulent diffusion. The measure of the neutrino flux appeared then as one of the key of solar structure.

1. INTRODUCTION

1.1 - Purpose of the paper

It is intended to give here a self consistent presentation of the relation between the internal structure of the sun and the solar neutrinos problem. It means that except for the most technical questions, the careful reader would hopefully get the understanding of the basic physics of the problem.

There are now several books and review papers available on the market, to which we shall refer in due time. However, they are not always easily readable for a physicist who is unaware of the problems which worry the astrophysicist, or who ignores the usual astrophysicist's slang. The only way of remaining understandable is to always come back to the basic physics, which represents the commun background of physicists and astrophysicits.

1.2 - The basic physics

The sun is very slowly rotating. At the equator, the ratio of the centrifugal force to gravity

$$\chi = \frac{GM}{R^2} \cdot \omega^2 R \simeq 1.87 \cdot 10^{-5}$$

is very small, and the shape of the sun is very close to sphericity. The effect of rotation is to generate very small departures from the sphere. As a first and very good approximation, the sun can be considered as spherically symmetric.

As a consequence, the sun can be described to a high degree of approximation with only two variables, radius and time, every physical quantity being a function of r and t.

The equations which describe the standard model of the structure and evolution of the sun are the classical macroscopic equations of conservation :

(1) conservation of mass (and chemical elements),

(2) conservation of momentum,

(3) conservation of energy.

to which we add the equation of state $P = P(\rho,T,X,Y,Z...)$ where X,Y,Z... symbolizes the chemical composition*, the chemical conductivity $\Lambda(\rho, T, X.Y.Z...)$ which includes mainly the radiative transfer, the molecular heat transfer being

*) In astrophysical slang, X.Y.Z represents respectively the concentration, in weight, of hydrogen, helium and other elements. Z refers to a standard chemical composition of the most abundant element from Carbon to Iron.

negligible with respect to the radiative transfer, the rate of energy production by thermonuclear reactions, including the neutrino energy losses. We shall come back later to the question of the validity of this various functions.

Due to the very slow evolution of the sun from its formation up to the present time, a number of simplifications, due to proper scaling, are obvious.

Respectively :

(1) The conservation of mass and chemical elements can be respectively restricted to the effect of mass loss (through the conversion into radiated energy), and to the effect of the balance between element formation and element destruction through nuclear reactions.

(2) Conservation of momentum can ignore the inertial term, and the viscous force : we are then left with the equation of hydrostatic equilibrium.

(3) Conservation of energy includes naturally the energy production through thermonuclear reactions, but it must include also a small term which represents the gravitationnal energy gains or losses which are due to the slow structural changes of the sun. We thus have for the energy balance of the sun the local expression :

$$\text{div } F = - T \frac{\partial S}{\partial T} - \sum_i \mu_i \frac{\partial}{\partial t} \frac{n_i}{\rho}$$

where F is the energy flux per unit surface, S the entropy per unit of mass, μ_i and (n_i/ρ) respectively the chemical potential and the number per unit of mass of the i^{th} kind of particles, and the summation is extended over all relevant kinds of particles.

1.3 - Local physical quantities

Equation of state. It seems quite reasonable, at first look, to accept the relation

$$P = \frac{k\rho T}{\mu} + \frac{1}{3} a T^4 = P_G + P_R$$

which express the fact that the pressure is the sum of the perfect gas pressure and of the radiation pressure. In the solar conditions,

$$\frac{P_R}{P_G + P_R} \equiv 5.10^{-4}.$$

However, it turns out that for the purpose of precise studies of the solar interior, it is necessary to take into account several corrections. According to

Ulrich (1982) the following corrections lead to appreciable differences in the solar models :

(1) The most obvious correction is due to the Coulomb interaction between ions and electrons. This leads to the well known Debye - Hückel modification to the pressure. The Debye - Hückel modification is small, and $(-\delta P_c/P) \simeq 0.03$.

(2) It is well known that partition functions of bound states diverge if the higher terms are not eliminated. This can be achieved by including the effect of "pressure ionization". This can be easily introduced by a proper description of the motion of the electrons in the neighborhood of an ion. The free electrons are not described by plane waves, but rather are described by scattering states. As pointed by Larkin (1960) the difficulty of the treatment of the high temperature bound states is largely eliminated by the effect of the scattering states. Scattering states compensate for the bound states and are treated in lowest order by a general replacement of factors of the form

$$\exp \frac{E}{kT}$$

by

$$\exp \frac{E}{kT} \quad - 1 - \frac{E}{kT}$$

where $E > 0$ is the binding energy of a state. Further more, according to Ebeling (1974) it is necessary to use for the binding energies E the screened energies, which take into account the effect of the screening of the Coulomb potential by the distributions of spaces charges ;

(3) The change of pressure which would have been brought by the bound states is replaced by the effect of the scattering states. Ulrich (1982) gives the contribution to the second virial coefficient of the scattering states, (P_{sc}/P) is of the order several 10^{-3}.

Absorption coefficient. The energy transport is governed in most of the interior of the sun by the radiative transport. The molecular conductivity is completely negligible compared to the radiative transport of heat.

The series of improvements in the theory of radiative transport is a long story. The present situation is not fully satisfactory. We shall mention here only the major difficulties :

a) The numerical code must deal with a chemical composition with a large number of elements. The largest is the number of photoionization which is included, the larger is the blocking of radiation (10 elements in the Livermore code, 20 elements in the Los Alamos code).

b) The computation must include all possible ionization stages of the atoms and all singly and multiply excited states for each ion.

c) The computation of the photoelectric cross section has to take into account the fact that the ions are not isolated, but are imbedded into a plasma. A comparison has been carried by Bahcall et al. of the different treatment of the problem (Hartree-Fock, Thomas - Fermi). It is necessary also to use non-hydrogenic photoelectric cross sections, to deal correctly with the line wings, and include a large number of weak absorptions lines.

d) A correction has to be included, due to collective effects, to the Thomson scattering cross section. Cross section for photon scattering is decreased by about 35 %.

Nuclear Cross sections. The basic quantity of interest for all the nuclear reactions of interest, is the low-energy cross-section factor S(E) defined by

$$S(E) = \sigma(E)\ E \exp\ (2\pi\ Z_1\ Z_2\ e^2 / \hbar\ v)$$

where $\sigma(E)$ is the cross section at the center-of-mass energy E ; $\exp(-2\pi Z_1 Z_2 e^2/\hbar v)$ represent the tunnel effect, and in the product $\sigma(E)\ \exp(2\pi\ Z_1 Z_2 e^2/\hbar v)$ the exponential compensates for the quick decrease of the cross section $\sigma(E)$ when v (or E) decreases. Similarly, the E term compensates for the decrease of the cross section like $\pi\ \lambda^2 \sim E^{-1}$. The factor S(E) is a slowly varying functions of the energy which includes only the effects of nuclear structure and details in the shape of the potential barrier.

Bahcall et al. (1982) give a detailed description of the present situation concerning the determination of S(E) for the various reactions which are involved. The table (table I) is a reminder of the major properties of these reactions.

The cross sections have been measured, or can be derived directly from measurements, except for the p - p reaction.

$$(1)\ p + p \rightarrow {}^2H + e^+ + \nu_e$$

The largest uncertainty comes from the value of the neutron half-life (about 10 %) ; next comes the uncertainty in the nuclear matrix element, and the uncertainty from the imperfectly known corrections for mesonic exchanges. Bahcall et al. (1982) give

$$S_{p-p}(E = 0) = 3.88(1 \pm 0.09)10^{-25}\ \text{Mev} \times \text{barns}$$

A slight connection for $E \neq 0$ has to be applied, which comes from the slow variation, $(dS/dE) \neq 0$.

(2) $p + e^- + p \rightarrow {}^2H + \nu_e$

The rate for pep is proportionnal to the rate of the basic p - p reaction. Bahcall and May (1969) have given a satisfactory approximation for the ratio of the rates R(pep)/R(pp).

(3) ${}^2H + p \rightarrow {}^3He + \gamma$

The cross section for this reaction has been measured (see Bahcall et al. 1982 for reference),

$S_{12}(0) = (2.5 \pm 0.4)10^{-4}$ KeV b.

The value of S_{12} is finally unimportant, as all ${}^2H$ is immediately converted into ${}^3He$.

(4) ${}^3He + {}^3He \rightarrow {}^4He + 2p$

This reaction is the dominant way of terminating the proton-proton chain in the sun. It has been considered simultaneously for the first time by Fowler (1951) and by Schatzman (1951). The low-energy cross section has been measured accurately in an energy range from about 1.3 MeV to 33 KeV (Bahcall et al. 1982 for references). With :

$S(E) = S(0) + S_1(0)E + S_2(0)E^2$

Bahcall et al. (1982) give

$S(0) = 4.7(1 \pm 0.17)$ MeV b

$S_1(0) = -0.9$

$S_2(0) = 0.1$

(5) ${}^3He + {}^4He \rightarrow {}^7Be + \gamma$

The result of the Caltech and Münster groups (see Bahcall et al. 1982) are not consistant with each other. Bahcall et al. adopt

$S_{34}(0) = 0.52 \pm 0.15$ KeV b

whereas the Münster group gives $S_{34}(0) = 0.30 \pm 0.03$ KeV b.

The main discussion rests on the value of the slope $S^{-1}dS/dE \simeq -0{,}50$ MeV^{-1}. If the curve S(E) is flat, its extrapolation to E = 0 leads to the results of the Münster groups. The direct-capture- model calculation and Caltech measurements seem to agree with the above mentionned value of the slope, thus confirming the Caltech S(0) cross-section.

The value of $S_{34}(0)$ is important as the formation of ${}^7Be$ is the key of the door to the neutrinos detected in the Davis experiment.

(6) $e^- + {}^7B_e \rightarrow {}^7li + \nu_e$

The rate at which B_e captures an electron in a stellar interior is fairly well known.

(7) $p + {}^7B_e \rightarrow {}^8B + \gamma$

This is the major reaction leading to the production of the neutrinos actually detected by the Davis experiment. The extrapolation to E = 0 of the curve S(E) nead a reliable theory. The direct capture model suggests a slow rise of the cross section for E < 100 KeV. This leads to

$$S_{17}(0) = 0.029 \pm 0.010 \text{ KeV b}$$

$$\frac{dS_{17}}{dE}(0) = -3.10^{-5} \text{ b}$$

Thermonuclear reaction rates.

The major contribution for a non-resonant reaction comes from the peak of the exponential

$$\exp\left[-\frac{2MZ_1Z_2e^2}{\hbar(2E/m)^{1/3}} - \frac{E}{kT}\right]$$

The first term comes from the cross section, the second term from the Maxwell distribution function. The integral $S\sigma(E)\nu_{12}\, f(E)dE$ can be approximated near the maximum by a gaussian. The leading term is usually written exp(-τ), with

$$\tau = \left(\frac{27\pi^2 Z_1^2 Z_2^2 e^4 m}{2\hbar^2 kT}\right)^{1/3}$$

A correction has to be included, which takes into account the modification of the electrostatic potential by the plasma itself. For weakly correlated plasmas, the correction, found by Salpeter (1954) is

$$\exp \frac{Z_1 Z_2 e^2 \chi_D}{kT}$$

where χ_D^{-1} is the Debye length for the plasma. The screening factor for the pp reaction in the center of the sun is exp(0.015). For the helium reactions, it is exp(0.060). The increased rate factors are included in all the calculations.

2. MODEL COMPUTATION

The procedure is always the same. Due to the fact that an evolutionnary model loses quickly the memory of the initial conditions, the method consists

in starting at t = 0 with an homogeneous model in hydrostatic equilibrium. The equations are then

- equation of hydrostatic equilibrium,
- equation of radiative transfer,
- equation of energy balance.

The physical quantities which are involved in these three equations are respectively

- the equation of state,
- the absorption coefficient,
- the thermonuclear reaction rate.

A slight difficulty comes from the existence of a Rayleigh-Benard instability in the outer layers. In this region, the heat transfer takes place through radiative and convective transfer. Convective transport in compressible fluids (in the solar convection zone, the density varies from bottom to top by a factor of the order of 1000) is still dealt with in a phenomenological way. It uses mainly a phenomenological parameter $\alpha = (\ell/H_p)$ which describes the efficiency of turbulent transport in a highly turbulent region. H_p is the pressure scale height, $-(dz/d \log P) \equiv H_p$, and ℓ is the "mixing length", using the phenomenological terminology of Prandtl. The sensitivity of the model, and especially of the central regions, to the phenomenological parameter α is small. However, we shall see that when we look for a complete consistency of the solar model the depth of the convective zone has a significant importance and then depends on the value of α. The properties of the surface pressure modes of oscillation are also influenced by the properties of the surface convective zone.

Technically, the procedure follows an explicit code. The structure at a step $t + \Delta t$ is supposed to differ very little from the structure at the preceding step t. The change in structure defines the amount of gravitationnal energy which is available. The assumption that the difference in structure is small allows a linearization of the equations. The sphere being divided in a number of mesh points, the internal structure is obtained at each step by the inversion of a matrix, the boundary conditions defining the solution.

The problem is to obtain at $t = 4.6.10^9$ years, for a mass of $1.989.10^{33}$ g a star with a luminosity $L = 3.86.10^{33}$ ergs sec^{-1} cm and a radius $6.9598.10^{-10}$ cm. Three parameters are available, when considering standard models : the Helium content Y (in weight), the heavy elements content Z (in weight) and the phenomenological parameter α which describes the efficiency of turbulent transport in the convective zone.

Table 1

Nuclear reactions of the hydrogen cycle

Reactions	Q (MeV)	Maximum energy of the neutrinos (MeV)	Branching ratio (%)
$^1H + {}^1H \rightarrow {}^2H + e^+ + \nu$	1.442	0.42	
$^1H + {}^1H + e^- \rightarrow {}^2H + \nu$	2.464	1.44 a)	
$^2H + {}^1H \rightarrow {}^3He + \gamma$	5.493		
$^3He + {}^3He \rightarrow {}^4He + 2^1H$	12.859		
or			
$^3He + {}^4He \rightarrow {}^7Be + \gamma$	1.587		
$^7Be + e^- \rightarrow {}^7Li + \nu$	0.860	0.860	90
$^7Li + {}^1H \rightarrow 2^4He$	17.346	0.383	10
or			
$^7Be + {}^1H \rightarrow {}^8B + \gamma$	0.133		
$^8B \rightarrow {}^8Be^* + e^+ + \nu$	17.980	14.06	
$^8Be^* \rightarrow 2^4He$			

a) Monokinetic.

Table 2

A typical solar model (Bahcall et al , 1982)

Contribution to the luminosity : pp cycle 0.985
CNO cycle 0.015

Hydrogen convective zone (bottom) : radius 0.73 R_{Sun}
temperature $2 . 10^6$ °K
density 0.15 g cm^{-3}

Center : temperature $15.5 .10^6$ °K
density 156.3 g cm^{-3}

neutrino flux (Cl experiment) , predicted : 7.6 (1 ± 0.43) SNU
observed : 2.2 ± 0.4

With these three parameters and two constraints (L, R), a full range of stellar models can be obtained (fig. 1), but the neutrino flux constraint leads to a large anomaly in the chemical composition (Iben 1969, Abraham Iben, 1971, Bahcall-Ulrich, 1971, Christensen Dalgaard, Gough and Morgan, 1979). As an example, we give the characteristics of the standard model calculated by Bahcall et al. (1982) (Table II). It should be noticed, however that the predicted range of values of the detectable neutrino flux, even for standard models, is very large, and depends appreciably from the physical input.

For the Davis experiment, Bahcall et al. (1982) give for the predicted rate, with the standard S_{34} cross sections, with a 3σ confidence :

$$\phi_\nu(^{37}\mathrm{Cl}) = 7.6 \text{ SNU}(1 \pm 0.43)$$

If the Münster value of S_{34} is taken,

$$\phi_\nu(^{37}\mathrm{Cl}) = 4.9 \text{ SSNU}(1 \pm 0.42)$$

It is necessary here, to explain briefly the notion of the self-regulation which takes place inside the sun. The situation is the following :

The central pressure of the sun depends very little on its structure, therefore

$$\rho\, T \simeq \text{const.}$$

The luminosity of the sun depends on the rates of the various reactions which are involved. In the neighborhood of $T = 15.10^6$ °K, it is possible to write

$$L \simeq W_1\, X_1^2\, \rho\, T^4 + W_2\, X_1\, X_4\, \rho\, T^7 \qquad (1)$$

where the exponents 4 and 7 are simply the result of applying an interpolation formula. W_1 and W_2 include both the rate of the reactions and the energy available in each reaction. When changing W_2 into $0.6\, W_2$ (from the Caltech value to the Münster value) this implies a raise in the temperature, of about 0.6 %. The ^8B neutrino flux grows in the same temperature range like T^{20},

$$\phi\,(^8\mathrm{Be}) \sim T^{20}. \qquad (2)$$

With the Münster cross section, the change in the neutrino flux is the combination of two factors, the decrease in the cross section, by a factor 0.576, and an increase due to the adjustment of the temperature, by a factor 1.131, which corresponds to the slight increase in temperature mentionned above and hence, the reduction of the neutrino by only a factor 0.65.

3. NON STANDARD MODELS

As can be seen from eqn. 2, the reduction of the predicted neutrino flux can be obtained by a model in which the central temperature is lower.

This can be obtained in several ways, leading to a variety of non-standard models of the internal structure of the sun. However, the assumptions which are at the basis of each of these models raise a number of difficulties which makes them more or less unacceptable.

3.1 - Mixed models

During the evolution of the sun, the central regions, burning their hydrogen, become helium rich. The decrease in the concentration of available fuel is compensated by an increase in temperature, which is further enhanced by a luminosity increase due mainly to the change of the absorption coefficient due it self to the increase in the Helium concentration.

It is possible to avoid, at least partly, this temperature increase, by assuming that a certain mass fraction $m = qm_\odot$ is fully mixed and remains fully mixed during the evolution of the sun. This kind of solution has been considered by several authors. Ezer and Cameron (1968), assuming a sun mixed at 95 % obtained a reduction of the neutrino flux by a factor 5 ; Shaviv and Beaudet (1968) noticed that Ezer and Cameron did not use the proper luminosity of the actual sun and, after corrections found, for a fully mixed sun a reduction of the neutrino flux by a factor 2.5. Immediately after, Bahcall et al. (1968) showed that a 95 % mixed sun has a neutrino flux reduced by about a factor 4.

There are several difficulties with these models. For example, Shaviv and Salpeter assumed that the ^3He concentration has its local equilibrium value, the mixing time being longer than the equilibrium time of ^3He. This assumptions ignores the fact that in the outer regions, $m_s > 0.6$, ^3He is being built up and not destroyed.

It should be noticed that there is no physical indication that the sun can be fully mixed. The meridional circulation due to rotation has a characteristic time of the order of

$$\tau \simeq \frac{1}{\chi} \tau_{KH} \simeq \frac{1}{\chi} \frac{Gm^2}{LR} \simeq 2.10^{12} \text{ years}$$

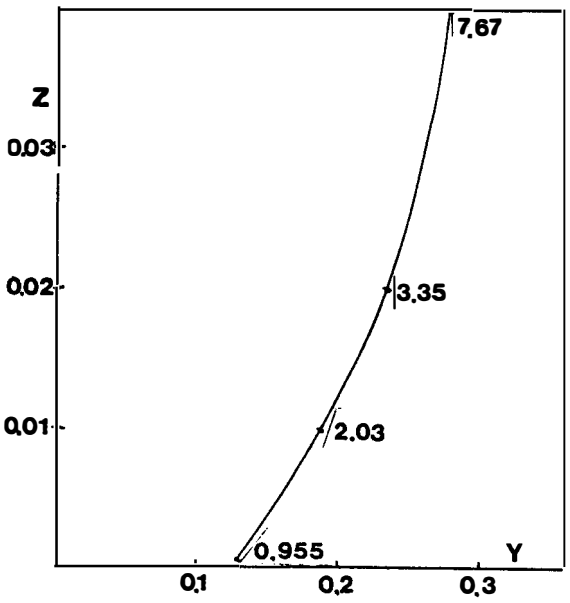
where the Kelvin-Helmotz time scale compares the luminosity of the sun to its internal gravitationnal energy. Mixing prevents a star of evolving towards the giant branch and therefore mixing must stop some time.

Spin-down mixing has been considered by Ezer and Cameron (1968). Spin-down of stars, due to loss of angular momentum (Schatzman, 1962) is a well established fact (Kraft, 1967). Considering the discussion carried by Iben (1968, 1969), it is quite clear that spin-down mixing cannot generate such a kind of homogeneous mixing over a large fraction of the sun. This would produce a number of abundance anomalies (excess of ^{13}C dredged up from the central regions of the sun, equal destruction of berylium and Lithium through passage at the fast burning layer) which are not observed.

Mixing can take place, but in a more subtle way, and this will be consider later.

3.2 - Low Z model

Assuming a low concentration Z of heavy elements and a low concentration of helium leads to an acceptable model, as far as the neutrino flux is concerned. This has been considered by Iben (1969) (see fig. 1), Joss (1974), Christansen-Dalsgaard (1979) and by Christansen-Dalsgaard and Gough (1980). However, such a low Z contradicts the spectroscopic observations at the surface of the sun. The possibility that the atmosphere abundances of heavy elements can be different from the internal abundances has been discussed by Michaud (1977) on the ground that microscopic diffusion induced by gravitationnal drag would carry the heavy elements inside the sun in a time scale which is incompatible with an realistic rate of accretion.



3.3 - Large magnetic field model

The possibility that the pressure of a large magnetic field in the central regions of the sun would reduce the predicted neutrino flux has been considered by Iben (1969) and then by many other authors, Bahcall and Ulrich (1971) Chitre, Ezer and Stothers (1973), Bartenwerfer (1973), Ulrich (1974). The point is that a contribution of the magnetic pressure, $(B^2/8\pi)$, to the total pressure, would allow a lower gas pressure and hence a lower central temperature.

Iben considered the effect of a magnetic field of 10^9 gauss in the center, decreasing outwards like $\rho^{2/3}$, so that the ratio of the magnetic pressure to the gas pressure is roughly constant. The effect on the neutrino flux is small, due to the self-adjustment of the sun on radiative transfer and energy generation.

The effect of the magnetic fields is more subtle than its would seem from such an elementary argument, which implies in fact the presence of a random field. Bachcall and Ulrich (1971) have considered the case of a slowly decaying magnetic field, according to the model of Cowling (1945), with as a surface boundary condition, a dipole field. Including the magnetic pressure as $\underline{j} \times \underline{B}$, with a central magnetic field $B_o = 3.18^8$ gauss. Ulrich and Rhodes (1983) obtain a reduction of the neutrino flux by 30 %. The questions of the stability of such a magnetic field and of its extension are open.

A tangled magnetic field, as considered by Chitre et al. (1973) and by Bartenwerfer (1973) is unstable, due to buoyaucy forces, as shown by Parker (1974, 1979), with a time scale of the order of 10^8 years.

3.4 - High turbulence

The presence of a high level of turbulence, with $\frac{1}{3}\rho v^2$ of the order of a few percent of the gas pressure is highly speculative. The decay of such a turbulence has a time scale which is comparable to $(\ell/v_{th}) \simeq 1$ hour, and need a very powerful driving mechanism in order to maintain it. This can be considered as a very highly speculative hypothesis.

3.5 - Fast rotating case

Dicke (1967) derived from his observations of the solar oblatness that the central regions of the sun have a period of rotation of the order of 1.6 days (16 - 17 faster than the surface rotation). His interpretation (1967) is that the microscopic viscosity is so small that the fast rotating case is uncoupled to the outer part of the sun. This statement has been critized on observationnal and theoretical grounds. Observations by Hill (1975) have not confirmed the re-

sult of Dicke, and the discussion on instabilities and transfer of vorticity shows that the presence of turbulent viscosity allows an efficient transfer of vorticity (see, for example Bretherton and Spiegel, 1968).

As far as the neutrino problem is concerned, a period of rotation of 10^5 seconds in the central region supplies a fraction of the pressure of the order of only 10^{-5} ans is not sufficient to have any appreciable effect on the neutrino flux. Any large velocity of rotation is excluded on observationnal grounds.

4. TURBULENT DIFFUSION MIXING

The problem of turbulent diffusion mixing is considered here under a different paragraph, as it is the result of a consistent physical assumption concernong the effect of the instabilities associated with meridional circulation and differential rotation generated by the solar rotation ; the model is supposed to be valid in all stars, and it leads to various consequences which can be tested observationnally. It is based on the physics of fluids and is by no means and ad hoc assumption.

According to Zahn (1983 a,b), the differential rotation can generate a 2D turbulence if the angular velocity of the rotating star is larger than a critical value, which is determined by the Reynolds condition

$$\frac{\ell \Delta v}{\nu} > R_e$$

where R_e is the critical Reynolds number, and Δv the differential velocity over a distance ℓ on an equipotential surface. This can be written

$$\Omega^2 \geqslant (g^2/2c^2)\left(\nu_{Rad}/(\nu_{mol} + \nu_{Rad})\right) R_e(\nabla_{ad} - \nabla_{Rad})$$

with $R_e \simeq 1000$ and $\nabla = (\mathrm{DlogT/dlogP})$. This provides in the case of the sun the condition

$$P_{crit} \leqslant 30 \text{ days}$$

According to the experiments carried by Hopfinger et al. (1982), the 2-D turbulence decays into a 3-D turbulence for the large wave numbers, as soon as the inertial force exceed the Cariolis force. This provides a turbulent diffusion coefficient

$$D = Re^* \nu$$

where Re^* is appreciably smaller than the critical Reynolds number, because the 3-D turbulence is present only in the tail of the turbulence spectrum. Assuming that the distribution of the angular velocity Ω^2 is given by the condition of

marginal stability, as described by Knobloch and Spruit (1983) this gives

$$Re^{*} \cong 8 \frac{r}{H_p}$$

where H_p = (dr/dlog P) is the pressure scale height.

This approximation is certainly not valid in the central regions, where the conditions for applying the local stability criteria are not fullfilled. Other effects, like pseudo-stochastic motions, can take over the turbulence, and generate mixing in the central regions.

The tests of turbulent diffusion mixing are the following

(a) surface abundance of nuclearly processed elements. In the case of the sun, it concerns , going inwards, ^{7}Li, ^{9}Be, ^{3}He ;

(b) solar neutrino flux

(c) solar sismology data : pressure modes (in the 5 minutes range) and gravity modes (in the 360-160 min range).

We shall consider now each of these tests.

4.1 - Nuclearly processed elements

A short description of the standard solar structure is needed, before describing the effect of turbulent diffusion mixing on the surface abundance of nuclearly processed elements.

The very outer layer of the sun are in radiative equilibrium. At a depth of about 300 km begins a convective zone (Rayleigh Benard instabilty) which extends to a depth of about 200 000 km. From the bottom of the convective zone, to the center, the sun is radiatively stable. The motions of the convective zone extend slightly in the radiatively stable region. This is called "penetrative convection". These motions are not very important as far as the structure of the sun is concerned, but are important as far as mixing is concerned.

The amplitude of the motions due to the penetrative convection decreases very quickly downwards, and, in fact do not penetrate below a finite distance. This defines a fully mixed region, where the time scale of complete mixing is of the order 10 days. The location of the bottom of the fully mixed region is not known with a great certainty ; however, the properties of the pressure modes give some indication on the depth of the convective zone (see below).

The fully mixed region is chemically homogeneous. Transport of elements away

from the convective zone or towards the convective zone generates changes in the chemical abundances which involve the diffusion coefficient and the distance between the region of nuclear processing and the bottom of the convective zone.

Lithium burning. The solar lithium deficiency is not an isolated case, and the discussion of the lithium depletion in the sun has to be compatible with other evidences of lithium burning.

We have to consider the following equation :

$$\rho \frac{\partial X_7}{\partial t} = \text{div } (\rho \text{ D grad } X_7) - K_{17} X_1 X_7$$

where D is the turbulent diffusion coefficient, and $K_{17}(\rho,T)$ the rate of lithium burning. The boundary conditions express the physical constraints : at great depth, ^{7}Li is entirely burnt and $X_7 = 0$; at the boundary of the fully mixed region, the rate of depletion results from ^{7}Li burning in the fully mixed region and from diffusion out of the fully mixed region (FMR)

$$-D\rho \text{ grad } X_7 - \int_{FMR} K_{17} X_1 X_7 \, dz = \int_{FMR} \rho \frac{\partial X_7}{\partial t} \, dz$$

In order to get an idea of the physics of the problem, it is useful to consider a simplified description of lithium burning (fig. 2) (Schatzman, 1981).

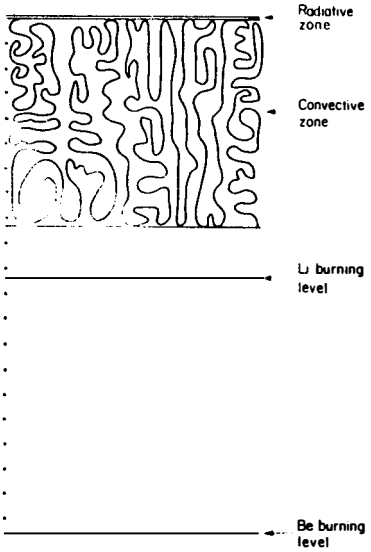


Fig. 2 :

A sketch of the structure of the outer layers of the sun, showing the distance of the bottom of the convective zone to the regions of Li and Be burning.

Due to the high dependance of the rate of lithium burning on temperature an interpolation around $T \simeq 2.5.10^6$ °K gives $K_{17} \sim T^{20}$, the scale height of lithium burning is of the order of $(H_P/10)$, where H_P, the pressure scale height is given by

$$H_P = \frac{dr}{d\log P} = \frac{kT}{g\mu} .$$

It is then a fair approximation to replace the actual z-dependant lithium burning rate by a step-function, $K_{17}\ X_1\ X_7 = 0$ for $T < T_{burning}$ and to write that for $T = T_{burning}$, the lithium concentration is zero. This provides a solution

$$X_7 = X_7 \text{ initial } \exp\left(-\frac{t}{\tau}\right)$$

where the caracteristic time of lithium burning is given by the solution of an eigen-value problem,

$$\frac{h}{H_P} = \frac{h}{(D\tau)^{1/2}}\ tg\ \frac{h}{(D\tau)^{1/2}}$$

The lithium depletion at the solar surface is of the order of 10^{-2} ; for an age of the sun of $4.6.10^9$ years, this provides a value of

$$\tau = 0.217\ t_{sun}$$

with a temperature at the bottom of the fully mixed region

$$T_{FMR} = 2.2.10^6$$

and a temperature of lithium burning

$$T_{Li} \simeq 2.5.10^6$$

we obtain

$$(h/H_P) = 0.32$$

$$h(D_\tau)^{-1/2} = 0.538$$

$$D_\tau = 3.455\ h$$

$$D = 600$$

$$\frac{D}{\nu} = Re^* \simeq 70$$

This analysis of lithium deplection seems to be confirmed by the measurements of lithium abundance (A. Boesgard, 1970 ; Duncan , 1981 ; Cayrel et al., 1984) especially in the Hyades, as shwon by Baglin and Morel (1983).

Beryllium burning. Beryllium burning taking place at a greater depth, beryllium depletion is less important than lithium depletion Beryllium depletion at the solar surface is not known with precision. It is of the order of 1/2 and is quite compatible with lithium depletion.

Helium abundance (^{3}He). The isotope ^{3}He of helium is produced inside the sun. In the outer half of the sun, ^{3}He is produced by the reactions

$$^2D + {}^1H + {}^3He + \gamma$$

but it is not until a temperature of the order of 8.10^6 °K is reached that the ^{3}He is destroyed by further nuclear reactions.

During the evolution of the sun a peak of concentration of ^{3}He is buildt (fig. 3), and this is true in all standard models.

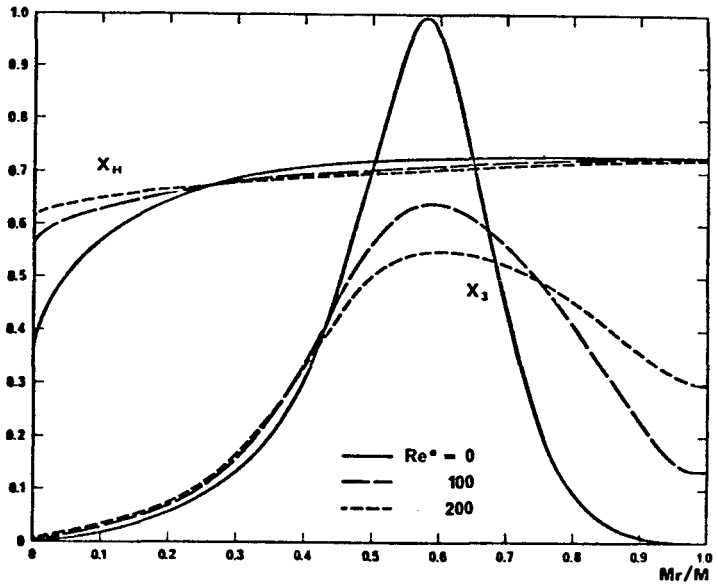


Fig. 3 : The hydrogen ^{1}H and ^{3}He concentrations in a 1 $M_\odot$ star at the age of 4.6×10^9 y (according to Schatzman and Maeder[26]). The curves are plotted for various values of the parameters Re^* which describes the efficiency of the turbulent diffusion.

When turbulent diffusion mixing is being introduced in the physics of solar evolution, the result is the production of a flux of ^{3}He towards the surface and a flux of ^{3}He towards the center. The flux of ^{3}He towards the surface produces an increase of the surface abundance of ^{3}He. In order to appreciate the signifi-

ficance of the surface abundance of ^3He it is necessary to compare it to the primordial abundance of ^3He and to the primordial abundance of ^2D. This last quantity is important, as the reaction

$$^2D + {}^1H \rightarrow {}^3He + \gamma$$

inside the convective zone (for T > 600 000 °K) may eventually generates the whole observed ^3He. The cosmic abundance of ^2D is badly known, as discussed by Laurent (1983), and is eventually as small as $(^2D/^1H) \simeq 10^{-6}$, in which case its contribution to the surface ^3He would be negligible. Previously Geiss (1973) has shown that the measurements of ^3He abundance in lunar samples suggest a rate of growth of at most 20 % during the last 1 or 2 billion years. The observed surface abundance, as discussed by Geiss and Reeves (1972) and by Hall (1975) suggest an abundance ratio $(^3He/^4He) \simeq 5.10^{-4}$. Interpolation between calculated values by Schatzman and Maeder (1981) gives the following results :

Re^*	$(^3He/^4He)$
30	2.8×10^{-4}
31	3.12×10^{-4}
32	3.44×10^{-4}

We shall conclude tha a value of Re^* of the order of 30 explains the present surface abundance of ^3He and the rate of growth of the abundance of ^3He as shown by the linear samples.

Solar neutrino flux

The effect of turbulent diffusion mixing is to bring to the central region hydrogen and ^3He along the concentration gradients of H and ^3He. To the difference with the partially mixed models of the sun, the turbulent diffusion mixing brings to the center ^3He which has been produced far away from the hot center in a region where the ^3He production is not balanced by ^3He burning. The ^3He which anyhow accumulates in the middle of the sun (around $(m_r/m) \simeq 0.5$) is partially driven to the center, changes the amount of fuel available and decreases the central temperature. It can be noticed on fig. 4 that the contribution of ^3He to the energy generation in the central regions of the sun is much larger in the case of turbulent diffusion mixing than in the standard models.

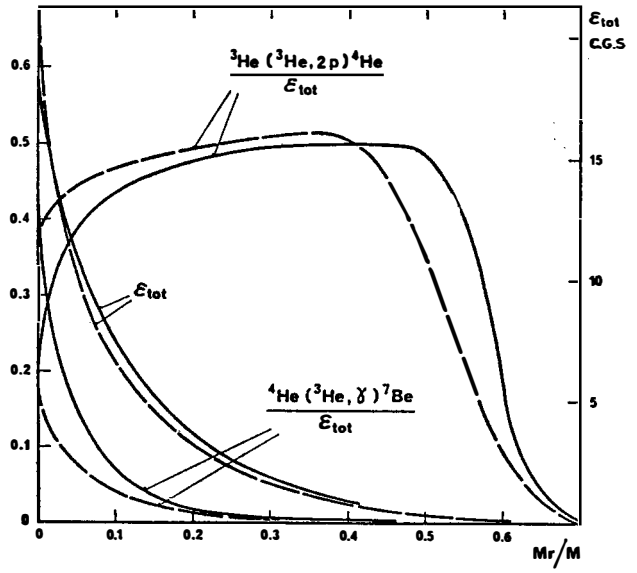


Fig. 4

From the presently available solar models, it is only possible to get estimates of the value of the turbulent diffusion coefficient which provides the proper value of the neutrino flux. A value of $Re^* \simeq 100$ seems to fall into the proper range of values. This is definitely larger than the values deduced from the surface abundance of ^3He and ^7Li.

This shows that the turbulent diffusion coefficient is certainly not a constant throughout the sun. A question comes up immediately : is the "high" value of Re^* close to the center of the sun compatible with the "low" values of Re^* which can be deduced from ^7Li and ^3He surface abundances ? It can be shown on simple mathematical examples that a large value of D_{int} near the center generates a large drag on the chemical inhomogeneities which compensates for the low value of D_{int} in the median and outer regions.

4.2 - Solar sismology

The linear analysis of the hydrodynamic motions of the sun shows the existence of two kinds of oscillatory modes, the pressure modes, in which the restoring force is the pressure, like in sound waves, and the gravity modes, in which the restoring force is the gravity, like in the surface sea waves.

Oscillatory modes are characterized by two numbers, the degree of the modes, ℓ, which corresponds to the decomposition in spherical harmonies $Y_{\perp}^{m}(\theta,\phi)$ and the order of the mode, n, which corresponds to the number of nodes from the center to the surface. To each couple of numbers (n,ℓ) corresponds a frequency. It should be noticed that for a given ℓ, the frequency increases with n for the pressure modes, and decreases with n for the gravity modes.

The velocity of sound increases inwards, and therefore the sound rays (the eikonals, orthogonal to the acoustic waves) are refracted inside. The larger is ℓ, the closer to the surface are trapped the pressure modes. However, the pressure modes of low degree are influenced by the deep layers of the sun and can be used, in principle, to determine the inner structure of the sun.

The mention "in principle" is due to the fact that the final word in solar models has not been said, and that the interpretation of the pressure modes frequencies meets still some difficulties.

The principle is the following. The time of propagation of an acoustic wave from the center to the surface

$$t_{prop} = \int_0^R \frac{dr}{c}$$

defines a characteristic frequency $\nu_o = (2t_{prop})^{-1}$

For $n \gg \ell$, an asymptotic expansion obtained by Tassoul (1980) yields :

$$\nu = \frac{\nu_o}{2}(2n + \ell + \bar{\mu} + \frac{1}{2}) - \Lambda[\ell(\ell+1) + \delta]\,\nu_o^2\,\nu^{-1} + \ldots$$

where $\bar{\mu} = (d\log\rho / d\log T)$ (outer layers) describes the density-temperature behaviour of the outer layers and is called a polytropic index.

Λ and δ are more complicated constants which depends on the equilibrium model.

It is interesting to notice that when making the difference

$$\delta_\nu = (n,\ell) - \nu(n-1, \ell+2)$$

the major term disappears, and we are left with the internal structure number Λ,

$$\delta_\nu(n,0) = 6\,\Lambda\,\nu_o^2\,\nu^{-1} + 0\,(\nu_o^{-2})$$

$$\delta_\nu(n,1) = 10\,\Lambda\,\nu_o^2\,\nu^{-1} + 0\,(\nu_o^{-2})$$

The exact computation of the differences $\delta\nu$ (where the frequencies are obtained directly as eigenvalues, and not as the result of an asymptotic formula) is a powerful test of the model. However, considering the high precision of the observations of Claverie et al. (1981) and Grec et al. (1983), the agreement is far from being satisfactory. The table III, reproduced from Gough (1983) shows that the frequency differences in microhertz are in agreement with the models only in order of magnitude and not to the precision of the microhertz.

Table III

Solar sismology : observations and models

Observations			$\delta\nu_0$	$\delta\nu_1$
Claverie et al (1981)			8.3*	-
Grec et al (1983)			9.4*	15.3*
Theory	**Y (Helium in mass)**	**Z**		
Christensen-Dalsgaard	0.25	0.020	10.1	16.0
and Gough (1980)	0.19	0.004	13.2	17.2
Shibahashi et al (1983)	0.23	0.020	10.7	11.9
	0.23	0.018	6.7	11.7
Ulrich and Rhodes (1983)		0.021	8.3	16.3
	0.27	0.018	9.2	10.0
	-	0.005	9.7	17.5

* These values are averages

It is readily seen from the asymptotic expressions of Tassoul (1980), that a decrease in the μ-gradient generates an increase in $\delta\nu(n,\ell)$'s. Such a change could eventually bring the values given Shibahashi et al. (1983) to the observed values, but certainly not to the values given by Ulrich and Rhodes (1983).

In the case of pressure waves, the asymptotic formula for the periods, is

$$P = \frac{P_o}{\sqrt{\ell(\ell+1)}} \left(n + \frac{\ell}{2} - 0.25 + \theta \right) + \frac{P_o^2}{P\ell(\ell+1)} \left(\ell(\ell+1)\ V_1 + V_2 \right)$$

with

$$P_o^{-1} = \frac{1}{2\pi^2} \int_0^{x_c} \frac{N}{x}\ dx$$

$$P_o\ V_1 = \lim_{\varepsilon \to o} \left(\int_0^{x_c} \frac{dx}{Nx} - \frac{1}{N(\varepsilon)} \right)$$

the coefficient V_2 is given by a more indicate formula. N is the Brunt-Väisälä frequency, defined by the relation

$$N^2 = g \left(\frac{\partial \rho}{\rho dn} - \frac{1}{\Gamma} \frac{1}{p} \frac{dp}{dn} \right)$$

$$\Gamma = \left(\frac{\partial \log P}{\partial \log \rho} \right)_{ad}$$

P, ρ, Γ are respectively the pressure, the density, the adiabatic exponent, $x = (r/R)$, and ℓ and n are, as above respectively the degree and the radial order. There is still some difficulty in the determination of the observed period P_o. According to Delache and Scherrer (1983) P_o = 38.8 minutes. The standard models give $P_o \simeq$ 35 minutes. Turbulent diffusion mixing decreases the BRUNT-VÄISÄLÄ frequency. According to Berthomieu et al. (1984) a turbulent diffusion mixing $D_T = Re^* \nu$, with $Re^* \simeq 25$ could being the theoretical period P_o to the observed one.

CONCLUSION

Whereas the basic physics of the internal structure of the sun seems to be now well established, the effects of rotation and mixing are still in an evolutionnary state. Surface abundance, solar sismology are, or can be, very important tests of the internal structure of the sun. But the solar neutrino deficiency, despite the fact that it can potentially be explained by turbulent diffusion mixing, remains the key of the solar structure problem.

Bibliography

Classics are :

Eddington A., Internal Constituion of the Stars , Cambridge 1926

Chandrasekhar S., Stellar Structure, Chicago 1939

Schwarzschild M. Structure and Evolution of the Stars, Princeton 1958.

Clayton D. Principles of stellar evolution and nucleosynthesis, Mc Graw Hill 1968

Here are the papers mentionned in the lecture :

Abraham Z., Iben I.Jr. 1971, Astrophys. J. 170, 157.

Baglin A., Morel P., 1983, I.A.U. Symposium 106, A.Maeder Ed., Reidel, 1984.

Bahcall J.N., Bahcall N.A., Ulrich R.K., 1968; Astrophys. L. 2,91.

Bahcall J.N., Ulrich R.K.,1971, Astrophys.J. 170,593.

Bahcall R.N., May, R.M., 1969, Astrophys.J. 155,501.

Bahcall J.N., Huebner W.F., Lubow S.H., Parker P.D.,Ulrich R.K., 1982, Rev.Mod Phys. 54,767.

Bartenwerfer D., 1973, Astr.Astrophys. 25, 455.

Berthomieu G., Provost J., Schatzman E.,1984, Nature,

Boesgard A., 1970, Publ.Ast.Soc.Pac. 88,153.

Bretherton F.P., Spiegel E.A., 1968, Astrophys.J.Letters 153,L 77.

Cayrel R., Cayrel de Strobel G., Campbell B., Däppen W.,1983, submitted to Astronomy and Astrophys.

Chitre S.M., Ezer E.,Stothers R., 1973, Astrophys L. 14, 37.

Christansen-Dalsgaard J., Gough D.O., Morgan J.G.,1979, Astron.Astrophys.73, 121; 79, 260 .

Christansen-Dalsgaard J., Gough D.O., 1980, Nature, 288,544.

Claverie A., Isaak G.R., Mc Leod C.P., van der Ray H.B., Rica-Cortes T., 1981 Nature, 293, 443.

Cowling T.G., 1945 Monthly Notives R.A.S. 105, 166.

Delache P., Scherrer P.H., 1983, Nature 306, 651 .

Dicke R.H., 1967, Annual Rev. Astron. Astrophys. 8 , 297.

Duncan D.K., 1981, Astrophys. J. 248, 651.

Ebeling W., 1974, Physica 73, 573.

Ezez D., Cameron A.G.W., 1968, Astrophys. L. 1, 177.

Fowler W., 1951, Phys. Rev., 81, 655.

Geiss J., 1973, 13th International Cosmic Ray Conference, Denver .

Geiss J., Reeves H., 1972, Astron. Astrophys. 18, 126.

Gough D.O., 1983, E.S.O. Workshop on "Primordial Helium" , Shaver P.H., Kunth D.,Kjär K., Eds. Garching ; R.F.A..

Grec G., Fossat E., Pomerantz M., 1981

Grec G., Fossat E., Pomerantz M., 1981, Nature 288, 541.

Hall D.N.B., 1975, Astrophys.J., 197, 509.

Hill H.A., Stebbins R.J. , 1975, 200, 471.

Hopfinger E.J., Browand F.K., Gagne Y., 1982, J. Fluid. Mech. 125, 505.

Iben I.jr., 1968, Phys. Rev. Letters 21, 1208.

Iben I.Jr., 1969, Ann. Phys. 54, 164.

Joss P.C., 1974, Astrophys. J. 191, 771.

Knobloch .,Spruit ., 1983, Astron. Astrophys.

Kraft R., 1967,

Larkin A.I., 1960, Sov. Phys. J.E.T.P. , 11, 1363.

Laurent C., E.S.O. Workshop on "Primordial Helium" , p.335, Shaver P.H., Kunth D.
Kjär K., Eds., ES.S.O. , Garching, R.F.A.

Michaud G., 1977, Nature, 266, 433.

Parker E., 1974, Astrophys. Space Sci., 31, 261.

Parker E., 1979, in Cosmic Magnetic Fields, Oxford, Clarendon Press, pp. 147-150.

Salpeter E.E., 1954, Australian J. Phys. 7, 373.

Schatzman E., 1951, Comptes Rendus Acad.Sci., 232, 1740

Schatzman E., 1962, Ann d'Astrophys.

Schatzman E., 1981, Turbulent diffusion and the Solar neutrino problem,
CERN 18-11 , Geneva .

Shaviv G., Beaudet G., 1968, Astrophys. L. , 2, 17.

Shibahashi H., Noels A., Gabriel M., 1983, Astron. Astrophys. 123, 283.

Tassoul M., 1980, Astrophys.J. Suppl., 43, 469.

Ulrich R.K., 1974, Astrophys. J. 188, 369.

Ulrich R.K., 1982, Astrophys J., 258, 404.

Ulrich R.K., Rhodes E.J.Jr., 1983, Astrophys J., 265, 551.

Zahn J.P., 1983 a, Cours de Saas Fe , Société Suisse d'Astronomie, Maede A.Ed.
1983 b, Cours de Goutelas, Société Fran*aise des Spécialistes en
Astronomie , Baglin á. Ed. (published in 1984).

PRINCIPLES AND APPLICATIONS OF A NEUTRAL CURRENT DETECTOR FOR NEUTRINO PHYSICS AND ASTRONOMY

A. Drukier and L. Stodolsky
Max-Planck-Institut für Physik und Astrophysik
- Werner-Heisenberg-Institut für Physik -
Munich (Fed.Rep.Germany)

We study detection of MeV range neutrinos through elastic scattering on nuclei and identification of the recoil energy. The very large value of the neutral current cross section due to coherence indicates a detector vould be relatively light and suggests the possibility of a true "neutrino observatory". The recoil energy which must be detected is very small ($10-10^3$eV), however. We examine a realization in terms of the superconducting grain idea, which appears in principle feasible through extension and extrapolation of presently known techniques. Such a detector could permit determination of the neutrino energy spectrum and should be insensitive to neutrino oscillations, since it detecst all neutrino types. Various applications and tests are discussed, including spallation sources, reactors, supernovas, solar and terrestrial neutrinos. A preliminary estimate of the most difficult backgrounds is attempted.

A full discussion is in Drukier and Stodolsky MPI-PAE/PTh 36/82 (to be published in Phys. Rev.).

THE DOUBLE BETA DECAY

— Neutrino Masses and Right-handed Current —

T. Kotani
Institute of Physics, College of General Education
Osaka University, Toyonaka 560, JAPAN



ABSTRACT

The present status of our knowledge of neutrino mass parameters and right-handed parameters obtained from studies of double beta decay is reviewed. Their upper limits are compared with other results from neutrino oscillations, the tritium β decay, cosmological constraints on neutrino masses and the $\pi^+ \to \mu^+ \to e^+$ decay. Some possible models consistent with all these informations are presented, though there is no confirmed evidence for the finite neutrino mass and the existence of the right-handed current.

1. Introduction

Questions whether neutrinos have finite masses and whether the right-handed weak current exists are of great interest. They are the important issues to provide evidence for possible new physics beyond the minimal standard model of electroweak interaction [the $SU(2)_L \times U(1)$ model with left-handed fermion doublets, right-handed singlets and no right-handed neutrino]. At present all known results, such as lepton and baryon number conservations, lepton universality, the absence of neutrino mass and mixing and so on, do not show the large deviations from the minimal standard model. Neutrino mass plays also a crucial role in astrophysics as well as in cosmology. However, the above questions could shed light on the validity of more encompassing theoretical schemes such as grand unified theories.

I shall summarize the present status of various experimental results on the basis of the following more explicit forms of questions:

[Q1] Do neutrinos have mass ($m_\nu \neq 0$)? If so, why is m_ν much smaller than the electron mass (m_e)?

[Q2] If $m_\nu \neq 0$, are neutrinos Dirac or Majorana particles?

[Q3] If $m_\nu \neq 0$, do the weak eigenstate neutrinos differ from their mass eigenstates? Are there neutrino mixings?

[Q4] Why does the Nature like to have only the left-handed (V-A) current, i.e., $SU(2)_L$? Isn't it natural to consider[1] that the (V-A) current appears at the present low energy region, although there should be the left-right symmetry above some higher energy? If so, we have again the question whether neutrinos are Dirac or Majorana particles even for the case with $m_\nu = 0$.

As for the smallness of m_ν in [Q1], we know one possible explanation; that is, the see-saw mechanism proposed by Gell-Mann-Ramond-Salnsky and independently by Yanagida in 1979.[2] Namely, it takes advantage of the fact that, if neutrinos are Majorana types, their left- and right-handed parts (ν_L and ν_R) themselves can acquire masses separately. By assuming the existence of the heavy right-handed neutrino, the mass (m_{ν_L}) of the presently observed left-handed neutrino is given by the relation $m_{\nu L}\, m_{\nu R} \approx m_\ell^2$, m_ℓ being the mass of the charged lepton (or quark). This idea can be realized in the models which include the $SU(2)_L \times SU(2)_R \times U(1)$ gauge group.[1] From the experimental point of view, the neutrinoless double β decay, the $(\beta\beta)_{0\nu}$ mode, appear to be one of experiments presently accessible for testing these questions directly.[3]

1-1. Why do we consider the $(\beta\beta)_{0\nu}$ mode?:

Let us consider, as an example, the 2n-mechanism where the successive transitions of two neutrons (n_1 and n_2) trigger the $\beta\beta$ decay. According to the standard model, an antineutrino ($\bar{\nu}_{eL}$) is emitted in the n_1 decay and a neutrino (ν_{eL})

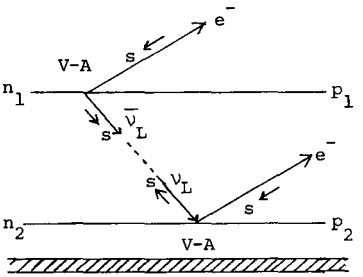


Fig. 1. The mass term for the $(\beta\beta)_{0\nu}$ mode.

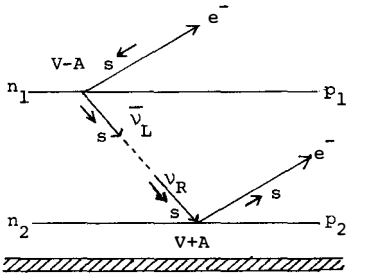


Fig. 2. The V+A term for the $(\beta\beta)_{0\nu}$ mode.

is absorbed in the transition of n_2. Therefore, if the $(\beta\beta)_{0\nu}$ mode, $A \to B + 2e^-$, is observed, it means that at least the electron-neutrino (ν_e) should be a Majorana type ($\nu_e = \bar{\nu}_e$) [*condition* (1): *the lepton number non-conservation*]. However, we need the other condition: The main helicity of neutrino is decided by the one for the case of $m_\nu = 0$, because $m_\nu \ll \omega$, ω being the neutrino energy. The main helicity states of two virtual neutrinos in the $(\beta\beta)_{0\nu}$ mode are opposite, as shown by allows ($s \leftarrow$) in Fig. 1. Therefore, these two virtual neutrinos can not be connected. However if $m_\nu \neq 0$, there should be a minor helicity state which is proportional to (m_ν / ω). The requirement of the helicity matching [*condition* (2)] means that the transition amplitude for the $(\beta\beta)_{0\nu}$ mode should be proportional to (m_ν/m_e) [the m_ν term], where the electron mass m_e is introduced to represent the order of the typical energy appearing in the $\beta\beta$ decay. In addition, there is the other possibility to satisfy this condition (2). It is the existence of the V+A interaction (RHC), for example, the $SU(2)_L \times SU(2)_R$ model. As shown in Fig. 2, if the second vertex is the V+A type, the second neutron n_2 absorbs the RH neutrino (ν_{eR}). Since the condition (2) is satisfied already for the main parts of helicity even for the $m_\nu = 0$ case, the transition amplitude in this case is proportional to the V+A parameters, say λ, but need not to be $m_\nu \neq 0$ [the V+A term]. Thus, we have to consider both the m_ν and V+A terms simultaneously. In other words, if ν_e is a Majorana type, the observation of the $(\beta\beta)_{0\nu}$ mode offers us the information on both m_ν and λ.[3)]

1-2. Parameters due to the V+A weak current:

Since there is some confusion about RHC parameters and mixing matrices among quarks and neutrinos at present, let us start from the weak gauge interactions. By assuming both the *left-right symmetry* and the *lepton-quark universality*

as in the grand unified theories, the Yukawa interaction between the charged gauge boson (W) and the fermion current ($\mathcal{J}$) is defined as

$$\mathcal{L}_W = -(g/2\sqrt{2})\,(\mathcal{J}_{L\rho}\,W_L^{\rho} + \mathcal{J}_{R\rho}\,W_R^{\rho}) + \text{h.c.}, \tag{1.1}$$

where g is a gauge coupling constant, and L and R stand for the left- and right-handedness (LH and RH), respectively. The current $\mathcal{J}$ consists of the leptonic (j) and quark (hadronic)(J) currents, $\mathcal{J} = j + J$, i.e., the lepton-quark universality.

Next let us assume that these weak gauge bosons are in mixed states between two mass eigenstate bosons (W_1 and W_2) with masses M_1 and M_2 ($M_2 \gg M_1$);[4] namely, independently of the CP invariance, we have

$$W_L = W_1 \cos\zeta + W_2 \sin\zeta \qquad \text{and} \qquad W_R = -W_1 \sin\zeta + W_2 \cos\zeta\,. \tag{1.2}$$

Then, if the momentum transfer in the weak process is much smaller than M_1,*) the effective lepton-hadron charged weak interaction Hamiltonian can be expressed in the four-fermion approximate form as[3]

$$H_W = (G/\sqrt{2})\,[j_{L\rho}(J_L^{\rho} + \kappa J_R^{\rho}) + j_{R\rho}(\eta J_L^{\rho} + \lambda J_R^{\rho})] + \text{h.c.}, \tag{1.3}$$

where couplings G, κ, η and λ are defined as[5]

$$(G/\sqrt{2}) = (g^2/8)(\cos^2\zeta + \alpha \sin^2\zeta)/M_1^2 \xrightarrow{\zeta \to 0} (g^2/8M_1^2), \tag{1.4}$$

$$\lambda = (\alpha + \tan^2\zeta)/(1 + \alpha\tan^2\zeta) \longrightarrow \alpha = (M_1/M_2)^2, \tag{1.5}$$

$$\eta = \kappa = -(1-\alpha)\tan\zeta/(1 + \alpha\tan^2\zeta) \longrightarrow 0. \tag{1.6}$$

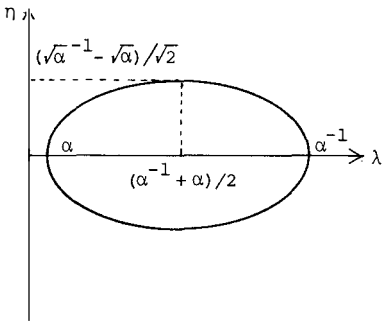


Fig. 3.
The relation between λ and η.

Note that if $\lambda = 0$, then we have $\eta = \kappa = 0$. The relation between λ and η is shown in Fig. 3.[5] In general, $\eta \neq \kappa$, if there is a mixing between the left-handed fermions and their mirror particles (the right-handed particles interacting with $W_{L\rho}$) which appear, for example, in the SO(12) grand unified model. In this talk, we assume no mirror particle for simplicity. However, as shown

*) In the $(\beta\beta)_{0\nu}$ mode, there is a closed loop due to two gauge bosons (W), as shown in Table I. This is a feature different from the ordinaty weak processes. However, we need not worry about the effect due to the momentum part in the W-propagator, because of the finite nuclear size.

in the practical application later on, contributions from the κ term can be neglected, because of its appearance as the combination $(1-\kappa) \simeq 1$.[3)]

The hadronic current J_ρ in the β decay is expressed as

$$J_{L\rho} = \bar{\psi}_N \tau^{(+)} \gamma_\rho (g_V - g_A \gamma_5) \psi_N + (\text{weak magnetism etc.}), \tag{1.7a}$$

$$J_{R\rho} = \bar{\psi}_N \tau^{(+)} \gamma_\rho (g'_V + g'_A \gamma_5) \psi_N + (\text{weak magnetism etc.}), \tag{1.7b}$$

where $\psi_N^T = (p, n)$, $\tau^{(+)}$ is a isospin raising operator. Here g_α's include both the generalized Cabbibo (Kobayashi-Maskawa)mixing angles among quarks and the renormarization effects due to the strong interaction; for example $g_V = \cos\theta_C$, $g'_V = \cos\theta'_C$ and $(g_A/g_V) = (g'_A/g'_V) = 1.24$.*) We may expect that $\theta'_C \simeq \theta_C$ (the Cabbibo angle). The leptonic current j_ρ is defined as

$$j_{L\rho} = \Sigma_\ell \bar{\ell} \gamma_\rho (1-\gamma_5) \nu_{\ell L} \quad \text{and} \quad j_{R\rho} = \Sigma_\ell \bar{\ell} (1+\gamma_5) \nu'_{\ell R}, \tag{1.8}$$

where ℓ represents n charged leptons $(e^-, \mu^-, \tau^-, \cdots)$, n being the number of generations, and $\nu_{\ell L}$ $(\nu'_{\ell R})$ is the left-(right-)handed weak-eigenstate of neutrino.

1-3. Mixing matrices in the lepton sector:

The weak eigenstate neutrinos $\nu_{\ell L}$ and $\nu'_{\ell R}$ are assumed to be the superposition of the mass eigenstate neutrinos N_j's with their masses m_j's:[3)]

$$\nu_{\ell L} = \sum_{j=1}^{2n} U_{\ell j} N_{jL} \quad \text{and} \quad \nu'_{\ell R} = \sum_{j=1}^{2n} V_{\ell j} N_{jR}, \tag{1.9}$$

Both the Dirac and Majorana neutrino system are incorporated in our H_W simultaneously by an appropriate choice of the $n \times 2n$ mixing matrices $U = (U^{(1)}, U^{(2)})$ and $V = (V^{(1)}, V^{(2)})$.

For the ordinary Dirac neutrino system (*case D*), it is convenient to choose that there are n neutrinos (N_k's) and no N_{n+k} for k=1,$\cdots$,n. In this choise, we have $U^{(2)} = V^{(2)} = 0$ and $U^{(1)}$ and $V^{(1)}$ are unitary matrices separately; Eq.(1.9) is

$$\nu_{\ell L} = \begin{pmatrix} \nu_e \\ \nu_\mu \\ \nu_\tau \\ \cdot \\ \cdot \\ \cdot \end{pmatrix}_L = U^{(1)} \begin{pmatrix} N_1 \\ N_2 \\ \cdot \\ \cdot \\ \cdot \\ N_n \end{pmatrix}_L \quad \text{and} \quad \nu'_{\ell R} = \begin{pmatrix} \nu_e \\ \nu_\mu \\ \nu_\tau \\ \cdot \\ \cdot \\ \cdot \end{pmatrix}_R = V^{(1)} \begin{pmatrix} N_1 \\ N_2 \\ \cdot \\ \cdot \\ \cdot \\ N_n \end{pmatrix}_R . \tag{1.10}$$

*) The generalized Cabbibo mixing angle should be included in the definition of g_α's from the view point of the gauge theory, because it is originated from mixings among quarks. In refs. (3) and (10), we showed it explicitly to avoid the confusion for nuclear physicists.

It is also possible to use a complicated representation: An ordinary Dirac neutrino consists of a left-handed (N_k) and a right-handed ($N_{n+k'}$) Majorana neutrinos which have the equal mass ($m_k = m_{n+k'}$) and the opposite CP values, if a Dirac neutrino has a definite CP value.[6] In this choice, the neutrino part of the mixing matrix (U^T, V^+) has a special form to construct a Dirac neutrino from two Majorana neutrinos in addition to the neutrino mixing.

In the general Majorana neutrino system (*case M*), let us assume that N_k and N_{n+k} with $k \leq n$ represent the LH and RH neutrinos, respectively. Then, $m_k \neq m_{n+k}$ in general and there are 2n neutrinos. Eq. (1.9) is expressed as

$$\begin{pmatrix} \nu_{eL} \\ \nu_{\mu L} \\ \vdots \\ (\nu'_{eR})^C \\ (\nu'_{\mu R})^C \\ \vdots \end{pmatrix} = \begin{pmatrix} U \\ \\ V^* \end{pmatrix} (N)_L = \begin{pmatrix} U^{(1)} & U^{(2)} \\ \\ V^{(1)*} & V^{(2)*} \end{pmatrix} \begin{pmatrix} N_1 \\ \vdots \\ N_n \\ N_{n+1} \\ \vdots \\ N_{2n} \end{pmatrix}_L , \tag{1.11}$$

where the charge conjugate state is defined as $(\psi_R)^C \equiv C(\bar{\psi}_R)^C \equiv (\psi^C)_L$. Let us consider two extreme cases: Case (M-I) All masses of Majorana neutrinos are smaller than the charged lepton mass (m_ℓ),

$$m_k \ll m_\ell \quad \text{and} \quad m_{n+k} \ll m_\ell \quad \text{for } k \leq n. \tag{1.12}$$

Then, $|V^{(1)}|$ and $|U^{(2)}|$ are not necessarily small. The previous case D is included as a special one, if $m_k = m_{n+k} \ll m_\ell$ for all $k \leq n$ and requirements on CP and flavor are satisfied. Case (M-II) The masses of RH neutrinos are much heavier than m_ℓ, though m_k is still lighter, i.e.,

$$m_k \ll m_\ell \quad \text{but} \quad m_{n+k} \gg m_\ell \quad \text{for } k \leq n. \tag{1.13}$$

Then, it is expected generally that $|V^{(1)}| \ll 1$ and $|U^{(2)}| \ll 1$, because they are mixing angles between light and heavy neutrinos. The see-saw mechanism[2] explained before is allowed in this case.

2. The $(\beta\beta)_{0\nu}$ decay.

The double β decay takes place in two modes: The $(\beta\beta)_{0\nu}$ mode for $A \to B + 2e^-$ and the $(\beta\beta)_{2\nu}$ mode for $A \to B + 2e^- + 2\bar{\nu}_e$. The typical nuclear energy levels for the ββ decay are shown in Fig. 4. Following Primakoff and Rosen,[7] three approximations have been made to estimate their transition rates. *Assumption* (I): The second order perturbation of the weak interaction H_W is applied. Then the

transition amplitude is

$$f_{\beta\beta} \sim \Sigma_i \frac{\langle F|H_W|i, e_1, \bar{\nu}_1\rangle\langle i, e_1, \bar{\nu}_1|H_W|A\rangle}{E_i + \varepsilon_1 + \omega_1 - M_A}, \quad |F\rangle = |B, 2e, (2\bar{\nu})\rangle, \qquad (2.1)$$

where E_i, ε_k and ω_k are energies of the intermediate nucleus, k-th electron and k-th neutrino, respectively, and M_A is the mass of initial nucleus.(See the footnote in §1-2.) *Assumption* (II): The energy E_i is replaced with the appropriate average value $\langle E_i\rangle$, so that the closure property $\Sigma_i |i\rangle\langle i| = 1$ is applied.

$$f_{\beta\beta} \sim \frac{\langle F|H_W|e_1, \bar{\nu}_1\rangle\langle e_1, \bar{\nu}_1|H_W|A\rangle}{\langle E_i\rangle + \varepsilon_1 + \omega_1 - M_A}. \qquad (2.2)$$

This closure approximation makes $f_{\beta\beta}$ to be larger, say a few 10%.[8),9)] Therefore, the use of this closure approximation gives some ambiguity, but if it is not applied, the expressions become complicated,especially for the $(\beta\beta)_{0\nu}$ mode, because of the Coulomb wave functions for electrons. For simplicity, expressions under this assumption (II) are shown here. *Assumption* (III): According to the standard β decay theory, the non-relativistic impulse approximation is adopted for hadronic currents $J_{L\rho}$ and J_{R_ρ} without taking terms due to the weak magnetism and so on into account;

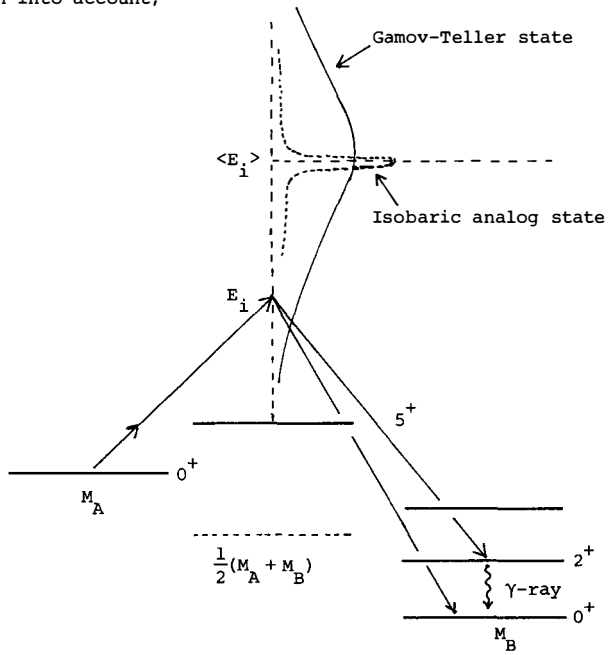


Fig. 4. The typical nuclear energy levels for the ββ decay.

$$J_{L\rho} \Rightarrow \Sigma_n \phi^*(\vec{r}_n)\tau^{(+)}[g_V \delta_{\rho 0} - g_A \delta_{\rho j}\sigma_n^j]\phi(\vec{r}_n)\delta(\vec{r}-\vec{r}_n), \tag{2.3}$$

where $\phi(\vec{r}_n)$ is the nucleon wave function at the position $\vec{r}_n$, and σ_n^j is the j-th component of spin operator acting on the n-th nucleon (j = 1,2,3).

2-1. Qualitative characters of the $(\beta\beta)_{0\nu}$ mode:

Let us explain briefly how the m_ν and V+A terms show different characters in the $(\beta\beta)_{0\nu}$ mode of the $0^+ \to J^+$ transition.[3),10)] Since the virtual neutrino propagator $S_F(q)$ in the momentum representation is proportional to $(\not{q} + m_j)$, the lepton part of the transition amplitude is expressed as

$$(\text{lepton part of } f_{\beta\beta}) \sim \bar{e}_2 \gamma_\rho (1 \mp \gamma_5)(\not{q} + m_j)(1 - \gamma_5)\gamma_\sigma e_1^C , \tag{2.4}$$

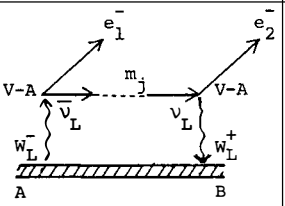
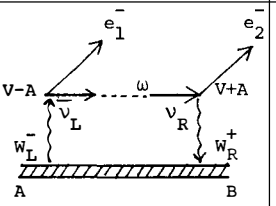
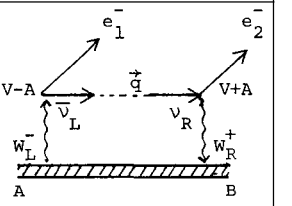
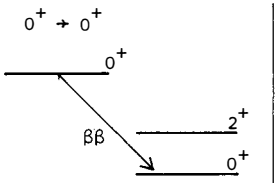
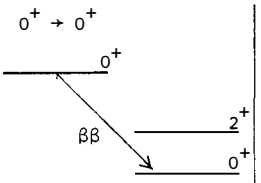
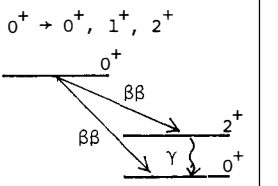
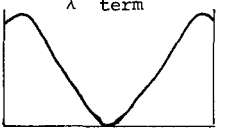
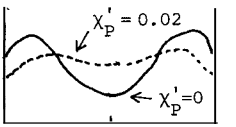
where e_k is the k-th electron field operator and $(1 \mp \gamma_5)$ correspond to the (V∓A) verticies. Therefore, if there is only the (V-A) current, then the apmlitude $f_{\beta\beta}$ is proportional to m_j linearly, because of $(1 - \gamma_5)(1 + \gamma_5) = 0$. While, if the (V-A) and (V+A) currents coexist, then the four momentum q^μ part contributes.

For the m_ν term, it is favorable that two final electrons are in the S-wave state and the total angular momentum of two electron system (J_{2e}) is 0 or 1. Therefore, only the $0^+ \to 0^+$ transition takes place, but the $0^+ \to 1^+$ transition is forbidden because of no operator to change the nuclear spin. Furthermore, since both electrons have negative main helicities as shown in Fig. 1, their angular correlation should be the $(1 - \cos\theta)$ type, θ being the angle between two emitted electrons. This correlation means that the energy spectrum of the single e^- should be the mountain type, because of the 3 body decay.[10)] These features are summarized in Table I. [We have two nuclear matrix elements defined later in Eqs.(2.10) and (2.13).]

As for the (V+A) term, two completely different situations appear due to the energy (ω) and space momentum ($\vec{q}$) parts of the virtual neutrino. It is worthwhile to note that the averages of neutrino energy and momentum appeared in the (V+A) term are $\langle q^0 \rangle \simeq \langle \vec{q} \rangle \simeq 70\, m_e$,[7)] while the corresponding (m_ν/m_e) in the m_ν term is of order of 10^{-5}.

For the ω part, it is expected to have the similar features to the m_ν term, because of the scalar property of ω. For example, only the $0^+ \to 0^+$ transition is allowed and the additional two new nuclear matrix elements are the similar ones.[10)] However, the main helicities of two electrons are opposite as shown in Fig. 2, so that their angular correlation should be the $(1 + \cos\theta)$ type in order to minimize J_{2e}. Accordingly, the kinematical factors of this part includes a factor $(E_1 - E_2)$, because of the Pauli exclusion principle. Thus, the single electron energy spectrum is expected to be a valley type, which reduces the

Table I. The m_ν and V+A terms in $(\beta\beta)_{0\nu}$ mode.

m_ν-term	(V+A) term	
mass-part	ω-part ($\omega = q^0$)	$\vec{q}$-part
		
both e^- : S-wave	both e^- : S-wave	one e^- : S-wave other e^- : P-wave
total $J_{2e} = 0, 1$	$J_{2e} = 0, 1$	$J_{2e} = 0, 1, 2$
The allowed nuclear transitions ($0^+ \to J^+$)		
		
Main angular correlation between $2e^-$ in the $0^+ \to 0^+$ transition		
$(1-\cos\theta)$ type	$(1+\cos\theta)$ type	approximately $\sim (1+\cos\theta)$ type
Energy spectrum of single e^- for the $0^+ \to 0^+$ transition		
		
Mountain type spectrum	Valley type spectrum	[χ'_p is defined in Eq. (2.14)]

transition rate. Fortunately, the spectrum obtained for the RH parameter λ^2 term retains this character for the ^{76}Ge case, which is shown in Table I as the λ^2 term.

For the $\vec{q}$ part, the situation becomes complicated, because $\vec{q}$ is a parity-odd and rank 1 tensor and appears between the initial and final nuclear wave functions with the same parity. Since we are considering only the $0^+ \to J^+$ transition,

we need to have one more parity-odd operator: Namely, one of emitted electrons should be in the P-wave state or the nucleon recoil effect should be taken into account. Let us consider the electron P wave case, where J_{2e} can take 0,1 and 2. First, it should be noticed that the $0^+ \to 2^+$ transition is allowed only for this $\vec{q}$ part.[10),11)] In other words, if the $0^+ \to 2^+$ transition in the $(\beta\beta)_{0\nu}$ mode is observed, then we can say definitely that the RH current exists in addition to the Majorana character of neutrino. [See Table I of ref.(3a).] Since the electron P wave in this case must have $j = 3/2$ (the simple P wave, g_{-1} and f_{+1}) to get $J_{2e} = 2$, the angular correlation in the $0^+ \to 2^+$ transition is the type like $[1 + \alpha \cos\theta + \beta(\cos^2\theta - 1/3)]$. Second, of course, the $0^+ \to 0^+$ transition is also allowed, where the total angular momentum of this electron P wave should be $j = 1/2$, because of $J_{2e} = 0$. This type of P-wave Coulomb wave function in the uniform charged distribution of nucleus is

$$\begin{pmatrix} g_1 \\ f_{-1} \end{pmatrix} \simeq \pm A_{\pm 1} \left[\frac{3}{2}\alpha Z + (\varepsilon \pm m_e) R \right] \left(\frac{r}{3R}\right) , \tag{2.5}$$

where α is a fine structure constant, Z the atomic number of the daughter nucleus, R the nuclear radius and $A_{\pm}$ the normalization factor. [See Eq.(A.9) of ref.(3a).] As it is well-known, it is expected that the P wave contribution is smaller by a factor of $pR \sim 1/10$ than the S wave one, i.e., $|\omega\text{-part}| \gg |\vec{q}\text{-part}|$. However, the first term in Eq.(2.5) is of order of $(3\alpha Z/2) \sim 1/2$ for the typical $\beta\beta$ decay.[12)] In addition, the factor $(E_1 - E_2)$ is not appeared in this case. While, note that the nucleon recoil effect is quite large, because both electrons are in the S wave state.

In the λ^2 term, the dangerous αZ terms in Eq.(2.5) are canceled each other in the coefficients.[10)] For ^{76}Ge case, the ω part give the main contributions, as mentioned before. On the other hand, in the η^2 term, complicated situations happen from two origins: One is the cancellation among terms in the ω part, so that the contributions from the second term in Eq.(2.5) of the $\vec{q}$ part become relatively important. Therefore, the single electron energy spectrum is not a simple form, as shown by the η^2 term with $\chi_P' = \chi_R' = 0$ in Table I. These situations depend on relative magnitudes and signs of various nuclear matrix elements. However, the other complications due to the αZ-term and the nucleon recoil effect are serious. The former appears only with a P-wave nuclear matrix element (χ_P') defined later in Eq.(2.14), while the latter nuclear matrix elements χ_R' is defined in Eq.(2.10) of ref. (10). These coefficients become larger by factor of $10^3 \sim 10^5$ than others, e.g., as you will see in Eq.(2.24). This means that if $|\chi_P'| > 10^{-2}$ and/or $|\chi_R'| > 10^{-3}$, the plane wave approximation for electrons[7)] can not be used even to discuss the qualitative features of the η term, as shown by the η^2 term with $\chi_P' = 0.02$ and $\chi_R' = 0$ in Table I, although all previous calculations for the η term had used this approximation.

So far, we have considered only the $2\tilde{\nu}$ mechanism, but, in the $0^+ \to 2^+$ transition, there is another competing mechanism,[3] i.e., the N^*-mechanism[13] where the $\beta\beta$ decay occurs through the transition of $\Delta(1232)$ inside the nucleus. The correction due to the exchange pion current may also be taken into account.[14]

2-2. Estimates of nuclear matrix elements:

Whenever the LH(RH) vertex exists, the neutrino mixing matrix U_{ej} (V_{ej}) should appear there. Therefore, we have to introduce three following parameters;

$$x \equiv \left|\Sigma_j'(m_j/m_e)U_{ej}^2\right| = \langle m_\nu \rangle / m_e \quad \text{for mass term} \tag{2.6}$$

$$y \equiv \lambda\left|\Sigma_j' U_{ej} V_{ej}\right| \quad > 0 \tag{2.7}$$

$$z \equiv \eta\left|\Sigma_j' U_{ej} V_{ej}\right| \quad \text{for V+A term} \tag{2.8}$$

where Σ' means the sum over only neutrinos with $m_j \lesssim 1$ MeV by neglecting contributions from the heavier neutrinos, as discussed in Appendix A of ref. (3b). It should be noted that if there is no neutrino mixing, then we have in general $U_{ej} = \varepsilon_j \delta_{jl}$ and $V_{ej} = \varepsilon_j \delta_{j,n+1}$ where ε_j is the relative CP value of the j-th Majorana neutrino ($\varepsilon_j = 1, i$ under the CP invariance). Therefore, we obtain that $m_\nu = m_l$, $x = (m_l/m_e)$ and $y = z = 0$. However, it is possible to be $y = \lambda$ and $z = \eta$, if one LH neutrino N_l happens to be identical to one RH neutrino, say N_{N+1},[13a] though this choice is not taken in the framework of the gauge theory.

The inverse of the half-life of the $(\beta\beta)_{0\nu}$ mode is expressed as[10]

$$[T_{0\nu}(0^+ \to 0^+)]^{-1} = \left|M_{GT}^{(0\nu)}\right|^2 \Xi ,$$

$$\Xi = [C_1 x^2 + C_2 xy + C_3 xz + C_4 y^2 + C_5 z^2 + C_6 yz] , \tag{2.9}$$

where coefficients C_i's consist of known kinematical factors*) G_{0j}'s and nine nuclear matrix elements $M_\alpha^{(0\nu)}$'s which are determined theoretically. The $M_\alpha^{(0\nu)}$ is normalized by $M_{GT}^{(0\nu)}$, the double Gomow-Teller type nuclear matrix element defined as

$$M_{GT}^{(0\nu)} \equiv \langle B \left| \Sigma_{nm} \tau_n^{(+)} \tau_m^{(+)} \vec{\sigma}_n \cdot \vec{\sigma}_m h_+ \right| A \rangle , \tag{2.10}$$

where $h_+ = R(H_1 + H_2)/2$ and H_k is the potential due to the neutrino propagation in the case where the k-th electron is emitted first in the old fashion perturbation theory:

$$H_k(r) \equiv \int \frac{d^3q}{2\pi^2} \frac{e^{i\vec{q}\cdot\vec{r}}}{\omega(\omega + D_k)} \equiv \frac{\phi(D_k r)}{r} , \tag{2.11}$$

where $D_k = \langle E_i \rangle + \varepsilon_k - M_A$ in Eq. (2.2) and $r = \left|\vec{r}_n - \vec{r}_m\right|$ is the distance of the neutrino propagation, $\phi(D_k r)$ is the deviation from the Coulomb type potencial due to $D_k \neq 0$.

*) There is a list of the numerical values of 12 G_j's as Osaka University preprint, OS-GE 84-09, which is sent on request.

In the case of the m_ν term, there are only two nuclear matrix elements, $M_{GT}^{(0\nu)}$ and $M_F^{(0\nu)}$, so that the coefficient C_1 is simple as follows,[10]

$$C_1 = G_{01}|1 - \chi_F|^2, \tag{2.12}$$

where G_{01} is a kinematical factor and the double Fermi type nuclear matrix element is

$$\chi_F \equiv [M_F^{(0\nu)}/M_{GT}^{(0\nu)}](g_V/g_A)^2, \qquad M_F^{(0\nu)} \equiv <B|\Sigma_{nm}\tau_n^{(+)}\tau_m^{(+)}h_+|A>. \tag{2.13}$$

On the other hand, in the V+A case, there are seven additional $M_\alpha^{(0\nu)}$'s. For example, one of them in the $\vec{q}$ part which gives the complicated situation is

$$\chi_p' = <B|i(r_{+nm}/r_{nm})\vec{\sigma}_n\cdot(\hat{r}_{nm}\times\hat{r}_{+nm})h_+'|A>(g_V/g_A)/M_{GT}^{(0\nu)}, \tag{2.14}$$

where

$$h_+' = -Rr_{nm}(H_1' + H_2')/2 \ . \tag{2.15}$$

Here the derivative of $H_k' = (dH_k/dr_{nm})$ is due to the 3-momentum $\vec{q}$ which gives rise to the relative direction $\hat{r}_{nm} = \vec{r}_{nm}/r_{nm}$. The electron P wave leads to the additive vector direction $r_{+nm} = (\vec{r}_n + \vec{r}_m)/|\vec{r}_n + \vec{r}_m|$ in this χ_p'. [The other six are defined in Eqs.(2.3), (2.6), (2.7) and (2.10) of ref.(10).]

The estimation of $M_\alpha^{(0\nu)}$ becomes complicated because of the existence of h_+. In order to check the reliability of theoretical calculation for $M_\alpha^{(0\nu)}$, it is convenient theoretically to consider the $(\beta\beta)_{2\nu}$ mode, because this decay mode is allowed for either Dirac or Majorana neutrino within the standard minimal model ($m_\nu = \lambda = \eta = \kappa = 0$). The inverse of the half-life for the $(\beta\beta)_{2\nu}$ mode is given by

$$[T_{2\nu}(0^+ \to 0^+)]^{-1} = \xi_p\left|\left((g_V/g_A)^2 M_F^{(2\nu)} - M_{GT}^{(2\nu)}\right)/\mu_0\right|^2 G_{GT} \ , \tag{2.16}$$

where G_{GT} is a known quantity[3),*)] and

$$\xi_p = 2\Sigma_{i\leq j}'\varepsilon_{ij}^2|U_{ei}U_{ej}|^2 \ , \tag{2.17}$$

$$M_{GT}^{(2\nu)} \equiv <B|\Sigma_{nm}\tau_n^{(+)}\tau_m^{(+)}\vec{\sigma}_n\cdot\vec{\sigma}_m|A> \ , \tag{2.18}$$

$$M_F^{(2\nu)} \equiv <B|\Sigma_{nm}\tau_n^{(+)}\tau_m^{(+)}|A> \ , \tag{2.19}$$

$$\mu_0 \equiv [<E_i> - (M_A + M_B)/2]/m_e \ . \tag{2.20}$$

Here ξ_p is due to neutrino mixings and a statistical factor [$\varepsilon_{ij} = (1/\sqrt{2})$ for $i = j$ and $\varepsilon_{ij} = 1$ for $i \neq j$]. We shall assume $\xi_p = 1$ in this talk. Some examples are shown in Table II. Concerning the detail of recent experimental results, see the review papers in ref. (15). The value of $|M_F^{(2\nu)}|$ should be much smaller than $|M_{GT}^{(2\nu)}|$, because of the isospin conservation (through the isobaric analogue state in Fig. 3).[7),22)] In Table II, values of $|M_{GT}^{(2\nu)}|$ are obtained by using the listed values of μ_0 by Haxton, Stephenson and Strottman.[22)]

*) Numerical values of G_{GT} in Table II are a little different from those in ref.(22). We used $\cos\theta_C = 0.9737$, $G = 1.16632\cdot10^{-5}$ GeV^{-2} and 1 year$=3.1558\cdot10^7$ sec.

Many theoretical estimates for $M_{GT}^{(2\nu)}$ have been made.[23] Let us consider the case of ^{82}Se and ^{130}Te measured by the geochemical experiments.[19] In a simple shell model calculation, Vergados[24] obtained $M_{GT}^{(2\nu)}(^{130}Te) = -0.496$ which is the same order as the "geochemically experimental" value shown in Table II. However, by doing the more elaborate computation with an extended model space, Haxton et al.[22] found -2.966 (-1.876) for ^{130}Te (^{82}Se), which is larger by factor of 12.4 (2.4) than in Table II. They did not take into account contributions from the Gammow-Teller state shown in Fig. 4, but Zamick and Auerbach[25] showed that by applying the Nilsson pairing model for ^{76}Ge and including the Δ particle-nucleon hole states, contributions from different shell transitions add coherently to give the large value similar to $M_{GT}^{(2\nu)}(^{76}Ge) = -2.556$ obtained by Haxton et al.. Also, without using the closure approximation (II) mentioned before, Grotz, Klapdor and Matzinger[9] evaluated the half-life by using the BCS pairing model, and got $T_{2\nu} = 1.14 \cdot 10^{19}$ ($3.51 \cdot 10^{18}$) for ^{130}Te (^{82}Se). Discrepancies between theory and geochemical experiment become worse. On the other hand, Abad et al.[26] and Grotz et al.[9] found that these geochamical results can be explained, if only the lowest 1^+ state of the intermediate nuclide is assumed to make the dominant contribution.

As a conclusion, in order to check the reliability of theoretical treatments such as the closure approximation and the nuclear model, it is quite disirable to determine the finite results for the $(\beta\beta)_{2\nu}$ mode by direct counting experiments. From the theoretical point of view, it is necessary to understand whether the discrepancy between the present theoretical estimate and the geochemical result

Table II. Some examples for the $(\beta\beta)_{2\nu}$ mode.

Transition	Experiment (year)		$(G_{GT})^{-1}$ (year)	μ_0	$\lvert M_{GT}^{(2\nu)} \rvert$
	Geochemical	Direct Counting	ref. (3)	ref. (22)	
$^{48}Ca \rightarrow {}^{48}Ti$		$> 3.6 \cdot 10^{19}$ (a)	$2.6 \cdot 10^{16}$	15.10	<0.41
$^{76}Ge \rightarrow {}^{76}Se$		$> 2.8 \cdot 10^{19}$ (b) $> 4 \cdot 10^{18}$ (c)	$7.9 \cdot 10^{18}$	18.42	< 9.8
$^{82}Se \rightarrow {}^{82}Kr$	$1.45 \cdot 10^{20}$ (d)	$(1.0 \pm 0.4) \cdot 10^{19}$ (e)	$2.3 \cdot 10^{17}$	19.73	0.79
$^{130}Te \rightarrow {}^{130}Xe$	$2.55 \cdot 10^{21}$ (d)		$2.1 \cdot 10^{17}$	25.98	0.24
$^{150}Nd \rightarrow {}^{150}Sm$		$> 5 \cdot 10^{18}$ (f)	$8.7 \cdot 10^{15}$		

(a): ref. (16), (b): ref. (17), (c): ref. (18), (d): ref. (19),
(e): ref. (20), (f): ref. (21)

exists really. Since the method of theoretical calculation is not established even for the absolute value of $M_{GT}^{(2\nu)}$, further investigations are needed for the more complicated $M_{GT}^{(0\nu)}$ in Eq.(2.10).

In order to find order of magnitudes of three parameters, m_ν, λ and η, we shall make the following assumptions: Ratios of theoretical values for various nuclear matrix elements $M_\alpha^{(0\nu)}$'s may be more reliable than absolute values themselves. Therefore, ratios obtained theoretically by Haxton et al.[22] will be used. Concerning the absolute values of M_α's, in addition to estimates by them,[22] we shall use the reduced values which are consistent with the geochemical results: Namely, since the reduction factor to match the ^{82}Se geochamical result is 1/2.4, the value $|M_{GT}^{(2\nu)}| = 2.556/2.4 = 1.07$ for ^{76}Ge is also considered.[3] There are no published theoretical estimates for $M_\alpha^{(0\nu)}$'s related with the V+A term. Therefore, we shall use values based on the simple spherically symmetric nuclear model as an educated guess.

2-3. Estimates of $\langle m_\nu \rangle$, λ and η:

Experimental data for the $(\beta\beta)_{0\nu}$ mode are not reviewed here.[15] We shall discuss only two results; namely, the geochemical data on the ratio ^{128}Te/^{130}Te and the direct counting experiments on ^{76}Ge.

[I] $\underline{R_T = \left[T_{1/2}(^{128}\text{Te}) \Big/ T_{1/2}(^{130}\text{Te}) \right]}$

Since this ratio is measured by the geochemical method, the half-life consists of two modes, $(1/T_{1/2}) = (1/T_{2\nu}) + (1/T_{0\nu})$. Then, we have

$$R_T = \rho_{2\nu} r_{2\nu} \left(\frac{1 + {}^{130}(\xi_\mu^2 \Xi / G_{GT})}{1 + {}^{128}(\xi_\mu^2 \Xi / G_{GT})} \right), \qquad \rho_{2\nu} r_{2\nu} = \left(\frac{T_{2\nu}(128)}{T_{2\nu}(130)} \right), \tag{2.21}$$

where we have defined from $T_{2\nu}$ in Eq.(2.16) for the $(\beta\beta)_{2\nu}$ mode,

$$\rho_{2\nu} = \left| \frac{^{130}\left(M_{GT}^{(2\nu)}/\mu_0 \right)}{^{128}\left(M_{GT}^{(2\nu)}/\mu_0 \right)} \right|^2, \qquad r_{2\nu} = [G_{GT}(130)/G_{GT}(128)], \tag{2.22}$$

and from ratio of $T_{2\nu}$ to $T_{0\nu}$ in Eq.(2.9),

$$\xi_\mu(A) = \xi(A)\mu_0(A) \quad \text{with} \quad \xi(A) = [M_{GT}^{(0\nu)}(A)/M_{GT}^{(2\nu)}(A)]. \tag{2.23}$$

By substituting 12 kinematical factors G_{0j}'s given in Table I of ref.(10) and numerical values of 8 nuclear parameters χ's,*) $\Xi(128)$ and $\Xi(130)$ in Eq.(2.9) are

*) For 8χ's defined in ref.(10), we use tha following real values for both ^{128}Te and ^{130}Te: $\chi_F = -0.23$ [from ref.(22)], $\chi_{GT}^{(0)} = 0.65$, $\chi_F^{(0)} = 0.65\,\chi_F$, $\chi_{GT}' = 1.25$, $\chi_F' = 1.25\,\chi_F$, $\chi_T' = 0$, χ_P' = free and χ_R' = free. In ref.(3), we assumed $\chi_{GT}' = 1$, $\chi_F' = \chi_F$, $\chi_{GT}^{(0)} = \chi_F^{(0)} = \chi_T' = \chi_P' = \chi_R' = 0$.

$$\Xi(128) = 10^{-15}\left[\begin{array}{l} 2.7\,x^2 - 0.37\,xy\cos\psi + 0.39\,y^2 - 0.026\,yz \\ -(0.56 + 1.18\cdot10^2\chi_P' - 5.9\cdot10^2\chi_R')\,xz\cos\psi \\ +(0.133 + 3.0\cdot10^3\chi_P'^2 - 2.9\cdot10^4\chi_P'\chi_R' + 7.3\cdot10^4\chi_R'^2)z^2 \end{array}\right] \text{(year)}^{-1}, \quad (2.24)$$

$$\Xi(130) = 10^{-14}\left[\begin{array}{l} 6.5\,x^2 - 2.4\,xy\cos\psi + 8.3\,y^2 - 4.6\,yz \\ -(1.19 + 1.69\cdot10^2\chi_P' + 8.2\cdot10^2\chi_R')\,xz\cos\psi \\ +(1.27 + 6.7\cdot10^3\chi_P'^2 - 6.4\cdot10^4\chi_P'\chi_R' + 1.50\cdot10^5\chi_R'^2)z^2 \end{array}\right] \text{(year)}^{-1}, \quad (2.25)$$

where the relative phase ψ is

$$\psi = \arg[(\Sigma_j'(m_j/m_e)U_{ej}^2)(\Sigma_j' U_{ej} V_{ej})^*], \quad (2.26)$$

and χ_P' is defined in Eq.(2.14) and χ_R' is the nucleon recoil parameter defined in Eq.(2.10) of ref. (10). If the CP invariance is assumed, then $\psi = 0$ or π, because $(U^T, V^\dagger)$ is an orthogonal matrix.

If we take $\xi(130) = 1.70$, $\xi(128) = 1.69$ and $\mu_0(128) = 24.53$ obtained by Haxton et al.,[22] then we obtain $^{130}(\xi_\mu^2/G_{GT}) = 4.2\cdot10^{20}$ and $^{128}(\xi_\mu^2/G_{GT}) = 2.1\cdot10^{24}$ from $G_{GT}(128)^{-1} = 1.2\cdot10^{21}$ and Table II. Therefore, an unequal relation $^{128}(\xi_\mu^2\,\Xi/G_{GT}) > {}^{130}(\xi_\mu^2\,\Xi/G_{GT})$ is always satisfied. To get this conclusion, we have assumed $T_{0\nu}(0^+\to0^+) < T_{0\nu}(0^+\to2^+)$. For ^{128}Te, this may be reasonable because of the factor of 10 due to the available phase space, cf., G_{01} with G_{22} in Table III of ref.(3a). But we should carefully investigate the unestablished contribution due to the N^*-mechanism[13] for the $0^+\to2^+$ transition. [See Table I of ref.(3a).] For ^{130}Te, although the phase space factors, say G_{01} and G_{22}, are the same order, this contribution is not serious because of $^{130}(\xi_\mu^2\,\Xi/G_{GT}) < 10^{-2}$ for the $0^+\to2^+$ transitions where there is no dangerous αZ Coulomb correction.[3),10)] Here we have supposed that parameters x, y and z are of order of or less than 10^{-5}. Thus, we conclude that if no $(\beta\beta)_{0\nu}$ mode, $(\rho_{2\nu}r_{2\nu}/R_T) = 1$ and in general

$$(\rho_{2\nu}r_{2\nu}/R_T) \simeq 1 + {}^{128}(\xi_\mu^2\,\Xi/G_{GT}) \geq 1. \quad (2.27)$$

Now let us consider two results for R_T from the geochemical experiment:

$$R_T = (1.59 \pm 0.05)\cdot10^3 \quad \text{by the Missouri group,}[27] \quad (2.28)$$

$$R_T^{-1} = (1.03 \pm 1.13)\cdot10^{-4} \quad \text{by the Heidelberg MPI group.}[28] \quad (2.29)$$

The ratio of kinematical factors[3] is $r_{2\nu} = (5.62 \pm 0.25)\cdot10^3$. If we take $\rho_{2\nu} = 0.902$ by Haxton et al.,[22] then $\rho_{2\nu}r_{2\nu} = 5.1\cdot10^3$ means that the Missouri data satisfies the unequal relation (2.27), while the central value of the Heidelberg data does not. The theoretical ambiguity in the $(\beta\beta)_{2\nu}$ mode is only in $\rho_{2\nu}$, which Pontecorvo[29] supposed to be unity. Klapdor and Grotz[9] found $\rho_{2\nu}r_{2\nu} = 4.0\cdot10^3$

without assuming the closure approximation (II) and by including the effect of Δ-h excitations. This makes worser. Therefore, in the following, we shall require that theoretical estimates lie within two standard deviation of the Heidelberg data.

By substituting Eqs.(2.24) and (2.25) with $\psi = 0$ into Eq.(2.21), we find

$$\langle m_\nu \rangle = |\Sigma_j' m_j U_{ej}^2| < 5.6 \text{ eV} \qquad \text{for } \lambda = \eta = 0. \tag{2.30}$$

$$y = \lambda |\Sigma_j' U_{ej} V_{ej}| < 3.0 \cdot 10^{-5} \qquad \text{for } m_j = \eta = 0, \tag{2.31}$$

$$|z| = |\eta \Sigma_j' U_{ej} V_{ej}| < 5.0 \cdot 10^{-5} \qquad \text{for } m_j = \chi_P' = \chi_R' = 0 \text{ and } \lambda \ll |\eta|. \tag{2.32}$$

If $|\chi_P'| > 10^{-2}$ and $|\chi_R'| > 10^{-3}$, then we have

$$|z| < 3.3 \cdot 10^{-7} / |\chi_P' - 4.9 \chi_R'| \qquad \text{for } m_j = 0 \text{ and } \lambda \ll |\eta|. \tag{2.33}$$

[II] The $(\beta\beta)_{0\nu}(0^+ \to 0^+)$ transition in ^{76}Ge

Three upper limits for the half-life of this decay mode by the direct counting method have been reported:

$$T_{0\nu} > 5 \cdot 10^{22} \text{ (y)} \qquad \text{by the Milano group}^{30)}, \tag{2.34}$$

$$> 1.7 \cdot 10^{22} \text{ (y)} \qquad \text{by the Barttle-South Carolina group}^{31)}, \tag{2.35}$$

$$> 1.0 \cdot 10^{22} \text{ (y)} \qquad \text{by the Caltech group.}^{32)} \tag{2.36}$$

The theoretical estimate for the inverse of the half-life of the $(\beta\beta)_{0\nu}(0^+ \to 0^+)$ transition is by assuming $\psi = 0$ and numerical values χ's,*)

$$[T_{0\nu}(0^+ \to 0^+)]^{-1} = |M_{GT}^{(0\nu)}|^2 \cdot 10^{-15} \times \left[\begin{array}{l} 8.9 x^2 - 3.0 xy + 8.3 y^2 - 6.1 yz \\ - (1.04 + 2.2 \cdot 10^2 \chi_P' - 1.66 \cdot 10^3 \chi_R') xz \\ + [1.79 + 5.8 \cdot 10^3 (\chi_P')^2 - 8.6 \cdot 10^4 \chi_P' \chi_R' + 3.2 \cdot 10^5 (\chi_R')^2] z^2 \end{array} \right] \text{(year)}^{-1}. \tag{2.37}$$

By assuming $M_{GT}^{(0\nu)} = -1.76$ (-4.19), the value inside bracket being obtained by Haxton et al.[22], we get from the Milano data,**)

$$\langle m_\nu \rangle < 14 \text{ eV} \quad (5.8 \text{ eV}) \qquad \text{for } \lambda = \eta = 0, \tag{2.38}$$

$$y < 2.8 \cdot 10^{-5} \quad (1.2 \cdot 10^{-5}) \qquad \text{for } m_\nu = \eta = 0, \tag{2.39}$$

$$|z| < 6.0 \cdot 10^{-5} \quad (2.5 \cdot 10^{-5}) \qquad \text{for } m_\nu = \chi_P' = \chi_R' = 0 \text{ and } \lambda \ll |\eta|. \tag{2.40}$$

If $|\chi_P'| > 10^{-2}$ and $|\chi_R'| > 10^{-3}$, we have

$$|z| < 1.1 \cdot 10^{-6} (\chi_P' - 7.4 \chi_R')^{-1} \left(4.4 \cdot 10^{-7} (\chi_P' - 7.4 \chi_R')^{-1} \right) \text{ for } m_\nu = 0 \text{ and } \lambda \ll |\eta|. \tag{3.41}$$

*) For 6 χ's, we use the following values: $\chi_F = -0.20$ [from ref.(22)], $\chi_{GT}^{(0)} = 0.8$, $\chi_F^{(0)} = 0.8 \chi_F$, $\chi_{GT}' = 1.2$, $\chi_F' = 1.2 \chi_F$ and $\chi_T' = 0$.

**) The expression including $\langle m_\nu \rangle$ and η which is obtained by Haxton et al. is given in ref.(31). However, we do not use it, because we can not check whether their derivation includes the αZ term in Eq.(2.5) for the η term.

3. Neutrino mass and the pseudo Dirac neutrino

3-1. Experimental results on m_ν

As we saw in §2-3, although there are some ambiguities for the theoretical treatment of the $(\beta\beta)_{0\nu}$ mode, we get the following upper limits for the neutrino mass:

$$\langle m_\nu \rangle = \left|\Sigma_j' m_j U_{ej}^2\right| \begin{cases} < 6 \text{ eV} & \text{from geochemical experiment,} \\ < (14 \sim 6)\text{eV} & \text{from direct counting experiment.} \end{cases} \tag{3.1}$$

We shall use these results in the following discussion.

On the other hand, there is a long history to determine the neutrino mass from the single β decay directly. In order to simplify the presentation, let us assume that only two mass eigenstate neutrinos are emitted in the single β decay $(A \to B + e + N_j)$. Then, the energy spectrum is expressed as

$$N(E) \sim pE(W-E)\left[\cos^2\theta \sqrt{(W-E)^2 - m_1^2} + \sin^2\theta \sqrt{(W-E)^2 - m_2^2}\right], \tag{3.2}$$

where θ is a mixing angle between two mass eigenstate neutrinos, E(p) is the energy (momentum) of electron and $W = (M_A^2 + m_e^2 - M_B^2)/2M_A$. The recent results from the ^3H decay under the assumption $\theta = 0$ are the following;

$$m_{\bar{\nu}_e} < (55 \sim 60) \text{ eV} \qquad \text{by Bergkvist,}^{33)} \tag{3.3}$$

$$14 \le m_{\bar{\nu}_e} \le 46 \text{ eV} \qquad \text{by the Moscow group (1980)}^{34)}, \tag{3.4}$$

$$(0 \le m_{\bar{\nu}_e} \le 41 \text{ eV} \quad \text{by Simpson}^{35)}),$$

$$20 \text{ eV} < m_{\bar{\nu}_e} \qquad \text{by the Moscow group (1983)}^{36)}. \tag{3.5}$$

The value in the bracket of Eq. (3.4) is derived from the old Moscow data by taking into account the instrumental correction. While, the Moscow group[36] pointed out that their results may also be interpreted as $0 \le m_1 \le 30$ (eV), $80 \le m_2 \le 120$ and $\cos^2\theta \simeq 0.75 \sim 0.95$.

In writing the status of neutrino oscillations, we shall use a 2 parameter model with a mass parameter $\Delta m^2 = |m_1^2 - m_2^2|$ (eV^2) and a mixing amplitude $\sin 2\theta$. Thus transitions between two weak eigenstate neutrinos, ν_{ℓ_1} and ν_{ℓ_2}, take plece with a probability,

$$P(\nu_{\ell_1} \to \nu_{\ell_2}) = \sin^2 2\theta \ \sin^2\xi \qquad \text{with} \quad \xi = 1.26\,\Delta m^2 (L/\omega), \tag{3.6}$$

where L (meter) is the distance between the source of ν_{ℓ_1} and detector, ω (MeV) is the neutrino energy. Until now, various laboratory experiments show no visible oscillation.[37] For example, the Grenoble-Gösgen results[38] shows that

$$\Delta m^2 < 0.014 \text{ eV}^2 \qquad \text{at } \sin^2 2\theta = 0, \tag{3.7}$$

or

$$\sin^2 2\theta < 0.15 \qquad \text{at large } \Delta m^2. \tag{3.8}$$

They will be referred to, respectively, as $\Delta m^2 = 0$ and no mixing in Table III symbolically. One exception which may show the neutrino oscillation is the solar

Table III. Consistency of 3 experimental resutls.

Type of ν / Experiment	$m_\nu \ll$ 10eV	$m_\nu \simeq$ a few 10eV		
	Majorana or Dirac	Majorana		Dirac
no neutrino oscillation	acceptable	$\Delta m^2 = 0$	no mixing	$\Delta m^2 = 0$ or no mixing
$(\beta\beta)_{0\nu}$ mode $<m_\nu> < 6$eV or $<m_\nu> < 14$eV	acceptable	neutrino is PDν	not acceptable	acceptable
^{3}H-decay $m_\nu > 20$eV	not acceptable			acceptable
case	A	B	C	D

neutrino experiment ($L = 10^{11}$).[39] If it is indeed telling us the large mixing angle, then the Δm^2 value must lie between 10^{-2} and 10^{-10} eV^2. However, I shall not take it seriously, because of the flux ambiguity for $\omega > 0.236$ MeV.

Finally, from the view point of cosmology, it has been reported[40] that the number of generations for the light neutrinos is less than 4, and that the sum of their masses is

$$\Sigma_j m_j \leq 100 \text{ eV}. \tag{3.9}$$

These situations may be summarized as in Table III.[41] If all neutrinos are Dirac fermions (case D in §1-3), there is no $(\beta\beta)_{0\nu}$ mode, but there remains a theoretical problem how to explain $m_\nu \ll m_e$. On the other hand, in the Majorana case where there is a possibility to explain it by the see-saw mechanism, the case C in Table III is not allowed, because $<m_\nu> = m_1 < 20$ eV and $m_{\bar{\nu}_e} > 20$ eV from Eqs.(3.1) and (3.5). If the new Moscow result Eq.(3.5) is considered seriously, one possible scenario is the case B. That is, some of the Majorana neutrinos are the pseudo Dirac neutrino (PDν). Let us explain it in the next subsection.

3-2. The pseudo Dirac neutrino (PDν)

It was recognized first by us that the "neutrino mass" appeared in the $(\beta\beta)_{0\nu}$ mode may possibly be suppressed.[42] Later, Wolfenstein pointed out that it can be interpreted as the existence of two neutrinos with equal mass but opposite CP values, if CP is conserved.[43] Finally, it has been realized that it is due to the character of a pseudo Dirac neutrino.[6),44] The idea of PDν itself had been proposed by Wolfenstein before.[45]

In order to show typical features of the PDν, let us consider the simplest example: (i) Only 2 generations exist (ℓ=e and μ), (ii) there is no RH neutrino and (iii) 2 LH Majorana neutrinos have equal mass ($m_1 = m_2$). Then, by using only $U^{(1)}$ in Eq.(1.11), the weak eigenstate neutrinos are expressed as

$$\begin{pmatrix} \nu_{eL} \\ \nu_{\mu L} \end{pmatrix} = \begin{pmatrix} \cos\theta & \sin\theta e^{i\beta} \\ \sin\theta & -\cos\theta e^{i\beta} \end{pmatrix} \begin{pmatrix} N_{1L} \\ N_{2L} \end{pmatrix} . \tag{3.10}$$

If the CP invariance is assumed, then we have $\beta = 0$ or $\pi/2$ (mode π). Thus, $\langle m_\nu \rangle$ in Eq.(2.6) is expressed as follows:

β	CP values for N_{1L} and N_{2L}	$\langle m_\nu \rangle = \lvert \Sigma_j' m_j U_{ej}^2 \rvert$
0	same	$m_1(\cos^2\theta + \sin^2\theta)$
$\pi/2$	opposite	$m_1\lvert\cos^2\theta - \sin^2\theta\rvert$

On the other hand, if $\beta = \pi/2$, one "Dirac" neutrino can be constructed from 2 LH Majorana neutrinos with the opposite CP values:[6)]

$$\psi_L = [N_{1L} + i N_{2L}]/\sqrt{2}, \tag{3.11a}$$

$$\psi_R = [(N_{1L})^C + i(N_{2L})^C]/\sqrt{2}. \tag{3.11b}$$

By substituting Eq.(3.11) into Eq.(3.10), we find

$$\nu_{eL} = \cos\varepsilon\,\psi_L + \sin\varepsilon\,(\psi_R)^C, \tag{3.12a}$$

$$\nu_{\mu L} = -\sin\varepsilon\,\psi_L + \cos\varepsilon\,(\psi_R)^C, \tag{3.12b}$$

where $\cos\varepsilon = (\cos\theta + \sin\theta)/\sqrt{2}$ and $\sin\varepsilon = (\cos\theta - \sin\theta)/\sqrt{2}$.

If $\theta = \pi/4$ (mode $\pi/2$), i.e., $\varepsilon = 0$, then the weak interaction Hamiltonian in Eq.(1.3) becomes

$$H_W = (G/\sqrt{2})[\bar{e}\gamma_\rho\psi_L + \bar{\mu}\gamma_\rho(\psi_R)^C]\,J_L^\rho + \text{h.c.}, \tag{3.13}$$

There is no RH current in this example. This is exactly the Konopinski-Mahmoud scheme proposed in 1953, where the difference of lepton numbers ($L_e - L_\mu$) is conserved.[46)] Thus, the $(\beta\beta)_{0\nu}$ mode is forbidden, i.e., $\langle m_\nu \rangle = 0$, while the conversion $\mu^- + A \to B + e^+$ is allowed. Therefore, I would like to call this "Dirac" neutrino the "Dirac in Konopinski-Mahmoud (KM) scheme". While, the usual Dirac neutrino which consists of one LH and one RH Majorana neutrinos with a definite

Table IV. The "Dirac in KM scheme" neutrino and the PDν.

θ	$-\pi/4$	$\longrightarrow$	0	$\longrightarrow$	$\pi/4$
ε	$\pi/2$	$\longleftarrow$	$\pi/4$	$\longleftarrow$	0
$L_e - L_\mu$	conserved	not conserved			conserved
$\nu_{\alpha L}$	Dirac in KM scheme	pseudo Dirac neutrino			Dirac in KM scheme
$(\beta\beta)_{0\nu}$ $\lambda=\eta=0$	forbidden	$\longleftarrow$	no suppression factor	$\longrightarrow$	forbidden
$\mu^- \to e^+$	no suppression factor	$\longrightarrow$	forbidden	$\longleftarrow$	no suppression factor

flavor is distinguished by calling it an "ordinary Dirac" neutrino. In the latter case, the lepton number for each flavor is conserved separately.

If $\theta \neq \pi/4$, then the mass degeneracy is broken by a tiny mass difference[41),45)] which is generated by the radiative correction due to H_W ($\Delta m_1 \neq \Delta m_2$; $(\Delta m_j/m_j) \ll 1$). Thus, we have two Majorana neutrinos, though their mass difference is too small to be measured experimentally. In the extreme case with $\theta = 0$, the $(\beta\beta)_{0\nu}$ mode has no suppression factor because $\langle m_\nu \rangle = m_1$, while the $\mu^- \to e^+$ conversion is forbidden. These situations are shown in Table IV.

Conditions for the pseudo Dirac neutrino are summarized as follows:[41)] (i) At least in zeroth-order, a pair of mass degenerate neutrinos form a "Dirac" neutrino, ψ. (ii) For the mass matrix of neutrino systems, there is a phase transition of ψ, which characterizes the "lepton number" assigned to ψ. (iii) Both ψ and ψ^C couple to charged leptons with different flavours through either gauge boson or Higgs boson coupling, i.e., $\varepsilon \neq 0$ (mode $\pi/2$) in the weak interaction of Eq.(3.12). Thus, ψ splits into two Majorana neutrinos with different masses due to the higher-order (radiative) corrections. (iv) This mass splitting should be finite. (v) If the CP invariance is assumed, the composing Majorana neutrinos should have opposite CP values.

Finally, let us show one example of PDν in the framework of SU(5) GUTS with 3 generations.[6)] In order to get both the reasonable Kobayashi-Maskawa mixing matrix and the appropriate mass relations among quarks and charged leptons, we had to introduce 6 Higgs bosons. It was also required for a PDν mass to be $m_D = m_1 = m_2$. Thus, two neutrino masses, m_D and M_3, are remained as fee parameters. Only the final results are listed here.

For the β *decay* from Eq.(3.2):

$$N(E) \sim \left(1 - \frac{m_e}{m_\tau}\right)\sqrt{\Delta^2 - m_D^2}\;\theta(\Delta - m_D) + \left(\frac{m_e}{m_\tau}\right)\sqrt{\Delta^2 - m_3^2}\;\theta(\Delta - m_3), \tag{3.14}$$

where $\Delta = W - E$, $\theta(x) = 1$ for $x > 0$ and $\theta(x) = 0$ for $x < 0$.

For the neutrino oscillation from Eq.(3.6):

$$P(\nu_e \to \nu_\tau) \simeq 4(m_e/m_\tau)\,\sin^2\xi\,, \tag{3.15}$$

$$P(\nu_\mu \to \nu_e) \simeq 4(m_e m_\mu/m_\tau^2)\,\sin^2\xi\,, \tag{3.16}$$

$$P(\nu_\mu \to \nu_\tau) \simeq 4(m_\mu/m_\tau)\,\sin^2\xi\,. \tag{3.17}$$

In the first two cases, we can say $\sin^2(2\theta) \sim 0$. But the third $P(\nu_\mu \to \nu_\tau)$ gives $\sin^2(2\theta) \simeq 4(m_\mu/m_\tau) \simeq 0.24$, which leads to the following limit from the $\nu_\mu - \nu_\tau$ experiment,[47]

$$\Delta m^2 = |m_D^2 - m_3^2| < 5\ \mathrm{eV}^2. \tag{3.18}$$

For $\langle m_\nu \rangle$ *in the* $(\beta\beta)_{0\nu}$ *mode* from Eq.(2.6):

$$\langle m_\nu \rangle \simeq 2\sqrt{m_e/m_\mu}\; m_D + (m_e/m_\tau)\, m_3\,. \tag{3.19}$$

The suppression factor for the $(\beta\beta)_{0\nu}$ mode becomes $2\sqrt{m_e/m_\mu} \simeq 0.14$. If the lower limit ($m_\nu > 20$ eV) in Eq.(3.5) is combined with Eq.(3.18), then we have $m_D \approx m_3 > 20$ eV, so that $\langle m_\nu \rangle$ should be larger than 2.8 eV from Eq.(3.19) in this example.

4. Right-handed parameters ; λ and η

Many experimental searchs for non-zero right-handed parameters within the framework of the gauge theory have been carried out.[48] They are obtained from the μ decay, the polarization of $e^\pm$ in the β decay and the ν - N scattering. In these processes, lighter neutrinos appear in the real state and heavier neutrinos are missing, because of the energy conservation. All results before June of 1983 are beautifully summarized in Fig. 1 of ref.(48). Data analyses in these experiments have been done without taking the neutrino mixing into consideration. This mixing effect is included hereafter. On the other hand, in the $(\beta\beta)_{0\nu}$ mode, all neutrino contributions are in the virtual state. We found upper limits on y and z in Eqs.(2.31-33) and (2.39-41). Let us discuss the consistency between these two different approaches.

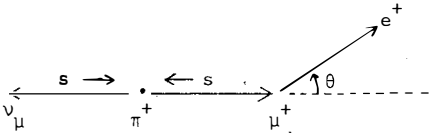
As an example among former approaches, we shall consider the Berkeley[48] experiment in which the deviation from the minimal standard model is measured on the e^+ spectrum end point in μ^+ decay. The effective lepton-lepton weak interaction Hamiltonian corresponding to H_W in Eq.(1.3) is

$$H_{W\ell} = (G/\sqrt{2})[j^{\dagger}_{L\rho}\, j^{\rho}_{L} + \eta(j^{\dagger}_{L\rho}\, j^{\rho}_{R} + \text{h.c.}) + \lambda\, j^{\dagger}_{R\rho}\, j^{\rho}_{R}]\,. \tag{4.1}$$

The partial decay rate of μ^+ decay is expressed as [5),49)]

$$d\Gamma = \left(\frac{G^2 m_\mu E_0}{24\pi^3}\right)[N(E) + S(E)\, P_\mu \cos\theta]\, pE\, dE\, d\cos\theta\,, \tag{4.2}$$

where N(E) and S(E) are spectra for no polarized μ^+ and polarization parts, respectively, P_μ is the absolute magnitude of μ^+ polarization in π^+ decay and $E_0 = (m_\mu^2 + m_e^2)/(2m_\mu)$ and $E_{max} = E_0 - (m_j + m_k)^2/(2m_\mu)$, m_k being the mass of the k-th mass eigenstate neutrino. The decay angle θ is defined as follows:



The Berkeley group measured the ratio

$$R(E, \theta) = [N(E) + S(E)\, P_\mu \cos\theta]/N(E)\,. \tag{4.3}$$

After subtracting the radiative corrections and terms proportional to m_e, they defined the limiting value

$$R(E \to E_{max},\ \theta \to 0) = 1 - C_\mu\,, \tag{4.4}$$

and found the upper limit [48)]

$$C_\mu \equiv \left(\frac{A - \lambda^2 B}{A + \lambda^2 B}\right) P_\mu > 0.9959, \tag{4.5}$$

where A and B are defined as follows in terms of neutrino mixing matrices in Eq.(1.9) under the assumption that all masses of *emitting* neutrinos are much smaller than m_μ, [49),5)]

$$A = \Sigma''_{jk} |U_{ej}|^2 |U_{\mu k}|^2\,, \tag{4.6a}$$

$$B = \Sigma''_{jk} |V_{ej}|^2 |V_{\mu k}|^2\,, \tag{4.6b}$$

Here the primed sum extends over all energetically allowed neutrino pairs, i.e., $(m_j + m_k)^2 < m_\mu^2 + m_e^2 - 2 m_\mu E$.

Next, we have to know the μ^+-polarization P_μ in the $\pi^+ \to \mu^+$ decay. In this case, as there are the effects due to the hadronic current $J_{L(R)\rho}$ in Eq.(1.3), the relation $\langle 0|J_L|\pi^+\rangle = -\langle 0|J_R|\pi^+\rangle$ is assumed.[49)] By assuming again that masses of neutrinos *emitted* in π^+ decay are much smaller than m_μ, we have [49)]

$$P_\mu = \left[1 - \frac{2(\lambda - \eta)^2 v_\mu}{(1 - \eta)^2 u_\mu + (\lambda - \eta)^2 v_\mu}\right] \tag{4.7}$$

where

$$u_\mu \equiv \Sigma_j' |U_{\mu j}|^2 \quad \text{and} \quad v_\mu \equiv \Sigma_j' |V_{\mu j}|^2. \tag{4.8}$$

Here the primed sum extends over all energetically allowed neutrinos, $m_j < (m_\pi - m_\mu)$.

Now, we are ready to find the physical meaning of the Berkeley data. Let us consider two extreme cases: One corresponds to the case D or (M-I) in §1-3, and the other is the case (M-II).

In the case D or (M-I), let us assume that all neutrinos are light enough to be emitted and their masses are much smaller than m_μ, i.e., $\Delta_j = (m_j/m_\mu) \ll 1$ like in Eq. (1.12). Then the unitarity condition requires that

$$A \cong B \cong u_\mu \cong v_\mu \cong 1 \quad \text{for all } \Delta_j \ll 1. \tag{4.9}$$

where deviations from unity are proportional to m_j.[5] Then the Berkeley group found

$$2(2\lambda^2 - 2\lambda\eta + \eta^2) < 0.0041. \tag{4.10}$$

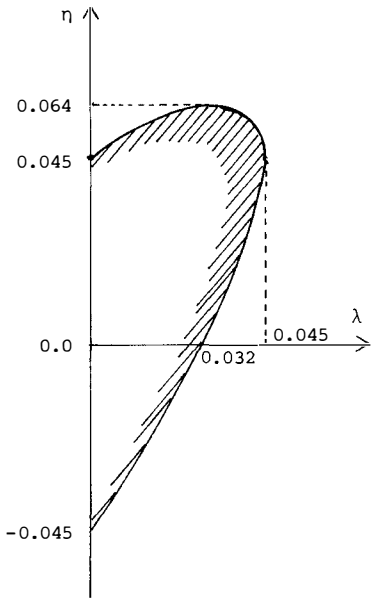


Fig. 5 Constraints on λ and η from $\pi^+ \to \mu^+ \to e^+$ decay

As shown in Fig. 5, we have

$$\lambda \simeq \alpha \equiv \left| \frac{M_1}{M_2} \right|^2 < 0.045, \tag{4.11}$$

or

$$|\eta| < 0.064. \tag{4.12}$$

Note that $\eta \simeq -\tan\zeta$. The Berkeley group concluded from Eq. (4.11) that if $M_1 \simeq 81$ GeV,[50] then we have $M_2 > 380$ GeV. These limits are correct for both Dirac and Majorana neutrino. [Note that strictly speaking, there are tiny different terms between the Dirac and Majorana cases, if there is a RH current.[5),49)] However, since the deviations due to both the finite m_j and the Majorana case may be small enough, we need not worry about them, if all $\Delta_j \ll 1$.]

Let us compare these constraints on λ and η with the upper limit on y and z from the $(\beta\beta)_{0\nu}$ mode, say, Eqs. (2.39) and (2.40). Of course, if the electron-neutrino (ν_e) is a Dirac neutrino, there is no $(\beta\beta)_{0\nu}$ mode. Even in the Majorana case, upper limits on y and z give no useful information in this $\Delta_j \ll 1$ case. The reason is as follows: In the framework of gauge theory, all

neutrinos should be distinguishable. The electron-neutrino shows a Dirac-like character, because the deviation from the unitarity condition $\Sigma_j U_{ej} V_{ej} = 0$ is of order of $m_j/\langle\omega\rangle$, $\langle\omega\rangle$ being the average energy of the propagating neutrino. In definitions of y and z, this m_j dependence has been neglected. [See Fig. 5 of ref. (3b).] Thus, limits on y and z may be compatible with Eqs. (4.11) and (4.12). If we assume phenomenologically that one LH neutrino is identical with one RH neutrino,[13a] the constraints from the $(\beta\beta)_{0\nu}$ mode give much severe limits on λ and η than the μ^+ decay. One example is shown in Table V.

On the other hand, the situation is completely different in the case (M-II), where $\Delta_k \ll 1$ but $\Delta_{n+k} \gg 1$ for $k \leq n$ in Eq. (1.13). The unitarity condition is not satisfied, because of the missing heavy RH neutrinos. In general, we may expect that $|V_{\ell k}| \ll 1$, as mentioned in §1-3. Concerning the off-diagonal elements of $U_{\ell j}$, a large number of experiments on nuclear beta decay and π and k decays have reexamined their data. These limits have been compiled by Shrock[51] and others.[37] Including the information from neutrino oscillation experiments, we find that all off-diagonal elements squared $|U_{\ell j}|^2$ are much smaller than unity. Therefore, we have the following approximate expressions;

$$A \simeq 1 - 2\bar{u}^2, \quad B \simeq \bar{v}^4, \quad u_\mu \simeq 1 - \bar{u}^2 \quad \text{and} \quad v_\mu \simeq \bar{v}^2, \tag{4.13}$$

where the barred quantities mean the small deviation from the unitarity. Then, by substituting Eq. (4.7) into Eq. (4.5), C_μ is expressed as

$$C_\mu \simeq 1 - 2\bar{v}^2 \{ \lambda^2 [1 + (B/\bar{v}^2)] - 2\lambda\eta + \eta^2 \}. \tag{4.14}$$

Table V. Constraints on λ and η in extreme cases.

Dirac ν ($j \leq n$)	Majorana neutrino ($j \leq 2n$, $k \leq n$)		
case D	case (M-I)		case (M-II)
all $\Delta_j = (m_j/m_\mu) \ll 1$			$\Delta_k \ll 1$ for LHν $\Delta_{n+k} \gg 1$ for RHν
no $(\beta\beta)_{0\nu}$ mode	if gauge theory is assumed, effectively no $(\beta\beta)_{0\nu}$ mode	if $\nu_e = N_1 = N_{n+1}$ and no mixing	from μ^+ decay $\lvert\bar{v}(\lambda-\eta)\rvert < 4.5\cdot10^{-2}$
from μ^+ decay or $\lambda < 0.045$ $\lvert\eta\rvert < 0.064$		from $(\beta\beta)_{0\nu}$ mode $\lambda < 2.8\cdot10^{-5}$ or $\lvert\eta\rvert < 6.0\cdot10^{-5}$	from $(\beta\beta)_{0\nu}$ mode $\lambda\lvert\bar{v}\rvert < 2.8\cdot10^{-5}$ or $\lvert\eta\bar{v}\rvert < 6.0\cdot10^{-5}$

Note that if $\bar{\nu} = B = 1$, this formula reduces to Eq.(4.10). However, in the present case (M-II), we obtain from the Berkeley data in Eq.(4.5),

$$|\bar{\nu}(\lambda - \eta)| < 0.045, \tag{4.15'}$$

where the small term $|B/\bar{\nu}^2| = \bar{\nu}^2$ has been neglected. Contrary to the previous case, bounds on λ and η become less severe by the factor of $|\bar{\nu}| \ll 1$. Since there are three unknown parameters in Eq.(4.15), we can not draw any direct information on the mass of the second gauge boson (W_2).

Concerning the upper limits on y and z from the $(\beta\beta)_{0\nu}$ mode, each term in the sum $|\Sigma'_j U_{ej} V_{ej}|$ of Eqs.(2.7) and (2.8) includes either $|V_{ek}|$ or $|U_{e,n+k}|$ for $k \leq n$, both of which are expected to be much less than unity ($\sim |\bar{\nu}|$). Therefore, we can reexpress their limits as follows from Eqs.(2.39) and (2.40);

$$y \simeq \lambda|\bar{\nu}| < 2.8 \cdot 10^{-5} \quad \text{or} \quad |z| \simeq |\eta\bar{\nu}| < 6.0 \cdot 10^{-5}. \tag{4.16}$$

These latter bounds are much tighter than the one from μ^+ decay in Eq.(4.15). These results are listed in Table V. In other words, if μ^+ decay data give us some finite constraint on $|\bar{\nu}(\lambda - \eta)|$ which is of order of $10^{-2} \sim 10^{-3}$, then we have to abandon the case (M-II), e.g., the idea of the see-saw-mechanism to explain the smallness of neutrino mass.

5. Concluding remarks

For the question whether neutrinos are Dirac or Majorana fermions, the observation of the $(\beta\beta)_{0\nu}$ mode seems to be the most prominant process.[52),*)] Until now, there is no positive result for it.

As it is well-known, we can distinguish the $(\beta\beta)_{0\nu}$ mode from the $(\beta\beta)_{2\nu}$ mode experimentally by observing the sum of two emitting electron energies. But there are some problems. One is whether this energy spectrum is disturbed by the majoron emission.[55)] Another is the pure theoretical problem of reliabilities on the closure approximation and the estimates of nuclear matrix elements. To understand the latter problem, the experimental observation of the $(\beta\beta)_{2\nu}$ mode is quite useful, because this mode takes place within the framework of the standard electroweak model. If the $0^+ \to 0^+$ transition in the $(\beta\beta)_{0\nu}$ mode is observed, it will tell us not only the Majorana character of neutrinos but also their chracters like mass, mixing scheme and the CP properties in addition to the information on the RH current.

---

*) Enqvist et al. have claimed that the $(\beta\beta)_{0\nu}$ mode can take place even for the Dirac neutrino.[53)] Their formalism needs to include some special symmetry to prevent the Majorana mass term derived from the higher order loop diagram. This symmetry requires that some unknown and unusual quarks (nucleus) should be participated, when their $(\beta\beta)_{0\nu}$ decay takes place by exchanging their Dirac neutrinos.[54)] Therefore, their $(\beta\beta)_{0\nu}$ mode is not included in my terminology of the $(\beta\beta)_{0\nu}$ mode connected between the ordinary nuclei.

Concerning the neutrino mass, we consider three extreme cases from present experimental data, i.e., cases A, B and D in Table III. For case A where all $m_j \ll 10$ eV, we need other ^{3}H experiments. In the case B where at least one pair of neutrinos is in the PDν type (two Majorana neutrinos), the combination of lepton numbers are conserved. While, in the case D where neutrinos are Dirac fermions, each lepton number associated with different charged leptons is conserved separately. Of course, it is possible to consider other cases where Dirac and Majorana neutrinos coexist due to mixings or where there are one light and one heavy ν_e's.[56] Anyway, we have to wait for the further experimental information to say something definetely.

As for the right-handed parameters (λ and η), the $0^+ \to 2^+$ transition in the $(\beta\beta)_{0\nu}$ mode gives us the definite information on the existence of the V+A current, if some of neutrinos are Majorana fermions.[11] In order to get the more detailed numerical values on λ and η, it needs to know the number of different neutrinos and their mixing scheme in addition to values of nuclear matrix elements. At present, we can not reach the definite conclusion for the right-handed parameters too.

The contents of this talk are the results obtained by coworking with Drs. E. Takasugi, M. Doi and H. Kenmoku. I would like to express my sincere thanks to them for their valuable discussions and criticisms, and also for reading this manuscript carefully. I also thank Professors E. Fiorini, T. Kirsten and H. V. Klapdor for their suggestive comments. As usual, I am indebted to Miss Y. Hinohara for her hard work to make this manuscript.

References

1) J. C. Pati and A. Salam, Phys. Rev. D10 (1974), 275;
R. N. Mohapatra and J. C. Pati, Phys. Rev. D11 (1975), 566; D11 (1975), 2599;
G. Senjanovic and R. N. Mohapatra, Phys. Rev. D12 (1975), 1502;
Riazuddin, R. E. Marshak and R. N. Mohapatra, Phys. Rev. D24 (1981), 1310.

2) T. Yanagida, *Proc. Workshop on Unified Theory and Baryon Number in the Universe*, eds. Sawada and Sugamoto, KEK (1979);
M. Gell-Mann, P. Ramond and R. Slanski, in "*Supergravity*", edited by van Nieuwenhuizen and Freedman (North-Holland, Amsterdam, 1979).

3a) Doi et al., Prog. Theor. Phys. 69 (1983), 602 and previous references cited.
3b) Doi et al., Prog. Theor. Phys. 66 (1981), 1765; 68 (1982), 348 (E).

4) M. A. B. Bég et al., Phys. Rev. Lett. 38 (1977), 1252 and previous references cited therein.

5) M. Doi et al., Prog. Theor. Phys. 67 (1982), 281; Sci. Rep. Col. Gen. Educ. Osaka Univ. 30 (1981), 119.

6) M. Doi et al., Prog. Theor. Phys. 70 (1983), 1331.

7) H. Primakoff and S. P. Rosen, Rep. Prog. Phys. 22 (1959), 121; Proc. Phys. Soc. 78 (1961), 464.

8) W. C. Haxton, G. J. Stephenson, Jr. and D. Strottman, Phys. Rev. Lett. 47 (1981), 153.
A. H. Huffman, Phys. Rev. C2 (1970), 742.

9) K. Grotz, H. V. Klapdor and J. Metzinger, J. Phys. 69 (1981), L169;
H. V. Klapdor and K. Grotz, Heidelberg MPI preprint, MPI H-1983-V34.

10) M. Doi et al., Prog. Theor. Phys. 70 (1983), 1353.

11) M. Doi et al., Phys. Lett. 103B (1981), 219;
S. P. Rosen, *Proc. of Orbis Scientiae* 1981, Coral Gables, 1981, p.333.

12) E. Takasugi, in *"Neutrino Mass and Gauge Structure of Weak Interactions"*, ed. by Barger and Cline, Telemark, October, 1982, (AIP Conference Proceedings, No. 99), p. 207.

13a) H. Primakoff and S. P. Rosen, Phys. Rev. 184 (1969), 1925.
13b) A. Halprin, Phys. Rev. D24 (1981), 2988.

14) D. Bryman and C. Picciotto, Rev. Mod. Phys. 50 (1978), 11 and previous references cited therein;
J. D. Vergados, Phys. Rev. D25 (1982), 914; Nucl. Phys. B218 (1983), 109.

15) L. Zanotti, Milano Univ. preprint for ICOMAN 83 Conference, Frascati, January, 1983.
C. S. Wu, in *"Science Underground"*, ed. by Nieto, Haxton, Hoffman, Kolb, Sandberg and Toevs, Los Alamos, September, 1982, (AIP Conference Proceedings, No. 96), p. 374.
Yu. G. Zdesenko, Sov. J. Part. Nucl. 11 (1980), 542.
New data: F. Leccia, et al., Nuov. Cim. 78A (1983), 50.

16) R. K. Bardin et al., Nucl. Phys. A158 (1970), 337.

17) F. T. Avignone et al., in AIP Conf. Proc. No. 96, p. 419.

18) E. Bellotti et al., in AIP Conf. Proc. No. 99, p. 219.

19) T. Kirsten, in AIP Conf. Proc. No. 96, p. 396.

20) M. K. Moe and D. D. Lowenthal, Phys. Rev. C22 (1980), 2186;
M. K. Moe and A. A. Hahn, in AIP Conf. Proc. No. 96, p. 411.

21) G. R. Smith, Phys. Rev. C4 (1971), 1344.

22) W. C. Haxton, G. J. Stephenson, Jr. and D. Strottman, Phys. Rev. D25 (1982), 2360.
W. C. Haxton and G. J. Stephenson, Jr., Los Alamos preprint LA-UR-83-417.

23) V. B. Beliaev and B. N. Zakhar'rev, Sov. Phys. JETP 7 (1958), 347;
L. Meichsner, Phys. Rev. 117 (1960), 489; 120 (1960), 552;
V. A. Khodel, Phys. Lett. 32B (1970), 583; Sov. J. Nucl. Phys. 12 (1971), 499; 20 (1975), 169;
S. A. Fayans and V. A. Khodel, Nucl. Phys. 3 (1977), 359;
J. D. Vergados, Phys. Rev. C24 (1981), 640;
P. Minkowski, Nucl. Phys. B201 (1982), 269;
L. D. Skouras and J. D. Vergados, Phys. Rev. C28 (1983), 2122.

24) J. D. Vergados, Phys, Rev. C13 (1976), 865.

25) L. Zamick and N. Auerbach, Phys. Rev. C26 (1982), 2185.

26) J. Abad et al., Univ. Zaragoza preprint IFNAE Z/83-1.

27) E. W. Hennecke, O. K. Manuel and D. D. Sabu, Phys. Rev. C11 (1975), 1378.

28) T. Kirsten, H. Richter and E. Fessberger, Phys. Rev. Lett. 50 (1983), 474;
Z. Phys. C 16 (1983), 189.

29) B. Pontecorvo, Phys. Lett. 26B (1968), 630.

30) E. Bellotti et al., paper presented at EPS 83, Brighton, July, 1983;
L. Zanotti, talk in this Proceedings.

31) F. T. Avignone et al., Phys. Rev. Lett. 50 (1983), 721.

32) A. Forster et al., Cal. Inst. Tech. preprint, CALT-83-412.

33) K. E. Bergkvist, Nucl. Phys. B39 (1972), 317; talk in this Proceedings.

34) V. A. Lubimov et al., Phys. Lett. 94B (1980), 266.

35) J. J. Simpson, paper presented at ICOMAN 83, Frascati, January, 1983.

36) S. Boris et al., paper presented at HEP 83, Brighton, July, 1983.

37) M. Shaevitz, *Proc.* 1983 *Int'l Symp. Lepton and Photon Int. at High Energies*, ed. by Cassel and Kreinick (Cornell Univ., Ithaca, 1983), p. 132.
See also F. Vannucci, talk in this Proceedings.

38) J. L. Vuilleumier et al., Phys. Lett. 114B (1982), 298;
F. Boehm, talk at APS Annual Meeting of the Div. of Particle and Field, Virginia, Sept. 1983, (Cal. Inst. Tech. preprint, CALT-63-413);
J. L. Thenard, talk in this Proceedings.

39) J. N. Bahcall, *Proc. Neutrino* 81, ed. by Cence, Ma and Roberts, Maui, Hawaii, July, 1981, p. 1;
M. Spiro and Schatzman, talks in this Proceedings.

40) M. S. Turner, *Proc. Neutrino* 81, p. 95;
G. Steigman, talk in this Proceedings.

41) Doi et al., Osaka Univ. preprint OS-GE 84-03.

42) Doi et al., Phys. Lett. 102B (1981), 323.

43) L. Wolfenstein, Phys. Lett. 107B (1981), 77.

44) S. T. Petcov, Phys. Lett. 110B (1982), 245;
C. N. Leung and S. T. Petcov, Phys. Lett. 125B (1983), 461;
J. W. F. Valle, Phys. Rev. D27 (1983), 1672;
J. W. F. Valle and M. Singer, Phys. Rev. D28 (1983), 540.

45) L. Wolfenstein, Nucl. Phys. B186 (1981), 147.

46) E. J. Konopinski and H. Mahmoud, Phys. Rev. 92 (1953), 1045;
S. M. Bilenky and B. Pontecorvo, Phys. Lett. 102B (1981), 32.

47) N. Ushida et al., Phys. Rev. Lett. 47 (1981), 1694;
N. J. Baker et al., Phys. Rev. Lett. 47 (1981), 1576;
A. E. Asratyan et al., Phys. Lett. 105B (1983), 301;

48) J. Carr et al., Phys. Rev. Lett. 51 (1983), 627;
References for other experiments are cited in this paper.

49) M. Doi, T. Kotani and E. Takasugi, Osaka Univ. preprint OS-GE 84-02.

50) G. Arnison et al., Phys. Lett. 122B (1983), 103;
M. Banner et al., Phys. Lett. 122B (1983), 476.

51) R. E. Shrock, Phys. Lett. 96B (1980), 159;
R. Prieels, talk in this Proceedings.

52) J. Schecher and J. W. F. Valle, Phys. Rev. D25 (1982), 2951.

53) K. Enqvist, J. Maalampi and K. Mursula, Phys. Lett. 124B (1983), 89.

54) M. Doi, T. Kotani and E. Takasugi, Osaka Univ. preprint OS-GE 84-08.

55) H. M. Georgi, S. L. Glashow and S. Nussinov, Nucl. Phys. B193 (1981), 297;
J. D. Vergados, Phys. Lett. 109B (1982), 96.

56) J. D. Vergados, Phys. Rev. D28 (1983), 2887;
S. P. Rosen, talk in this Proceedings; Los Alamos preprint LA-UR-83-3096.

COMMENT ON THE LIGHT-HEAVY MAJORANA NEUTRINO MECHANISM IN NO-NEUTRINO DOUBLE BETA DECAY

S. P. Rosen
T-Division, Los Alamos National Laboratory
Los Alamos, New Mexico 87545



ABSTRACT

We review the cancellation mechanism between light and heavy neutrinos in no-neutrino double beta decay, and the limits on the mass and mixing angle for the heavy neutrino. We emphasize that the effective mass for no-neutrino double beta decay varies with atomic weight, being heavier the lighter the parent nucleus. A search for double beta decay in ^{48}Ca will be an excellent test of this mechanism.

As an alternative to what have become known as "Pseudo-Dirac" neutrinos[1], Halprin, Petcov and I[2] have proposed the "light-heavy" mechanism for cancellations in double beta decay. The idea is inspired by the "see-saw" mass matrix of Gell-Mann, Ramond, and Slansky[3], and by an earlier observation that experimental limits on double beta decay lifetimes yield lower limits on "heavy" neutrino masses[4], as well as upper limits on "light" neutrino masses. Thus we proposed that in the amplitude for no-neutrino double beta decay, the exchange of a light neutrino, with mass a few times 10 ev, is almost cancelled by the exchange of a heavy neutrino, with opposite CP and mass anywhere from a few times 10 Mev to 5 Gev or more. In our case, both neutrinos must have the same helicity if they are to interfere coherently with one another.

The exchange of a light neutrino between two nucleons inside a nucleus gives rise to an effective Coulomb-like potential in the nuclear matrix element, whereas the exchange of a heavy neutrino gives rise to an effective Yukawa-like potential[4]. Therefore the "effective mass" in the no-neutrino decay amplitude has the form[2]

$$M_{\beta\beta} = |M_\ell \cos^2\theta - F(M_h,A) M_h \sin^2\theta| \qquad (1)$$

where M_ℓ and M_h are the light and heavy masses respectively, and θ is the mixing angle between them. The function $F(M_h,A)$ is the ratio of the Yukawa-like and Coulomb-like potentials,

$$F(M_h,A) = \langle \exp(-M_h r)/r \rangle \Big/ \langle 1/r \rangle \qquad (2)$$

and the argument A is inserted to emphasize that the value and functional form of F varies from one nucleus to another. Its value and form also depends upon the two-nucleon correlation functions used to evaluate the numerator and denominator in eq. (2).

We have found, in our investigations, that this mechanism gives us two general, qualitative results[2]. One is an upper bound on the mass of the heavy neutrino: M_h cannot be so large in eq. (2) that there is virtually no cancellation in eq. (1). The other is that the effective double beta decay mass, $M_{\beta\beta}$, varies with atomic mass, the general tendency being for $M_{\beta\beta}$ to become larger as the parent nucleus becomes lighter.

Exactly what the upper bound on M_h is, or what the values of $M_{\beta\beta}$ are, can depend sensitively upon the two-nucleon correlation function being used. In a model with a hard core at 0.5 fermi[2], we have obtained a bound of 3.5 Gev, while in another model[5] the bound is only 500 Mev. The light neutrino mass M_ℓ falls in the ITEP-80 range[6] in both cases, and $M_{\beta\beta}$ is bounded by the latest Tellurium

ratio results[7]. As for the effective double-beta decay mass for lighter nuclei, we find similar results in both models:

$$\begin{aligned} 5 \text{ ev} &< {}^{82}(M_{\beta\beta}) < 16 \text{ ev} \\ 13 \text{ ev} &< {}^{48}(M_{\beta\beta}) < 43 \text{ ev} \end{aligned} \tag{3a}$$

for the first model, and

$$\begin{aligned} {}^{82}(M_{\beta\beta}) &\simeq 18 \text{ ev} \\ {}^{48}(M_{\beta\beta}) &\simeq 45 \text{ ev} \end{aligned} \tag{3b}$$

for the second. In eq. (3) the superscripts 82 and 48 stand for the parent isotopes ^{82}Se and ^{48}Ca.

Besides an upper bound on M_h, one can also use this analysis to mark out an "allowed" region in that part of the $\sin^2\theta$ - M_h plane for which $\sin^2\theta$ is small. From eq. (1), one finds that for small mixing angles, the allowed region is determined by the condition:

$$(M_\ell + M_{\beta\beta}) > M_h \, F \, (M_h, A) \sin^2\theta > (M_\ell - M_{\beta\beta}) \tag{4}$$

For illustrative purposes we take M_ℓ = 30 ev, $M_{\beta\beta}$ = 5 ev, and A = 130, corresponding to Tellurium. In the first model mentioned above, the limit in eq. (4) takes the form:

$$35 > 1.4 \times 10^6 \sin^2\theta \exp [-M_h/400] > 25 \tag{5}$$

where M_h is measured in Mev. Numerical values are given in Table I:

Table I: Mass ranges versus $\sin^2\theta$ for Model I

$\sin^2\theta$	10^{-2}	10^{-4}	3×10^{-5}
M_h	$2.50 > M_h > 2.36$ Gev	$674 > M_h$ 540 Mev	$197 > M_h > 64$ Mev

As long as the heavy neutrino is not identified with ν_τ, the final column will not be in conflict with the CHARM experiment[8].

In the second model, the bounds are given by

$$35 \text{ ev} > M_h \sin^2\theta \exp (-M_h/33) > 25 \text{ ev} \tag{6}$$

where again M_h is measured in Mev. The corresponding numerical ranges are now:

Table II: Mass ranges versus $\sin^2\theta$ for Model II

$\sin^2\theta$	10^{-2}	10^{-4}	3×10^{-6}
M_h (Mev)	$395 > M_h > 383$	$224 > M_h > 211$	$70 > M_h > 43$

The mass values in Table II are significantly smaller than the corresponding ones

in Table I, and the final column is no longer in conflict with the CHARM experiment. Thus it is possible to identify the heavy neutrino with ν_τ in this second model.

The crucial test of these ideas is the variation of $M_{\beta\beta}$ with atomic mass. It is therefore necessary to study double beta decay in a variety of isotopes to determine whether such a variation does or does not occur in nature. Of special interest is the decay of ^{48}Ca for which one expects the largest value of $M_{\beta\beta}$ (see eq. (3)), and for which there is general agreement regarding the magnitude of the matrix element. We therefore urge that a new effort be made to search for the no-neutrino double beta decay of ^{48}Ca.

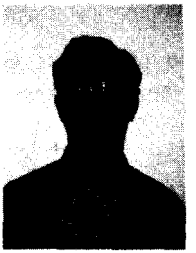
References

(1) See T. Kotani, these proceedings, for a complete set of references.
(2) A. Halprin, S. Petcov, and S. P. Rosen, Phys. Lett. 125B, 335 (1983).
(3) M. Gell-Mann, P. Ramond, and R. Slansky, Rev. Mod. Phys. 50, 721 (1978).
(4) A. Halprin, P. Minkowski, H. Primakoff, and S. P. Rosen, Phys. Rev. D13, 2567 (1976).
(5) M. Doi et al, Prog. Theoret. Phys. 66, 1739 and 1765 (1981).
(6) V. A. Lubimov, et al, Phys. Lett. 94B, 266 (1980).
(7) T. Kirsten, H. Richter, and E. Jessberger, Phys. Rev. Lett. 50, 474 (1983).
(8) C. Santoni, these proceedings.

DOUBLE BETA DECAY EXPERIMENT IN THE MONT BLANC TUNNEL

E. Bellotti, O. Cremonesi, E. Fiorini, C. Liguori, A. Pullia, P.P. Sverzellati, and L. Zanotti
Dipartimento di Fisica - Università di Milano and I.N.F.N. Sezione di Milano - Italy.

Presented by L. Zanotti



ABSTRACT

A result is presented of a 10068 h measurement on $^{76}_{32}Ge$ neutrinoless double beta decay in the Mont Blanc Tunnel with a carefully studied shielding.

A limit of $\tau_{1/2}(0^+-0^+) \geq 4.7 \cdot 10^{22}$y (68 % c.l.) can be quoted, leading to a limit on the effective neutrino mass

$$\langle m_\nu \rangle_{eff} \leq 14 \text{ eV}$$

in the most conservative theoretical framework.

A new setup for $^{76}_{32}Ge$ is then discussed, leading to a considerable background reduction, together with the features of a new measurement on inclusive Te double beta decay on 2^+ excited levels. Preliminary limits on both measurements are given.

INTRODUCTION

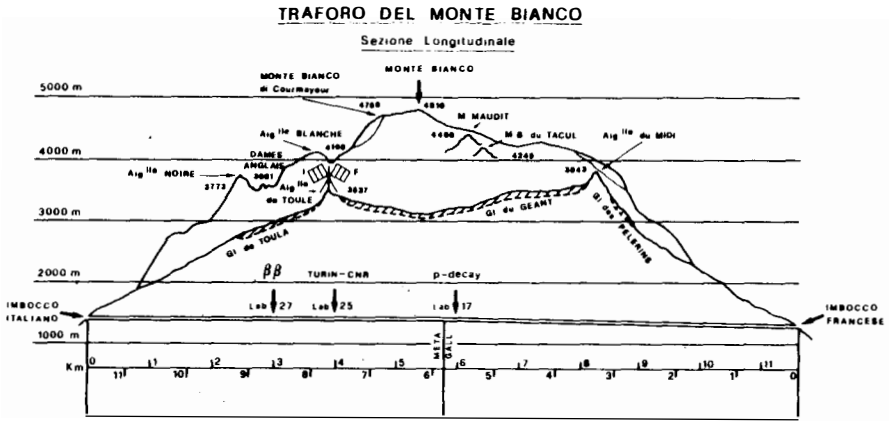
After the exhaustive theoretical discussion of double β decay presented by T. Kotani [1], in this paper only the experimental results of our measurement will be discussed, in two separated sections.

Old experiment: in this section experimental features and results will be discussed, concerning the study of neutrinoless double β decay of ^{76}Ge in a 10068 h measurement.

New experiment: a new experiment has been started, both on ^{76}Ge decay (as in the previous case) and on Te decay.

In both cases Ge(Li) detectors have been used; in the new setup two of them are operating simultaneously.

In Fig. 1 the location of the laboratories in the Mont Blanc Tunnel is shown; the old setup has been working for ∿70 % of the time in laboratory 17 and for ∿30 % of the time in laboratory 27, while the new setup is working in laboratory 27.



OLD EXPERIMENT

The following two transitions of ^{76}Ge have been considered:

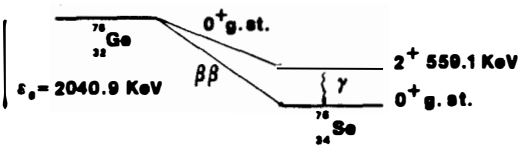


Fig.2

$$^{76}_{32}Ge \rightarrow {}^{76}_{34}Se + 2e^- \quad (0^+ - 0^+, \text{ neutrinoless})$$

$$^{76}_{32}Ge \rightarrow {}^{76}_{34}Se^*(2^+, 559.1 \text{ keV}) + 2e^- \quad (0^+ - 2^+, \text{ neutrinoless}).$$

To perform the measurement we used a Ge(Li) crystal with these properties:

Total volume = 143 cm^3
Active volume = 125 cm^3
Fiducial volume = 116 cm^3

taking advantage of the crystal being simultaneously both source and detector with a very good energy resolution, of the order of $\Delta E/E \simeq 1.5 \cdot 10^{-3}$ at E ≃ 2 MeV.

A drawback is however the rather poor isotopic abundance of ^{76}Ge in natural germanium (i.a. = 7.76 %).

Transition energies and efficiencies for the two transitions described above are reported in the following Table.

TABLE I

Transition	Energy	Efficiency
$0^+ - 0^+$	2040.9 keV	1.0
$0^+ - 2^+$	1481.8 keV	0.5 (*)

(*) Note: the efficiency concerns the detection of $2e^-$ with photon escaping without interaction in the crystal.

In both cases we expect to find a sharp line in the detector energy spectrum, at the energy values quoted above and with a shape quite similar to that of natural radioactivity γ lines which are also present in the spectum and will be discussed further.

The main problem to face in double β decay experiments is the very low counting rate that we expect as due to the decay itself.

Solution in the actual setup is a rejection of background as good as possible.

Three main sources of background can be listed:

1. Cosmic rays.
2. Natural radioactivity of the environment.
3. Internal radioactivity of the various elements assembled in the detector.

These backgrounds have been reduced in the following way:

1. Detector has been placed deep underground in the Mont Blanc Tunnel (which means an overburden of ∿ 5000 m w.e. of rock). The reduction in cosmic ray flux achieved in this way is of the order of $\sim 10^7$, with respect to the ground

level. Neutron flux is lower than 10^{-6} sec^{-1} cm^{-2} sr^{-1}, as measured at lab. 17.

2. The detector has been heavily shielded; during the first 1560 h with 5 cm OFHC (Oxigen Free High Conductivity) Copper and ∿20 cm Lead in all directions, for the remaining time with 5 cm highly purified (tridistilled) Hg in a nylon bag, and ∿20 cm Lead in all directions. The setup used in the latter part of the measurement is shown in Fig.3.

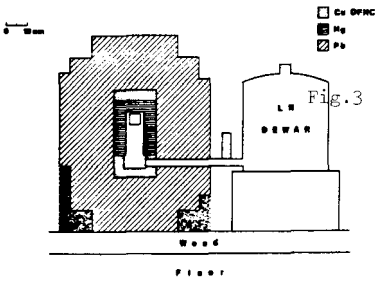


Fig.3

3. Materials for the detector parts have been carefully choosen, to reduce inner contamination. After having considered many configurations, we at last decided for a 0.5 mm OFHC Copper crystal holder and a 1.0 mm Ti end cap.

All these choices allowed us to achieve a background reduction, with respect to a measurement performed with shielded detector, but at ground level, of a factor 20 at 0.5 MeV to a factor >100 at 2 MeV.

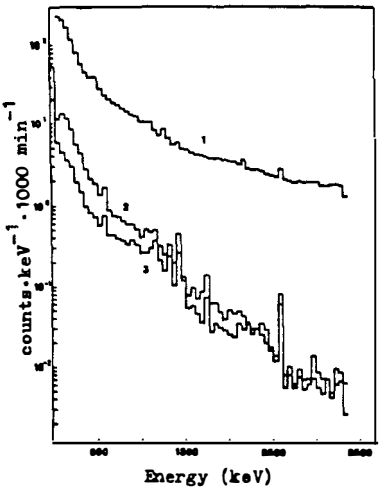


Fig. 4 reports a comparison of the counting rate (in units of counts·keV^{-1}·1000 min^{-1}) at ground level (1), in Mont Blanc laboratory with the first shielding (2), in Mont Blanc laboratory with the second shielding (3).

Notwithstanding the strong reduction in background (the counting rate at 2 MeV is ∿2·10^{-2} counts·keV^{-1}·1000 min^{-1}), no evidence has been found for both 0^+-0^+ and 0^+-2^+ transitions as it can be seen in Fig.5, showing spectra obtained in 8600 h for both transitions.

We can state therefore that there is no evidence for neutrinoless double β

decay of $^{76}_{32}Ge$ in both channels.

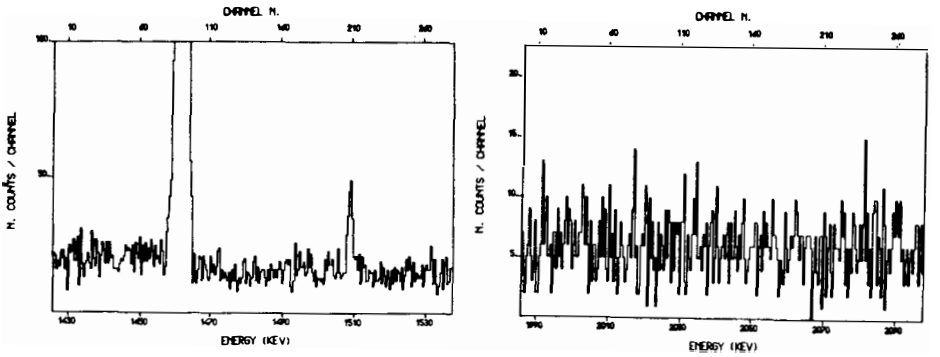


Fig. 5

Limits reported at various stages of the experiment have been summarized in the following Table II.

TABLE II

Hours	Conference	0^+-0^+(68 %)	0^+-0^+ (90 %)	0^+-2^+(68%)	0^+-2^+(90%)
4400	[2] Icoman '83	$2.3\cdot10^{22}$	-	$8.7\cdot10^{21}$	-
6824	[3] Brighton '83	$(2.5\text{-}5.0)\cdot10^{22}$	$(2.0\text{-}3.0)\cdot10^{22}$	$4.5\cdot10^{21}$	$2.7\cdot10^{21}$
6824	Fixed energy	$3.3\cdot10^{22}$	$1.8\cdot10^{22}$	$7.8\cdot10^{21}$	$4.4\cdot10^{21}$
8599	-	$4.2\cdot10^{22}$	$2.1\cdot10^{22}$	$1.2\cdot10^{22}$	$6.0\cdot10^{21}$
10068	Moriond '84	$4.7\cdot10^{22}$	$2.5\cdot10^{22}$	$6.9\cdot10^{21}$	$4.6\cdot10^{21}$

$\tau_{\frac{1}{2}}$(years)

A few comments are necessary about Table II.

First the limits at 6824 h have been obtained both letting the transition energy vary over an interval of 5 keV centered on the nominal transition energy [4] for the Brighton Conference, and fixing the transition energy at the nominal value for the second unpublished result.

Second, while limits on the 0^+-0^+ transition are reasonably scaled with the measuring time, on the contrary limits on the 0^+-2^+ transition fluctuate with time; this trend is not clear and we are considering now possible different background contaminations in the two locations (lab. 17, lab. 27) of the experiment. We can therefore assume at this stage as "final" limit for the 0^+-0^+ transition:

$$\tau_{\frac{1}{2}} \geq 4.7 \cdot 10^{22} \text{ y (68 \% c.l.)}$$

-though data have not yet been completely reanalyzed-, on which basis the following limits on effective neutrino mass can be quoted:

$\langle m_\nu \rangle_{\text{eff.}} \leq 6$ eV (according to theoretically computed nuclear matrix elements $|M^{0\nu}_{GT}|$: Haxton [5]).

or

$\eta(\text{RHC}) \leq 1.3 \cdot 10^{-5}$

$\langle m_\nu \rangle_{\text{eff}} \leq 14$ eV (according to nuclear matrix elements scaled to match geochemical result [6] on 2ν double β decay of $^{82}_{34}Se$;

or

$\eta(\text{RHC}) \leq 3.0 \cdot 10^{-5}$ $\tau_{\frac{1}{2}}(\text{Geochemical}) \simeq (1.45 \pm 0.15) \cdot 10^{20}$y; Kotani [7]).

both at 68 % c.l..

NEW EXPERIMENT

A careful analysis of the data collected during the experiment just described has led us to the conviction that a new detector was needed with a larger volume of the crystal and an improved set of building materials.

The new detector, having:

Total volume:	169 cm^3
Active volume:	148 cm^3
Fiducial volume:	140 cm^3

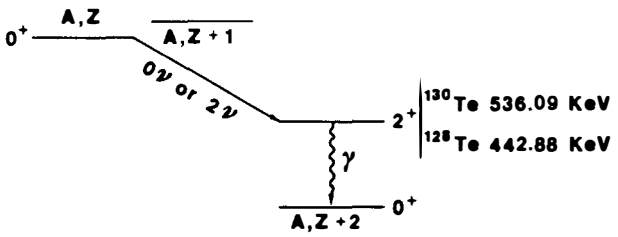
is now employed to measure $^{76}_{32}Ge$ double beta decay, while the old one is used to measure an external sample of Tellurium weighting $\sim$0.5 Kg.

Te has in fact two double β decay candidate isotopes

^{130}Te i.a. = 34.49 % transition energy = 2.533 MeV(0^+) 1st level = 536 keV(2^+)

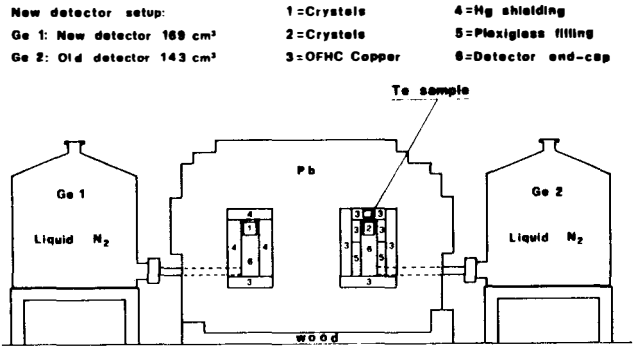
^{128}Te i.a. = 31.79 % transition energy = 0.869 MeV(0^+) 1st level = 443 keV(2^+)

on which an "inclusive measurement" can be performed, looking for the (0^+-2^+) transition on the first excited level through the detection of the deexcitation γ ray, according to the scheme reported in Fig.6.



The term "inclusive" means that there is no way of distinguishing decays with and without neutrinos.

To perform the measurements quoted above the same shielding has been used for both detectors, with the following characteristics (Fig.7).



1. Both detectors are shielded on every side by more than 20 cm Pb.
2. New Ge(Li) (Ge 1) is surrounded on top and sides by 5 cm Hg (the same of the old measurement) while on the bottom a slab of 5 cm OFHC Copper has been placed.
3. Old Ge(Li) (Ge 2) is surrounded by 5 cm OFHC Cu on all sides, plus 5 cm OFHC Cu around the detector, plus PVC filling the holes.

This setup has been operating since the end of September '83, up to the end of December '83, when a further improvement has been planned and realized for the Te measurement; in fact Te mass all around Ge 2 has been brought to 5 Kg, and measurement is starting just now.

In Table III results are reported of a preliminary analysis of data collected with the new detector, concerning the background of the most significant radioactive decays.

TABLE III

Energy (keV)	Series	Transition	Old Ge (counts/h)	New Ge (counts/h)	Reduction
583.14	^{232}Th	^{208}Tl → ^{208}Pb	0.447 ± 0.012	0.038 ± 0.011	11.8 ± 3.4
609.31	^{238}U	^{214}Bi → ^{214}Po	1.042 ± 0.017	0.351 ± 0.023	3.0 ± 0.2
1460.75	-	^{40}K → ^{40}Ar	0.966 ± 0.015	0.736 ± 0.030	1.3 ± 0.05
1764.50	^{238}U	^{214}Bi → ^{214}Po	0.149 ± 0.010	0.049 ± 0.014	3.0 ± 0.9
2614.47	^{232}Th	^{208}Tl → ^{208}Pb	0.165 ± 0.006	0.022 ± 0.005	7.5 ± 1.7

A substantial reduction has been achieved on the ^{232}Th series (a factor 8 ÷ 10) and on the ^{238}U series (a factor ∿3), that is possibly due to:

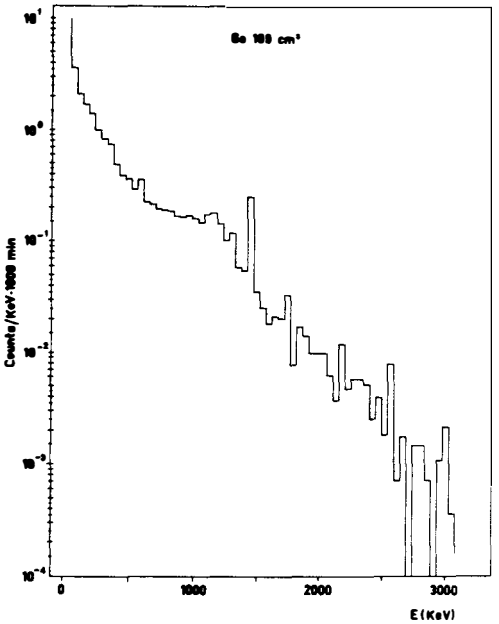
a) Crystal holder in OFHC Cu 0.5 mm thick.

b) End cap in OFHC Cu 0.8 mm thick.

c) Sapphire supports of the holder instead of BN.

d) OFHC Cu used for the final part of the cryostat rod.

The resulting spectrum (counts·keV^{-1}·1000 mm^{-1}) is shown in Fig.8, and should be compared with that reported in Fig.4.



PRELIMINARY RESULTS

In conclusion, after 941 h of operation of the new detector we can quote the following (conservative) limits:

$$\tau_{\frac{1}{2}}(0^+ \to 0^+) \geq 1.3 \cdot 10^{22} y \quad (68\ \%\ c.l.)$$
$$\tau_{\frac{1}{2}}(0^+ \to 2^+) \geq 2.7 \cdot 10^{21} y \quad (68\ \%\ c.l.)$$

while after 1470 h of operation with the Te sample we get:

$$\tau_{\frac{1}{2}}(0^+ \to 2^+) \geq 6.7 \cdot 10^{18} y \quad (68\ \%\ c.l.) \text{ for } ^{128}Te$$
$$\tau_{\frac{1}{2}}(0^+ \to 2^+) \geq 3.0 \cdot 10^{19} y \quad (68\ \%\ c.l.) \text{ for } ^{130}Te$$

REFERENCES

1) T. Kotani, this Conference.
2) L. Zanotti, ICOMAN '83, Frascati (January 17-21 1983) p.263.
3) E. Bellotti, HEP '83, Brighton (July 20-27 1983).
4) H. Wapstra, private communication, Transition energy for $^{76}_{32}Ge$ double β decay is ΔE = 2040.9 ± 2.5 keV. Recent revision of previous data gives ΔE=2039.6±2.2 keV.
5) W.C. Haxton, G.J. Stephenson, preprint La-UR-84-396.
6) T. Kirsten, Proceedings of Workshop on Science Underground, Los Alamos, AIP 96 (1982) 396.
7) T. Kotani, this Conference.

PROGRESS REPORT ON THE UCSB/LBL NEUTRINOLESS DOUBLE BETA DECAY EXPERIMENT

Robert Eisberg
University of California at Santa Barbara

ABSTRACT

Eight 170 cm^3 high purity Ge detectors provide the parent nuclei ^{76}Ge and detect the emitted electrons. They are surrounded with 15 cm thick NaI detectors that veto various forms of background and detect γ's emitted in decays to the first excited state of the ^{76}Se daughters (to distinguish between massive neutrinos and right-handed currents). A graded shield of boron-loaded plastic, copper, and lead surrounds the detector array, on the outside of which is a set of plastic scintillation counters that veto cosmic ray background. Each component of the apparatus involves custom design and fabrication, using materials carefully chosen to minimize background. It is sensitive enough to set a lifetime limit of $\sim 1 \times 10^{24}$ years, corresponding to an upper limit of $\sim$ 1 eV on the ν_e mass.

This is a report on progress made in the design and construction of an experiment to study the neutrinoless double β decay of ^{76}Ge. The work is being done by a group from the University of California at Santa Barbara, consisting of D. Caldwell, R. Eisberg, D. Grumm. D. Hale, and M. Witherell, and a group from the Lawrence Berkeley Laboratory, consisting of F. Goulding, D. Landis, N. Madden, D. Malone, R. Pehl, and A. Smith. The experimental technique is derived from the pioneering work of Prof. Fiorini and the Milano group. But the amount of Ge being used is much larger to increase the "signal" and number of background-reducing innovations are being used to decrease the "noise."

One of the purposes of the experiment is, of course, to set a more strict upper limit on the mass of the ν_e (or, if we are lucky, to actually measure the mass of the particle). Since all the preceeding papers speak to the question of neutrino mass, it is hardly necessary here to describe the current theoretical or experimental situation concerning this purpose. Two other purposes of the experiment are to study the possible admixture of right-handed currents in the weak interaction and to try to determine if the ν_e is a Dirac or a Majorana particle. These purposes are more specific to the neutrinoless double β decay technique. But the theory underlying them has been discussed amply in the papers by Kayser, Rosen, Kotani, and Zanotti, and the experimental situation has been described by Kotani and Zanotti. Because the author last mentioned has explained the Milano technique in detail, and because our experiment is based on that technique, this paper need only describe what we do to improve the technique.

The Milano groups is currently quoting a lower limit of 2.5×10^{22} years for the half-life of the ground state to ground state neutrinoless double β decay of ^{76}Ge to ^{76}Se. This result is based on 10068 hours of running time and has a 90% confidence limit. If translated to an upper limit on the ν_e mass, it corresponds to 6 eV or 14 eV, depending on whether the Haxton or the Doi nuclear matrix element is used. We would like to be able to drop the upper limit on the mass to 1 or 2 eV. Since the half-life is inversely proportional to the square of the mass, this means we want to raise the lower limit on the half-life by about a factor of 40; that is, we are want to be sensitive enough

to see the decay if its half-life is about 1 x 10^{24} years. The natural isotopic mixture of Ge is 7.76% ^{76}Ge. This number leads to the conclusion that 1 kg of natural Ge would produce approximately 0.5 decays per year if the half-life is 1 x 10^{24} years. It is clear that we need of the order of 10 kg of Ge.

There is, at present, no way to produce a single Ge detector with this much mass. The largest that have been made have a volume of about 170 cm^3 or, since the specific gravity is 5.5, a mass of about 0.94 kg. Hence we must use an array containing many Ge detectors. This precludes the use of Ge(Li) because that material must <u>always</u> be kept at liquid nitrogen temperature, once it has been fabricated, so there is no technically feasible way to go through the many cycles of assembly and disassembly involved in getting a complicated device into operation.

Our apparatus employs eight ultra-high purity (often called intrinsic) Ge detectors. Such detectors are not damaged by being at room temperature, although they are operated at liquid nitrogen temperature to reduce electronic noise. Each has a coaxial geometry and a volume of approximately 170 cm^3, for a total Ge mass of around 7.5 kg. We obtain the single-crystal Ge cylinders, with rectifying and non-injecting junctions and an overlying metalization to reduce thermal emissivity, from Ortec.

The increased amount of Ge we use enhances our potential signal by not quite a factor of 10 over the Milano experiment. To achieve our sensitivity goal, we must also reduce the expected noise by a factor of 4, or so. We use a number of different means to do this.

One is to use active, as well as passive shielding. The work of the Milano group, and of other groups doing similar experiments, have shown that one potentially serious source of the continuum of counts in the region of where the neutrinoless double β decay summed electron energy peak is expected, 2.041 Mev, arises from the 2.6 Mev γ's produced at the last step of the Th radioactive series from materials in this series present in the apparatus as contaminants. If one of these γ's undergoes a Compton scattering on the Ge in a detector, fortuitously depositing about 2.0 Mev on an electron, that electron will look to the detector like a double β decay event. We prevent this

from happening by surrounding the eight Ge detectors with a set of ten NaI scintillation detectors, the polycrystalline NaI(Tl) for which we have obtained from Harshaw. They form an almost complete shield that is 15 cm thick. The approximately 600 keV γ recoiling from the Compton scattering has a high probability of being detected in one of the NaI detectors -- or in one of the other seven Ge detectors. This allows us to veto the event.

The array of Ge and NaI detectors also make the apparatus well suited to looking for neutrinoless double β decay to the 2^+ first excited state of ^{76}Se. As Rosen first pointed out, this process is specifically sensitive to the presence of right-handed currents in the weak interaction. The detector array allows us to look for the deexcitation γ of energy 559 keV in one detector, in coincidence with a summed electron energy of 1.482 Mev for the ground state to first excited state decay in the other detector. This gives us an easily-recognized identification of the decay.

Figure 1 is a cut away drawing of the UCSB/LBL apparatus. Not shown are a set of plastic scintillation "paddle" counters surrounding the apparatus, used to detect cosmic ray events. A view with all but the bottom layer of scintillator shield removed is shown in Figure 2.

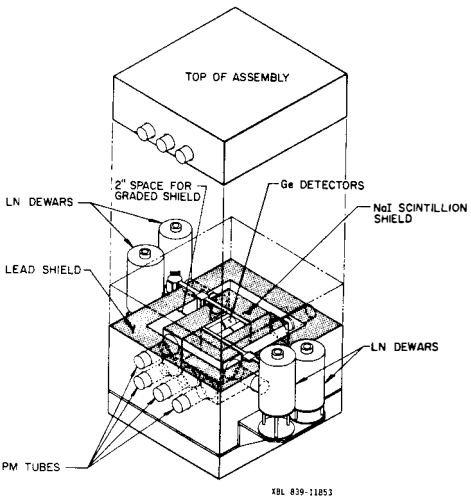
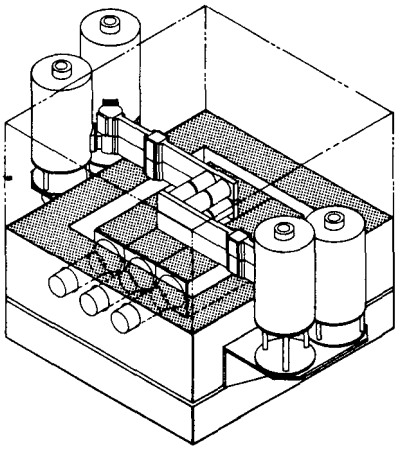


Fig. 1: Cut away drawing of the UCSB/LBL neutrinoless double β apparatus. Plastic scintillation counters surrounding the lead shield are not shown.



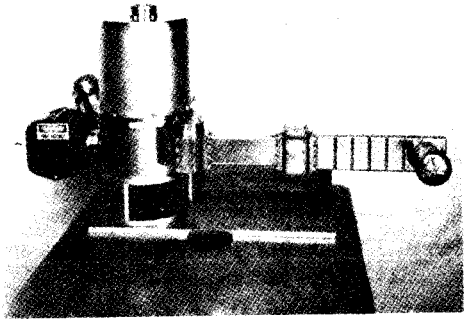
XBL 839-11852

Fig. 2: View of the UCSB/LBL system with all but the bottom layer of sodium iodide counters removed.

Returning to the task of vetoing background with the recoiling Compton γ's, it is clear that every precaution must be taken to reduce the probability that they can experience a photoelectric absorption on structural material in the system before they enter one of the detectors of the array. This means that the amount of structural material must be minimized and that it must be of as low a Z as is possible. And, of course, it also must be extremely free from radioactive contamination. As a consequence, we have employed a number of special design and fabrication techniques.

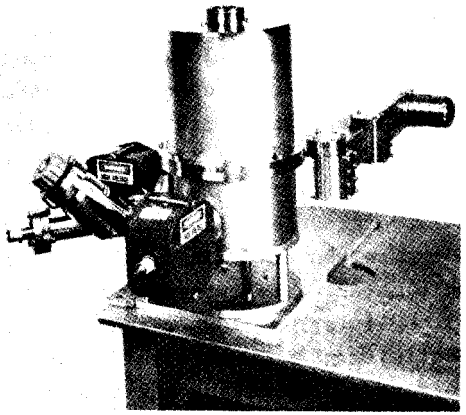
For example, the vacuum jackets surrounding each Ge detector and each cold finger connecting these detectors to the liquid nitrogen dewars (there are two detectors per cold finger) are made from OFHC Cu by a sophisticated electroforming procedure that results in material that is only about 1/4 mm thick except for a few small reinforcing ribs that are about 1 mm thick. The cold fingers themselves are made from single crystal Si, about 4 mm thick. This material is extremely free of contamination, very strong (albeit brittle), of low Z, and has about three times more thermal conductivity than Cu at liquid nitrogen temperature. Much of the effort in the design and construction of the apparatus has been involved in finding "exotic" materials and fabrication procedures. And every critically located piece of the apparatus has been tested for radioactivity with very sensitive equipment.

Figures 3 and 4 show a prototype (single detector per cold finger) version of one of the four cryostats that comprise the system. Each cryostat is independent of the others, and each is evacuated by two independent ion pumps. The intent is to achieve greater reliability in long, remote runs. A detector mounted on a cold finger is shown in Figure 5.



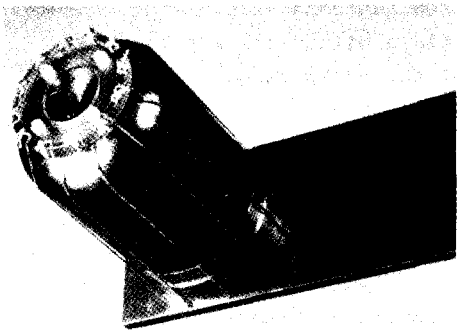
CBB 839-8161

Fig. 3: Photograph of a prototype single detector version of the germanium detector system used in the UCSB/LBL experiment.



CBB 839-8159

Fig. 4: Same as Fig. 3 but from a different angle.



CBB 839-8163

Fig. 5: Photograph of a detector mounted on a single-crystal silicon cold finger.

Several different electronic means are being used to reduce background. Contaminants in the U radioactive decay series commonly produce 3.26 Mev electrons from the β decay of ^{214}Bi. These can enter the Ge detectors through their outer surfaces and produce counts in the energy range where they will look like double β decays. But these detector surfaces are moderately thick (about 1/2 mm) Li-diffused regions in which the electric field is appreciably lower than in the bulk of the detector. Hence, if an electron passes through the surface there will be a slow component in the signal it produces. Our electronics recognizes the presence of such a component, and allows us to reject the background event.

A more sophisticated form of pulse-shape analysis will be used to discriminate against multiple Compton scattering, which Monte Carlo calculations indicate constitute a significant fraction of the Compton scattering background mentioned above. The Ge detector current waveform of each interesting event will be sampled every 20 ns, digitalized, and stored with the event record. The calculations show that the pulse shape should allow us to reject events in which all the energy is not deposited in a single region whose size is the ~ 1 mm range of the double β decay electrons, and thereby discriminate against multiple Compton scatterings where it is deposited in two regions, provided those regions are separated by more than 3 mm and provided at least 20% of the total energy is deposited in each region.

Capture γ's from thermalized neutrons originating in cosmic ray μ-induced reactions taking place within the apparatus are expected to form a major part of the background. We have designed the experiment to reduce this problem by electronic means. Any μ which enters the apparatus through one of the surrounding plastic scintillation counters, and does not exit through another, starts a clock which records elapsed times in an interval extending to 0.1 sec. Subsequent events have this time as part of the event record. It allows us to look for, and reject, a sequence of events following a μ-induced reaction in the time interval during which the neutrons are thermalized. Also, any large deposition of energy in a Ge of NaI detector will be flagged as an indicator of the passage of a cosmic ray μ.

Although the procedure just described should reduce our difficulties with cosmic rays, its efficiency cannot be 100%. Thus we plan eventually to go underground to a depth sufficient to reduce the μ flux to a negligible value. The data-collection scheme has been designed in anticipation of long runs at a remote location. It involves a pair of matched Hewlett-Packard series 200 computers, one at the equipment for data acquisition and the other in Santa Barbara for data analysis. To avoid any chance of data contamination, each event record will be written directly on hard-disk storage and then read back into the data acquisition computer for on-line diagnostics. The contents of the hard disk will periodically be removed by streaming magnetic tape for transportation to the data analysis computer. A high degree of automation is built into the data acquisition program to allow calibration, etc., as often as experience proves it to be necessary, without human intervention more often than once a week to check everthing and change data tapes. But it is planned to do the final analysis of all original event records of interest in a very nonautomated way, just to be sure.

The first Ge detector was successfully tested in February 1984. Essentially all other components were complete at that time. We expect to have the full system in operation in a low background counting facility at LBL by the summer of 1984. Present plans call for running there for some months before moving underground to an as yet unchosen site.

SINGLE PHOTON DETECTION WITH CELLO AT PETRA

F. PIERRE
Departement de Physique des Particules Elémentaires, CEN-Saclay,
91191 Gif-sur-Yvette Cedex, France.

ABSTRACT

An upgrading of the calorimetry of CELLO at PETRA is described. It will be used for the detection of single photons produced in association with pairs of neutrinos and/or photinós.

Counting the number of light neutrinos, N_ν, is one of the most promising probes of the number of generations. Recent results from Z and W production at the CERN $p\bar{p}$ collider [1] have limited N_ν to about ~ 10. Improvements are expected at the $p\bar{p}$ collider, and precise measurements ($\Delta N_\nu \lesssim 1$) seem feasible at future e^+e^- colliders [2] near the Z^0 pole. A rare decay mode of the charged Kaon is also expected to provide useful constraints [3].

Here we describe an experiment which is going to be performed at the PETRA e^+e^- collider, well below the Z^0 pole.

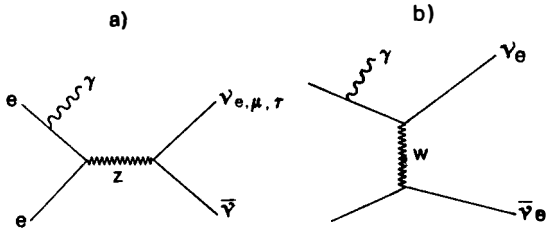


Fig.1 - Graphs for the radiative production of neutrinos via Z_0 (a) or W (b) exchange

The mechanism by which we can "detect" the neutrinos is the radiative annihilation [4] of the incoming electrons into a Z^0 (fig. 1a). In addition, electron neutrinos can be produced by W exchange (fig. 1b). The differential cross section is [5] :

$$\frac{d\sigma}{dxdy} = \frac{G_F^2\alpha}{6\pi^2}\left[\frac{M_Z^4\{N_\nu(g_V^2+g_A^2)+2(g_V+g_A)[1-s(1-x)/M_Z^2]\}}{[s(1-x)-M_Z^2]^2+M_Z^2\Gamma_Z^2}+2\right] \qquad (1)$$

$$\times \frac{s}{x(1-y^2)}\left[(1-x)(1-\tfrac{1}{2}x)^2+\tfrac{1}{4}x^2(1-x)y^2\right]$$

G_F is the Fermi Constant

S is the square of the center of mass energies

G_A, G_V are the electron weak coupling constants :

$$g_V = \frac{1}{2} + 2\sin^2\theta_W \quad , \quad g_A = -\frac{1}{2} \qquad (2)$$

x is the γ energy divided by $\sqrt{S}/2$

y is the cosine of the polar angle of the photon with respect to the beam

M_Z is the Z° mass

Γ_Z is the Z° width

$$\Gamma_Z = \frac{M_Z^3 G_F}{12\pi\sqrt{2}} (21+N_\nu -48\sin^2\theta_W+64\sin^4\theta_W) \qquad (3)$$

θ_W is the Weinberg angle

Detecting this reaction requires a trigger on the single photon, and a veto on background processes. This is possible in the CELLO detector at PETRA. A sketch is in fig.2. Four pieces of equipment are important :

1) The barrel calorimeter is used for both purposes : trigger and measurement of the γ, and veto against other particles in the region ~ 30° - 150°.

2) The endcap calorimeters are used only for veto in the region 8° - 21° (and 150° - 172°).

3) A new piece of equipment covers the intermediate region, the hole tagger, made of one Pb layer (4 radiation lengths) sandwiched between 2 layers of Altustipe scintillator. Light read-out is achieved by means of wave length shifter. Inefficiency on the detection of 2 GeV electro magnetic showers is at the level of 10^{-3}. It is ~ 20 % on minimum ionising particles.

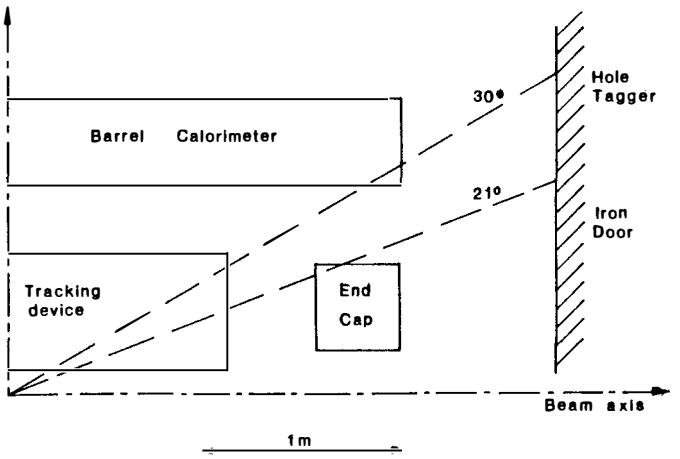


Fig.2 - Sketch of the CELLO detector

4) The central tracking device can reject $\gamma\mu\mu$ events where the muons would escape detection in calorimeters.

The main background to be expected is the QED process $e^+e^- \to \gamma\gamma\gamma$.

The experiment will be performed at $\sqrt{s}$ = 40 GeV, for single photons above 4 GeV ($x > 0.2$) in the polar angular range 30° - 150° ($|y| < .86$). Under these conditions we have

$$\sigma\left(e^+e^- \to \gamma\gamma\gamma \begin{cases} \to \text{barrel} \\ \to \text{Hole} \\ \to \text{Beam pipe} \end{cases}\right) \sim 8 \text{ Pb},$$

to be compared to

$$\sigma\left(e^+e^- \to \gamma \begin{cases} \to \text{barrel} \\ + \sum_{e,\nu,\tau} \nu_\ell \bar{\nu}_\ell \end{cases}\right) \sim .03 \text{ Pb}$$

Those 2 numbers demonstrate the necessity of the hole tagger. With it, the contamination of the annihilation into 3 photons becomes comparable to the production of 3 species of neutrinos. Assuming an integrated luminosity of 100 Pb^{-1}, we therefore could detect an excess of ~ 10 species.

Such a sensitivity may be outmoded by the $p\bar{p}$ collider results. It must be said that the main goal of this experiment is to detect the pair-production of light photinos via a similar radiative process [6], fig. 3, where a scalar electron S_e is exchanged. Lower limit on its mass, which is presently around 22 GeV [7], could be raised to ~ 50 GeV. A preliminary result from single γ detection has been presented by the MAC collaboration [8]. A dedicated experiment has been approved at PEP on the same subject [9].

Technical performances of the CELLO system have been recently obtained [10].

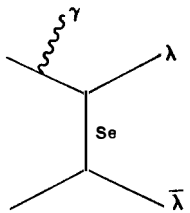


Fig.3 - Graph for the radiative production of photinos

REFERENCES

1) UA1 Coll. B. Sadoulet, presentation to this Workshop
UA2 Coll., A.F. Rothenberg, presentation to this Workshop

2) G. Barbiellini et al., Phys. Lett. 106B, 414 (1981)
T. Bartels et al., DESY 83-090 (1983)

3) I.H. Chang et al., A study of the Decay $K^+ \to \pi^+ \nu\bar{\nu}$,
proposal at BNL, (1983) unpublished.

4) E. Ma and J. Okada, Phys. Rev. Lett. 41, 287 (1978)

5) J.F. Gaemers, R. Gastmans and F.M. Renard,
Phys. Rev. D19, 1605 (1979)

6) P. Fayet, Phys. Lett. 117B, 460 (1982)

7) MAC Coll., E. Fernandez et al., Phys. Rev. Lett. 52, 22 (1984)
MARK II Coll., L. Gladney et al., Phys. Rev. Lett. 51, 2253 (1983)

8) S. YAMADA, 1983 Intern. Symposium on lepton and photon interactions
at high energies, Cornell Univ. (D.G. Cassel and D.L. Kreinick, ed.)

9) Proposal PEP-21

10) E. Ros Martinez, Thèse de 3ème cycle, Université Paris-Sud,
march 1984.

LIMITS ON THE NUMBER OF LIGHT NEUTRINOS

The UA2 Collaboration

Bern - CERN - Copenhagen (NBI) - Orsay (LAL) -
Pavia - Saclay (CEN) Collaboration

presented by

Allan Rothenberg
CERN



ABSTRACT

The recent discovery of the intermediate vector bosons at the CERN $\bar{p}p$ collider allows us to put limits on the number, Δn_ν, of additional types of light neutrinos. The standard model gives a simple relationship between the width of the Z^0, Γ_Z, and Δn_ν. When we determine Γ_Z directly from the experimentally measured mass of four of our eight events we find $\Delta n_\nu < 22$ ($\Delta n_\nu < 41$) with 90% (95%) confidence. If we determine Γ_Z indirectly from the ratio of the number of $Z^0 \rightarrow e^+ + e^-$ to $W^\pm \rightarrow e^\pm + \nu$ ($\bar{\nu}$) events we find that $\Delta n_\nu = 0$ ($\Delta n_\nu < 2$) with 90% (95%) confidence. All of these limits are somewhat better than one might have expected.

1. INTRODUCTION

We have recently reported [1] the observation of eight events which were interpreted in terms of the reaction

$$\bar{p} + p \rightarrow Z^0 + \text{anything}$$
$$\rightarrow e^+ + e^- \quad \text{or} \quad e^+ + e^- + \gamma$$

where Z^0 is the neutral intermediate vector boson. These events were found in a data sample corresponding to a total integrated luminosity of 131 nb^{-1} collected during 1982 and 1983 at the CERN $\bar{p}p$ collider ($\sqrt{s}$ = 540 Gev). At the same time we have observed events containing an electron-neutrino pair in the final state as expected for the charged intermediate vector boson $W^{\pm}$ [2,3].

Limits on the number of additional types of light neutrinos, Δn_ν, can be set by comparing the width of the Z^0, Γ_Z, to the theoretically expected value which is a function of Δn_ν. We have two ways of determining Γ_Z, directly from the width of the experimentally measured Z^0 mass distribution, or indirectly using the observed ratio of the cross-section for Z^0 production followed by e^+e^- decay to the cross-section for $W^{\pm}$ production followed by $e^{\pm}\nu$ ($\bar{\nu}$) decay.

2. DIRECT LIMITS ON Γ_Z

The UA2 electron analysis will not be discussed in this article. We will simply use the results. The parameters of the Z^0 events can be found in Table I. Four events (A,B,C and E) are judged to be measured well enough to be used for the mass calculation. They give the result

$$M_Z = 92.7 \pm 1.7(\text{stat.}) \pm 1.4(\text{syst.}) \text{ GeV}/c^2$$

with a weighted r.m.s. deviation from the mean of 2.0 Gev/c^2 and a weighted r.m.s. mass error of 2.1 Gev/c^2.

In order to get limits on Γ_Z it will be important for us to understand the error on the mass for these events. This error is obviously dominated by the

Table I

Parameters of the Z^0 events

Event	A	B	C	D	E	F	G	H
E_1(GeV)	71.5±1.8	48.4±1.7	69.9±1.8	104.5±6.4	60.0±2.0	55.6±2.1	45.1±1.5	46.3±1.6
E_2(GeV)	49.7±1.6	72.1±2.6	11.5±0.7	51.3±1.6	38.6±1.4	46.6±1.6	47.6±1.5	42.1±1.4
k (GeV)			24.4±1.0					
M(GeV/c^2)	91.6±1.9	94.6±2.4	90.6±1.9	91.9±3.2	95.5±2.3	92.0±2.3	83.4±1.9	88.0±2.1
p_T(GeV/c)	0.4±1.4	12.7±1.8	1.4±0.6	2.7±1.7	6.2±1.1	5.5±2.0	10.4±1.8	6.7±0.9

errors on the individual electron energies. The energy errors have two terms that have been added in quadrature. The first term is a systematic error due to the cell-by-cell uncertainty in the final calibration of the elements of the electromagnetic calorimeters. The second is a "statistical" error on the energy measurement dominated by the effect of sampling fluctuations in the calorimeter.

For the forward electrons (E_1 of events A,C and E) the systematic error $\Delta E/E = 1.5\%$ has been determined from the residual variation of the calorimeter's response to a Co^{60} source measured five times over a 2.5 year period. It is actually an upper limit on this error. The "statistical" error $\Delta E/E = 17\%/\sqrt{E}$ (Gev) is a result of measurements of the calorimeter's response in electron beams at the SPS and PS.

For central electrons and the photon of Event C the systematic error $\Delta E/E = 2.2\%$ has been determined [4] from the residual variation of the change in the calorimeter's response from the original 10 Gev electron beam calibration performed between the end of 1980 and March 1981 and a recalibration of eight of the modules in December 1982. It is the number applicable to the full central calorimeter which contains an additional sixteen modules that have not been recalibrated. This error is larger than that found for the forward calorimeters because not all of the central units were equipped for a Co^{60} source measurement when their initial calibration was made. The "statistical" error has a dominant component that is taken to be $\Delta E/E = 15\%/\sqrt{E}$ (Gev) in agreement with test beam results. However, there are additional contributions to the error which depend on the electron's angle and impact point on the calorimeter. All of these effects combine to give an overall "statistical" error that can be approximated to be $\Delta E/E = 18\%/\sqrt{E}$ (Gev).

A complete discussion of the validity of these error estimates is beyond the scope of this paper. It might be useful, however, to show limiting cases and observe the effect of changes in the errors on the physics results of interest. It should be noted that the weighted r.m.s. mass error for the four events used from Table I is $\sigma_{exp} = 2.1$ Gev/c². If we assume that both calorimeters had "statistical" energy errors of $\Delta E/E = 15\%/\sqrt{E}$ and that the systematic errors were as described above we would have had $\sigma_{exp} = 1.8$ Gev/c². Similarly, if we err in the direction of worse energy resolution we might have had $\sigma_{exp} = 2.4$ Gev/c².

As can be calculated from Table I the weighted r.m.s. deviation from the mean of the mass of events A,B,C and E is $\omega_0 = 2.0$ Gev/c². Since this number is less than the weighted r.m.s. mass error $\sigma_{exp} = 2.1$ Gev/c² it is clear that we cannot do a very good job of measuring the width Γ_Z. Given the small number of events we cannot expect the maximum likelihood method to give us reasonable confidence intervals for Γ_Z. Instead we resort to a Monte-Carlo technique in order to determine the expected distribution of ω from "experiments" containing four events taken from a relativistic Breit-Wigner distribution of width Γ_Z and using experimental resolutions for each of the events as measured. We can then determine α confidence level upper bounds on Γ_Z from the relationship $P(\omega<\omega_0|\Gamma_\alpha) = \alpha$ where P is the probability that $\omega<\omega_0$ in the Monte-Carlo distribution generated with the width Γ_α. In this way we determine that $\Gamma_{90\%} = 6.5$ Gev/c² and $\Gamma_{95\%} = 9.9$ Gev/c². These numbers are sensitive to the values of σ_{exp} used. If we use the smaller $\sigma_{exp} = 1.8$ Gev/c² we would have found $\Gamma_{90\%} = 6.8$ Gev/c² and $\Gamma_{95\%} = 10.3$ Gev/c². This illustrates the annoying fact that if we underestimate (overestimate) the experimental errors we get less (more) stringent limits on the Z^0 width. A further complication is introduced because we have chosen to use the weighted r.m.s. If our experimental errors are wrong the relative weights on each of the events may be wrong too. In this way we can get reductions of $\omega_0 = 0.1$ Gev/c² which can make $\Gamma_{90\%} = 6.2$ Gev/c² and $\Gamma_{95\%} = 9.4$ Gev/c².

In a similar way we can combine the results of the UA1 and UA2 experiments. The UA1 experiment [5] has four Z^0 events with an r.m.s. of 3.38 Gev/c². If we assume that the UA1 events have been measured with the same errors as the UA2 events we find that $\Gamma_{90\%} = 5.3$ and $\Gamma_{95\%} = 7.3$ Gev/c².

3. CROSS SECTION RATIO LIMIT ON Γ_Z

To determine Γ_Z from the ratio of cross-sections for W and Z we need the following information. There are $N_Z = 8$ decays of $Z^0 \rightarrow e^+e^- + e^+e^-\gamma$. This means that the $Z^0 \rightarrow e^+e^-\gamma$ is assumed to be due to bremsstrahlung and not to be an indication of new physics. Also, we are taking Event D in which an electron appears to have struck a magnet pole face as a good event falling inside of our acceptance. Furthermore, we are assuming that events G and H which contain small amounts of energy in the hadronic calorimeter behind one of their electrons are really normal e^+e^- decays. Finally, event F which exhibits an anomaly in the ratio of the signals from the two light guides of the impact cell in the electromagnetic calorimeter is also taken to be an e^+e^- decay. It must be emphasized that considerable effort has been made to understand these last three events and there are no known explanations for their surprising characteristics. The background to the eight events is only 0.03 events.

There are $N_e = 37$ electrons with transverse momentum $p_T > 25$ Gev/c in the final W sample of the UA2 electron analysis. We expect a background contribution, N_b, of 4.9 events coming from misidentified electrons, electrons from $Z^0 \rightarrow e^+e^-$ decays with one electron undetected and electrons from $W \rightarrow \tau\nu_\tau$ followed by $\tau \rightarrow e\nu_e\nu_\tau$. The first contribution of 2.3 events is calculated from the data while the other two are the result of Monte-Carlo simulations.

To determine the final cross-section ratio, R, we need the ratio of the overall W to Z acceptance and identification efficiency. Monte-Carlo calculation is used to get the geometric acceptance and calculate the effect of the cut on p_T. The electron detection efficiency is 0.77 ± 0.05. We find

$$R = \sigma_Z B_Z/\sigma_W B_W = (0.85 \pm 0.03)\, N_Z/(N_e - N_b).$$

We can now determine confidence limits on the value of R. A correct statistical treatment of this problem [6] gives confidence levels that differ significantly from those one would calculate using simple Gaussian errors. We get that with 90% (95%) confidence R is greater than 0.116 (0.098). Note that if we just use the naive result $R = 0.21 \pm 0.08$ we would have said $R > 0.072$ with 95% confidence.

Continuing the analysis we use the relationship

$$\Gamma_W/\Gamma_Z = (\sigma_Z B_Z/\sigma_W B_W)C$$

where $C = (\sigma_W/\sigma_Z)(\Gamma_{W\to e\nu}/\Gamma_{Z\to ee}) = 9.3$

is a proportionality constant that is determined in a calculation using the standard model, QCD methods and the measured proton structure functions. A detailed analysis [7] shows that the biggest uncertainty in C is ≈ 10% and comes from uncertainty in the ratio σ_W/σ_Z depending on which structure functions are used. The second biggest variation is ≈ 3 % coming from the error in the ratios of the Z and W masses. Therefore, we find that with 90% (95%) confidence Γ_W/Γ_Z is greater than 1.08 (0.91) with a possible 10% error on these numbers due to uncertainty in structure functions.

The final step to get limits on Γ_Z can only be done using our theoretical expectations of Γ_W. We chose to evaluate Γ_W with a top mass $m_t = m_Z/2$. This is the least favourable value of m_t when one wants to set upper limits on Γ_Z because it corresponds to the lowest values of Γ_Z and Γ_Z/Γ_W. For this choice of m_t in the standard model with first order QCD corrections [8] we get $\Gamma_W = 2.77$ Gev/c². This implies 90% (95%) confidence level upper bounds on Γ_Z of 2.57 Gev/c² (3.05 Gev/c²). With this choice of m_t we also find $\Gamma_Z = 2.67$ Gev/c².

4. LIMITS ON THE NUMBER OF ADDITIONAL LIGHT NEUTRINOS

In the preceeding sections we have obtained two limits on Γ_Z. If we write

$$\Gamma_{Z(exp)} = \Gamma_{Z(SM)} + \Gamma_{Z\to\nu\nu}\ \Delta n_\nu$$

where $\Gamma_{Z(SM)} = 2.67$ Gev/c² for $m_t = m_Z/2$

and $\Gamma_{Z\to\nu\nu} = 0.17$ Gev/c² for $\sin^2\theta_W = 0.22$

we can use limits on $\Gamma_{Z(exp)}$ to determine Δn_ν, the number of additional generations of light neutrinos. It should be noted that we assume that an additional generation contains only ν and $\bar{\nu}$ and no other quarks or leptons which could affect the standard model values of Γ_Z or Γ_W.

In this framework we find that, using the width as determined directly from our four Z^0 events, $\Delta n_\nu < 21$ (40) with 90% (95%) confidence. The uncertainty

in our knowledge of the energy resolution of the detector could change Δn_ν by $\approx$ 3(4) generations. This result is surprisingly good considering the small number of events. However, this should be attributed to the fortuitous clustering in the measured mass values.

If we combine the UA1 and UA2 events we can get a better limit, $\Delta n_\nu < 15$ (27) with 90% (95%) confidence.

Similarly, using the width as measured from the cross-section ratio we find that with 90% confidence there is no room for additional neutrino generations and that with 95% confidence there cannot be more than two additional generations. Even if we invoke a maximal 10% error in the theoretical ingredients of the calculation we find that $\Delta n_\nu < 1$ (4) at 90% (95%) confidence. Here, the surprisingly good result comes from the large number of $Z \rightarrow e^+e^-$ decays observed. If there are no new physics mechanisms responsible for our $Z \rightarrow e^+e^-$ events it may be many years before better limits can be set on the number of additional generations of light neutrinos. Given more data we can expect that the limits will become less strict if they are the result of a statistical fluctuation.

REFERENCES

1. P. Bagnaia et al., Phys. Lett. 129B (1983) 130.

2. M. Banner et al., Phys. Lett. 122B (1983) 476.

3. P. Bagnaia et al., A study of high transverse momentum electrons produced in $\bar{p}p$ collisions at 540 Gev, CERN-EP/84/39, submitted to Zeitschrift für Physik C.

4. A. Beer et al., The central calorimeter of the UA2 experiment at the CERN $\bar{p}p$ Collider, CERN-EP/83-175 (1983) to be published in Nucl. Instr. Meth.

5. G. Arnison et al., Phys. Lett. 126B (1983) 398 and private communication.

6. F. James and M. Roos, Nucl. Phys. B172 (1980) 475.

7. K. Hikasa, Counting neutrino species at high-energy proton-antiproton collisions, University of Wisconsin preprint MAD/PH/144 (Nov. 1983).

8. D. Albert, W.J. Marciano, D. Wyler and Z. Parsa, Nucl. Phys. B166 (1980) 460.

AMPLIFICATION OF FLUXOIDS BY METASTABLE SUPERCONDUCTING GRANULES
PROPOSAL FOR AN ALL-BETA MONOPOLE DETECTOR

L.Gonzalez-Mestres, D.Perret-Gallix
Laboratoire d'Annecy-le-Vieux de Physique des Particules
B.P. 909, 74019 Annecy-le-Vieux Cedex, France

(Presented by D.Perret-Gallix)

Monopole magnetic effects on superheated metastable type I superconductors are discussed, as well as the effect of energy losses. Superheated granules detectors offer a new way to search for monopoles in the whole range $0 < \beta < 1$ and provide simultaneously a high background rejection. The speed of the monopole can equally be measured with good accuracy.

1. INTRODUCTION

The problem of slow monopole energy loss in metals has recently been addressed by a number of authors[1),2)] and has led to proposals[3),4)] for detecting monopoles through magneto- and thermo- acoustic wave creation in bulk type I superconductors. On the other hand superconducting loops are already a well established technology to detect the (β-independent) magnetic flux variation produced by a monopole[5)]. Other possible processes leading to different detector techniques are ionisation[6)] and atomic excitation by Zeeman effect[7)].

Acoustic detection of monopoles is β-dependent and in any case requires the use of very powerful noise-reduction techniques. Superconducting loops have brought a candidate event[5)] which has led to some controversy. The very high sensitivity of the detector leads to sophisticated shielding techniques difficult to implement on large area apparatus. Moreover, no timing information can be provided by this type of detectors. Ionisation and Zeeman effects are, of course, limited by β-dependence, even if the best suited materials are used.

We propose, here, a unique way to turn a fluxoid into a macroscopic effect: namely, the superconducting to normal state transition of a metastable granule. Since the main flipping mechanism is independent of the size of the grain, large tin granules (15 μm radius) can be used producing signals that can be detected with conventional electronics (no SQUID needed).

We will discuss mainly two points:

The surface effect due to the flux quantum injected by the monopole traversing the granule. This amounts to creating a macroscopic defect on the surface and breaks metastability in a β-independent way. Furthermore such an effect does not depend on the size of the grain: it provides the most efficient mechanism to flip large granules.

The energy loss of the monopole in a superconductor. We conclude that, for low β, it is too small to flip thermically a 15 μm granule. To detect by thermal effects $\beta = 10^{-4}$ monopoles, one should use grains of radius $R \simeq 6$ μm which corresponds to the lower limit for standard electronics. It remains, however, that even for big grains energy losses can help to break metastability at the surface of the granule, near the normal zone created by the monopole flux line.

Granules then appear to provide a very efficient way to detect magnetic monopoles for all values of β. The use of 15 μm grains allows for a very good background rejection due the high amount of energy required to flip the grains.

2. BASIC CONCEPTS

The principle of superheated granules detectors has been presented several years ago[8] and since then, prototypes have been used in X-ray detection (X-ray imaging[9]) and electron detection (transition radiation[10]).

A tiny granule, a few microns diameter, plunged in a magnetic field at superconducting temperature can reach the metastable superheated state for $H_c < H < H_{sh}$ where H_c is the critical field and

$$H_{sh} \simeq \phi(\kappa) H_c \underset{(\text{low } \kappa)}{\simeq} 2^{-1/4} \kappa^{-1/2} H_c \qquad (1)$$

is the superheating critical field[11]. $\phi(\kappa)$ is a function of the Ginzburg-Landau parameter, $\kappa = \lambda/\xi$, λ is the London penetration length and ξ the coherence length. We are interested in good type I superconductors, which means $\kappa << 1/\sqrt{2}$. For tin, $\kappa = 0.16$, $H_{sh} = 2.17\ H_c$ and $H_c(T=0) = 300$ Gauss. H_c depends on the temperature T through the formula:

$$H_c(T) \simeq H_c(0) \left[1-(T/T_c)^2\right] \qquad (2)$$

where T_c is the critical temperature in the absence of magnetic field ($T_c = 3.7°K$ for tin). Superheated states are usually difficult to obtain for large samples, as surface defects prevent metastability. For spherical granules, it is reasonable to fix a maximal size of about $R \simeq 15\ \mu m$ [8]. The Meissner effect modifies the magnetic flux measured by a close-by current loop. If the granule falls back to normal state, the magnetic flux changes locally and a current variation can be detected at the loop terminals. A way to make this transition happen is to raise the temperature by irradiation[8]. X-ray energy as low as 30 Kev allows to flip a granule of a size large enough ($R \simeq 6\ \mu m$) to generate a signal detectable by conventional electronics. Josephson junctions and cryo-electronics can be used to increase the signal over noise ratio and lower the detection energy threshold.

A practical detector is constituted of a large number of granules embedded in an insulating material (paraffin) with a dilution factor of 10 to 20 %. Thin mixture foils are sandwiched in loops planes.

3. INTERACTION OF MONOPOLES WITH METASTABLE GRANULES

When a heavy monopole goes through a type I superconducting granule, it leaves behind a magnetic flux tube trapped into the superconductor[3),4)]. This flux equals $2n\phi_0$, where n is the monopole charge measured in elementary units of magnetic charge (n = integer $\geq$ 1) and $\phi_0 = 2.067 \times 10^{-7}$ Gauss.cm^2. The size of this flux tube can be computed as follows. Asssume n = 1, which means a total flux $\Phi = 2\phi_0$. If the granule can be superheated, the metal will become normal everywhere the magnetic field is larger than H_{sh}. We can then write the approximate equation ($\lambda << \xi$):

$$\pi\rho^2 H_{sh} \simeq 2\phi_0 \tag{3}$$

where ρ is the radius of the flux tube. Taking H_{sh} = 600 Gauss, one gets $\rho = 1.45 \times 10^{-5}$ cm, which is to be compared with the coherence length of tin, $\xi = 2.3 \times 10^{-5}$ cm. We then have a normal tube of about 3000 Å diameter where most of the flux is trapped.

At the ends of the flux tube, the monopole has created in the surface of the grain two normal windows, whose diameter is of the same order as the size of Cooper pairs. Moreover, there is a magnetic field of order H_{sh} acting on the two surface normal domains.

If the granule is in a metastable state, the surface normal zones can expand and the whole granule will then fall to normal state. This is thermodynamically favoured since the type I superconductor surface energy is positive and a sphere with a cylindrical hole is not a configuration that minimizes the surface, even locally. Therefore, provided that the flux tube is not created too close to the poles of the grain (where the external magnetic field vanishes by Meissner effect), it will originate a normal zone that propagates and rapidly flips the granule.

To be more precise, note that if $\vec{H}_0$ is the applied magnetic field, the field at the surface of the sphere in the absence of monopole flux effects is always tangent to the surface and equals in module for a point $\vec{r}$ on the sphere:

$$H_{ext}(\vec{r}) \simeq 3/2\ H_0 |\sin\theta| \tag{4}$$

where we use H_{ext} for "$H_{external}$" and θ is the angle between $\vec{H}_0$ and $\vec{r}$. If $H_{sh} \simeq 2.17\ H_c$ and H_{ext} at the equator is close to H_{sh}, we have $H_{ext} \simeq H_c$ for $|\sin\theta| \simeq 0.46$. We can then roughly estimate that, at the surface of the granule, the region for which the local parameters (H_{ext}, T) lie in the super-

heated part of the phase diagram corresponds to $|\sin\theta| > 0.46$. This represents about 80% of the surface of the granule. If we make the pessimistic assumption that the monopole flips the granule only when it creates a normal hole in this region, the probability that none of the ends of the flux tube flips the grain is:

$$P_{\text{non-flip}} \simeq 0.2^2 = 0.04$$

So that we can safely expect 95% efficiency each time the monopole traverses a granule. Since the monopole will encounter several metastable granules in the same foil, the inefficiency turns out to be very low.

Finally, the trapped magnetic field will of course add vectorially to $\vec{H}_{ext}$, but since the flux tube will be arbitrarily oriented with respect to $\vec{H}_{ext}$, we do not expect this effect to go in average in the wrong direction.

In conclusion, surface effects due to the trapped magnetic flux provide a very efficient all-β monopole detection.

4. ENERGY LOSS BY SLOW MAGNETIC MONOPOLE IN SUPERCONDUCTING GRANULES

To complete the discussion, let us turn to energy losses. These have been studied by G.W. Ford[2] and S.P. Ahlen and K. Kinoshita[1], and the low frequency cutoff has been discussed by C. Bernard et al.[3]. The energy loss per unit length of a $n = 1$ monopole is given by:

$$-dE/dX \simeq g^2\omega_p{}^2 v/c^2 v_F \left[\ln 4E_F v/v_F - \ln 2\Delta\right] \qquad (5)$$

where v is the monopole speed, v_F the Fermi velocity, E_F the Fermi energy, g the monopole magnetic charge, ω_p the plasma frequency and Δ the superconductor energy gap. Numerical computation for tin ($E_F = 10.2$ eV, $\Delta = 5 \times 10^{-4}$ eV), gives:

$$-dE/dX \simeq 50 \quad \text{KeV}/\mu\text{m} \quad \beta = 10^{-3}$$

$$-dE/dX \simeq 4 \quad \text{KeV}/\mu\text{m} \quad \beta = 10^{-4}$$

$$-dE/dX \simeq 0.25 \quad \text{KeV}/\mu\text{m} \quad \beta = 10^{-5}$$

This is to be compared with the local heating model[12),13)], which leads to good predictions for large grains, and givesthe formula[13)]:

$$\Delta H/\Delta E = 1/R^3 \times 97.4/(1.5+0.22T^2) \qquad (6)$$

with ΔH in Gauss, ΔE in KeV, R in microns and T in Kelvin. For $R = 15$ μm, $\Delta H = 10$ Gauss, $T = 2°K$, we get $\Delta E \simeq 700$ KeV whereas the energy deposited by a monopole with $\beta = 10^{-3}$ along a distance $d = 4/3\ R = 20$ μm is of about 1 MeV. This makes clear that slower monopoles ($\beta < 4\times10^{-4}$) will not flip thermically grains of 15 μm radius. Detecting thermically monopoles with $\beta \simeq 10^{-4}$ would require using $R \simeq 6$ μm granules, pushing conventional electronic detection to its limit. Going lower in β with only the thermal effect would imply the use of Josephson technology. The magnetic flux effect is therefore crucial for the design of the detector, if one wants it to work for all values of β. However, energy losses can play a role in the expansion of the surface normal domain. A monopole with $\beta = 10^{-4}$ deposits an energy of about 1 KeV in a distance of the order of the coherence length. This will heat the surface of the grain near the flux line and help to break the metastability.

To study the phenomenon from a microscopic point of view, note that in formula (5) the upper and lower energy cutoffs have been explicitely separated and the photons are emitted according to a logarithmic law. Each scale contributes with the same amount of energy, which means that the number of emitted photons varies as the inverse of the frequency. For $R = 15$ μm, the electrons excited by these photons will spread over the whole granule in a time $t \sim 0.5\times10^{-11}$sec. But, before, there will be local energy losses in the form of phonons that remain more localized.

The inverse of a quasiparticle lifetime of energy E in normal metal is[14]:

$$\tau_{el}(E) = 2\omega_D\{0.25(r_s/a_0)^{1/2}(\omega_D/E_F)(E/\omega_D)^2 + 0.174(r_s/a_0)\min[(E/\omega_D)^3,1]\} \qquad (7)$$

where some $\hbar$ factors are to be understood, r_s is the radius of the free electron sphere, ω_D is the Debye frequency and a_0 the Bohr radius. The formula can be used for superconductor as long as $E >> \Delta$. For tin, and with $\beta = 10^{-4}$, the upper cutoff in (5) starts at:

$$E \simeq 3E_F/50 \simeq 0.6 \text{ eV} \simeq 1200\Delta$$

At this energy $\tau_{el}(E)$ is of about 10^{13} sec^{-1}, and both terms in (7) contribute to a sizeable amount. The first term is due to electron-electron collisions, whereas the second one comes from electron-phonon interactions. Electron-electron relaxation is very rapid and dominates for high energy quasiparticles

(beyond the eV scale).

At $E \simeq \hbar \omega_D \simeq 0.02$ eV, relaxation by phonons completely dominates and electron-electron collisions can be neglected. This corresponds to a lifetime of 2.5×10^{-13}sec. If we go lower in energy, τ_{el} falls very rapidly because of the E^3 factor. At $E = 0.3\, \hbar \omega_D \simeq 6 \times 10^{-3}$ eV $\simeq 12\, \Delta$, the lifetime is about 10^{-11} sec.

In conclusion, we can say that about 50% of the energy is deposited in the form of quasiparticles with lifetimes of 2.5×10^{-13} sec. or less. These quasiparticles relax most of their energy in the form of phonons. In 10^{-13} sec., a Fermi electron travels over about a coherence length. Since phonons travel much slower than Fermi electrons, a sizeable part of the energy deposited by the monopole near the surface will remain close to it and contribute to local heating, essentially in a radius of about three coherence lengths around the flux tube. Typically, for $\beta \sim 10^{-4}$, the local increase in temperature will be of a few tenths of °K, which is not a negligible effect. At $T \simeq 2$ °K, a $\Delta T = 0.2$ °K amounts to a variation of about 20 Gauss in H_c (43 Gauss in H_{sh}). The discussion is relevant for monopoles, but also for a complete understanding of background, since we cannot exclude the possibility that events due to cosmic rays or natural radioactivity flip granules through surface heating.

5. PROPOSAL FOR A MONOPOLE DETECTOR

A review of the present status of the experimental limit for monopole flux[15] shows that the only competitor experiments for the same β range are the superconductive loop experiments. The flux limit, at present time[16] is $F < 3.2 \times 10^{-2}$ Monopole/(m^2.d.sr) for 90% C.L.. This leaves plenty of room for improvement to reach the astrophysical limits (for example: modified Parker bound[17] $F < 10^{-4}$ Monopole/m^2.d.sr for monopoles with mass $M \sim 10^{19}$ GeV).

A simple detector could be formed by at least three groups of sensitive planes, each group giving position informations (two planes with detection loops oriented in the X and Y direction). Time of flight will be recorded triggered by a coincidence of any two X-Y planes. The relative error on β induced by timing and spatial resolution is less than 1% for $\beta = 10^{-4}$ with 50 cm spacing between groups of X-Y planes.

The signature for a monopole would be a large flip signal (several granules) in each of the 6 planes, the three points being aligned and the timing consistent with the flight of a single particle. In this way one will observe the trajectory of the monopole and determine its speed.

The cosmic background is dominated by charged particles (75% muons). The mean energy loss of a charged particle in a 15 μm grain is about 22 KeV, whereas, the flip energy threshold is, as we have seen, of the order of 700 KeV. The probability for such a Landau energy loss fluctuation is about 1.5 ‰. Furthermore, this high energy tail is mainly due to δ-rays whose range in tin is larger than 300 μm, therefore this energy will not be dissipated in one 15 μm grain. The trigger (X and Y planes) rate will then be less than 1 Hz/m^2 for an average of 10 granules per plane. Moreover, such charged particles can be identified by a set of hodoscope scintillators.

The low probability for ionisation flip, added to the tracking and timing information, gives us confidence in the possibility to reduce the background to a negligible amount. A complete simulation program is under way to give precise data related to detector efficiency and background rejection. We are also studying various quantum flux generation processes that could be used as a calibration system.

6. CONCLUSION

We are proposing a new method to detect $0 < \beta < 1$ monopoles. This technique based on the universal feature of metastability, widely used in high energy physics (bubble chambers, emulsions), offers an independent checking, and eventually an alternative, to superconducting loops detectors. In addition this system provides timing information and the monopole speed can be measured. The quite high built-in background rejection (only dictated by the granule size) and the use of conventional electronics make possible the development of large area detectors.

7. ACKNOWLEDGEMENTS

We would like to thank G. Waysand for introducing us to the world of small granules as well as for constant help and encouragement. We are indebted to N. Perrin for a discussion on quasiparticle relaxation in metals and to M. Werlen for contribution to the study of energy loss fluctuations.

REFERENCES

1) S.P. Ahlen and K. Kinoshita, Phys. Rev. D26, 2347 (1982).
2) G.W. Ford, Phys. Rev. D26, 2519 (1982).
3) C. Bernard, A. De Rujula and B. Lautrup, preprint CERN TH-3694.
4) A.M. Allega, N. Cabibbo, preprint ROMA 1983.
5) B. Cabrera, Phys. Rev. Lett. 48, 1378 (1982).
6) S.P. Ahlen, Rev. of Mod. Phys. vol. 52 n 1 121 (1980).
7) S.D. Drell, N.M. Kroll, M.T. Mueller, S.J. Parke and M.A. Ruderman, Phys. Rev. Lett. 50, 644 (1983).
8) H. Bernas, J.P. Burger, G. Deutscher, C. Valette and S.J. Williamson, Phys. Lett. 24A, 721 (1967). See also G. Waysand, these Proceedings, and A. Hrisoho, G. Waysand, Nucl. Inst. Meth. 214, 415 (1983).
9) J. Behar, J.M. Cardi, B. Herszberg, D. Hueber, C. Valette, G. Waysand, J. Phys. Coll. 39, C6-1201 (1978).
D. Hueber, C. Valette, G. Waysand, Cryogenics, July 1981, 387.
10) A.K. Drukier, C. Valette, G. Waysand, L.C.L. Yuan and F. Peters, Lett. al Nuovo Cimento 14, 300 (1975).
11) J. Matricon, D. Saint-James, Phys. Lett. 24A, 241 (1967).
12) D. Hueber, C. Valette and G. Waysand, Physica 108B, 1229 (1981);
D. Hueber, Université Paris-Sud, Thèse de 3e cycle (1980).
13) G. Waysand, to appear. We are grateful to G. Waysand for communicating this formula prior to publication.
14) J.R. Schrieffer, Theory of superconductivity (Benjamin, New-York, 1964);
For a detailed study of quasiparticle relaxation in superconductors, see:
S.B. Kaplan, C.C. Chi, D.N. Langenberg, J.J. Chang, S. Jafarey and D.J. Scalapino, Phys. Rev. B14, 4854 (1976).
J.J. Chang, D.J. Scalapino, Phys. Rev. B15, 2651 (1977).
15) P. Musset, preprint CERN-EP/83-131 and references therein.
16) B. Cabrera, M. Taber, R. Gardner and J. Bourg, Phys. Rev. Lett. 51, 1933 (1983).
17) E. Parker, Ap. J. 160, 383 (1970), 163, 225 (1971), 166, 295 (1971);
M.S. Turner, E.N. Parker and T.J. Bogdan, Phys. Rev. D26, 1296 (1982);
E.E. Salpeter, S.L. Shapiro and I. Wassermann, Phys. Rev. Lett. 49, 114 (1982).

SEARCH FOR SUPERHEAVY MAGNETIC MONOPOLES WITH USE OF A SUPERCONDUCTING COLLOID DETECTOR

A. K. D r u k i e r

Max-Planck-Institut für Physik und Astrophysik
- Werner-Heisenberg-Institut für Physik -
Munich (Fed. Rep. Germany)

The energy deposition by superheavy magnetic monopole in metals is expected to be a few orders of magnitude larger than in insulators, say 1 GeV/cm. A detector based on the change of state from superconducting to normal should be sensitive to monopoles. In our opinion, it is possible to develop the detector with the following properties :

- millimetric spatial resolutions for a surface up to 100 m^2;
- temporal resolution of hundreds nanoseconds,
- measurement of specific ionization with precision of ca. 20%.

By time of flight method, the velocity of monopoles can be ascertained with uncertainty of 1% for $\beta \leq 0.001$. We should like to point out that using the superconducting colloid the background suppression is possible. The expected background due to cosmic rays is of the order of 3×10^{-8} per m^2 x year. The background due to radioactivity is negligible, e.g. due to typical β^- emitting contaminant K40 it is 10^{-23} per m^2 x year.

Introduction

In the following we suggest that the superheavy magnetic monopoles may be detected by a superconducting colloid consisting of a collection of normal metal grains coated with thin layer of superconductor. Optionally one can use somewhat smaller, but homogeneous superconducting grains. The monopoles of velocity $\beta \gtrsim 10^{-5}$ can be detected, but to reject the background it may be necessary to restrict the search to monopoles with $10^{-5} \lesssim \beta \lesssim 10^{-3}$.

In the first chapter we present the justification for use of this "exotic" detector. In the next two chapters the physics of superconducting colloid as particle, and more specifically, as monopole detector is discussed. In chapter 4 we discuss one possible configuration: two cylindrical position sensitive superconducting colloid detectors placed within a big liquid helium-4 cryostat. Last but not least, different sources of background are discussed. We should like to point out that using the superconducting colloid the background suppression is excellent due to:

- hundreds nanoseconds time resolution;
- millimetric spatial resolution;
- good energy resolution which permits to reject single charged cosmic rays and most of the natural radioactivity.

Astrophysical limits and experimental searches for monopoles

Investigations of grand unification theories have suggested the existence of magnetic monopoles whose mass may be comparable to the unification scale 10^{16} GeV[1]. Although many experimental searches for fast monopoles have reported negative results, there still remains a possibility[2] that a massive monopole might have evaded detection if their velocity is $\beta \lesssim 10^{-3}$. Actually, using liquid helium detectors, i.e. Superconducting Quantum Interference Device (SQUID) Cabrera[3] observed the quantized change of magnetic flux consistent in magnitude with the passage of a particle possessing a single Dirac unit of magnetic charge.

The limits to flux and velocity of magnetic monopoles have been obtained using cosmologic and astrophysical arguments (see refs. 1, 3-9). The quoted papers suggest that:

- either the velocity is $\beta \gtrsim 10^{-3}$ and fluxes very small,
- or the flux of monopoles is locally enhanced and $\beta \lesssim 10^{-4}$.

In the first case, monopole search requires the detectors with size of ... "football field". Conventional cosmic rays installations (usually plastic scintillators and gas detectors) should be considered, but conventional detectors may be sensitive only for monopoles with $\beta \gtrsim 10^{-3}$.

On the other hand, the local density of monopoles in a solar system may be enhanced; the velocity of such monopoles may be as small as $\beta = 10^{-4}$. The big importance of the induction searches is that they can detect arbitrarily slow monopoles. However, they have also some disadvantages, namely the small surface, relatively slow response and bad spatial resolution. Truely, the signal is very specific but the velocity cannot be measured and the direction (straight line!!!) is difficult to ascertain. It should be pointed out that these disadvantages

of induction method are not fundamental but connected to use of very sensitive but also very costly sensor, the SQUID. Recently, much higher surface, up to 10 m^2 searches have been suggested using many SQUID's systems.

It was soon realized that when using the conventional detectors, it is important to have the one with smallest energy gap. The experiment[11] with array of semiconducting detectors followed. Furthermore, it has been pointed out that the magnetic field of a slow monopole interacting with atomic electrons yields Zeeman energy splitting equal in magnitude to normal electrostatic atomic binding[12,13]. Similarly, the presence of very slow monopole ($\beta \lesssim 10^{-4}$) may lead to local magnetization in soft ferromagnets; the effect can be stabilized and detected by appropriate magnetooptic read-out[15]. Finally, some very special phosphore with very small energy gap was discussed[11]. Unfortunately, calculating the response of any quantum-mechanical system to such a point magnetic field seems to be extremely difficult. Thus, below some velocity, the uncertainty of the magnetic monopole energy losses is a major problem of the above described detection schemas.

Since the existence of monopoles is rather speculative, one would like to employ a detection scheme which depends as little as possible on the monopole properties. It is fairly certain that the monopole energy losses in conductors are due to induced eddy currents. The conduction electrons in a metal have low lying excitation levels which even a slow monopole can excite. It is important to take in account the nonlocal metal response[15,16]. We should like to point out two aspects of these calculations:

- the energy losses in metal are many orders of magnitude higher than in other materials,

$$-\frac{dE}{dX} \approx 6 \times \sigma \times (\beta/10^{-3}) \text{ GeV/cm}^2 \qquad (1)$$

  where σ is the conductivity

- it is strongly dependent on the metal temperature (see Fig. 1).

Monopole induced eddy currents may produce the thermo-acoustic signals. Unfortunately, for typical metal (Al) the signal will be severely limited by noise even in liquid helium temperature[14] (see however refs. 17 and 21).

It should be pointed out that the use of low temperature facilities the detection of monopoles

- the losses are much bigger and almost independent of velocity for $5 \times 10^{-5} \lesssim \beta \lesssim 10^{-3}$ (see Fig. 1),
- the specific heat of metals is much lower

  $C_v(T) \approx \gamma T + aT^3$

  wherein γT term dominates below 1°K,

- the thermal noise is smaller.

In the following, we suggest a new method of detecting superheavy monopoles. The detector should consist of a collection of small, diameter $\lesssim 50$ microns, grains of normal metal coated with thin layer of superconductor. The eddy currents are generated and dissipated in the normal metal which leads to an increase of temperature of the whole grain and thus to the change of state of coat from superconducting to normal state. Optionally, one can use smaller superconducting grains.

It should be pointed out, that for electrically charged particles, ionization losses leads to change of state of homogeneous superconducting grains. The new particle detector based on this effect is called superconducting colloid detector, and is described in the next chapter.

Superconducting colloid - a new particle detector

In the superconducting colloid, metal superconducting grains of micron dimensions are held in a dielectric filler material under a magnetic field. The field and temperature are so adjusted that a definite small temperature jump δT will flip the grain into the normal state. Due to the very low value of the specific heat at low temperature, the energy deposed by a single particle can flip the grain. Now, as the grain goes normal, the magnetic field in and around the grain changes due to the disappearance of the Meissner effect. This in turn leads to an electromagnetic signal which can be picked up by a read out loop.

The method is essentially calorimetric. Due to the Kapitza resistance between the metal and filler material, the sharing of heat can be neglected, at least in a first few hundreds of nanoseconds. Thus the setting of a temperature barrier, δT, means that a certain minimum deposited energy E_{min} is necessary to flip the grain.

In the last few years, the superconducting colloid has been tested as particle detector using alpha and beta sources, relativistic electrons, gamma emitters and neutrons[18]. The electronic read-out was developed[19] and methods of small grains production and selection established.

The electronic read-out of superconducting colloid was discussed in details elsewhere[19]. We should like to point out, however, that with R = 5 microns grains placed in the loop of 0.3 mm width (spacing = 2L) and 20 cm length, the signal/noise of the order of ten was achieved. From experience of the Orsay group one can estimate that the change of state of grain is detectable (S/N $\gtrsim$ 5) if

$$2\pi R^3/L \geqslant 2 \times 10^{-6}\ \mathrm{Gcm}^2 \approx 10\phi_0 \qquad (2)$$

The physics and some applications of superconducting colloid are discussed in this volume in contributions of L. Stodolsky and G. Waysand.

Superconducting colloid as monopoles detector

To detect superheavy magnetic monopole we propose to use a superconducting colloid detector, wherein grains consist of normal core coated with a thin layer of superconducting metal. The typical size of the grains will be $20 \lesssim R \lesssim 30$ microns and the thickness of superconducting coat only a few microns.

Let us consider the response of nonhomogeneous grain to the energy deposition by monopole. The eddy currents will be created in both superconducting and normal material due to magnetic equivalent of EMF. It should be pointed out that the eddy currents in superconductor are only partially dissipated. However, in the normal metal core the eddy currents are dissipated and this energy deposition leads to heating of the grain. The normal and superconducting metal are well coupled thermically, whereas there is a big Kapitza resistance between the metal and the diaelectric. Thus the superconducting layer is heated

and can change state due to monopoles.

In the following, we will assume that the normal metal is Aluminium coated with type I superconductor. Specific heat of Al at T = 1.2, 2.0, and 4.2°K is given in Table 1. It should be pointed out that the thickness of coat is only a few micron, i.e. the specific heat of the superconductor can be neglected. As the coat is a few penetration depths, the proximity effect, i.e. influence of normal metal on superconductor is small. Furthermore, the thermal conductivity between normal metal and superconductor is much better than between superconductor and filler material, i.e. the superconducting coat gets heated due to deposition of energy in normal metal.

The change of state takes place when

$$E_{deposed} \geq \frac{4}{3} \pi R^3 C_v(T) \delta T \qquad (3)$$

wherein δT is characteristic temperature barrier. However,

$$E_{deposed} \approx \sqrt{2} R \left(-\frac{dE}{dx}\right) \qquad (4)$$

and the maximal radius of grain which can change state due to average energy deposition is

$$R_{max} \approx 0.6 \times \sqrt{\left(-\frac{dE}{dx}\right)/C_v(T)\delta T} \qquad (5)$$

In our calculation we use the energy losses of monopoles according to refs. 15 and 16 (see Tab. 2). Actually, the Ford's data are for room temperature; improved conductivity in low temperature leads to bigger losses predicted by Akerlof. It should be pointed out that the energy losses of monopoles in metals are about 500 times bigger than the losses due to minimum ionization, single charge particle. Thus if with relativistic electrons we observed the change of the state in a few micron grains, the losses by monopole should be able to flip much bigger, say a few tens micron grains. The maximum size of grains which flips are quoted in Tab. 3 for 1.2 and 4.2°K, respectively. The typical temperature stability of liquid helium is a few millikelvin and we assumed δT = 10 mK.

From formula (2) and grain radii one can calculate the minimum spacing of the read-out line necessary to detect the change of state of grain crossed by the monopole. They are quoted as L/cm/ in Tab. 3. We see that both in 1.2°K and 4.2°K, the read-out lines spacing of one centimeter permits to detect the grains flipped by monopole, if Akerlof estimates are right. This is valid for all ranges of velocities of interest, $\beta \geq 10^{-5}$. Even for very conservative (based on room temperature conductivity) energy losses calculated by Ford, this detection method is valid for T = 1.2°K and $\beta \geq 5 \cdot 10^{-5}$. Taking into account that Al is not the metal with optimal properties, we are confident that in all cases the read-out problem is not too difficult.

For a monopole traversing a superconductor, one would at first sight not expect an energy loss. However, this is true only for low frequency electromagnetic signals, say $\nu \lesssim 10$ GHz. For signals above a certain frequency, the energy in the quanta is sufficient to overcome the energy gap and to break up the Cooper pairs responsible for superconductivity. It was recently pointed out (see ref. 21 for detailed calculations) that

$$\left(-\frac{dE}{dx}\right)_{supra} \approx 0.5 \left(\frac{n_c}{3}\right)^{2/3} (\beta/10^{-3}) \text{ GeV/cm} \qquad (6)$$

In Fig. 2 the data for superconducting Al(n_c = 3) are compared with

energy deposition in other materials. It should be noted that for $\beta \geq 5 \times 10^{-5}$ this energy losses are much higher than due to minimum ionizing particle, but about a factor hundred smaller than in normal metal. For other superconductors with density ρ, the multiplicative factor of the order of $\rho / \rho(Al)$ should be accounted for.

Most of the studies of SSC have been with tin grains ($T_c \approx 3.3°K$). Specific heat of superconducting tin is, especially for $T \geq 2°K$ much higher than for normal Al. Thus using tin, the grains with diameter smaller than 15 microns should be used. The change of state of such grains is easily detectable, but requires a bigger number of channels (see Tab. 3).

Following our suggestion in April 83, the use of metastable superconducting granules as monopole detector was considered by L. Gonzalez-Mestres and D. Perret-Gallix (see this volume). They point out the "surface effect due to the flux quantum injected by the monopole traversing the granule. This amounts to creating a macroscopic defect on the surface and breaks metastability in a ß-independent way ... Such an effect does not depend on the size of the grain: it provides the most efficient mechanism to flip large granules". Actually, the thermal and magnetic effects of monopole are complementary, which enhance the probability of change of state of large grains. The use of very large grains improves background rejection and makes electronic read-out simpler.

Search for superheavy magnetic monopoles using the superconducting colloid detector

Large surface detector is one of the requirements of any search for superheavy monopoles. The size of SSC detector suggested for the monopoles search is limited by:

- size of existing cryostats
- need of modest, say 200 Gauss field with homogenuity of a few percent;
- cost of electronic read-out, say 50¢ per channel;
- background.

We believe that in practice, the size of the cryostat is the limiting factor. Thus in the following we consider SSC position sensitive detectors placed in a cryostat similar to the biggest existing cryostats. Obviously, the search for magnetic monopoles using superconducting colloid should be initiated with cryostats available commercially, which are much smaller, say 1 m high and 25 cm in diameter.

In Fig. 3 is presented the Stanford cryostat used for gravitational antenna[20]. In the following we will consider a modification of this cryostat, wherein the 0.5 m diameter warm bore is introduced. The dimensions of the liquid helium chamber are 1.4 and 4.0 meters for diameter and length, respectively.

In Fig. 4 is presented the suggested detector configuration. The magnetic field is provided by superconducting magnet. Inside the magnet are two cylindrical position sensitive superconducting colloid detectors with diameters of 1.3 and 1.0 m, respectively. The space between the detectors is partially filled with high density material, say 200 g/cm^2. Inside of the warm bore are placed two conventional position sensitive detectors, e.g. cylindrical MWPC. Furthermore, all of the set-up is

covered by anticoincidance detector, say plastic scintillator.

Let us assume that the thickness of the superconducting colloid detectors is ca 0.5 cm and that the filling factor is 0.1%. With grain size of about 20 microns, the monopole will cross about 50 grains within the same pixel of about 1cc. The read-out of superconducting colloid detector is somewhat similar to MWPC; one can cover the surface of detector with grid of perpendicular readout lines. One requires about 1000 amplifiers with spacing of 2 cm. However, in our case the signal/noise $\gtrsim$100 and the change of state will be sensed by all read-out loops within some 50 cm. The height of the signal is proportional to the distance from the loop to grain and the event position can be estimated from the pulse heights analysis (see center of gravity method in MWPC). With ca 400 amplifiers spaced each 5 cm the spatial resolution of ca 0.5 cm is expected.

For the signal of the magnetic monopole we will accept the coincidance of 4-events on the surface of two coaxial superconducting colloid detectors. These 4-points should be on a straight line. Furthermore, no signal from classical detectors is expected, i.e. we assume that our search is for slow monopoles only.

The geometrical cross-section is ca 28 m^2 str, i.e. some 10^3 times higher than for big induction coil search of IBM group. Furthermore, the velocity of "monopole candidate" can be measured. The time of flight should be ca 4.7 nsec/ß. The superconducting colloid detector provides the timing precision of about 200 nsec, and for monopoles with ß = 10^{-3} the velocity should be measured with precision of about 5%.

Background

Let us consider the background in our detector. The most important source of background in most searches are the cosmic rays, e.g. relativistic protons and/or electrons. However, for grains with R = 20 microns, the energy losses of monopoles should be above 1 MeV, i.e. the grains energy threshold will be set at a few hundreds of keV. The minimum ionization single charged particles leaves ca 0.6 keV/micron in Al, (ca 1.6 keV/μm in Sn) and the energy deposed in the grain is smaller than 50 keV. Thus the minimum ionization particles will not be detected in superconducting colloid when appropriate threshold is used (see ref. 22). Furthermore, the flux of cosmic rays with energy much smaller than $\approx$ GeV/nucleon is suppressed by earth magnetic field. Thus all cosmic rays are relativistic. Good timing of SSC detector permits very good rejection of particles with ß $\lesssim 10^{-3}$.

He^4 and the particles of iron peak, say Z = 26, are non-negligible components of cosmic rays. They will depose over 10 MeV in grain and can flip the grains. However, they are strongly suppressed by anticoincidence counters and by time for flight. Nonrelativistic, say ß $\lesssim 10^{-2}$, particles are rare due to geomagnetic cut-off. Furthermore, if they have velocity of ß $\lesssim 10^{-3}$, their total energy is below 100 MeV. They will be stopped by 200 g/cm^2 of material placed between the superconducting colloid detectors.

The background due to cosmic rays is discussed in (ref. 22). At sea level muons are dominating; with four detector planes, the expected background is ca 8×10^{-4} per m^2 x year. With six detector planes the contribution of He^4 component becomes important and the expected background is ca 7×10^{-8} per m^2 x year. Under ground only muons are

of importance and with 4 detector planes, the expected background is 3×10^{-8} per m^2 x year (at 1000 m H_2O equivalent).

Let us consider the background due to natural radioactivity. The electrons with $E \gtrsim 500$ keV are already relativistic and will leave less than 20 keV/grain. Thus both beta and gamma emitting impurities will only rarely change the state of the grains. The background due to typical ß-emitting contaminant K^{40} is ca $10^{-23}/m^2$ x year. Alpha sources and fission will influence our detector. Actually, the few MeV alpha will not be stopped within a single grain, but can be rejected because we assumed that some ten of grains within a pixel of one cubic centimeter are required as monopole signal. Actually, fission seems to be a more important source of background than α particles. However, even in this case background is negligible. We expect that with 4- detector planes the background due to natural radioactivity is below 10^{-10} per m^2, i.e. much smaller than background due to cosmic rays.

Neutrons are not suppressed by external anticoincidence detectors. Grains can flip due to:

- absorption of thermal neutrons and the induced radioactivity;
- scattering and/or nonelastic interactions of energetic neutrons.

The analysis shows (see ref. 22) that the background due to neutrons is small. We should like to point out that the superconducting colloid provides for a very good rejection of background. This is possible due to:

- good energy resolution (threshold);
- excellent time resolution;
- good spatial resolution.

Acknowledgements

It is a pleasure to thank L. Stodolsky and G. Raffelt for discussions. Furthermore, my thanks go to C.W. Akerlof and B. Lautrup; Fig. 1 and 2 are from their papers.

References

(1) J.P. Preskill, Phys.Rev.Lett. 43, 1365 (1979);
Y.D. Zeldovitch, M.Y. Klopov, Phys.Lett. 79B, 239 (1978).

(2) B. Cabrera, P. Trower, "Magnetic Monopoles: Evidence since the Dirac conjecture", August 1982 (preprint VPI-EPP-82-4);
G. Giacomelli, "Experimental status of monopoles", in "Magnetic Monopole Workshop", Racine, U.S.A. (October 1982), (preprint IFUB 82-36).

(3) B. Cabrera, preprint BC19-82, Stanford University (to be published in Proc. of 3rd Workshop on Grand Unification, April 1982).

(4) J.P. Ostriker, P.J.E. Peebles, Astrophys.J. 186, 467 (1973);
J.A.R. Caldwell, J.P. Ostriker, ibid. 251, 61 (1981).

(5) E.N. Parker, Astrophys.J. 160, 383 (1970);
M.S. Turner et al., Phys.Rev.D 26, 1296 (1982);
E.E. Salpeter et al., Phys.Rev.Lett. 49, 1114 (1982).

(6) J. Arons, R.D. Blandford, Phys.Rev.Lett. 50, 544 (1983);
N. Meyer, in "Les Monopoles Magnetiques", preprint LAL/83-20.

(7) S. Dimapovlos et al., Nature 17, 135 (1979);
S.L. Glashow, III. Workshop on Grand Unification; Chapel Hill, April 1982.

(8) See discussions during "Magnetic Monopole Workshop", Racine, U.S.A.-October 1982 and
K. Freese, M.S. Turner, Physics Letters 123B, 293 (1983).
(9) A.K. Drukier, "The limit to the cross-section for monopoles creation obtained from the persistance of the magnetic field of white dwarfs", Acta Astronomica, vol. 32, No. 1 (1983);
A.K. Drukier, in Proceedings of Trieste Conference on Magnetic Monopoles, Trieste, December 1981.
(10) D.E. Morrison, preprint Berkeley, September 1982;
M. Price, Proceedings of Monopole 83 Conf., Oct. 83, Ann Arbor.
(11) R. Hagström, Proceedings of 1982 Proton Decay Workshop, June 82, Argonne.
(12) D.J. Ullman, Phys.Rev.Lett. 47, 289 (1981);
S.D. Drell et al., Phys.Rev.Lett. 50, 644 (1983);
see however R. Hagström, Proc.Monopole 83 Conference for less optimistic calculus.
(13) P. McIntyre, Proceedings of 1982 Proton Decay Workshop, June 1982, Argonne;
G. Tarlé et al., Proceedings of Monopole 83, Oct. 83, Ann Arbor.
(14) L. Stodolsky, A.K. Drukier, unpublished;
see also T. Datta, Proceedings of Monopole 83, Oct. 83, Ann Arbor.
(15) C.W. Akerlof, Phys.Rev. D26, 1116 (1982).
(16) G.W. Ford, Phys.Rev. D26, 2519 (1982).
(17) B. Barish, private information;
A.M. Allega, N. Cabibbo; Lett.Nuovo Cimento 38, 263 (1983).
(18) A.K. Drukier, C. Valette, NIM, 105, 285 (1972);
A.K. Drukier et al., Lett.Nuovo Cimento 14, 300 (1975);
A.K. Drukier, L.C. Yuan, NIM, 138, 213 (1976);
A.K. Drukier et al., NIM, 154, 253 (1978);
A.K. Drukier, NIM, 173, 259 (1980);
A.K. Drukier, NIM, 201, 77 (1982);
A.K. Drukier et al., Proceedings, Symposium: Radioaktive Isotope in Klinik und Forschung, Bad Gastein 1982, p. 213-219;
D. Hueber et al., NIM, 167, 201 (1979).
(19) R.L. Chase et al., Proceedings of Int. Conference, ISPRA 1978;
D. Hueber, Ph.D. thesis, University of Paris-6, Orsay, 1981.
(20) W.O. Hamilton et al., Cryogenics, p. 107-112, March 1982.
(21) C. Bernard et al., preprint Th 3694-CERN, summer 1983.
(22) A.K. Drukier, preprint MPI-PAE/PTh 58/83.

NIM = Nuclear Instruments and Methods

Figure Captions

Fig. 1: Energy loss of slow monopole in Al (according to C.W. Akerlof ref. 15)
a) 300°K, Drude-Lorentz approximation for phonon spectrum;
b) 300°K, realistic phonon spectrum;
c) 4.2°K, Drude-Lorentz approximation;
d) 4.2°K, realistic phonon spectrum.

Fig. 2: Thermal energy loss of monopoles in different materials (according to C. Bernard et al., ref. 21; data for Al at 4.2°K according to C.W. Akerlof, realistic phonon spectrum).

Fig. 3: The cryostat used to house Stanford gravitational antenna.

Fig. 4: The magnetic monopole hodoscope based on SSC detector.
1) Veto detector, e.g. plastic scintillator;
2) cryostat; 3) superconducting colloid detector;
4) absorber; 5) warm bore detector, e.g. gas MWPC.

Table 1: Thermal properties of Aluminium and Tin (for T = 10 mK)

T(°K)	C_v(keV/μm^{3}x°K)	E_{th}(keV/μm^3)	C_v(keV/μm^{3}x°K)	E_{th}(keV/μm^3)
1.2	2.1	0.021	3.8	0.038
2.0	3.6	0.036	25.	0.25
4.2	9.3	0.093		
	Al (normal)		Sn (supra)	

Table 2: Energy deposition in Aluminium and Tin (keV/μm)

ß =	10^{-5}	5 x 10^{-5}	10^{-4}	10^{-3}
Al(Akerlof)	50	55	60	80
Al(Ford)	0.3	1.65	3	30
Al(Bernard et al.)	0.2	0.6	1.	10.
Sn(Bernard et al.)	0.54	1.6	2.7	27.

Table 3: Maximum radius of grains flipped by monopole (R/μm/) and spacing of read-out lines (L/cm/)

ß	T/ °K/	R/μm/	L/cm/	R/μm/	L/cm/	R/μm/	L/cm/
10^{-5}	1.2	28	41	2.2	0.1	3.8	1
	4.2	13	4	1.0	0.1		
5x10^{-5}	1.2	29	46	5.2	0.25	6.5	0.85
	4.2	13.6	4.6	1.5	0.1		
10^{-4}	1.2	31	56	6.9	0.6	5.1	2.4
	4.2	15	6	3.3	0.1		
10^{-3}	1.2	36	88	22.	20.	16.	8
	4.2	17	9	10.	2.2		
		Al (Akerlof)		Al (Ford)		Sn (Bernard et al.)	

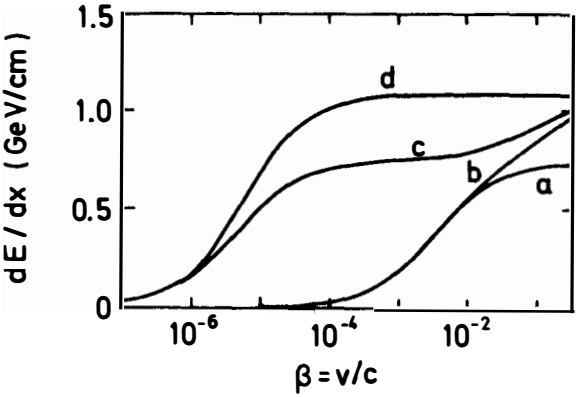

1.5
1.0
0.5
0
dE / dx (GeV/cm)
d
c
b
a
10^{-6}
10^{-4}
10^{-2}
β = v/c

Fig. 1

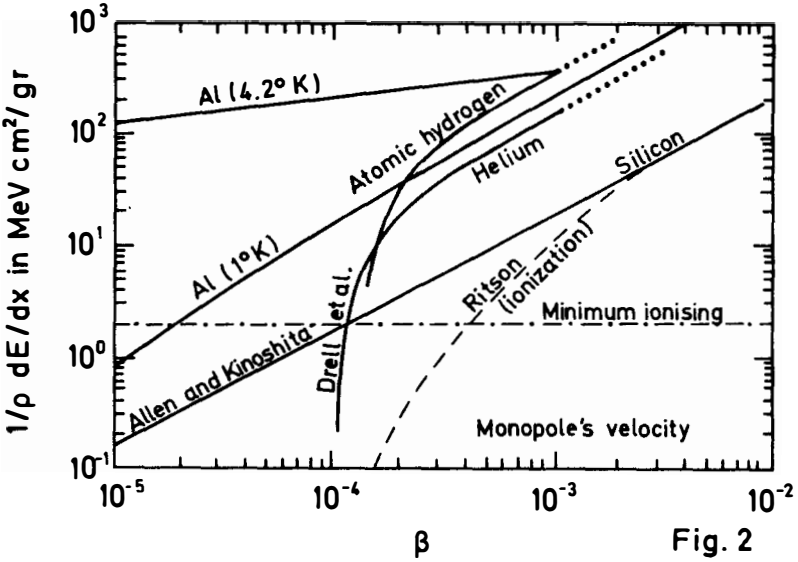

10^3
10^2
10^1
10^0
10^{-1}
1/ρ dE/dx in MeV cm²/ gr
Al (4.2° K)
Atomic hydrogen
Helium
Silicon
Al (1°K)
Ritson (ionization)
Minimum ionising
Allen and Kinoshita
Drell et al.
Monopole's velocity
10^{-5}
10^{-4}
10^{-3}
10^{-2}
β

Fig. 2

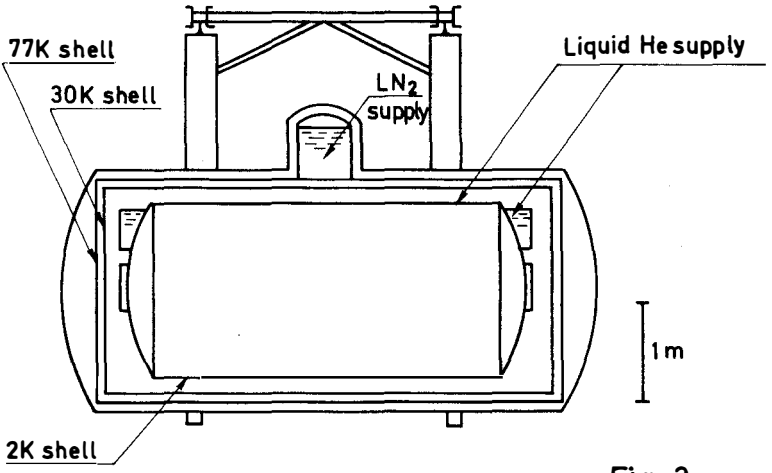

77K shell
30K shell
LN_2 supply
Liquid He supply
1m
2K shell

Fig. 3

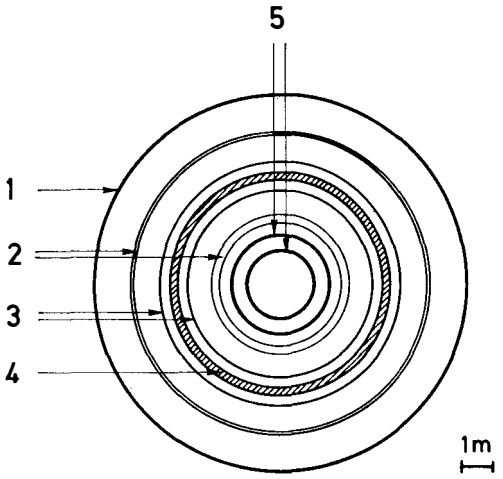

5
1
2
3
4
1m

Fig. 4

XIX RECONTRE DE MORIOND

Fourth Moriond Workshop on Massive Neutrinos in Particle- and Astro-Physics

SUMMARY TALK

S. P. Rosen
T-Division, Los Alamos National Laboratory
Los Alamos, New Mexico 87545



The theoretical arguments for neutrino mass are reviewed, and the present status of searches for neutrino mass in neutrino oscillations, direct measurements and other experiments are summarized.

§ I. Introduction

We have heard many interesting talks at this Moriond Workshop on Massive Neutrinos in Particle- and Astro-Physics, and I will try my best to summarize the main themes. Please keep in mind that, of necessity, the views expressed are purely personal ones.

Let me begin by characterizing the excellent introductory talks of Vanucci[1], Kayser[2], and Steigman[3] with a few words from "Notre Père":

"Que ta volonté soit faite
"Sia fatta la tua voluntá — VANNUCCI
"Thy will be done

sur la terre
come in terra — KAYSER
on Earth

comme au ciel."
cosi in cielo." — STEIGMAN
as it is in Heaven."

As for me, should I omit something of importance, then please:

"forgive us our trespasses, as we forgive them that trespass against us."

Now to the physics! I shall first discuss the present-day theoretical prejudice about the mass of neutrinos, and the experimental methods for detecting it. Then I shall review the limits on masses and mixing angles as presented during the Workshop, and the plans for new experiments. Finally I shall summarize the present status of the field, as I see it.

(a) Theoretical Prejudice

In Grand Unified Theories (GUTS) of strong, electromagnetic, and weak interactions, it is natural for neutrinos to have mass! Zero is a special number, and there is no obvious reason why neutrinos should be different from other fermions, all of which do have mass. However, we must beware that the GUTS do not give us any firm predictions about the likely values of neutrino masses, as they did in the case of the proton lifetime. Indeed, as Kayser[2] has warned us, what predictions there are point toward much smaller masses, in the range $(10^{-6}\text{-}1)$ev, than are contemplated in most experiments today! Nevertheless it is important to pursue the question to the limits of present experimental sensitivity.

For all fermions f, we can construct a mass term by coupling the left-handed and right-handed chirality projections in the usual way:

$$M_D = M_D \bar{f}_L f_R + h.c \qquad (1)$$

Such terms conserve total lepton number and require that both fields f_L and f_R exist in the theory being considered. For neutrinos, and for certain other neutral fermions, we can construct a second type of mass term in which the left-handed field f_L coupled to its own charge-conjugate field f_{LC}, which is right-handed ($f_{LC} \equiv f_{CR}$):

$$M_M \equiv M_M \bar{f}_L f_{CR} + h.c \qquad (2)$$

This term does not conserve lepton number (and for charged fermions it would not conserve charge), but it has the advantage that it can be constructed even when the right-handed field f_R does not occur in the theory. It has become customary to call the total lepton number conserving mass term of eq. (1) the Dirac mass term, and the lepton number violating term of eq. (2) the Majorana mass term.

In the simplest version of the Weinberg-Salam electro-weak theory, and in the simplest GUT (SU(5)), the right-handed neutrino does not occur. This suggests that if the neutrinos that take part in ordinary weak interactions (e.g. β-decay, μ-capture, τ-decay) do have mass, it must be of the Majorana variety. Morever, this suggestion carries through into those GUTS which do have room for right-handed neutrinos; the mass of the right-handed neutrino is assumed to be very large in the Gell-Mann-Ramond-Slansky[4] mechanism, and the effective low-energy theory still contains only left-handed neutrino fields. Thus, in addition to the prejudice that neutrinos are massive (or massious[5]) particles, GUTS also lend support to the notion that neutrino mass is, at least in part, of the Majorana variety.

Neutrino mass matrices which are either dominated by Majorana mass terms, or contain a significant component of such terms, have as their eigenstates, the so-called Majorana neutrinos. Strictly speaking, Majorana neutrinos are eigenstates of CPT, but it is often a good approximation to treat them as CP eigenstates; for some practical applications one can even work with eigenstates of charge conjugation.

Most of the experimental methods for detecting neutrino mass do not distinguish between the Dirac and Majorana varieties, but there is one phenomenon which does, namely no-neutrino double beta decay. This phenomenon is sensitive only to Majorana mass terms and provides no information about Dirac terms. We now turn to a discussion of these methods.

(b) Searching for Neutrino Mass (sur la terre).

Neutrino flavor oscillations will occur if the neutrino flavor eigenstates produced by weak interactions are actually linear combinations of mass eigenstates with different masses. As each flavor eigenstate evolves in time, these

mass differences induce changes of phase between the mass eigenstates of which the original flavor eigenstate is composed, and in turn the changes of phase introduce into the neutrino state-vector components of flavor eigenstates which were not present when the particle was born. Detection of these additional flavors (appearance experiments), or of a depletion in the original flavor (disappearance experiments) would demonstrate qualitatively that there exists at least one neutrino with non-zero mass.

The simplest and most common way of analysing oscillation experiments is a two-state model in which the lepton flavors ℓ and ℓ' are assumed to be orthogonal combinations of the mass-eigenstates ν_1 and ν_2. The probability for the appearance of the second flavor ℓ' in a beam which is initially pure ℓ flavor is given by the familiar and oft-quoted formula:

$$P(\nu_\ell \to \nu_{\ell'}) = \sin^2 2\theta \, \sin^2 (\pi R/L) \tag{3}$$

and the probability for the disappearance experiment is

$$P(\nu_\ell \to \nu_\ell) = 1 - P(\nu_\ell \to \nu_{\ell'}) \tag{4}$$

In these formulae, the oscillation length expressed in kilometres is given by

$$L = 2.5 \, [E(\text{Gev})/\Delta m^2(\text{ev}^2)] \text{ km} \tag{5}$$

where $\Delta m^2 = m_1^2 - m_2^2$ is the squared-mass difference between ν_1 and ν_2.

When the distance R between neutrino source and detector is very large compared with L, then the oscillatory function $\sin^2(\pi R/L)$ goes through many cycles, and we detect its average value of $\frac{1}{2}$. This situation gives us great sensitivity to very small mixing angle factors, $\sin^2 2\theta$, and it usually arises when Δm^2 is relatively large. When R is small compared with L, we can achieve great sensitivity to very small squared-mass differences Δm^2 as long as $\sin^2 2\theta$ is reasonably large (say $\geqq 0.2$). Thus, neutrino oscillations provide us with a very effective means for exploring those regions of the Δm^2 - $\sin^2 2\theta$ parameter space in which one parameter is extremely small while the other is quite large; in fact, oscillations are probably the best means for exploring mass differences down to the 10^{-10}ev^2 level.

At first sight, direct determination of the neutrino mass in two- and three-body decays would seem to be the best way of determining whether the neutrino has a mass, and if so how large it is. In practice, however, experimental problems limit the sensitivity of the experiments, or create difficulties of interpretation. The tritium beta decay experiments, for example, have definitely established an upper limit of 55 ev on the mass of the electron-neutrino ν_e [6], and the

present question is whether they also establish a lower limit. The claim of the ITEP group that this lower limit is 20 ev[7] has yet to be confirmed; a new round of experiments should be sensitive to a level somewhere in the 1-5 ev range, but there may be questions as to whether any effect observed would be due to the mass of the neutrino, or to the environment in which the daughter nucleus finds itself. As for the ν_μ and ν_τ masses, present techniques of two-body, or quasi-two-body decays have not gone lower than 500 kev for ν_μ and 170 Mev for ν_τ.

Besides the predominantly left-handed, and presumably light neutrinos ν_e, ν_μ, ν_τ, there could exist within the same families other, heavier neutrinos, which might be right-handed. There could also exist entirely new families of fermions with their attendant neutrinos, which might also be heavy. As Gronau[8] emphasized, the theoretical motivation for such neutrinos arises from attempts to understand the mass matrix. In the mechanism of Gell-Mann, Ramond, and Slansky[4] all neutrinos are Majorana particles, and each light left-handed neutrino has a heavy right-handed one associated with it. In other models, the light neutrinos are actually massless because of some discrete symmetry, and the right-handed ones become heavy Dirac particles. Whatever the model, we expect that all of the mass eigenstates become admixed into the flavor eigenstates, and we must try to determine, or set limits on the masses and mixing matrices.

One way of doing this is to search for secondary peaks in two-body decays such as $K, \pi \to \mu\nu$, and another is to look for "kinks" in three-body decay spectra, signifying the kinematic limits for heavy neutrinos. Other methods include searches for decays of heavy neutrinos in conventional beams, in beam dump experiments, and even in the decays of B-mesons and Z^o-mesons; some care must be excercized in the interpretation of such experiments because the lifetimes of heavy mesons could be very long (see talks by Kayser[2] and Levy[9]). From these types of experiment we can set extensive limits on the masses and mixing matrices of heavy leptons, as has been discussed by Gronau[8].

The methods for detecting neutrino mass that we have discussed so far are not sensitive to the nature of that mass, to whether it is Dirac or Majorana. One method which is sensitive to this question is the phenomenon of no-neutrino double beta decay:

$$(A,Z) \to (A, Z + 2) + 2e^- \qquad (6)$$

This process can occur as a second-order effect of the usual beta-decay interaction only if:

(i) lepton number is not conserved; and

(ii) the helicity rule associated with (V-A) currents breaks down.

The Majorana mass term satisfies both of these conditions, whereas the Dirac mass term satisfies only the second one; hence no-neutrino double beta decay is sensitive to the Majorana mass term but not to the Dirac one. As we learned from the comprehensive review by Professor Kotani[10] and the experimental report from Dr. Zanotti[11], present experiments (which have not yet detected the no-neutrino decay) on Tellurium isotopes limit the mass to about 5 ev, and those on ^{76}Ge limit the mass to 5 ev or 14 ev, depending upon the theoretical nuclear matrix elements being used:

$$\begin{aligned} (M\nu_e)_{\text{Majorana}} &\leqq 5 \text{ ev} \quad (Te^{128,130}) \\ &\leqq 5 \text{ or } 14 \text{ ev } (Ge^{76}) \end{aligned} \tag{7}$$

It should be noted that, even if the no-neutrino decay were observed, we could only set limits on the neutrino mass because small admixtures of right-handed currents in the weak interaction, of order 10^{-4} -10^{-5}, can mimic the effects of neutrino masses of the size given in eq. (7), insofar as the total rates are concerned. Angular correlations are needed to pick out the mass contribution.

Double beta decay is, of course, a low energy phenomenon. An interesting high-energy phenomenon which is also sensitive to the Majorana mass is a process I would like to call the "Grand Prix de Kayser". One takes very energetic positive pions ($E_\pi \sim$ 600 Gev), and looks to see whether the neutrinos produced in their decay will give birth to positive muons when they strike a nucleus, rather than to negative muons. This two-step process has the effect of producing two positive muons and no neutrinos from an initial state that contained no leptons, and so it violates lepton number conservation in exactly the same way as no-neutrino double beta decay.

If one made no attempt to select the neutrinos in the "Grand Prix", then one could set a limit on the parameter $(M_\nu/\langle E_\nu \rangle)$. For energetic pions, the average energy of the neutrino will be high, and hence the limit obtained would not be very severe. However, Kayser[2] argues that if one selects those neutrinos which travel backwards in the pion center-of-mass frame, then the Lorentz transformation into the laboratory frame will flip the neutrino helicity (provided that $M_\nu \neq 0$) and thereby enhance the probability for the neutrino to create a μ^+ at the second stage of the process. This enhancement, Kayser hopes, can greatly tighten the limit on M_ν.

(c) Astrophysical Limits (comme au ciel).

We heard from Steigman[3] that arguments concerning the age of the Universe, its expansion, and the existence of dark matter on various scales indicate that the neutrino mass should fall within the broad range:

$$M_\nu \sim 10 - 100 \text{ ev} \tag{8}$$

Stable neutrinos with masses between a few ev and a few Gev would dominate the Universe, but there are problems, especially for light neutrinos. Such particles could stream freely through the Universe and damp out the perturbations responsible for galaxy and galactic cluster formation. Thus neutrinos with masses in a range somewhere between 25 to 100 ev at the lower end and 2 to 5 Gev at the upper end must be unstable.

These arguments do not distinguish between Dirac and Majorana masses; moreover, some of them appear to be quite controversial. For example, we heard from Lafon[12] that on the scale of galaxies the roughly constant behaviour of rotation curves does not necessarily imply a halo of dark matter. Lafon has found distributions of visible matter that yield rotation curves consistent with those actually seen; to distinguish between distributions of visible matter and dark haloes, one will have to study the distribution of angular momentum in galaxies.

§ II. The Experimental Situation

Let me now review the experimental data presented at this Workshop. I shall begin with neutrino oscillations, direct measurements, and the solar neutrino problem, and then move on to a discussion of limits on masses and mixing angles for heavy neutrinos.

(a) Neutrino Oscillation Limits.

In order to summarize the limits on oscillations, I shall make use of the ΔM^2 - $\sin^2 2\theta$ plot and look for any trends indicated by the data. Thus I shall not pay too much attention to the wiggles that occur in the data from individual experiments, but concentrate instead upon the limits of small $\sin^2 2\theta$ obtained when ΔM^2 can be large, and upon the limits of small ΔM^2 obtained when $\sin^2 2\theta$ is itself quite large. As indicated in fig. (1), the narrow allowed region along the ΔM^2-axis is called "La Manche", and that along the $\sin^2 2\theta$-axis is called "Le Doigt."

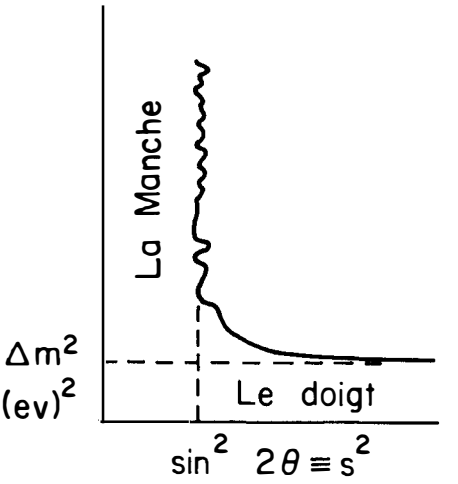


Figure (1) Neutrino Oscillation Limits in the Δm^2 - $\sin^2 2\theta$ Plane.

The tendency of much of the data is to push us more and more into the region of La Manche - low $\sin^2 2\theta$ (henceforth called s^2) and possibly large ΔM^2. In

TABLE I, I have assembled the limits presented by various experiments to the Workshop, and one can see that, while the limits on ΔM^2 obtained from accelerator experiments tend to remain in the range of 0.2 → 1 ev^2, the limit on s^2 gets down to 5 x 10^{-2} in both the CDHS and Fermilab ν_μ disappearence experiments, and in the CHARM $\nu_\mu \to \nu_e$ appearence experiment. At Brookhaven, the limit on s^2 for $\nu_\mu \to \nu_e$ has been pushed down to the level of 5 x 10^{-3}, but at a cost of a much larger mass difference, $\Delta M^2 \simeq 10$ ev^2.

Reactor experiments on $\bar{\nu}_e$ disappearence are not so sensitive to small s^2, but they do yield much tighter limits on ΔM^2. The Goesgen reactor experiment has

TABLE I: Neutrino Oscillation Limits

	$\nu_\mu \to \nu_x$		$\nu_\mu \to \nu_e$		$\bar{\nu}_e \to \bar{\nu}_x$		Notes
	Δm^2	s^2	Δm^2	s^2	Δm^2	s^2	
CHARM[13]	0.3	0.2	0.2	0.05			
CDHS[14]	0.25	0.05					"Best fit" $\Delta^2 = 0.32$ $1^2 = 0.2$
BNL[15]			10	0.005			
FNAL[16]	1	0.05					Room for osc. in large Δ^2
Goesgen[17]					10^{-2}	0.15	small s^2
	(A change in τ_n could raise to 0.2)						$\Delta^2 = 500$, s^2=0.06
Le Bugey[18]					0.1	0.10	High statistics Hint at $\Delta^2 = 0.6, s^2 \lesssim 0.1$
Beam Dump[19] Oh Brave New World!	G. Conforto						$\nu_e \to \nu_\tau$ with $\Delta = 360 \pm 40$ $s^2 = 0.32^{+018}_{-0.08}$

pushed ΔM^2 down to 10^{-2} ev^2 for $s^2 \gtrsim 0.2$, while Le Bugey has achieved a level of 10^{-1} ev^2 in a relatively short period of running. Le Bugey, a large power reactor near Lyons, is a promising newcomer to the field: it has very high power (2750 MW), and offers an excellent location for a detector just 13.6 m below the core! A second position to the right of the first and 18.7 m from the core is also being used. One looks forward to a significant improvement in statistics and

sensitivity with this experiment[18].

Almost all of these experiments report hints that there may be an oscillation in the data. In the case of ν_μ- disappearence, for example, CDHS gives a "best fit" to the data with $\Delta^2 = 0.32 ev^2$ and $s^2 = 0.2$, while the Fermilab experiment could accommodate an oscillation with large mass difference and small mixing angle, namely $\Delta^2 = 500\ ev^2$, $s^2 = 0.06$. Similarly Le Bugey has a hint of an oscillation in $\bar{\nu}_e$- disappearence with parameters $\Delta^2 = 0.6 ev^2$ and $s^2 \lesssim 0.1$. In none of these experiments, however, do the experimentalists make any strong claims for the existence of oscillations because of uncertainties in their knowledge of such items as normalizations, backgrounds, and theoretically calculated spectra. There is, in another type of experiment, one exception to this cautious attitude.

Gianni Conforto[19] has analysed a series of Beam Dump Experiments carried out by the BEBC, CDHS, and CHARM detectors at CERN between 1977 and 1982, and by the FMOWW group at Fermilab in 1981-82, and he believes that there is clear evidence for neutrino oscillations. He argues that: (i) the ratio of "prompt" electron-type neutrinos to "prompt" muon-type neutrinos is definitely smaller than unity in certain groups of experiments; and (ii) that the ratio shows a definite dependence on the distance between dump and detector. From a statistical analysis of the data, he concludes that the probability that no oscillation is taking place is about 2×10^{-4}, while the probability for an oscillation is approximately 35%.

To fit the data, which is summarized in the following table, Conforto adopts the admittedly simple hypothesis that ν_μ does not undergo oscillations, while the

TABLE II: Summary of Beam Dump Data

Experiments (n = number of detectors)	Distance	$\langle \nu_e/\nu_\mu \rangle$	χ^2
CERN (77-79) (n = 3)	~ 900 m	0.57 ± 0.09	0.58
CERN (1982) (n = 2)	~ 450 m	0.74 ± 0.10	4.5
Fermilab (81-82) (n = 1)	~ 60 m	1.09 ± 0.09 ± 0.10	-

ν_e oscillates into some unspecified neutrino ν_x. He then finds that the best fit to the data is an oscillation with parameters

$$\Delta^2 = (360 \pm 40)\ ev^2$$
$$\sin^2 2\theta = 0.32\ ^{+0.18}_{-0.08} \qquad (9)$$

The value for $\sin^2 2\theta$ is just within two standard deviations of the Goesgen limit on $\bar{\nu}_e$-disappearence.

Conforto believes that $\nu_e \leftrightarrow \nu_\tau$ oscillations provide the most reasonable interpretation of this data, but he would be glad to examine other hypotheses. He is presently engaged in a more refined analysis.

b) Direct Mass Measurements

On the subject of the direct measurement of neutrino mass, we heard about new experiments on the muon- and tau- neutrinos, and a discussion of the preparations for new efforts to measure the mass of the electron-neutrino in tritium beta decay. Le Coultre[20] described an experiment at SIN in which pions decaying in flight are used to set an upper bound on the ν_μ mass. The energies and decay angle of the parent pion and daughter muon are measured with the aid of an 180° degree magnetic spectrometer, the decay point being determined by time-of-flight. The neutrino momentum, as determined from the vector difference between pion and muon momenta, is then compared with the momentum expected for a zero-mass neutrino and a limit of

$$M_{\nu_\mu} < 0.50 \text{ Mev/c}^2 \quad (90\% \text{ C.L.}) \tag{10}$$

is extracted from the data with 90% confidence limit.

By far the hardest part of the experiment is the measurement of the decay angle between the pion and muon, and it will require a significant improvement in this measurement in order to improve the above limit by a factor of 2-3. It is interesting to note that, at this time, the limits on $M\nu_\mu$ from decay in flight are very similar to those obtained from decay at rest. Deutsch[21] has suggested that one may be able to push these limits much farther down by looking at the "Concorde Edge" of the Dalitz plot for $\mu^- + Li^6 \rightarrow 2H^3 + \nu_\mu$; this is analogous to studying the end-points of β-spectra.

The previous limit on the tau-neutrino mass of 250 Mev/c^2 has now been reduced to 173 Mev/c^2 in an experiment by the Mark II collaboration[22] at PEP. Whereas the earlier limit was obtained from the decay of the tau-lepton into relatively light systems ($\tau \rightarrow e\ \nu_e\ \nu_\tau$, $\pi\ \nu_\tau$), the new one comes from decay into a heavy system, $\tau \rightarrow 3\ \pi^{\pm}\ \pi^o\ \nu_\tau$. The experiment has been carried out at a PEP beam energy of 14.5 Gev, and a search was made for τ-decays in which the four pions have a total energy of at least 8 Gev. Of the 55 events found to satisfy the cuts, some 14 have an invariant four-pion mass greater than 1.5 Gev. The distribution of these events is compared with the theoretical distribution for $\tau \rightarrow \rho'\ \nu_\tau$, appropriately smeared by the experimental resolution, and the result

$$M_{\nu_\tau} < 173 \text{ Mev/c}^2 \quad (95\% \text{ C.L.}) \tag{11}$$

is obtained at the 95% confidence level. Under certain conditions this limit can be reduced to 160 Mev/c^2, but it is generally stable against variations of the parameters used in the analysis.

Given the enormous interest in the latest results on $M\nu_e$ obtained by the Moscow group[7] (ITEP-83), it is a great shame that no member of the group has come to the workshop to discuss the details of their tritium β-decay experiment and to respond to questions. The fact that, with greatly improved statistics, background rejection, and resolution, they can set a lower limit of 20 ev on $M\nu_e$ is a result of primary significance, and we are all eager to see whether other experiments will confirm it. In the meantime, questions have been raised about the response function used in the analysis of ITEP-83[23], and it would have been most useful to learn the answers to them. I hope the experts in the field will forgive me if I record my own "gut feeling" that this line of questioning represents the last obstacle to general acceptance of the ITEP-83 result.

Besides the lower limit on $M\nu_e$, there are other very interesting results from the Moscow experiment, in particular the "best fit" of

$$M_{\nu_e} = 33 \pm 1.1 \text{ ev} \tag{12}$$

and the hint, arising from the break in the spectrum at approximately 18,560 ev, that two neutrino mass-eigenstates may be emitted in β-decay. Robertson[24] gave a verbal report of the following two possibilities for the masses and mixing angles:

$$M_1 = 0 \quad ; \quad M_2 = 80 \text{ ev} \qquad 80\% \quad 20\% \tag{13a}$$

and

$$M_1 = 22 \quad ; \quad M_2 = 114 \text{ ev} \qquad 95\% \quad 5\% \tag{13b}$$

The first possibility is not consistent with the Goesgen limit on mixing angles and ΔM^2 ($\sin^2 2\theta < 0.2$ implies that $\sin^2 1\theta < 0.05$), but the second one is consistent, falling as it does within La Manche.

A number of new tritium decay experiments are under construction. Bergkvist[23] has rebuilt the electrostatic-magnetic high-luminosity spectrometer that he used to set the original upper limit of 55 ev on $M\nu_e$, and he has already achieved order of magnitude improvements in the control of the electric and magnetic fields, and in background rejection. He will use a large source of tritium embedded in aluminum, and he hopes to develop a source of better quality than the original one. His game plan is to try and confirm that $M\nu_e$ must be

different from zero before attempting a precision measurement of its actual magnitude.

Robertson[24] described an experiment under way at Los Alamos in which the source of tritium is an atomic beam and the decay electrons are analysed by an improved version of the Tretyakov spectrometer used in the Moscow experiment. Because the tritium comes in the form of free atoms, the final-state effects are well understood and there are no problems associated with source backing. Ultimately the experiment hopes to achieve an unambiguous result at, or below the mass level of 10 ev.

An experiment which is generally expected to produce the first new results in the near future is being performed by a Zurich group at S.I.N.[25] It makes use of a "secret" source and a Tretyakov-type spectrometer. The resolution function can be calculated with some confidence, and measurements have been made to check the calculations. The group hopes to reach a level of ~ 10 ev for the neutrino mass, which is certainly sufficient to check the ITEP result.

Fackler and Mugge[26] talked about an experiment at the Lawrence Livermore National Laboratory which makes use of frozen molecular tritium as its source. Fackler discussed the extensive calculations that have been performed in order to elucidate the final state problem, and Mugge described the experimental set-up, including the electrostatic spectrometer. They hope to have preliminary results by late 1984, and expect to determine the neutrino mass to within ± 2 ev as long as $M\nu_e > 4$ ev.

The considerable attention devoted by the Livermore group to the problem of final states serves to underline the importance of understanding the environment of the tritium source when it is embedded in some matrix, or frozen into a molecular state. Because the environment can engender small shifts in the final state energy levels of the decaying nucleus, it can simulate the effects of a non-zero neutrino mass in the Kurie plot. Therefore, without a thorough understanding of the final state energy levels, one cannot decide whether signals for a non-vanishing neutrino mass found in Kurie plots are real or spurious. For experiments with free atoms, the environmental problem is much less severe than it is for atoms bound in molecules or other matrices.

A different method of measuring the neutrino mass is provided by the phenomenon of "Inner Bremstrahlung Electron Capture" (IBEC) or "Radiative EC Beta Decay"[27]:

$$Z + e_{n\ell j} \rightarrow (Z - 1) + \nu_e + \gamma \qquad (14)$$

The end-point of the γ spectrum is sensitive to a non-zero neutrino mass in much the same way as is the Kurie plot, and the effect can be strongly enhanced if the

capture takes place from a P-state[27]. A recent experiment on ^{193}Pt verified the basic theory of the process developed by Glauber and Martin (1956) and by de Rujula (1981), and it set a limit of 500 ev/c^2 on $M\nu_e$. The nucleus ^{163}Ho is regarded as the most promising case for neutrino mass measurements and an experiment described by Ravn is being performed at CERN. Bennett is using this isotope at Princeton, and Raghavan[28] has suggested ^{158}Tb as another favorable case.

(c) The Solar Neutrino Problem

The solar neutrino problem, which led Pontecorvo to revive his original idea of neutrino oscillations in 1967[29], is still with us, some seventeen years later! We still cannot say for sure whether the discrepancy between the rate observed in the Davis experiment and the theoretically calculated rate is due to neutrino oscillations, or to a faulty model of the sun, or to some subtle error in the experiment.

To indicate the gravity of the problem, let us recall that there are three major components of the solar neutrino flux:[30]

(i) pp neutrinos with energies in the range $0 \leq E_\nu \leq 420$ kev and a flux of 6×10^{10} ν_e/cm^2 sec;

(ii) Be^7 neutrinos which are monochromatic with $E_\nu = 861$ kev and have a flux of 4×10^9 ν_e/cm^2 sec; and

(iii) B^8 neutrinos with energies in the range $0 \leq E \leq 14$ Mev and a relatively small flux of 3×10^6 ν_e/cm^2 sec.

The $\nu_e + Cl^{37} \rightarrow e^- + Ar^{37}$ reaction has a threshold of 814 kev, and so it is sensitive predominantly to the B^8 neutrinos and partially to the Be^7 ones; it has no sensitivity to the major component of the spectrum, namely the pp neutrinos. Averaged over the last three or four years of observation, the experimental rate for the reaction as measured by Davis and his colleagues is[30]:

$$< \text{Exp tl Rate} > = 2.2 \pm 0.4 \text{ SNU} \tag{15}$$

and the theoretical rate is[30] either

$$< \text{Theor. Rate} >_{\text{Bahcall}} = 7.6\ (\pm 40\%) \text{ SNU} \tag{16a}$$

or

$$< \text{Theor. Rate} >_{\text{Münster}} = 4.95\ (\pm 40\%) \text{ SNU} \tag{16b}$$

depending upon whether one uses the Cal Tech value for the parameter S_{34} describing the reaction $He^3 + He^4 \rightarrow Be^7$ (eq. 16a) or the Münster value for it (eq. 16b). The former tends to be the more favored value, but in either case, there is a significant difference between theory and experiment.

According to Schatzman[30], it is possible to change the solar model in such a way that: (i) it is still consistent with what is understood about Li burning,

and with both pressure and gravity modes of solar oscillations; and (ii) the flux of B^8 neutrinos is a factor two smaller than in the standard calculations. However, it would be much harder to reduce this flux by the factor ~4 required by eqs. (15) and the Bahcall rate of eq. (16a). Schatzman also emphasises that the flux of pp neutrinos is proportional to the solar luminosity and subject to no more than a 10% uncertainty; consequently, if the pp neutrinos should not be observed at the theoretically predicted rate, then they must oscillate into flavors which do not undergo charged current nuclear reactions at low energies. It follows that the search for pp neutrinos is the most important next step in the effort to resolve the solar neutrino neutrino problem. Because of the very long baseline, it could also be the oscillation experiment most sensitive to extremely small mass differences ($\Delta^2 \gtrsim 10^{-12} ev^2$).

Spiro[31] described a new effort to mount the indium experiment originally proposed by Raghavan. The reaction

$$\nu_e + {}^{115}In \rightarrow e^- + {}^{115}Sn^{**}(7/2) \qquad (17)$$

has a threshold of 120 kev, and so it is sensitive to both the pp neutrinos and the ^7Be neutrinos. By measuring the energy of the electron, Spiro hopes to separate these two components of the neutrino spectrum and thereby gain some information about nuclear reactions in the sun.

Unfortunately, the estimated rates are low, being 0.25 events/ton In/day for pp neutrinos and 0.05 events/ton In/day for ^7Be neutrinos. The major background comes from the β-decay of ^{115}In to the ground-state of ^{115}Sn which has a half-life of 5×10^{14} years! Spiro and his colleagues are looking for clever ways to overcome this difficulty, and one technique they are considering is that of superconducting granules. A typical granule is of order 10 microns in diameter and, when it is cooled to a sufficiently low temperature, the energy deposited by a single neutrino is sufficient to restore it to the normal state. The major experimental problem is being able to read out magnetic flux changes in every granule in the detector; Waysand[32] described some ways by which it might be overcome.

Superconducting granules represent an exciting new possibility for detectors of all kinds. Stodolsky and Drukier[33] would like to use them as a "neutral current" detector for all types of neutrino, including solar, reactor, terrestrial, and supernova neutrinos; their basic idea is to make the granules sensitive to the coherent forward scattering of neutrinos arising from the neutral current interactions of the standard model. Gonzalez-Mestres and Perret-Gallix[34] would like to use them to detect monopoles, and to measure their velocities. In addition, it may be possible to apply the superconducting granule technique to detectors at accelerators.

Returning to the solar neutrino problem, we note two other experiments which are being seriously pursued. One is the gallium experiment, based upon neutrino capture in ^{71}Ga giving rise to ^{71}Ge, and the other is the bromine experiment, in which neutrino capture by ^{81}Br gives rise to the noble gas isotope ^{81}Kr. The gallium experiment has a threshold of 236 kev and it is sensitive to both pp and ^{7}Be neutrinos; however, because the detection method is radiochemical in nature, it cannot distinguish directly between these two components of the neutrino spectrum. Like the original chlorine experiment, the bromine experiment is sensitive only to the ^{7}Be and ^{8}B neutrinos, but in a different combination; since ^{81}Kr is metastable, with a half-life of ~200,000 yrs., one cannot use radiochemical detection, and so G. S. Hurst[35] is planning to make use of Resonance Ionization Spectroscopy, a very sensitive laser detection technique.

(d) Double Beta Decay

Of the two anticipated modes of nuclear double beta decay, one, the two-neutrino mode, is expected to occur as a second-order effect of the effective Hamiltonian for single β-decay, and the other, the no-neutrino mode, will occur only if lepton number and the (V-A) helicity rule are both violated. The expectation in most grand unified theories is that these violations will occur through a Majorana mass term for neutrinos, but right-handed currents (V+A) may also be present. Kotani[10] has given us a thorough review of the present status of the subject and its relationship to the other phenomena discussed here, and I will try to summarize the situation.

There are several important and presently unresolved problems in double beta decay, some theoretical and some experimental: let me begin with the experimental ones. The earliest definitive evidence for the actual occurrence of the double beta decay phenomenon came from geochemical experiments on ^{130}Te and ^{82}Se. Even though the lifetimes observed in these experiments are consistent with expectations for the two-neutrino mode ($\sim 10^{21\pm2}$ yrs), they cannot be used to rule out the existence of the no-neutrino mode because only the daughter nuclei are detected in the geochemical method. Many laboratory experiments to detect the emitted electrons have been attempted, but only one, by Moe and Lowenthal[36] has claimed any success. Using a cloud chamber and a source of ^{82}Se, they have detected about fifteen candidates which fit the pattern for the two-neutrino mode and correspond to a lifetime of $\sim 10^{19}$ years. Unfortunately, however, this lifetime is an order of magnitude shorter than that measured geochemically: thus the debate rages as to whether the events seen by Moe and Lowenthal are actually due to some very low level background contamination, or whether the geochemical method is inaccurate.

There is also a problem within the geochemical method itself. Many years

ago Pontecorvo[37] invented the tellurium ratio argument as a test for which double beta decay mode might be the dominant one. His argument was that, as long as the nuclear matrix elements for the decays of the isotopes ^{128}Te and ^{130}Te can be taken to be approximately equal, the ratio of their lifetimes will be given by the ratio of the appropriate phase spaces; moreover the ratio for the no-neutrino mode is small (of order 10), while that for the two-neutrino mode, with four fermions in the final state instead of two, is much larger (~7000). The first significant measurement of this ratio in 1974 gave a value of ~1600, which is intermediate between the two extremes and which was interpreted by Bryman and Picciotto[38] as implying that the no-neutrino mode occurs through a right-handed current of strength 10^{-4} times that of the left-handed current. Dr. Kotani and his colleagues[39] subsequently re-interpreted the same result as implying a Majorana mass of order 40 ev. Last year, however, the Heidelberg group re-measured the ratio and found it to be much larger[40], which implies an upper limit of only 5.4 ev on the neutrino mass. On grounds of caution alone, one should favor the smaller limit, but it would be helpful to have another measurement.

The most significant theoretical problem is the calculation of the nuclear matrix elements for double beta decay. Primakoff and I originally made a very crude estimate of 0.1, but allowed ourselves an order of magnitude lee-way on either side. More sophisticated calculations by Vergados suggest that they are much closer to unity, while Haxton, Stephenson, and Strottman find values in the range of 2-3. While the former authors calculate lifetimes for the two-neutrino mode that are consistent with the geochemical measurements, the latter obtain much shorter lifetimes. For example the Haxton et al lifetime for ^{82}Se is 6 times shorter than the geochemical value and within a factor of 2 of the laboratory value obtained by Moe and Lowenthal; for ^{130}Te, the Haxton et al lifetime is 150 times shorter than the geochemical one! Recent calculations by Zamick and Auerbach, Huffman, and Klapdor and Grotz all tend to confirm the Haxton et al matrix elements.

Despite these problems, one can still gain some valuable insights from mass limits in double beta decay. As mentioned above, the tellurium ratio argument gives an upper limit of less than 6 ev on the Majorana mass. If we take the latest bound on the no-neutrino decay of ^{76}Ge as given in the talk by Zanotti[11], we find that the Majorana mass must be less than 14 ev if we use the Kotani matrix element, or less than 6 ev if we use the Haxton et al matrix element. In all cases, these upper bounds are smaller than the lower bound of 20 ev obtained by ITEP-83. Therefore, to the extent that we accept these experiments, there appears to be a conflict between the mass limits from no-neutrino double beta decay and those from tritium beta decay.

One way out of this conflict is to say that the Majorana mass term is zero and the neutrino is a pure Dirac particle. This, however, runs counter to the prevailing theoretical prejudice that neutrinos are Majorana particles. Therefore it behooves theorists to find a clever way out of this dilemma.

The way out was implicit in an early remark of Kotani et al[41] that the contributions of different mass-eigenstates to the no-neutrino amplitude could cancel one another. Thus was born the "Pseudo-Dirac" neutrino, which is a coherent linear combination of two Majorana neutrinos with opposite CP eigenvalues and almost degenerate masses -- the analogue, in fact, of the K_1-K_2 system. The opposite CP eigenvalues ensure that the neutrinos interfere destructively in the no-neutrino decay, and the near degeneracy ensures a very small amplitude. Another realization of this idea is to have one light neutrino and one heavy neutrino, again with opposite CP eigenvalues. In the Pseudo-Dirac case the "effective mass" extracted from the measured lifetimes will be the same for all parent isotopes, whereas in the light-heavy scenario it will vary from isotope to isotope because of the propagation of the heavy neutrino through the nucleus[47]. Thus, if the no-neutrino decay mode is eventually discovered, it will be important to measure its rate and extract an effective mass for several parent nuclei.

Two experiments which hope to detect the no-neutrino double beta decay of ^{76}Ge are the "new set-up" in the Mont Blanc Tunnel[11] and the Santa Barbara-LBL experiment[43]. The "new set-up" has a total volume of 169 cc of high purity germanium as compared with 143 cc in the original experiment, and it sits in a much cleaner vessel. In 941 hours of running it has achieved a lifetime limit (1.3×10^{22} years at 68% confidence level) which compares very favorably with the limit (4.7×10^{22} years at 68% c.l.) ahieved by the old detector in 10,068 hours of operation! The old detector is now being used in an attempt to find the $0^+ \to 2^+$ transitions in ^{128}Te and ^{130}Te; for no-neutrino decay these transitions would signal the presence of right-handed currents.

The Santa Barbara-LBL experiment is a much larger one[43], involving eight detectors each of which is comparable in size with the new Mont Blanc detector. Special care has been taken to improve the purity of the germanium and to reduce the activity in the materials from which the detector housing is fabricated. Discrimination against external β-particles, multiple Compton scattering, and cosmic ray neutron induced backgrounds is achieved by surrounding each germanium crystal with ten 15 cm thick Na I detectors. In one year of running, it is hoped to set a limit of 1×10^{24} years on the ground-state to ground-state ($0^+ \to 0^+$) transition, and a comparable limit on the $0^+ \to 2^+$ transition; in the absence of right-handed currents, this corresponds to a mass limit of 2 ev with the Kotani matrix element, and 1 ev with the Haxton et al matrix element.

Some other experiments on ^{76}Ge were not discussed at this meeting. They include one by the South Carolina-Battelle group (Avignone et al), and one by a Cal Tech-S.I.N. collaboration (Boehm et al).

(e) Search for Heavy Neutrinos.

As Gronau emphasized in his talk[8], the theoretical motivation for continuing to search for heavy neutral leptons includes the possible existence of a fourth generation, each of whose members would be significantly heavier than their partners in present generations, and the necessity for heavy partners for the known light neutrinos as envisaged in the Gell-Mann-Ramond-Slansky and Yanagida mass mechanisms. Shrock[44] has pioneered the notion of searching for anomalous spikes in two-body decays and kinks in three-body decay spectra, as a means of setting limits on masses and mixing matrix elements, and several experiments of this type were discussed at this workshop.

We heard from Schreckenbach[17] about the search for kinks in the spectra of the $\beta\pm$-decays of ^{64}Cu; the experiment yields limits on $\sin^2\theta$ ($\equiv |U_{eH}|^2$) in the range 10^{-2} to 10^{-3} for a heavy neutrino mass in the range $100 \leqq M_H \leqq 400$ kev. If the heavy neutrino is a Majorana particle, then the limits on $\sin^2\theta$ obtained by Simpson from double beta decay are about an order of magnitude more stringent.

Olin and Prieels[45] discussed the search for spikes in $\pi \to e\, \nu_H$. From the Triumf experiment, Olin extracts limits on the mixing matrix element $|U_{eH}|^2$ in the range 10^{-5} to 10^{-6} for $20 \leqq M_H \leqq 120$ Mev. Prieels, in an experiment at SIN, hopes to push these limits down by an order of magnitude. In another Louvain - SIN collaboration, this time on μ-capture in ^3He, Prieels and his colleagues hope to push the limits on muon-heavy neutrino mixing matrix elements $|U_{\mu H}|^2$ down to the 10^{-3} to 10^{-4} level for masses in the range $20 \leqq M_\mu \leqq 100$ Mev. This will help to fill in the gap between the limits obtained at SIN from $\pi \to \mu\nu$ ($|U_{\mu H}|^2 \leqq 10^{-4}$ to 10^{-5} for $M_H \leqq 20$ Mev) and those found by KEK in $K \to \mu\nu$ ($|U_{\mu H}|^2 \leqq 10^{-5}$ to 10^{-6} for $100 \leqq M_\mu \leqq 200$ Mev).

Eventually we may be able to apply the "spike and kink" approach directly to D-mesons and B-mesons (and even to T-mesons if the top quark ever shows itself) as a way of exploring mass regions beyond a few hundred Mev. But for the moment we can best search for neutral leptons in this mass range through their presumed production as primary or secondary products of high energy neutrino and hadron reactions, followed by their decay into some specific final state. It is impressive how well one can do with this method.

The CHARM detector at CERN has been used in a series of experiments in which various pseudoscalar mesons M ($\equiv \pi$, K, D, ...) are produced in the primary collision of the proton beam and then decay into a heavy neutrino[46]:

$$M \to \nu_H + \ell + X \qquad (18)$$

where X represents the vacuum (two-body decay) or some system of hadrons. In its turn, the heavy neutrino is then assumed to decay into an electron-positron pair, for example:

$$\nu_H \to e^- e^+ \nu_e \tag{19}$$

The probability for the occurrence of the sequence in eqs. (18) and (19) is proportional to the product $|U_{\ell H}|^2 \, |U_{eH}|^2$. When $\ell = e$, a limit on $|U_{\ell H}|^2$ can be extracted from the data, and when $\ell = \mu$, a limit on the product $|U_{\mu H}| \cdot |U_{\ell H}|$ is obtained.

In one experiment[46], the CHARM collaboration makes use of the Wide Band Beam and assumes that the heavy neutrino comes only from the decays of π and K mesons; limits on $|U_{eH}|^2$ and $|U_{eH}| \cdot |U_{\mu H}|$ of the order of 10^{-6} are obtained for heavy neutrinos in the 200-300 Mev range. The beam dump is used in a second experiment and the mass range up to ~1750 Mev is explored through the decays of D- and F-mesons; limits of order 10^{-7} are then found for $|U_{eH}|^2$ and $|U_{eH}| \cdot |U_{\mu H}|$ when the heavy neutrino mass is in the vicinity of 1500 Mev.

It is also possible in this second experiment to set very tight limits on $|U_{e\tau}|^2$ through the sequence

$$\begin{aligned} P &\to F + \ldots\ldots \\ &\to \nu_\tau + \tau \\ &\to e^- e^+ \nu_e \end{aligned} \tag{20}$$

The probability for this sequence is proportional to $|U\tau\tau|^2 |U_{e\tau}|^2 \sim |U_{e\tau}|^2$, and so, if one makes "reasonable" assumptions about the production cross-section and branching ratio for F in eq. (20), one obtains a limit on $|U_{e\tau}|^2$ rather than on $|U_{eH}|^4$ directly from the data. If the production cross-section for F is assumed to be 20% of that for D-mesons, and the branching ratio for $F \to \nu_\tau \, \tau$ is 3%, then the limits on $|U_{e\tau}|^2$ are 10^{-9} for $M_{\nu\tau} \sim 100$ Mev and 10^{-10} for $M_{\nu\tau} \sim 170$ Mev, its new upper bound! When the most recent 1983 run is analysed, it is hoped to improve these remarkable limits by one or two orders of magnitude.

We summarize these results in Table III; for a more detailed picture the reader should turn to the various $|U_{\ell H}|^2$ - mass plots given by the speakers to whom I have made reference. As a point of comparison, we note that the Conforto oscillations[19] occur at $\sin^2 \theta \sim 0.1$, $M \sim 20$ ev.

According to Gronau[8], new beam dump experiments and the decays of b-quarks produced in e^+e^- collisions should be able to push the mass limits to ≥ 3 Gev with $|U_{\ell H}|^2 \leq 10^{-6} - 10^{-5}$, while high statistics neutrino experiments may extend the excluded mass range to 5 Gev. W and Z decays will eventually push the mass limits out to ~ 50 Gev, and the SSC could even venture as far as 10 Tev! The

theoretical "see-saw" reciprocity between heavy and light neutrinos makes the search for high mass leptons as important as the search for light ones.

TABLE III: Summary of $|U_{\ell H}|^2$ - mass limits

$\|U_{\ell H}\|^2$	limits	Mass Range	Method
$\|U_{eH}\|^2$	10^{-2} - 10^{-3}	100 - 400 kev	β-decay
$\|U_{eH}\|^2$	10^{-5} - 10^{-6}	$10 \leqq M_H \leqq 120$ Mev	$\pi \to e\nu$
$\|U_{\mu H}\|^2$	10^{-3} - 10^{-4}	$20 \leqq M_H \leqq 100$ Mev	μ-capture
$\|U_{\mu H}\|^2$	10^{-4} - 10^{-5}	$M_H \leqq 20$ Mev	$\pi \to \mu\nu$
$\|U_{eH}\|^2$ / $\|U_{eH}\| \cdot \|U_{\mu H}\|$	10^{-6}	200 - 300 Mev	$K \to \nu_H \to ee\nu$
$\|U_{eH}\|^2$ / $\|U_{eH}\| \cdot \|U_{\mu H}\|$	$\sim 10^{-7}$	~ 1500 Mev	$D \to \nu_\mu \to ee\nu$
$\|U_{e\tau}\|^2$	~ 10^{-9}	~ 100 Mev	$F \to \nu_\tau \to ee\nu$
-"-	~ 10^{-10}	~ 170 Mev	-"-

§III. What To Make Of All This?

Que Faire?

What sense can one make of all this information? Let me try to give you a personal view, which may, or may not, coincide with other points of view.

1) Neutrino oscillation limits continue to move into the regions "La Manche" and "Le Doigt" of the Δ^2 - s^2 plane (see fig. 1). My own preference is for La Manche, and so I hope that experimentalists will not give me "Le Doigt" in the next round of experiments. As a word of caution, let me admonish you to "Ricorda Conforto", who believes that oscillations are here to stay.

2) The case for non-zero $\bar{\nu}_e$ mass from tritium β-decay seems to be still "Not Proven". But help is on the way with several new experiments which may have something to tell us next year! Unfortunately molecular and environmental corrections in the source render these experiments not quite as clean as one would like in relation to the qualitative question: does $\bar{\nu}_e$ have a non-vanishing mass? In principle, the experiments are simple, but in practice environmental energy shifts may imitate or mask the effect for which one looks. An attractive exception to this is the atomic experiment described by Robertson[24], in which the

final states are well understood. It may well be, however, that oscillations are a better qualitative demonstration of non-zero mass, especially if the masses are very small (Kayser's Warning!).

3) The solar neutrino problem is still with us, and there is a crying need for more experiments, especially those that will detect the pp neutrinos! The flux of these neutrinos is proportional to the solar luminosity, and any significant deviation from the predicted reaction rate would be a sure sign of oscillations. Thus solar neutrino experiments could make or break the oscillation hypothesis.

4) Double beta decay experiments are getting to a point where limits on the effective Majorana mass begin to be in conflict with the tritium experiment. If the latter is confirmed, it could either mean "the end" for Majorana neutrinos, or an enrichment of the spectrum. One form of enrichment is the pseudo-Dirac hypothesis according to which the electron-type neutrino is an admixture of two almost degenerate Majorana neutrinos with opposite CP eigenvalues. Another is the light-heavy option in which ν_e is still an admixture of Majorana neutrinos with opposite CP, but now one is light and the other heavy; the mass and mixing angle of the heavy neutrino should be located in La Manche region of the oscillation plot.

5) Mixing matrix elements for heavy neutrinos have now reached the general level of $|U_{\ell H}|^2 \leq 10^{-6}$ and are still falling! Future experiments should push this down by one or two orders of magnitude, and extend the range of excluded masses considerably. We may have to wait for W and Z factories, or even the SSC before we see a heavy neutral lepton!

6) We have, at present, no definitive evidence for the existence of neutrino mass, either of the Dirac kind, or the Majorana kind. We must therefore begin to face the ultimate question: could it be that neutrinos are massless Dirac particles which neither oscillate nor behave in any other exotic ways?

FIN

I began my talk on a religious note, so let me end on a poetic one. "We are such stuff as dreams are made of," said William Shakespeare; and for us the dream is a universe filled with neutrinos, a world of powdery snow.

Many thanks to our hosts for giving us such a wonderful week. May they give us many more!

References

The abbreviation t.p. is used for talks included in "these proceedings", and the reader is referred to such talks for a complete set of references.

(1) F. Vannucci, t.p.
(2) B. Kayser, t.p.
(3) G. Steigman, t.p.
(4) M. Gell-Mann, P. Ramond, R. Slansky, Rev. Mod. Phys. 50, 721 (1978).
(5) F. W. Stecker, Neutrino '81 Vol. I p. 124 (1981).
(6) K. E. Bergkvist, Nucl. Phys. B39, 317 (1972).
(7) V. A. Lubimov, Proceedings of HEP 83, Brighton, England (1983).
(8) M. Gronau, t.p.
(9) J.-M. Levy, t.p.
(10) T. Kotani, t.p.
(11) L. Zanotti, t.p.
(12) J. P. Lafon, t.p.
(13) C. Lanceri, t.p.
(14) J. Wotschack, t.p.
(15) H. White, t.p.
(16) C. Haber, t.p.
(17) K. Schreckenback, t.p.
(18) J. Thenard, t.p.
(19) G. Conforto, t.p.
(20) P. le Coultre, t.p.
(21) J. Deutsch, t.p.
(22) C. Matteuzzi, t.p.
(34) K. Bergkvist, t.p.
(24) M. Robertson, t.p.
(25) J. Peterson, t.p.
(26) O. Fackler and M. Mugge, t.p.
(27) H. Ravn, t.p.
(28) R. Raghavan, Phys. Rev. Lett. 51, 975 and 1395 (1983).
(29) B. Pontecorvo, JETP 26, 984 (1968).
(30) A. Schatzman, t.p.
(31) M. Spiro, t.p.
(32) G. Waysand, t.p.
(33) L. Stodolsky and A. Drukier, t.p.
(34) D. Perret-Gallix, t.p.
(35) G. S. Hurst, Oak Ridge National Laboratory.
(36) M. Moe and D. Lowenthal, Phys. Rev. C22, 2186 (1980).
(37) B. Pontecorvo, Phys. Lett 26B, 630 (1968).
(38) D. Bryman and C. Picciotto, Rev. Mod. Phys. 50, 11 (1978).
(39) M. Doi et al, Phys. Lett. 102B, 323 (1981).
(40) T. Kirsten, M. Richter, and E. Jessberger, Phys. Rev. Lett. 50, 474 (1983).
(41) M. Doi et al, Phys. Lett 103B, 219 (1981). See also Valle, and Petcov.
(42) A. Halprin, S. Petcov, and S. P. Rosen, Phys. Lett. 125B, 355 (1983).
(43) R. Eisberg, t.p.
(44) R. Shrock, Phys. Rev. D24, 1232 (1983).
(45) S. Olin and R. Prieels, t.p.
(46) C. Santoni, t.p.

LIST OF PARTICIPANTS

ANDERHUB Hans	IHP, ETH-Z Institut Honggerberg 8093 ZURICH SWITZERLAND
BERGKVIST Karl	Research Inst. for Physics Roslagsvagen 100 104 05 STOCKHOLM SWEDEN
BERNARDI Gregorio	LPNHE, Univ. P. & M. Curie Tour 32, 4 Place Jussieu 75230 PARIS Cedex 05 FRANCE
BJORKEN James	FERMILAB P.O. Box 500 60510 BATAVIA IL USA
BOSETTI Peter	III Physikalisches Inst. RWTH Aachen Physikzentrum 5100 AACHEN FEDERAL REP. GERMANY
BOUCHEZ Jacques	D.Ph.P.E. CEN Saclay 91191 GIF SUR YVETTE Cedex FRANCE
CHARDIN Gabriel	D.Ph.P.E/SECB CEN Saclay 91191 GIF/YVETTE Cedex FRANCE
CHAUVEAU Jacques	Lab. Phys. Corpusculaire Collège de France 75231 PARIS Cedex 05 FRANCE
CONFORTO Gianni	I.N.F.N. - Univ. di Firenze Largo Enrico Fermi 2 50125 FIRENZE ITALY
DE BELLEFON Alain	Lab. Phys. Corpusculaire Collège de France 75231 PARIS Cedex 05 FRANCE
DE-RUJULA Alvaro	C.E.R.N. TH Division 1211 GENEVA 23 SWITZERLAND

DECLAIS Yves	CPPM - UER de Luminy Case 907 13288 MARSEILLE Cedex 02 FRANCE
DEUTSCH Jules	Inst. de Physique Univ Catholique de Louvain 1348 LOUVAIN LA NEUVE BELGIUM
DIEMOZ Marcella	Ist. di Fisica, Univ. di Roma Pzale A. Moro 2 00185 ROMA ITALY
DOMINGUEZ-TENREIRO Rosa Maria	Dept de Fis. Téorica, Mod C-XI Univ. Autonoma de Madrid 34 Canto Blanco MADRID SPAIN
DRUKIER Andrzej K.	Max Planck Inst. fur Physik Postfach 40 12 12 8000 MUNCHEN 40 FEDERAL REP. GERMANY
EISBERG Robert	Physics Dept. Univ. of California 93106 SANTA BARBARA CA USA
ESCOUBES Bruno	Centre de Recher.Nucléaires Div. des Hautes Energies 67037 STRASBOURG CEDEX FRANCE
FACKLER Orrin	Phys. Dept., Rockefeller Univ. 1230 York Ave. 10021 NEW YORK NY USA
FERRONI Fernando	Ist. di Fisica, Univ. di Roma Pzale A. Moro 2 00185 ROMA ITALY
GIRARDI Georges	L.A.P.P. Boite Postale 909 74019 ANNECY LE VIEUX Cedex FRANCE
GONZALEZ MESTRES Luis	L.A.P.P. Boite Postale 909 74019 ANNECY LE VIEUX Cedex FRANCE

GRONAU Michael
Dept of Physics
Syracuse University
13210 SYRACUSE NY
USA

GUYOT Claude
C.E.R.N.
EP Division
1211 GENEVA 23
SWITZERLAND

HABER Carl
Nevis Laboratory
P.O. Box 137
10533 IRVINGTON NY
USA

HALPRIN Arthur
Physics Dept.
University of Delaware
19716 NEWARK DE
USA

HARRIS Frederick
Dept of Phys. & Astronomy
Hawaii University
96822 HONOLULU Hawaii
USA

HOUMMADA Abdeslam
Inst des Scie Nucleaires
Université de Grenoble
38026 GRENOBLE Cedex
FRANCE

KAYSER Boris
Division of Physics
National Scie. Foundation
20550 WASHINGTON DC
USA

KITAGAKI Toshio
Dept of Physics, Tohoku Univ.
Aramaki Aoba
980 SENDAI
JAPAN

KOANG Dy-Holm
Inst. des Sciences Nucléaires
Univ. de Grenoble
38026 GRENOBLE Cedex
FRANCE

KOTANI Tsuneyuki
Phys. Inst-Gal Educat. College
Osaka Univ., Toyonaka
560 OSAKA
JAPAN

LABERRIGUE-FROLOW Jeanne
LPNHE, Univ. P.& M. Curie
Tour 32, 4 Pl. Jussieu
75230 PARIS Cedex 05
FRANCE

LAFON Jean Pierre	DESPA - Obs. de Paris Meudon Meudon Principal 92195 MEUDON Cedex FRANCE
LANCERI Livio	C.E.R.N. EP Division 1211 GENEVA 23 SWITZERLAND
LE COULTRE Pierre	IHP, ETH-Z Inst.of Honggerberg 8093 ZURICH SWITZERLAND
LEVY Jean Michel	LPTHE, Univ. P & M Curie Tour 12, 4 Place Jussieu 75230 PARIS Cedex 05 FRANCE
LUSIGNOLI Maurizio	Dipt di Fis.,Univ. La Sapienza INFN, Pzale Aldo Moro 2 00185 ROMA ITALY
MATTEUZZI Clara	S.L.A.C. P.O. Box 4349 94305 STANFORD CA USA
MERRITT Frank	Enrico Fermi Lab, Chicago Univ 5640 S. Ellis Ave. 60637 CHICAGO IL USA
MERRITT Wyatt	FERMILAB P.O. Box 500 60510 BATAVIA IL USA
MORALES Angel	Dept.de Fis. Atom. y Nuclear Fac. Scie., Ciudad Univ. 9 ZARAGOZA SPAIN
MUGGE Marshall	FERMILAB P.O. Box 500 60510 BATAVIA IL USA
O'HALLORAN Thomas	Loomis Phys. Lab-Illinois Univ 1110 West Green Str. 61801 URBANA IL USA

OLIN Art	TRIUMPH, 4004 Wesbrook Hall UBC Campus V6T 2A6 VANCOUVER BC CANADA
PERRET-GALLIX Denis	L.A.P.P. Boite Postale 909 74019 ANNECY LE VIEUX Cedex FRANCE
PESSARD Henri	L.A.P.P. Boite Postale 909 74019 ANNECY LE VIEUX Cedex FRANCE
PETERSEN Jon Wulff	Inst. of Physics - Zurich Univ Schonbergas. 9 8001 ZURICH SWITZERLAND
PETROFF Pierre	CERN / L.A.L. Bat 200, Univ. Paris Sud 91405 ORSAY CEDEX FRANCE
PEVSNER Aihud	Jonhs Hopkins Univ, Phys. Dept 34 th & Charles Streets 21218 BALTIMORE MD USA
PIERRE Francois	D.Ph.P.E CEN Saclay 91191 GIF/YVETTE Cedex FRANCE
PONS Yvette	L.P.N.H.E, Univ. Paris VII Tour 32, 4 Place Jussieu 75230 PARIS Cedex 05 FRANCE
PRIEELS René	Inst. de Physique Univ Catholique de Louvain 1348 LOUVAIN LA NEUVE BELGIUM
RAVN Helge	C.E.R.N. EP Division 1211 GENEVA 23 SWITZERLAND
ROBERTSON Hamish	Los Alamos Nat. Laboratory P-3, MS D456 87545 LOS ALAMOS NM USA

ROSEN Peter	Los Alamos Nat. Laboratory T-Do, Ms B 288 87545 LOS ALAMOS NM USA
ROTHENBERG Allan	C.E.R.N. EP Division 1211 GENEVA 23 SWITZERLAND
SADOULET Bernard	C.E.R.N. EP Division 1211 GENEVA 23 SWITZERLAND
SANTONI Claudio	INFN Sanita (Roma) & C.E.R.N. EP Division 1211 GENEVA 23 SWITZERLAND
SCHATZMAN Evry	Lab. de Radio Astronomie Ecole Normale Supérieure 75231 PARIS CEDEX 05 FRANCE
SCHRECKENBACH Klaus	Dept. de Phys., Inst Langevin Ave des Martyrs, BP 156X 38042 GRENOBLE CEDEX FRANCE
SHAEVITZ Michael	Nevis Lab. P.O. Box 137 10533 IRVINGTON NY USA
SPIRO Michel	D.Ph.P.E CEN Saclay 91191 GIF/YVETTE Cedex FRANCE
STEIGMAN Gary	Bartol Research Foundation University of Delaware 19711 NEWARK DE USA
STODOLSKY Léo	Max Planck Inst. Kernphys Postfach 40 12 12 8000 MUNCHEN 40 FEDERAL REP. GERMANY
THENARD Jean Michel	L.A.P.P. Boite Postale 909 31500 ANNECY LE VIEUX Cedex FRANCE

TRAN THANH VAN Jean	L.P.T.P.E. Bat 211, Univ. Paris Sud 91405 ORSAY Cedex FRANCE
VANNUCCI Francois	LPNHE - Univ. P. & M. Curie Tour 32 - 4 Place Jussieu 75230 PARIS CEDEX 05 FRANCE
VIGNON Bernard	Inst. des Sciences Nucléaires 53 Ave des Martyrs 38026 GRENOBLE CEDEX FRANCE
WALKER James K.	C.E.R.N. EP Division 1211 GENEVA 23 SWITZERLAND
WAYSAND Georges	Lab. de Phys. des Solides, ENS Univ. Paris 7 Tour 23 75231 PARIS Cedex 05 FRANCE
WHITE Hywel	Physics Dept. Brookhaven Nat. Lab. 11973 UPTON NY USA
WOTSCHACK Jorg	C.E.R.N. EP Division 1211 GENEVA 23 SWITZERLAND
ZANOTTI Luigi	Dipt di Fis, Univ. di Milano Via Celoria 16 20133 MILANO ITALY